REPORT MDC E1248
JSC 09651

NASA CR-
141925

DATA CORRELATION AND ANALYSIS OF ARC TUNNEL AND WIND TUNNEL TESTS OF RSI JOINTS AND GAPS

PHASE II FINAL REPORT

VOLUME I — TECHNICAL REPORT

NAS9-14012 DRD MA-384T 19 MAY 1975

MCDONNELL DOUGLAS ASTRONAUTICS COMPANY - EAST

MCDONNELL DOUGLAS CORPORATION

FOREWORD

This report summarizes the work conducted by McDonnell Douglas Astronautics Company-East (MDAC-E) in St. Louis, Missouri for the Structures and Mechanics Division of the NASA Johnson Space Center (NASA-JSC) under Contract NAS9-14012, "Data Correlation and Analysis of Arc Tunnel and Wind Tunnel Test of RSI Joints and Gaps, Phase II." This final report consists of two volumes: Volume I - Technical Report and Volume II - Data Base, Part 1 and Part 2. The period of performance was from 20 May 1974 thru 19 May 1975.

Mr. Donald J. Tillian was the NASA Technical Monitor for this study; Messrs. H. E. Christensen and H. W. Kipp were the MDAC Principal Investigator and Study Manager, respectively. Significant contributions to this study were made by A. E. Bruns, M. B. Donovan, L. H. Ebbesmeyer, E. A. Eiswirth and T. W. Parkinson. The cooperation of numerous NASA Personnel at Ames Research Center, Johnson Space Center and Langley Research Center in providing experimental data, supplemental calculations and valuable counsel was instrumental to the successful completion of this study. Data used in Section 4.2 are based on an analysis originally performed for Rockwell International Corp. under the direction of P. C. Merhoff. We are appreciative of the cooperation from the following for supplying test data; C. D. Scott and L. P. Murray of JSC, W. K. Lockman and F. J. Centolanzi of Ames, D. A. Throckmorton and I. Weinstein of LaRC, and G. W. Mauss and C. B. Blumer of Rockwell International. Special acknowledgement is made of assistance and support provided by the NASA Ames Research Center under Contract NAS2-7897 (Rev 4) for the RSI sizing calculations using current Shuttle design philosophy which are presented in Section 7 of this report.

The International System of Units is used as the primary system for all results reported herein. The results are also reported in the British Engineering System of Units which was used for calculations made during the course of this study.

TABLE OF CONTENTS

TABLE OF CONTENTS
(Continued)

TABLE OF CONTENTS
(Continued)

LIST OF PAGES

Title Page
ii thru vi
1 thru 307
A1 thru A3
B1 thru B3
C1 thru C24
D1

ABSTRACT

Heat transfer data measured in gaps representative of those being employed for joints in the Space Shuttle RSI thermal protection system have been assimilated, analyzed and correlated. The study reported herein is the second phase of an earlier study of gap heating phenomena reported in Reference 1. Portions of these results are included herein for completeness.

The body of data under study was obtained in six NASA facilities, the Ames 3.5 Foot Hypersonic Wind Tunnel, the Ames 20 Megawatt Turbulent Duct, the JSC 10 Megawatt Arc Tunnel, the LaRC Mach 10 Continuous Flow Hypersonic Tunnel, the LaRC Mach 8 Variable Density Tunnel, and the LaRC 8 Foot High Temperature Structures Tunnel. Several types of gap were investigated with emphasis on simple butt joints. Gap widths ranged from 0.0 to 0.76 cm and depths ranged from 1 to 6 cm. Laminar, transitional and turbulent boundary layer flows over the gap opening were investigated. The angle between gap axis and external flow was varied between 0 and $\pi/2$ radians. The "contoured" cross section gap performed significantly better than all other wide gaps and slightly better than all other narrow gap geometries. Three-dimensional heating variations were observed within gaps in the absence of external flow pressure gradients. Interactions between heating within gaps and heating of adjacent top tile surfaces were observed in several tests. Also, gaps aligned with the flow were observed to promote boundary layer transition in tests conducted in the Ames 3.5 Foot Hypersonic Wind Tunnel. Heat transfer correlation equations were obtained for many of the tests. TPS thickness requirements with and without gaps were computed for a current Shuttle entry trajectory. Experimental data employed in the study are summarized in Volume II.

1.0 INTRODUCTION

The reusable surface insulation (RSI)* thermal protection system (TPS) for Space Shuttle requires gaps at RSI joints to accommodate structural deflection resulting from loads and thermal expansion. In addition, allowance must be made for manufacturing and assembly tolerances. At room temperature, gap widths under current consideration range from 0.127 cm to 0.254 cm (0.050" to 0.10") $\pm$ 0.038 cm to 0.076 cm (0.015" to 0.030"). In orbital operation, these may shrink to near zero during cold soak or grow by as much as 25%. Candidate tile edge radii range from 0.076 to 0.254 cm (0.030" to 0.1").

The successful application of RSI material for Shuttle thermal protection is significantly affected by entry heating within the RSI gaps. Gap width, depth, cross section geometry, gap orientation, boundary layer state and surface mismatch are all known to affect convective heating within the gap and heat leakage to the protected substructure. For instance, present study results indicate a 0.254 cm wide flush transverse butt gap increases TPS thickness requirements by approximately 33% above the thickness required for a TPS without gaps.

During 1972 and 1973, extensive tests of various gap configurations were run by NASA to provide a data base for accurate assessment of gap heating Data were taken in both wind tunnels and in arc tunnels. A large segment of these data were analyzed and correlated to obtain methods for predicting heating in RSI gaps on Shuttle. Based on the correlations, the effect of gap heating on Shuttle lower surface TPS requirements was determined for a typical reentry trajectory. The results of these Phase I studies are documented in Reference 1 .

Subsequently, additional tests were run by NASA to clarify prior data and to address unresolved questions. The analysis of these data on a consistent basis with the earlier analysis was the objective of the Phase II study documented herein. The test data sources utilized in this study are identified in Figure 1. Data sources used in the earlier Phase I study are also shown, identified with an asterisk.

NASA is continuously improving and adding test facilities. Throughout this report we refer to testing in the JSC 10 Mw Arc Tunnel facility using a laminar duct configuration. This duct was operated at TP2 (test position number 2). Similarly, the NASA personnel at Ames have several duct test facilities, and the test programs evaluated in this study were performed using the 2"x9" turbulent duct facility.

---

* Also referred to as HRSI (High Temperature Reusable Surface Insulation)

GAP HEATING TEST SUMMARY - OCTOBER 1974

TEST FACILITY	INVESTIGATORS	BOUNDARY LAYER STATE	M_∞	Re_∞/m	TYPE MODEL	TYPE GAPS	GAP WIDTHS (cm)	GAP DEPTH (cm)	STEP HEIGHTS (cm)	FLOW ORIENT. (DEGREES)	EDGE RADIUS (cm)
JSC 10 MW ARC TUNNEL CHANNEL NOZZLE (TP2) **	H.E. CHRISTENSEN D.J. TILLIAN (1972 - 1973)	LAMINAR	4.2-4.7	6×10^4	MULLITE RSI (6")	BUTT, CONTOURED INCLINED OVERLAP BLOCK	0.127, 0.254 0.381, 0.762 (COLD WALL)	3.175 5.08 6.35	0. ±0.381	0	
JSC 10 MW ARC TUNNEL WEDGE ($15^\circ\alpha$)	CARL SCOTT (1974)	LAMINAR	9.6	1741	6" THIN SKIN TILES	INLINE BUTT	0.127 0.254 0.381	4.1275	~.	0	0. 0.3175 0.635 1.27
JSC 10 MW ARC TUNNEL CHANNEL NOZZLE	ROCKWELL INT. (GARY HAUSS) 1973	LAMINAR	3.7-4.5	$4.5\text{-}8.2\times10^4$	SILICA HRSI (5.8")	STAGGERED BUTT AND OVERLAP BLOCK	0.127 0.254	2.54 5.08	0.	0	
LaRC MACH 8 * VARIABLE DENSITY (WALL & FREESTREAM)	C. B. JOHNSON (1972)	LAMINAR TRANSITIONAL TURBULENT	8.0	1.1×10^6 TO 40×10^6	4"X8" THIN SKIN TILES	INLINE AND STAGGERED BUTT	0.159 0.318 0.476	2.54	0.	0	
AMES 3.5 FOOT * HWT (FREESTREAM)	W.K. LOCKMAN C.B. BLUMER (1973)	LAMINAR TRANSITIONAL TURBULENT	5.1	1×10^6 TO 4.6×10^6	FLAT PLATE THIN SKIN	INLINE, TRANSVERSE, SWEPT BUTT	0, 0.064 0.127, 0.254 0.508	0, 1.016 2.032 4.064	+0.318 ±0.159 0.	0	
AMES 3.5 FOOT HWT (FREESTREAM)	W.K. LOCKMAN C.B. BLUMER (1973)	LAMINAR TRANSITIONAL TURBULENT	5.1	1.64×10^6 3.28×10^6 6.56×10^6	FLAT PLATE THIN SKIN	SINGLE INLINE BUTT (12"&40" LENGTH)	0.0 0.127 0.254	0.0 1.0 2.0 3.81	0.	0 5 10 15	
LaRC MACH 10 * CFHT (WALL)	H.E. CHRISTENSEN D.A. THROCKMORTON (1973)	TURBULENT	10	3.28×10^6	6" THIN SKIN TILE	INLINE AND STAGGERED BUTT	0.13 0.23 0.46 0.71	6.35	+0.254 0 -0.168	0, 7.5, 15, 30 45, 60 75, 82.5, 90	0.3175
LaRC MACH 10 CFHT (WALL) (SUPPLEMENTAL RUNS)	H.E. CHRISTENSEN D.A. THROCKMORTON (1974)	TURBULENT	10	3.28×10^6 7.4×10^6	6" THIN SKIN TILE	INLINE AND STAGGERED BUTT	0.0 0.13 0.23	0.0 6.35	0.	0, 90	0.3175
LaRC 8 FOOT HTST (0° 7.5° $15^\circ\alpha$)	IRVING WEINSTEIN (1974)	TURBULENT	6.2-7.0	1.9×10^6 4.8×10^6	6" THIN SKIN TILE	INLINE AND STAGGERED BUTT	0.0 0.10, 0.18, 0.30, 0.41	6.35	0.0 +.254	0	0.254
AMES 20 MW TURBULENT DUCT (2" x 9")	FRANK CENTOLANZI (1974)	TURBULENT	3.5	0.3×10^6	SILICA RSI (4"X8")	TRANSVERSE BUTT	0.0 0.127, 0.180, 0.254, 0.381, 0.508	5.08	0.	0	0.153 0.635 + OTHERS

* DATA SOURCES UTILIZED IN REPORT MDC E1003 (PHASE I)

** TP2 - TEST POSITION NUMBER 2

Figure 1

The following major tasks were performed during the study:

- o Assimilation of gap heating data from NASA facilities
- o Analysis of the data to determine heating rates and sensitivities; comparison of the various candidate joints
- o Correlation of the assimilated data and the development of a gap heating procedure which was applied to a current Shuttle trajectory.

This volume describes the assimilation, analyses and correlations resulting from the study as well as the conclusions derived therefrom. Volume II of this report presents the basic gap heating data including information relating to each test facility, run schedule, test conditions and models.

2.0 SUMMARY

This study of heat transfer within RSI gaps builds upon the Phase I study results documented in Reference 1 . As in Phase I, the Phase II work described herein was performed in three tasks, namely, data assimilation, data analysis and correlation of results. Highlights of these tasks are summarized in this section.

The data assimilation task entailed compilation and evaluation of the gap heating data from the new sources listed in Figure 1. Also, errors in some of the thin skin heat transfer data assimilated during Phase I were eliminated by a new data reduction employing corrected specific heat values. In addition, skin conduction corrections were established for portions of the data. The experimental data were read from magnetic tapes provided by the various test facilities and transcribed into a uniform format in a gap heating data bank. To facilitate data retrieval and analysis, 24 attribute words were assigned to each heating data point. These attribute words consisted of information such as test and geometry identifiers, instrumentation locations, flow orientation, inviscid flow conditions and boundary layer parameters. The SELECT computer program, prepared during the Phase I study was used to assess the data bank and to prepare specific data for the subsequent multiple regression analysis. The assimilated data are compiled in a test data document which is the second volume of this report.

The data analysis task entailed performing a number of diverse subtasks. Included were reduction of temperature histories measured on RSI tiles in the JSC 10 MW Tunnel and in the LaRC 8 Foot HTST to heat flux by means of an inverse solution. Subsequently these data were incorporated in the data bank. Additional subtasks included graphic data presentation, data-theory comparison, sensitivity analysis and boundary layer calculations. End results of the analysis task included the identification of significant phenomena observed in the test program and the preparation of data for correlation.

Reinforcement of many of the Phase I conclusions resulted from the additional data obtained during Phase II.

Among the more significant observations made during Phase II is that gaps aligned with the flow promote transition. Examination of the data taken in the Ames 3.5 Foot H.W.T. indicates that the transition onset occurs within the gap. The parametric variation of edge radius tested in the JSC 10 MW indicates that increased convective heating results from increasing edge radius. Coupling these data with a complete RSI tile heat transfer analysis indicates, however, that the

increased convective heating is more than offset by increased radiation re obtained from the larger radius.

Correlation equations for several new classes of gap heating were obtained during Phase II and improvements were made on several developed during Phase I. The development of correlation equations benefited significantly by the use of multiple regression analysis. The correlation of transverse gap data obtained during Phase I has been updated by including a larger body of data. An improved correlation of in-line gaps to include flow incidence up to 51 degrees was developed using data from the Ames 3.5 Foot HWT. A correlation for the effect of edge radius on in-line and transverse gap heating was developed using data obtained in the JSC 10 MW Tunnel.

An automated gap heating subroutine incorporating the above correlations has been developed. This subroutine is described in Section 6 of this report.

A re-assessment of the influence of gap heating on TPS requirement was made during Phase II. The assessment included a parametric evaluation of gap width and radius effect. The increase in TPS thickness caused by the presence of gaps was found to vary between 12% and 42%. The calculations are described in Section 7.

3. TEST PROGRAMS AND DATA ASSIMILATION

Ten test programs constitute the principal data base for this study as summarized in Figure 1 . Four of these ten programs were previously reported in detail in Reference 1 , but are summarized herein for reader convenience. In addition, supplemental runs were made for the previous tests conducted in the LaRC Mach 10 Continuous Flow Hypersonic Tunnel (CFHT). The primary data assimilated during Phase II resulted from test programs conducted in the JSC Laminar Duct, the LaRC 8 foot High Temperature Structures Tunnel (HTST), the Ames 20 MW Turbulent Duct, the JSC 10 MW Laminar Duct and the Ames 3.5 foot Hypervelocity Wind Tunnel (HWT) facility.

A general description of each test program and the data assimilated follows. Additional information related to the test facilities, models, test conditions and data appears in Volume II of this report and Volume II of Reference 1 (Phase I data). The terminology used in this report to describe gap configurations and tile arrangements is depicted in Figure 2 .

3.1 Data Previously Assimilated (Phase I) - Gap heating tests were performed in the channel nozzle of the JSC 10 MW Arc Tunnel to provide heating data in the presence of a high enthalpy laminar boundary layer. The tests employed arrays of Mullite RSI tile which were heavily instrumented on gap surfaces and in depth at the center of one tile in each array. Thirteen models employing a variety of gap and tile configurations were tested. The gaps between the tiles were adjustable to study the effects of gap width using consistent sets of instrumentation. Four gap settings were employed (0.127, 0.254, 0.381 and 0.762 cm) with tile thickness of 3.175, 5.08 and 6.35 cm. Butt joint step heights of $\pm$0.381 cm were also investigated. Figure 3 summarizes the matrix of configurations tested in the channel nozzle. The figure also depicts the arc tunnel and shows a 5.08 cm butt joint model. Temperature response data from 36 gap locations were analyzed to obtain comparisons of heating rate distributions using the inverse solution technique.

Gap heating tests were conducted in the LaRC Mach 10 CFHT to provide data in the presence of a relatively thick turbulent boundary layer. The tests employed a wall-mounted stainless steel, thin skin "tile" model in which the instrumented thin skin tile was surrounded by an array of uninstrumented RSI tiles. The model was mounted on a turntable to permit variation of flow orientation relative to the tile array. A total of 157 runs was made at a unit Reynolds number per meter of

NOMENCLATURE

- SYSTEM INTERNATIONAL UNITS
- JOINT DESIGN

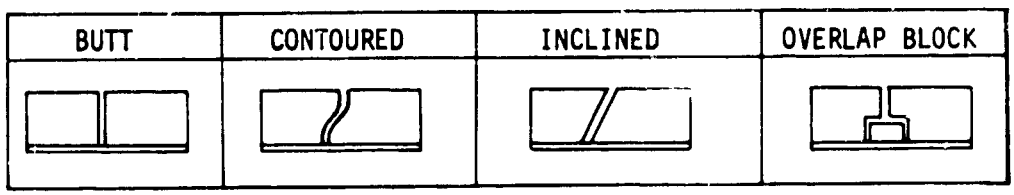

- DOWN STREAM SIDE OF GAP
- UPSTREAM SIDE OF GAP

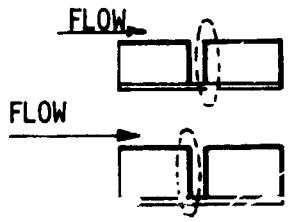

- IN-LINE GAP

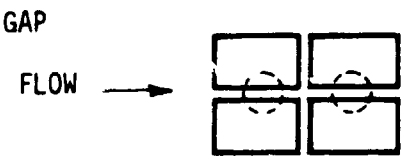

- TRANSVERSE GAP

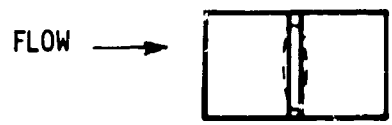

- BUTT JOINT FWD STEP
- BUTT JOINT AFT STEP

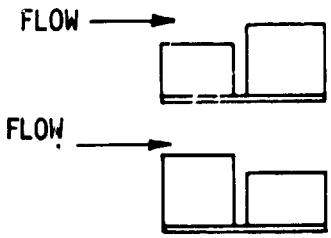

- IN-LINE TILES

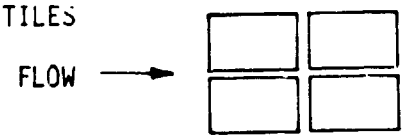

- STAGGERED TILES

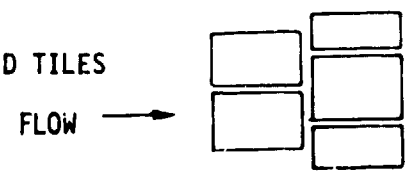

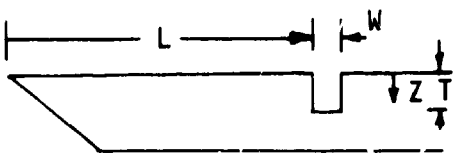

Figure 2

NASA JSC 10 MW ARC TUNNEL TESTS OF GAP HEATING MODELS (MISSION SIMULATION)

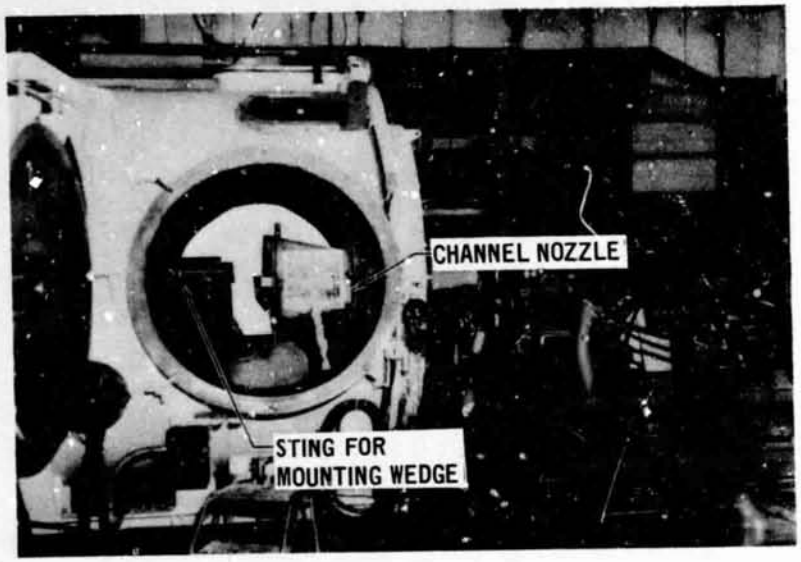

5.08 cm BUTT JOINT (0.381 cm AFT FACING STEP)

TESTING CONTOURED JOINT

(0.762 cm GAP)

	WEDGE CONFIGURATION W =0.127,0.254,0.762 cm	CHANNEL NOZZLE W = 0.127,0.254,0.381,0.762 cm
BUTT 3.175 cm 5.08 cm 6.35 cm	✓	✓ ✓ ✓
BUTT STEP 5.08 cm WITH 0.381 cm FORWARD STEP 5.08 cm WITH 0.381 cm AFT STEP	✓	✓ ✓
STAGGERED BUTT 5.08 cm		✓
OVERLAP BLOCK 5.08 cm 6.35 cm		✓ ✓
CONTOURED 3.175 cm 5.08 cm 6.35 cm	✓ ✓ ✓	✓ ✓ ✓
INCLINED 5.08 cm 6.35 cm		✓ ✓

W = GAP WIDTH

Figure 3

3.2×10^6. The test matrix included nine flow orientations (0 to $\pi/2$ radians), four gap widths (0.127, 0.229, 0.457 and 0.711 cm) and three step heights (0, +0.254 and -0.168 cm). Tile thickness was 6.35 cm. Figure 4 shows the instrumented tile, the surrounding array of uninstrumented RSI tiles and the installation in the CFHT tunnel wall. A photograph of the installation is shown in Figure 5 which also summarizes the test matrix. Temperature response data from 81 thermocouples were analyzed to obtain heat fluxes and to determine the effects of inline versus staggered tiles, gap width, flow orientation and steps.

Gap heating tests were conducted by C. B. Johnson (NASA, Langley Research Center) in the LaRC Mach 8 Variable Density Tunnel (VDT) to provide data in the presence of laminar and turbulent boundary layers. The tests employed models which simulated thin skin tiles which were mounted in a curved plate. Models were tested both in the free stream and mounted flush with the tunnel wall. In each model position, the test section unit Reynolds number was varied over the range of 1.1×10^6 to 40×10^6 per meter. Both in-line and staggered tile configurations were evaluated at gap widths of 0.159, 0.317 and 0.476 cm. The tile geometry is shown in Figure 6 . Temperature data from 22 test runs was assimilated and analyzed to obtain heating patterns on in-line and staggered tiles.

Gap heating tests were conducted by W. K. Lockman (NASA, Ames Research Center) and C. B. Blumer (Rockwell International) in the Ames 3.5 Foot H.W.T. facility to provide data in the presence of laminar, transitional, and turbulent boundary layers. The model consisted of a 68.6x152.4 cm carrier plate into which 61.0x106.7 cm instrumented thin skin test articles were inserted. The five insert configurations used in the test program are shown in Figure 7 . The configurations included a flat calibration plate, a single transverse gap with and without surface steps, multiple transverse gaps, staggered tiles, and skewed intersecting gaps. Five gap settings (0, 0.064, 0.127, 0.254 and 0.508) were investigated with tile thickness of 1, 2 and 4 cm. Butt joint step heights of $\pm$0.159 and $\pm$0.318 cm were also investigated. Figure 7 summarizes the variables tested in the HWT facility. Data from 81 test runs were assimilated and analyzed for gap heating distributions.

Analysis of the above data is documented in Section 4.1 and correlation in Section 5. The facility, model description, test conditions and data are documented in Volume II of Reference 1 .

3.2 Silica RSI Tile Tests in the JSC Laminar Duct - A test program was conducted by G. Mauss (Rockwell International) in the JSC 10 MW Arc Tunnel on test panels

LaRC CFHT GAP HEATING EVALUATION

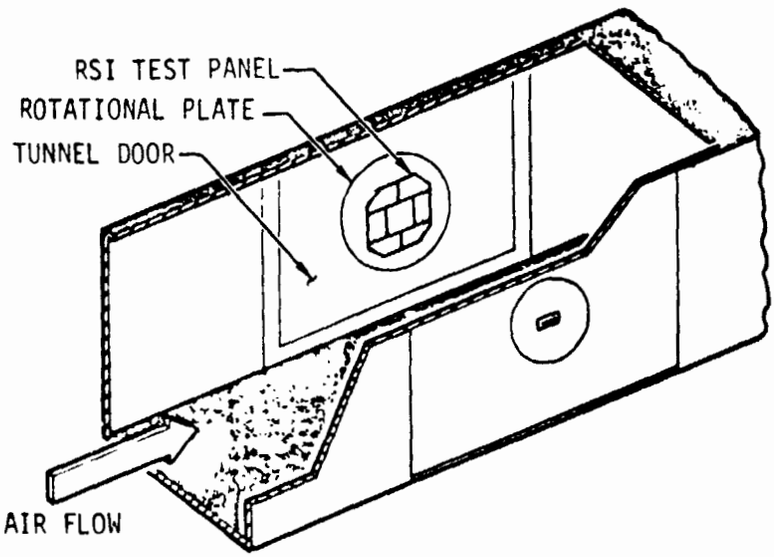

- o ADJUSTABLE GAP
- o SHIMS FOR STUDYING MISMATCH
- o 0 TO ±90° ORIENTATION

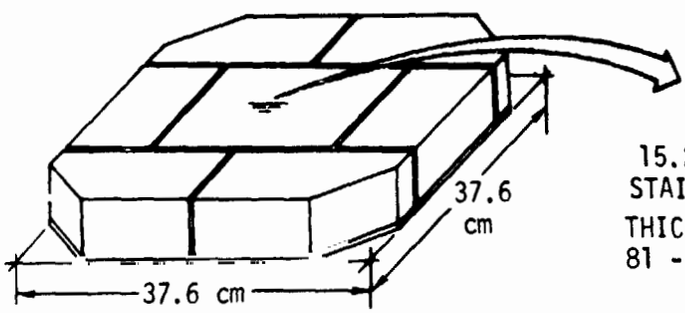

15.2 X 15.2 X 6.4 cm
STAINLESS STEEL (321)
THICKNESS = 0.0254 cm
81 - THERMOCOUPLES

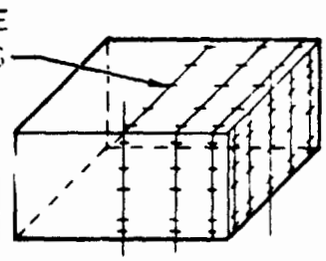

THIN SKIN TILE FOR MEASURING HEATING DISTRIBUTION

Figure 4

VIEW OF INSTRUMENTATION WITHIN THIN SKIN TILE TESTED IN CFHT, PART I

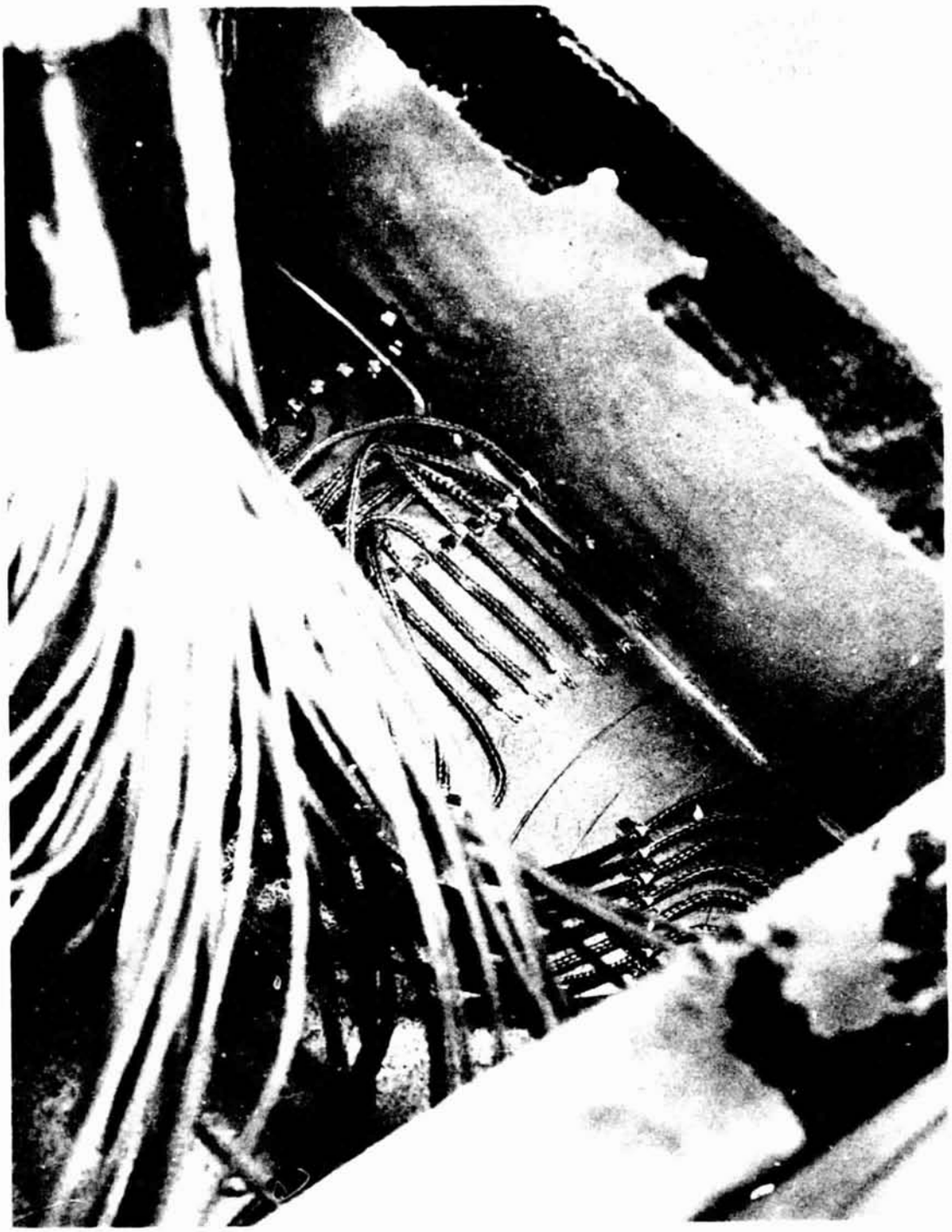

Figure 4

VIEW OF INSTRUMENTATION WITHIN THIN SKIN TILE TESTED IN CFHT, PART 2

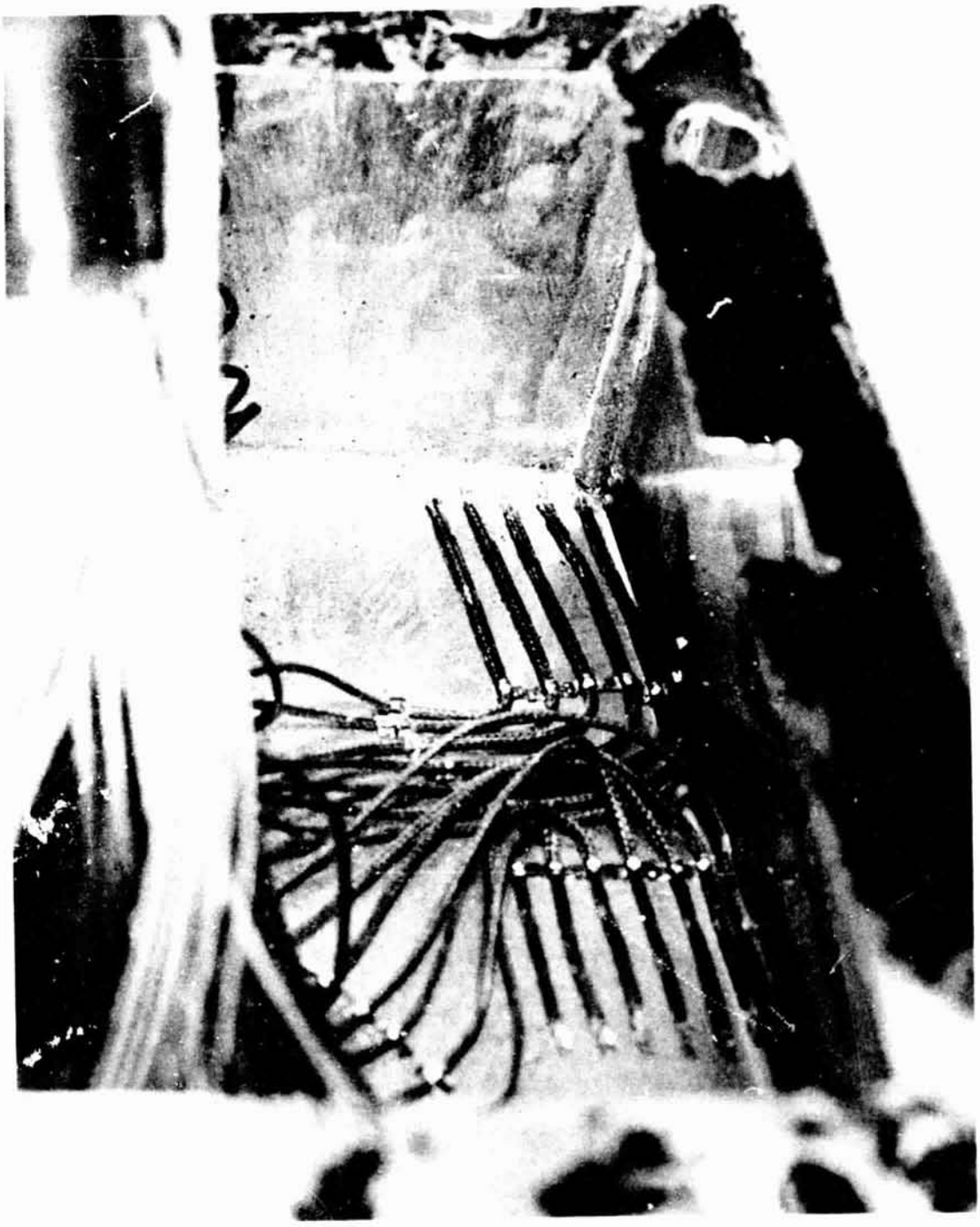

Figure 4

VIEW OF INSTRUMENTATION WITHIN THIN SKIN TILE TESTED IN CFHT, PART 3

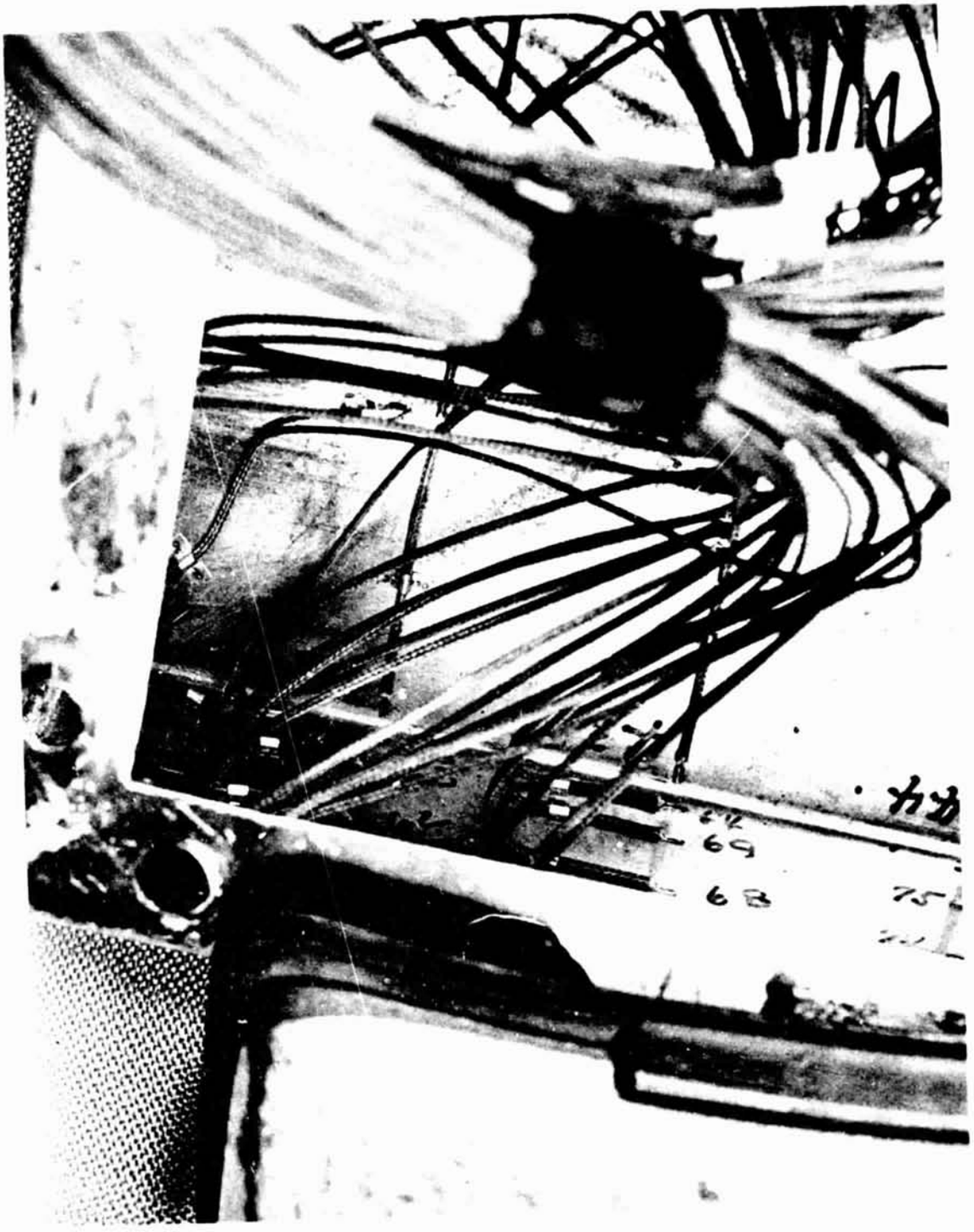

Figure 4
Conc.

LaRC CFHT GAP MODEL

9 FLOW ORIENTATIONS 0 TO $\pi/2$

4 GAP WIDTHS .127, .229, .457, .711 cm

STEPS = 0, + 0.254, - .168 cm

MACH = 10.3

$Re/_m = 3.28 \times 10^6$

157 TEST RUNS, DATA ASSIMILATED

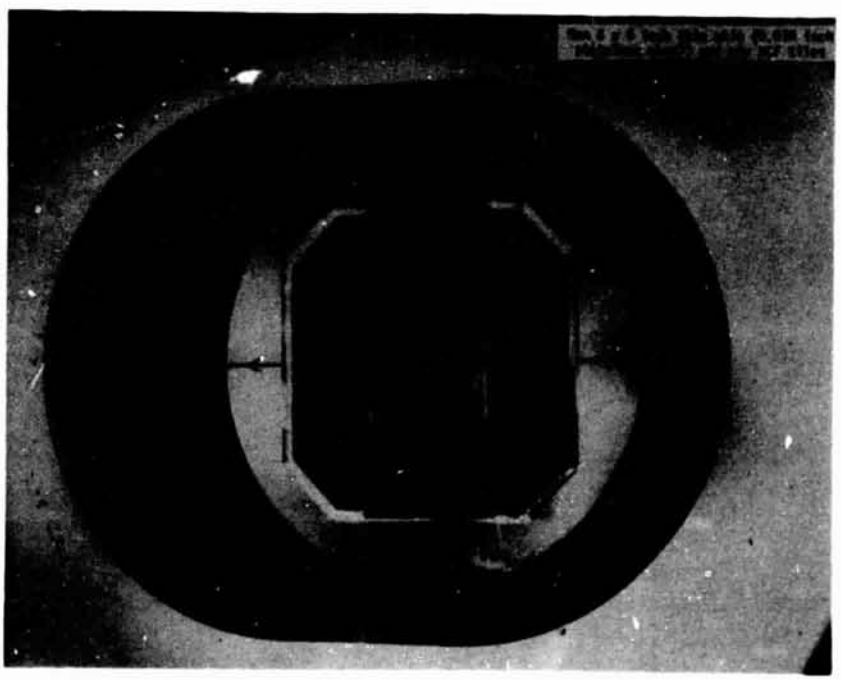

Figure 5

LaRC MACH 8 V.D.T. GAP HEATING TESTS

- FREE STREAM AND TUNNEL WALL TESTS
- GAP WIDTH = 0.159, 0.317 and 0.476 cm
- Re/meter = 1.1 X 10^6 TO 21.8 X 10^6

2.54 X 20.32 X 10.16 cm TILES

IN-LINE TILES

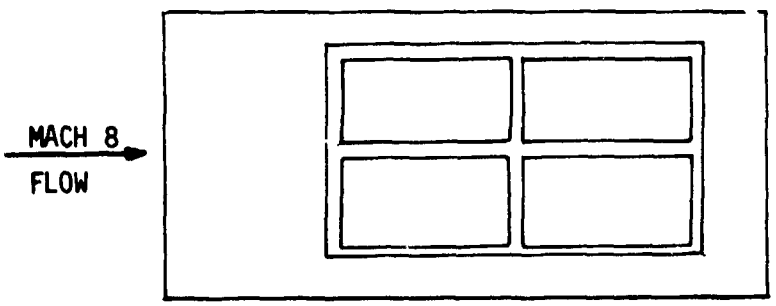

STAGGERED TILES

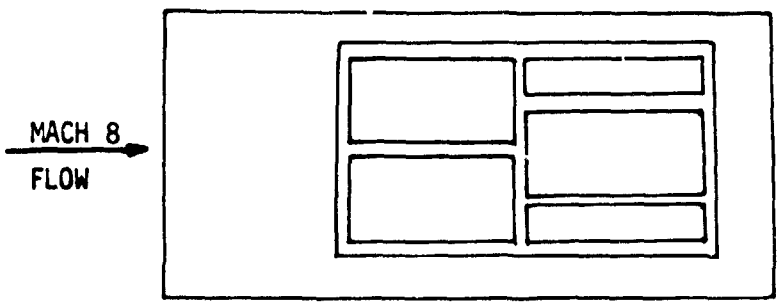

Figure 6

AMES 3.5 FOOT HWT GAP MODELS

CALIBRATION PLATE

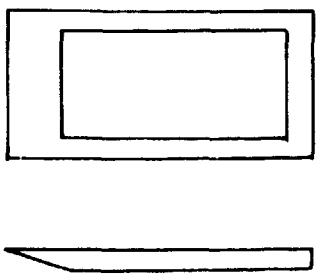

SINGLE TRANSVERSE GAP

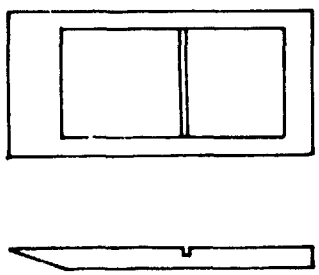

MULTIPLE TRANSVERSE GAP

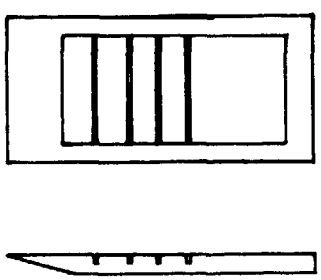

STAGGERED TILES

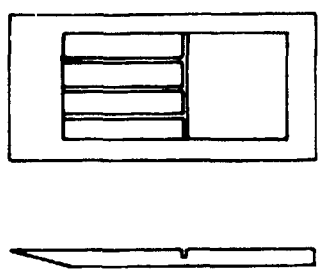

30^{o} ORIENTED TILES

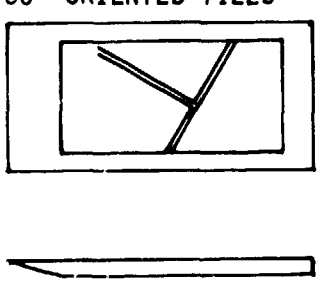

- TEST VARIABLES
  - $10^{6}Re/_{m}$ = 1.4, 2.2, 3.2 AND 4.5
  - m_{∞} = 5.1
  - GAP WIDTH = 0.064, 0.127, 0.254 AND 0.508 cm
  - GAP DEPTH = 1, 2, and 4 cm
  - STEPS = 0, ± .159 AND + .318 cm
- 81 TEST RUNS ASSIMILATED

Figure 7

using Silica RSI tiles fabricated and instrumented by NASA Ames. The purpose of the program was to obtain comparative thermal performance data on overlap and butt joint designs and the effect of tile thickness and gap width under simulated laminar flow conditions. Test panel overall dimensions were 33x33 cm.

Six runs from the test program were selected for analysis. All six runs were made with the staggered gap design (shown in Figure 8) consisting of 3 full and 2 half tiles with a perimeter of narrow guard tiles. Gap widths of 0.127 and .254 cm were evaluated with RSI thicknesses of 2.54 and 5.08 cm. Four of the six runs were made on butt joint models and two runs on overlap joint models, both of which are shown in cross-section in Figure 9 which also includes gap thermocouple locations. Thermocouple location and distances were measured from x-ray photographs of the instrumented tiles.

Test conditions for the six runs analyzed are summarized in Figure 10 . Arcjet mass flow rate was 45.4 grams/sec in all cases and enthalpy varied from 8.58×10^6 to 21.95×10^6 J/Kg. All runs were conducted in the channel nozzle of the JSC 10 MW Arc Jet Facility. The test panels were mounted in one wall of the channel nozzle and a calibration plate was mounted on the other wall. The calibration plate served as a basis for referencing data and as a basis for investigating anomalies. Test results used in the analysis consisted of gap and plug temperature histories, test section pressures and channel wall temperatures. Figure 11 is a typical set of gap temperature histories obtained from the JSC automated plotting output. Data were also recorded on magnetic tapes for direct reading into the CDC 6500 computer to obtain heating rate distributions via the inverse solution technique.

Analysis of the above data is reported in Section 4.2. The facility, model description, test conditions and data are documented in Volume II of this report.

3.3 Supplemental LaRC Mach 10 CFHT Tests - Additional gap heating tests were conducted in the LaRC Mach 10 CFHT to provide supplemental data to the previous tests reported in Section 3.1. The purpose of these additional tests was to substantiate the calibration data previously measured in the CFHT facility, to evaluate the effect of zero gap width, and to determine the effects on heating in the gaps between the tiles at higher Reynolds number.

The test program employed the same model as used in the previous tests (see Figure 4), namely, a wall-mounted thin skin "tile" model in which the instrumented thin skin tile was surrounded by an array of uninstrumented RSI tiles. Again, the model was mounted on a turntable to permit variation of flow orientation relative

STAGGERED TILE TEST PANEL CONFIGURATION

o SILICA RSI TILE TESTS IN JSC LAMINAR DUCT

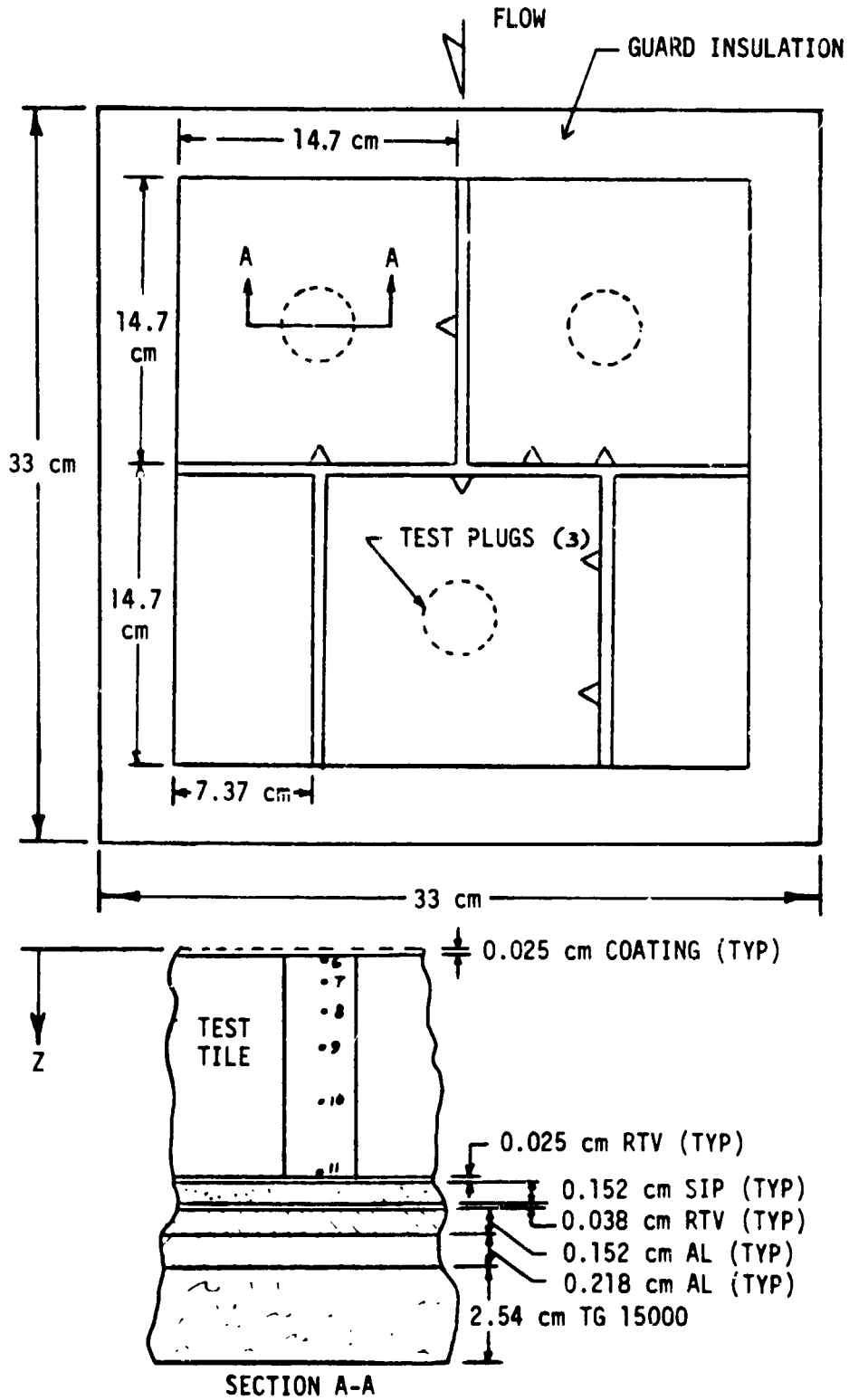

Figure 8

GAP THERMOCOUPLE LOCATIONS

o SILICA RSI TILE TESTS IN JSC LAMINAR DUCT

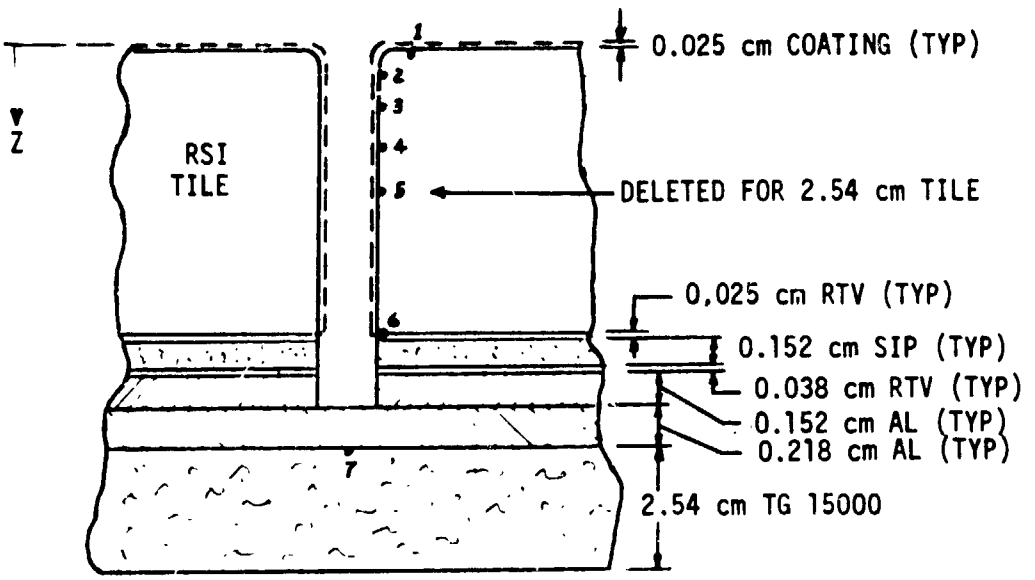

BUTT JOINT

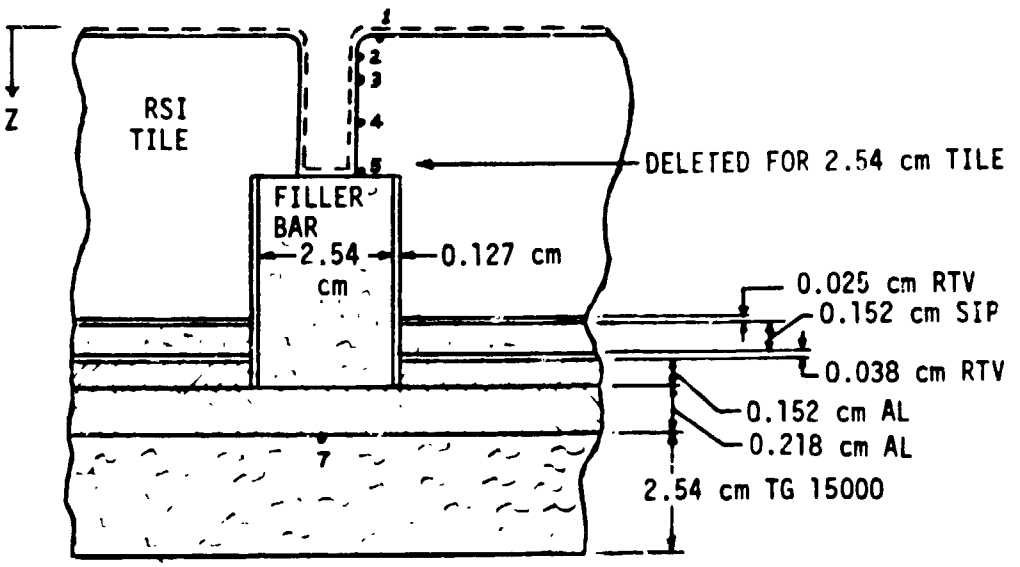

OVERLAP JOINT

Figure 9

TEST MATRIX
SILICA RSI TILE TESTS IN JSC LAMINAR DUCT

RUN NO.	MODEL	GAP WIDTH, cm	$\dot{m}$ grams/sec	CURRENT, [illegible]	ENTHALPY, J/kg
528	2.54 cm OVERLAP	0.127	45.4	[illegible]	8.582×10^6
533	5.08 cm OVERLAP	0.127	45.4	480	21.950×10^6
533	2.54 cm BUTT	0.127	45.4	375	11.578×10^6
539	2.54 cm BUTT	0.254	45.4	375	11.578×10^6
542	5.08 cm BUTT	0.127	45.4	480	21.950×10^6
544	5.08 cm BUTT	0.254	45.4	480	21.950×10^6

Figure 10

TYPICAL GAP TEMPERATURE HISTORIES

o SILICA RSI TILE TESTS IN JSC LAMINAR DUCT

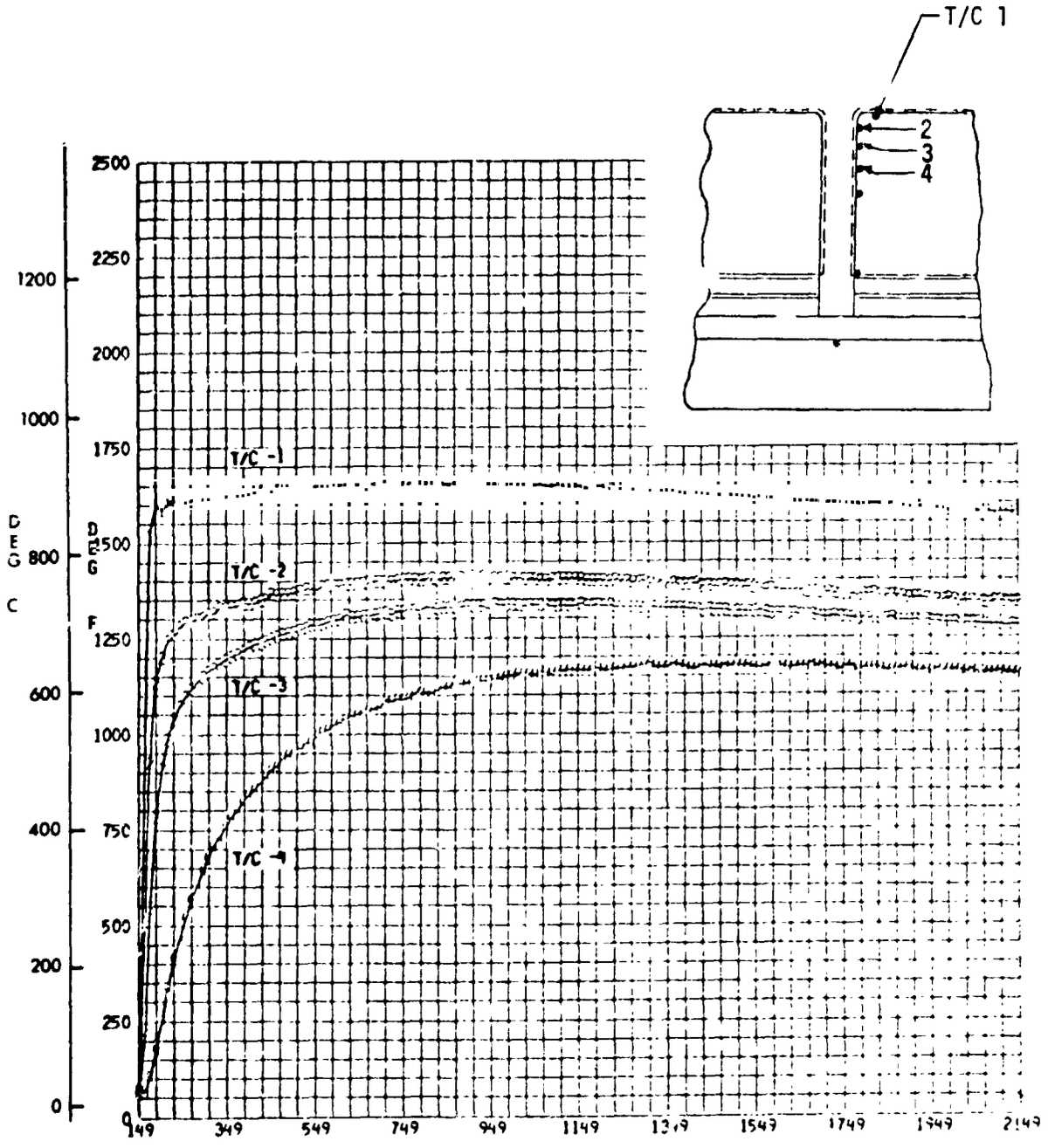

TIME - SECONDS

to the tile array. Results from ten runs were assimilated into the Data Bank for analysis. The test runs were conducted at unit Reynolds number per meter of both 3.28×10^6 and 7.38×10^6. The test matrix included flow orientations of 0 and $\pi/2$ radians, gap widths of 0, 0.127, and 0.229 cm, and gap depths of 0.0 and 6.35 cm. Both in-line and staggered butt joint designs were investigated. Figure 12 summarizes the test matrix.

Temperature response data from these runs was analyzed to obtain heating rate distributions using the inverse solution technique as discussed in Section 4.3. The facility, model description, test conditions and data are documented in Volume II of this report.

3.4 Edge Radius Tests at NASA JSC - Gap heating tests were conducted by C. D. Scott (NASA, Johnson Space Center) in the JSC 10 MW Arc Tunnel to provide heating data in the presence of a high enthalpy laminar boundary layer. The primary purpose of the tests was to investigate the effect of tile edge radius on gap heating.

The tests employed sets of thin skin metallic tiles mounted in a wedge test fixture. Four edge radii (0.157, 0.3175, 0.635, and 1.27 cm) were parametrically tested at gap widths of 0.127, 0.254, and 0.381 cm. It should be pointed out that the tile with the small edge radius was originally specified as a sharp edged tile and many of the correlations were initially developed using this specification. The joint configuration was an in-line butt, and the tile height was 4.1275 cm for all tests. The test panel configuration, edge radii and instrumentation are shown in Figure 13 .

Test data were received in tabular form. The analysis of the heating distributions is reported in Section 4.4 and correlation of the data in Section 5.3. Correlations for edge radius effects have been developed for both the vertical wall, and the edge-and-wall geometries. Test related information and data are documented in Volume II of this report.

3.5 Single In-Line Gap Tests at Ames 3.5 Foot H.W.T. - Gap heating tests were conducted by W. K. Lockman (NASA, Ames Research Center) and C. B. Blumer (Rockwell International) in the Ames 3.5 foot H.W.T. facility to obtain data in the presence of laminar, transitional and turbulent boundary layers. These tests were conducted on panels furnished by Rockwell International and provided additional data to the

CFHT TEST 92 - SUPPLEMENTAL RUNS - FEBRUARY 1974

RUN	GAP (cm)	ORIENTATION	Re_∞/m
161	.127	Staggered	3.28×10^6
162	↓	Staggered	7.38×10^6
163	↓	In-line	3.28×10^6
164	.127	In-line	7.38×10^6
165	.229	Staggered	3.28×10^6
166	↓	Staggered	7.38×10^6
167	↓	In-line	3.28×10^6
168	.229	In-line	7.38×10^6
169	Closed		7.38×10^6
170	Closed		3.28×10^6

Figure 12

TEST PANEL CONFIGURATION, EDGE RADIUS STUDY AT NASA JSC 10MW ARC TUNNEL

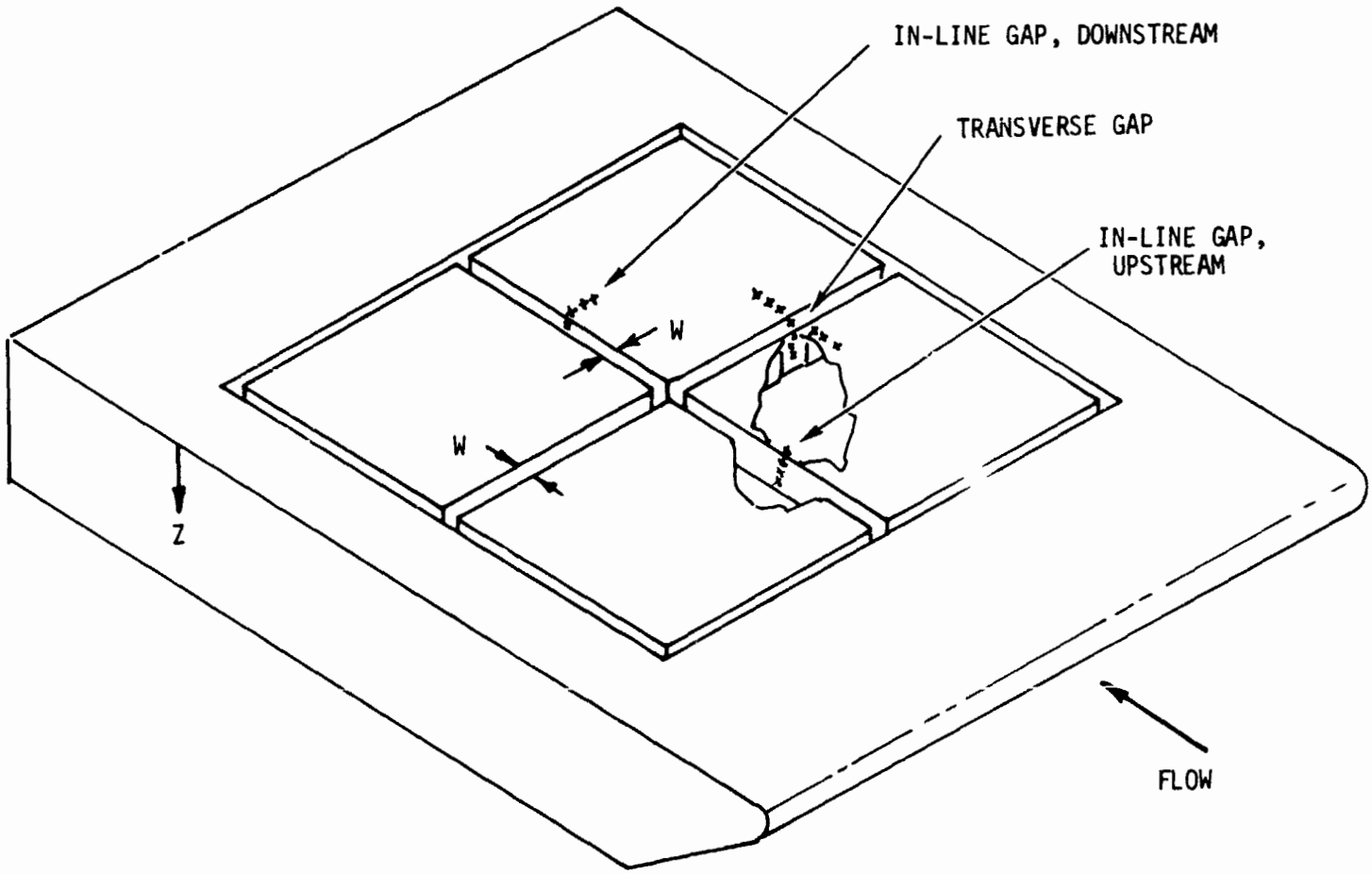

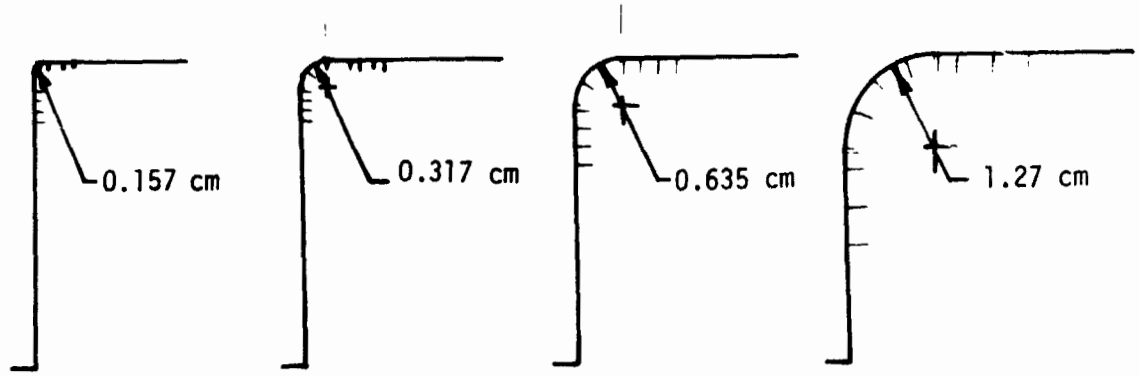

*INSTRUMENTATION LOCATIONS INDICATED BY TICK MARKS

Figure 13

previous tests at this facility described in Section 3.1. The primary test purpose was to investigate the effects of tile orientation for several gap width settings.

The tests employed a thin skin model inserted into a 68.6 x 152.4 cm carrier plate. The joint configuration was a single, in-line, gap of 30.48 and 101.6 cm length. Thermocouples were installed along the top of the panel and along the faces of the gap. The model is shown in Figure 14 . The test matrix included four orientations (0, 5, 10 and 15 degrees), three gap widths (0.063, 0.127 and 0.254 cm), four gap depths (0, 1.016, 2.037 and 3.81 cm), and two gap lengths (30.48 and 101.6 cm). Test runs were conducted at Reynolds numbers per meter of 1.64×10^6, 3.28×10^6 and 6.56×10^6. The complete matrix of 93 runs is listed in Figure 15 .

Information from these runs was assimilated into the Data Bank. Analysis of the heating rate distributions are described in Section 4.5. Correlations for long in-line gaps are contained in Section 5.3 for both zero flow orientation and orientation up to 15 degrees. Information relating to the test and data are documented in Volume II of this report.

3.6 Test of Large Gap Panel in LaRC 8 Foot HTST - Gap heating tests were performed in the LaRC 8 Foot HTST to obtain heating data on a large gap panel in the presence of a turbulent boundary layer. The same test panel was to be used in both the HTST and the AFFDL 50 MW Arc Tunnel Tests. The panel was originally scheduled for testing at AFFDL but was switched to the LaRC HTST due to fabrication difficulties with the test fixture by the vendor. The 50 MW tests were intended to determine the effects of higher enthalpy on the heating in a field of RSI gaps, and would have also provided a comparison of arc and wind tunnel gap heating data. The AFFDL test program was subsequently cancelled. The test program at LaRC was under the direction of I. Weinstien.

The test panel as shown in Figure 16 consisted of eleven LI 900 silica tiles with an interchangeable thin skin metallic center tile. Testing was planned for both the center LI 900 tile and the center metallic tile, but time permitted testing only of the metallic tile. The panel size was 46 x 46 x 6.5 cm.

Both the LI 900 and the metallic tiles were heavily instrumented with the thermocouple locations for the thin wall metallic center tile shown in Figure 17 . The RSI panel was mounted in a large test sled for free stream testing and permitted variation of angle of attack relative to the tile array. The panel was tested in both the in-line and staggered tile configurations. Gaps between the tiles were

AMES 3.5 FOOT H.W.T. IN-LINE GAP MODEL

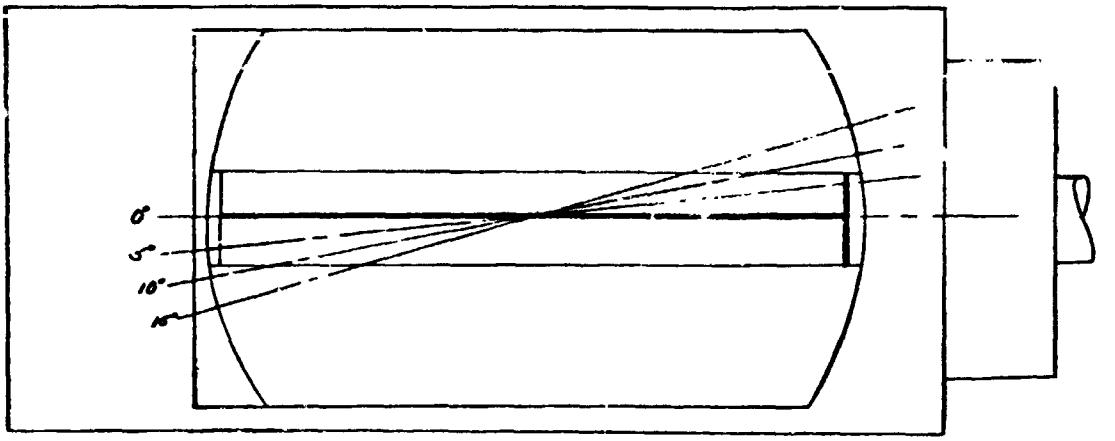

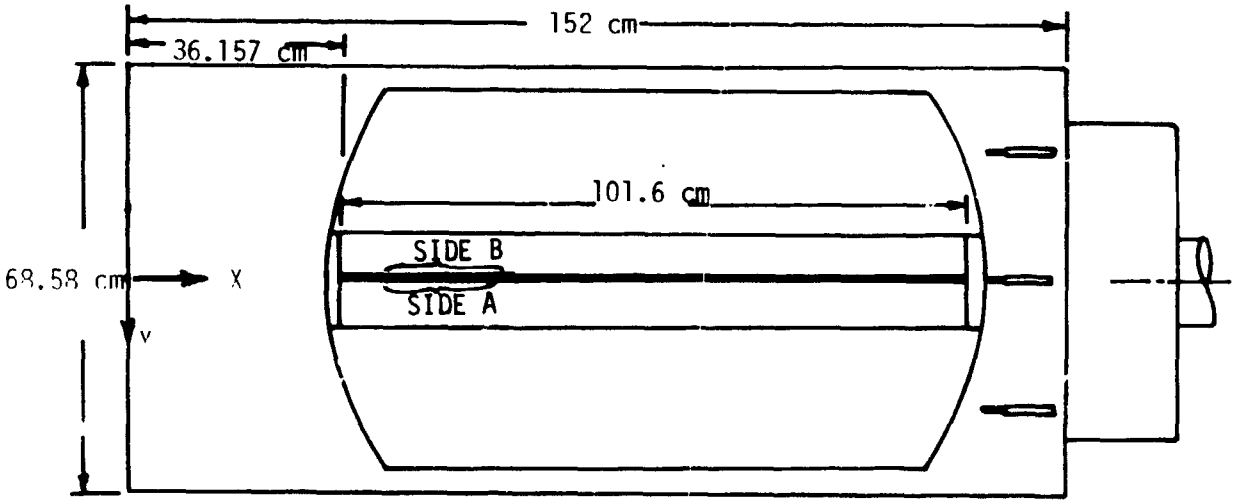

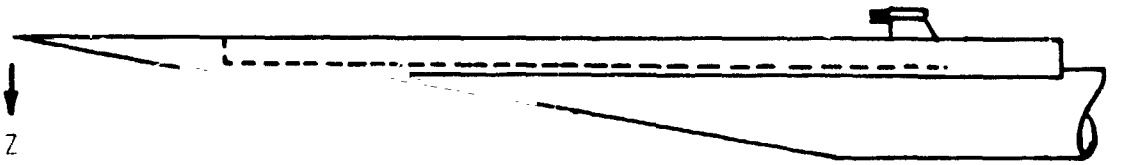

Figure 14

RUN SCHEDULE

SINGLE IN-LINE GAP TESTED IN THE AMES 3.5 H.W.T.
MODEL OH-43
TEST SUPERVISED BY C. B. BLUMER

RUN NO.	R_N ($X10^6$/m)	GAP WIDTH (cm)	GAP DEPTH (cm)	GAP LENGTH (cm)	GAP ORIENT. ANGLE (DEG)	T/C SCHEDULE	MODULE POSITION SCHEDULE	REMARKS
1	1.64	0.127	0	101.6	0	2	1	TUNNEL CONDITIONS
2	3.28	↓	↓	↓	↓	↓	↓	UNSTEADY, WILL RE-RUN
3	1.64	↓	↓	↓	↓	↓	↓	GAP FILLED WITH DENTAL PLASTER
4	1.64	↓	↓	↓	↓	↓	↓	L.E.1
5	3.28	↓	↓	↓	↓	↓	↓	L.E.1
6	1.64	↓	2.032	↓	↓	1	↓	
7	3.28	↓	↓	↓	↓	↓	↓	
8	6.56	↓	↓	↓	↓	↓	↓	
9	1.64	↓	↓	↓	↓	4	↓	L.E.1
10	3.28	↓	↓	↓	↓	↓	↓	
11	6.56	↓	↓	↓	↓	↓	↓	
12	6.56	↓	0	↓	↓	2	↓	
13	6.56	↓	3.81	↓	↓	5D	↓	
14	3.28	↓	↓	↓	↓	↓	↓	
15	1.64	↓	↓	↓	↓	↓	↓	
16	6.56	↓	1.016	↓	↓	3A	↓	
17	3.28	↓	↓	↓	↓	↓	↓	
18	1.64	↓	↓	↓	↓	↓	↓	
19	1.64	↓	2.032	30.48 (FWD)	↓	6H	2	
20	3.28	↓	↓	↓	↓	↓	↓	
21	1.64	0.254	↓	↓	↓	↓	↓	
22	3.28	↓	↓	↓	↓	↓	↓	
23	3.28	↓	↓	↓	5	6I	↓	
24	1.64	↓	↓	↓	↓	↓	↓	
25	1.64	0.127	↓	↓	↓	↓	↓	
26	3.28	↓	↓	↓	↓	↓	↓	
27	1.64	↓	↓	↓	10	↓	↓	
28	3.28	↓	↓	↓	↓	↓	↓	
29	1.64	0.254	↓	↓	↓	↓	↓	
30	3.28	↓	↓	↓	↓	↓	↓	
31	3.28	↓	↓	↓	15	↓	↓	
32	1.64	↓	↓	↓	↓	↓	↓	
33	3.28	0.127	↓	↓	↓	↓	↓	
34	1.64	↓	↓	↓	↓	↓	↓	
35	6.56	↓	↓	↓	↓	6J	3	
36	↓	0.254	↓	↓	↓	↓	↓	
37	↓	↓	↓	↓	↓	↓	↓	
38	↓	0.127	↓	↓	↓	↓	↓	
39	↓	↓	↓	↓	5	↓	↓	
40	↓	0.254	↓	↓	↓	↓	↓	
41	↓	↓	↓	↓	↓	↓	↓	
42	↓	0.127	↓	↓	↓	↓	↓	

Figure 15

RUN SCHEDULE

SINGLE IN-LINE GAP TESTED IN THE AMES 3.5 H.W.T.
MODEL OH-43
TEST SUPERVISED BY C. B. BLUMER

RUN NO.	R_N ($X10^6$/m)	GAP WIDTH (cm)	GAP DEPTH (cm)	GAP LENGTH (cm)	GAP ORIENT. ANGLE (DEG)	T/C SCHEDULE	MODULE POSITION SCHEDULE	REMARKS
43	1.64	0.254	1.016	101.6	0	3A	1	L.E.1
44	3.28	↓	↓	↓	↓	↓	↓	L.E.1
45	6.56							
46	1.64		2.037			1		
47	3.28		↓			↓		
48	6.56							
49	6.56					4		
50	1.64	↓	↓	↓		4		
51	3.28	0.254	2.032	101.6		↓		
52	1.64	0.063	↓	↓		5D		
53	3.28	↓	↓	↓		↓		
54	1.64	0.254	3.81	↓		15D		TOTAL TEMP. GAP PROBE IN
55	3.28	↓	↓	↓		↓		↓
56	6.56				↓			
57	3.28				10			
58	1.64				10			
59	3.28				5			
60	↓	↓			15			
61		0.127			15			
62	↓	↓			10			
63	6.56				10			
64	3.28	↓	↓		5	↓		
65	6.56	0.063	2.032		0	5D		
66	1.64		1.016			3A		
67	3.28		↓			↓		
68	6.56							
69	6.56		0.508					
70	1.64		↓					
71	3.28	↓						
72	1.64	0.127						
73	3.28	↓						
74	6.56			↓		↓	↓	
75	1.64	↓	0.381	30.48		5E	4	TOTAL TEMP.RAKE IN (MOD.6)
76	3.28	0.127	0.381	(FWD)		↓	↓	
77	6.56	↓	↓	↓	↓			
78	1.64				5	5F		
79	3.28				↓	5G		
80	3.28				10	↓		
81	1.64				↓			
82	1.64	↓	↓	↓	15	↓	↓	

Figure 15

RUN SCHEDULE

SINGLE IN-LINE GAP TESTED IN THE AMES 3.5 H.W.T.
MODEL OH-43
TEST SUPERVISED BY C. B. BLUMER

RUN NO.	R_N ($\times 10^6$/m)	GAP WIDTH (cm)	GAP DEPTH (cm)	GAP LENGTH (cm)	GAP ORIENT. ANGLE (DEG)	T/C SCHEDULE	MODULE POSITION SCHEDULE	REMARKS
83	3.28	0.127	0.381	30.48	15	5G	4	
84	3.28	0.254		(FWD)				
85	1.64							
86	1.64				0	5E		
87	3.28							
88	6.36							
89	1.64	0.127	2.032					
90	3.28							
91	6.56		3.81	30.48		5H	5	
92	6.56			(AFT)	15			
93	6.56	0.254						

Figure 15
Conc.

46 x 46 CM HRSI GAP HEATING EVALUATION PANEL (MINIMUM GAP SETTING)

- LaRC 8-FOOT HTST TESTS

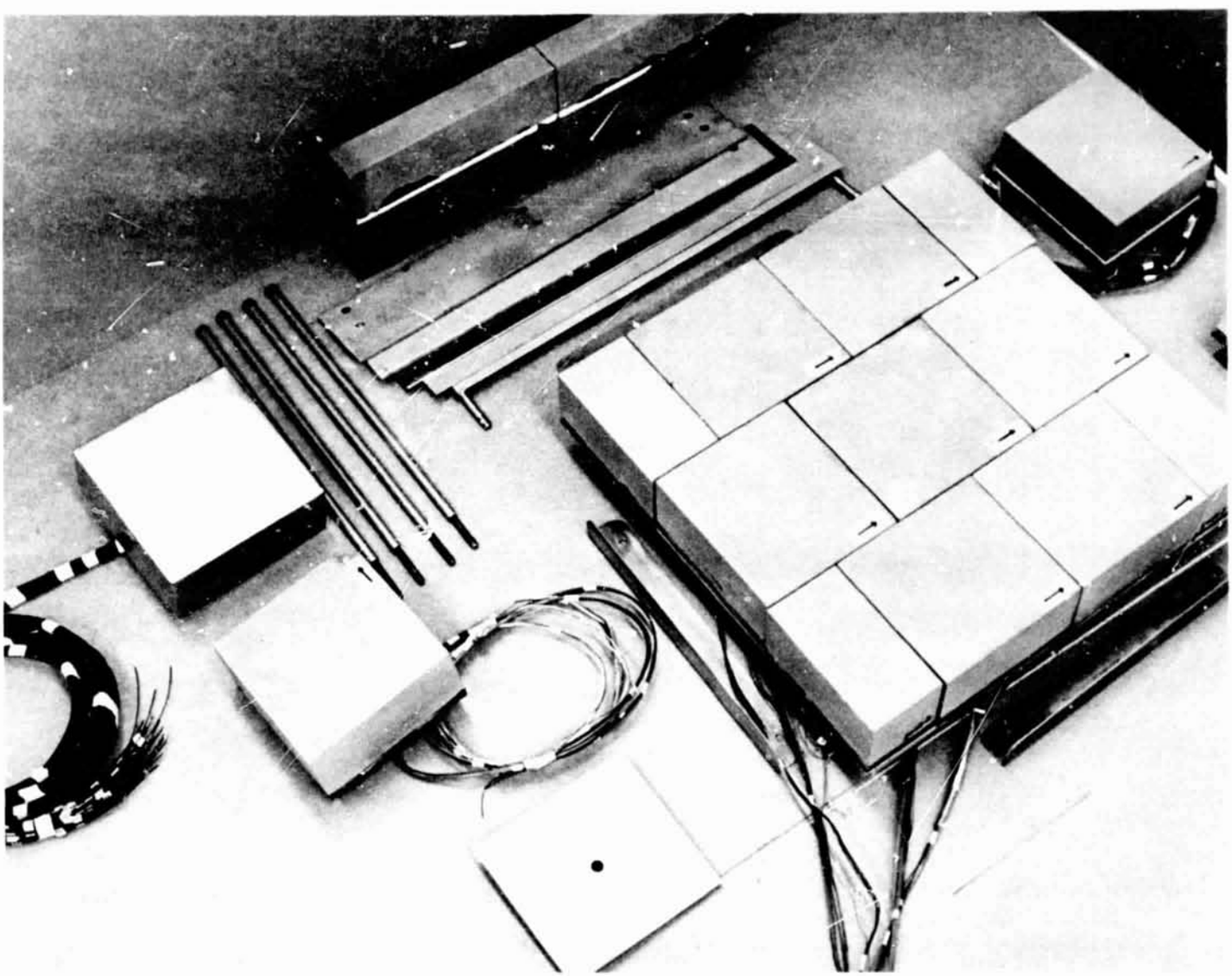

FIGURE 16

THERMOCOUPLE LOCATIONS ON THIN WALL METALLIC CENTER TILE

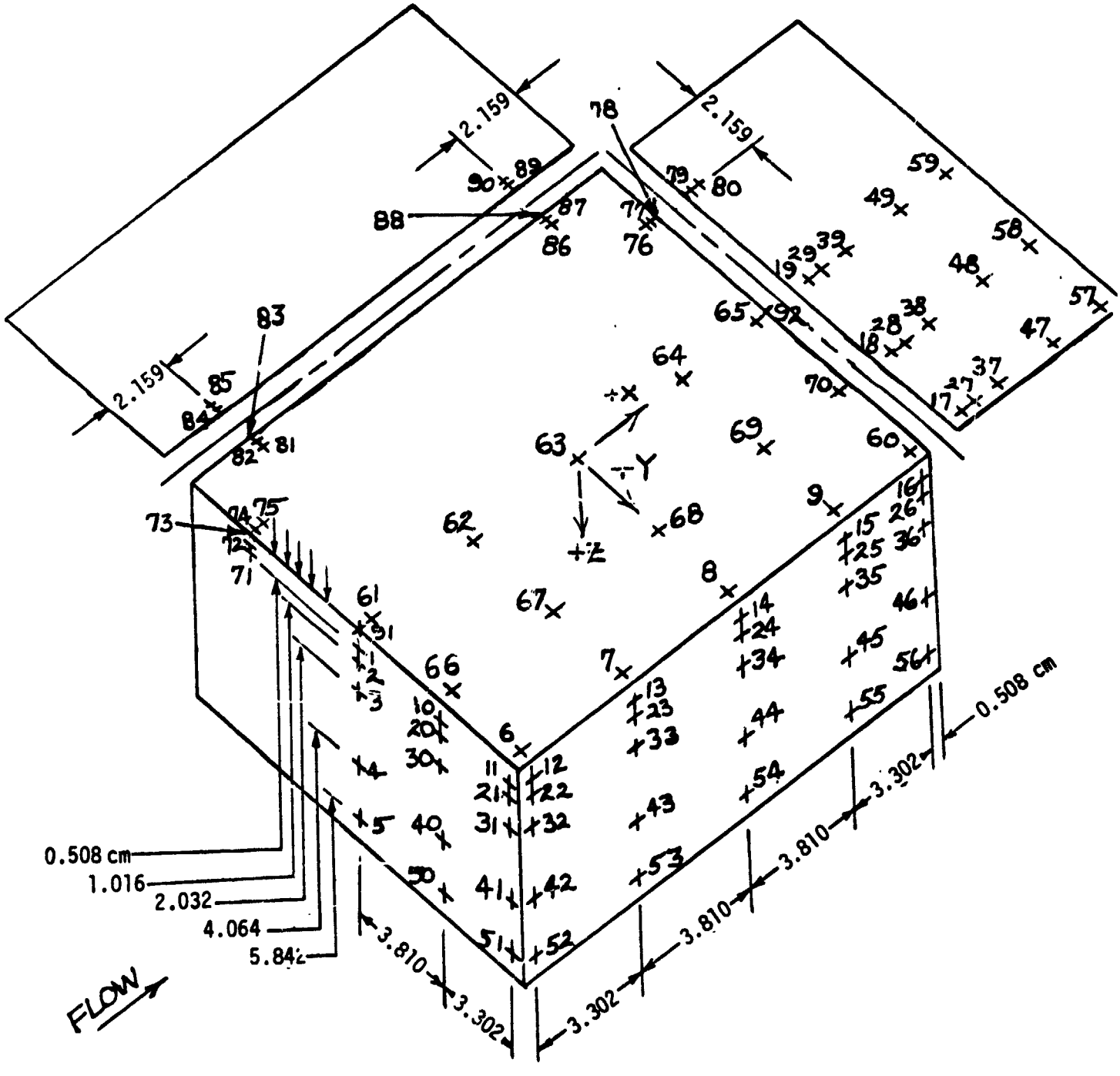

Figure 17

adjustable to study the effects of gap width, and shims were used under the tiles to study the effects of step heights. A companion plate that fitted into the same opening as the test panel was used for calibration purposes.

The test matrix for the 8 Foot HTST program is summarized in Figure 18 . Five gap settings were employed (0, 0.10, 0.18, 0.30, and 0.41 cm) with the tile thickness of 6.35 cm. Step heights investigated were 0 and +0.254 cm. Tests were run at Reynolds number per meter of 1.9×10^6 and 4.8×10^6, while the test sled angle of attack was varied from 0 to 15 degrees.

Problems specifically related to the model and facility occurred during the program. Figure 19 is a view of the panel prior to the first test and Figure 20 shows the panel following the same test. The time in the stream was 11 seconds and coating was removed in three locations from the LI 900 tiles. The erosion formed in the regions where the coating had been repaired prior to testing. Primary cause of the problem was that good bonding of the repair coating was prevented due to the silicone waterproofing on the tile. Also, the repaired coating could not be thermally fused in-place prior to testing.

The leading edge of the transverse gaps in the panel also experienced progressive erosion during the tests. The erosion was caused by a fine alumina dust originating at the combustor liner. Exposure duration per run was reduced to four seconds to minimize this erosion problem.

Finally, heating of the center, thin skin, metallic tile resulted in surface warping. Surface contour maps of the metallic tile are shown in Figures 21 and 22 following test runs 4 and 11 respectively.

Analysis of the above data is documented in Section 4.6 and correlation in Section 5. Information relating to the test and data are documented in Volume II of this report.

3.7 RSI Tile Tests in the Ames 20 MW Turbulent Duct - Gap heating tests were conducted by F. J. Centolanzi (NASA-Ames Research Center) in the Ames 20 MW Turbulent Flow Duct Facility to provide heating data in the presence of a high enthalpy turbulent boundary layer. The tests employed panels of Silica RSI tiles fabricated and instrumented by NASA Ames. The panels were placed in the wall of the Ames 2 x 9 inch turbulent duct which employs an arc heated air stream to produce turbulent flow. A schematic of the 2 x 9 inch duct facility is shown in Figure 23 . Panel sizes of 20.4 x 25.4 cm and 20.4 x 50.8 cm can be tested at a Mach number of 3.5. Figure 24 shows a photograph of the facility.

TEST CONDITIONS & MODEL CONFIGURATIONS FOR GAP HEATING TESTS IN 8-FT HTST

TEST NO.	RUN NO.	MODEL CONFIG.	NOMINAL GAP SETTING, cm	STEP, cm	α DEG.	TOTAL TEMP., °K	COMBUSTOR PRESSURE, N/m^2	MACH NO.	Re/m	TAW. °K
57	4	STAGGERED	.178	0.00	7.34	1533	7.1016×10^6	6.35	2.069×10^6	1423
↓	5	↓	↓	↓	-0.14	1656	7.1706	6.54	2.001	1529
	6				15.15	1700	7.2050	6.61	2.001	1591
	7				7.63	1733	18.0643	6.50	4.823	1608
	8		↓		-0.10	1822	17.9264	6.65	4.692	1691
	9		.102		7.64	1833	7.2050	6.87	1.969	1700
	10		.305		7.40	1639	7.3774	6.60	2.1	1520
	11		.406		7.49	1667	7.1706	6.58	2.001	1545
	12	↓	↓		0.14	1831	18.0643	6.64	4.692	1699
	13	IN-LINE	↓		7.56	1706	7.1706	6.65	2.001	1582
	14	↓	.305		7.53	1711	7.2050	6.65	2.001	1587
	15		.178		7.66	1772	7.1706	6.76	1.969	1643
	16		↓		-0.15	1844	7.0327	6.90	1.903	1702
	18			↓	14.96	1722	7.1361	6.70	2.001	1610
	19	↓		.254	7.63	1886	7.1361	7.00	1.870	1749
	20	STAGGERED	↓	.254	7.49	1767	7.2740	6.76	2.034	1638
	21	↓	0	0.0	7.53	1492	7.1016	6.21	2.001	1385
↓	22	↓	0	0.0	7.30	1689	7.1706	6.60	2.034	1566
58	1	CAL. PLATE	——	——	7.70	1694	7.1016	6.60	1.969	1572
↓	3	↓	——	——	0.10	1722	6.5500	6.70	1.870	1590
	4		——	——	0.08	1719	17.8574	6.45	4.692	1588

FIGURE 18

INSTALLATION OF 46x46x6.5 CM LI900 HRSI GAP HEATING PANEL (8 FOOT HTST)

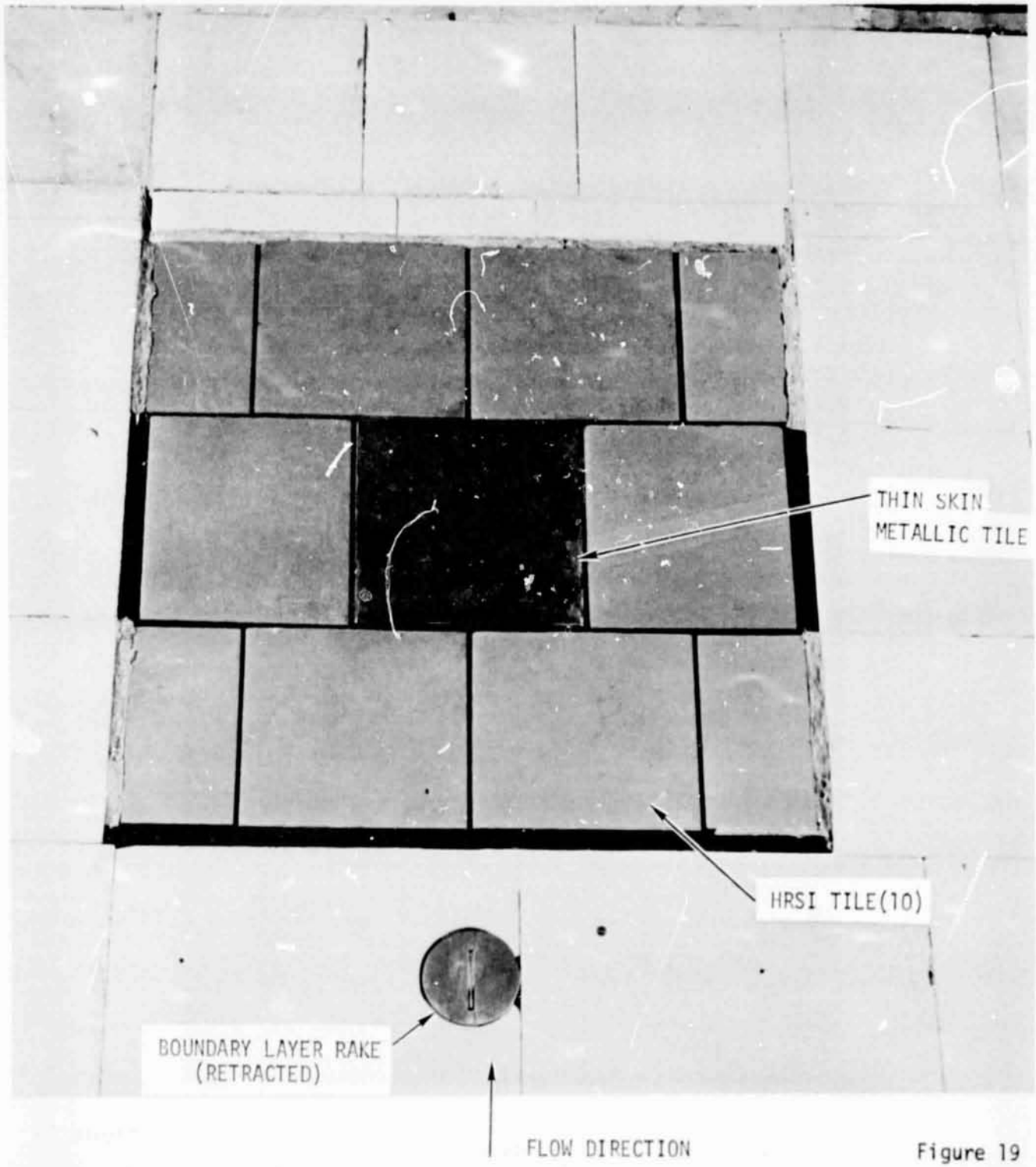

Figure 19

POST TEST CONDITION OF 46x46x6.5 CM LI900 HRSI GAP HEATING TEST (8 FOOT HTST)

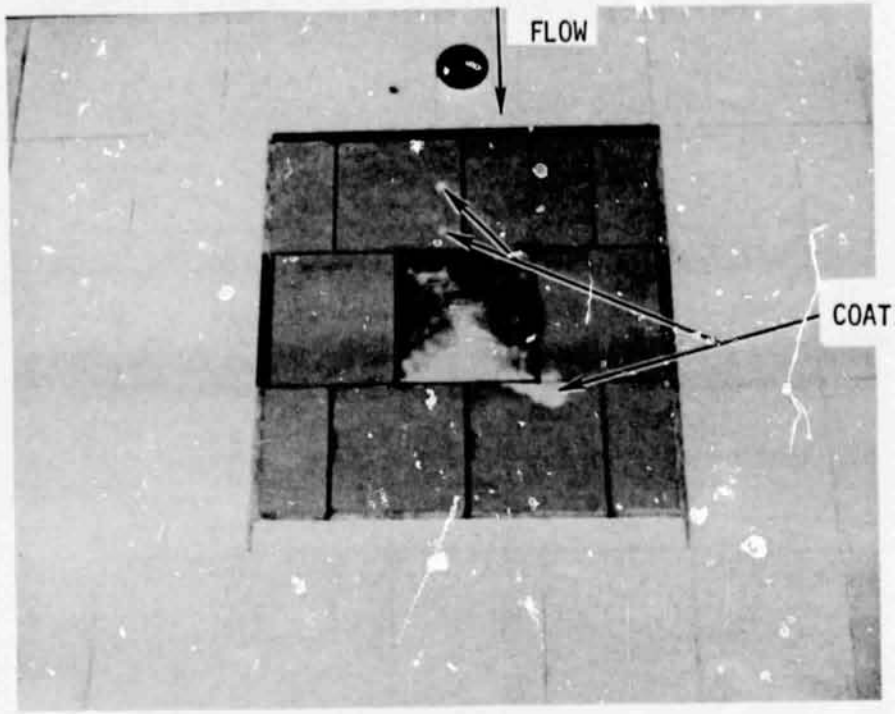

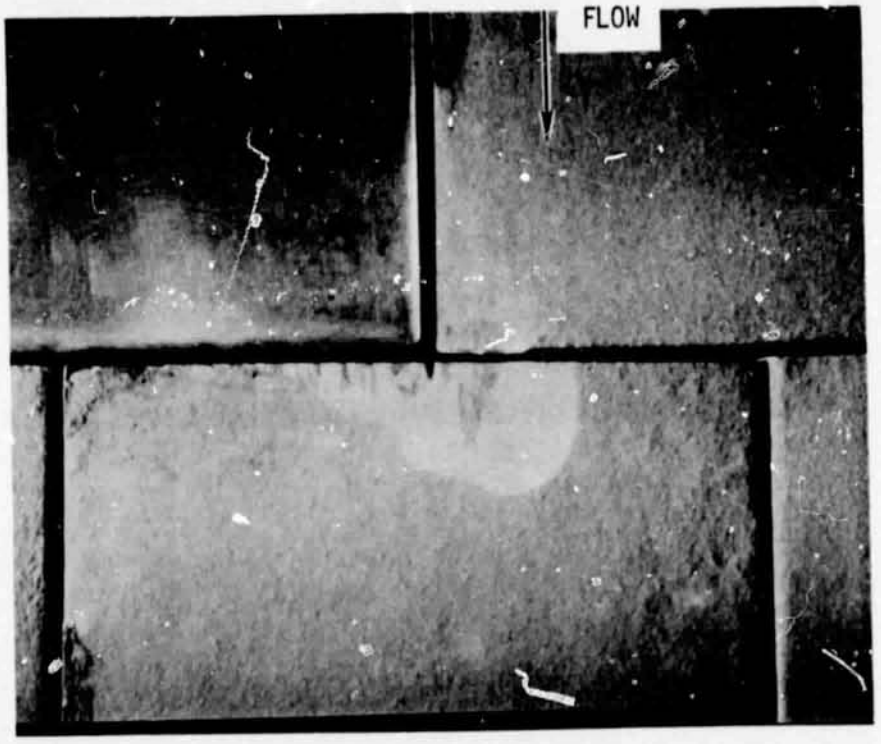

Figure 20

SURFACE CONTOUR MAP OF METALLIC TILE

AFTER RUN NUMBER 4

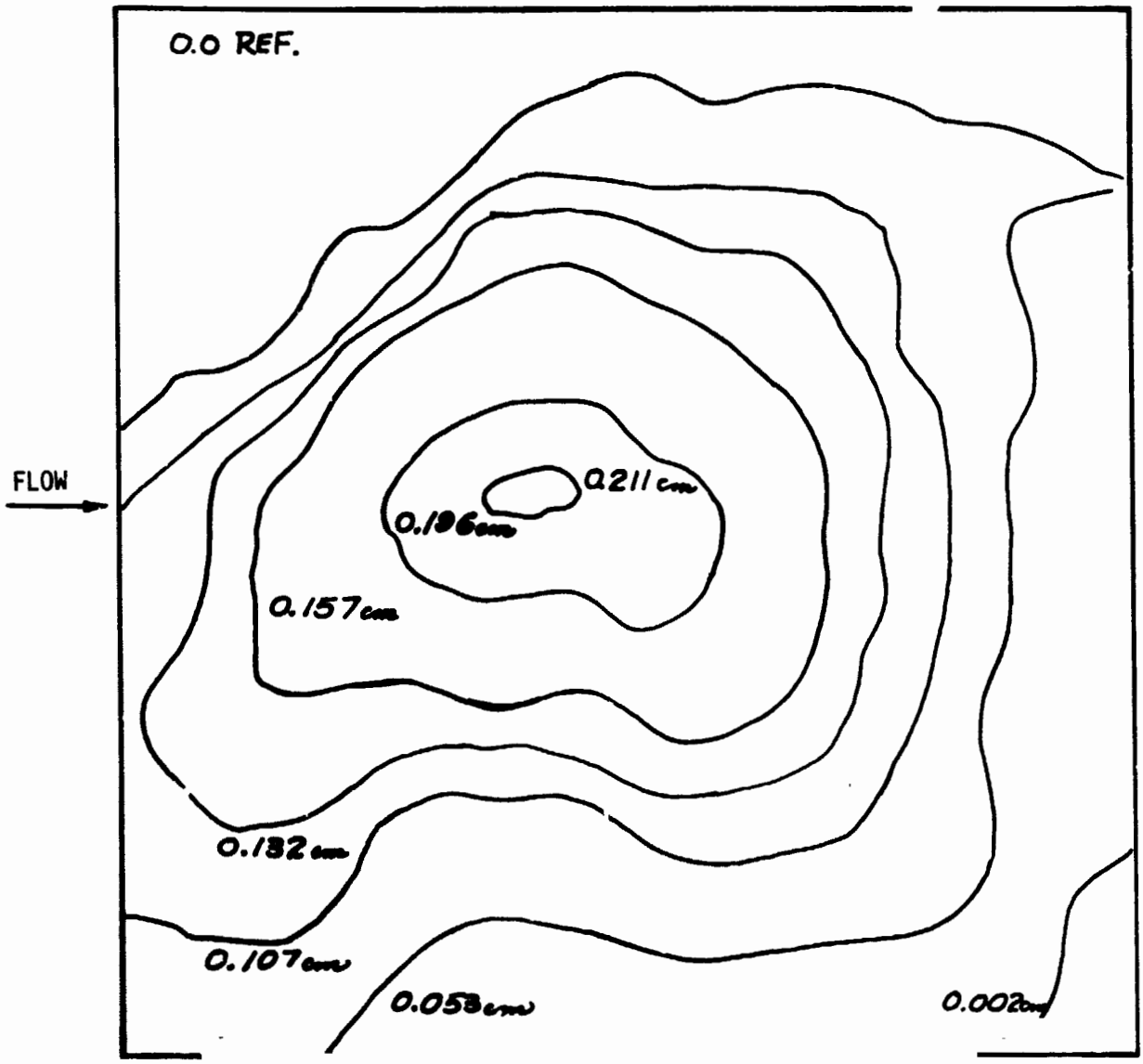

Figure 21

SURFACE CONTOUR MAP OF METALLIC TILE

AFTER RUN NUMBER 11

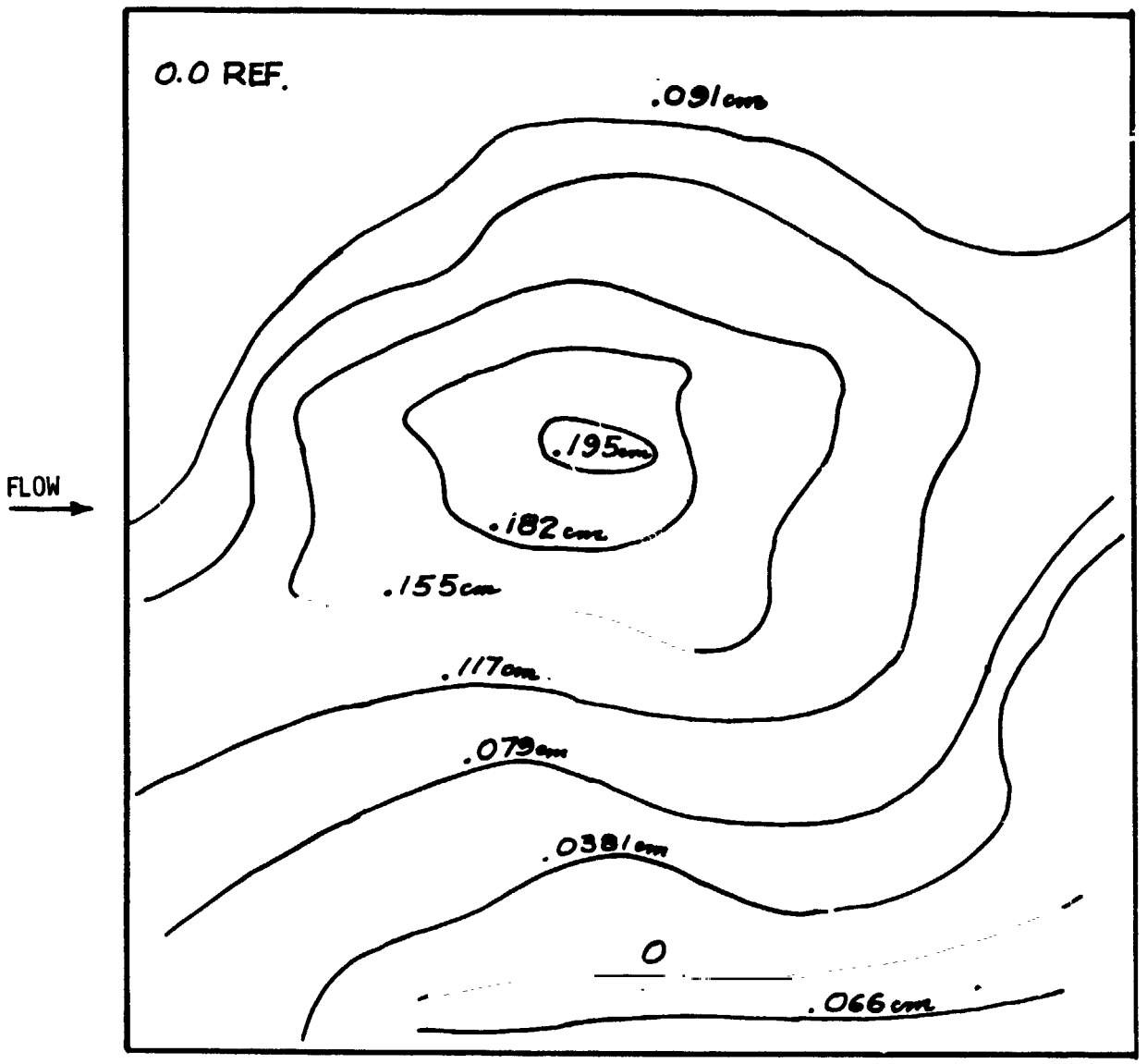

Figure 22

SCHEMATIC OF AMES 2x9 INCH TURBULENT FLOW DUCT FACILITY

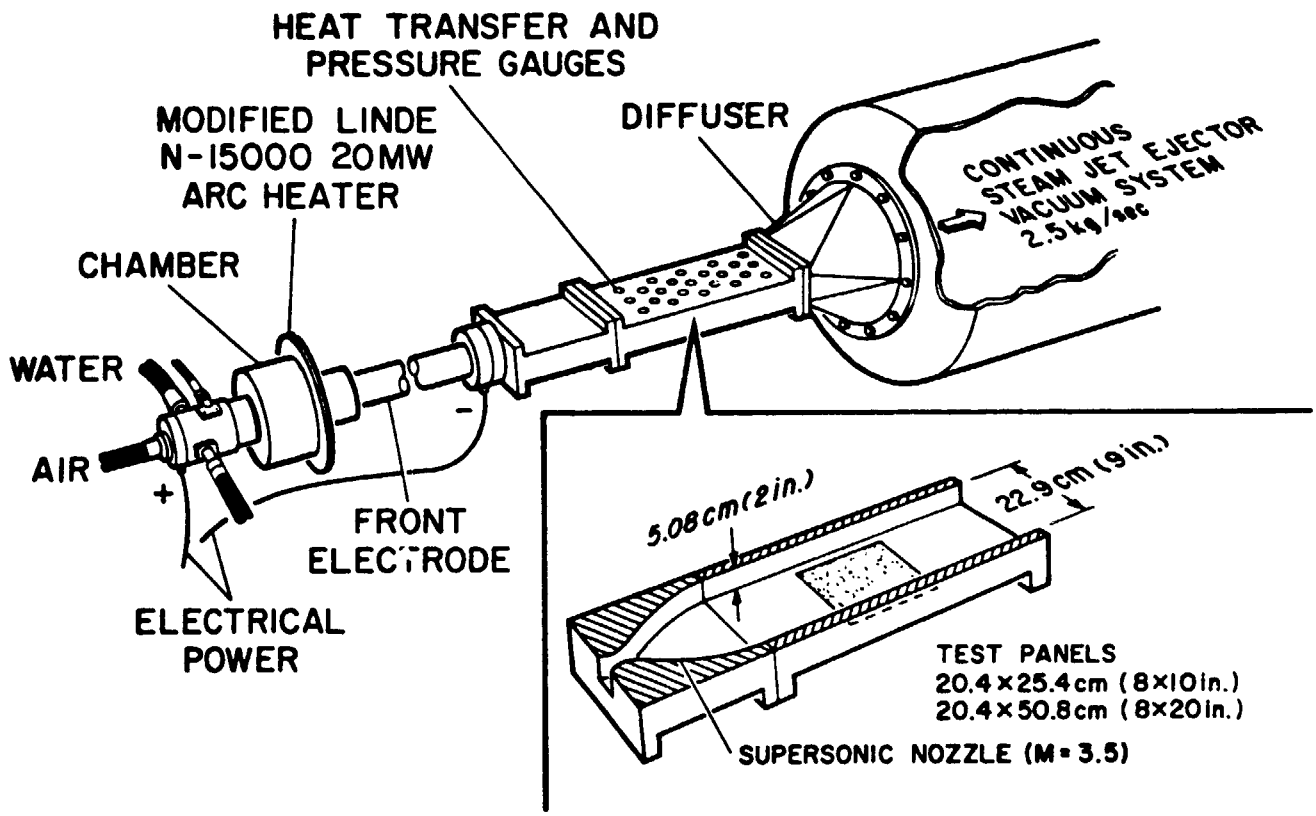

Figure 23

PHOTOGRAPH OF AMES 2x9 INCH TURBULENT FLOW DUCT FACILITY

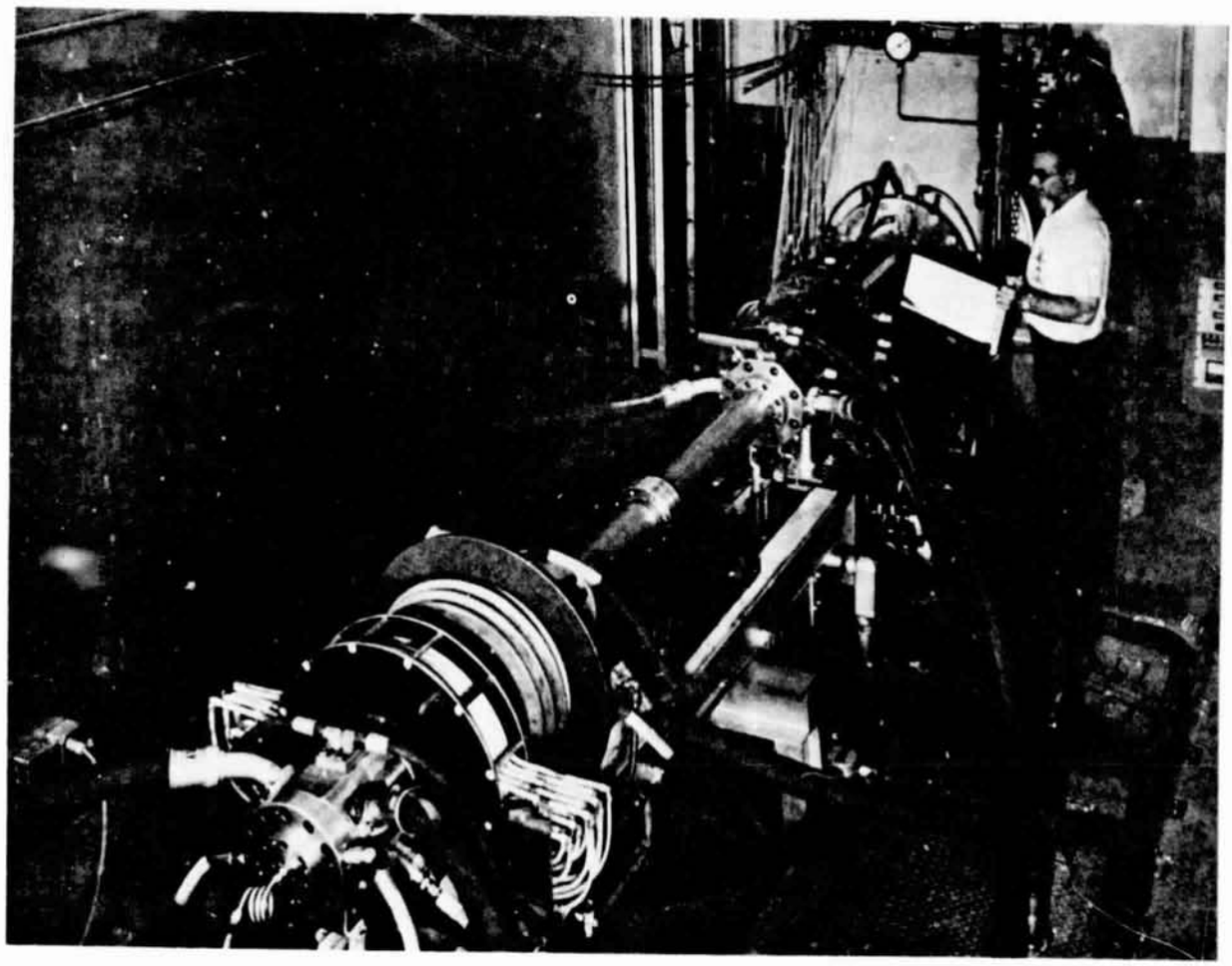

The test program investigated heating effects on a transverse butt joint design. Gap widths of 0, 0.127, 0.180, 0.254, 0.381 and 0.508 cm were evaluated for a RSI thickness of 5.08 cm and an edge radius of 0.635 cm. The test section Reynolds number was 0.3×10^6 per meter. The test specimen is shown in Figure A-25. As shown, the transverse gap was instrumented on both the upstream and downstream sides with thermocouples. The panel was tested twice at each gap width such that thermocouple number 1 (Figure 25) was located upstream and downstream of the instrumented gap.

Temperature response data were assimilated and analyses were performed including temperature history comparison and inverse solutions. The analyses are reported in Section 4.7.

AMES HRSI VARIABLE GAP MODEL, VG-2

THERMOCOUPLE LOCATIONS

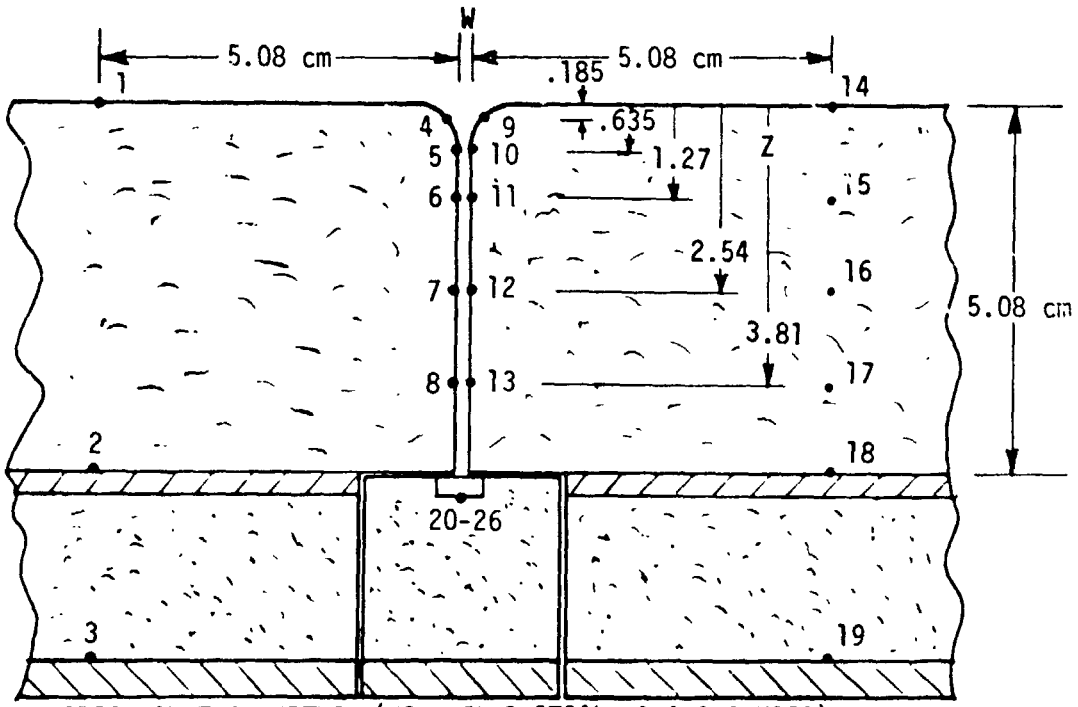

ORIGINAL T/C DEPTHS (USED IN INITIAL DATA ANALYSIS)

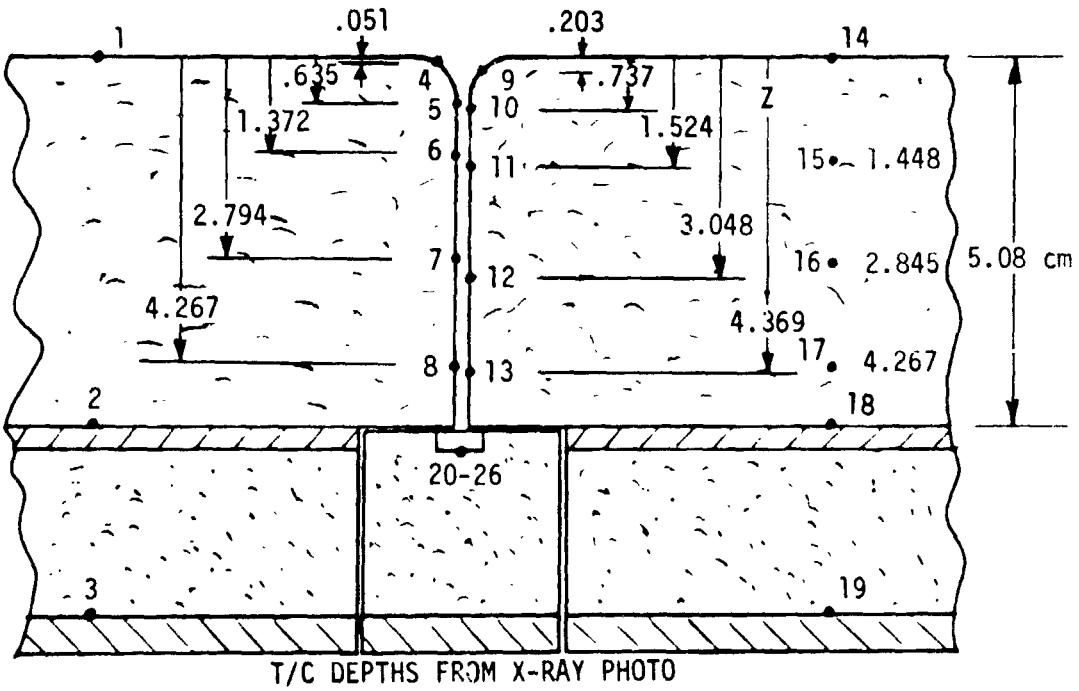

T/C DEPTHS FROM X-RAY PHOTO

Figure 25

4.0 DATA ANALYSIS

4.1 Analysis of Data Assimilated During Phase I - During Phase I efforts, heat transfer data were assimilated from tests conducted at the NASA JSC 10 MW Arc Tunnel, the LaRC Mach 10 Continuous Flow Hypersonic Tunnel, the LaRC Mach 8 Variable Density Tunnel, and the Ames 3.5 Foot Hypersonic Wind Tunnel. A detailed discussion of the analysis of these data is given in Section 4.0 of Reference 1 . However, significant results and conclusions are included in this report for reader convenience and report completeness.

4.1.1 Heat Protection Ability of Candidate Joints - The heat protection performance of candidate RSI joint configurations was compared based on maximum bondline heat-up (temperature rise) rates. The temperature responses were measured during tests in the NASA JSC 10 MW channel nozzle arc tunnel. Four joint configurations were tested (butt, contoured, inclined and overlap block). The butt joint was tested with forward- and aft-facing steps at the transverse joint and with gap wall emittances of 0.6 (white) and 0.9 (black). The other configurations were tested only with "white" walls. The term "white" walls refers to tiles having white gap walls ($\varepsilon = 0.6$) except for the first 0.635 centimeters down the gap, which is black ($\varepsilon = 0.9$). Gap widths of 0.127, 0.254, 0.381 and 0.762 centimeters were tested for each combination of other test variables. Tile thicknesses of 3.18, 5.08 and 6.35 centimeters were tested, but not for all joint configurations. The high cross range shuttle orbiter A2P entry heating rate-time history was simulated in the 10 MW channel nozzle for each test run. These test conditions resulted in a laminar boundary layer displacement thickness of approximately 1.02 cm, a Mach number of approximately 4.5, and a theoretical cold wall flat plate heating rate of up to 27.23 watts/cm^2. The conclusions drawn from the joint configuration comparisons are summarized below.

For the candidate joints, the rates of bondline heat-up in the transverse gap are shown in Figure 26 as functions of gap width. As seen, the contoured joint affords the best heat protection. At large gap widths the variation in heat protection ability among joint types is substantial with the forward-facing step model experiencing the largest temperature rise at the 0.762 cm gap width. This is in contrast to the aft-facing step which affords almost as much heat protection as the contoured joint. Thermal response for transverse gaps indicates that for small gaps (less than 0.381 cm), the forward-facing side of the gap experiences higher bondline

GAP CONFIGURATION CONTROLS
BONDLINE TEMPERATURE RESPONSE FOR WIDE GAPS

JSC 10 MW CHANNEL NOZZLE DATA

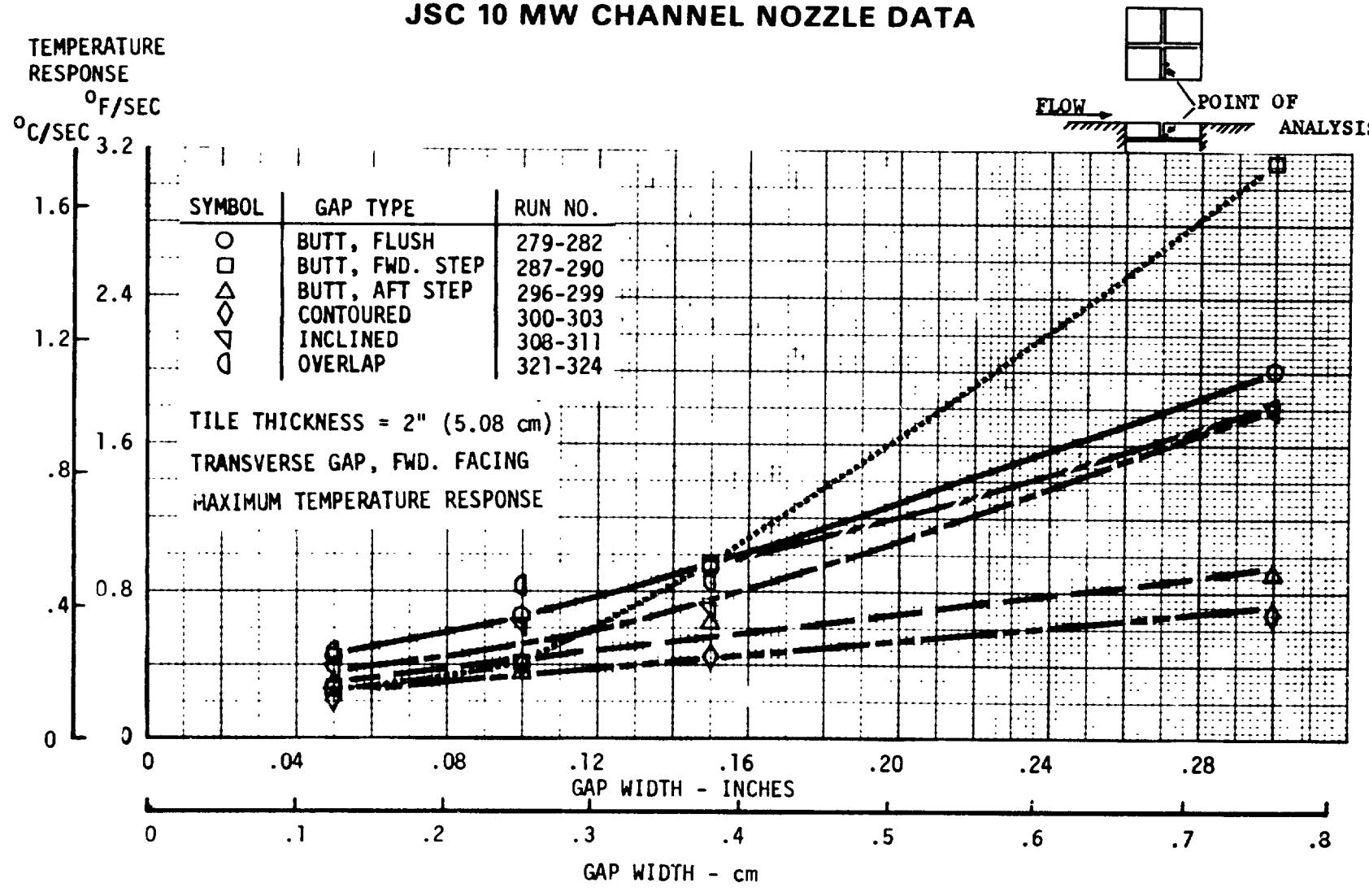

Figure 26

temperatures than the shielded aft-facing side of the gap. However, for the widest gap (0.762 cm), bondline heat-up rate is the same for both sides of the transverse gap.

The data generated with butt joint models having tile thicknesses of 3.18 and 6.35 centimeters and a gap wall emittance of 0.6 (white) are presented in Figures 27 and 28. As was expected, these data show a sharp increase in heat-up rate as the gap was opened. There was no clear differentiation of heating in the transverse gap as opposed to tne axial gap. The 6.35 centimeter thick tiles (Figure 28) provide more heat protection due not only to increased insulation, but also to a reduced sensitivity to gap width for most locations. Figure 28 shows that the downstream parallel gap location and both of the transverse locations were insensitive to the presence of the gaps for widths of 0.381 centimeters or less. Bondline heat-up rate (6.35 cm tile) at the upstream parallel gap location shows approximately the same sensitivity to increased gap width as do the parallel gap measurements for the 3.18 and 5.08 centimeter thick tiles.

Similarly, a comparison was made of data generated with butt joint models having tile thicknesses of 3.18, 5.08 and 6.35 centimeters and a gap wall emittance of 0.9. The joint bondline heat-up rate also shows a strong sensitivity to gap width. Neither the axial or transverse gap orientation appears to be consistently hotter.

A direct comparison of the "black" and "white" coatings indicated the bondline heat-up rates for a given tile thickness are similar for each coating. In general, the data showed that bondline heat-up rates were equal or slightly lower for the high emittance ($\varepsilon = 0.9$) walls. Consequently, it was concluded that increased gap wall emittance has little effect on bondline heat-up rate.

Either forward or aft-facing steps at the transverse gaps can be caused by manufacturing tolerances, structure deflection, etc. Both these configurations were tested by using two upstream butt-gap tiles of 5.08 centimeter thickness and two downstream tiles 5.46 centimeters thick to create forward-facing steps, or two downstream tiles 4.70 centimeters thick for aft-facing steps. The results of these tests are illustrated in Figure 29 and compared with results of the tests of 5.08 centimeter thick butt-joint tiles with flush surfaces. For small gap widths, both forward and aft facing steps produced bondline heat-up rates lower than those of the flush tiles. The aft-facing steps provide better thermal protection due to the shielding effect while the forward-facing step is cooler because of the thicker tiles (5.46 cm

3.18 CM (1.25") BUTT JOINT BONDLINE TEMPERATURE RESPONSE

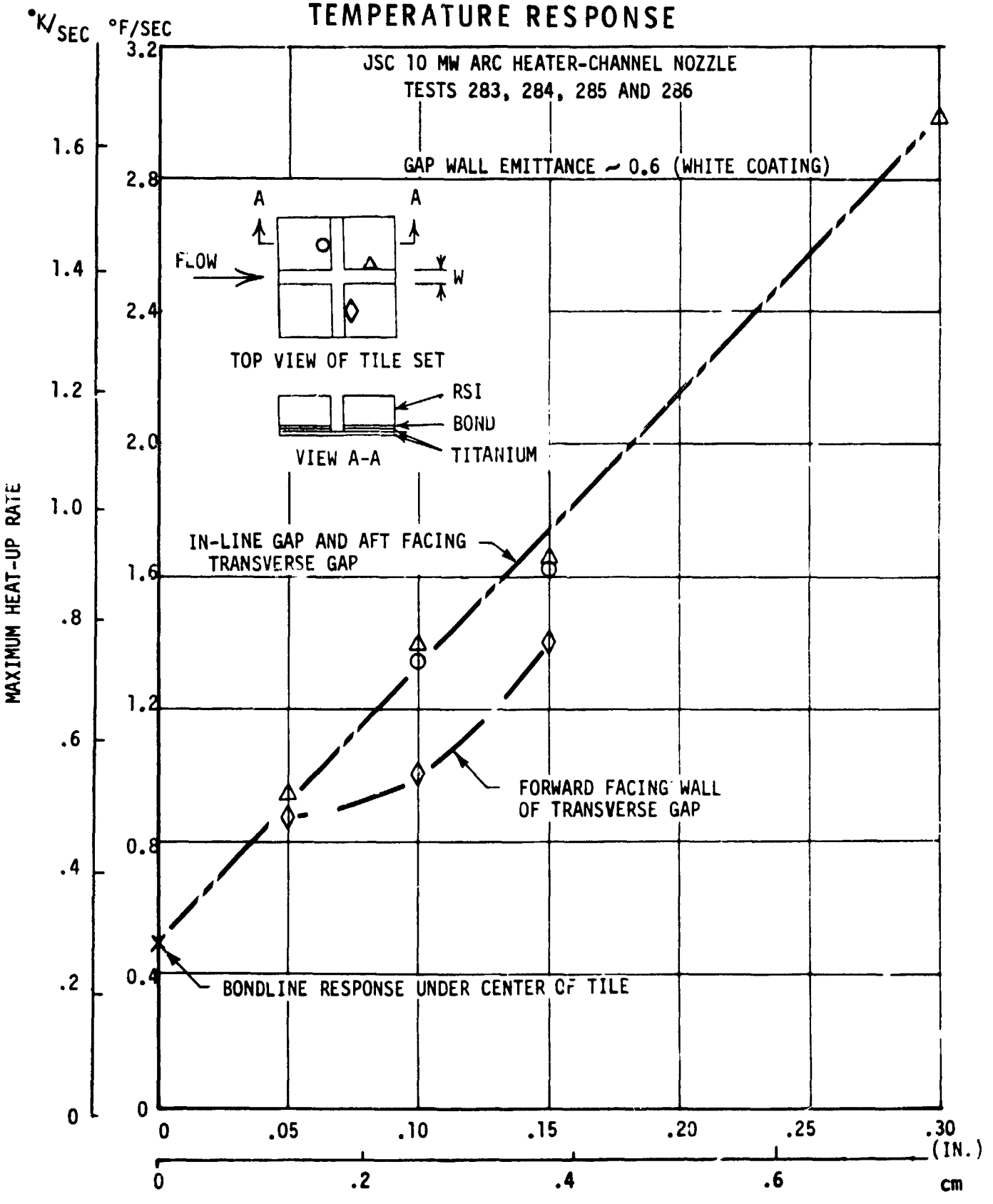

Figure 27

6.35 CM (2.5") BUTT JOINT BONDLINE TEMPERATURE RESPONSE

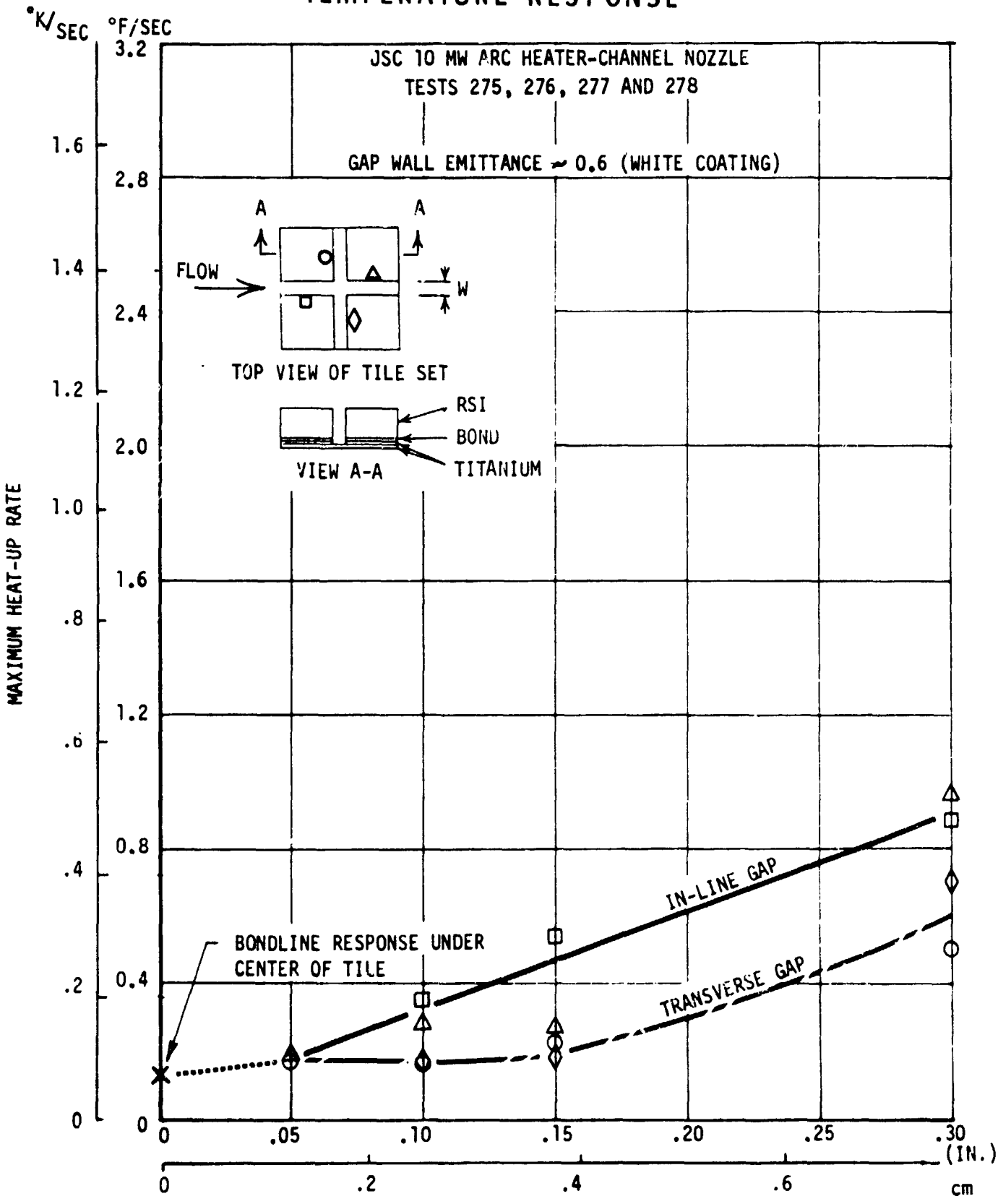

Figure 28

EFFECT OF FORWARD- AND AFT-FACING STEPS ON BONDLINE TEMPERATURE RESPONSE OF 5.08 CM (2") BUTT JOINTS

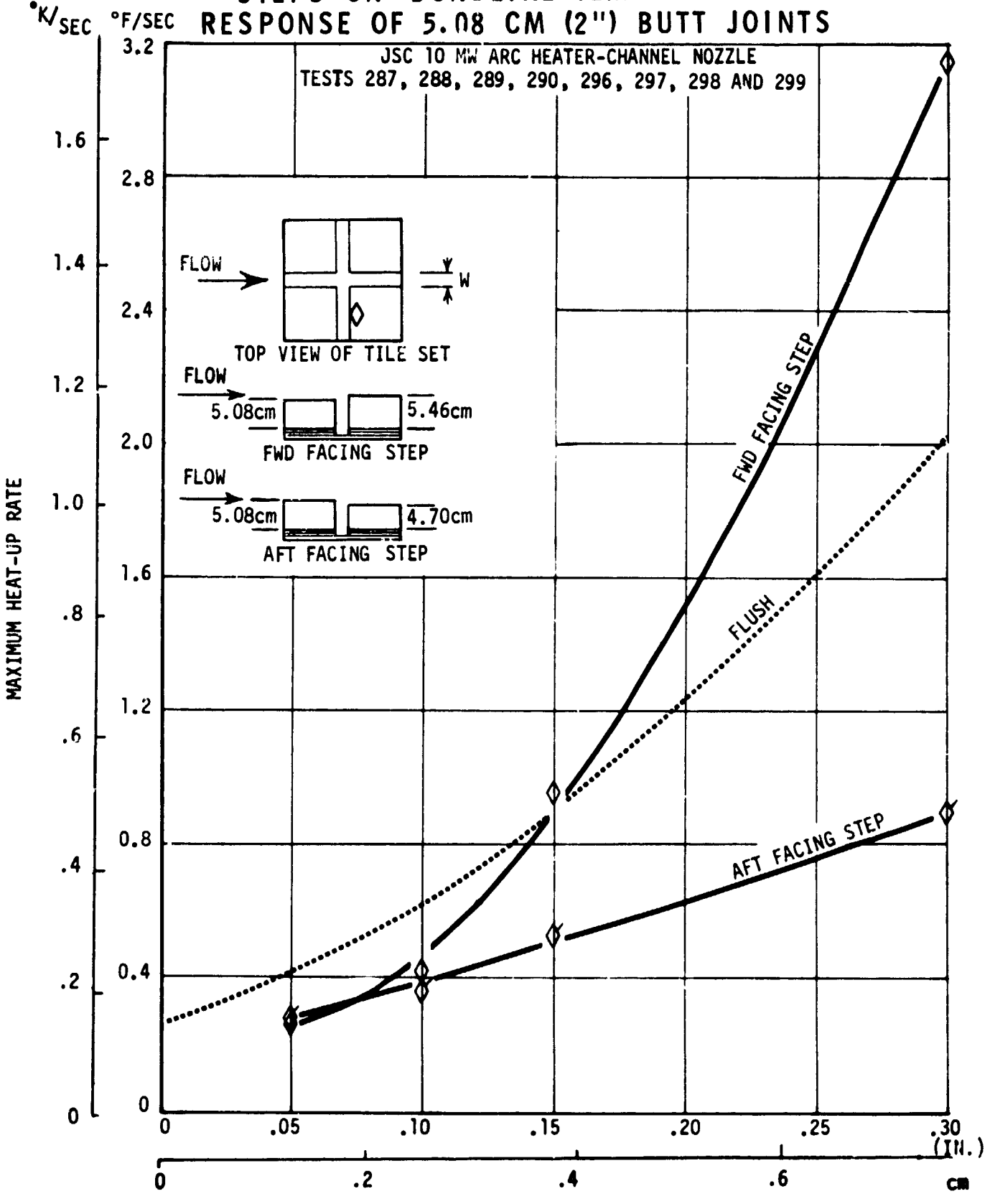

Figure 29

as opposed to 5.08 cm). As the gap is opened, the aft-facing step maintains lower response rates, but the forward-facing step experiences bondline heat-up rates which increase to levels well above those of the flush tiles.

Alternate gap configurations also offer an opportunity for reduction of gap heating. Three configurations, the contoured, inclined and overlap block in addition to the butt joint were tested. In each case the hot external flow is denied a direct path to the gap bottom. None of these configurations was an unqualified success, yet all achieved a reduction in bondline response at some instrumented location. Test data for 5.08 centimeter thick tiles of each candidate joint configuration are compared next and related to the 5.08 centimeter butt joint.

The measurements taken with the inclined joint tile set (Figure 30) exhibit a particularly wide range of sensitivity to gap width depending on instrument location. All locations are essentially equivalent to the butt joint performance (Figure 28) at a gap width of 0.127 centimeter. As the gap is opened, however, the heat-up rate of the upstream axial location quickly increases to a level well in excess of the heat-up rates experienced during the butt joint tests. The data taken at the bondline of the downstream-facing transverse gap wall remain at relatively low levels for all gap widths and data taken at the other two locations are roughly equivalent to those of the butt joint configurations.

The contoured joint configuration (which was more complicated) produced the least sensitivity to gap width of any of the configurations tested (Figure 31). It is also the only configuration for which bondline heat-up rate varies significantly with location for the 0.127 centimeter gap width. This configuration did, in fact, experience higher bondline heat-up rates in the downstream axial gap at widths of 0.127 and 0.254 centimeter than does the butt joint. With the largest gap width, though, the contoured joint provided significantly improved heat protection at all locations, compared to the butt joint.

The overlap block configuration creates a tortuous path for gas circulating from the surface to the bondline. Figure 32 , however, shows that the RSI filler block which is used to create that devious path suffers quite a high bondline heat-up rate. By comparison one may see that the other configurations hold no advantage over the simple butt joint.

The results of these tests indicate then, that if small gap widths can be achieved, little can be gained by use of joint configurations more complex than the butt joint. If gap widths approach the local boundary layer displacement thickness

5.08 CM (2") INCLINED JOINT BONDLINE TEMPERATURE RESPONSE

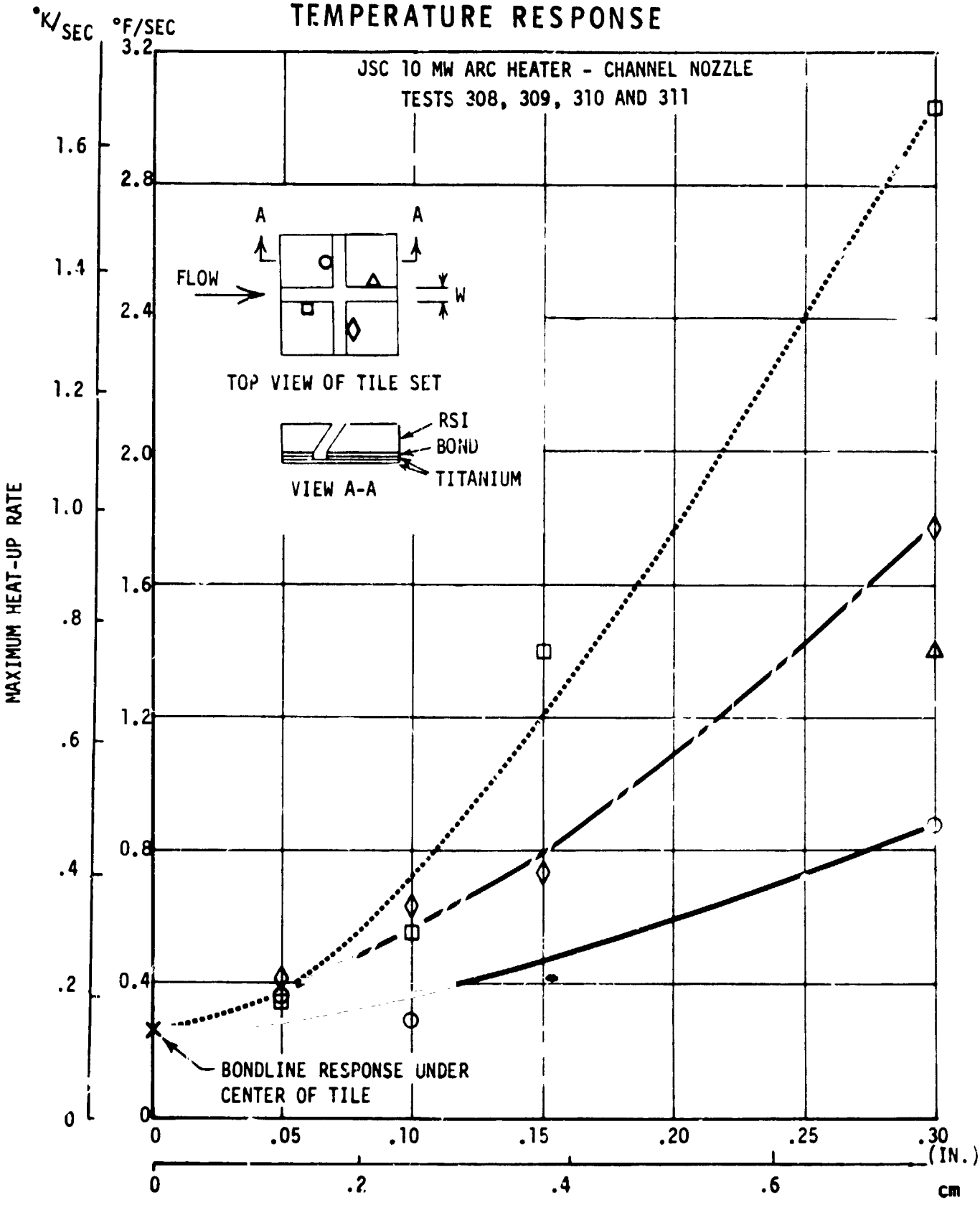

Figure 30

5.08 CM (2") CONTOURED JOINT BONDLINE TEMPERATURE RESPONSE

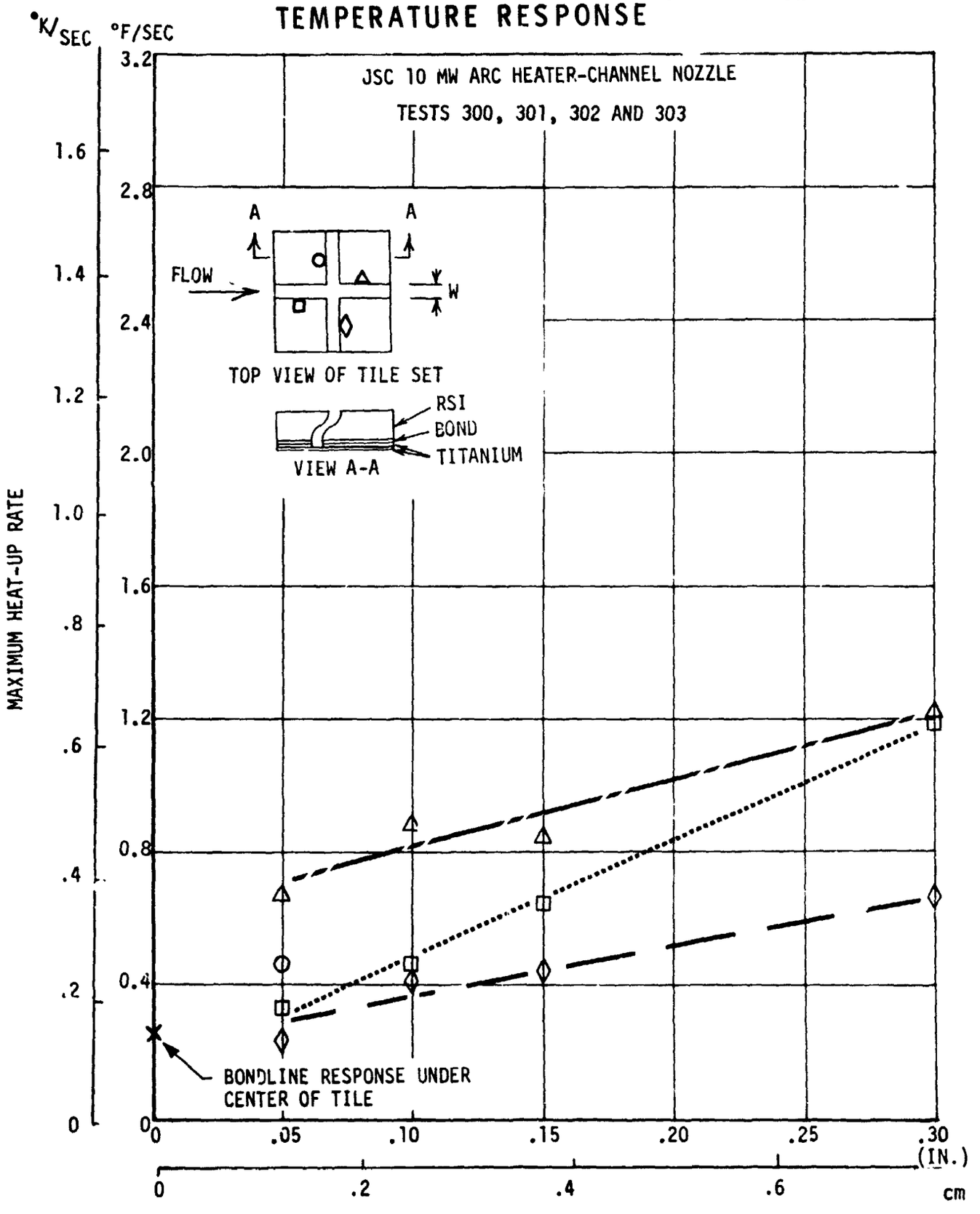

Figure 31

5.08 CM OVERLAP BLOCK BONDLINE TEMPERATURE RESPONSE

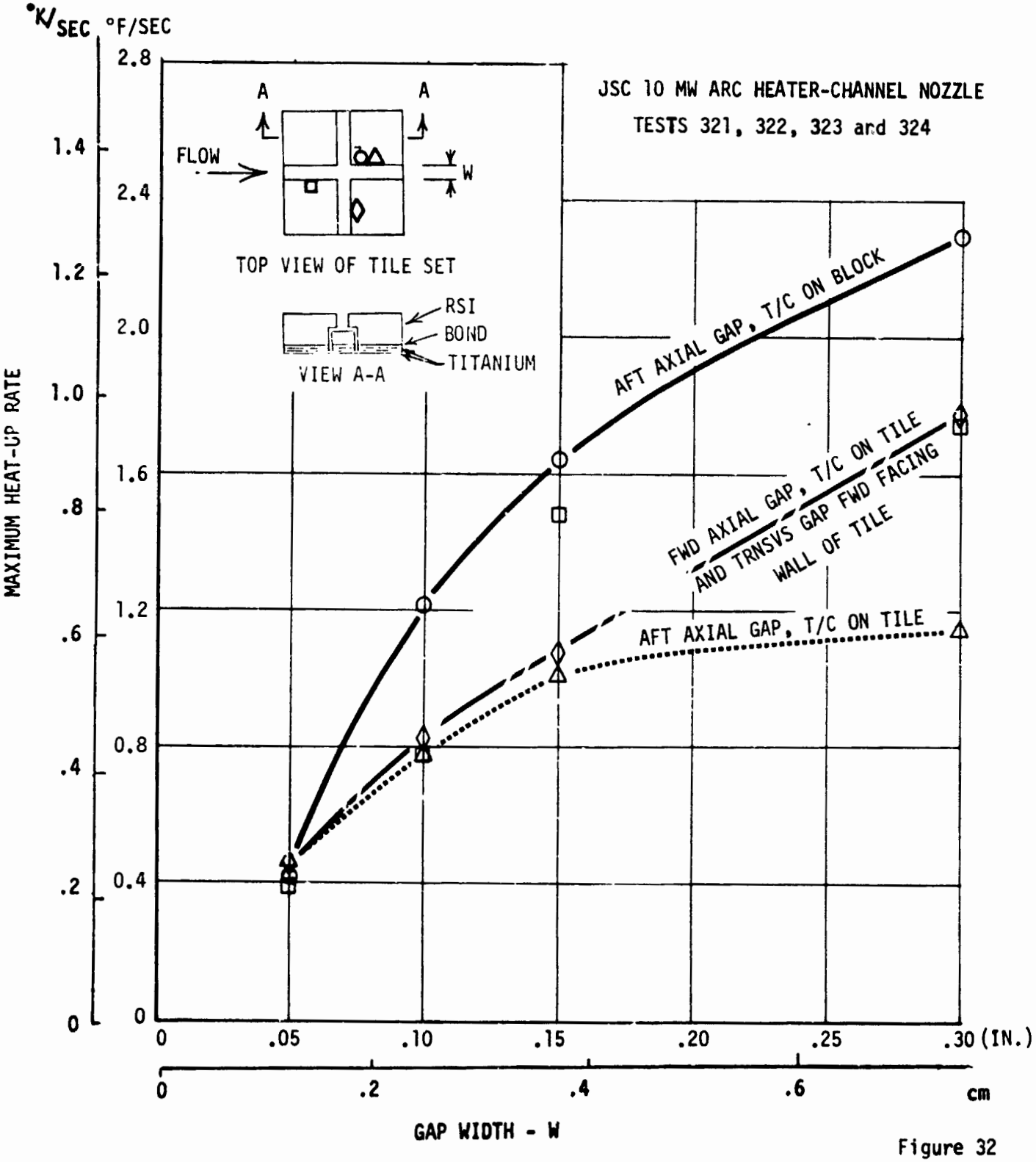

Figure 32

(about 1.016 centimeter for these tests), use of the contoured joint configuration may afford considerable relief and forward-facing steps at the joint may exact a considerable penalty.

4.1.2 Heating Rates in RSI Models of Gaps - Heating rates were calculated using RSI-gap thermal response histories measured during tests in the JSC 10 MW Arc Tunnel channel nozzle. The test conditions, model description and data assimilated are discussed in Section 3.1 of this report and in Volume II of Reference 1 . The analyses concentrated on a description of radiant heat exchange within the gap, a graphical description of the various modes of heat transfer in the gap, evaluation of data uncertainties, and comparison of convective heating distributions for transverse and in-line gaps for both butt and inclined joint configurations.

Radiant Heat Exchange - Radiation exchange between the faces of a gap is important because relatively high temperatures (816°C or more) are experienced at gap depths of more than 1.27 centimeter. Preliminary data indicated that convective heating at such depths was on the order of 0.113 watts/cm^2. For example a 8.3°C difference between two infinite plates (each with a 0.6 emittance) at 816°C produces about 0.113 watts/cm^2 net heat transfer. The 8.3°C represents only a 1% change in gap wall temperature. Initial thermal modeling employed a minimal number (8) of nodes within the gap. Consequently the radiation exchange modeling was refined by increasing the number of nodes on the gap wall from 8 to 18. Smaller area nodes are particularly helpful because they allow view factors and the nodal temperatures associated with them to approach the ideal condition of an infinitesimal element model. In modeling a 6.35 centimeter thick specimen, node lengths were decreased from 0.794 to 0.353 centimeters, alleviating the situation where large nodes are used in an analysis of a small gap. In the case of large nodes, the only significant view factor may be with the opposite node, virtually eliminating the opportunity for emitted or reflected energy to be transferred down the gap. Node size in the thermal model was varied so that the smallest nodes occurred in the region of highest temperature.

Graphical Description of Heat Transfer Modes - The heat transfer for the wall of a typical forward facing, transverse gap is segregated into its three components of convection, radiation and conduction in Figure 33. The analyses used an 18 node model down the gap and the inverse solution method. Temperatures for the uninstrumented wall of the gap were set equal to the values of the corresponding nodes on the instrumented wall. Heat fluxes less than zero indicate energy leaving the surface at that depth. The conductive flux consists of two parts, the conduction between adjacent coating nodes and conduction into the RSI, normal to the surface of the gap wall.

HEAT FLUX COMPONENTS COMPUTED FOR 3.18 CENTIMETER RSI BUTT JOINT MODEL

- o NASA JSC 10 MW CHANNEL FACILITY RUN 285
- o ANALYSIS @ PEAK HEATING (460 SECONDS)
- o INSTRUMENTATION ON FORWARD-FACING TRANSVERSE WALL
- o GAP EMITTANCE = 0.6
- o SURFACE HEATING RATE = 22.34 WATTS/cm^2

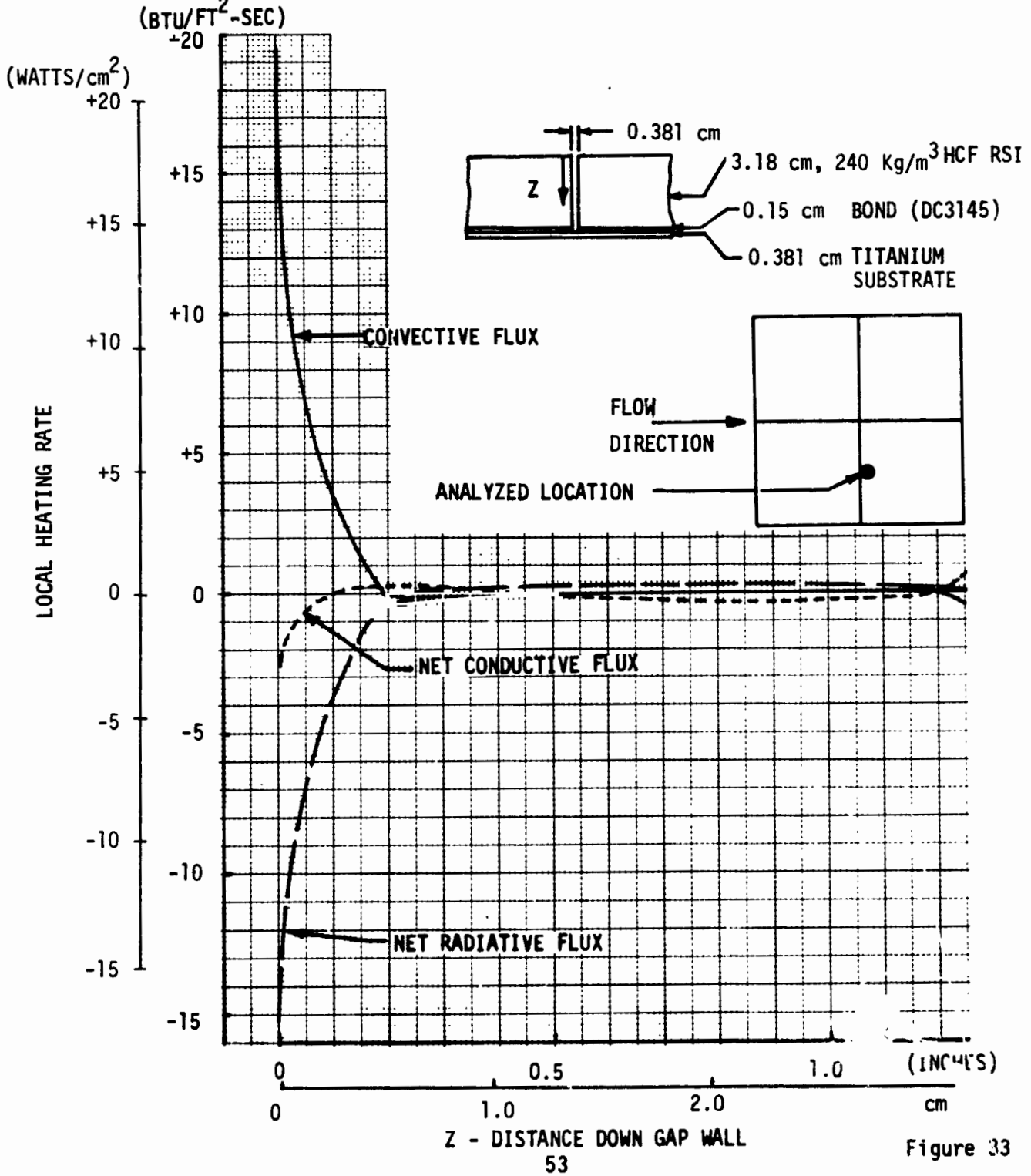

Figure 33

The convective heating and radiative flux shown in Figure 33 are large at the top of the gap and their distributions approximately mirror one another. At approximately 0.508 centimeters into the gap, the convective and radiative heat fluxes become minimal. The net conductive flux has the greatest magnitude near the top of the gap, as expected, but much smaller than either the radiative or convective components. The negative net conductive flux at the top of the gap is indicative of a temperature distribution which is approaching steady state and the remainder of the conduction curve is most likely due to the transient thermal response of the RSI. During peak heating, the gap wall is hotter at all locations than laterally adjacent RSI material so the conduction in the normal direction is always negative.

Impact of Uncertainties - Studies were conducted to determine the impact of uncertainties in gap heating rate distribution on Shuttle TPS performance. This is of importance since bondline temperature is a factor which must be controlled through proper TPS design, and the adhesives and strain isolation sponges available for this type of system have relatively low temperature capability compared with the RSI to which they are applied. The results of this analysis give an indication of the level at which gap heating ceases to be a significant factor in determining bondline temperature. Hypothetical cut-off points were assumed in the gap above which convective heating rates are known and below which they are uncertain. An extremely conservative design approach would then be to assume the heating value remains constant from that point. While a nonconservative approach would be to assume no heating below the cut-off point. The true heating rate distribution of course lies between these two assumptions. For the test case studied and for gap depths greater than 2.54 cm, the two assumptions gave comparative results. Thus, if the heating rate distribution is known accurately down to a depth of 2.54 cm, the ill effects of uncertainties below that gap depth are minimal.

Comparison of Heating Rate Distributions in RSI Models of Gaps - The convective heating analyses of gap tests contained in this section were performed on data obtained in the NASA-JSC 10 MW Arc Tunnel facility utilizing series of adjustable RSI models installed in one wall of a channel nozzle. Convective heating in the gaps between tiles was calculated using the MDC General Heat Transfer Program inverse solution technique. A description and the method of utilizing this technique are given in Section 4.2.1 of Reference 1 .

Convective heating results for the transverse and in-line gaps were obtained for the butt and inclined joint configuration. Four gap widths (0.127, 0.254, 0.381, and

0.762 centimeter) and three tile thicknesses (3.18, 5.08, and 6.35 cm) were analyzed for the butt joint configuration. The inclined joint was analyzed for the 6.35 cm tile and all gap widths.

Heating distributions for the downstream wall of the transverse gap for the butt joint configuration are shown in Figures 34 , 35 , and 36 . The data on Figures 34 and 35 are presented in rectilinear and semi-log coordinates to emphasize the low magnitude of convective heating in the transverse gap at depths beyond 0.762 centimeter for the arc heater environment produced by the 10 MW facility. In comparing these figures it is seen that heating drops off rapidly down the gap, heating increases with gap width and penetrates deeper into wide gaps, and that for a wide gap (0.762 cm) the heating rate ratio near the top of the gap can be higher than 1.0. Figure 37 is another way of presenting the above data, as a function of gap width, and indicates that for most conditions increasing gap depth lowers the gap heating distribution.

Similarly, in-line gap heating distributions were calculated for the butt joint configuration and gap depths of 3.18, 5.08, and 6.35 cm. The results are summarized in Figure 38 . A comparison of the data for the two type gaps (in-line versus transverse) indicates that heating in the in-line gaps is higher than for the transverse gaps at some combinations of gap width and depth. (See Figures 38 and 37 .) A comparison of these figures also indicates the in-line gap is more sensitive to gap width than the transverse gap for gap depths greater than 0.2 cm.

The effect of a forward facing step on heating distributions is shown in Figure 39 for a 5.08 cm tile and the whole range of gap widths. For the narrow gaps (0.127, 0.254, 0.381 cm) the heating near the top of the gap stagnates, increasing the heating rates. Since the gap is small, flow within the gap is impeded, therefore the heating falls off rapidly to 0.9 cm gap depth and then decreases gradually below that point. For the wide gap (0.762 cm) the heating takes on a different distribution which is also significantly higher than for the narrow gaps. Since the gap is wide the heating near the top gets relief from the wide gap below, which causes heating to recirculate and penetrate deep into the gap Because the step distorts the gap heating distribution, a significant increase in heating occurs when compared to a flush joint. Figure 40 shows a comparison of downstream transverse gap heating for a butt joint model with and without a forward facing step. As seen, heating along the gap wall of a forward facing step can be an order of magnitude or more greater than for flush tiles.

BUTT JOINT HEATING RATE DISTRIBUTION FOR 3.18 CM TILE

- o JSC 10 MW CHANNEL NOZZLE TEST
- o DOWNSTREAM TRANSVERSE GAP
- o HIGH EMITTANCE COATING 0.635 cm DOWN TILE GAP
- o LOW EMITTANCE COATING REMAINING GAP SURFACE

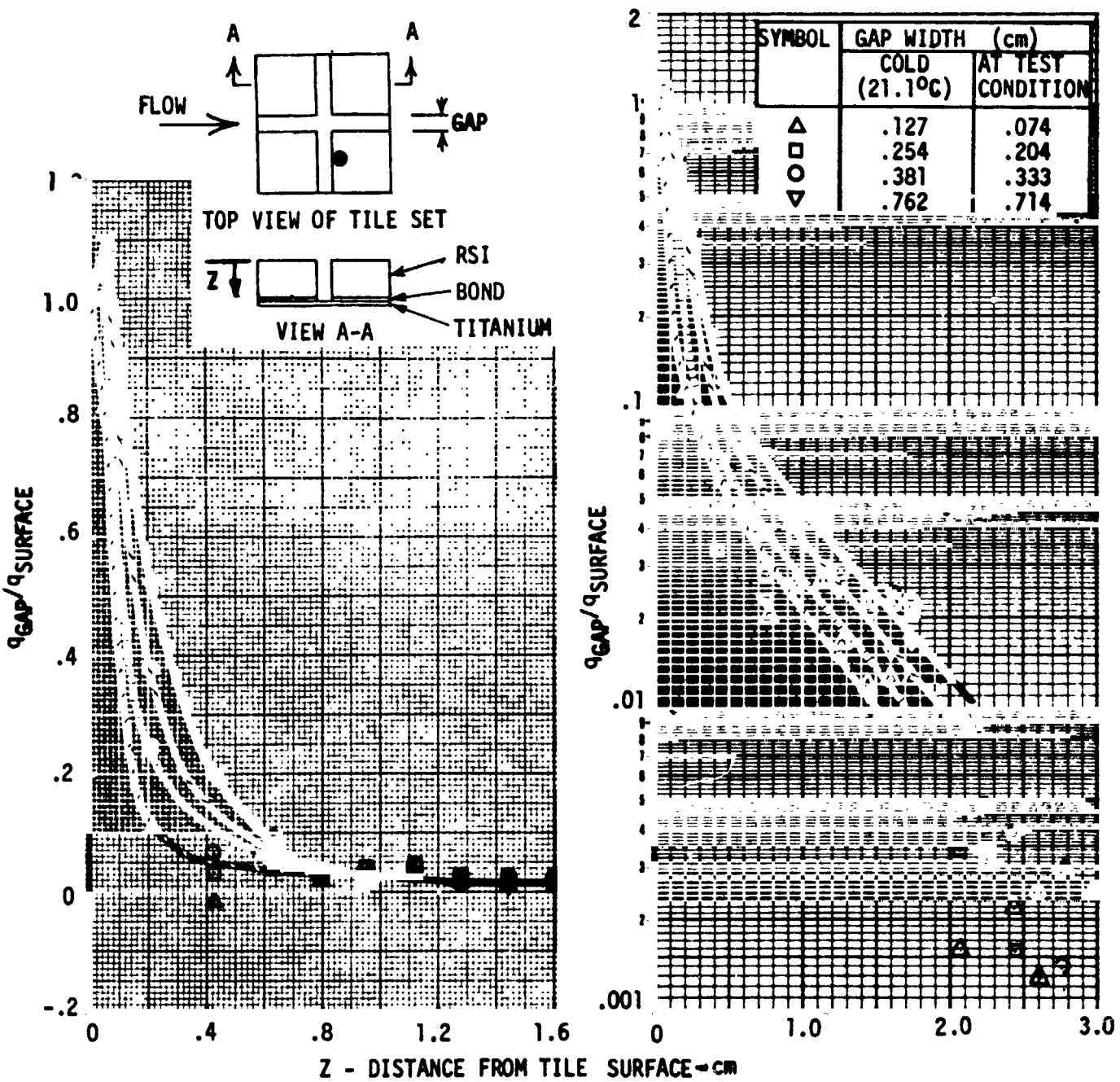

Figure 34

BUTT JOINT HEATING RATE DISTRIBUTION FOR 5.08 CM TILE

- o JSC 10 MW CHANNEL NOZZLE TEST
- o DOWNSTREAM TRANSVERSE GAP
- o HIGH EMITTANCE COATING ON GAP WALLS

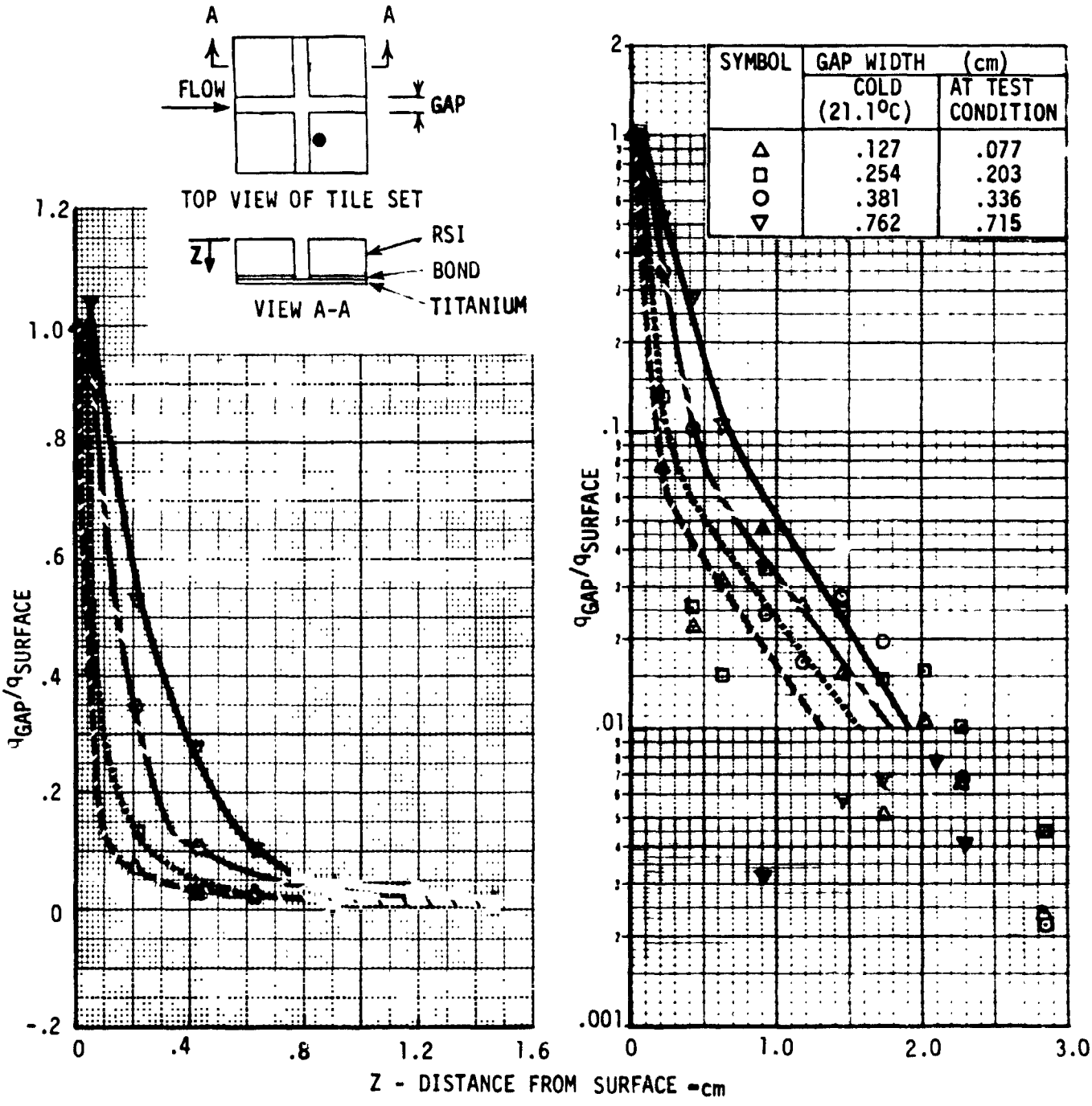

Figure 35

BUTT JOINT HEATING RATE DISTRIBUTION N DOWNSTREAM TRANSVERSE GAP 6.35 CM TILE

- o JSC 10 MW CHANNEL NOZZLE TEST
- o HIGH EMITTANCE COATING 0.635 cm DOWN TILE GAP
- o LOW EMITTANCE COATING REMAINING GAP SURFACE

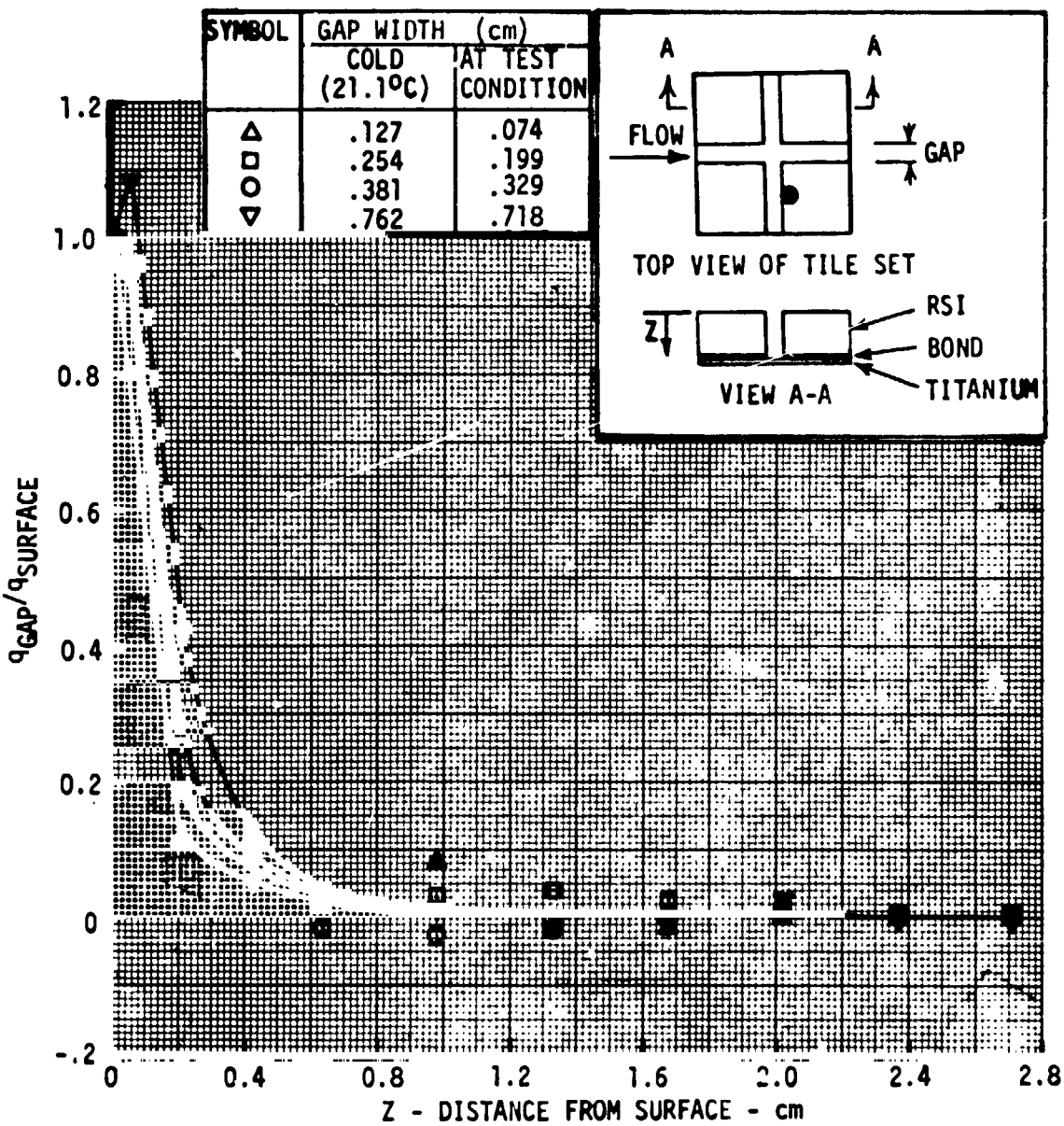

Figure 36

COMPARISON OF DOWNSTREAM TRANSVERSE GAP HEAT TRANSFER WITH GAP WIDTH FOR SEVERAL BUTT JOINT THICKNESSES

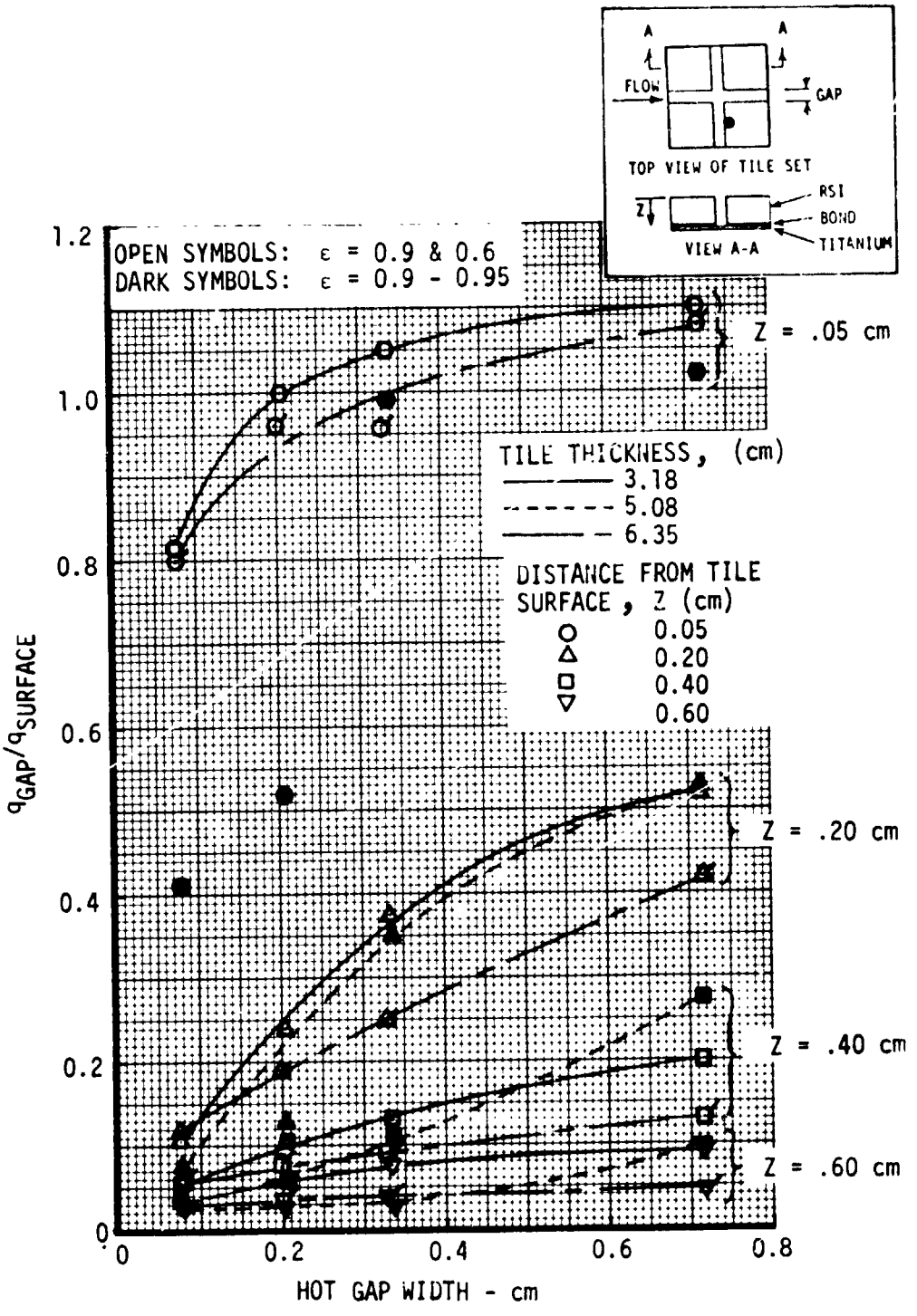

Figure 37

COMPARISON OF AXIAL GAP HEAT TRANSFER WITH GAP WIDTH FOR SEVERAL BUTT JOINT THICKNESSES

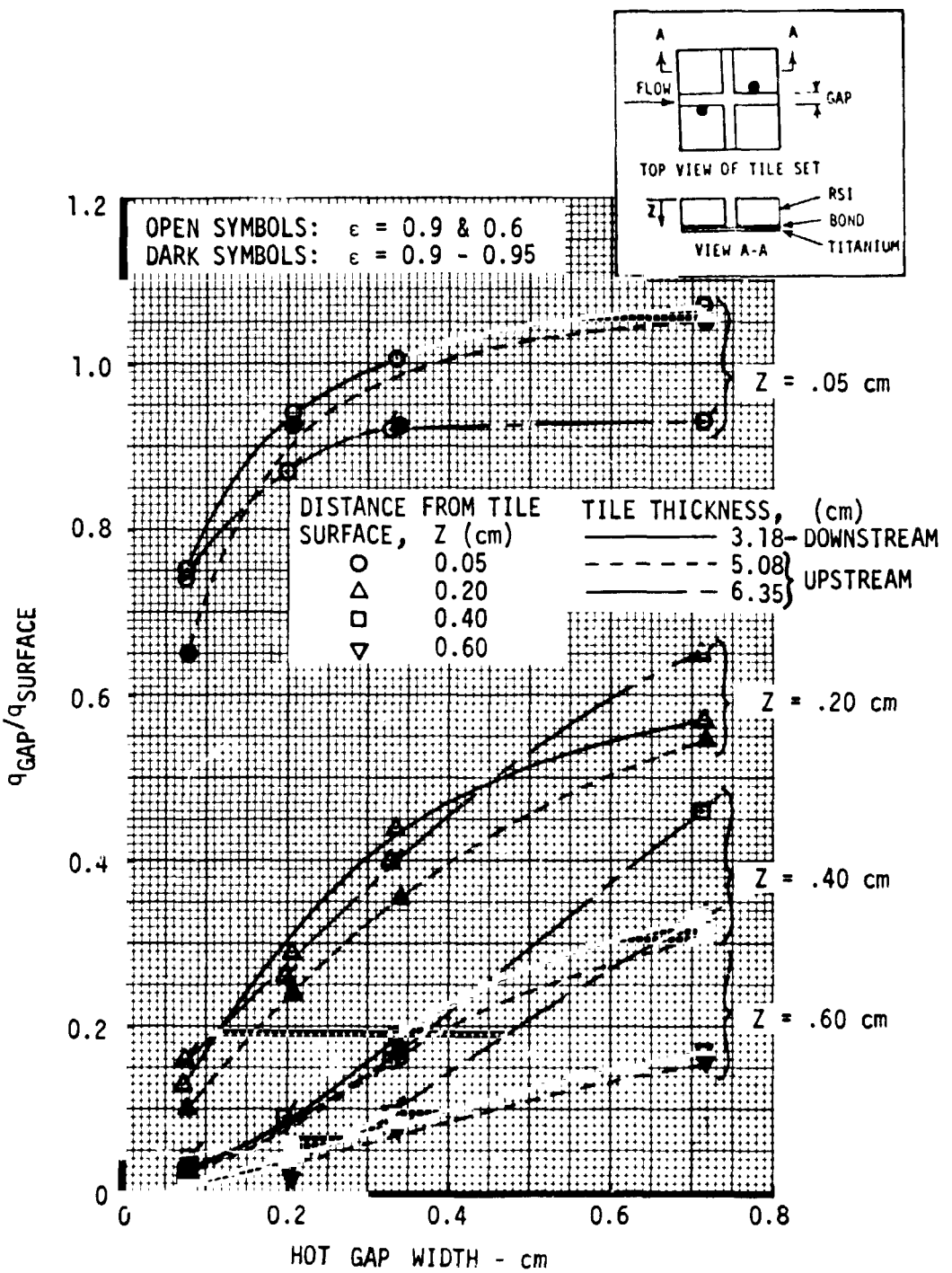

Figure 38

BUTT JOINT HEATING RATE DISTRIBUTION FORWARD-FACING STEP DOWNSTREAM TRANSVERSE GAP, 5.08 CM TILE

- o JSC 10 MW CHANNEL NOZZLE TEST
- o HIGH EMITTANCE COATING ON GAP WALLS

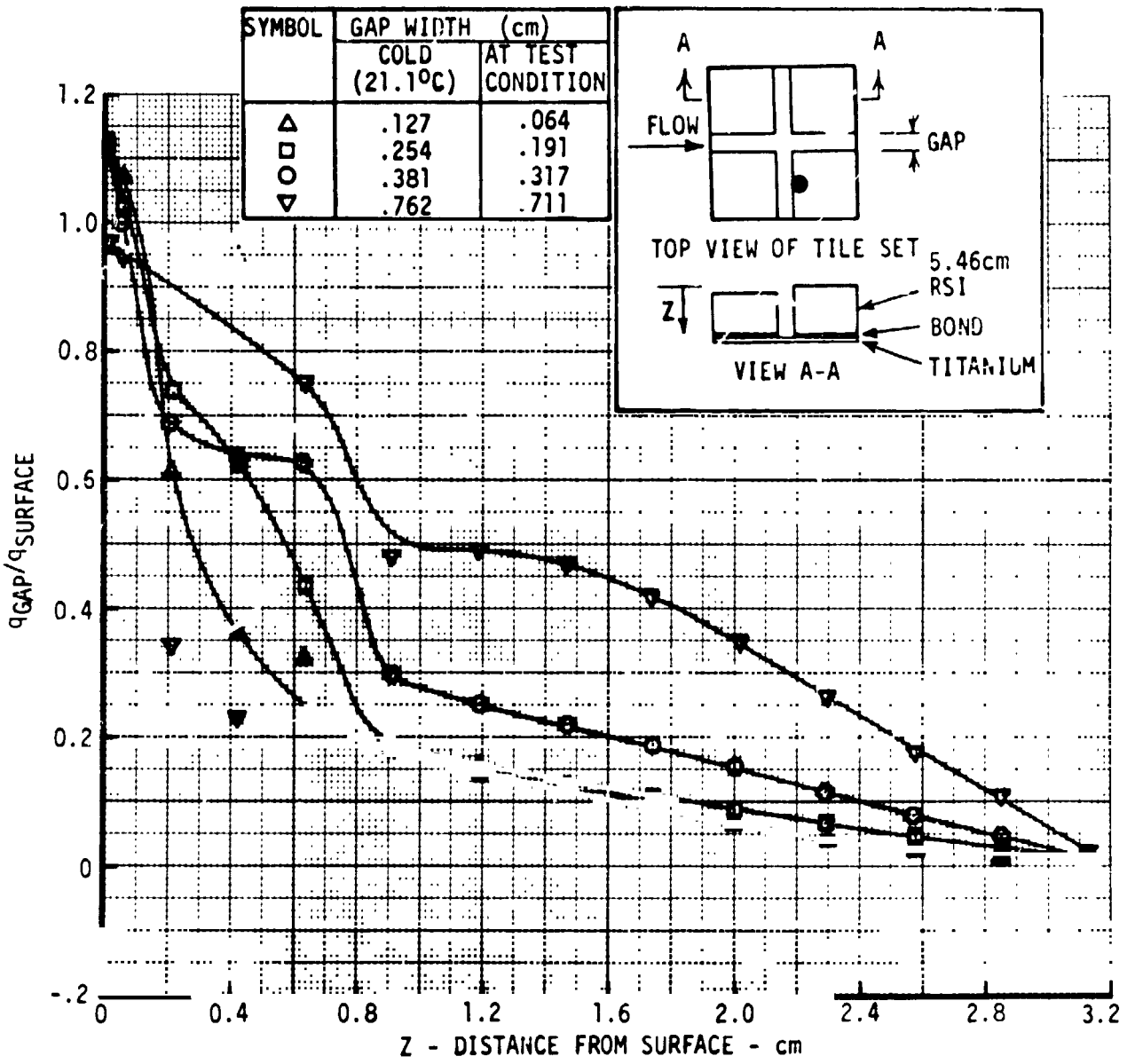

Figure 39

COMPARISON OF DOWNSTREAM TRANSVERSE GAP HEAT TRANSFER WITH GAP WIDTH BUTT JOINT WITH AND WITHOUT FORWARD STEP

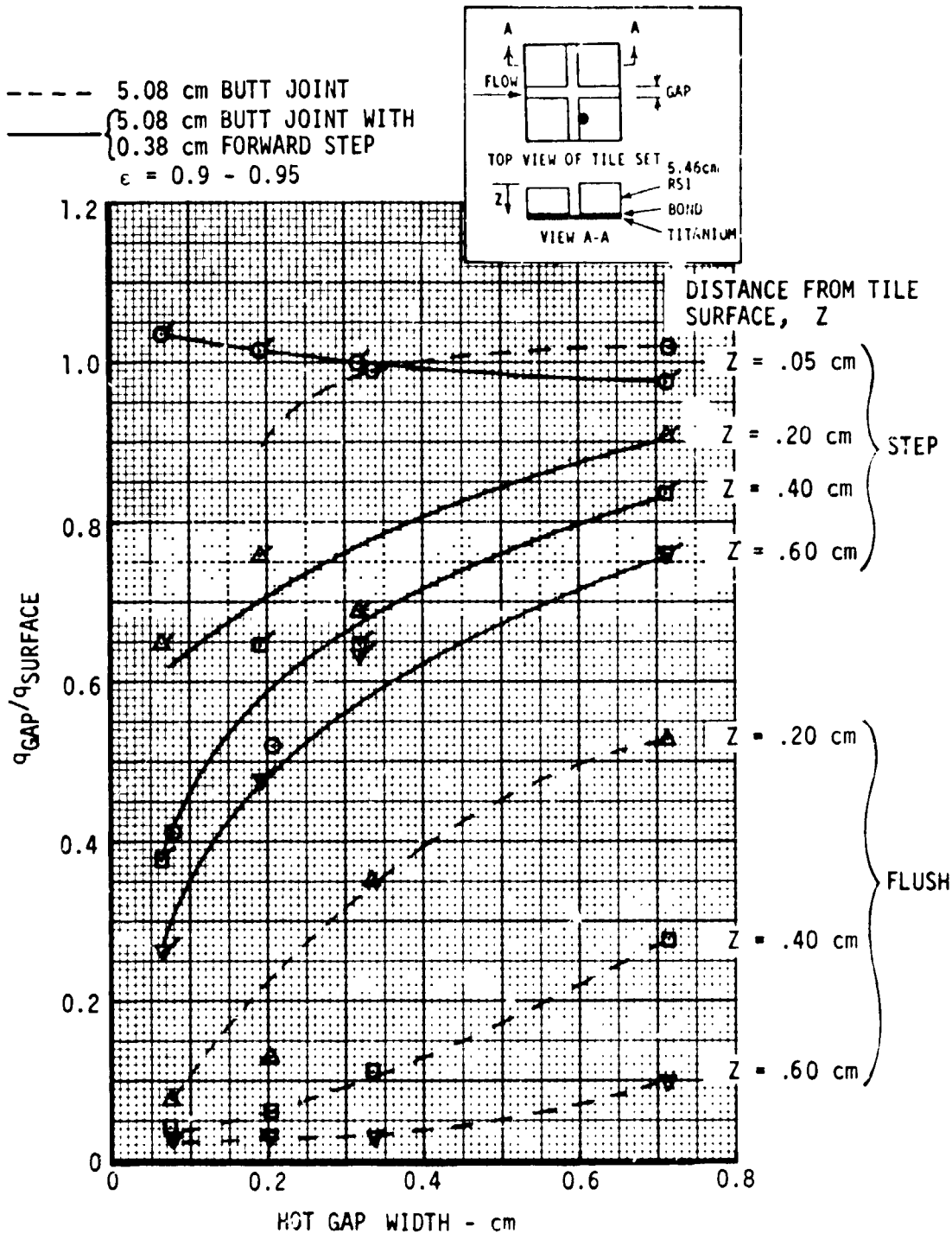

Figure 40

Convective heating analyses for an inclined joint model were also performed for both the downstream side of the transverse gap and for an in-line gap upstream of the transverse gap. The tiles were 6.35 centimeters thick. The heating distributions were found to be very similar to the butt joint distributions. For both in-line and transverse gaps, the heating for the inclined joint was slightly greater and more sensitive to gap width from 0.10 to 1.0 cm gap depths.

4.1.3 Analysis of Mach 10 CFHT Test of Gap Model - Analyses were performed on heat transfer data obtained on a wall-mounted, thin skin tile model tested in the LaRC Mach 10 Continuous Flow Hypersonic Tunnel. Test conditions, model description and data assimilated are discussed in Section 3.1 of this report and in Volume II of Reference 1 . The test article consisted of a panel with six RSI tiles surrounding a highly instrumented thin skin tile. The test panel was located on a rotational plate on the tunnel sidewall such that the flow angle could be varied over the test panel. The tests performed during the initial program were conducted at a Mach number of 10 and a unit Reynolds number of 3.3×10^6. Included in the data analyses are the following:

a) Evaluation of data reduction methods including calibration plate heating and the effect of considering conduction on measured heating rates.

b) In-line versus staggered tile heating patterns.

c) Effect of gap width on tile heating patterns.

d) Effect of flow angle on gap heating patterns.

e) Effect of steps on tile heating patterns.

Data Reduction Methods - LaRC performed calibration runs in support of a McDonnell Douglas sponsored program to measure heat transfer data on a corrugated panel model mounted on the tunnel sidewall. As part of that effort, flat plate heat transfer data were taken. Figure 41 presents the measured heat transfer distribution in the vertical direction on the flat plate mounted on the tunnel sidewall. The distribution shown is based upon three data runs. A significant variation in the heating across the flat plate is observed. This tunnel characteristic has been attributed to the square nozzle and test section which results in a slight flow convergence toward the center of the tunnel sidewall. Data taken on the corrugated panel exhibited a similar spanwise heating gradient to that observed on the flat plate. Normalizing the corrugated panel heat transfer coefficients by the flat plate coefficients resulted in successful collapsing of the data in the spanwise direction. Because of this previous experience in correlating the corrugated panel data, the gap heating data, taken at the same test condition were normalized by the measured flat plate heat transfer coefficients.

HEAT TRANSFER DISTRIBUTION [$H_{FP} = F_I(Y)$] ON FLAT PLATE MOUNTED ON CFHT SIDEWALL

$M_\infty = 10.33$ $Re_\infty/m = 3.28 \times 10^6$ TEST NO. 93

$Taw/T_T = 0.895$ X = 0.0

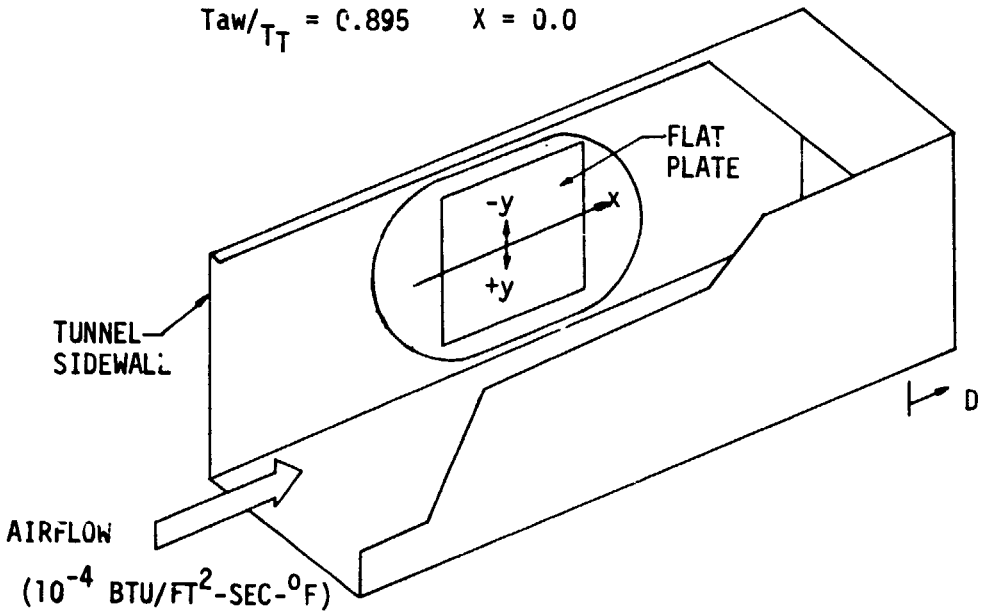

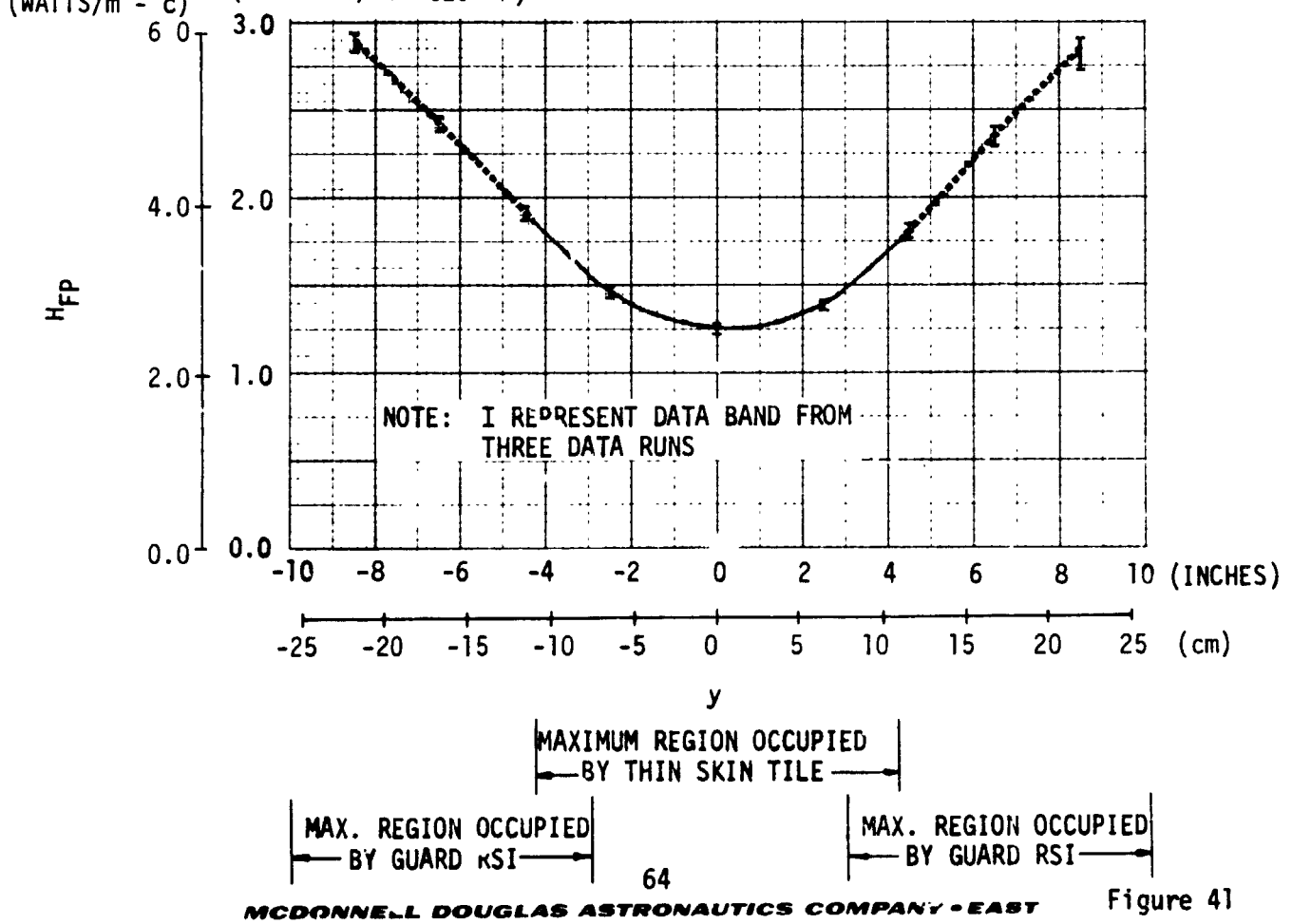

Figure 41

Data reduction for the thin skin tile tests employed the slope of the temperature-time curve at selected times to solve for the heat transfer coefficient using the following equation:

$$h = \frac{\rho C_p \; X \; (dTw/d\theta)}{(Taw-Tw)} \qquad \text{where } X = \text{skin thickness}$$

Two times were selected for data reduction for each thermocouple during these tests. The first time selected was 0.50 seconds after the test article reached the tunnel wall since during the first 0.35 to 0.45 seconds the temperature readings were erratic. A second time was also selected which was 0.50 seconds after the first time or 1.0 seconds after tile insertion. The temperature-time derivative ($dT/d\theta$) was obtained by taking the slope of a least squares quadratic curve fit through ten seconds of data obtained for each thermocouple. The initial point of the curve fit interval is the time selected for data reduction; i.e., 0.50 seconds and 1.0 second. Ten seconds was selected as the curve fit interval to obtain data deep in the gaps where heating levels are low. The curve fit expressions are of the form:

$$Tw = a + b\,\theta + c\,\theta^2 \text{ and } dT/d\theta = b + 2c\,\theta$$

where a, b, and c are constants. Two heat transfer coefficients were computed for each value of $dT/d\theta$ based upon two values of adiabatic wall temperature, i.e., Taw/T_T = 0.895 and 1.0. However, all data in this section are based upon Taw/T_T = 0.895 because the boundary layer was turbulent for all tests. Also all data presented in the following figures were evaluated at 0.50 seconds after test article insertion was complete.

The above method is graphically demonstrated in Figure 42 for two typically measured temperature histories on the downstream face of the thin skin tile. In the first curve (T/C Channel 20), the thermocouple was located in the gap 0.414 cm from the surface, and the two slopes are nearly equal indicating a linear temperature response. All thermocouples where a significant temperature rise occurred exhibited this type of temperature response. In the second curve (T/C Channel 55), the thermocouple is deeper within the gap (1.113 cm from the surface), and the temperature response was an order of magnitude lower than Channel 20. The temperature response was also low enough that "noise" from the data recording system

MEASURED TEMPERATURES IN GAPS AT CFHT

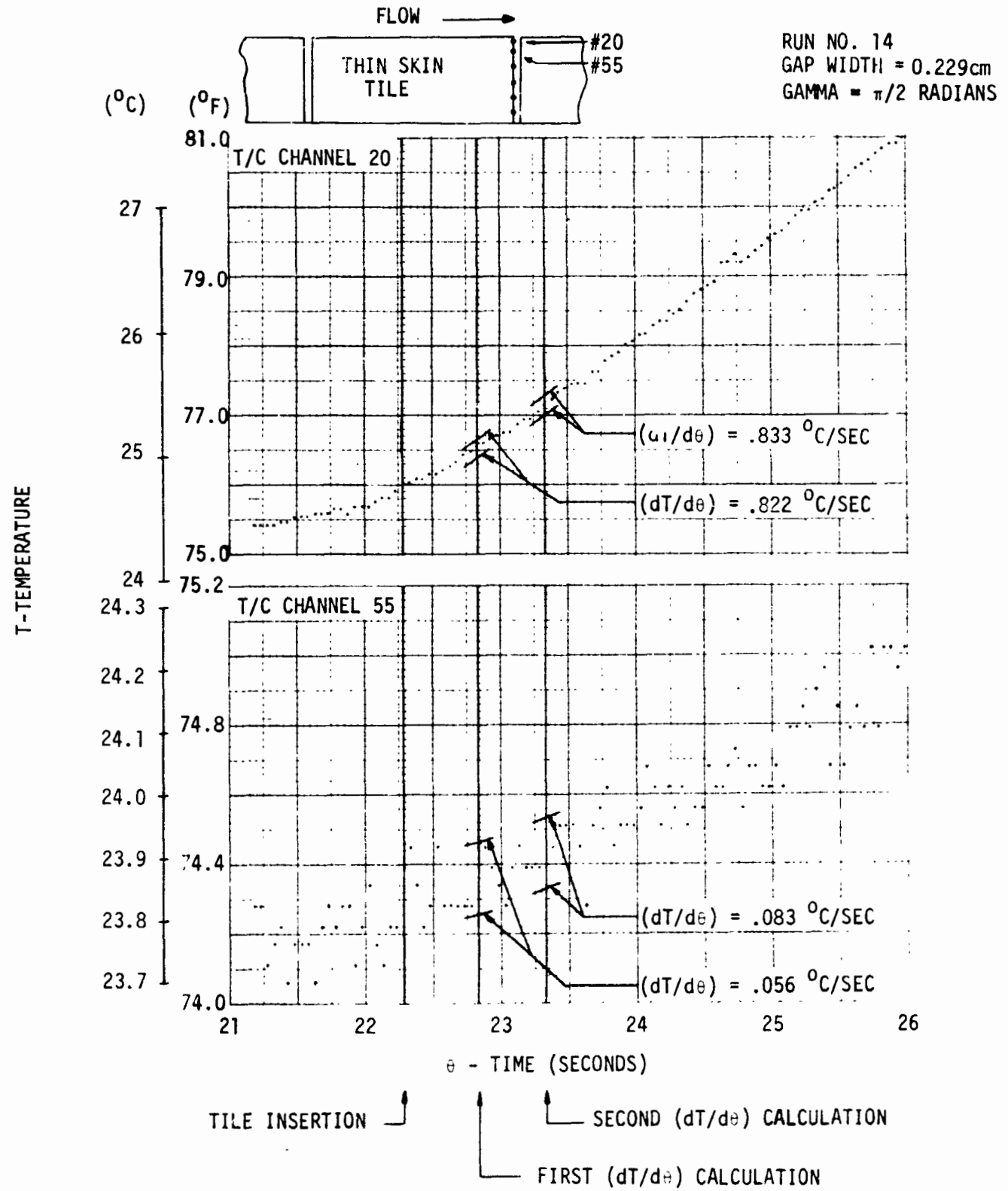

Figure 42

is observed in the data. The third through the sixth rows of thermocouples had a temperature response so low that the "noise" from the data recording system was greater than the temperature rise over a ten second time interval. Consequently, a significant number of thermocouples in the gaps had such a low signal to noise ratio that the data were not included in the analysis.

A study was made to examine the effect of including conduction in the calculation of heating rates from wind tunnel tests that employ thin skin tiles. Data from Run 14 of the CFHT were selected for this purpose. An eight node thermal model was formulated to describe the heat storage and heat conduction characteristics of a section through the thin skin tile for the temperature distributions shown in Figure 43 . For each node in the thermal model there was a corresponding thermocouple on the thin skin tile which was used to define the nodes' temperature history. Hand fairings of the temperature histories were input into the General Heat Transfer Computer Program along with the thermal model descriptors and an inverse solution was performed to calculate a heating rate for each node. Figure 43 depicts the spanwise temperature distribution across the top and down the side of the tile at 0.5 seconds after test article insertion. Two distributions are shown corresponding to "as received data" and "revised temperature data". The revised data resulted from applying a thermocouple calibration correction to the as-received-data. The correction was determined by NASA LaRC after initial efforts to examine the effects of conduction were unsuccessful (detailed discussion is given in Section 4.3 of Reference 1). The revised temperature distribution is seen to be much smoother than the original distribution with the resultant elimination of the "knee" in the curve that existed at node 4.

Figure 44 shows the effect on calculated heating rates of excluding and including conduction in the thermal model using the revised temperature distributions. The data shown in this figure is for 0.5 second after tile insertion. The heating rates for the "no conduction" case consider only the heat storage term and are comparable with the data reported by LaRC. The differences between these data are due to the techniques used in the fairing of the temperature histories. The technique used by LaRC consisted of least squares curve fit of the temperature histories while hand-faired histories were used with the eight node thermal model. When conduction is included in the thermal model analysis, the surface node near the top edge of the tile showed an increase in calculated heating rate of 8.5%. However, the calculated heating rates in the gap are generally lower when conduction is included. Consequently, it was concluded that the heating rates neglecting conduction (i.e., data

TYPICAL SPANWISE TEMPERATURE DISTRIBUTION ON TILE IN CFHT

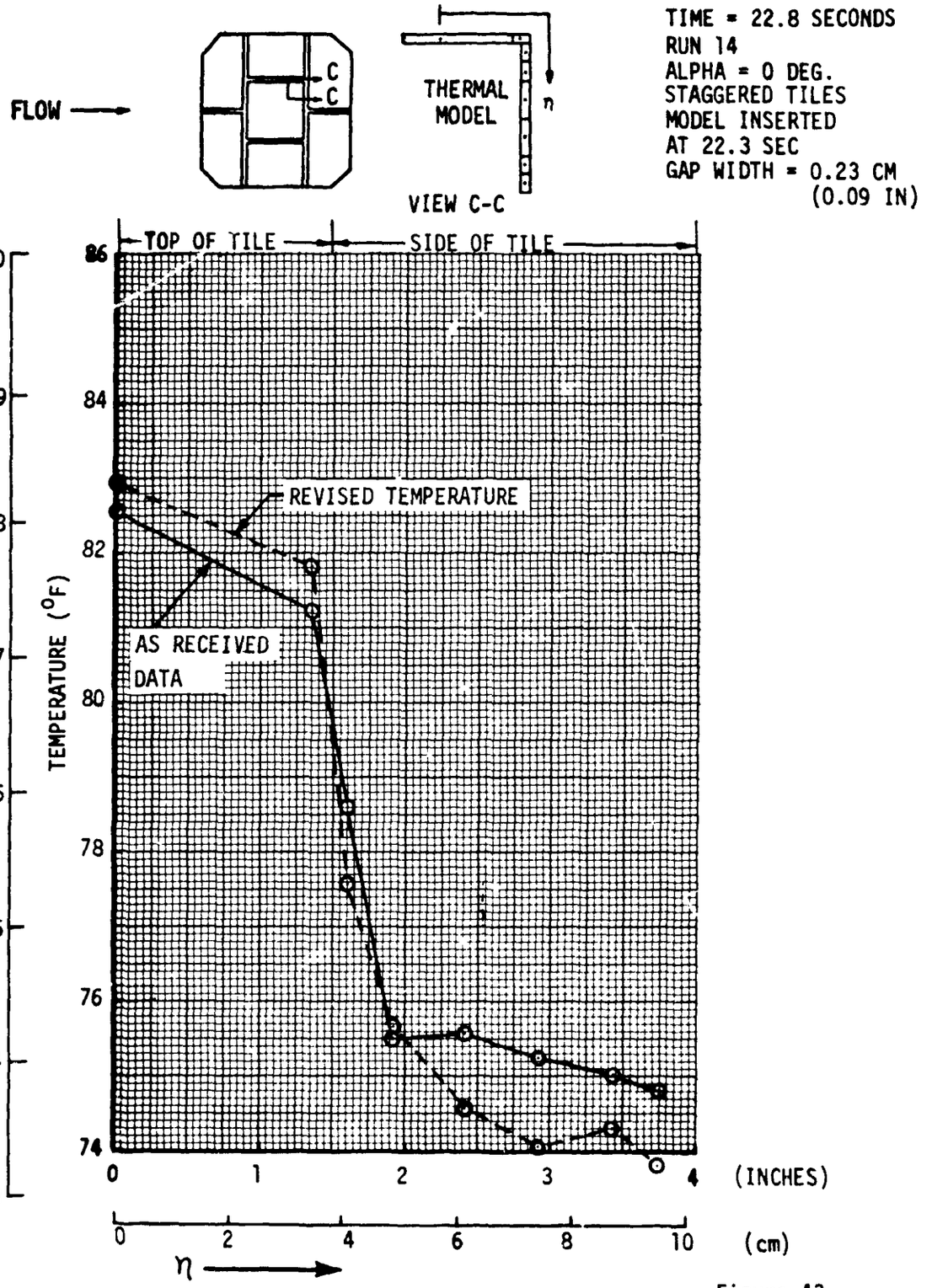

Figure 43

EFFECT OF INCLUDING CONDUCTION ON CALCULATED HEATING RATES IN CFHT

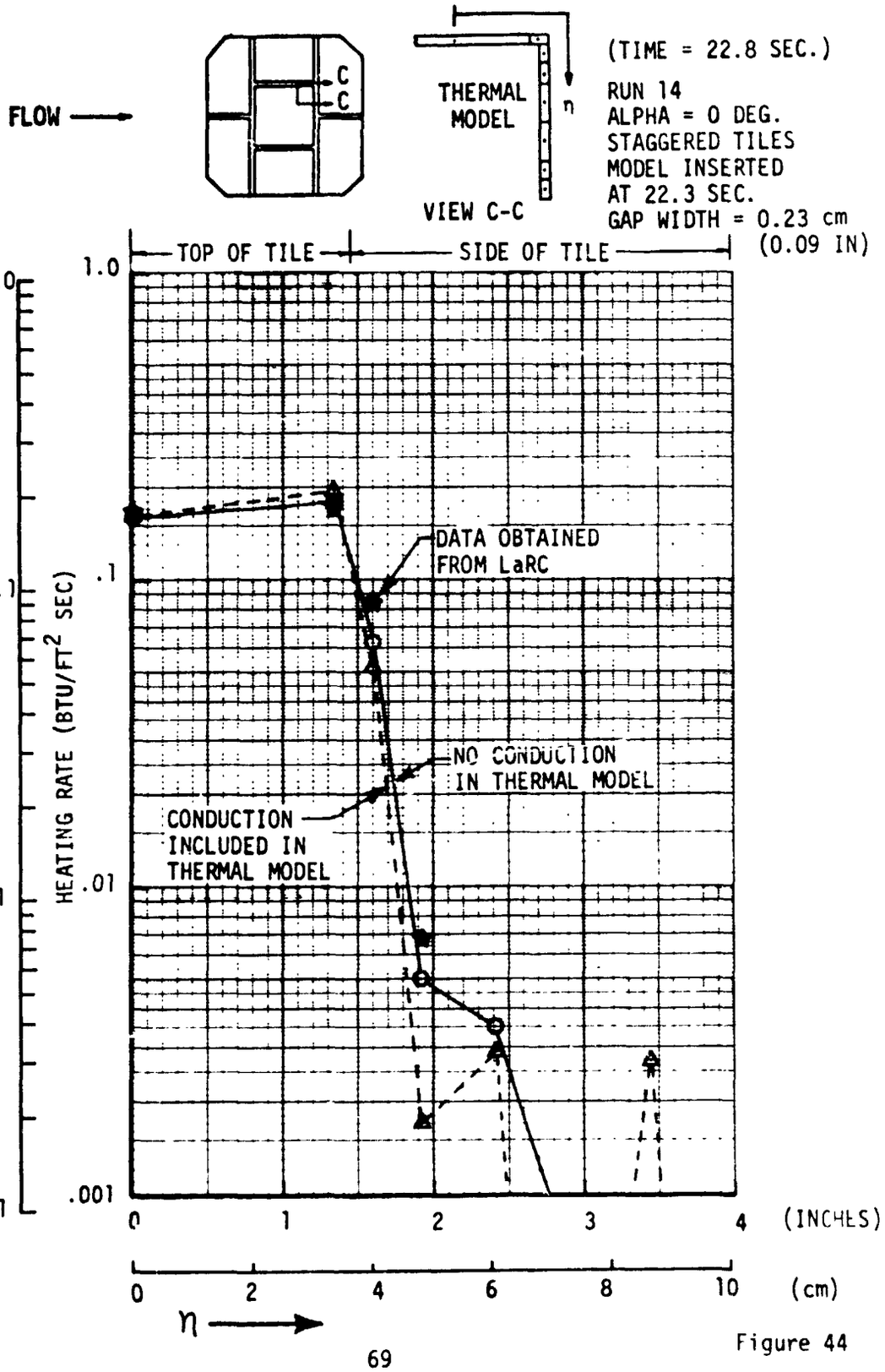

Figure 44

obtained from LaRC) be used in the gap heating data correlation since these data give conservative results.

Heating Patterns, In-line Versus Staggered Tiles - Data were taken on the thin skin tile with the two basic tile arrangements of staggered and in-line. Figure 45 shows the orientation of the test article with respect to the flow for both arrangements. The in-line arrangement is achieved by rotating the test article 90 degrees from the staggered tile orientation. It should be noted that for the in-line arrangement, the tiles are in-line in the axial direction only. In the spanwise direction (normal to the flow) the tiles are staggered. Comparisons of the axial heating distributions for the staggered and in-line tile arrangements at y = 0.0, -3.8 and -7.3 cm are presented in Figures 45 , 46 , and 47 respectively. These figures present data for a tile gap width of 0.23 cm. Heating on both the upstream and downstream faces of the tile does not appear to be significantly affected by the surrounding tile arrangement for a gap width of 0.23 cm. Heating on the top surface of the thin skin tile is higher (4% to 24%) for the staggered arrangement than for the in-line arrangement. This trend is most pronounced at the centerline (y = 0.0 cm) of the tile and decreases near the edge (y = -7.3 cm) of the tile. Also the magnitude of the heating on the top of both tile configurations decreases near the tile edges.

Effect of Gap Width - Comparisons of heating distributions for four gap widths at y = 0.0, -3.8 and -7.3 cm are presented for the staggered tile arrangement in Figures 48 , 49 , and 50 , respectively. Data for gap widths of 0.13, 0.23, 0.46, and 0.71 cm are shown in each figure. These figures show that the effect of gap width on tile heating changes with location on the tile. Figure 48 presents data along the centerline of the tile (y = 0.0). On the upstream face, the gap heating increases slightly with increasing gap width. This trend is reversed on the top surface and downstream face with the exception of the upstream edge of the tile top surface. Examination of the axial distribution at y = -3.8 cm shows a much greater increase in gap heating with increasing gap width on the upstream face than was shown at y = 0.0. On the top surface of the tile the heating at the upstream edge of the tile increased dramatically with increasing gap width. Over the rest of the top surface, the heating appears essentially independent of gap width. On the downstream face the trend is mixed with the gap heating either increasing or decreasing with gap width depending on the depth into the gap. The data near the outer edge of the tile (y = -7.3 cm) show the heating on the upstream face, top surface, and downstream face all increasing significantly with increasing gap width.

STAGGERED AND IN-LINE TILE HEATING DISTRIBUTIONS IN CFHT (Y = 0.0)

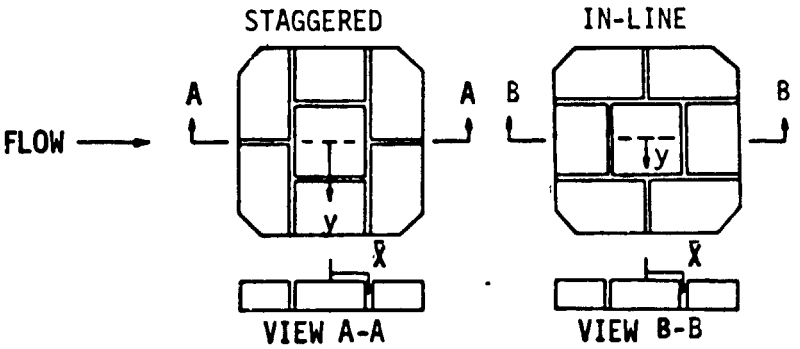

GAP WIDTH = 0.23 cm

M_∞ = 10

$Re_\infty/m = 3.3 \times 10^6$

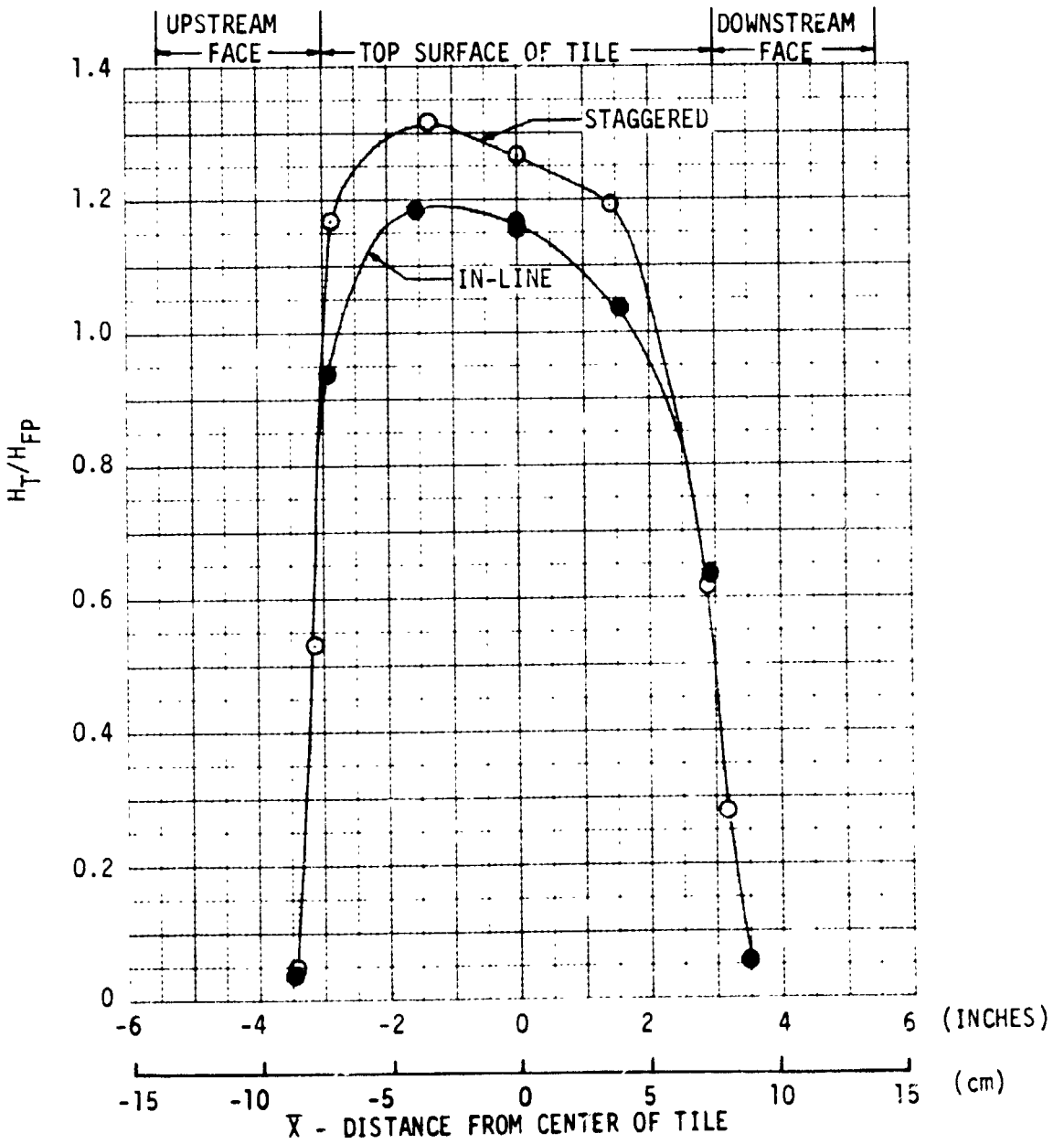

Figure 45

STAGGERED AND IN-LINE TILE HEATING DISTRIBUTIONS IN CFHT (Y = -3.8 CM)

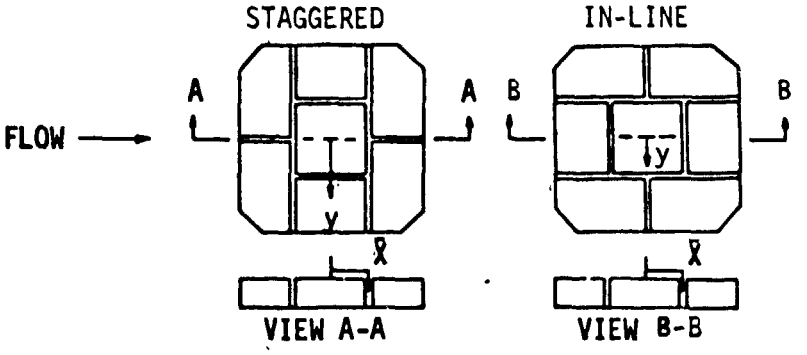

GAP WIDTH = 0.23 cm

M_∞ = 10

$Re_\infty/m = 3.3 \times 10^6$

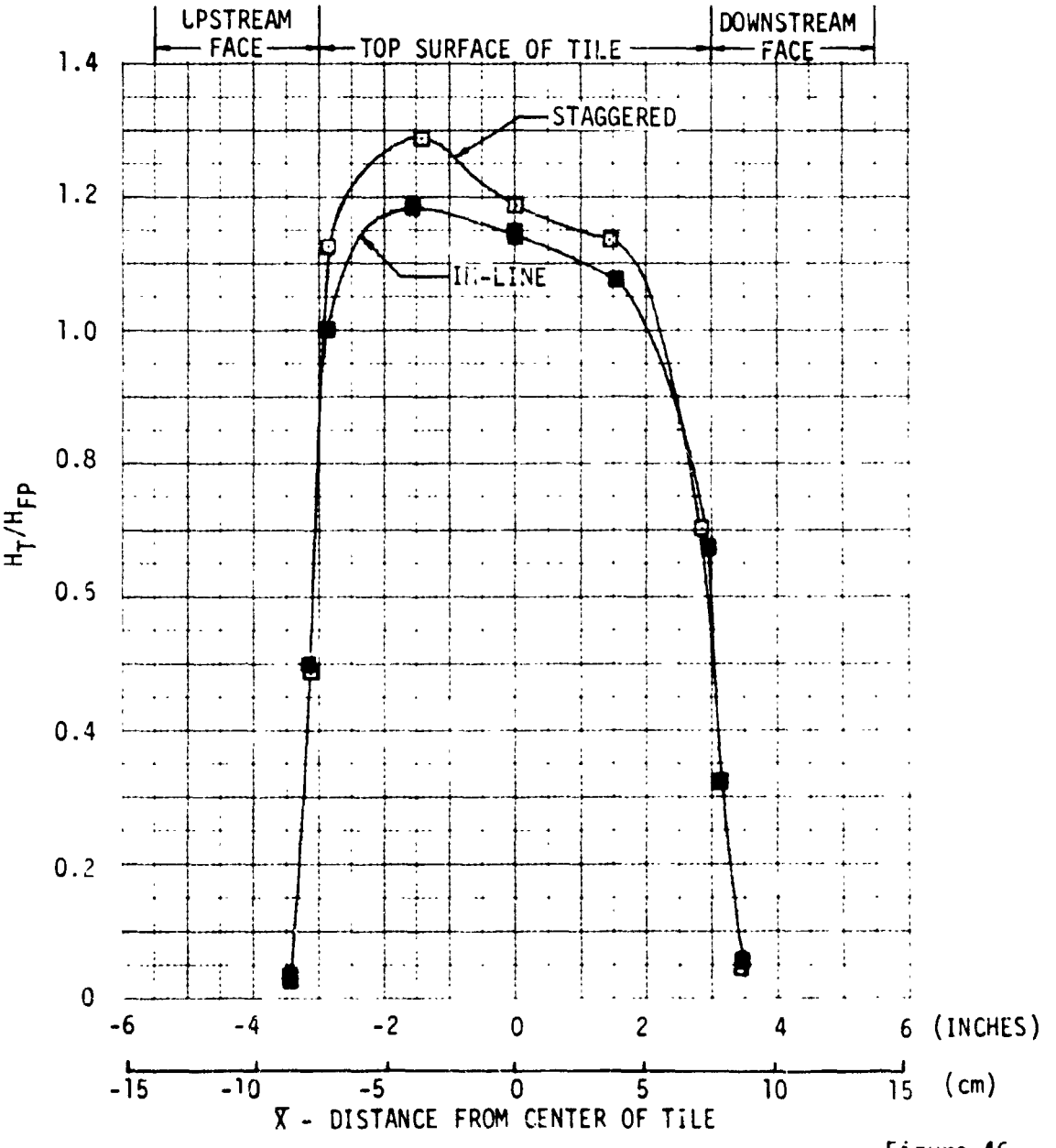

Figure 46

STAGGERED AND IN-LINE TILE HEATING DISTRIBUTIONS IN CFHT (Y = -7.3 CM)

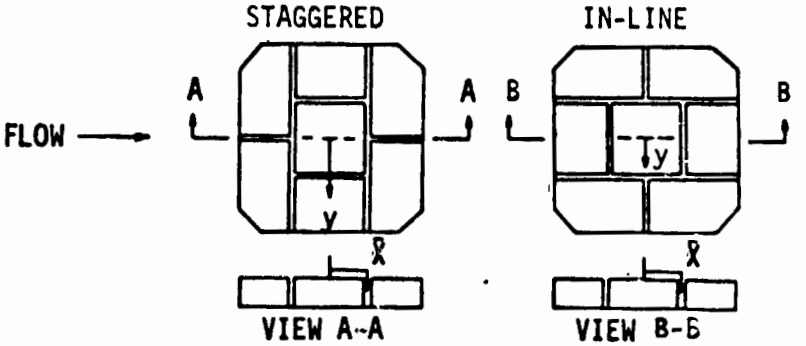

GAP WIDTH = 0.23 cm

M_∞ = 10

$Re_\infty/m = 3.3 \times 10^6$

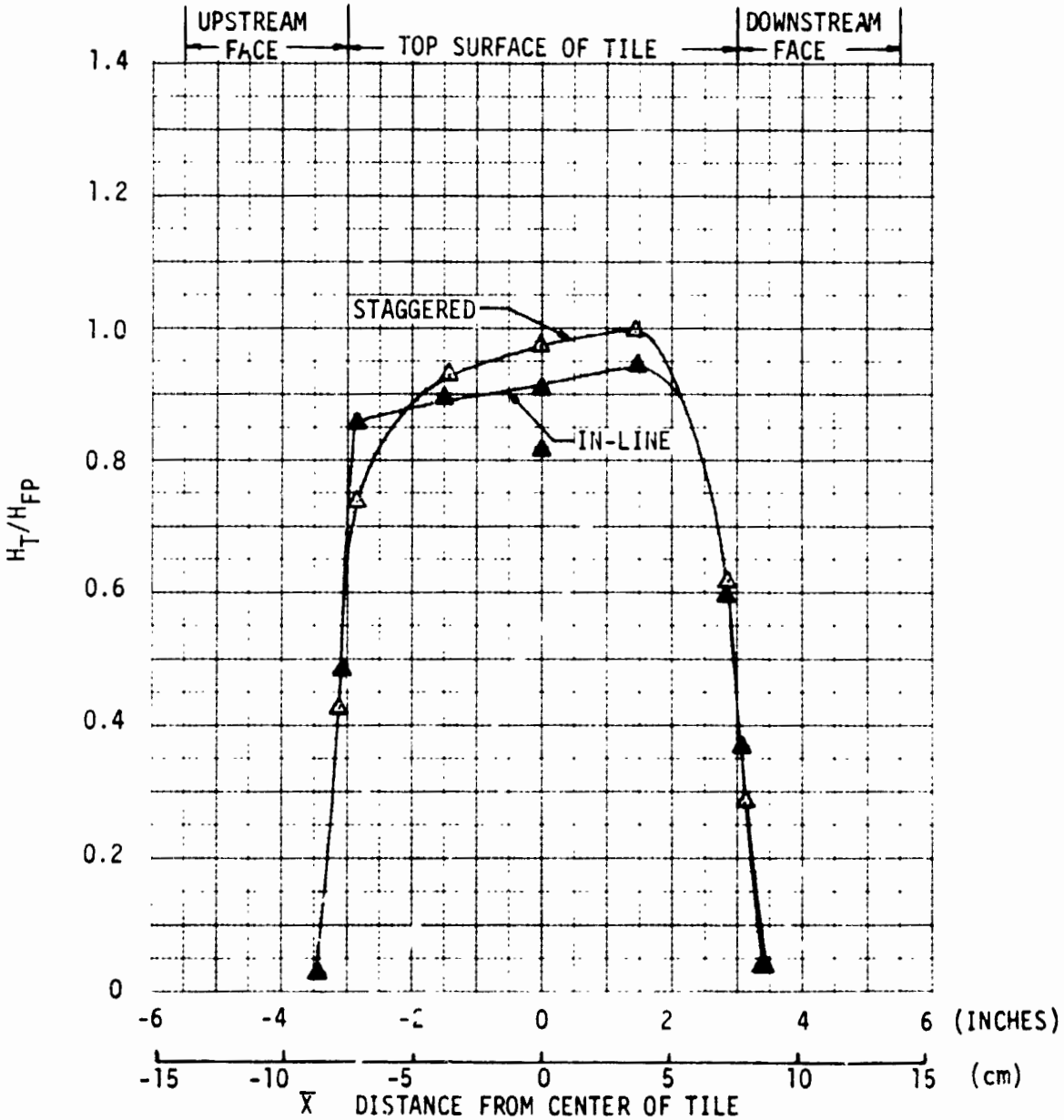

Figure 47

EFFECT OF GAP WIDTH ON STAGGERED TILE HEATING IN CFHT (Y = 0.0)

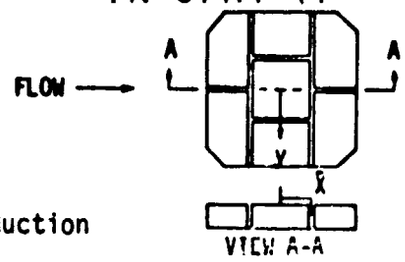

GAMMA = π/2 RADIANS

$Re_\infty/m = 3.3 \times 10^6$

$M_\infty = 10$

W = GAP WIDTH

Not corrected for C_p

Not corrected for conduction

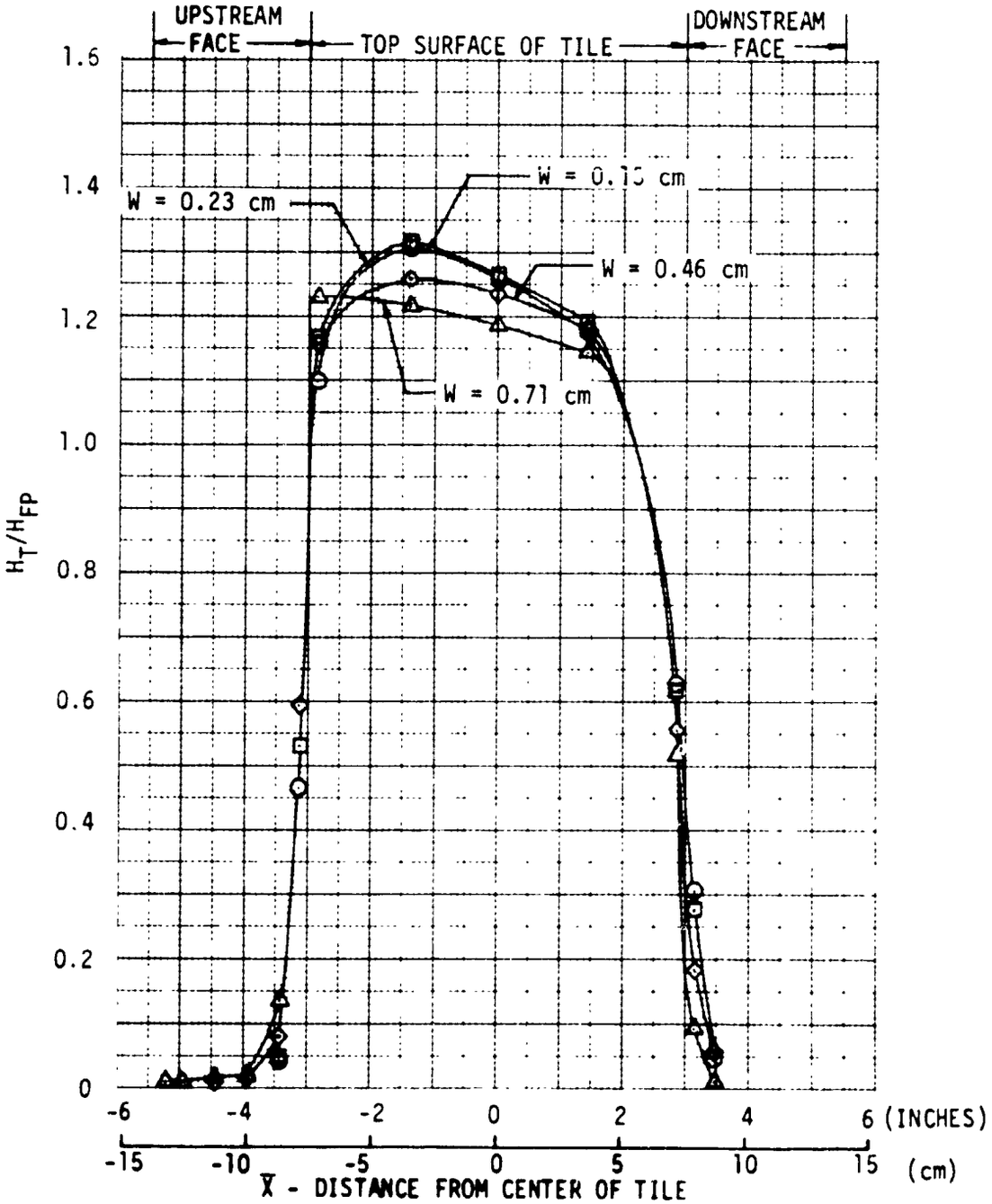

Figure 48

EFFECT OF GAP WIDTH ON STAGGERED TILE HEATING IN CFHT (Y = -3.8 CM)

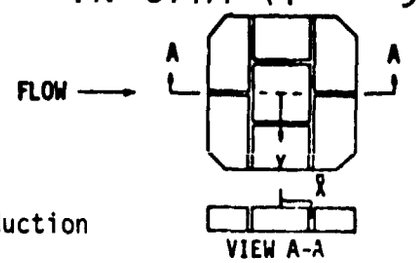

GAMMA = π/2 RADIANS

$Re_\infty/m = 3.3 \times 10^6$

$M_\infty = 10$

W = GAP WIDTH

Not corrected for C_p

Not corrected for conduction

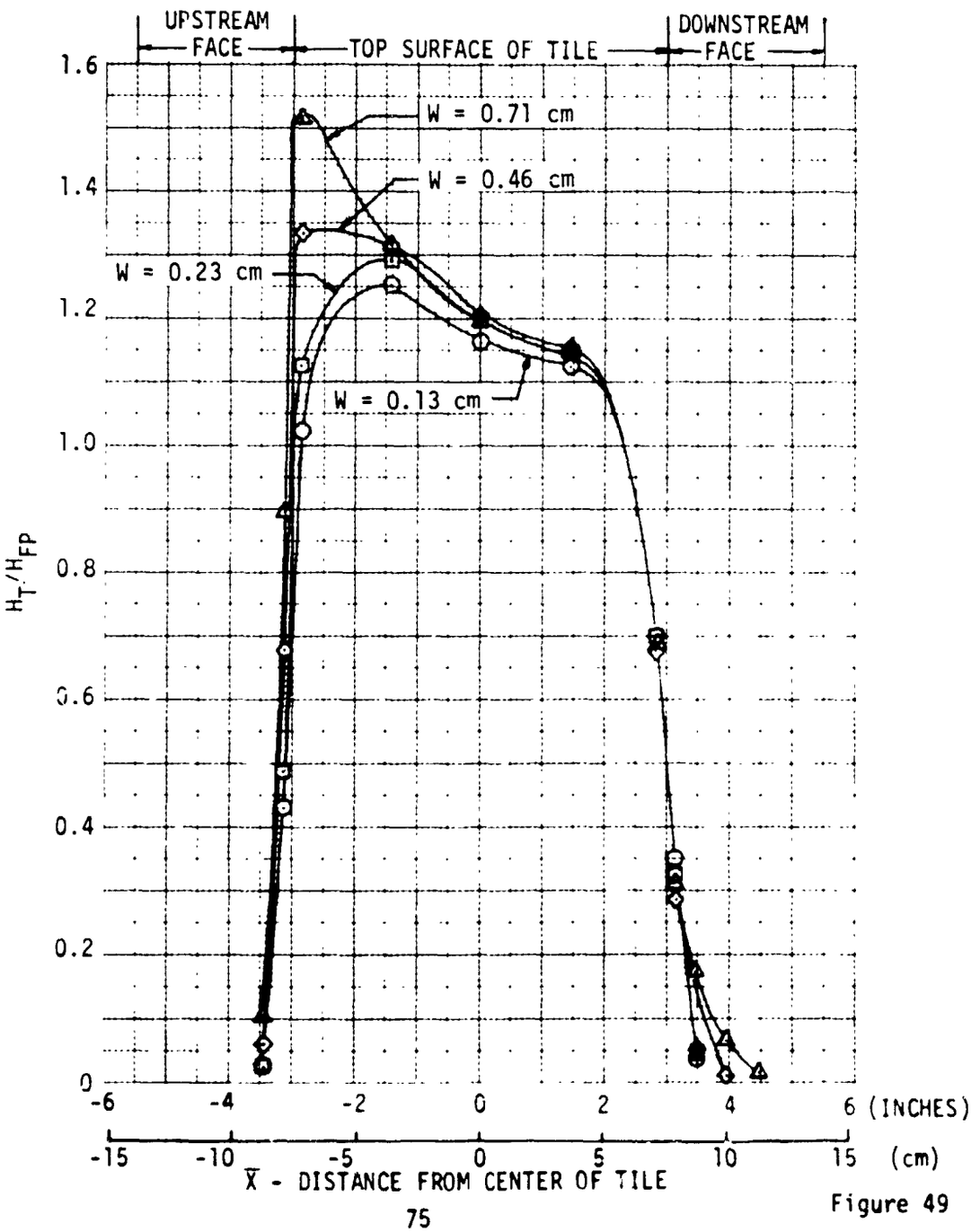

Figure 49

EFFECT OF GAP WIDTH ON STAGGERED TILE HEATING IN CFHT (Y = -7.3 CM)

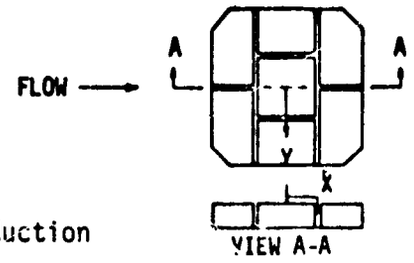

GAMMA = π/2 RADIANS

$Re_\infty/m = 3.3 \times 10^6$

$M_\infty = 10$

W = GAP WIDTH

Not corrected for C_p

Not corrected for conduction

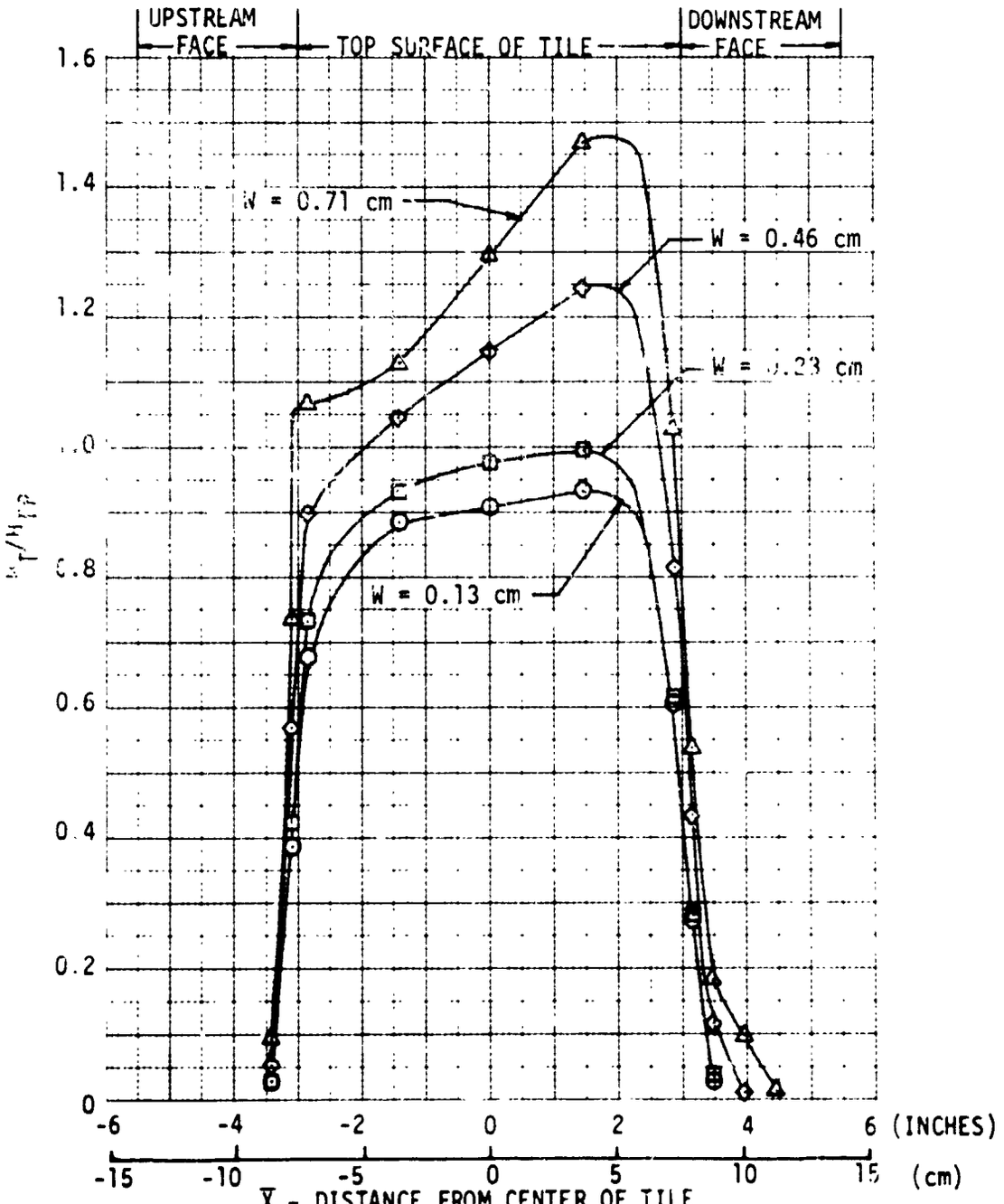

Figure 50

In general for the three (y) stations examined, it appears that the gap heating is related to the heating on the top surface near the gaps. The same trends that apply to the gap heating also apply to the top surface heating near the edges of the tile. This can be seen in all the figures presented for the staggered tile arrangement.

Similar comparisons of heating distributions for the in-line tile arrangement were made and are reported in Reference 1 (Section 4.3).

Review of gap width effects on both staggered and in-line tile arrangements indicates that the in-line tile arrangement results in lower and more uniform heating on the top surface of the tile. The gap heating on the upstream faces of the tile do not appear to be significantly different for the two tile arrangements and a similar conclusion can be drawn for the downstream face. As expected, gap width significantly affects gap heating; however, the magnitude of the effect is dependent on the location in the gap.

Effect of Flow Orientation - The effect of flow angle on gap heating was examined on two faces of the thin skin tile for 0.229 and 0.710 cm gaps. For ease of data handling, a consistent coordinate system was defined which is fixed in the thin skin tile. A flow angle (γ) was defined which varies from 0 radians at the in-line configuration to $\pi/2$ at the staggered configuration. The analyses indicated that either an in-line tile arrangement ($\gamma=0$) or a staggered tile arrangement ($\gamma=\pi/2$) is more desirable than other flow orientations. The spread in gap heating on the tile faces is minimized at $\gamma=0$ and $\pi/2$ radians, and the peak heating in the gaps are minima at these flow angles. These conclusions are based on data for both gap widths (0.229 and 0.710 cm). Figure 51 shows the locations and levels of maximum gap heating at various flow angles for the 0.710 cm gap. The data were measured approximately 0.3 cm from the tile surface. As seen, peak heating in the gaps are minima at 0 and $\pi/2$ radians flow angles.

The effect of gap width on heating rates at various flow orientations was also studied. The heating distributions along tile gaps at a flow angle of $\pi/4$ radians is illustrated in Figure 52 . The data was measured at a gap depth of 0.3 cm, and at gap widths of 0.23 cm and 0.71 cm. The heating rate gradients that occur at this flow angle become more severe as the gap width increases, as seen in this figure.

Effect of Steps - The effect of tile mismatch was examined by adding shims to raise and lower the thin skin tile. Tests were run with the tile raised 0.25 cm above the surrounding RSI tiles and lowered 0.168 cm below the surrounding tiles. Figure 53 presents in-line tile heating distributions ($Y_c = 0.0$)

LOCATIONS OF MAXIMUM GAP HEATING

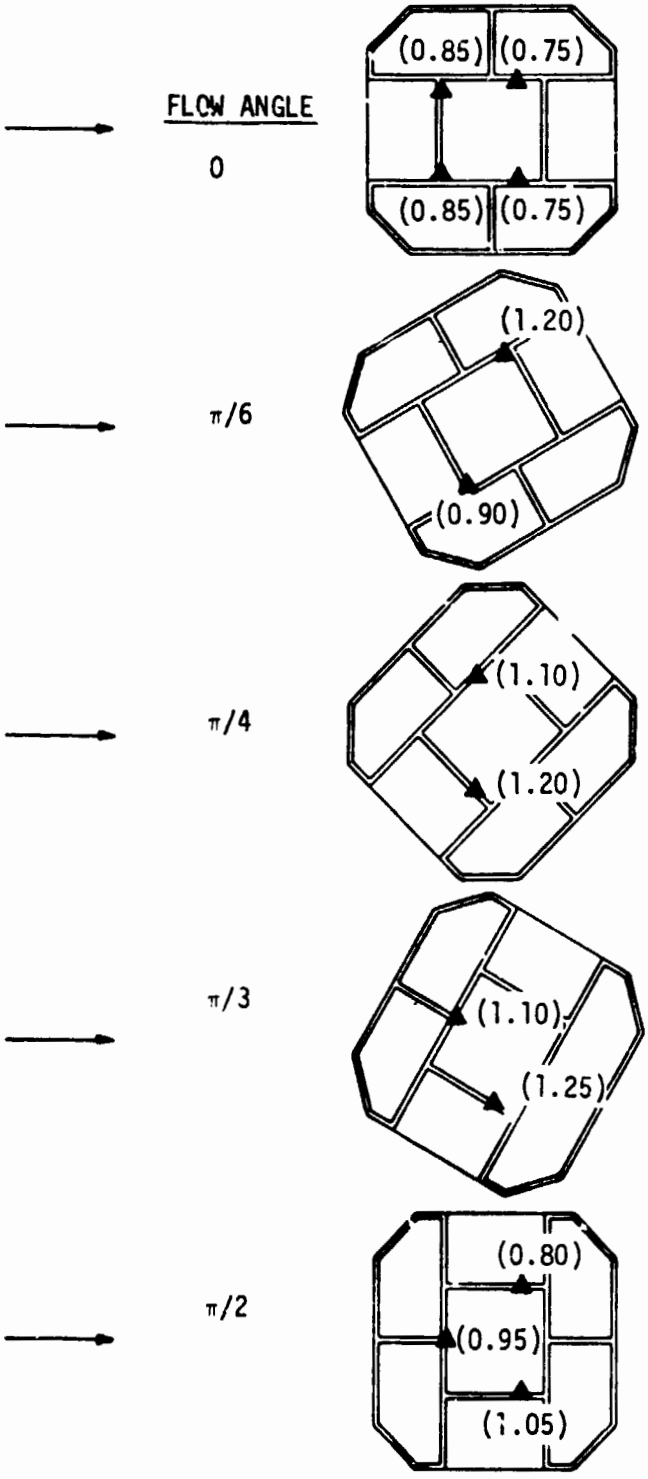

- CFHT DATA
- M_∞ = 10
- $Re_{\infty/m}$ = 3.27 x 10^6
- GAP WIDTH = 0.71 CM
- T/C LOCATED APPROXIMATELY 0.3 CM FROM TILE SURFACE
- (X.XX) = HT/H_{FP}

Figure 51

HEATING ALONG GAPS AT A DEPTH OF 0.3 CM

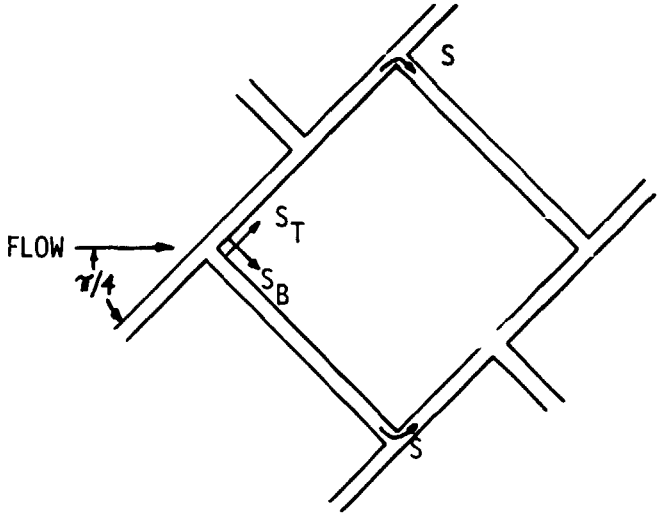

- FLOW ANGLE = π/4
- CFHT DATA
- M_∞ = 10
- $R_{e_{\infty/M}}$ = 3.26 x 10^6

LEGEND
GAP WIDTH = .71 CM
GAP WIDTH = .23 CM

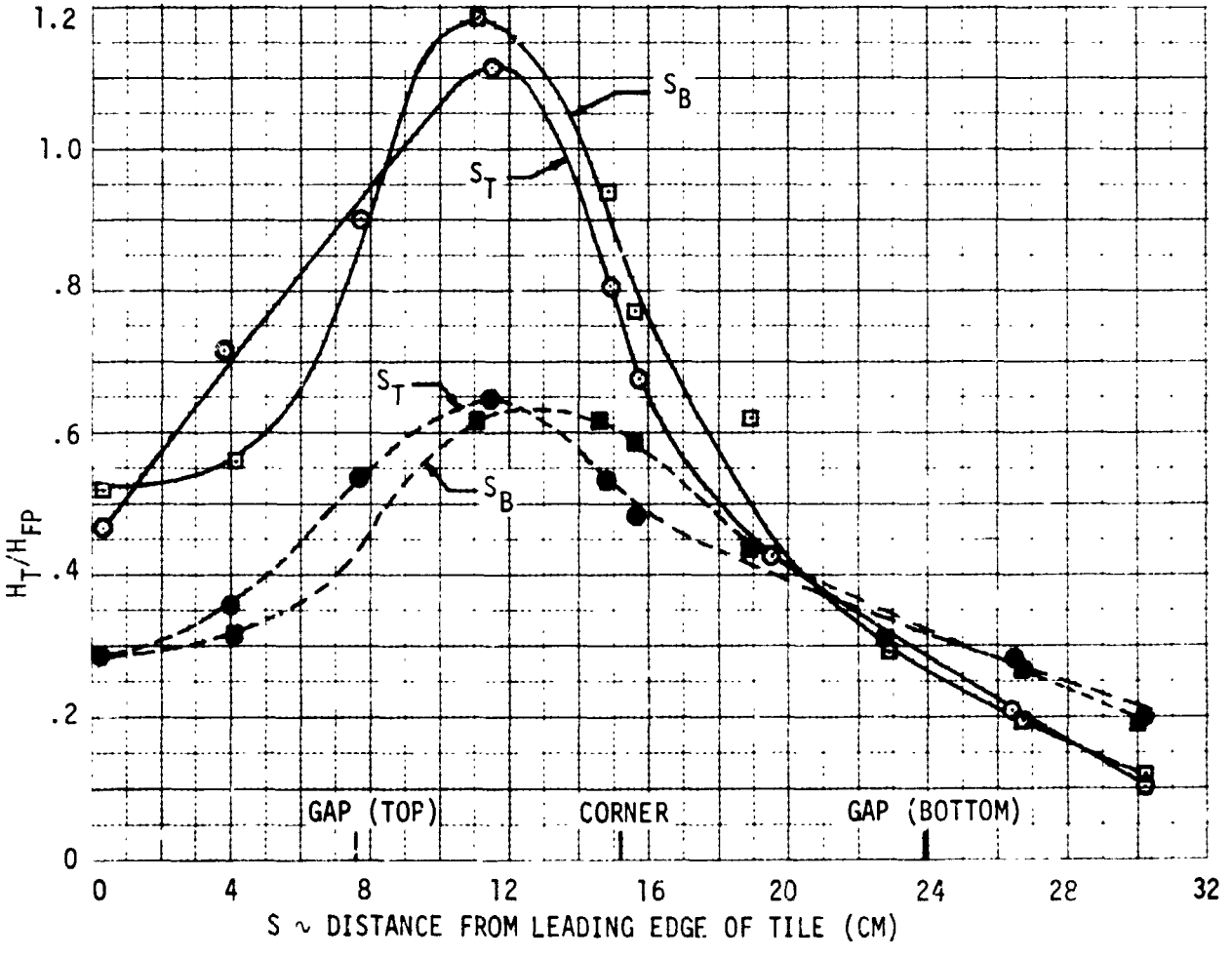

Figure 52

IN-LINE TILE HEATING DISTRIBUTIONS IN CFHT (Y_C = 0.0)

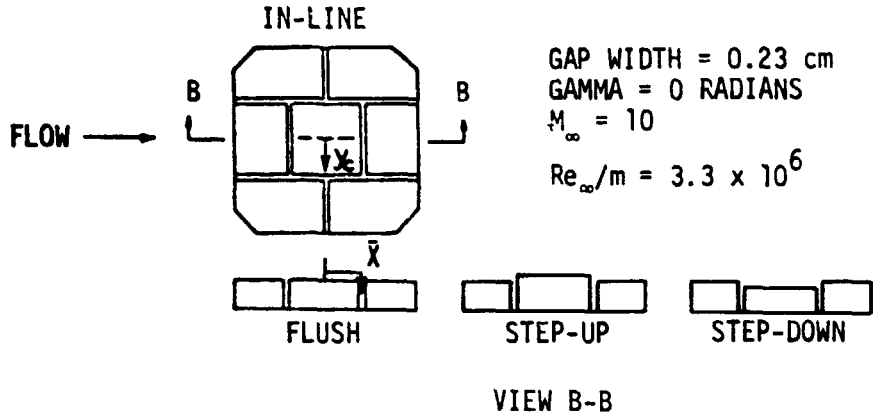

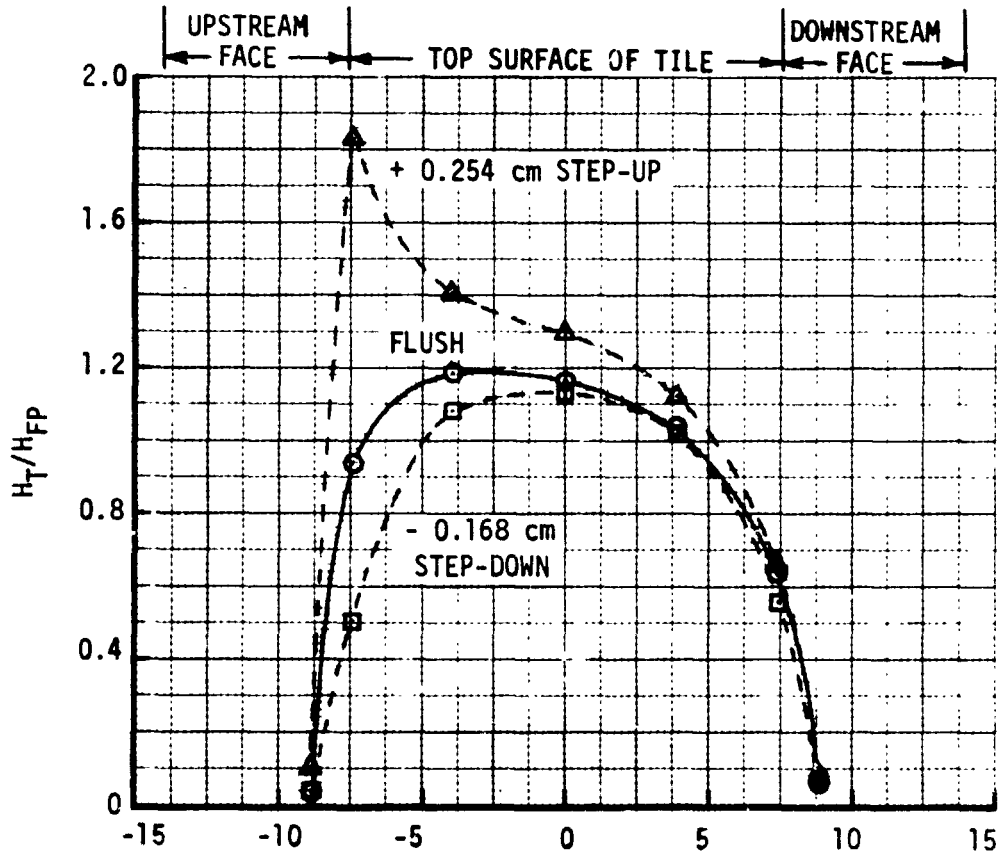

Figure 53

for the step-up, flush and step-down tile configurations with a gap width of 0.23 centimeters. The step-up configuration resulted in a 55% increase in the peak heating rate measured on the tile surface when compared to the flush tile. The peak heating location appears to move nearer the upstream edge of the tile as the tile is raised above the flush position. Raising the tile increased heating on the upstream face of the gap and entire tile surface while having little effect on the downstream face. The step-down tile configuration resulted in lower heating on the upstream half of the thin skin tile and similar heating on the downstream half when compared with the flush tile. The peak heating rate was only 4.5% lower for the step-down tile. Figure 54 presents heating distributions for the three tile positions when the surrounding tiles are in the staggered configuration ($\gamma = \pi/2$). Similar conclusions can be drawn from the staggered tile data as were found for the in-line tile data.

STAGGERED TILE HEATING DISTRIBUTIONS IN CFHT (X_C = 0.0)

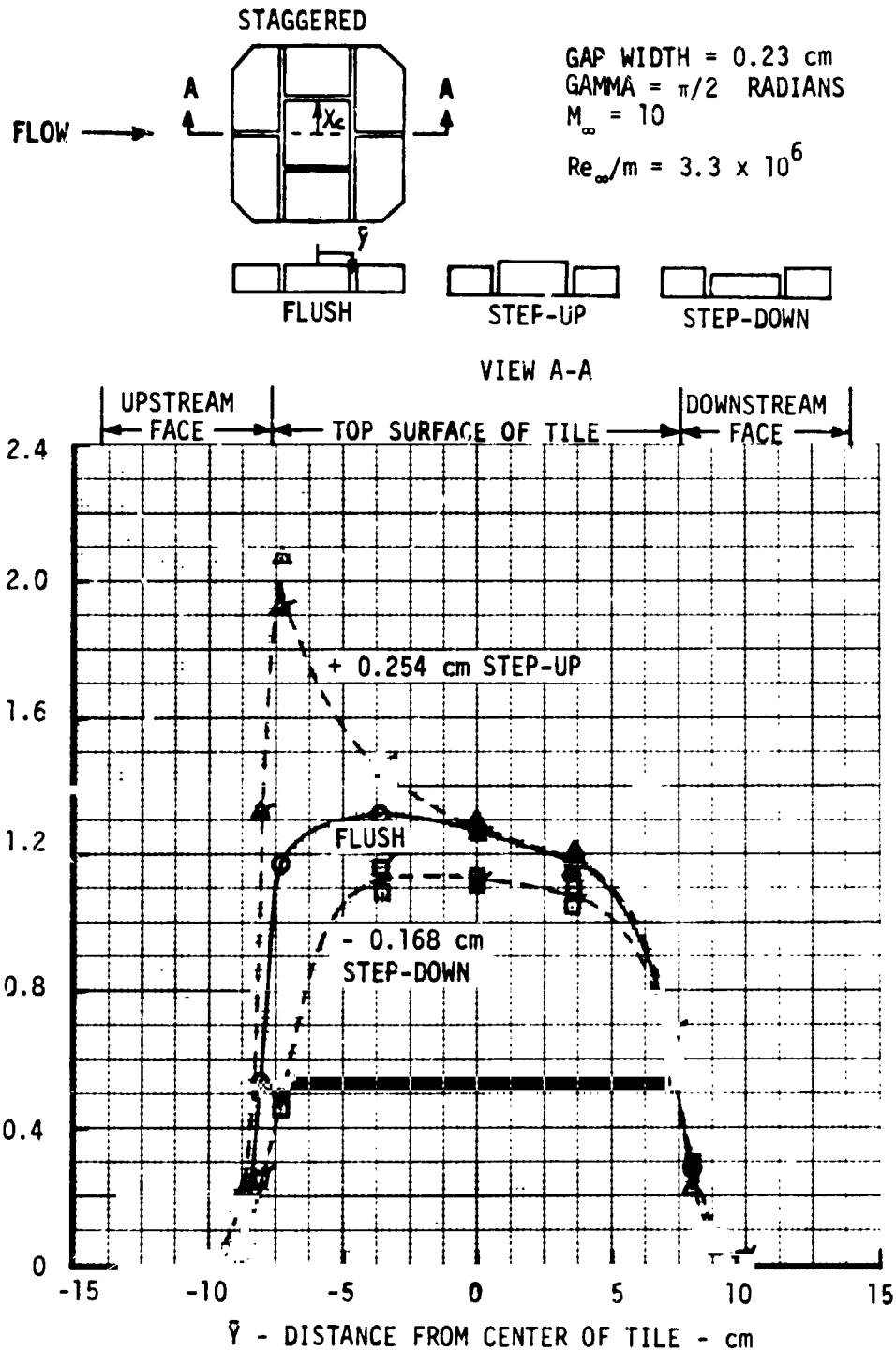

Figure 54

4.1.4 Analysis of Mach 8 Variable Density Tunnel Tests - Heat transfer measurements were performed on a thin skin tile panel in the LaRc Mach 8 Variable Density Tunnel to provide data in the presence of laminar and turbulent boundary layers. Model test position included both on the centerline (free stream) and on the tunnel wall (flush). Test conditions, model description and data are discussed in Section 3.1 of this report and in Volume II of Reference 1. Test output was recorded on tape to facilitate analysis and for use in the Multiple Regression Analysis computer program. The analysis included evaluation of:

a) a reference for data correlation
b) heating patterns on in-line tiles
c) heating patterns on staggered tiles
d) effect of Reynolds number on heating rates
e) effect of gap width on tile heating patterns

Reference for Correlation - Heat transfer rates on the top of the test panel were examined to establish either a laminar or turbulent flow reference for data correlation. Initially, a laminar recovery factor was used to compute a heat transfer coefficient (H_L) as well as laminar boundary layer theory to compute a referenced transfer coefficient (H_{ref}) which was based on distance from the model leading edge. The ratio of H_L to H_{ref} indicates the type of flow with a value of unity indicating laminar flow. Analysis indicated that for the free stream tests, conditions were laminar on the forward portion of the model at the low Reynolds number, and flow transition occurred on the aft portion of the panel. However, for the tunnel wall tests, Reynolds number and boundary layer thicknesses were characteristic of a turbulent boundary layer. For both the free stream and the flush wall tests, the referenced coefficient was that measured 2.582 cm from the forward tile leading edge.

Heating Patterns on In-Line Tiles - The measured heating distributions along the length of the panel for the in-line tile configuration are shown in Figure 55 for the free stream tests. Data are presented for unit Reynolds number per meter ranging from 2.3×10^6 to 21.8×10^6. A variety of heating patterns is exhibited on the top of the tiles indicating laminar flow on tile #1 for the lower Reynolds number and transitional flow for the higher Reynolds numbers. For tile #2, the two lower Reynolds number tests exhibit a trend toward transitional flow, while for $Re_\infty/m = 21.8 \times 10^6$ the data suggests that the flow is fully turbulent. The gap at the center of the panel did not affect the heating on the top of the panel except

HEATING DISTRIBUTION ALONG MACH 8 V.D.T. GAP MODEL, (IN-LINE GAP CONFIGURATION, FREE STREAM POSITION)

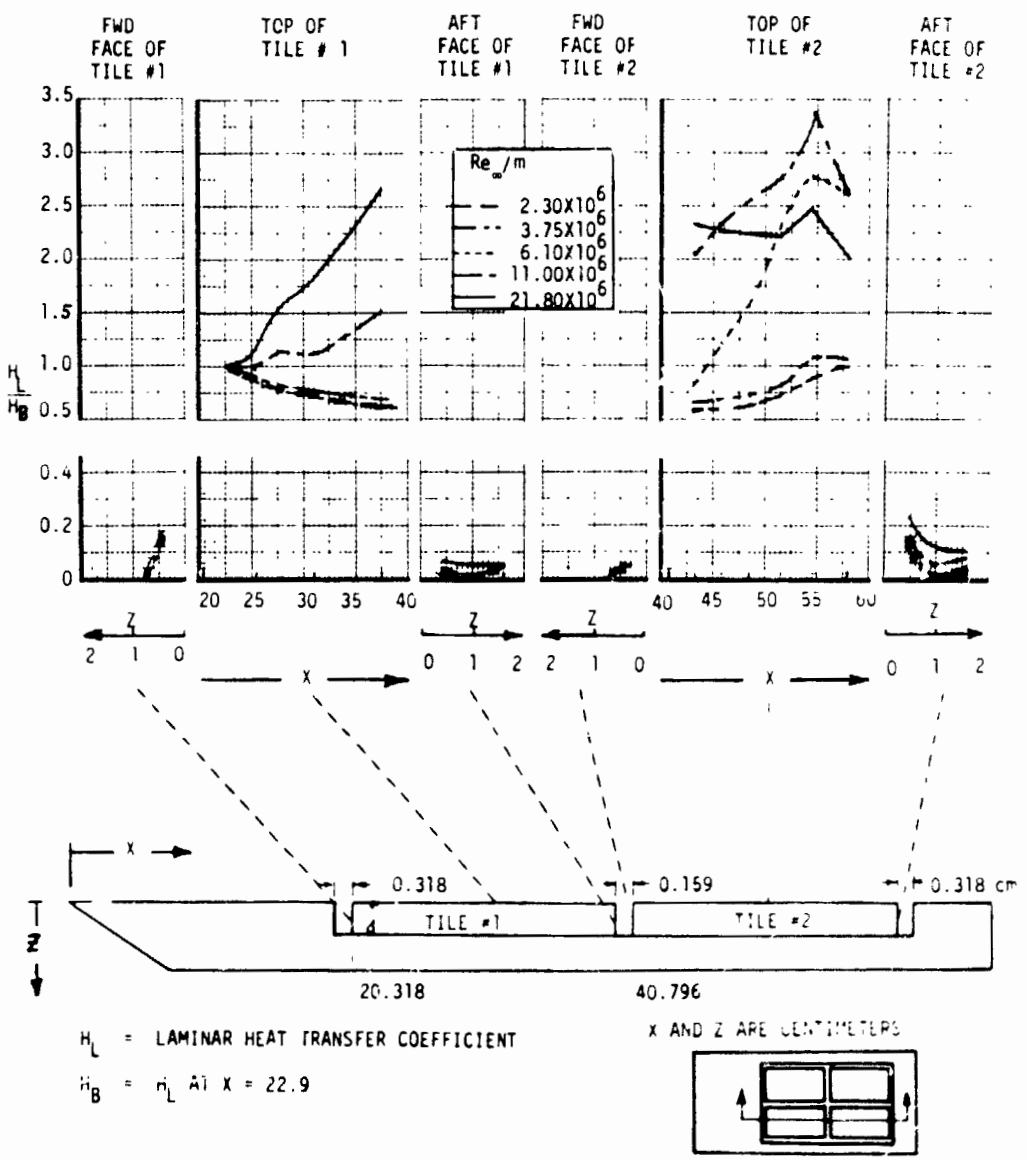

Figure 55

in the $Re_\infty/m = 6.1 \times 10^6$ test where the gap produced transition onset. Transverse gap heating is relatively low compared to that measured on top of the panel and does not show a strong dependence on Reynolds number for the forward facing wall. The aft facing walls experienced a slight change in heating distribution with Reynolds number. The larger gaps (0.318 cm) experience higher heating than the smaller gap (0.159 cm).

Heating distributions for the in-line gap model positioned flush with the tunnel wall are shown in Figure 56 . Tests were performed at unit Reynolds number/m from 1.16×10^6 to 41.4×10^6. Heating on top of the tiles is relatively uniform with the higher Reynolds number data being almost constant. The lower Reynolds number data show a 10% heating increase on the tile top. Heating in the transverse gaps does not decrease as rapidly with distance into the gap as for the free stream test. For both the free stream and tunnel wall position, the upstream side of the transverse gap experiences equal or higher heating than the downstream side of the gap. Again the heating is higher for the larger gap.

Heating Patterns on Staggered Tiles - Heating distributions were also measured for a staggered tile configuration with the model in the free stream position and flush with the tunnel wall. Figure 57 contains the heating data for the free stream tests. Heating distributions on the top surface of the tiles are similar to those obtained for the in-line gap model (Figure 55) over the range of Reynolds numbers investigated. The staggered tile configuration had twice the gap width of that tested in the in-line model, and only the downstream face of the center transverse gap was instrumented. Gap heating at the center of the model (stagnation region) is also presented in Figure 57 and shows a strong dependence on Reynolds number. For Reynolds numbers greater than 11.2×10^6 per meter, heating in the gap is greater than on the top surface.

Heating data for the staggered tile configuration flush with the tunnel wall (Figure 58) show that the turbulent boundary layer produced essentially uniform heating or the top of the panel similar to that experienced by the in-line tile model (Figure 56). As with the free stream tests of the staggered tiles, the downstream face of the transverse gap experienced significant heating with a distribution strongly dependent on Reynolds number.

Lateral heating distributions measured across the gap face of the downstream tile for the staggered tile configuration indicated that heating is almost constant across the half gap width and then decreases in the lateral direction similar to a "normal" distribution.

HEATING DISTRIBUTION ALONG MACH 8 V.D.T. GAP MODEL, (IN-LINE GAP CONFIGURATION, TUNNEL WALL POSITION)

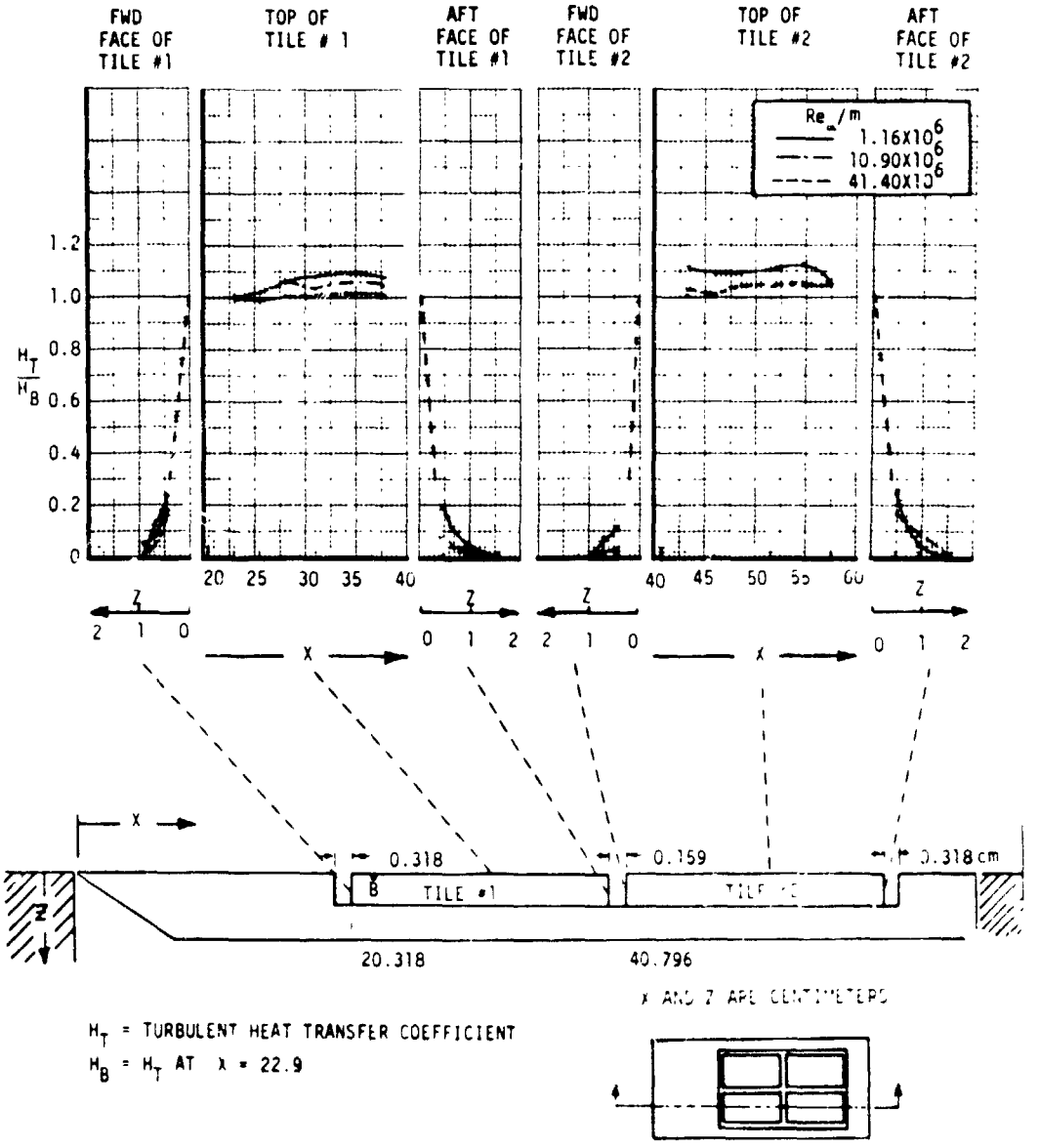

H_T = TURBULENT HEAT TRANSFER COEFFICIENT

H_B = H_T AT λ = 22.9

Figure 56

HEATING DISTRIBUTION ALONG MACH 8 V.D.T. GAP MODEL. (STAGGERED GAP CONFIGURATION, FREE STREAM POSITION)

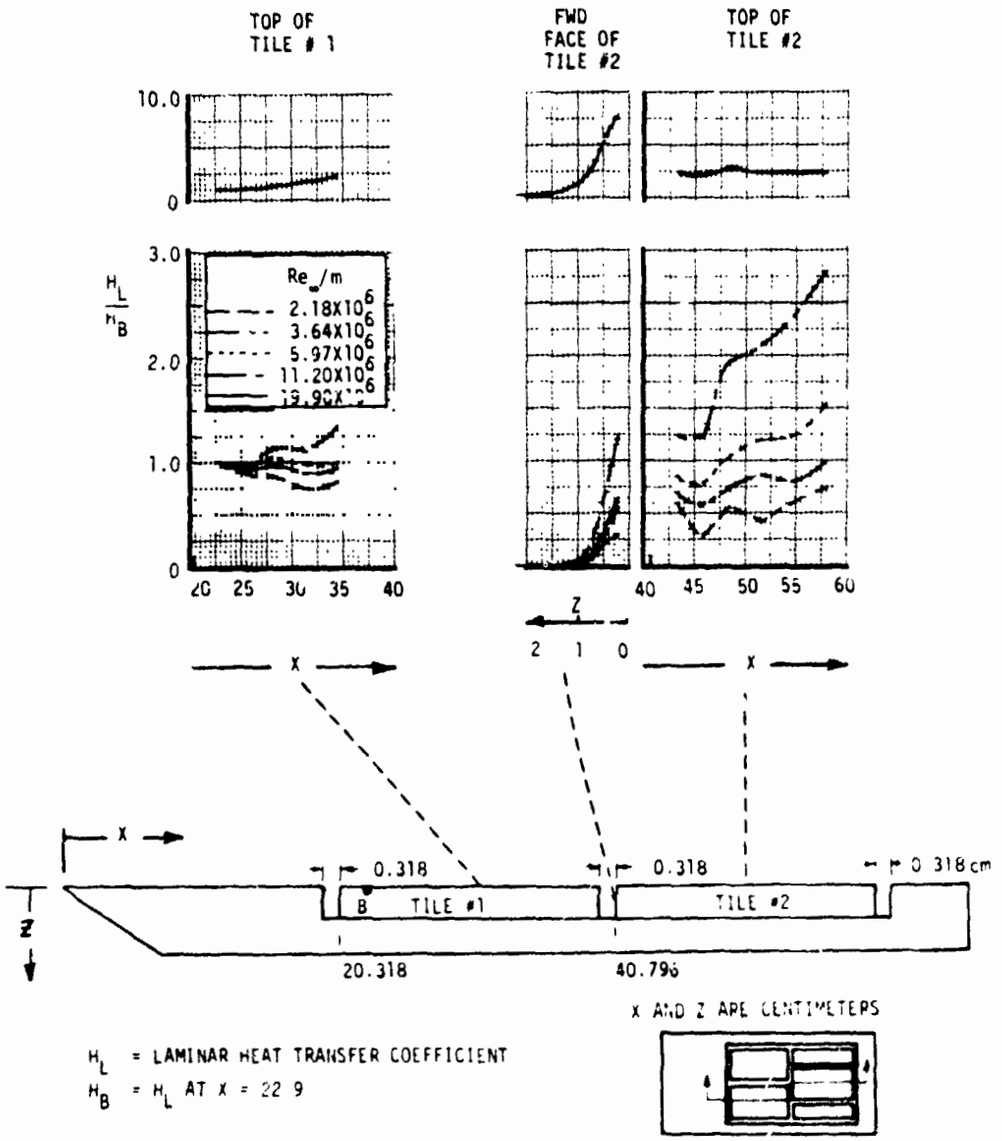

Figure 57

HEATING DISTRIBUTION ALONG MACH 8 V.D.T. GAP MODEL, (STAGGERED GAP CONFIGURATION, TUNNEL WALL POSITION)

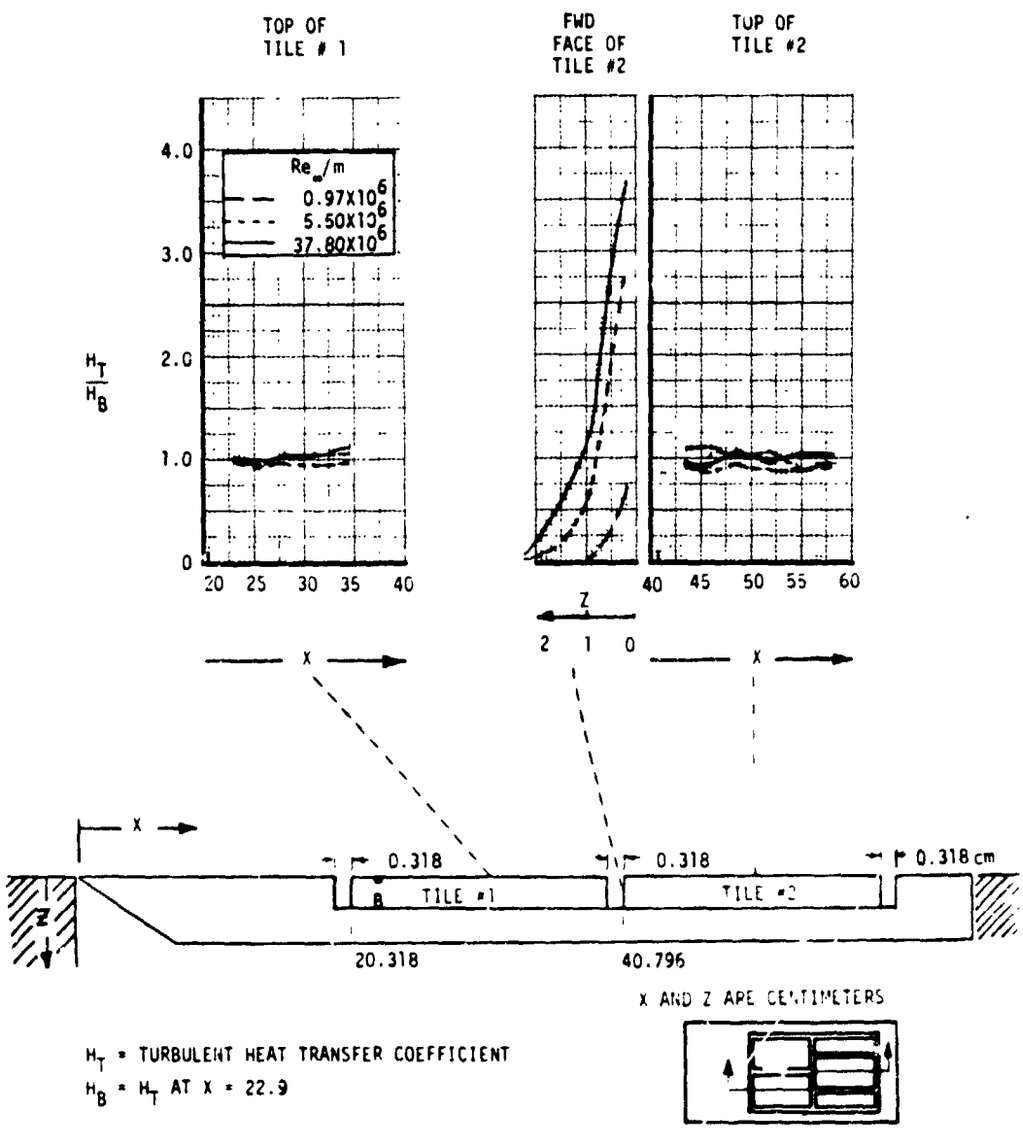

H_T = TURBULENT HEAT TRANSFER COEFFICIENT

H_B = H_T AT X = 22.9

4.1.5 Analyses of Ames 3.5 Foot HWT Tests - Analyses were performed on data obtained from the Rockwell International gap heating tests conducted in NASA-Ames 3.5 Foot Hypersonic Wind Tunnel. Data were obtained on thin skin test articles subjected to laminar, transitional, and turbulent flow conditions. Test conditions, model description and data are discussed in Section 3.1 of this report and in Volume II of Reference 1 . All tests used a flat plate model at zero angle-of-attack. Analyses included evaluation of:

a) calibration plate heating pattern
b) heating distributions in transverse gaps
c) heating distributions for in-line gaps
d) effect of Reynolds number on heating
e) effect of gap width on heating patterns
f) comparison of data trends to CFHT data

Calibration runs were made to characterize the flow over the test configuration utilizing a smooth heat transfer calibration plate. Three rows (located laterally at y = 0.0 and $\pm$ 20.54 cm) of thermocouples and three corresponding total temperature probes were used to measure the heating environment along and across the test article. Figure 59 presents the heat transfer coefficient along the calibration plate (y = -20.54) for the four test unit Reynolds numbers. The heat transfer coefficient (H_L) is based on a recovery factor of 0.874 The low Reynolds number heating data decreased approximately with the square root of distance along the panel which is characteristic of a laminar boundary layer. The higher Reynolds number data show a decrease and then a sharp rise in heating along the panel characteristic of transitional flow.

The heat transfer data measured on the thin skin inserts with simulated RSI gaps were referenced to the flat plate calibration data. For each test condition, a two-dimensional interpolation in the x and y directions was performed on the calibration data to determine the reference heat transfer coefficient at the specific locations where gap heating data were measured.

Gap Heating Distributions - Heating distributions in a single transverse gap model are shown in Figure 60 for three Reynolds number conditions. Gap width was 0.254 cm and gap depth was 2.03 cm. The heat transfer coefficients were normalized to the calibration plate coefficients at the same x and y locations. Heating distributions are shown on the surface of the model both forward and aft of the gap as well as both faces in the gap. The heating forward of the gap increases and then decreases with distance for all Reynolds number conditions, and the heating parameter

HEAT TRANSFER COEFFICIENT (LAM) ALONG AMES WEDGE

SYM	Re_∞/m	RUN
□	1.450800E+06	38
○	2.322100E+06	39
△	3.347600E+06	40
+	4.511900E+06	41

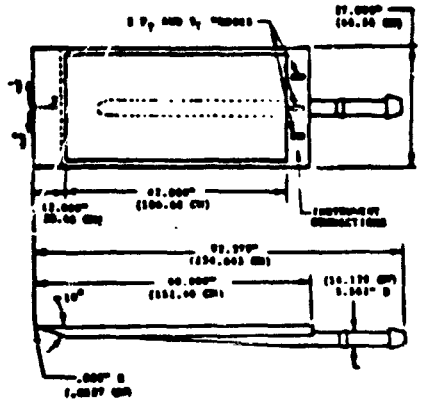

Y - LATERAL DISTANCE (CM) = -20.536

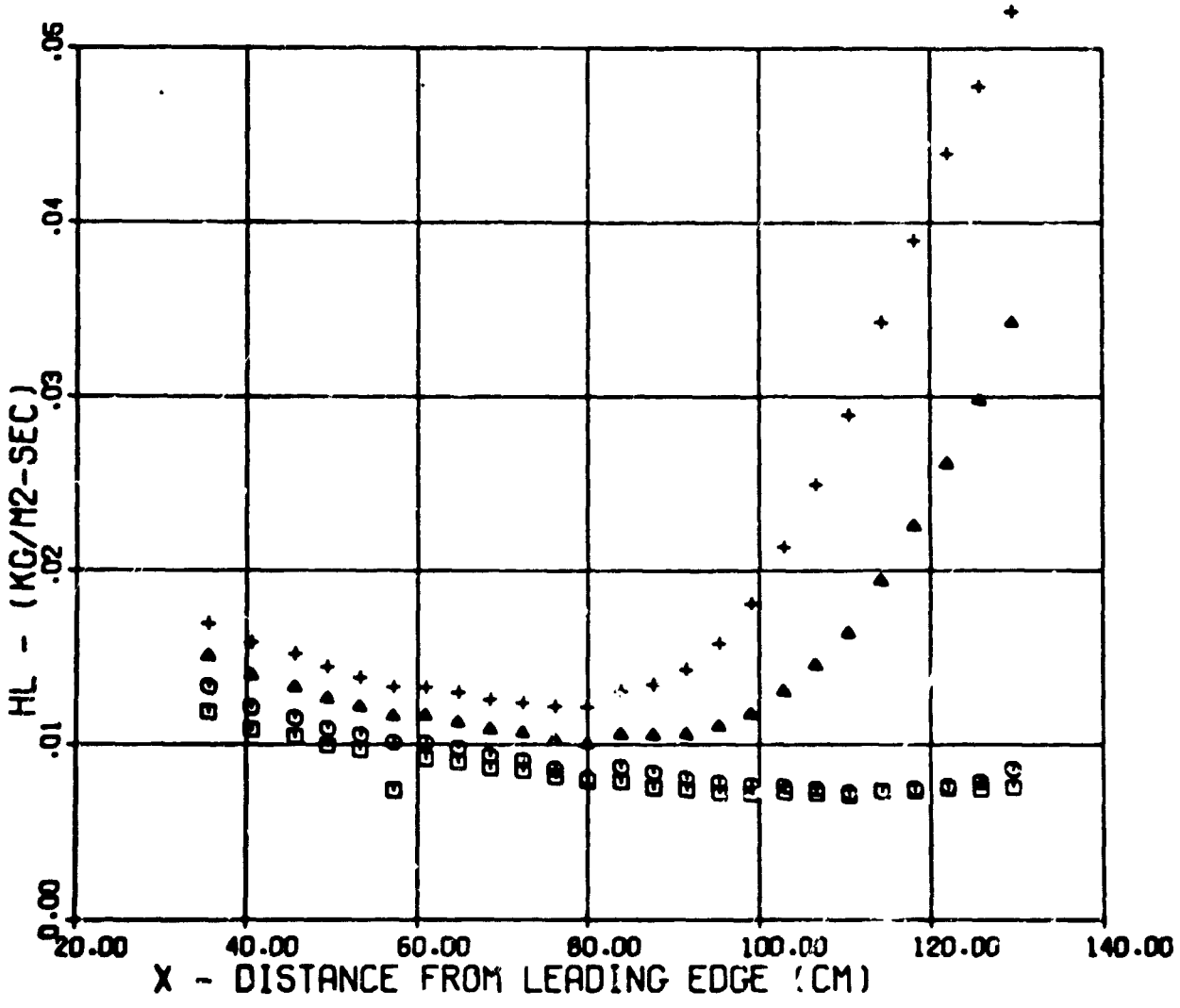

Figure 59

HEATING DISTRIBUTION MEASURED AT 0.254 CM TRANSVERSE GAP (AMES 3.5 FOOT HWT)

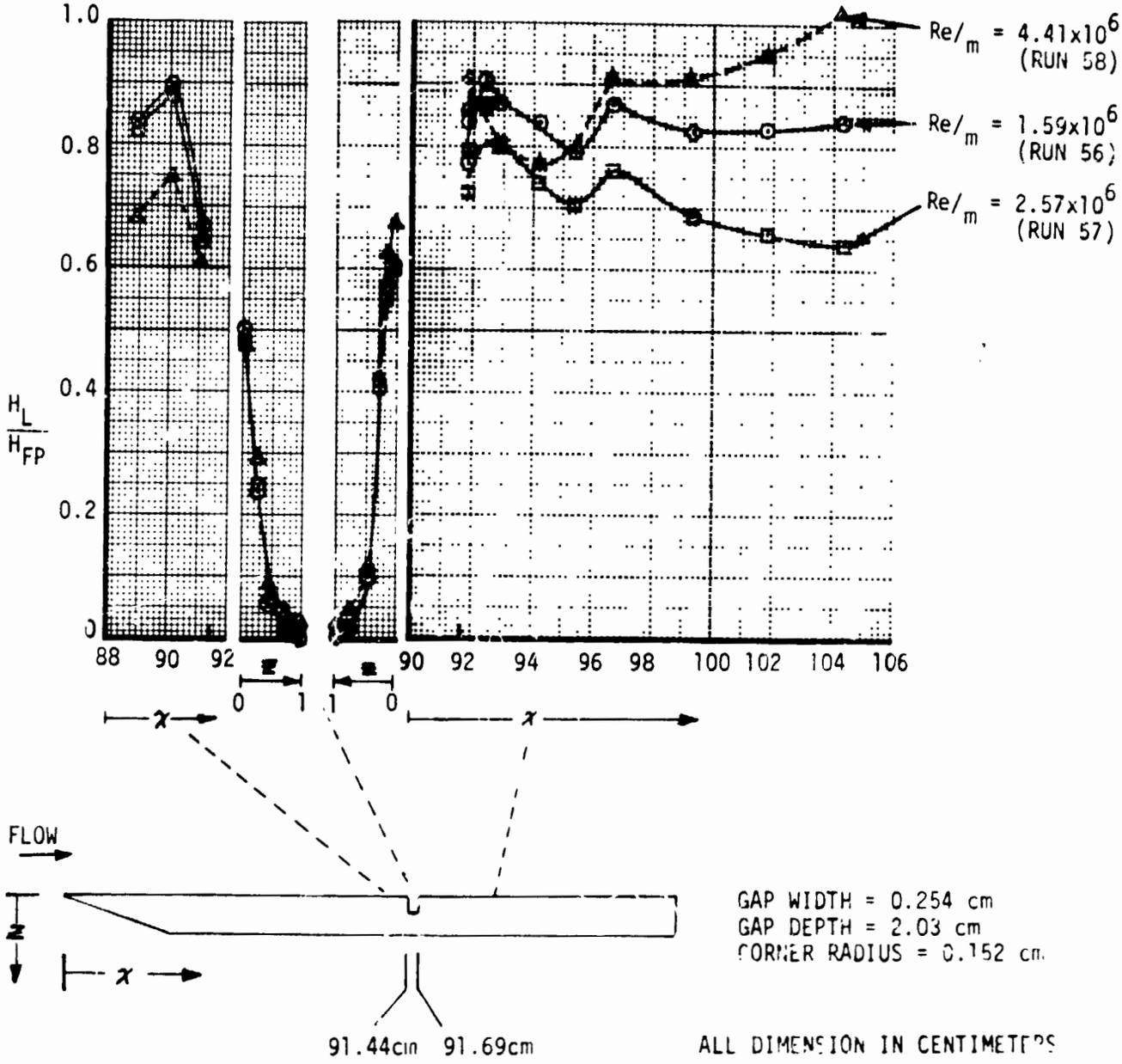

Figure 60

($H_L/H/_{FP}$) consistently decreases with increasing Reynolds number. The heating in the gap shows consistent Reynolds number trends with the effect of Reynolds number much less than is observed in the surface heating data. The surface heating aft of the gaps has irregular distributions with an apparent inconsistent Reynolds number trend. It can also be noted that the surface heating rates on the single transverse gap model were generally less than that measured on the calibration plate, i.e., $H_L/H_{FP} < 1.0$.

A comparison of surface heating distributions on the downstream side of a transverse gap is made in Figure 61 on data obtained from the Ames 3.5 foot HWT test and the LaRC CFHT test. The models used in the Ames tests had an ample number of thermocouples on the surface to define the heating rate distribution near the gaps while the model used in the CFHT tests did not. The Ames data indicate that the peak surface heating rate occurs approximately one edge radius downstream of the tile leading edge. A dashed curve has been added to the CFHT portion of the figure to illustrate a plausible heating distribution which would be consistent with the AMES data. In addition, the AMES data show a level of sensitivity to unit Reynolds number, i.e., as the Reynolds number is increased, the heating ratio (H/H_{FP}) increases.

Heating distributions for in-line gaps from the Ames 3.5 foot HWT and the CFHT were also compared (See Figure 62). These data are for the top of the tile near the gap where effects of gap flow should be evident. Both sets of data show an increase in (H/H_{FP}) with distance along the gap. Also, the in-line gap data increase with Reynolds number as do the other data measured at AMES.

Heating distributions for the upstream and downstream sides of gaps oriented at 30 degrees and 60 degrees to the flow (Figure 63 and 64) show similar dependence on unit Reynolds number. As the Reynolds number increases, the heating distribution intensifies. At 30 degrees, heating on the panel is monotonic with distance with a sharp drop near the gap. Heating on the downstream side of the gap shows a definite enhancement due to the gap. Reynolds number effects are evident on the downstream side of the gap. For the 60 degree orientation, heating on both sides of the gap is dependent on Reynolds number. It should be noted that the 60 degree data are downstream of the disturbance caused by the 30 degree gap. Also shown on both figures are comparable data measured during the CFHT tests. At the 30 degree orientation, the heating distributions from the CFHT and the AMES 3.5 foot tunnel are similar. At the 60 degree orientation the distribution measured at AMES is higher than measured at the CFHT. This is probably due to the transitional flow present in the AMES tests and the fully turbulent conditions in the CFHT.

C-2

HEATING DISTRIBUTION ON LEADING EDGE ON DOWNSTREAM SIDE OF GAP

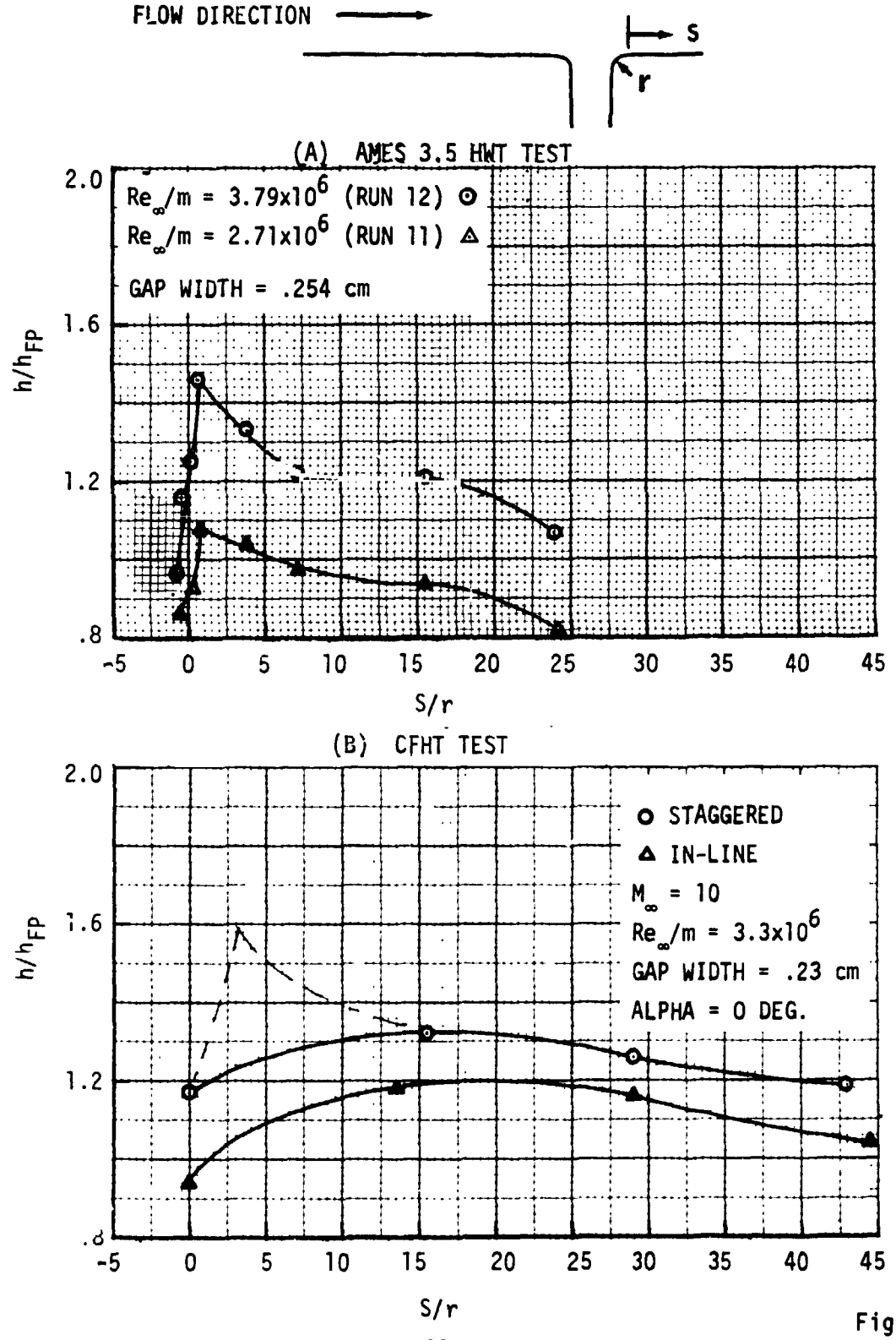

Figure 61

HEATING DISTRIBUTION ON TOP SURFACE OF GAP ALIGNED WITH FREE-STREAM FLOW DIRECTION

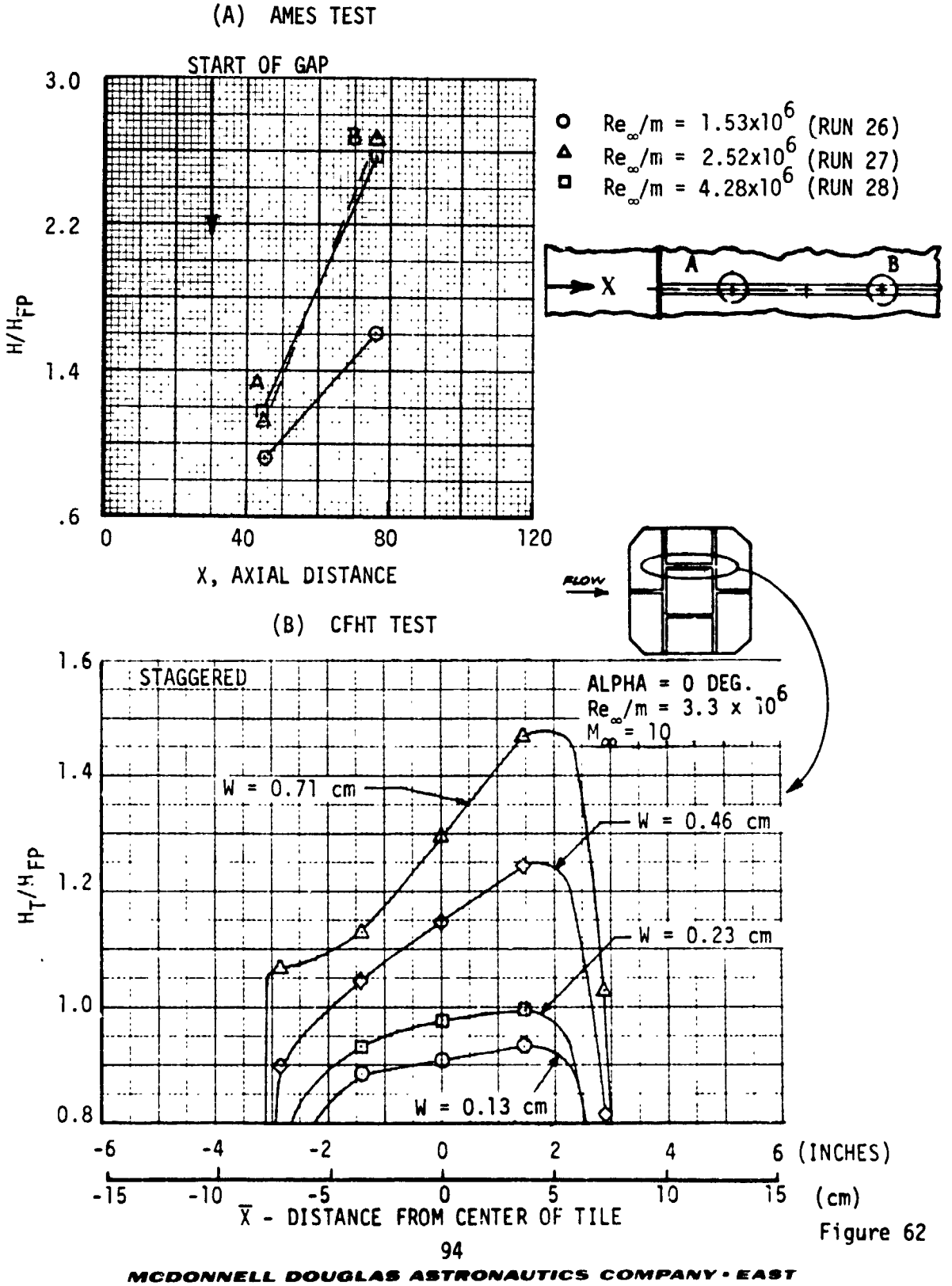

Figure 62

HEATING NEAR GAP AFFECTED BY REYNOLDS NUMBER AND BOUNDARY LAYER STATE
FLOW ANGLE = 30°

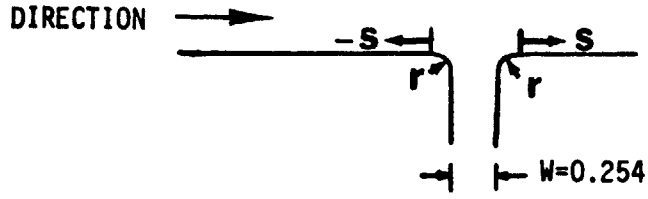

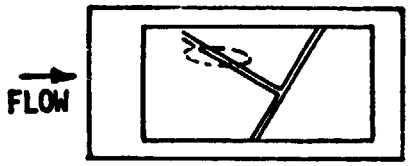

- ⊙ $Re_\infty/m = 1.688 \times 10^6$
- ▲ $Re_\infty/m = 2.815 \times 10^6$
- ⊡ $Re_\infty/m = 3.587 \times 10^6$
- ◇ $Re_\infty/m = 4.685 \times 10^6$

AMES $M_\infty = 5.1$

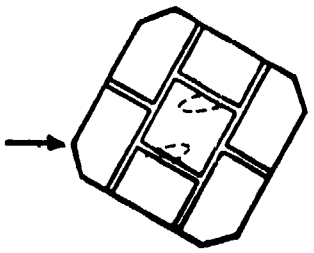

■ $Re_\infty/m = 3.3 \times 10^6$, $M_\infty = 10.3$, CFHT

(TURBULENT B.L.)

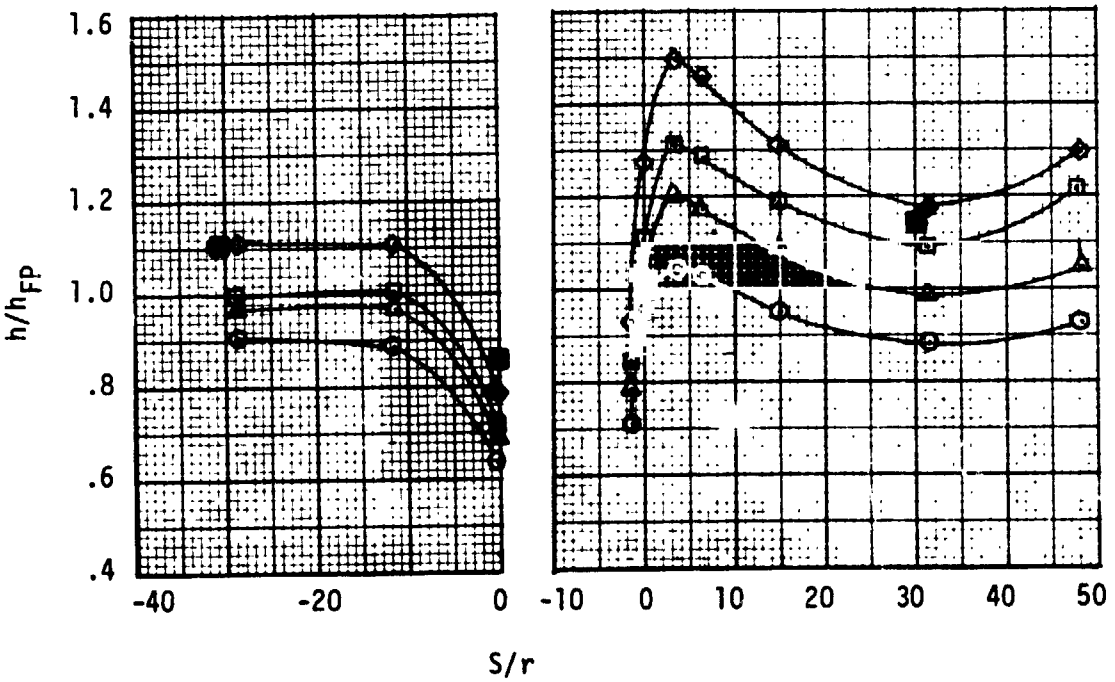

Figure 63

HEATING NEAR GAP AFFECTED BY REYNOLDS NUMBER AND BOUNDARY LAYER STATE FLOW ANGLE = 60°

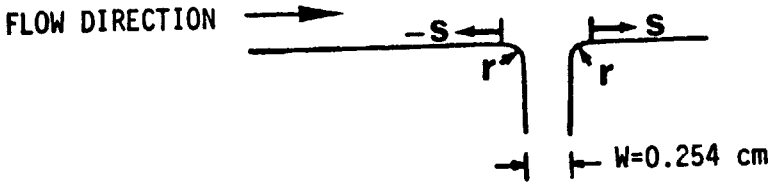

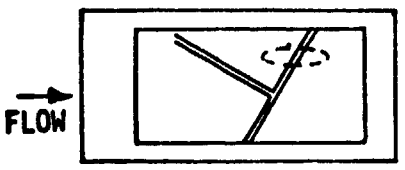

- ⊙ $Re_\infty/m = 1.688 \times 10^6$
- △ $Re_\infty/m = 2.8i5 \times 10^6$
- ⊡ $Re_\infty/m = 3.587 \times 10^6$
- ◇ $Re_\infty/m = 4.685 \times 10^6$

AMES $M_\infty = 5.1$

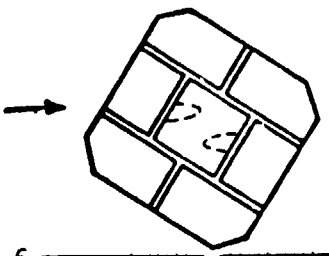

■ $Re_\infty/m = 3.3 \times 10^6$, $M_\infty = 10.3$, CFHT

(TURBULENT B.L.)

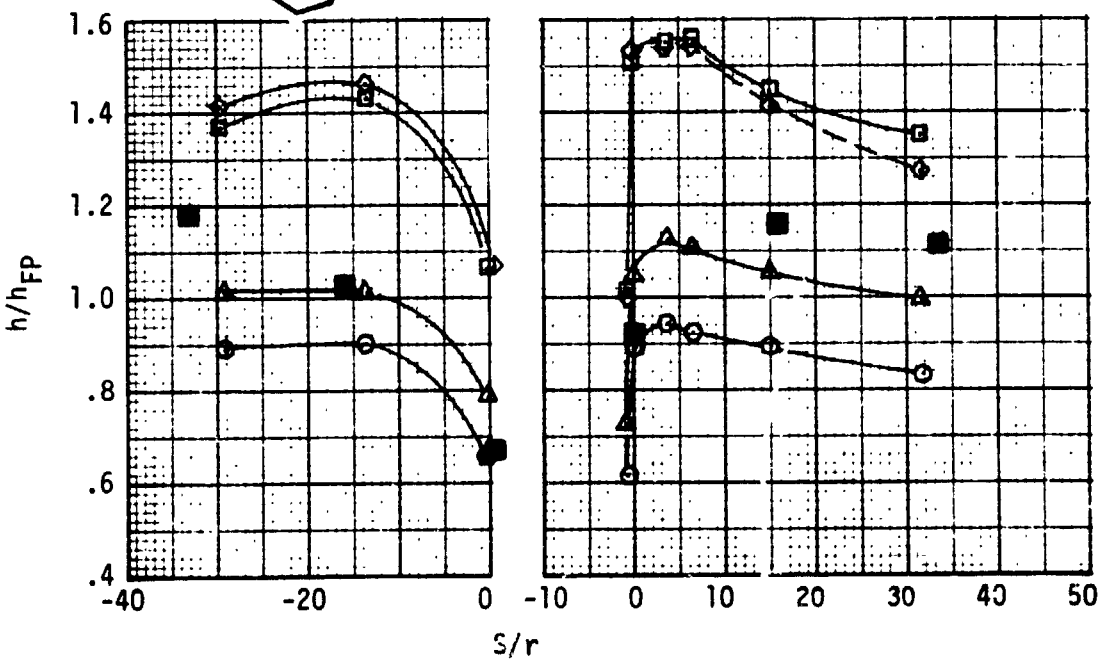

(UPSTREAM SIDE) (DOWNSTREAM SIDE)

Figure 64

4.2 Analysis of Silica RSI Tests in the JSC Laminar Duct - Analyses were performed on data from the Rockwell International gap heating tests in the NASA-JSC 10 MW Arc Tunnel (Reference 2). The tests employed silica RSI tiles fabricated and instrumented by NASA Ames. The test conditions, model description, and data assimilated are discussed in Section 3.2 and Volume II of this report. The purpose of the program was to obtain comparative thermal performance data on overlap and butt joint designs, and to evaluate the effect of tile thickness and joint gap width under laminar flow conditions.

Six runs from the test program were selected for analysis. All six runs were made with the staggered gap design consisting of three full and two half tiles with a perimeter of narrow guard tiles. Gap widths of 0.127 and 0.254 cm were evaluated with RSI thicknesses of 2.54 and 5.08 cm. Four of the six runs were made on butt joint models and two runs on overlap joint models. Mass flow rate was 45.4 grams/sec in all cases and enthalpy varied from 8.58×10^6 to 21.95×10^6 J/Kg. All runs were conducted in the channel nozzle of the JSC 10 MW Arc Jet Facility. The test panels were mounted in one wall of the channel nozzle and a calibration plate was mounted on the other wall.

Included in the data analysis are the following:

a) Selection of data for analysis
b) Analysis method including thermal models and thermal properties
c) Butt joint heating patterns
d) Overlap joint heating patterns
e) Comparison of butt and overlap joint heating patterns, and comparison to other test data
f) Sensitivity studies

4.2.1 Selection of Data for Analysis - Six runs from the test program and one thermocouple stack from each of the six runs were selected for analysis. The initial set of selected runs and thermocouple stack (T/C) are listed in Figure 65 as well as joint type, tile thickness, and gap width.

In reviewing the data it was found necessary to make certain substitutions as described below and indicated in Figure 66 . In Run 528, T/C stack 271 was analyzed instead of 159. By symmetry, conditions should be identical at these locations but measurements at locations 272 and 156 were desired in the analysis and no analogous data were available for stack 159.

SELECTED RUNS AND TEST CONDITIONS FOR DATA ANALYSIS

o SILICA RSI TESTS IN THE JSC LAMINAR DUCT

RUN	T/C STACK	JOINT TYPE	TILE THICKNESS (cm)	GAP WIDTH (cm)	GAP/FLOW ORIENTATION
528	159	OVERLAP	2.54	0.127	TRANSVERSE
533	68	OVERLAP	5.08	0.127	IN-LINE
538	164	BUTT	2.54	0.127	IN-LINE
539	164	BUTT	2.54	0.254	IN-LINE
542	262	BUTT	5.08	0.127	IN-LINE
544	262	BUTT	5.08	0.254	IN-LINE

Figure 65

TEST PANEL ORIENTATION

o SILICA RSI TILE TESTS IN THE JSC LAMINAR DUCT

□ ADDITIONAL GAP DATA USED IN ANALYSIS

△ LOCATION REQUESTED
▲ LOCATION USED

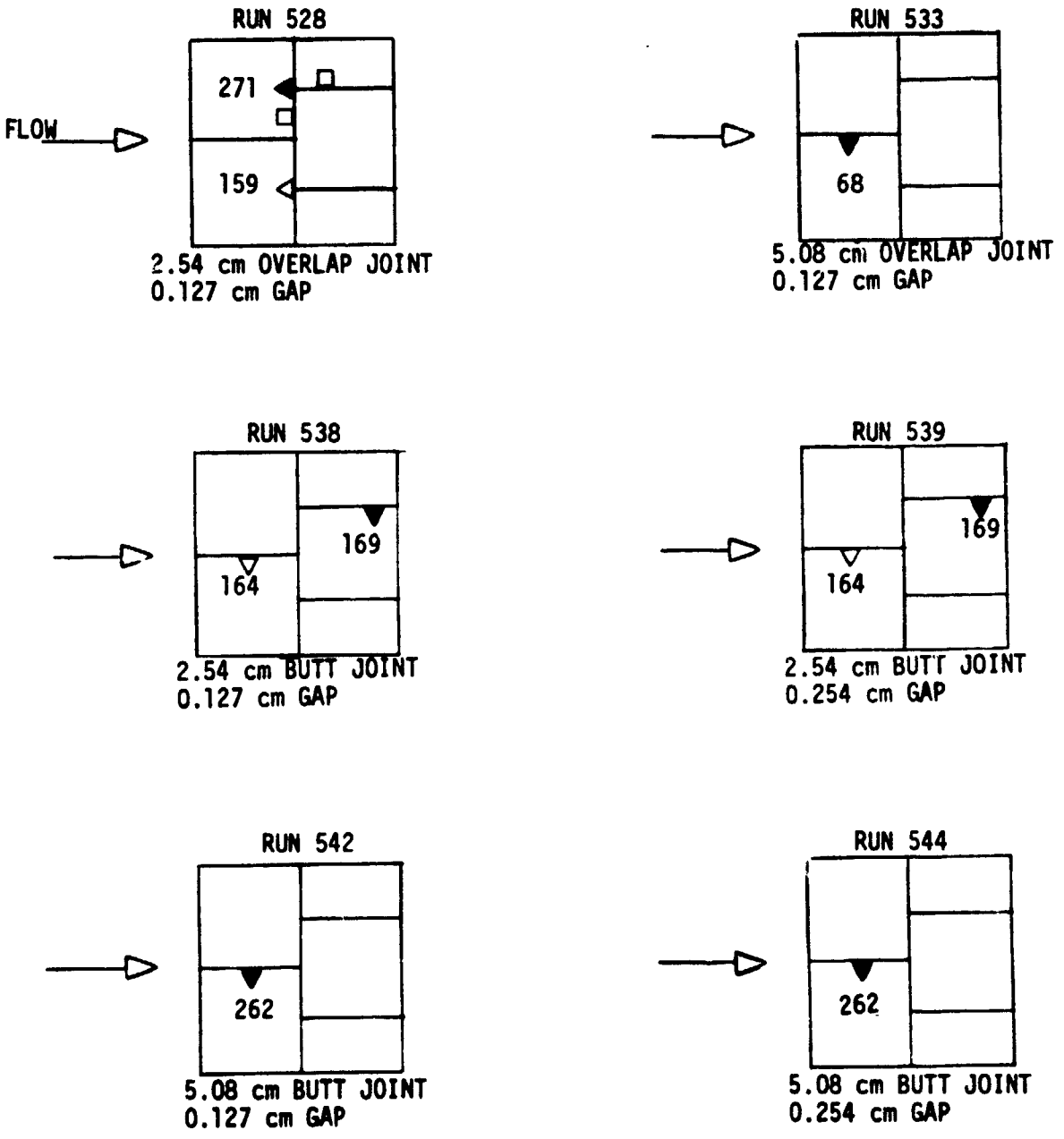

Figure 66

In runs 538 and 539, the requested T/C stack 164 is located in the upstream in-line gap but data for gap thermocouples 1 and 3 were missing. Since adequate temperature definition at and near the top of the gap is required for the inverse solution no attempt was made to compute heating at location 164. All data appeared good at location 169, and this location was used instead for the analysis of Runs 538 and 539. Plug data for this tile were largely missing for both of these runs, with only T/C No. 7 appearing valid; hence, indepth temperatures were computed and used in the place of the plug data.

For runs 542 and 544, data at locations 262 were complete and these runs were analyzed as requested, with temperature boundaries defined by plug measurements at the center of the tile.

4.2.2 Analysis Method - The MDAC HEATRAN inverse solution technique was used to obtain gap convective heating distributions from the test temperature data. Test results used in the analysis consisted of gap and plug temperature histories, test section pressures and channel wall temperature. The calibration plate served as a basis for referencing data and as a basis for investigating anomalies. Thermal models, material thermal properties and solution/test times are discussed below.

Thermal Models - Two thermal models were developed for this analysis--one for the butt joint configuration and one for the overlap joint with filler bar. The butt joint model is shown in Figure 67 and the overlap joint model in Figure 68 . Both models are modifications of an existing model described in Reference 1 .

In the butt joint model the RSI and waterproof coating are divided into 17 layers vertically and each RSI layer was divided into two sections laterally. All temperature node locations are defined in Figure 67 . Node spacing is constant between nodes 1 and 4, 4 and 15 and from 15 to 18; within these limits the spacing may be varied. The coating on top of the RSI is not shown in the sketch but was assumed to be the same thickness as in the gap and its effect is accounted for in the conduction and storage terms associated with nodes 22 and 43.

Radiation among the model components was accounted for as indicated by radiosity nodes 83 through 124 and 128 through 132. At each time step radiation view factors were computed using the crossed-strings method.

The 0.216 cm layer under the RSI tile consists of a 0.152 cm thick strain isolation pad with a 0.025 cm RTV bond on top and a 0.038 cm RTV bond on the bottom. Effective thermal properties were computed from the actual properties for this composite layer. Two conductivities were used, one defining resistances in parallel

THERMAL MODEL OF BUTT JOINT

o SILICA RSI TILE TESTS IN THE JSC LAMINAR DUCT

RADIOSITY NODES: 83 THROUGH 124,
128 THROUGH 132

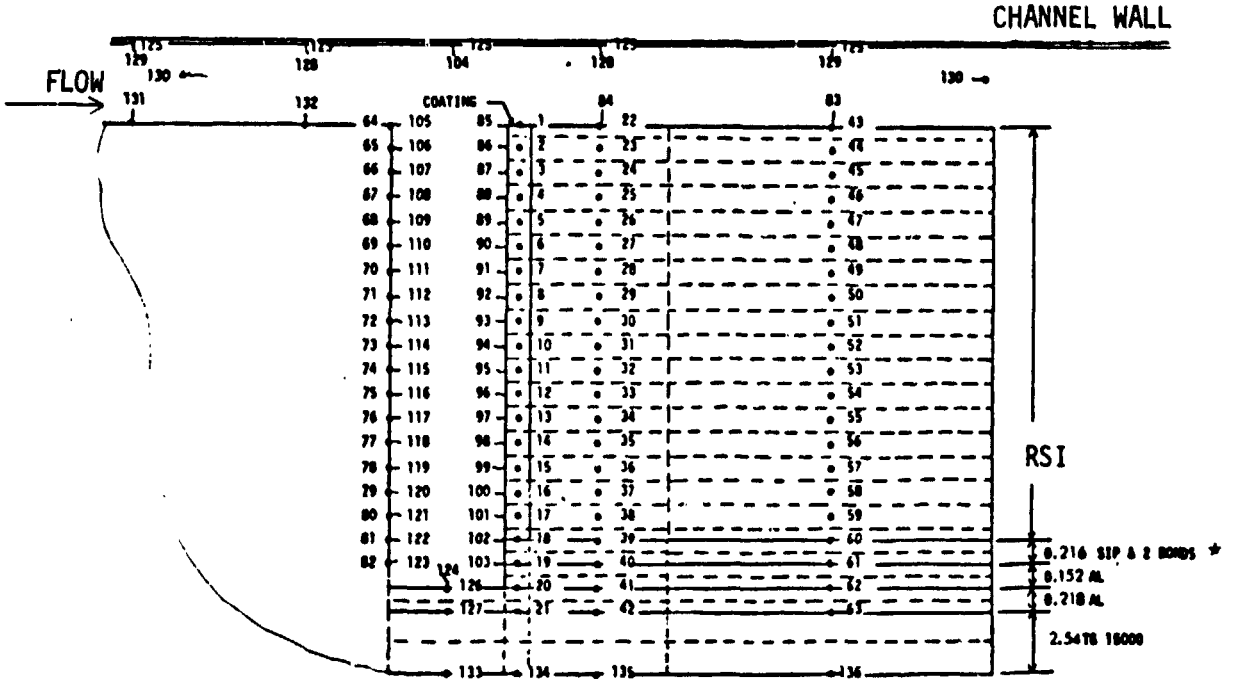

* NOTE: THICKNESS UNITS ARE cm.

Figure 67

THERMAL MODEL OF OVERLAP JOINT

o SILICA RSI TILE TESTS IN THE JSC LAMINAR DUCT

RADIOSITY NODES: 83 THROUGH 124,
128 THROUGH 132

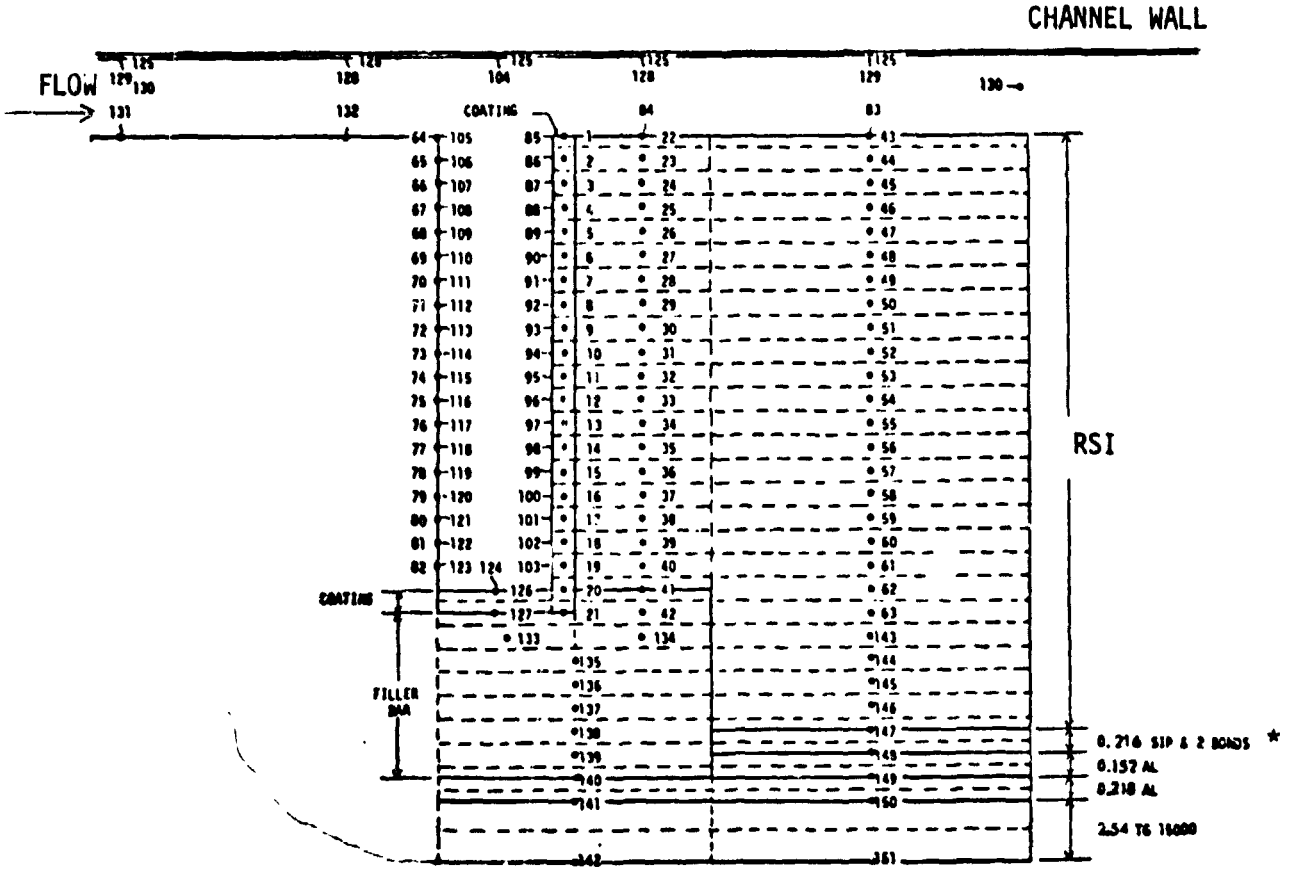

* NOTE: THICKNESS UNITS ARE cm.

Figure 68

for lateral conduction and one for vertical conduction in which the resistances were treated as in series. Under this layer is 0.152 cm of aluminum, extending to the edge of the gap and under this a 0.218 cm sheet of aluminum which functioned as a support plate for the entire panel. At the bottom is 2.54 cm of TG 15000 insulation.

Temperature nodes 43 through 60 are located to coincide with the plug thermocouple stack. Temperatures of these nodes were forced to follow the measured temperatures when the latter were available, i.e., a temperature boundary was defined by the data. When no plug data were available the temperatures of nodes 43 through 60 were computed. For gaps aligned parallel to the flow, temperature and heating conditions should be symmetrical on both sides of the gap and were so assumed in the analysis.

The foregoing discussion of the butt joint model is generally applicable to the overlap joint model, Figure 68 , except that the latter was expanded to include the filler bar and the waterproof coating on its exposed surface at the bottom of the gap. The filler material is FI 600 which is a lightweight fibrous material which was compressed at time of installation and hence is assumed to fill the gap closure alleviating the need to account for air gaps or contact resistance due to the low thermal expansion coefficient for silica RSI, 0.54×10^{-6} cm/cm, changes in gap width during a test were insignificant. Consequently, gap width was held constant during the analysis for each test.

Thermal Properties - Thermal properties were used in the analysis as provided by Rockwell International except that those for the RTV bond and strain isolation pad were combined to provide effective properties for a composite layer as discussed above in the Thermal Model section. Pressure remained relatively constant during test periods, hence pressure dependent properties were defined at a mean pressure obtained from measurements during each run along the centerline of the calibration plate in the opposite wall of the channel nozzle. Interpolation with pressure in the property tables was logarithmic.

A nominal emittance of 0.8 was used for the coating fired on the tiles by Ames. The channel wall emissivity was assumed to be 0.77 and that of the aluminum exposed at the bottom of the butt joint gap was assumed to be 0.35.

Inverse Solution Times versus Test Times - Test times for the six runs analyzed was from 269 to 2040 seconds, depending on tile thickness, gap size and gap configuration. The inverse solution was applied from the start of temperature rise to a time

at which temperatures near the tile top surface approached steady state conditions, or to the end of the test time if surface steady state conditions were not achieved. Test times and inverse solution times are tabulated in Figure 69 .

4.2.3 Butt Joint Heating Patterns - Of the four sets of butt joint data analyzed (See Figure 65) only that from runs 542 and 544 included nearly complete plug temperature distributions. For these runs no data were available for the second thermocouple from the top of the plug (T/C 7) but the remaining data appeared to provide adequate definition of the temperature distribution in the plug, hence were used to provide a temperature boundary for the inverse solution. Figures 70 and 71 show heating rate distributions normalized to the surface value. Figure 70 employs a linear scale and was used to fair curves through the computed points; Figure 71 presents the same information in log-log form.

The same instrumented 5.08 cm thick tiles were used in these two tunnel runs, with the gap width (0.127 and 0.254 cm) being the only parameter changed. The behavior of the solution for Run 542 as the heating rate approaches zero was found to be typical of those for the 0.127 cm gap data and considerable effort was devoted to understanding it. A curve was faired through the data assuming that the sharp drop to a negative heating rate is spurious. However, it was noted early in the study that the 0.127 cm gap data showed temperatures unexpectedly and significantly lower than plug temperatures at the same depth. Figure 72 shows the distribution of gap-plug temperature differences for runs 542 and 544. For the 0.254 cm gap, the plug and gap temperatures are within 14 C deg at the surface, the distribution varies smoothly and the gap temperatures are higher than the plug temperatures over most of the range. However, the 0.127 cm gap data shows plug temperature significantly higher than gap temperatures to a depth of 3.43 cm. This difference reaches a sharp maximum of 99°C at the same location as the spurious--appearing negative heating rate in Figure 70 and indicates an internal conduction from the plug toward the gap.

The cause of the anomaly has not been determined. The fact that surface temperatures are higher at the plug than at the gap for both runs 542 and 544 (see Figure 72) suggests a variation in heating conditions across the channel nozzle. Plug temperature histories are identical for both runs except for the initial steep rise period of about 40 seconds, indicating good run repeatability. The same instrumented tiles are used for both runs, so that differences in thermal properties tentatively may be ruled out. Gap width is the only known variable and Figure 72 suggests a possible variation or nonuniformity in gap width which might affect both the cavity

INVERSE SOLUTION TIMES AND TEST TIMES

o SILICA RSI TILE TESTS IN THE JSC LAMINAR DUCT

RUN NO.	MODEL	GAP WIDTH (cm)	TEST TIME SEC	INVERSE SOLUTION TIME, SEC
528	2.54 cm OVERLAP	0.127	600	330
533	5.08 cm OVERLAP	0.127	2040	590
538	2.54 cm BUTT	0.127	556	240
539	2.54 cm BUTT	0.254	269	220
542	5.08 cm BUTT	0.127	1724	1540
544	5.08 cm BUTT	0.254	562	460

Figure 69

IN-LINE BUTT JOINT HEATING DISTRIBUTION

NASA-JSC 10 MW CHANNEL NOZZLE
9 PCF AMES SILICA RSI

5.08 cm TILE - BUTT JOINT
0 RUN 542 - 0.127 cm GAP
Δ RUN 544 - 0.254 cm GAP

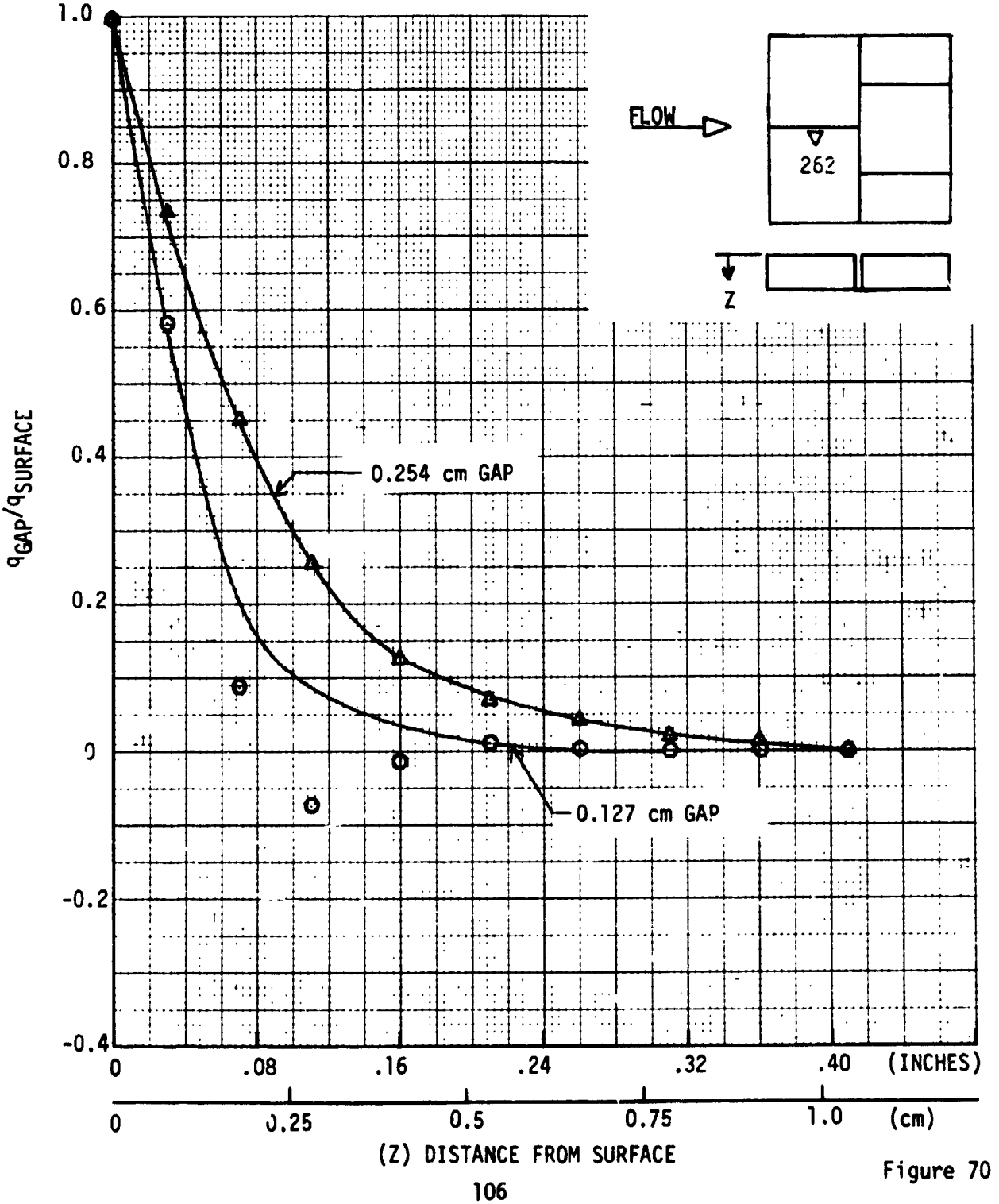

Figure 70

IN-LINE BUTT JOINT HEATING DISTRIBUTION

NASA-JSC 10 MW CHANNEL NOZZLE
9 PCF AMES SILICA RSI

5.08 cm TILE - BUTT JOINT
0 RUN 542 - - 0.127 cm GAP
Δ RUN 544 - - 0.254 cm GAP

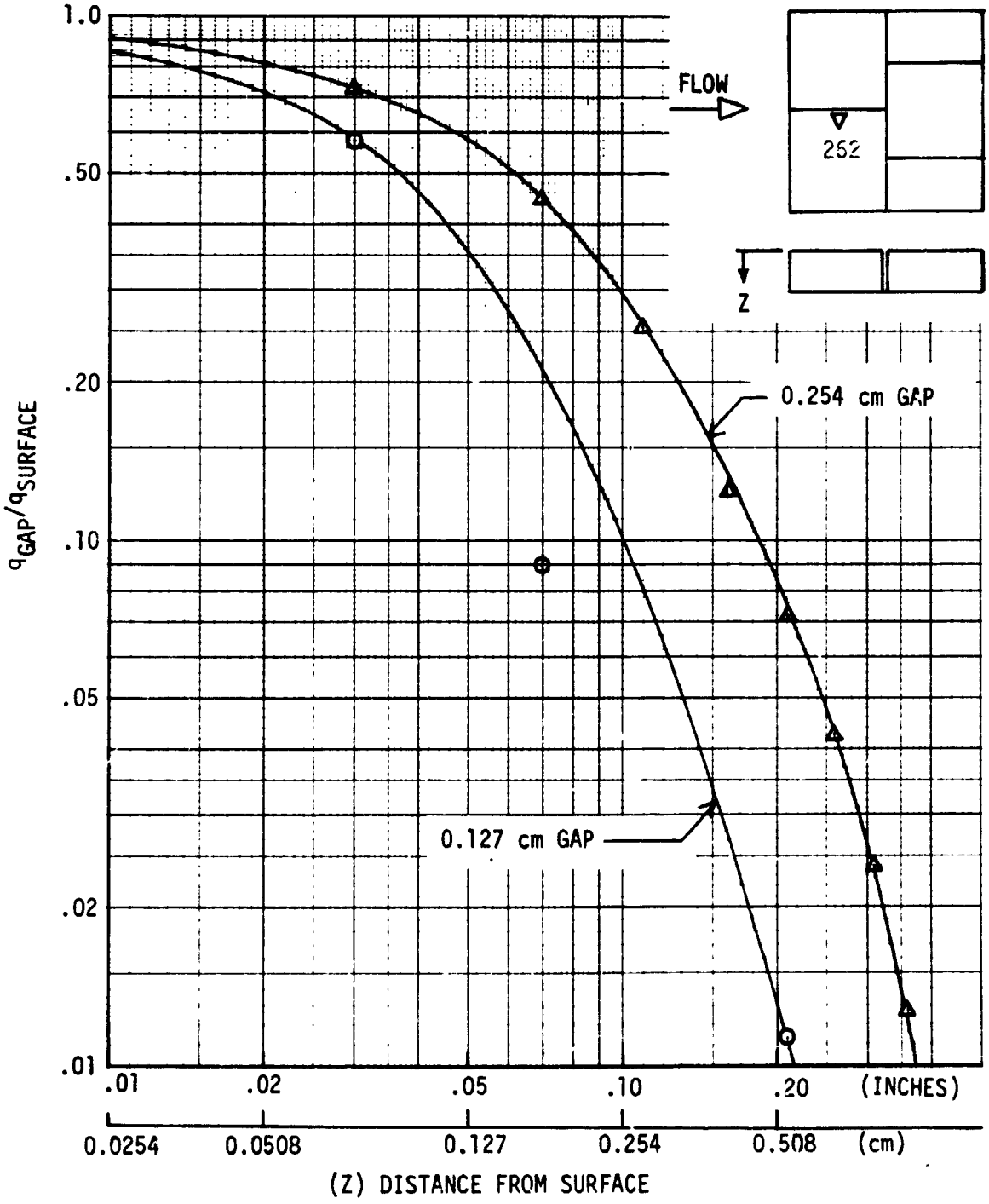

Figure 71

GAP-PLUG TEMPERATURE DIFFERENCES

NASA-JSC 10 MW CHANNEL NOZZLE
5.08 cm TILE - BUTT JOINT
MEASURED PLUG TEMPERATURES

9 PCF AMES SILICA RSI
0 RUN 542 - 0.127 cm GAP
Δ RUN 544 - 0.254 cm GAP

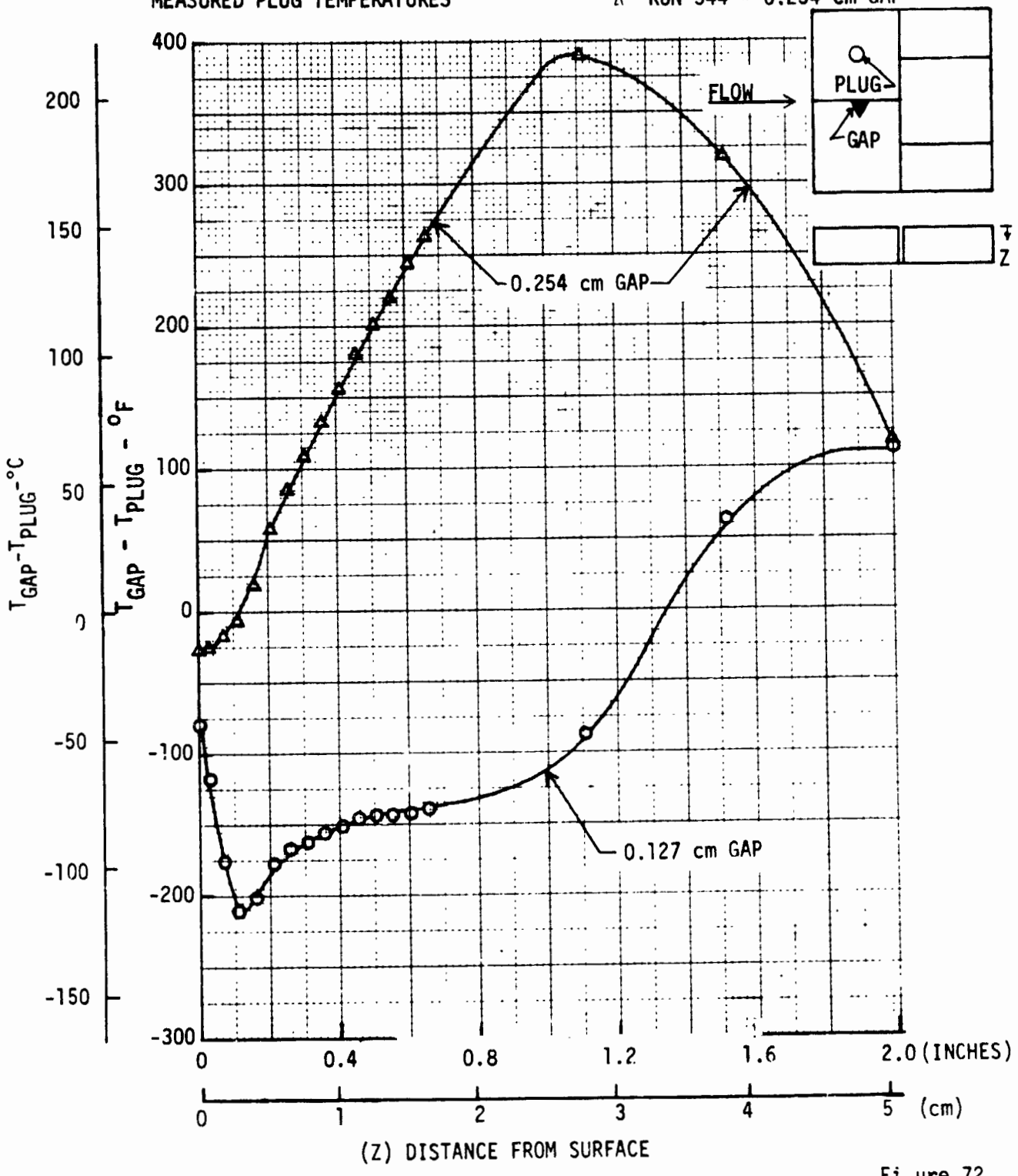

Figure 72

flow and radiation characteristics. A given variation might be a significant fraction of the smaller gap while having no obvious effect on the larger gap data.

Results of the analysis on the two 2.54 cm thick butt joint tests, runs 538 and 539, are shown in Figures 73 and 74 . For these runs, the data were inadequate at the requested location (no. 164) on an upstream tile and location 169 on the center downstream tile was substituted. Since data were available from only one RSI plug thermocouple, the temperature at the plug nodes were computed as a part of the solution. The surface temperature on the top of the tile was assumed uniform although this was found not to be the general case. For the 0.127 cm gap (run 538) data from the one functioning thermocouple indicate plug temperatures appreciably higher than gap temperatures at the same depth; the same thermocouple in the 0.254 cm gap run (run 539) indicates plug temperatures equal to or lower than corresponding gap temperatures. The heating distribution in the 2.54 cm tile and for the 0.127 cm gap exhibits the same form as that for the 5.08 cm tile, and the distribution of the 0.254 cm gap has a small irregularity at the same depth.

Gap/plug temperature differences are shown in Figure 75 for these runs. These distributions have the same form as those in Figure 72 for the 5.08 cm tiles. The initial irregularity (within 0.254 cm of the surface) is probably due to the assumption of constant surface temperatures between the gap and plug. The minima at a depth of 0.305 cm again correspond to the erratic points in the heating distribution curves in Figure 73 . These distributions both become asymptotic to the same slightly negative value, $q/q_{SURFACE} \sim -0.02$. Since both of these curves were obtained from the same instrumented tiles the effect is presumably associated with the tile or instrumentation, i.e., an error associated with a given thermocouple loading or location and/or a deviation in coating thickness.

4.2.4 Overlap Joint Heating Patterns - The heating distribution for run 533 is shown in Figure 76 and 77 and the gap/plug temperature difference distribution in Figure 78 . The test used a 5.08 cm tile with overlap in-line joint and 0.127 cm gap width. These figures exhibit the same phenomena observed in the other 0.127 cm gap results, with the plug temperature 130°C higher than the gap temperature 0.330 cm below the surface. The fact that the heating distribution is asympotic to the same value of ~ -0.02 as seen in Figure 73 is fortuitous since the temperature distributions are not analogous. In run 533 plug temperatures are higher than gap temperatures to a depth of 1.473 cm and the negative asympote involves conduction from plug to gap over that depth.

IN-LINE BUTT JOINT HEATING DISTRIBUTION

NASA-JSC 10 MW CHANNEL NOZZLE
9 PCF AMES SILICA RSI

2.54 cm TILE - BUTT JOINT
0 RUN 538 - - 0.127 cm GAP
Δ RUN 539 - - 0.254 cm GAP

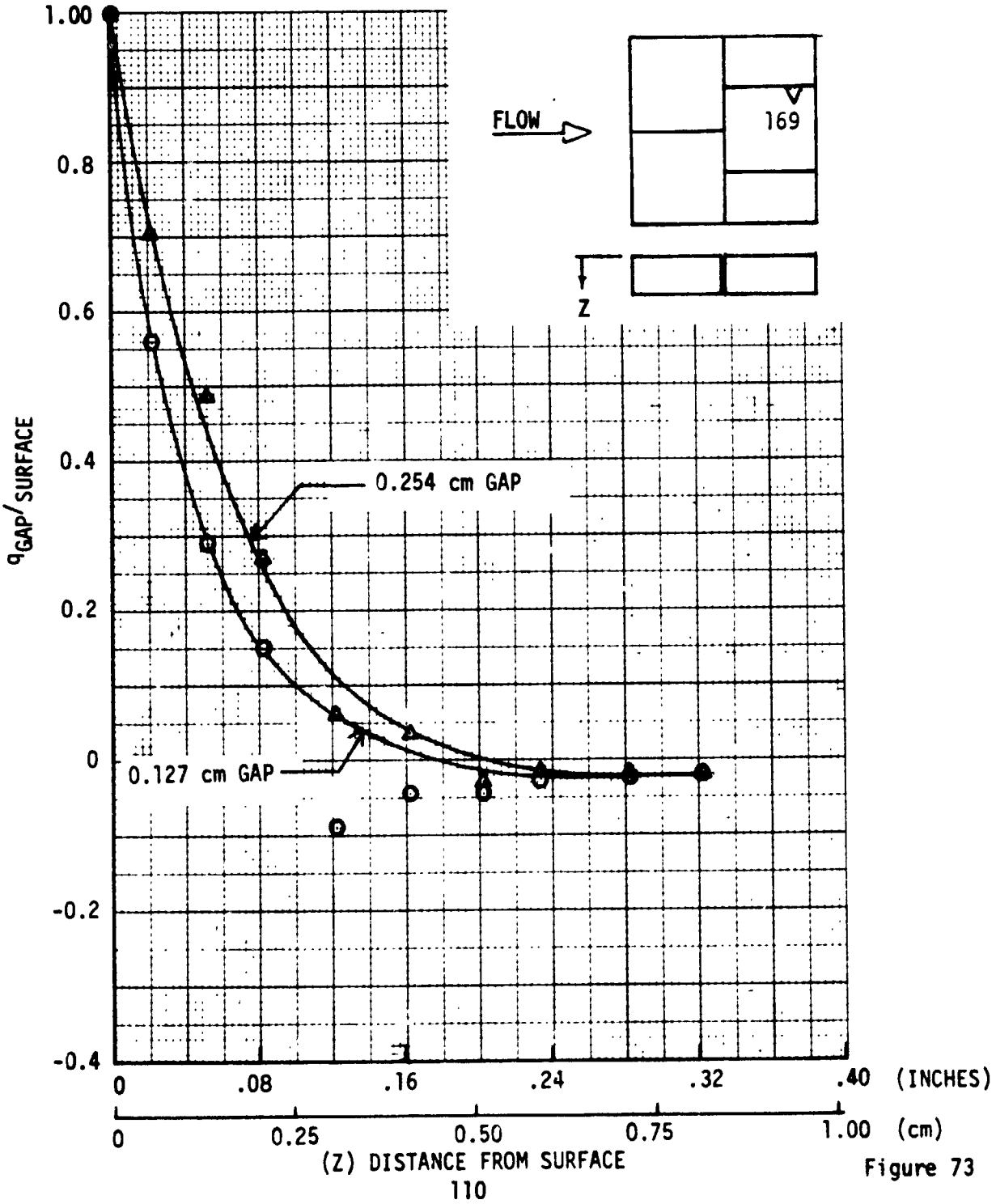

Figure 73

IN-LINE BUTT JOINT HEATING DISTRIBUTION

NASA-JSC 10 MW CHANNEL NOZZLE
9 PCF AMES SILICA RSI

2.54 cm TILE - BUTT JOINT
0 RUN 538 - - 0.127 cm GAP
Δ RUN 539 - - 0.254 cm GAP

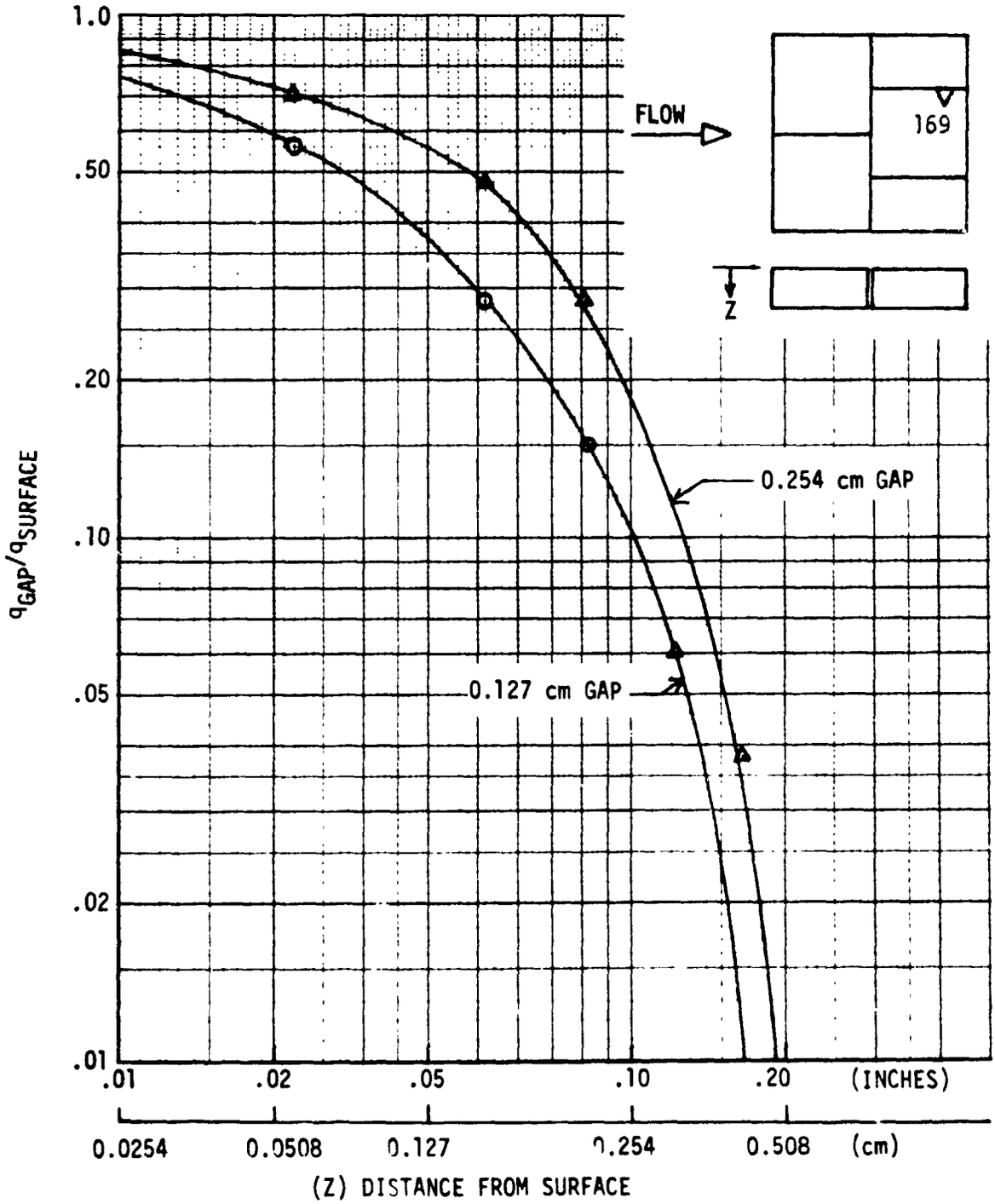

Figure 74

GAP-PLUG TEMPERATURE DIFFERENCES

9 PCF AMES SILICA RSI
2.54 cm TILE - BUTT JOINT
COMPUTED PLUG TEMPERATURES

NASA-JSC 10 MW CHANNEL NOZZLE
O RUN 538 - 0.127 cm GAP
Δ RUN 539 - 0.254 cm GAP

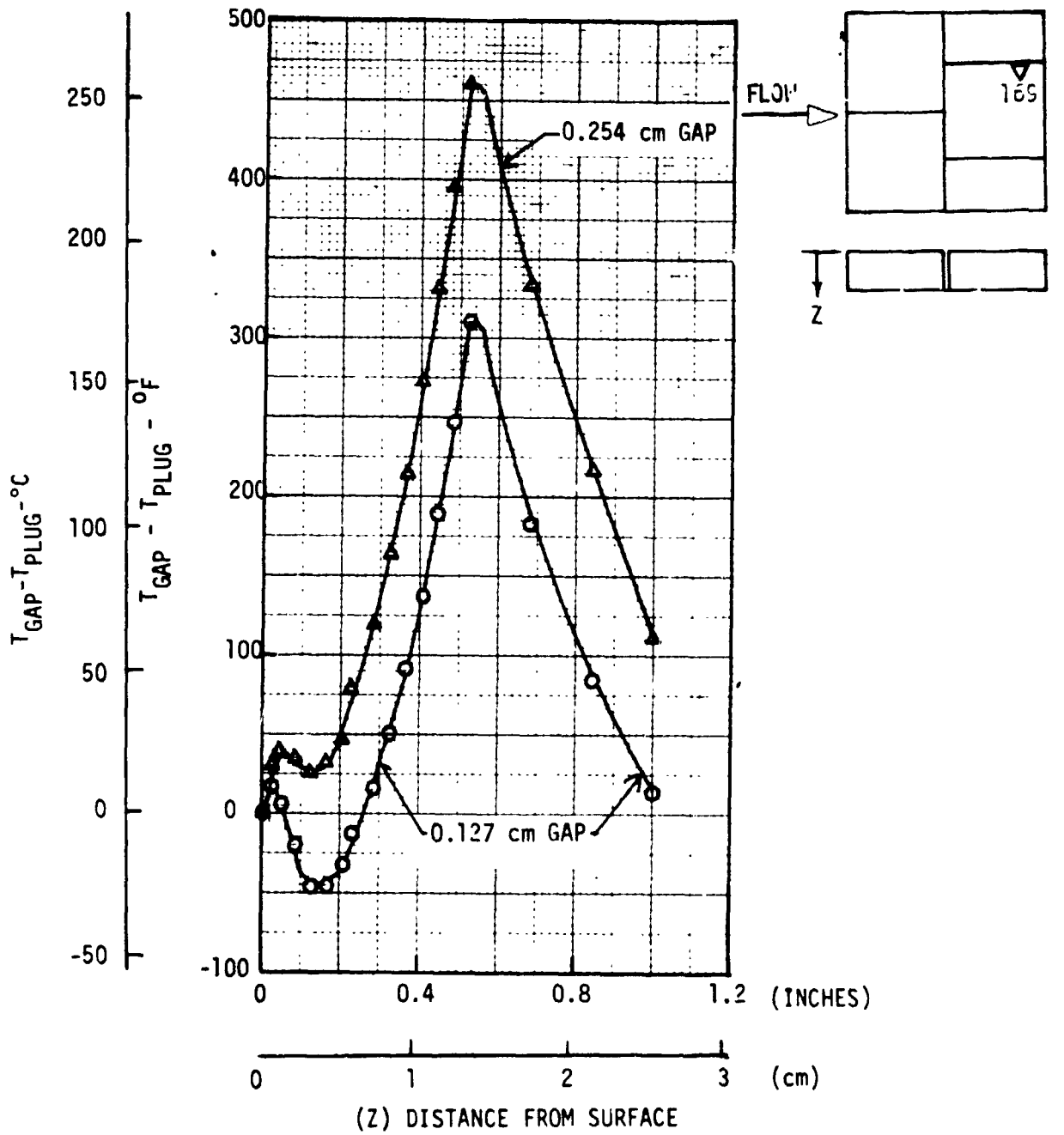

Figure 75

IN-LINE OVERLAP JOINT HEATING DISTRIBUTION

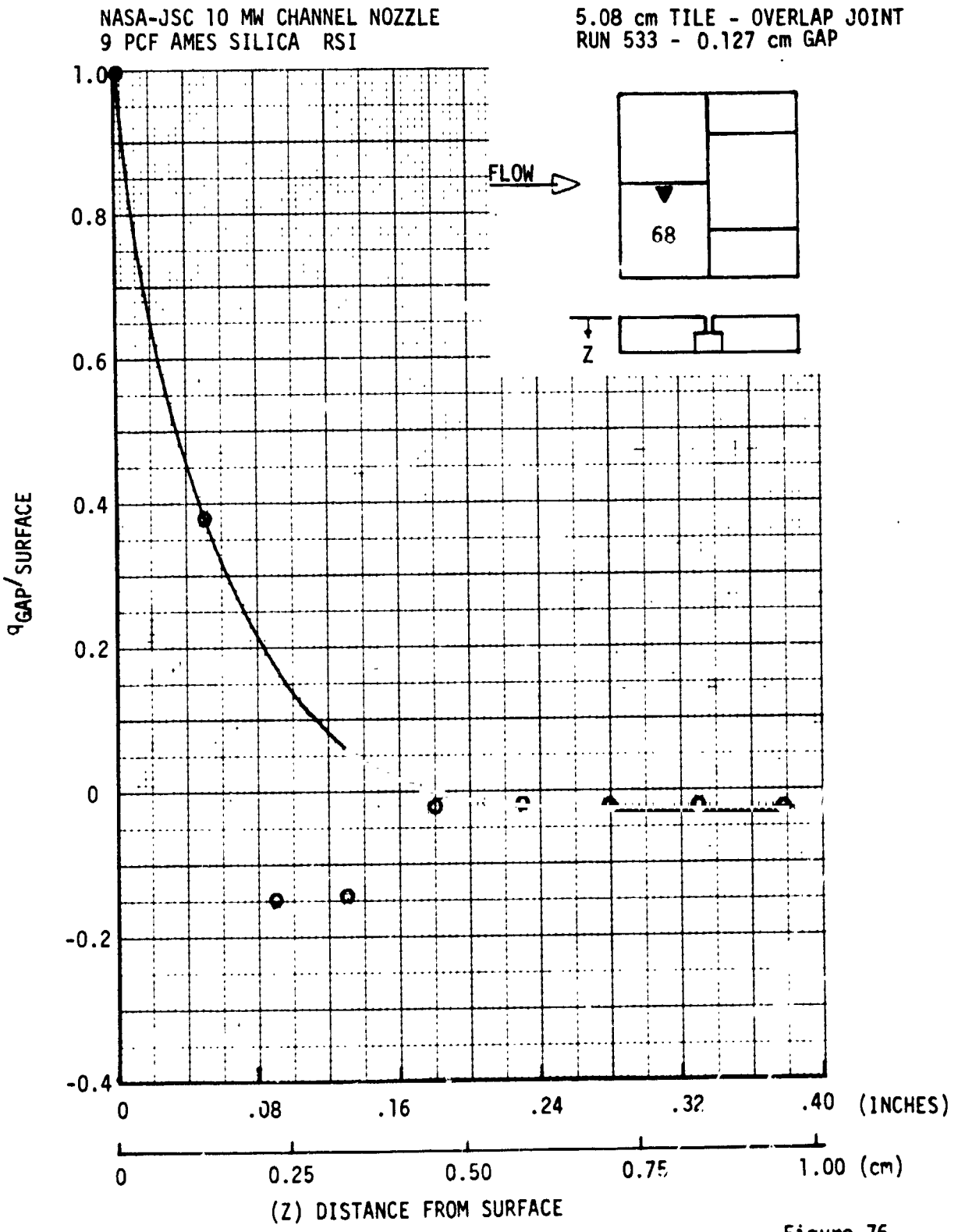

Figure 76

IN-LINE OVERLAP JOINT HEATING DISTRIBUTION

NASA-JSC 10 MW CHANNEL NOZZLE
9 PCF AMES SILICA RSI

5.08 cm TILE - OVERLAP JOINT
RUN 533 - 0.127 cm GAP

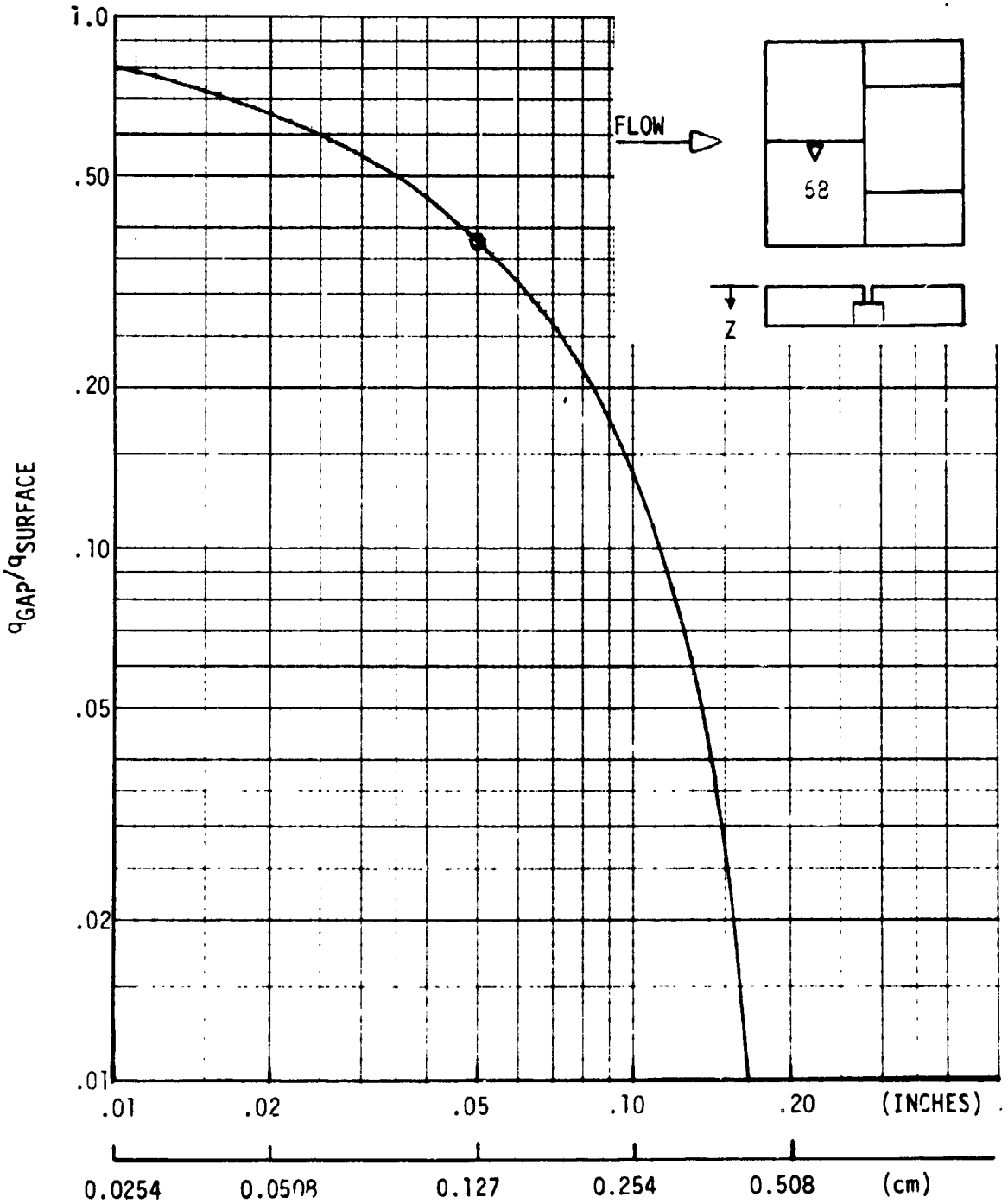

Figure 77

GAP-PLUG TEMPERATURE DIFFERENCES

NASA-JSC 10 MW CHANNEL NOZZLE
9 PCF AMES SILICA HRSI

RUN 533
5.08 cm TILE - OVERLAP JOINT
0.127 cm GAP WIDTH
MEASURED PLUG TEMPERATURES

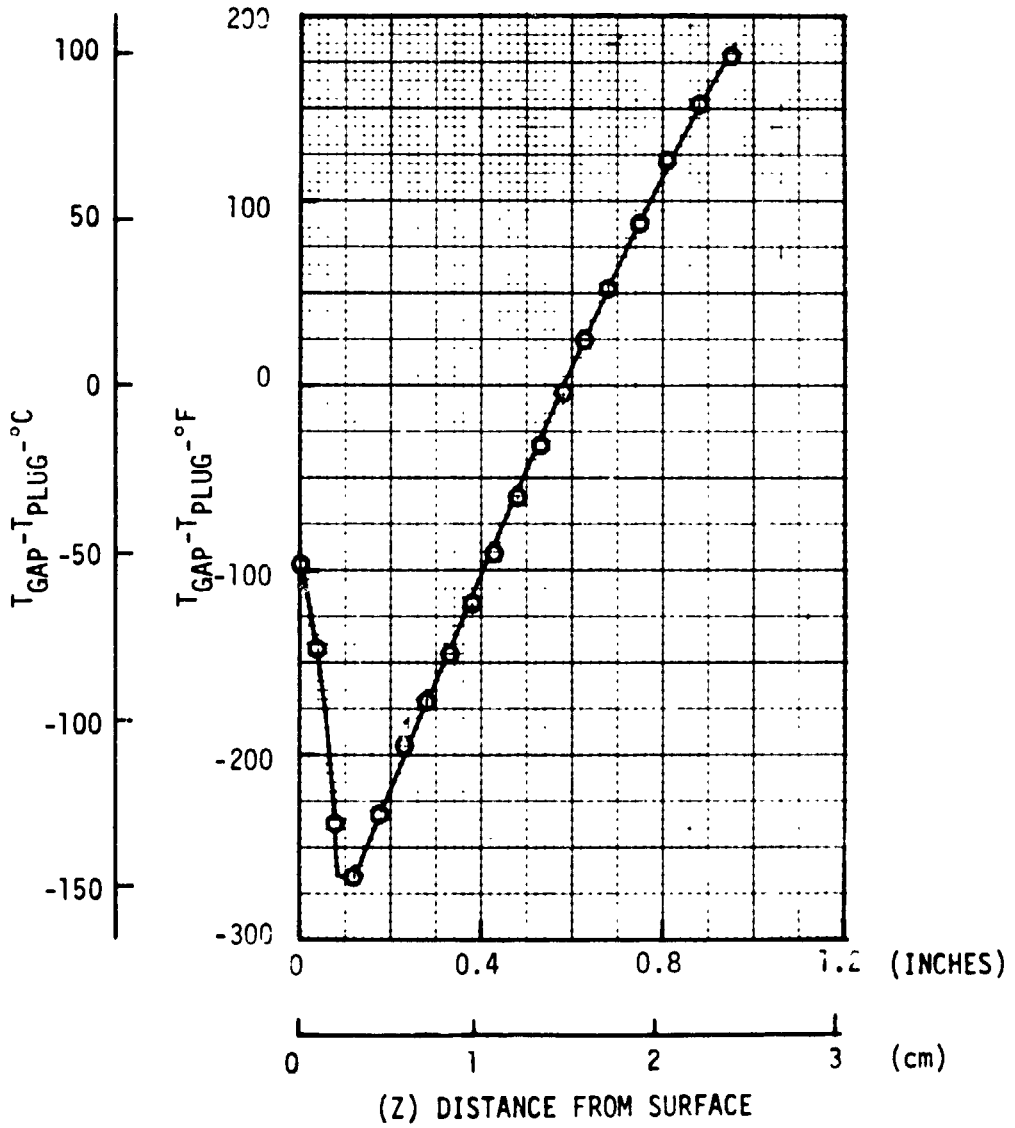

Figure 78

The second overlap joint analyzed was for run 528 at the location where the tiles form an aft facing T-slot. As noted previously for this run, location 271 rather than 159 (Figure 66) was used; since by symmetry, conditions should be identical at both locations and locations 156 and 272 provided additional data desired in the analysis. Proper analysis of the T-slot involved formulating a three-dimensional model with three-dimensional view factors and increasing the number of nodes. The scope of the study did not permit the formulating of such a model, so hypothetical conditions were analyzed using the two-dimensional thermal model to establish bounds for the heating at location 271. It was assumed that the gap wall at location 271 would see an opposite wall with temperature/view factors representing upper and lower limits. Figure 79 is an isometric sketch of the T-slot configuration, illustrating the locations where temperature histories were available. It was expected that reattaching flow would result in the highest temperatures at location 156 and that temperatures at location 271, which sees 156, would be intermediate between those at 156 and 272. Figure 80 shows actual temperature distributions at these locations. As expected, those at location 156 are the highest. Near the surface, location 271 temperatures are intermediate but crossover at a depth of 0.203 cm and then drop increasingly below those at 272. This trend probably results from the radiation relief provided by the increased view factor to the channel wall and, perhaps to some extent, to the bottom of the in-line gap.

Since temperature bounds were defined by measurements at locations 156 and 272 only to 0.254 cm below the surface and by measurements at locations 156 and 271 over the rest of the gap, three cases were computed using the two-dimensional model and the following assumptions:

a. Wall temperatures were assumed identical across the gap, as measured at location 271 and the nominal surface emissivity of 0.8 was used.

b. Wall temperatures opposite location 271 were assumed equal to those at 272 and the nominal surface emissivity used.

c. Wall temperatures opposite location 271 were assumed equal to those at 156 and an effective slot emittance of unity was assumed at 271.

The heating distributions obtained with these three assumptions are shown in Figure 81 . Using assumption (a) the gap heating distribution is reasonable although asymptotic to a slightly more negative value than was found in any of the other runs analyzed. The heating distributions obtained using assumptions (b) and

T-SLOT INSTRUMENTATION - RUN 528

o SILICA RSI TILE TESTS IN JSC LAMINAR DUCT

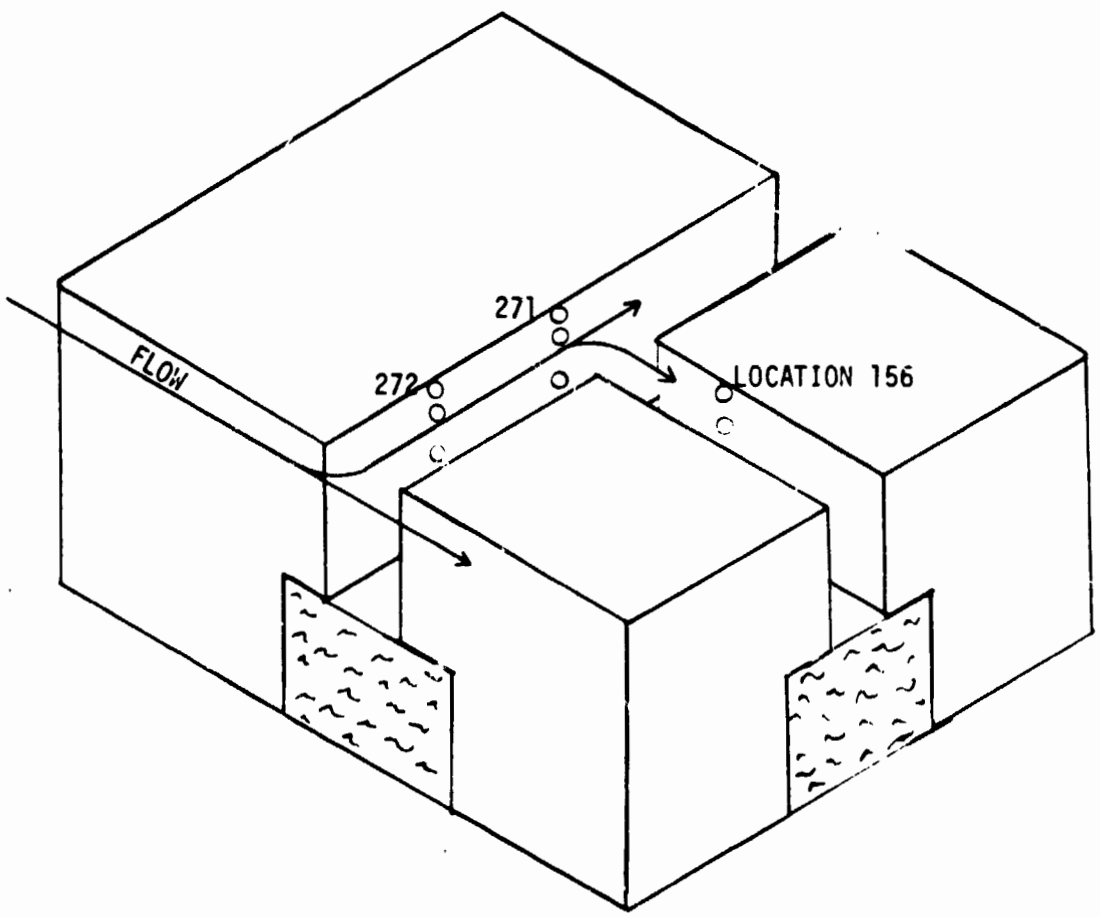

Figure 79

GAP TEMPERATURES IN THE T-SLOT

o SILICA RSI TILE TESTS IN JSC LAMINAR DUCT

RUN 528
TIME = 371 SEC
2.54 cm TILE - OVERLAP JOINT
0.127 cm GAP WIDTH

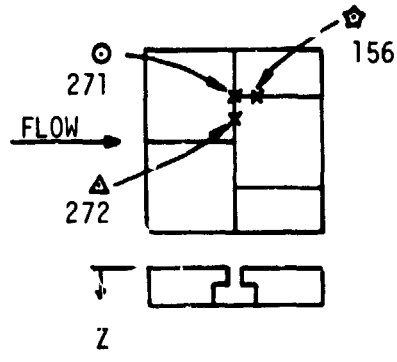

TEMPERATURE - °C: 0, 100, 200, 300, 400, 500, 600

TEMPERATURE - °F: 0, 200, 400, 600, 800, 1000, 1200

0, 0.1, 0.2, 0.3, 0.4 (INCHES)

0, 0.25, 0.50, 0.75, 1.00 (cm)

(Z) DISTANCE FROM SURFACE

Figure 80

HEATING IN AN AFT FACING T-SLOT GAP

NASA-JSC 10 MW CHANNEL NOZZLE 9 PCF AMES SILICA RSI
ASSUMED OPPOSITE WALL TEMPERATURES.

- □ LOCATION 272
- ◁ LOCATION 156
- ▽ LOCATION 271

2.54 cm TILE
OVERLAP JOINT (T-SLOT)
RUN 528 - - 0.127 cm GAP

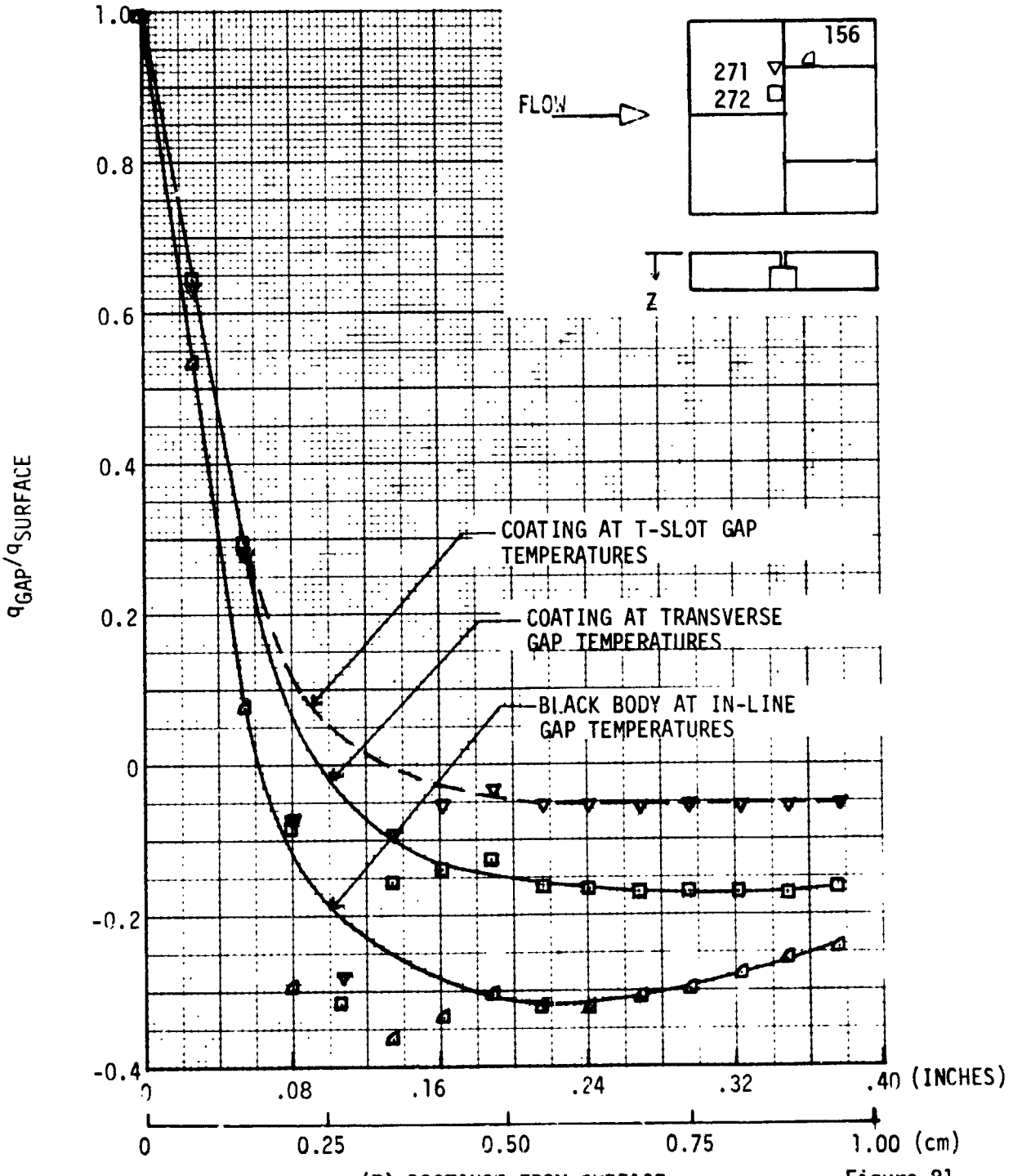

Figure 81

(c) show heating dropping to and remaining at significant negative values to the bottom of the gap.

The gap-plug temperature differences are shown in Figure 82 with the plug temperatures being higher at all depths. Taken together and in comparison with the other 0.127 cm gap runs, Figures 80 through 82 indicate that the T-slot configuration requires better radiation modeling and perhaps better temperature definition of radiating surfaces than are obtainable from the present data.

4.2.5 Comparison of Heating Distributions - A comparison of butt and overlap joint heating distributions is made in Figure 83 . Gap heating rate distributions for runs 542 and 533 are shown together to illustrate the effect of gap depth. Run 542 has a gap depth of 5.08 cm and run 533 (5.08 cm tile with 2.54 cm filler bar) has effectively a 2.54 cm deep gap. The curves coincide closely over most of the range with differences only near the bottom of the gap.

A comparison was also made between data from this test (runs 542 and 544) with previous gap heating tests in the JSC 10 MW channel nozzle. Figure 84 is adapted from Figure 31of Reference 1 and shows gap heating distributions on a 5.08 cm butt joint computed from a previous test reported in Section 4.1.2 and Reference 1 . Data from runs 542 and 544 of the present test program have been added and are seen to be in good agreement. Cold gap widths in the present test correspond to two of those from the earlier test. However at the test condition, the gap widths for the present test vary only slightly from the cold value because of the much lower RSI thermal expansion coefficient.

4.2.6 Sensitivity Studies - The effects of 1) the high sensitivity of the RSI thermal conductivity to pressure and 2) coating thickness variations on the computed heating distributions were briefly examined.

On noting the unexpectedly high plug temperatures, case 544 was rerun to 100 seconds assuming atmospheric pressure in the test section. This rerun was made assuming the internal pressure in the RSI might not have adjusted to the test section pressure resulting in higher RSI thermal conductivity (Ref. 2, Fig. 10). As expected, the gap heating was not significantly affected but the RSI temperatures between the gap and plug (nodes 23 to 39) were appreciably higher than obtained with the recorded test pressures. Figure 85 shows results for this rerun case. The temperature at node 22 was obtained by interpolating linearly between the gap and

GAP-PLUG TEMPERATURE DIFFERENCES AT AFT FACING T-SLOT GAP

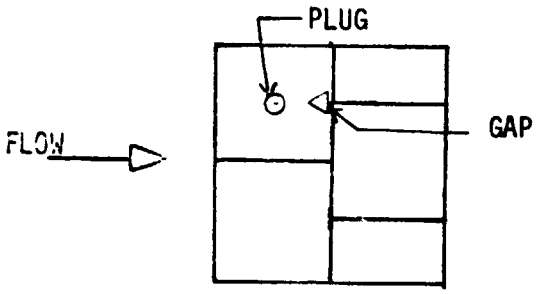

RUN 528
2.54 cm TILE - OVERLAP JOINT
0.127 cm GAP WIDTH
MEASURED PLUG TEMPEPATURES

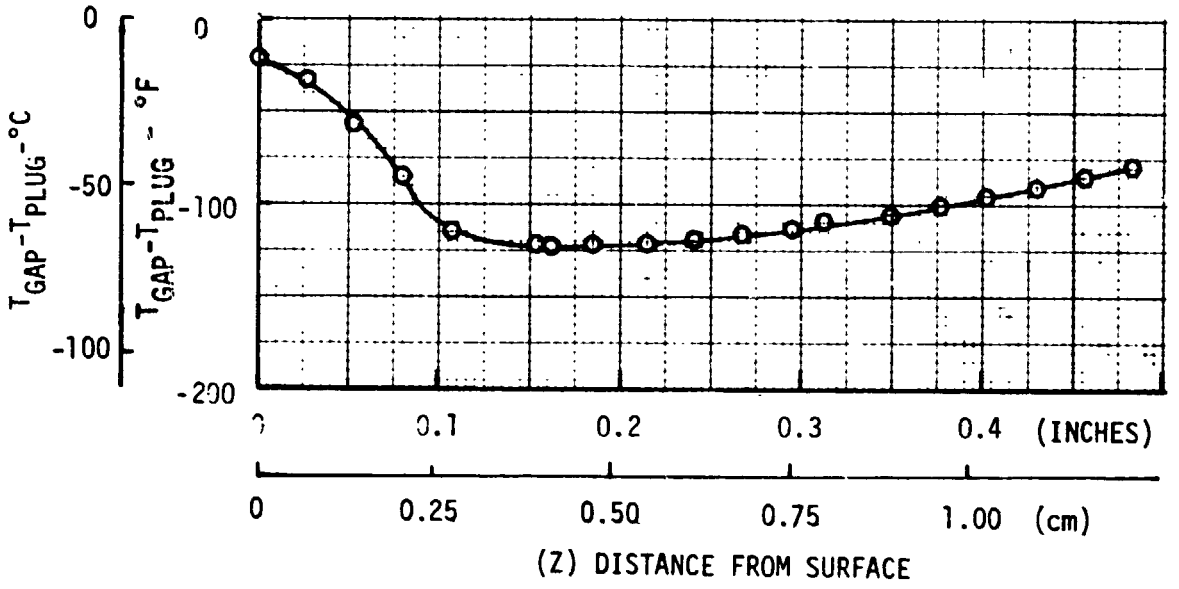

Figure 82

SENSITIVITY OF GAP HEATING DISTRIBUTION TO GAP DEPTH

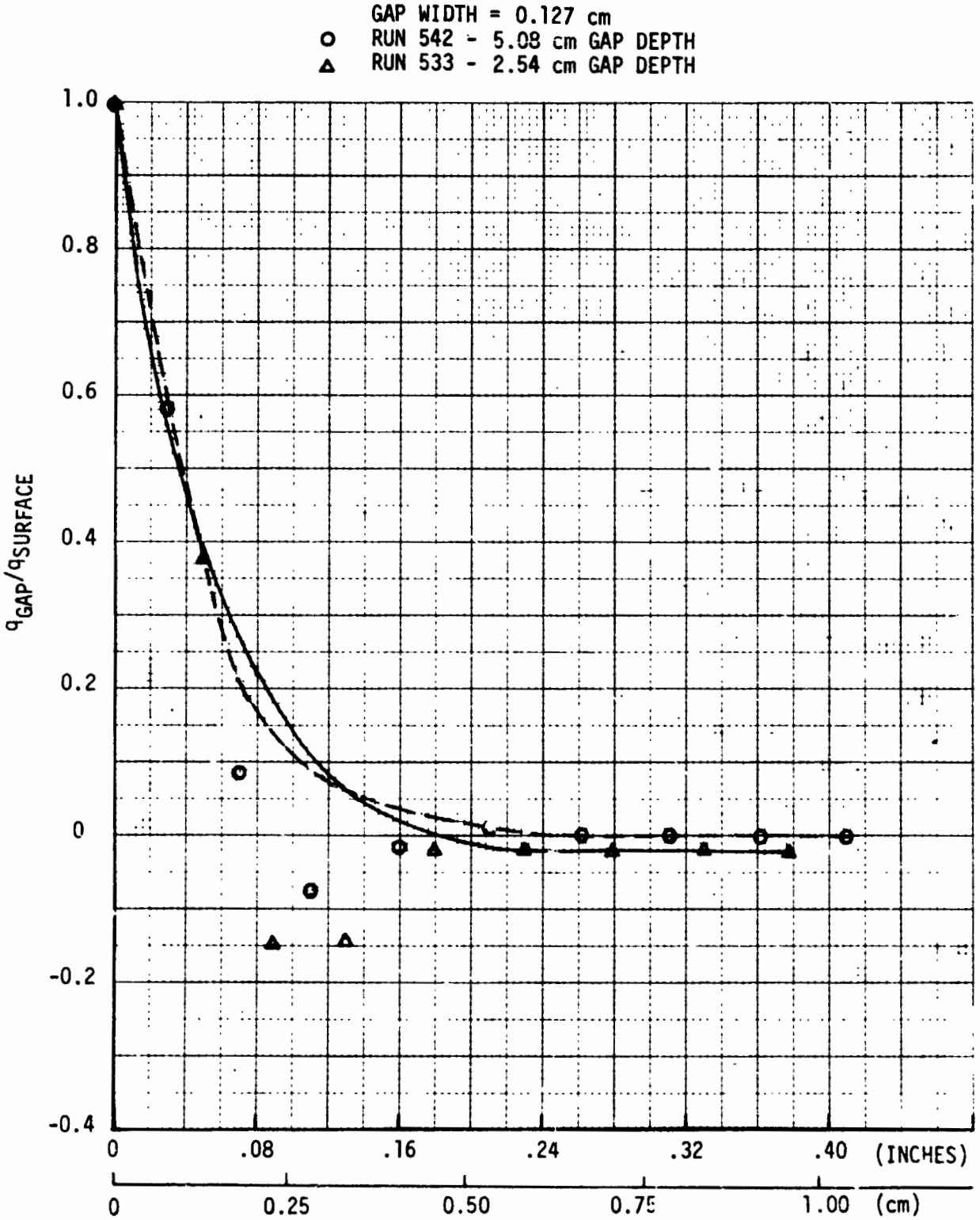

Figure 83

HEATING RATE COMPARISON WITH PHASE I RSI TESTS
5.08 CM TILE - BUTT JOINT

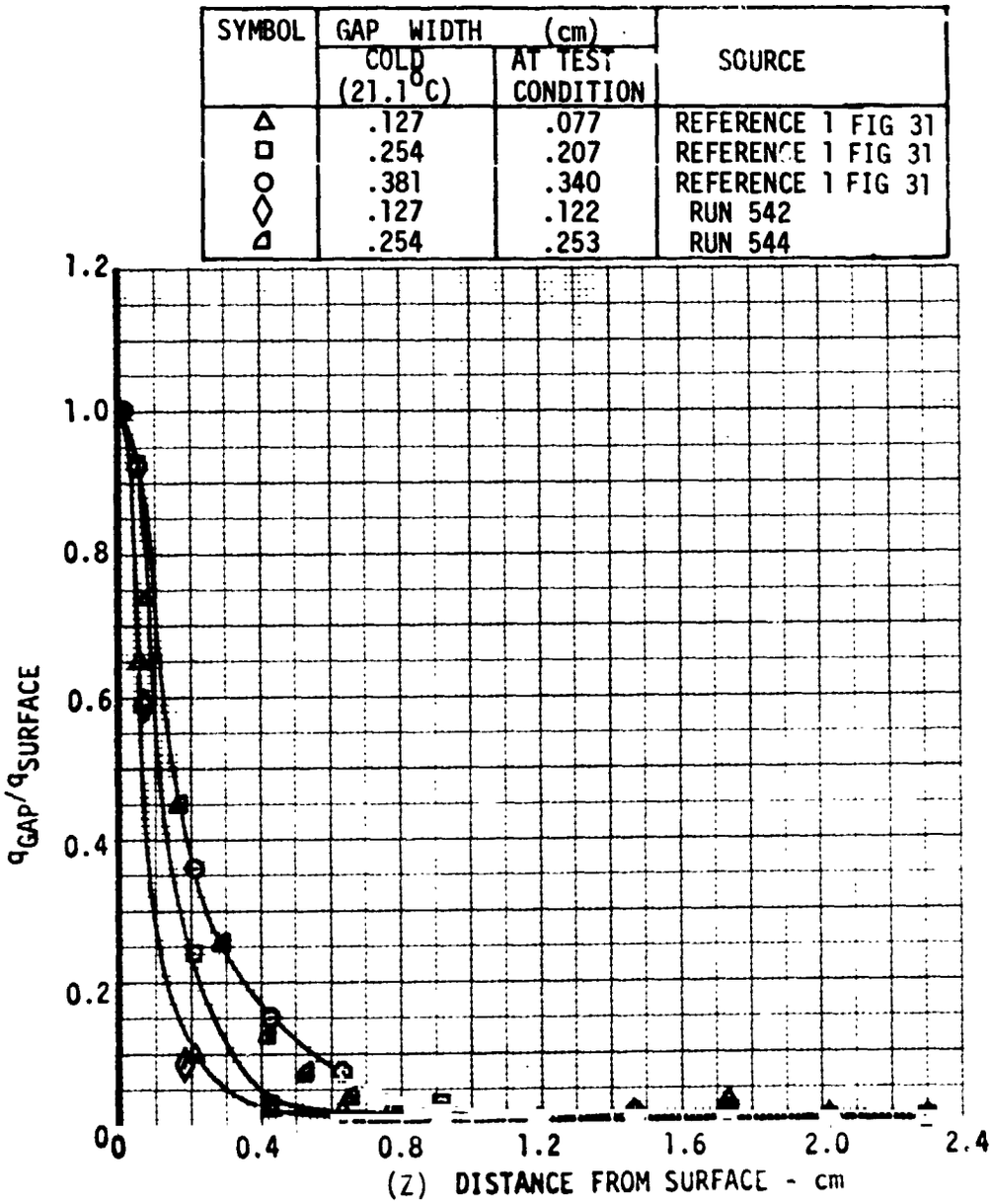

Figure 84

EFFECT OF PRESSURE ON INTERNAL RSI TEMPERATURE

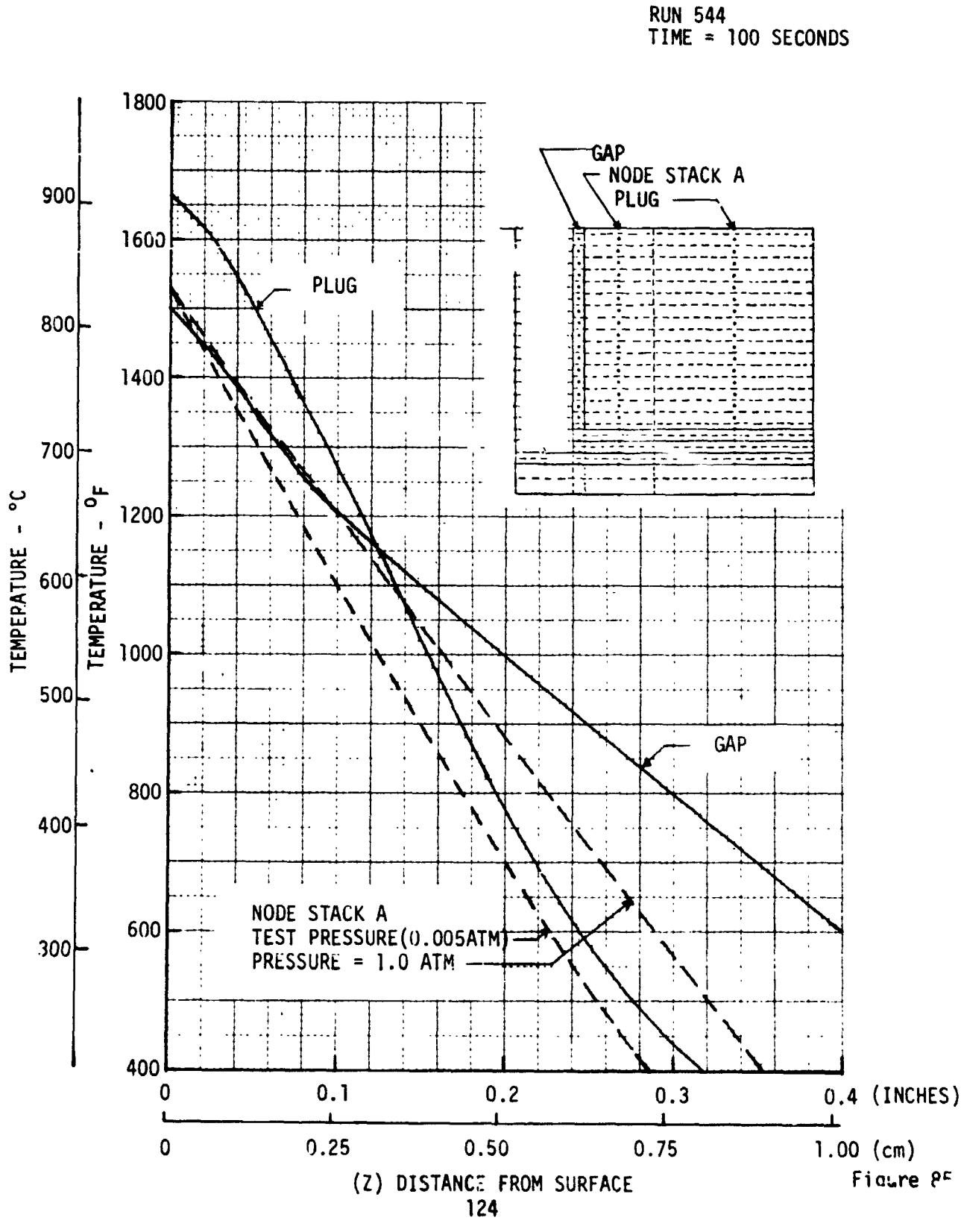

Figure 85

plug surface thermocouple data, and nodes 23 through 39 (Stack A) were computed by the program. For the test pressure (0.005 atmosphere) run, temperatures at these intermediate nodes were lower than either the gap or plug temperatures, indicating that the thermal properties are not consistent with the recorded data. While for the rerun, the resulting temperature distribution was much more realistic.

Run 542 was rerun to 250 seconds assuming a coating thickness of 0.038 cm rather than 0.025 cm, resulting in normalized heating rates up to 5.7% higher in the upper section of the gap than reported in Figures 70 and 71.

4.3 Analysis of Supplemental LaRC Mach 10 CFHT Tests - Analyses were performed of additional gap heating data obtained in the LaRC Mach 10 CFHT. Analyses of the original CFHT tests are reported in Section 4.1.3 herein. The purpose of the supplemental tests was to substantiate the calibration data measured previously, to evaluate the effect of zero gap width, and to determine the effects on heating in the tile gaps at higher Reynolds number. The tests employed the same model used in the previous tests, namely, a wall mounted instrumented thin skin tile surrounded by an array of uninstrumented RSI tiles. The test conditions, model description, and data assimilated are discussed in Section 3.3 and Volume II of this report. The test matrix is repeated in Figure 86 for convenience and gives run number, gap width, tile orientation and unit Reynolds number.

Included in the data analysis are the following:

a) Gap heating distributions for the supplemental tests including effects of gap width and in-line versus staggered tile orientation.

b) Comparison of supplemental and original heating patterns.

c) Effect of Reynolds number on heating rates

c) Investigation of anomalies in heating distributions; specifically, the decrease in surface heating near the edges of the thin skin tile and the greater heating rates on top of the tile than that measured on the flat calibration plate.

4.3.1 Supplemental CFHT Heating Analysis - The heating distributions across the top of the tile and within the gap are presented herein for the staggered tile pattern and the in-line tile orientations. Heating patterns were defined for both tile orientations for zero gap (no gap), 0.13 cm and 0.23 cm gap widths. The zero gap width was achieved by placing dental plaster in the gaps to an approximate depth of 0.64 cm above the top surface. The surface of the dental plaster was allowed to harden and then sanded until a smooth transition was achieved between the tiles. As for the previous CFHT tests, the in-line arrangement is achieved by rotating the test article 90 degrees from the staggered tile orientation (see Figure 45); and for the in-line arrangement, the tiles are in-line in the axial direction only. In the lateral direction (normal to the flow) the tiles are staggered. The unit Reynolds number per meter during these tests was 3.3×10^6. All heating data have been normalized by the flat plate calibration data.

Heating patterns for the staggered tile orientations are shown in Figures 87 , 88 and 89 . The data in Figure 87 were measured at the tile centerline (Y = 0), while Figure 88 and 89 data were recorded at the tile edges of Y = +7.2 cm and

CFHT TEST 92 - SUPPLEMENTAL RUNS - FEBRUARY 1974

RUN	GAP (cm)	ORIENTATION	Re_∞/m
161	.127	Staggered	3.28×10^6
162	↓	Staggered	7.38×10^6
163	↓	In-line	3.28×10^6
164	.127	In-line	7.38×10^6
165	.229	Staggered	3.28×10^6
166	↓	Staggered	7.38×10^6
167	↓	In-line	3.28×10^6
168	.229	In-line	7.38×10^6
169	Closed		7.38×10^6
170	Closed		3.28×10^6

Figure 86

EFFECT OF GAP WIDTH ON STAGGERED TILE HEATING IN CFHT (Y = 0.0)

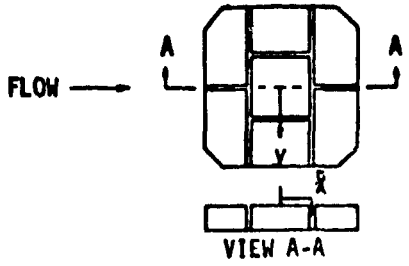

ALPHA = 0 DEG.
$Re_\infty/m = 3.3 \times 10^6$
$M_\infty = 10$

W = GAP WIDTH

Not corrected for C_p
Not corrected for conduction

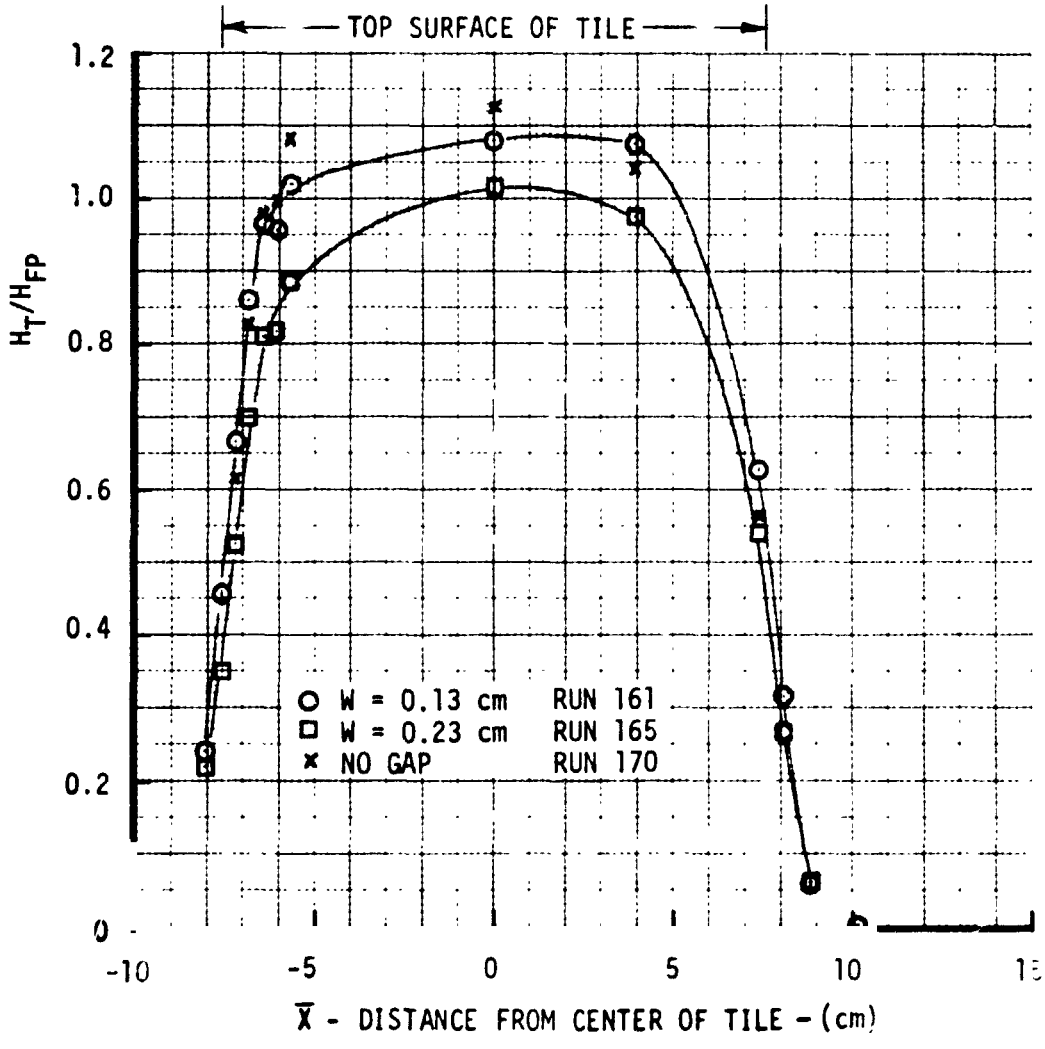

Figure 87

EFFECT OF GAP WIDTH ON STAGGERED TILE HEATING IN CFHT (Y = +7.2 CM)

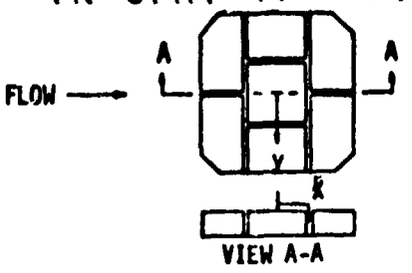

ALPHA = 0 DEG.
$Re_\infty/m = 3.3 \times 10^6$
$M_\infty = 10$

W = GAP WIDTH

Not corrected for C_p
Not corrected for conduction

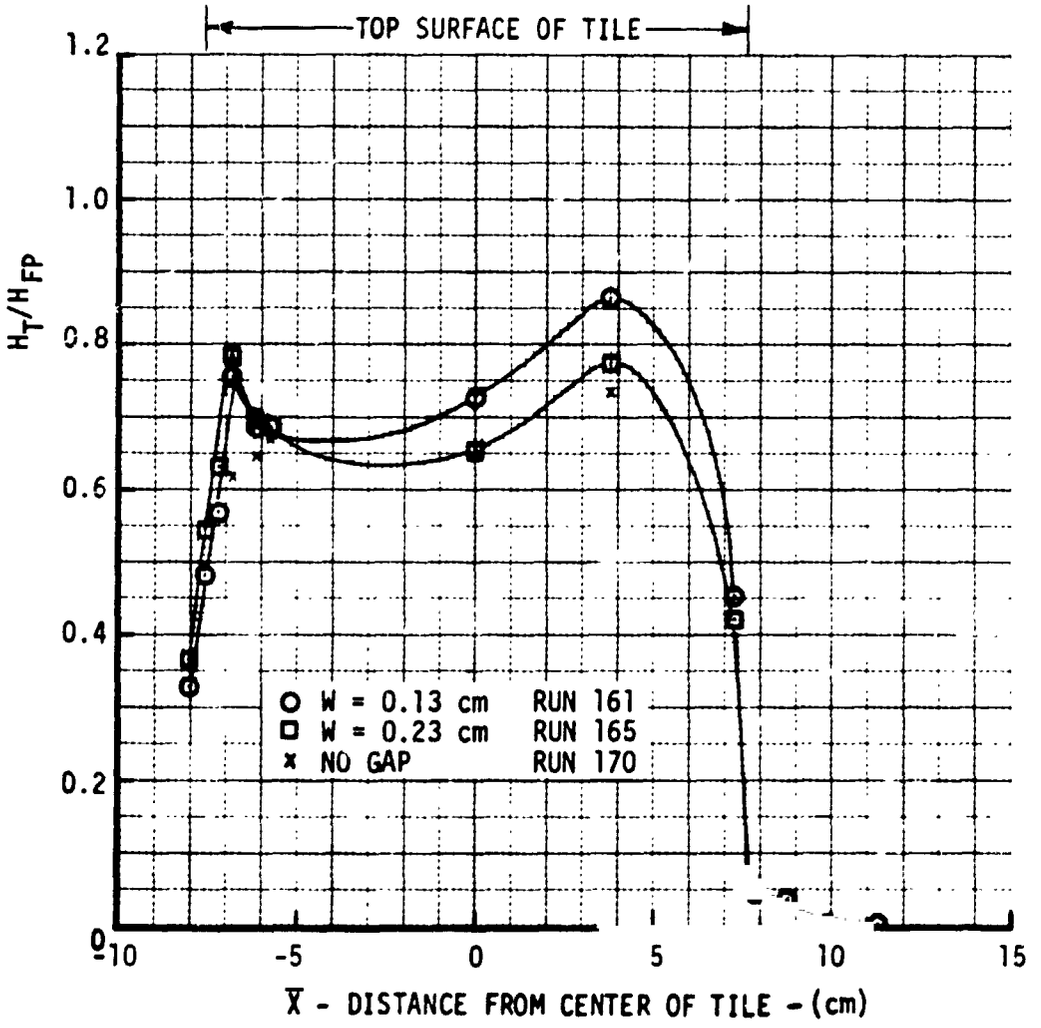

Figure 88

EFFECT OF GAP WIDTH ON STAGGERED TILE HEATING IN CFHT (Y = -7.3 CM)

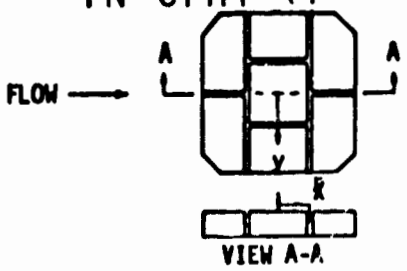

ALPHA = 0 DEG.
$Re_\infty/m = 3.3 \times 10^6$
$M_\infty = 10$

W = GAP WIDTH

Not corrected for C_p
Not corrected for conduction

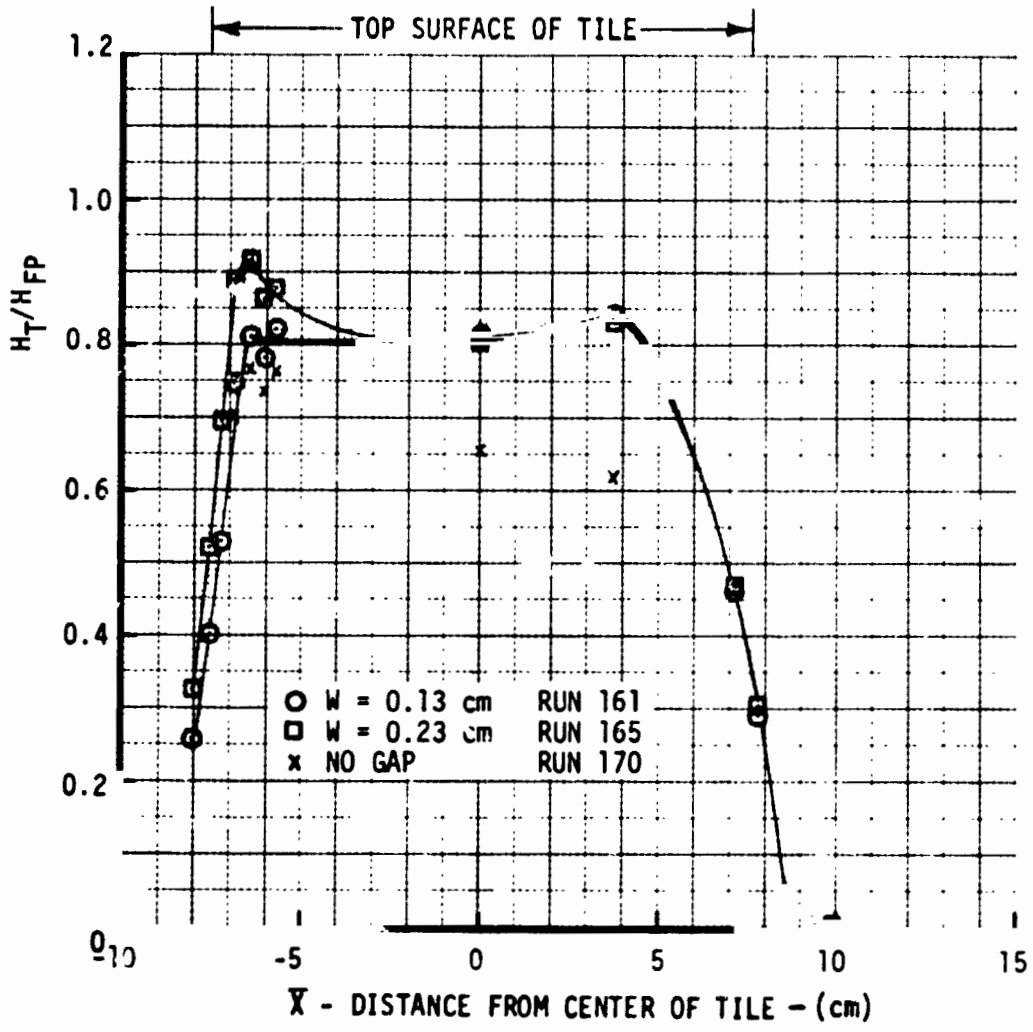

Figure 89

Y = -7.2 cm respectively. For each Y location, heating distributions are presented for the three gap widths investigated.

Similarly, results are presented for the in-line tile orientation in Figures 90 (Y = 0), 91 (Y = +7.2 cm), and 92 (Y = -7.2 cm).

Major conclusions drawn from these supplemental data are that the zero gap width condition shows a heating pattern very similar to that produced when a physical gap existed, heating ratios (H_T/H_{FP}) at the center of the tile exceeded the calibration plate heating, and surface heating decreases near the edges of the thin skin tile. The causes for these anomalies were investigated as reported in Sections 4.3.4 and 4.3.5. Also, the in-line gap configuration at all three lateral (Y) locations show a stronger sensitivity to gap width than does the staggered configuration. For both configurations, the heating patterns at the edges of the tile (Y = $\pm$ 7.2 cm) exhibit a lower level of heating which is also less sensitive to gap width than the centerline case.

A comparison of the data at the tile edges (Y = $\pm$ 7.2 cm) indicate the heating patterns deviate somewhat rather than being symmetric about the centerline. For both tile orientations (Figures 88 and 89 for staggered and Figures 91 and 92 for in-line), the heating at the leading edge is higher at Y = -7.3 cm than at Y = +7.2 cm. This deviation may be due to a slight mismatch in tile height causing a small step.

4.3.2 Comparison to Original CFHT Tests - The heating distributions obtained in these supplemental CFHT tests were compared to the original analyses reported in Section 4.1.3 of this report and also in Reference 1 . The comparison was made for the staggered tile configuration and for centerline (Y = 0) heating distributions. For both series of tests, tile thickness was 6.35 cm and the thin skin tile had an edge radius of 0.3775. Likewise, the test conditions were a Mach number of 10 and a unit Reynolds number per meter of 3.3×10^6. All data were corrected for thin skin tile specific heat variations (C_p) as described in Section 4.3.5.

The comparison between the supplemental and original distributions is shown in Figure 93 for gap widths of 0.127 and 0.229 cm. Both gap and top of the tile distributions are shown. Again, the tile heating has been normalized to the flat plate calibration heating. As seen, agreement is poor between the original and supplemental heating distributions, particularly on the top surface of the tile. The original data show a higher heating near the leading edge of the tile, while the supplemental test heating peaks near the center and aft edge of the tile. In

EFFECT OF GAP WIDTH ON IN-LINE TILE HEATING IN CFHT (Y = 0.0)

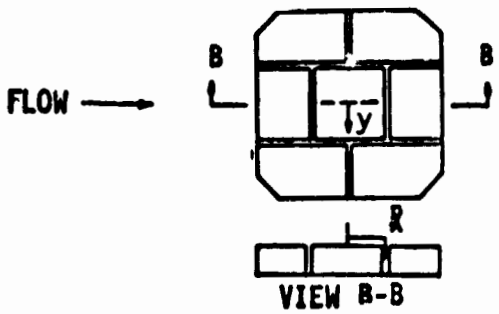

ALPHA = 0 DEG.
$Re_\infty/m = 3.3 \times 10^6$
$M_\infty = 10$

W = GAP WIDTH

Not corrected for C_p
Not corrected for conduction

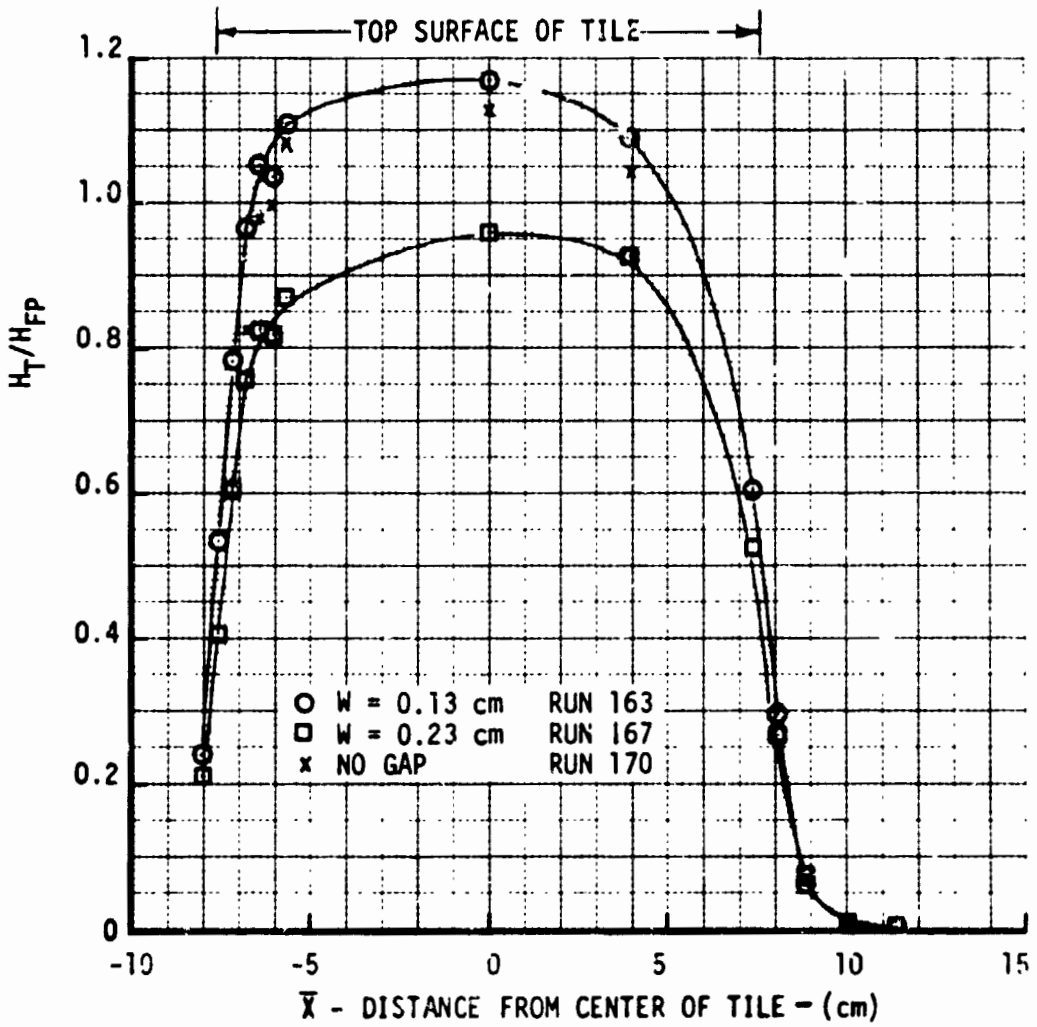

Figure 90

EFFECT OF GAP WIDTH ON IN-LINE TILE HEATING IN CFHT (Y = +7.2 CM)

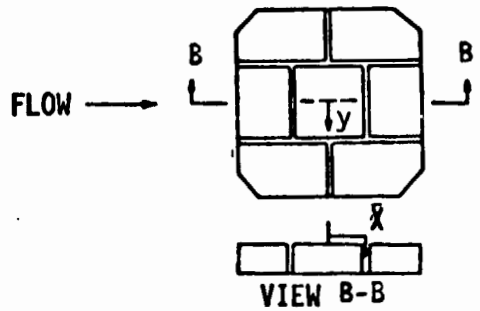

ALPHA = 0 DEG.
$Re_\infty/m = 3.3 \times 10^6$
$M_\infty = 10$

W = GAP WIDTH

Not corrected for C_p
Not corrected for conduction

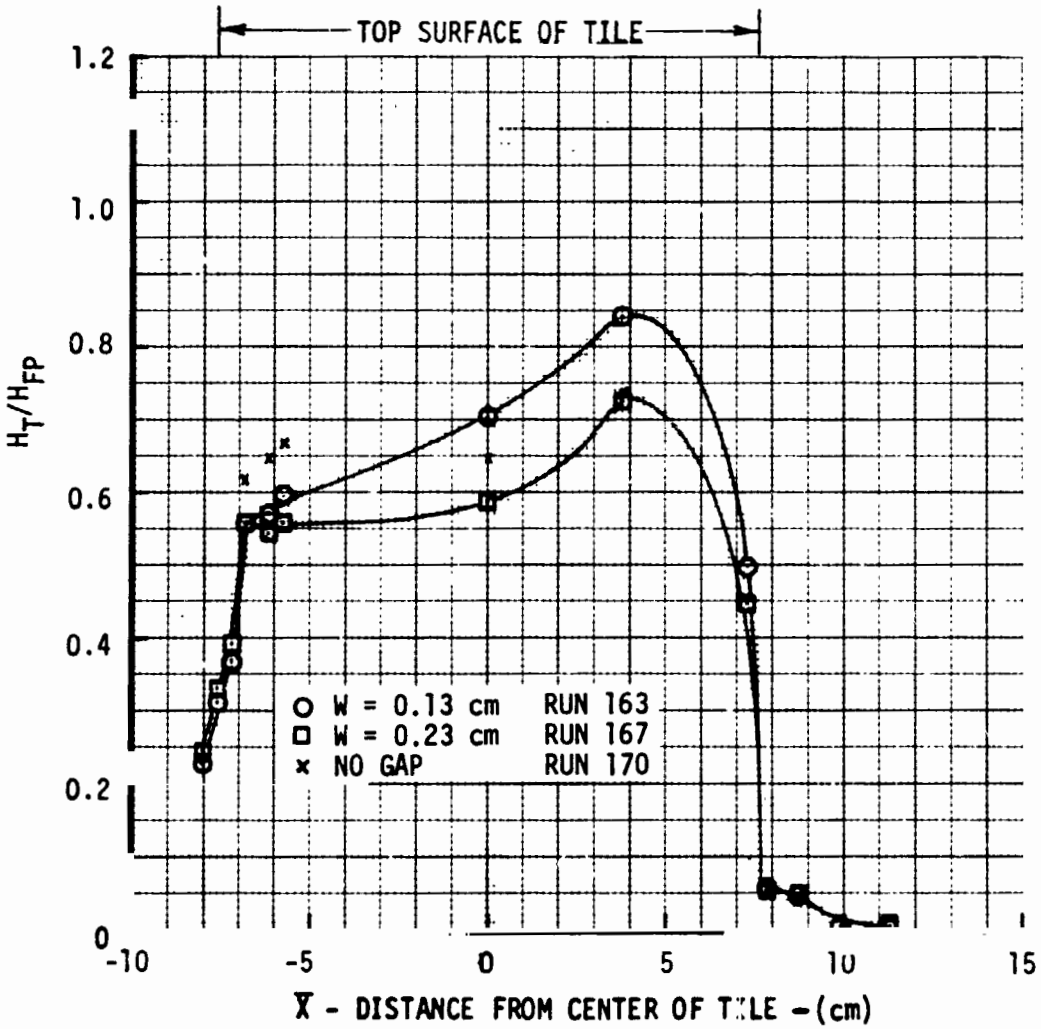

Figure 91

EFFECT OF GAP WIDTH ON IN-LINE TILE HEATING IN CFHT (Y = -7.3 CM)

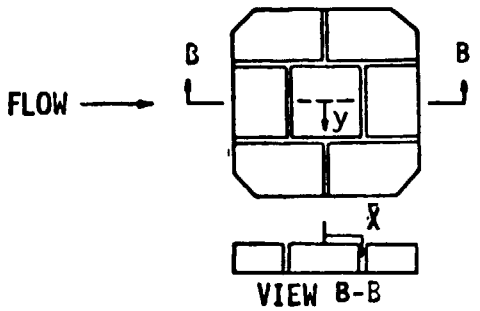

ALPHA = 0 DEG.
$Re_\infty/m = 3.3 \times 10^6$
$M_\infty = 10$

W = GAP WIDTH

Not corrected for C_p
Not corrected for conduction

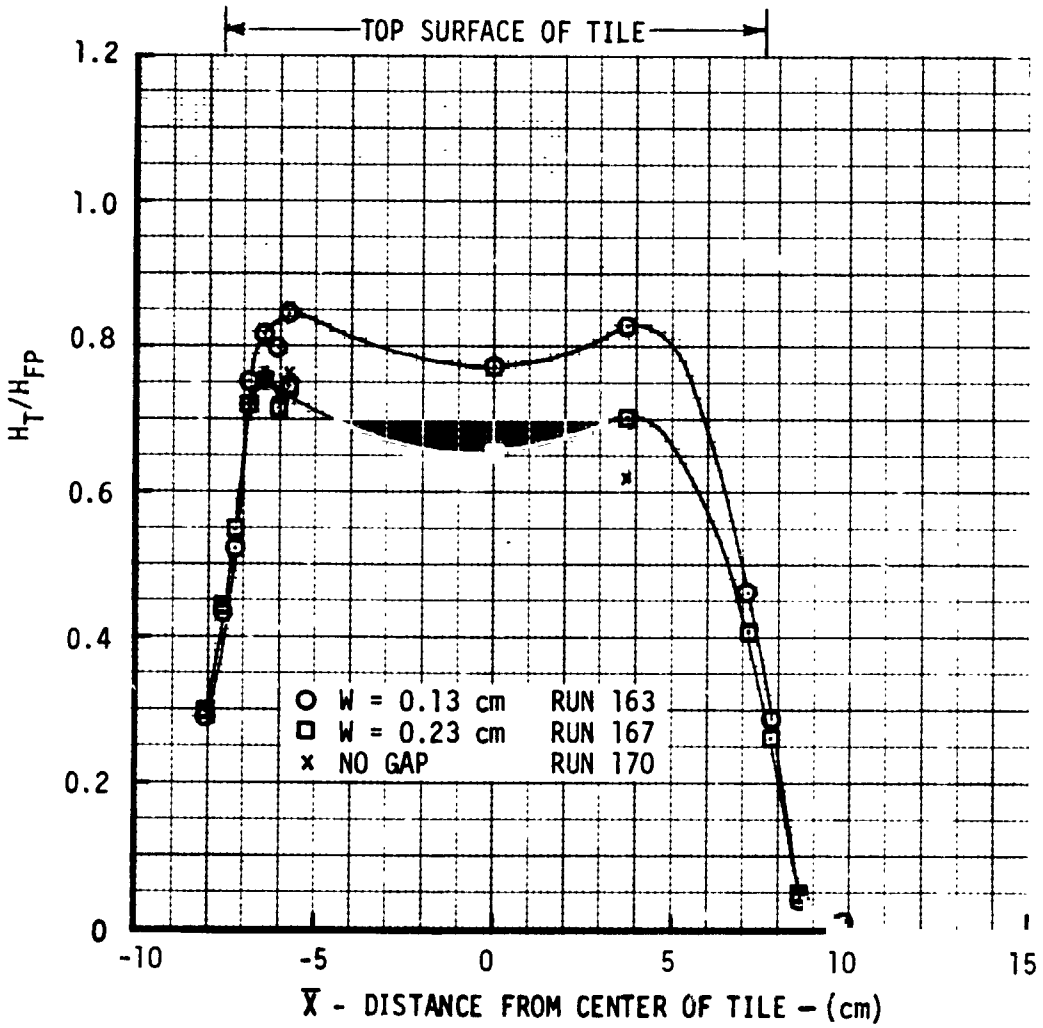

Figure 92

COMPARISON OF STAGGERED TILE HEATING FROM ORIGINAL RUNS AND SUPPLEMENTAL RUNS IN CFHT (Y=0.0)

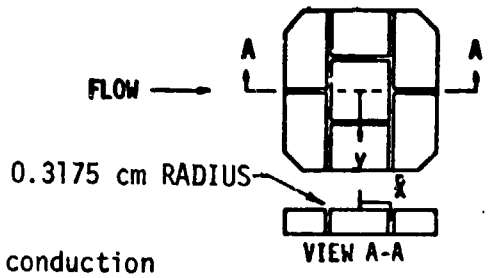

ALPHA = 0 DEG.
$Re_\infty/m = 3.3 \times 10^6$
$M_\infty = 10$

W = GAP WIDTH

C_p CORRECTED

Not corrected for conduction

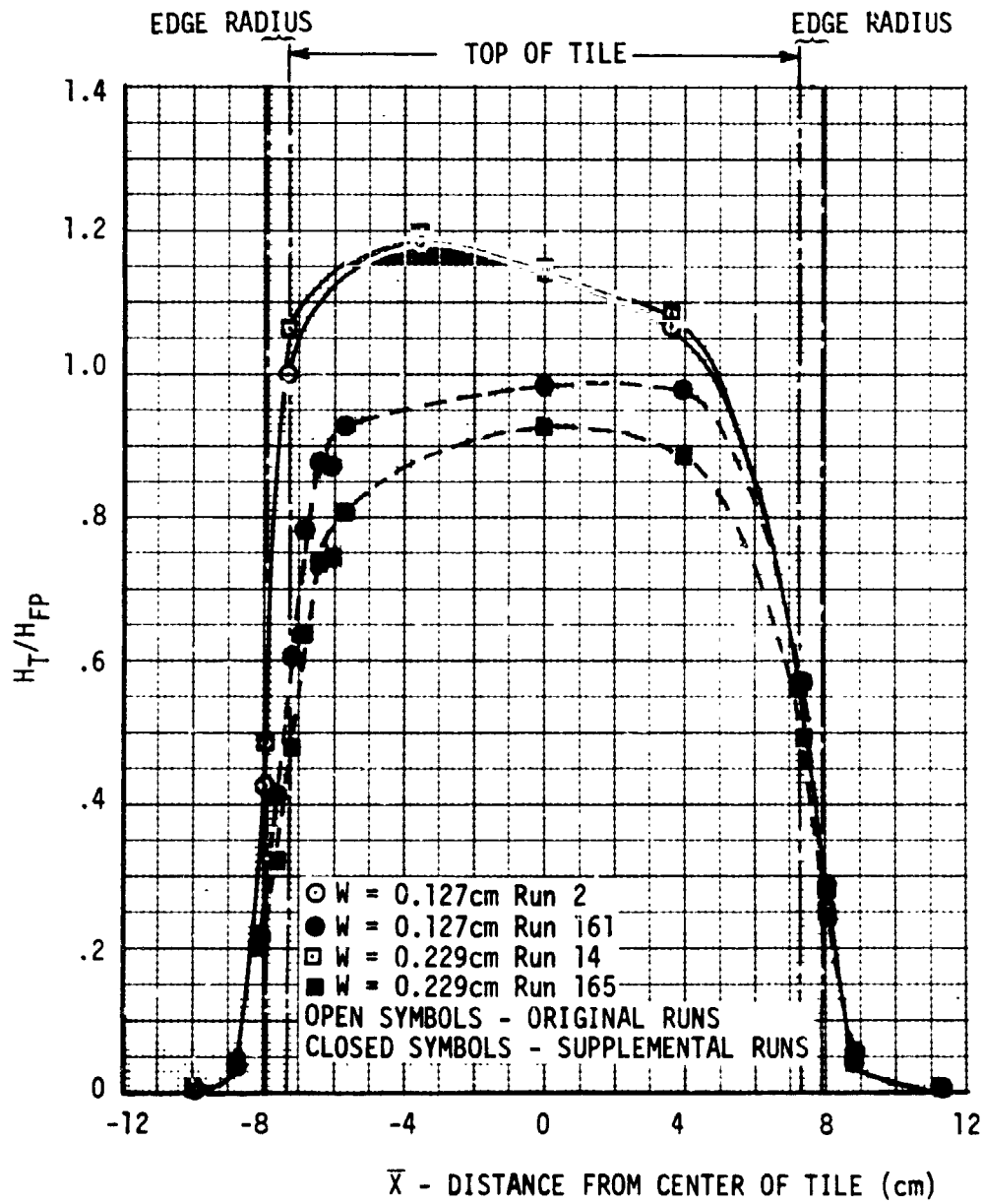

Figure 93

addition the original data are less sensitive to gap width variations. It is also noted that the original data, even after correction for specific heat variations, still exhibit higher heating on the top surface than the flat plate (i.e., $H_T/H_{FP} > 1.0$). The reason for the poor comparison between the supplemental and original heating distributions is unknown; possible causes could be tile mismatch, different instrumentation set points, and different test techniques.

The gap heating distributions were again compared using a different normalization parameter than flat plate heating. Since the heating in the gap and the heating on the top of the tile at the gap are interrelated, the feasibility of developing correlations in terms of H_T/H_{EDGE} was suggested. For example, by employing this parameter good agreement was obtained for gap heating (both the downstream and upstream face of the gap) between the supplemental and original data. These comparisons are made in Figures 94 and 95, again for the staggered tile orientation and center line distributions. In Figure 94, the Z distance into the gap is used as a reference, while in Figure 95 the distance down the gap is measured from the top of the tile and includes the edge radius. Using the latter reference improves the comparison, especially near the top of the gap.

4.3.3 Reynolds Number Effect on Heating Rates - One purpose of conducting additional tests was to determine the effect of higher Reynolds number on heating in the tile gaps. The original CFHT tests were all conducted at a Reynolds number per meter of 3.3×10^6, while supplemental tests were conducted at both 3.3×10^6 and 7.4×10^6. Test section Mach number was 10 for all runs.

The CFHT side wall heating was calibrated for both flow conditions used in the gap heating experiments. The heating distributions (Figure 96) are similar. Although the distributions are similar, individual calibration curves were used to normalize heating data for each Reynolds number test condition. The heat transfer coefficients (h_o) reported in the figure have been corrected for specific heat as discussed in Section 4.3.5.

The effect of increasing Reynolds number on tile heating is shown in Figure 97 for the staggered tile configuration and for the centerline (Y = 0) distribution. The heating at the higher Reynolds number flow condition has been referenced to the heating distributions at a Reynolds number of 3.3×10^6/m. For this reference case, the data were previously reported in Figure 87. Results are presented in the figure for gap widths of 0.0, 0.127 and 0.229 cm. As seen, the effect of higher Reynolds number is to double heat transfer coefficients on the tile surface. Within the gap the heating increases by factors varing from 1 to 3, depending upon gap width and location within the gap.

STAGGERED TILE GAP HEATING IN CFHT (Y ≃ 0.0)

⊙ W = 0.127cm Run 2
● W = 0.127cm Run 161
⊡ W = 0.229cm Run 14
■ W = 0.229cm Run 165
△ W = 0.457cm Run 31
◇ W = 0.711cm Run 120
OPEN SYMBOLS - ORIGINAL RUNS
CLOSED SYMBOLS - SUPPLEMENTAL RUNS

H_{EDGE} MEASURED AT S = 0.0
M_∞ = 10
$R_{e\infty}/m = 3.3 \times 10^6$
W = GAP WIDTH
EDGE RADIUS = 0.3175cm
Not corrected for conduction

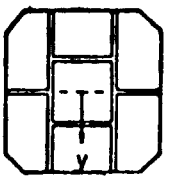

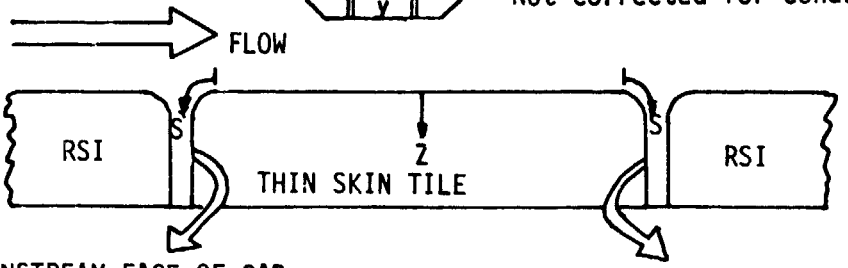

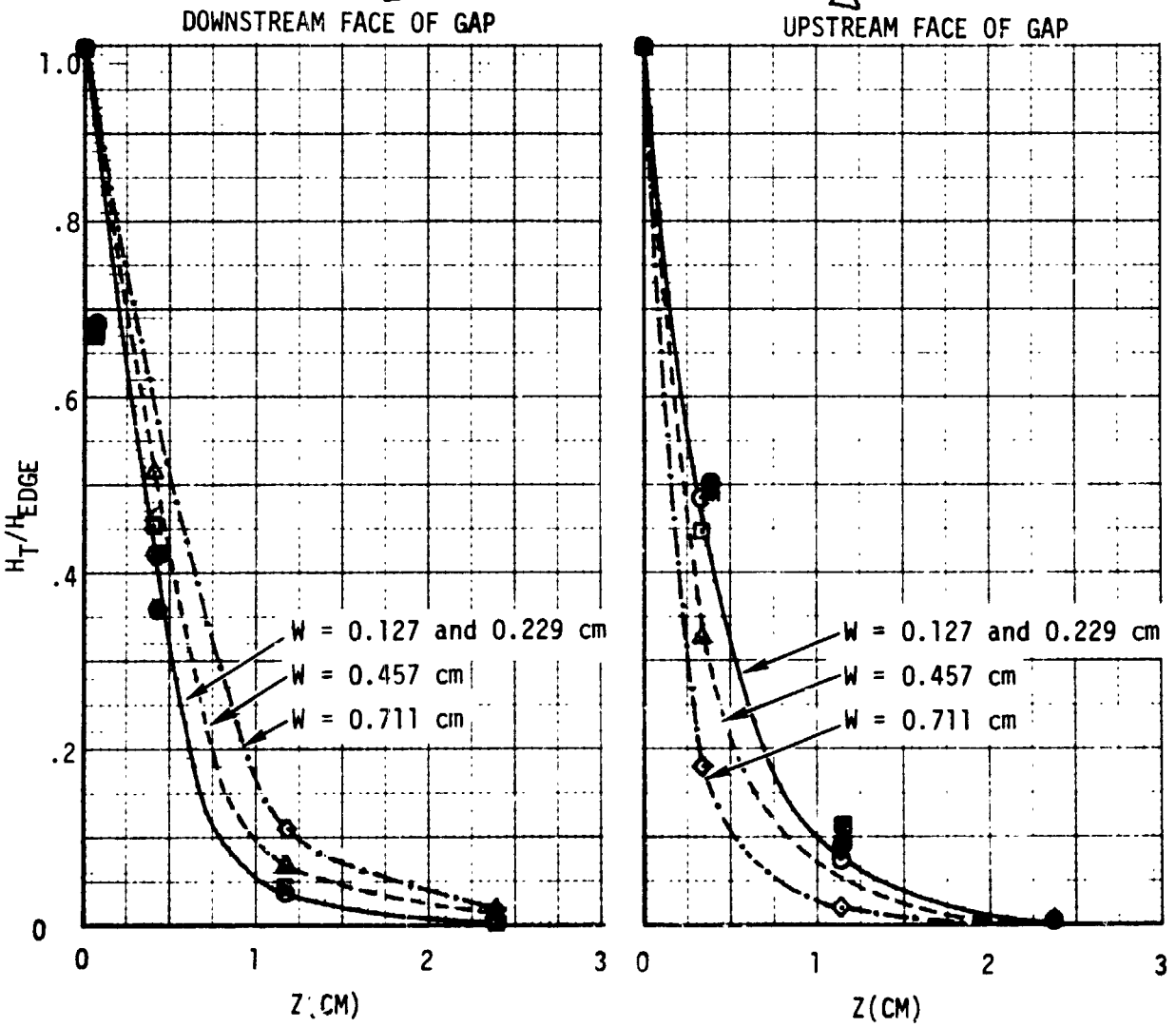

Figure 94

STAGGERED TILE GAP HEATING IN CFHT (Y = 0.0)

- ⊙ W = 0.127cm Run 2
- ● W = 0.127cm Run 161
- ⊡ W = 0.229cm Run 14
- ■ W = 0.229cm Run 165
- △ W = 0.457cm Run 31
- ◇ W = 0.711cm Run 120

OPEN SYMBOLS - ORIGINAL RUNS
CLOSED SYMBOLS - SUPPLEMENTAL RUNS

H_{EDGE} MEASURED AT S = 0.0
M_∞ = 10
$R_{e\infty}/m = 3.3 \times 10^6$
W = GAP WIDTH
EDGE RADIUS = 0.3175cm
Not corrected for conduction

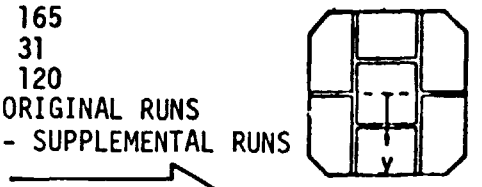

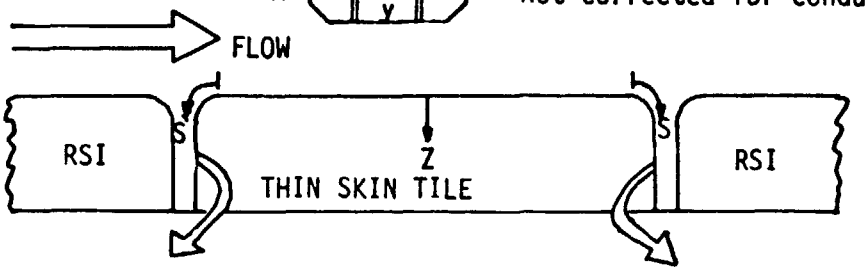

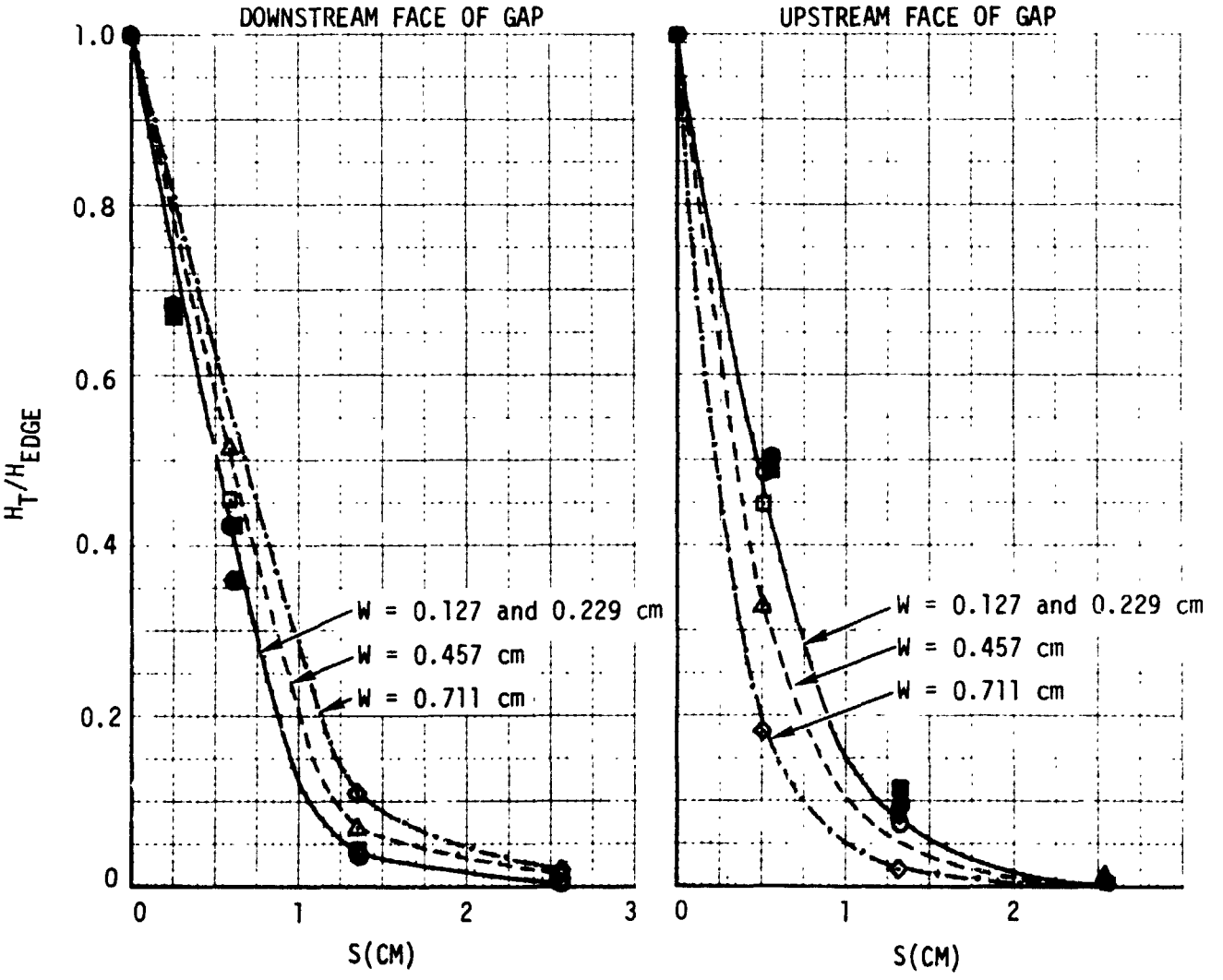

Figure 95

HEAT TRANSFER DISTRIBUTION [$H_{FP} \cdot F_I(Y)$] ON FLAT PLATE MOUNTED ON CFHT SIDEWALL

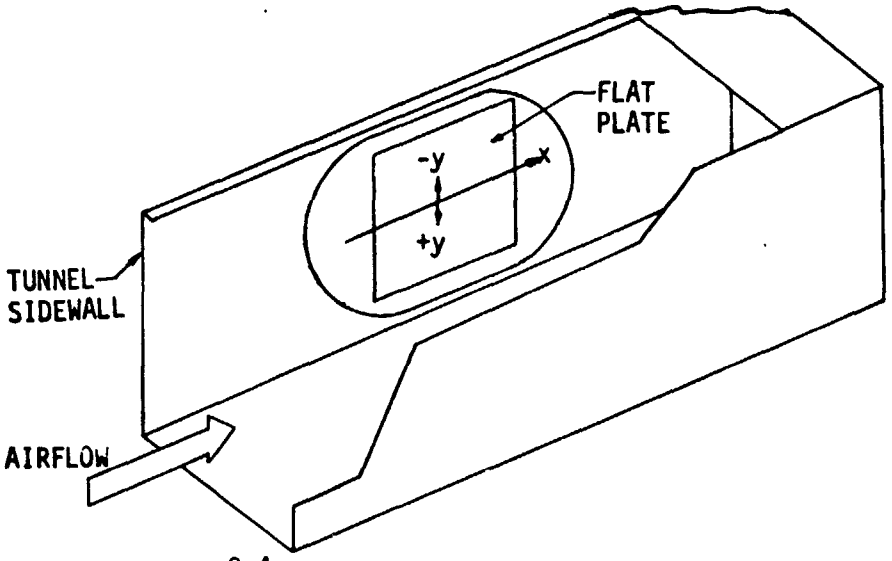

	○	□
M_∞	10.33	10.29
$Re_{\infty/m}$	3.28×10^6	7.38×10^6
$h_{y=o}$ $\left(\frac{W}{m^2\ ^oC}\right)$	2.718	5.003

$T_{AW}/T_T = 0.895$

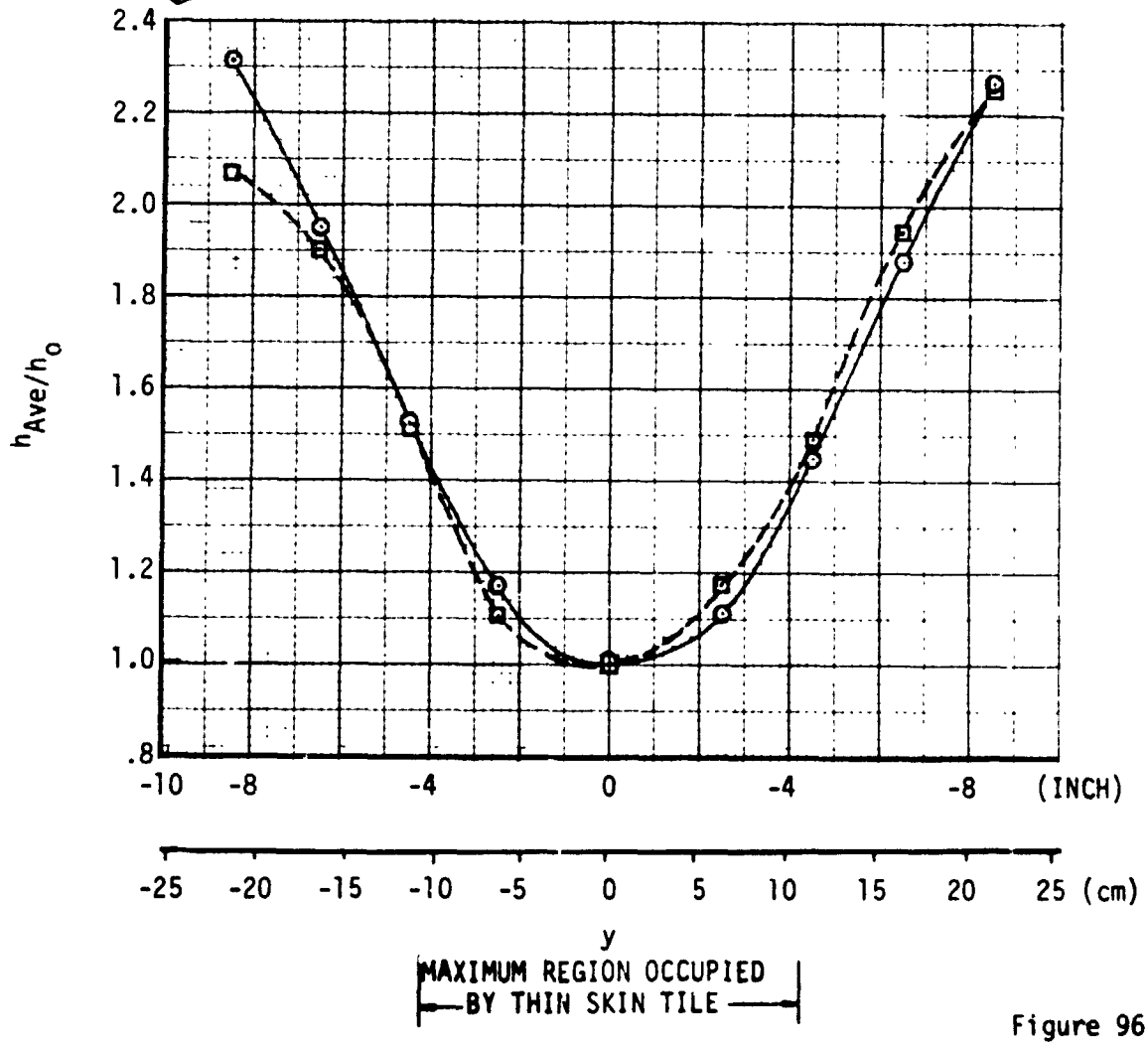

Figure 96

EFFECT OF REYNOLDS NUMBER ON STAGGERED TILE HEATING IN CFHT (Y = 0.0)

ALPHA = 0.0 DEG.
M_∞ = 10
W^∞ = GAP WIDTH
Cp CORRECTED
CONDUCTION CORRECTED

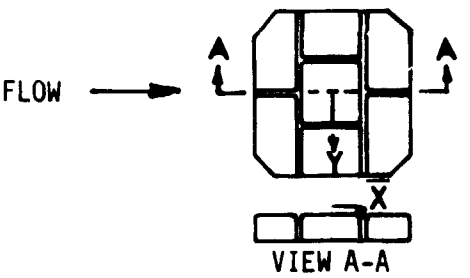

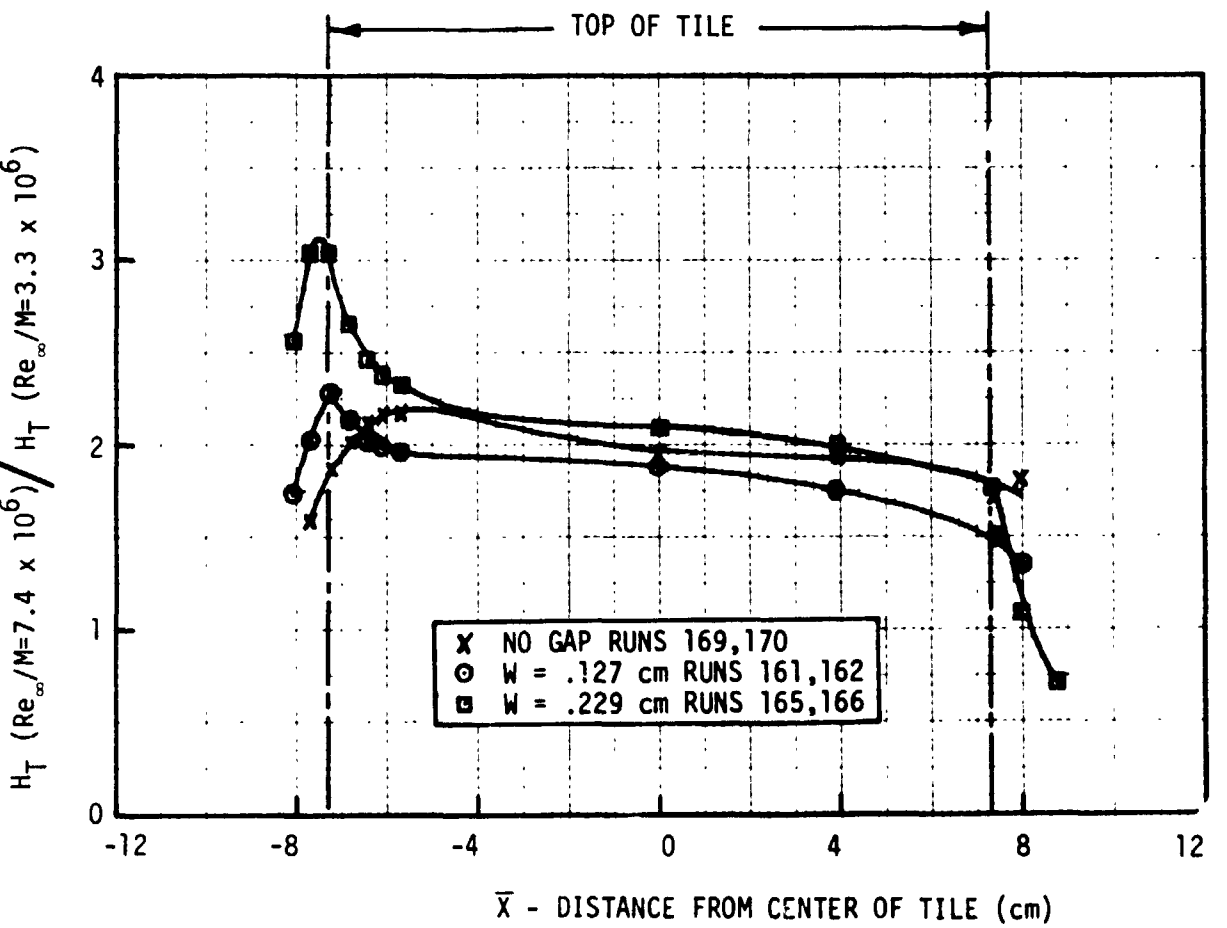

Figure 97

4.3.4 Investigation of Decrease in Surface Heating at Tile Edges - The heating data taken in the CFHT during both the original and supplemental test runs exhibited characteristics which have not been satisfactorily explained. This characteristic is a decrease in surface heating near the edge of the thin skin tile as seen in Figure 87 through 93 for both staggered and in-line tile configurations. Some of the possible reasons for this lower heating level are:

a) Flow phenomena produced by the presence of the gaps

b) Transient conduction effects in the thin skin tile

c) Thickness variations in the thin skin tile

Gap Flow Phenomena - Ten gap heating runs (See Figure 86) were made during the supplemental test program. Two of these runs were made with dental plaster in the gaps (zero gap width) to show the effect of gaps on tile surface heating. Figure 87 presents the measured heating distribution along the centerline of the tile for zero, 0.13 cm, and 0.23 cm gap width. It can be seen that the heating rate decreases near the front edge of the top surface for the zero gap run as well as for the runs with gaps present. This suggests that flow phenomena associated with gaps are not the cause of the decrease in measured surface heating rate near the tile edge. Since the filled gap runs did not produce a flat plate heating distribution on the tile surface, it was decided to take a detailed look at conduction in the thin skin tile for a filled gap run.

Temperature distributions along the centerline of the thin skin tile for a typical open gap run and the two filled gap runs are shown in Figure 98. These distributions were measured at the time when heating rates were evaluated. The open gap distribution shows a temperature gradient between the surface and the gaps which is due to preheating of the tile during the insertion procedure. This distribution is typical of the distributions existing in open gap tests. The filled gap was achieved by placing dental plaster in the gaps to an approximate depth of 0.64 centimeters from the top surface. The surface of the dental plaster was allowed to harden and then sanded until a smooth transition between tiles was achieved. It is apparent from the measured temperature distributions that the dental plaster was much cooler than ambient when the tests were run. The first filled gap run had measured gap temperatures as low as 6.1°C, while the top of the tile was at 27.6°C at its center. The second gap run (170) also had severe temperature gradients within the tile. These initial temperature gradients are the probable cause for failure of the filled gap tests to produce a flat plate heating distribution on the tile surface.

CFHT THIN SKIN TILE TEMPERATURE DISTRIBUTION

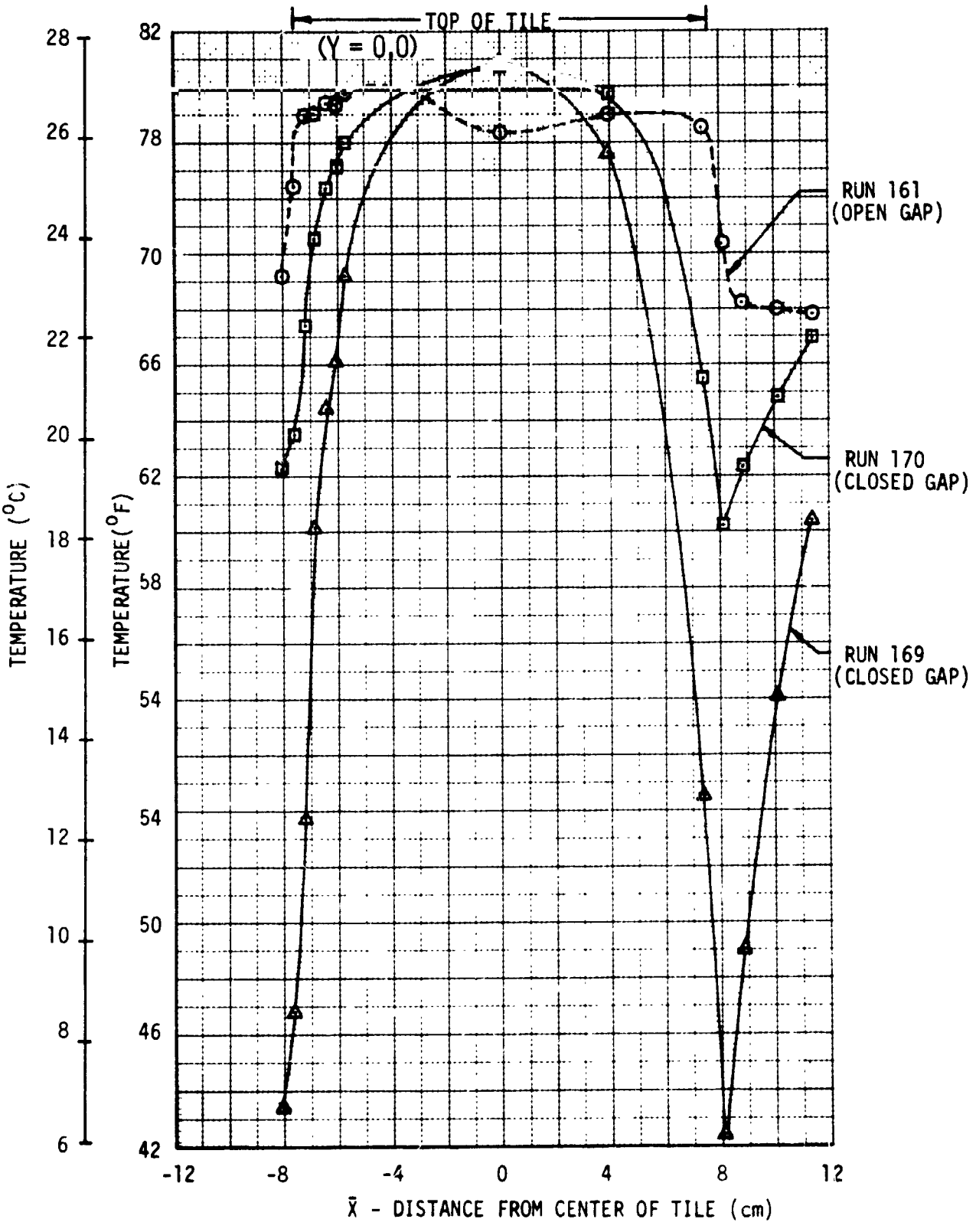

Figure 98

Transient Conduction Effects in Thin Skin Tile - Run 170 was evaluated to determine if correcting the measured heating rates for conduction would result in a uniform heating distribution on the tile surface. To evaluate the effect of transient conduction on the heating rate, the second derivative of temperature with respect to distance ($\partial^2 T/\partial \bar{X}^2$) must be determined. The methods used to calculate the second derivatives are shown in Figure 99. One method was to hand fair a smooth curve through the measured temperatures and numerically determine the second derivative using 3 points from the curve. A range of values was obtained due to uncertainties inherent in reading the hand faired curve. Another approach employed a fourth order least squares curve fit using seven data points to determine the temperature as a function of distance. The second derivative was then evaluated at the center data point. The third method used was a second order curve fit using three data points. The second derivative was evaluated at the center data point.

Figure 99 presents a summary of the second derivatives for the surface thermocouples. Also shown is the uncorrected and corrected nondimensionalized heat transfer coefficients (H_T/H_{FP}). These coefficients are presented in Figure 100 as a function of distance from the center of the tile. The conduction corrected coefficients are shown as a range of values as computed by the three methods. The open symbols display the characteristic surface heating distribution that has been observed in all the CFHT tests. In general, the conduction correction results in an insignificant change in the heat transfer coefficient. The thermocouple located at $\bar{X} \approx -7.62$ cm is known to be covered with dental plaster and thus should not have experienced convective heating. The conduction correction tends to reduce the coefficient toward zero at this location. The heating at locations -7.21 cm and +7.40 cm is not significantly affected by correcting for conduction. In addition, the level of heating at these locations is approximately the same as is measured with open gaps (See Figure 87).

It appears that neither conduction or gap flow phenomena (i.e., the presence of dental plaster) adequately explains the low heating measured at these locations. Correcting for conduction made a non-trivial change in the heat transfer coefficient at $\bar{X} = -6.85$ cm. The remaining thermocouples show very little effect of conduction on measured heating.

The above conclusions are reinforced by the comparison of conduction-corrected and uncorrected heating rates for Run 161 shown in Figure 101.

SUMMARY OF CONDUCTION CALCULATION METHODS CFHT RUN 170

$\bar{X}$ (cm)	H_T/H_{FP} UNCORRECTED	$\partial^2 T/\partial \bar{X}^2$			(H_T/H_{FP}) CORRECTED		
		HAND FAIRING ($^oC/cm^2$)	4TH ORDER CURVE FIT ($^oC/cm^2$)	2ND ORDER CURVE FIT ($^oC/cm^2$)	HAND FAIRING	4TH ORDER CURVE FIT	2ND ORDER CURVE FIT
-7.62	.358	-	7.824	8.891	-	.176	.152
-7.21	.615	1.111	-1.892	-1.300	.589	.659	.645
-6.85	.826	-2.222 to -8.333	-5.746	-5.822	.872 to 1.021	.960	.962
-6.43	.980	-1.389 to -3.056	-2.578	-3.322	1.013 to 1.051	1.040	1.058
-6.06	1.000	-0.556 to -1.667	-2.337	0.306	1.013 to 1.039	1.055	.993
-5.68	1.080	-0.556 to -0.833	-0.667	-0.347	1.093 to 1.100	1.096	1.088
0.0	1.126	-0.139 to -0.278	.020	-0.084	1.129 to 1.132	1.126	1.128
3.95	1.040	-0.278	-0.414	-0.406	1.046	1.050	1.050
7.40	.564	-1.944 to -2.778	-1.407	-1.336	.609 to .629	.597	.595

Not corrected for C_p

Figure 99

CFHT TILE SURFACE HEATING WITH CLOSED GAP

- RUN 170
- M_∞ = 10
- $Re_\infty/m = 3.3X10^6$

LEGEND
⊙ HEAT TRANSFER COEFFICIENT BASED ON HEAT STORAGE ONLY
I RANGE OF CONDUCTION CORRECTED HEAT TRANSFER COEFFICIENTS
—— ESTIMATED SURFACE HEATING
--- ESTIMATED SURFACE HEATING ± 5%

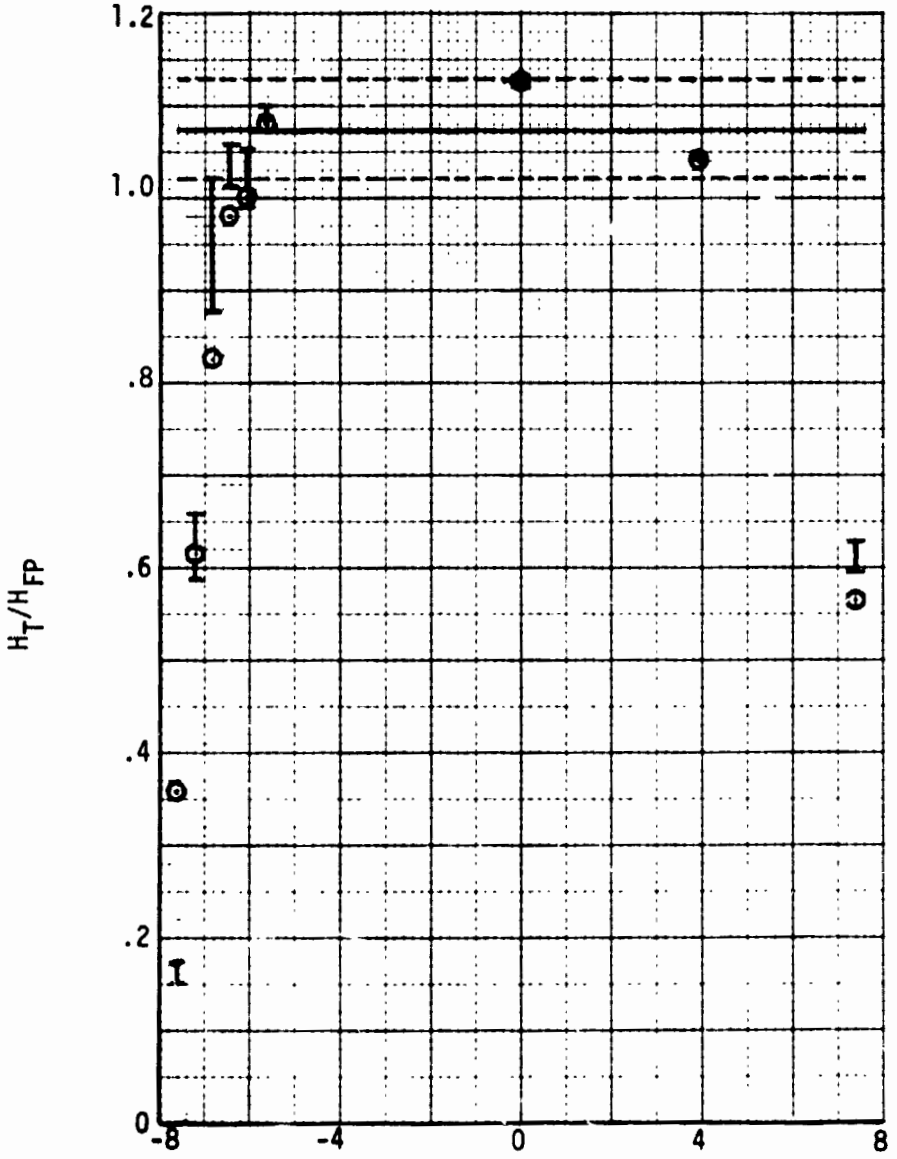

Not corrected for C_p

Figure 100

COMPARISON OF CONDUCTION CORRECTED AND UNCORRECTED HEATING IN CFHT (Y = 0.0)

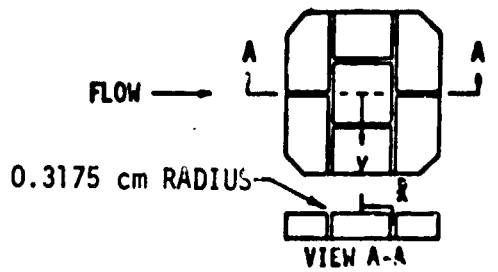

RUN 161
GAP WIDTH = 0.127 CM
C_p CORRECTED
M^∞ = 10
R_e /m - 3.3 x 10^6

CONDUCTION CORRECTED
UNCORRECTED

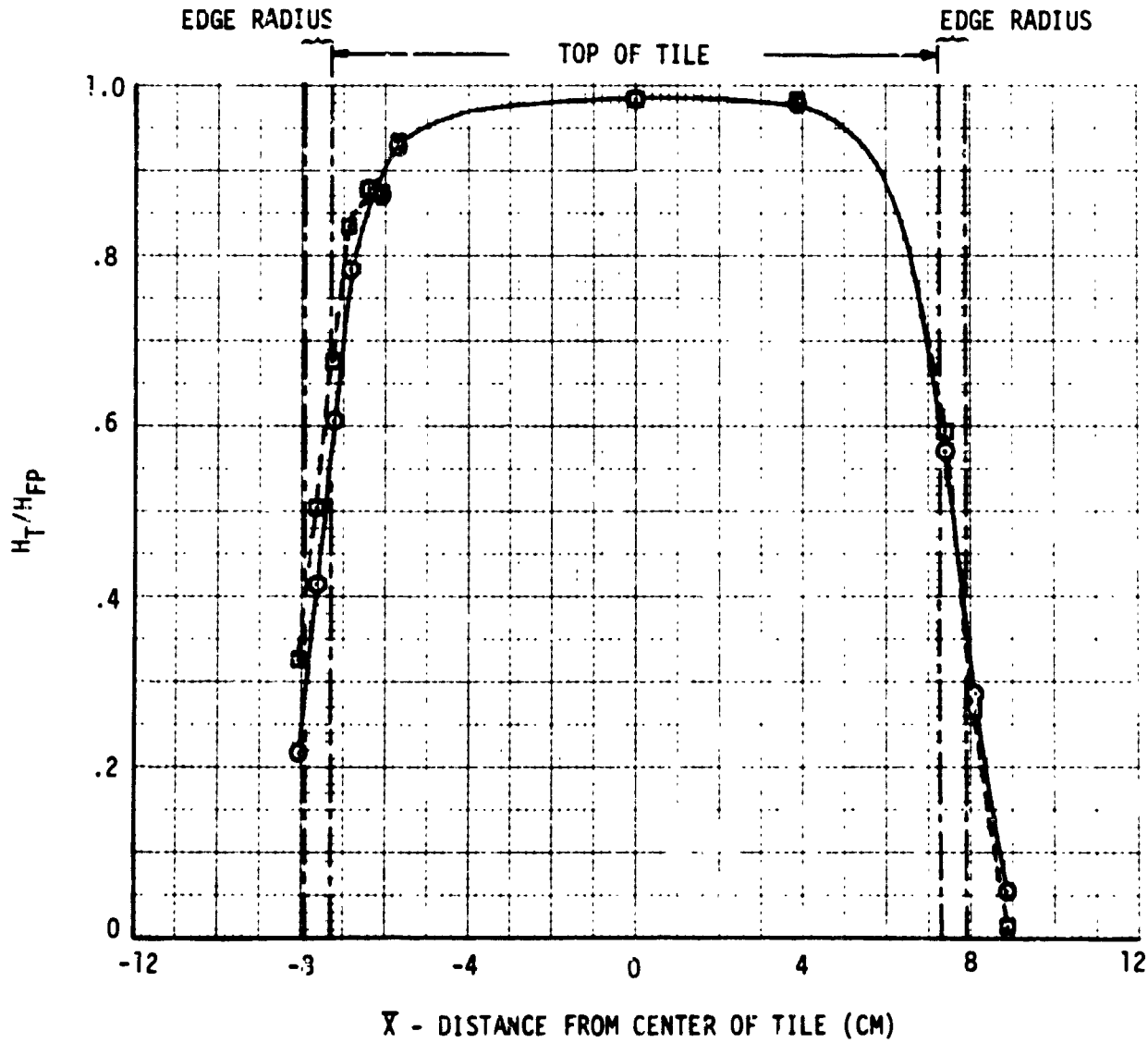

Figure 101

Concurrently with the above analysis, a calculation package was added to the data reading program used to input test results to the Data Bank. The package arranges data from adjacent instrumentation so that the second derivatives in both (x) and (y) directions can be computed. The correction on heat transfer coefficient is implemented as follows:

$$h_{corrected} = \frac{1}{T_{AW}-T_W}\left[\rho z C_p \frac{\partial T}{\partial \theta} - kz\left(\frac{\partial^2 T}{\partial x^2} + \frac{\partial^2 T}{\partial y^2}\right)\right]$$

$$h_{corrected} = h_{\substack{\text{HEAT}\\ \text{STORAGE}\\ \text{only-}}} - \frac{kz}{(T_{AW}-T_W)}\left(\frac{\partial^2 T}{\partial x^2} + \frac{\partial^2 T}{\partial y^2}\right)$$

Thickness Variations in the Thin Skin Tile - The expected variation in measured heat transfer coefficient due to tile skin thickness uncertainties is also shown in Figure 100. The thickness of the tile was measured by LaRC personnel and was found to be within $\pm$ 5 percent of the nominal thickness of .0254 cm. The dashed lines represent the possible heat transfer coefficient variation around an estimated surface heating level due to a 5% uncertainty in tile thickness. By including both conduction effects and tile skin thickness uncertainties, it is possible to conclude that uniform heating occurred on the surface for all locations but $\bar{X}$ = -7.21 cm and +7.40 cm. However, to do so one must assume worst-on-worst conditions.

In summary, no definite conclusion has been drawn as to the cause of the measured heating drop off near the edge of the thin skin tile. It has been shown that the heating distribution is similar for both the open and filled gap runs. This implies that the presence of gaps does not cause the drop off of measured heating near the edge of the tile. It also does not appear that conduction alone can explain the surface heating distribution. It should be noted that the thermocouples used in these tests were not calibrated as installed, thus, the temperature differences between thermocouples are not precisely known. Because of this, the conduction corrections that were calculated have an additional uncertainty.

It is suggested that the filled gap runs be neglected due to uncertainties in the conduction correction calculations and the measured temperatures. It was also shown that tile thickness uncertainties do not alone account for the surface heating variation. It is possible by combining conduction effects and thickness uncertainties, under the most favorable conditions, to conclude that uniform convective heating was experienced by the tile surface except for locations $\overline{X}$ = -7.21 cm and + 7.40 cm. These locations appear to have an additional heat sink which has not been explained.

4.3.5 Investigation of Tile and Calibration Plate Specific Heat Differences - Another characteristic exhibited by the heating data obtained in the CFHT tests was the greater heating rates on the tile top surface than that measured on the flat calibration plate. For both the original and supplemental tests, the measured heating rate on the top of the tile (away from the edge) was consistently from 10% to 20% higher than that measured on the companion calibration plate. It was determined that the specific heat of the thin skin tile (Type 304 stainless steel) used in data reduction was approximately 20% higher than that used in reducing the calibration plate (Type 321 stainless steel) data.

The calibration plate was fabricated from 0.0508 cm 321 stainless steel and the thin skin tile was made from a sheet of 304 stainless steel (0.0254 cm thick). Nominal values for the specific heat of both materials were used in the data reduction ($C_{P_{304}}$=0.12 and $C_{P_{321}}$=0.1019 Cal/gm^{o}C). To verify the correctness of these values the specific heat of a coupon cut from the two test articles was measured. The specific heat was measured at LaRC using the same equipment and technique on both specimens. Figure 102 contains the measurements and specific heat ratio. It was necessary to extrapolate down to 300^{o}K where the wind tunnel tests were conducted. The measured specific heat values used for correcting the data are $C_{P_{304}}$=0.112 and $C_{P_{321}}$=0.1045 Cal/gm^{o}C. This reduces the H_T/H_{FP} ratio by 9%. The computer program has been modified to automatically correct the CFHT data.

Figure 103 shows graphically the effects of the specific heat correction on tile heating. The correction was made on Runs 161 and 165 which are for the staggered tile configuration and gap widths of 0.13 and 0.23 cm. As seen in the figure, use of the C_p correction reduces the heating on top of the tile to less than that measured for the flat calibration plate. Subsequently, all test data have been corrected.

SPECIFIC HEAT MEASURED ON THIN SKIN MATERIALS USED IN LaRC CFHT TESTS

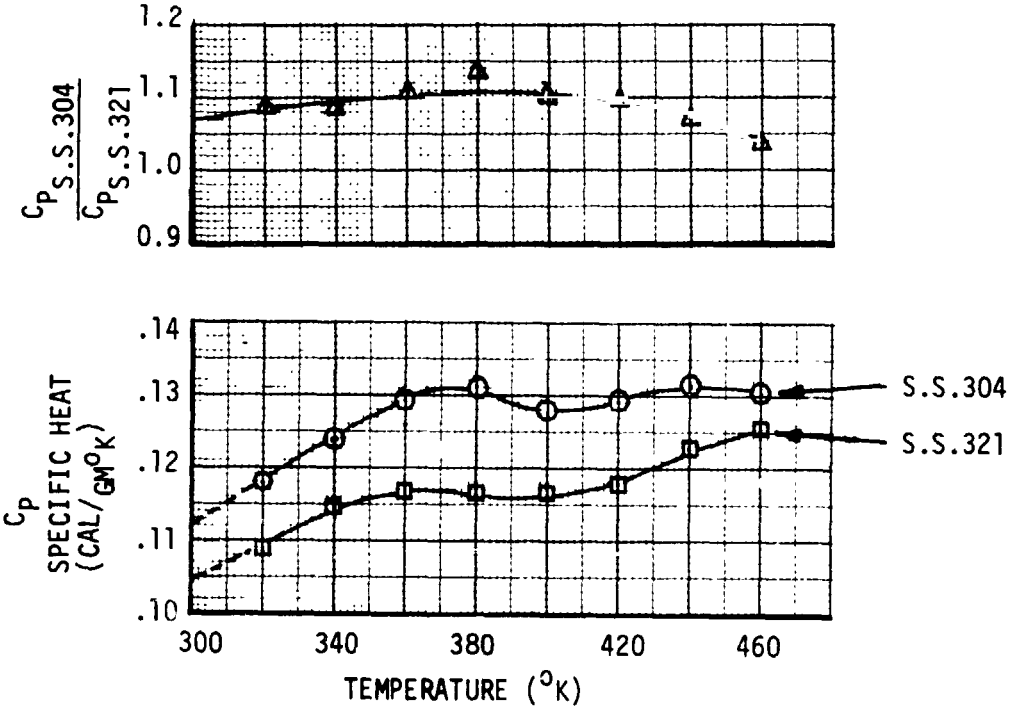

TEMPERATURE (°K)	SPECIFIC HEAT (CAL/GM°K)	
	TILE (S.S.304)	FLAT PLATE (S.S.321)
320	0.11808	0.10859
340	0.12368	0.11411
360	0.12948	0.11678
380	0.13131	0.11602
400	0.12797	0.11621
420	0.12922	0.11761
440	0.13147	0.12295
460	0.13053	0.12556

REFERENCE: D. A. THROCKMORTON NASA LaRC 8-21-74

Figure 102

EFFECT OF SPECIFIC HEAT CORRECTION ON STAGGERED TILE HEATING IN CFHT (Y = 0.0)

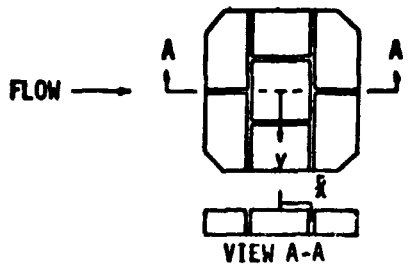

ALPHA = 0 DEG.
$Re_\infty/m = 3.3 \times 10^6$
$M_\infty = 10$

W = GAP WIDTH

Not corrected for conduction

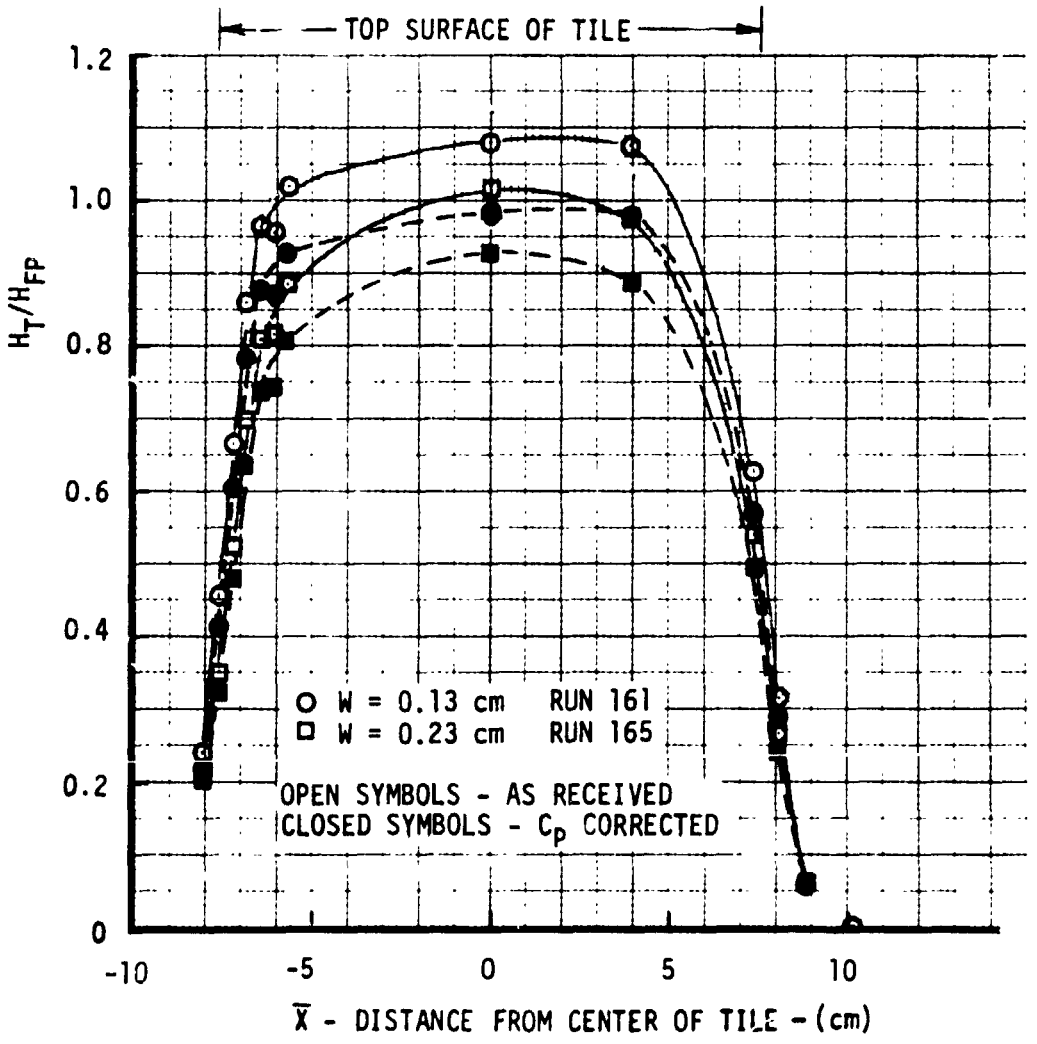

Figure 103

4.4 Analysis of Edge Radius Tests at NASA JSC - Analyses were performed on data obtained from gap heating tests on thin skin tiles with various edge radii. The tests were conducted by C. D. Scott of NASA, Johnson Space Center in the JSC 10 MW Arc Tunnel. Major purposes of the tests were to investigate the effect of tile edge radii on gap heating and to compare thin skin tile and RSI tile heating distributions obtained in the same tunnel. The test conditions, model description, and data assimilated are discussed in Section 3.4 and Volume II of this report.

The test employed sets of thin skin metallic tiles mounted in a wedge test fixture inclined at 15° angle-of-attack. The test article was inserted alternately with a calibration panel into the flow field produced by the 20 inch diameter conical nozzle. Four edge radii (0.157, 0.3175, 0.635, and 1.27 cm) were parametrically tested at gap widths of 0.127, 0.254, and 0.381 cm. The joint configuration was an in-line butt, and the tile thickness was 4.1275 cm for all tests.

In the following sections, results from these tests are reported and compared with gap heating distributions obtained in the same tunnel using RSI tiles.

4.4.1 Analysis and Comparison - Twelve tests were conducted on the thin skin tiles with four edge radii and three gap widths. Heating distributions for the minimum edge radius tiles are compared with data from RSI tiles in Figures 104 thru 107. The RSI tile heating distributions were computed from test data taken in the JSC 10 MW channel nozzle as reported in Reference 1 . Figures 104 and 105 present transverse gap data for gap widths of 0.381 and 0.254 cm respectively. Distributions are shown for the RSI tile thicknesses of 3.18 cm and 5.08 cm. The thin skin tile data are normalized by both flat plate and surface heating rates. The flat plate heating rate was measured on the calibration plate, while the surface heating rate was measured on the thin skin tile surface forward of the transverse gap. For both gap widths, the heating rates measured on the thin skin tile are shown to be higher than those derived from RSI tile data.

Figures 106 and 107 compare in-line gap heating data from thin skin and RSI tile tests for gap widths of 0.381 cm and 0.254 cm. The thin skin tile data are significantly higher than the RSI tile data for the in-line case.

A comparison of the heating to the upstream and downstream walls of a transverse gap are shown in Figure 108. These data are from the thin skin tile array having a corner radius of 0.318 cm and includes three gap widths (0.127, 0.254, and 0.381 cm). The heating on the downstream side of the gap is higher than that

COMPARISON OF THIN SKIN TILE AND RSI TILE TRANSVERSE GAP HEATING DATA

- GAP WIDTH = .381 cm
- DOWNSTREAM SIDE OF GAP
- JSC 10 MW ARC TUNNEL
- CORNER RADIUS = 0.157 cm

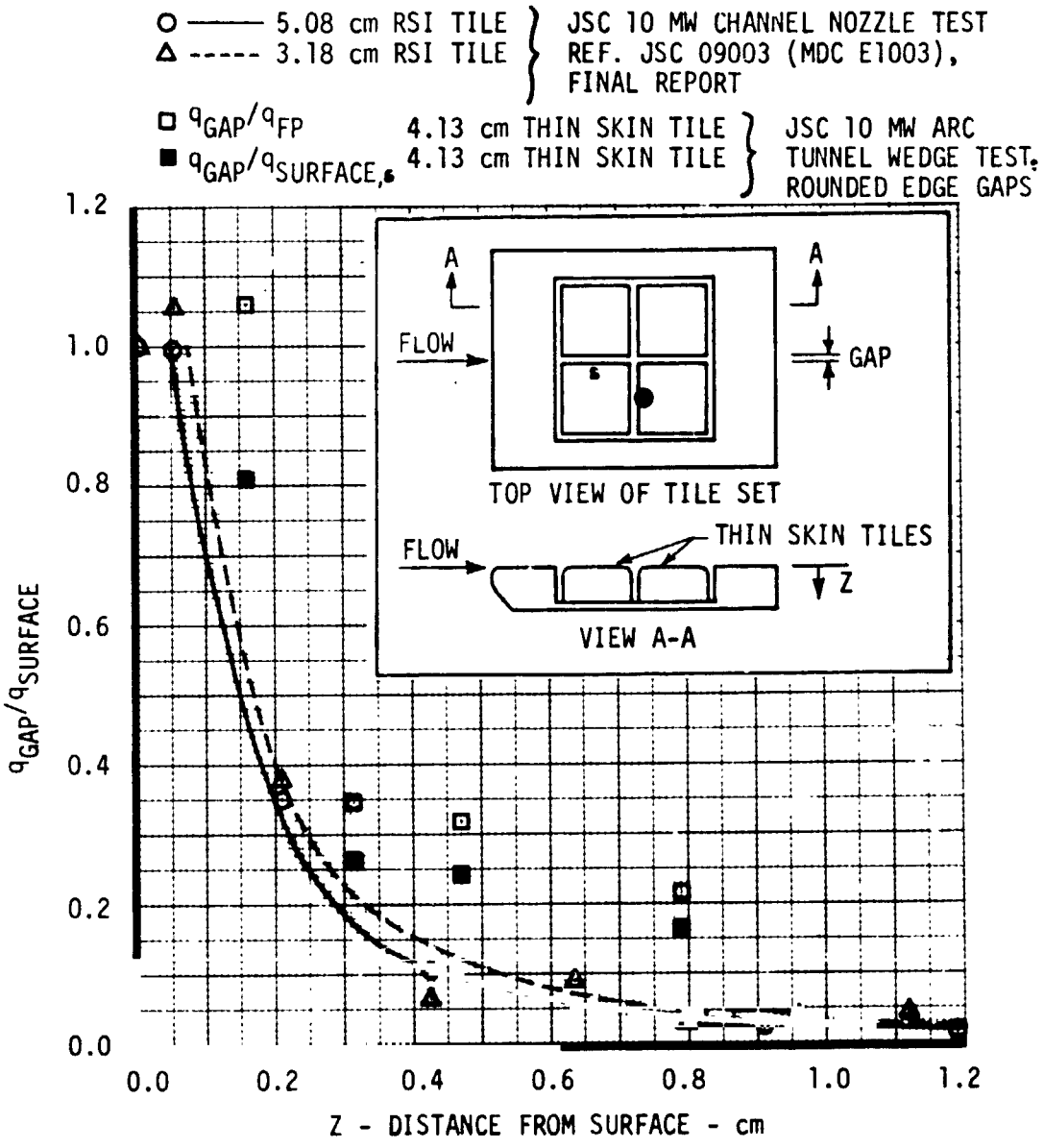

Figure 104

COMPARISON OF THIN SKIN TILE AND RSI TILE TRANSVERSE GAP HEATING DATA

- GAP WIDTH = .254 cm
- DOWNSTREAM SIDE OF GAP
- JSC 10 MW ARC TUNNEL
- CORNER RADIUS = 0.157 cm

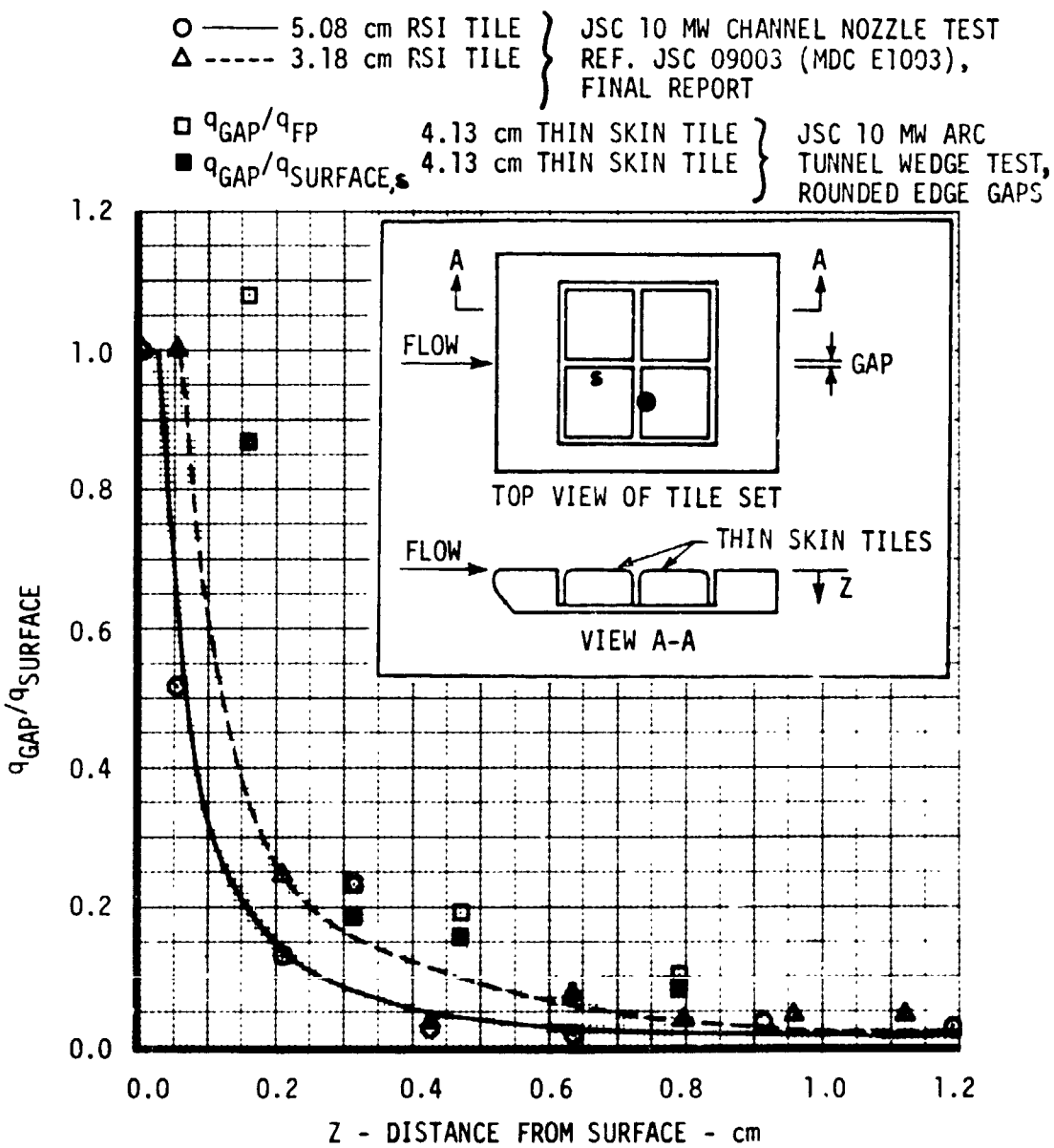

Figure 105

COMPARISON OF THIN SKIN TILE AND RSI TILE IN-LINE GAP HEATING DATA

- GAP WIDTH = .381 cm
- JSC 10 MW ARC TUNNEL
- CORNER RADIUS = 0.157 cm

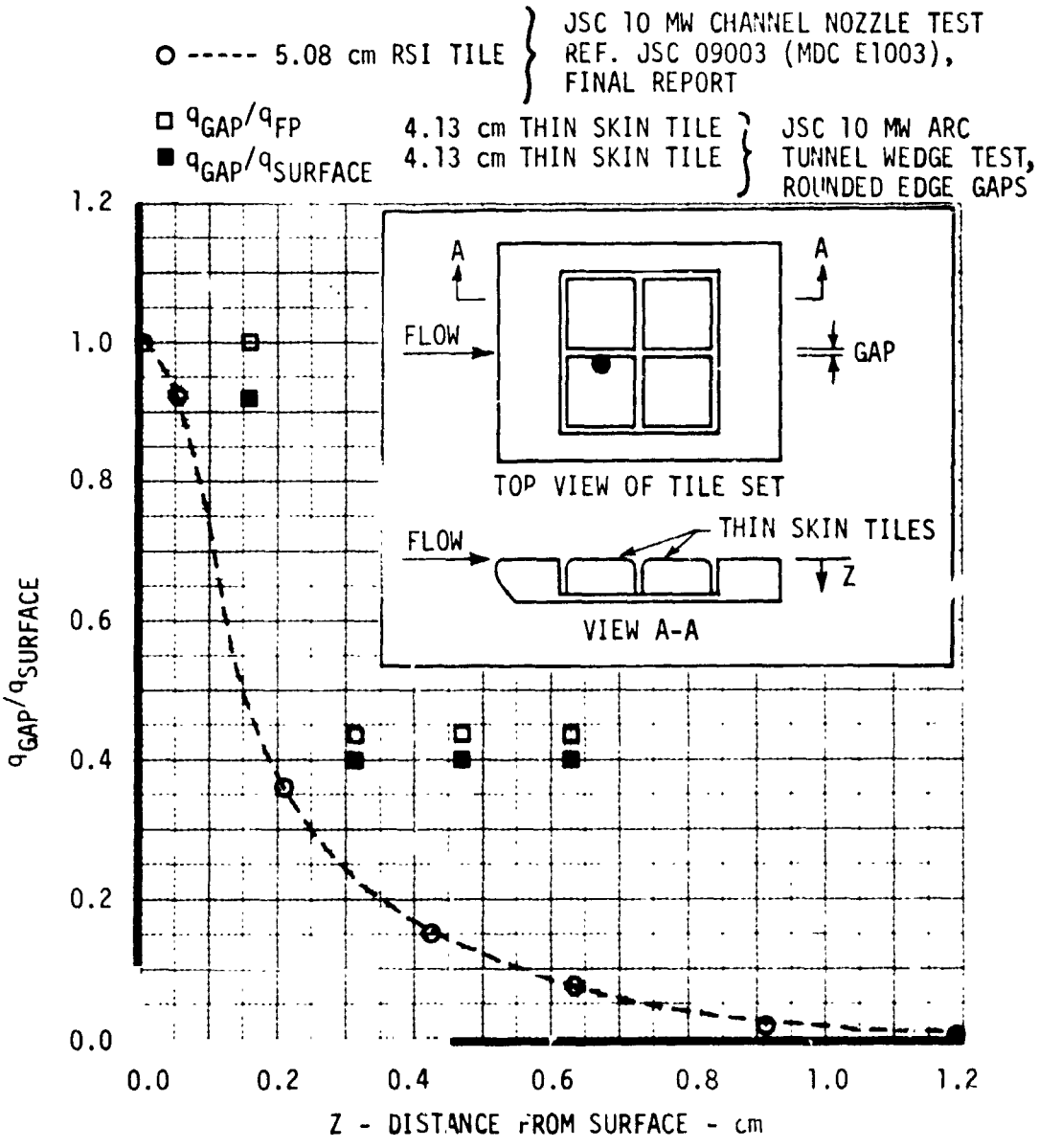

Figure 106

COMPARISON OF THIN SKIN TILE AND RSI TILE IN-LINE GAP HEATING DATA

- GAP WIDTH = .254 cm
- JSC 10 MW ARC TUNNEL
- CORNER RADIUS = 0.157 cm

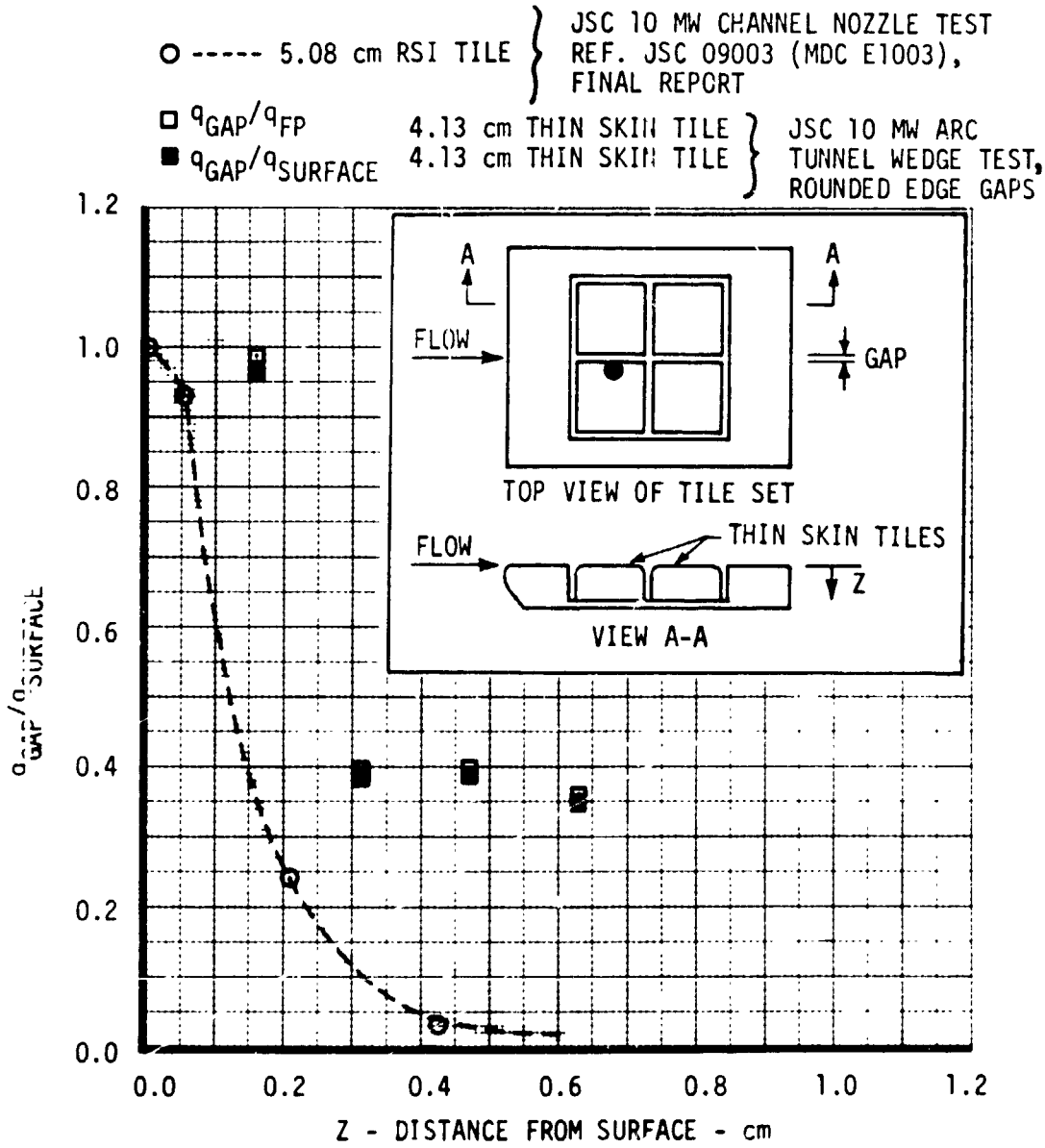

Figure 107

COMPARISON OF GAP HEATING TO UPSTREAM AND DOWNSTREAM WALLS OF TRANSVERSE GAP

- JSC 10 MW ARC TUNNEL WEDGE TESTS
- CORNER RADIUS = .318 cm

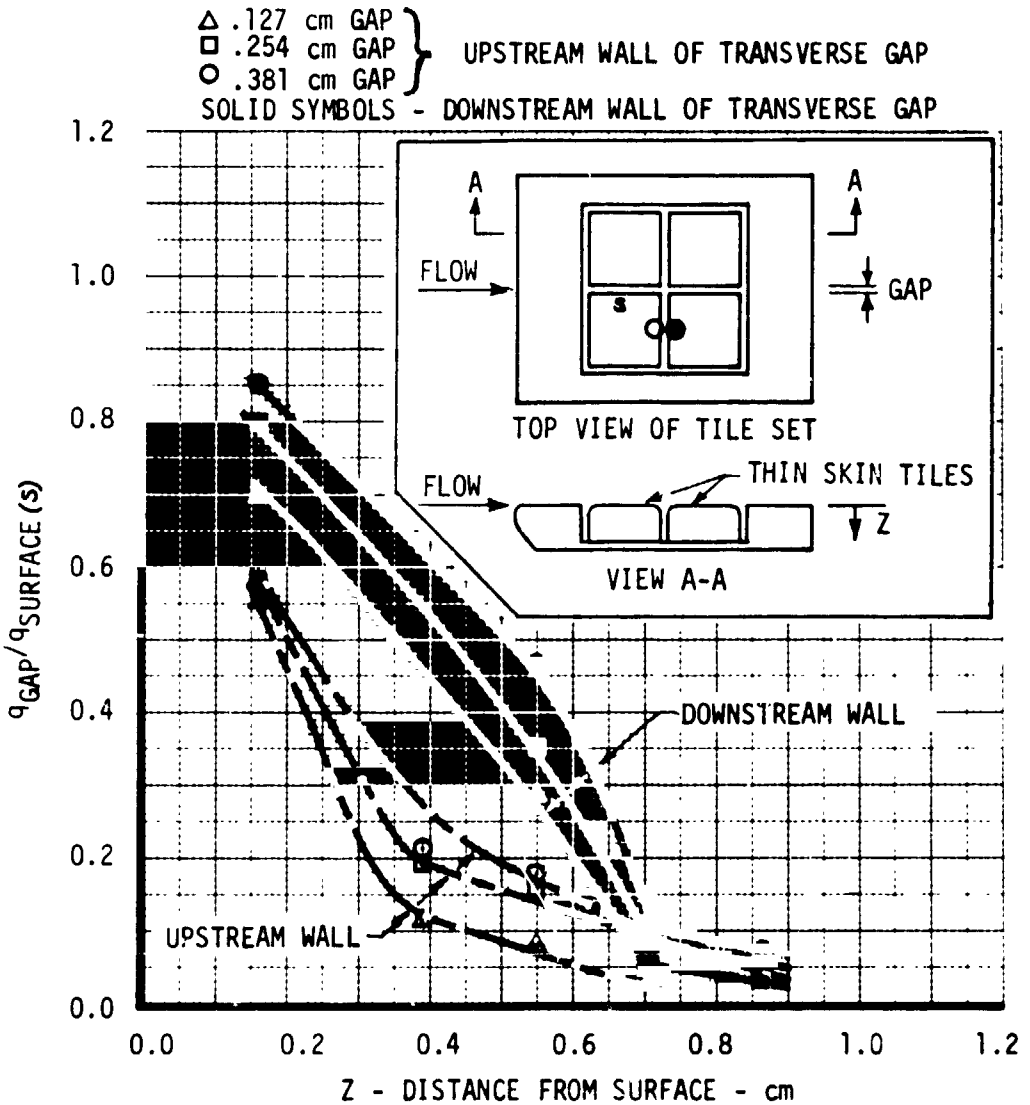

Figure 108

for the upstream side within 0.75 cm of the surface. Below this point the heating appears similar. The effect of width on gap heating is greater for the downstream side of the gap. Increasing gap width results in increased heating to the downstream wall. The effect of gap width on upstream wall heating appears to depend upon the distance into the gap. Near the surface and deep in the gap there is little affect of gap width. At Z = 0.39 and 0.55 cm the heating increases as the gap width varies from 0.127 cm to 0.254 cm. Further increases in gap width do not significantly increase gap heating at these locations.

4.4.2 Effect of Edge Radius on Heating to Top Surface of the Tile - The four tile sets tested by C. D. Scott in the 10 MW Arc Tunnel were instrumented on the top surface near the gap as well as in the gap. Data from the top of the tile near the transverse gap were examined in Figure 109 to determine the influence of the gap on surface heating. For the upstream side, all the tests except one (Edge Radius = 0.635 cm at a gap width of 0.127 cm) exhibited the same heating independent of the edge radius or gap width. This was as expected because the flow was supersonic and the influence of a disturbance should not be felt upstream.

Most of the tests showed an increase in heating across the gap. Heating on the downstream side of the gap showed as much as a 68% increase over the upstream data. However, not all the data showed such as increase. The data for the sharpest tile at the narrow gap actually show a slight decrease on the downstream gap side. This could be data scatter.

Examination of the downstream data shows no effect of edge radius on heating. There is however, an effect of gap width, with the intermediate gap being highest at the tangency point.

INFLUENCE OF EDGE RADIUS ON HEATING TO TOP OF TILE AT TRANSVERSE GAP

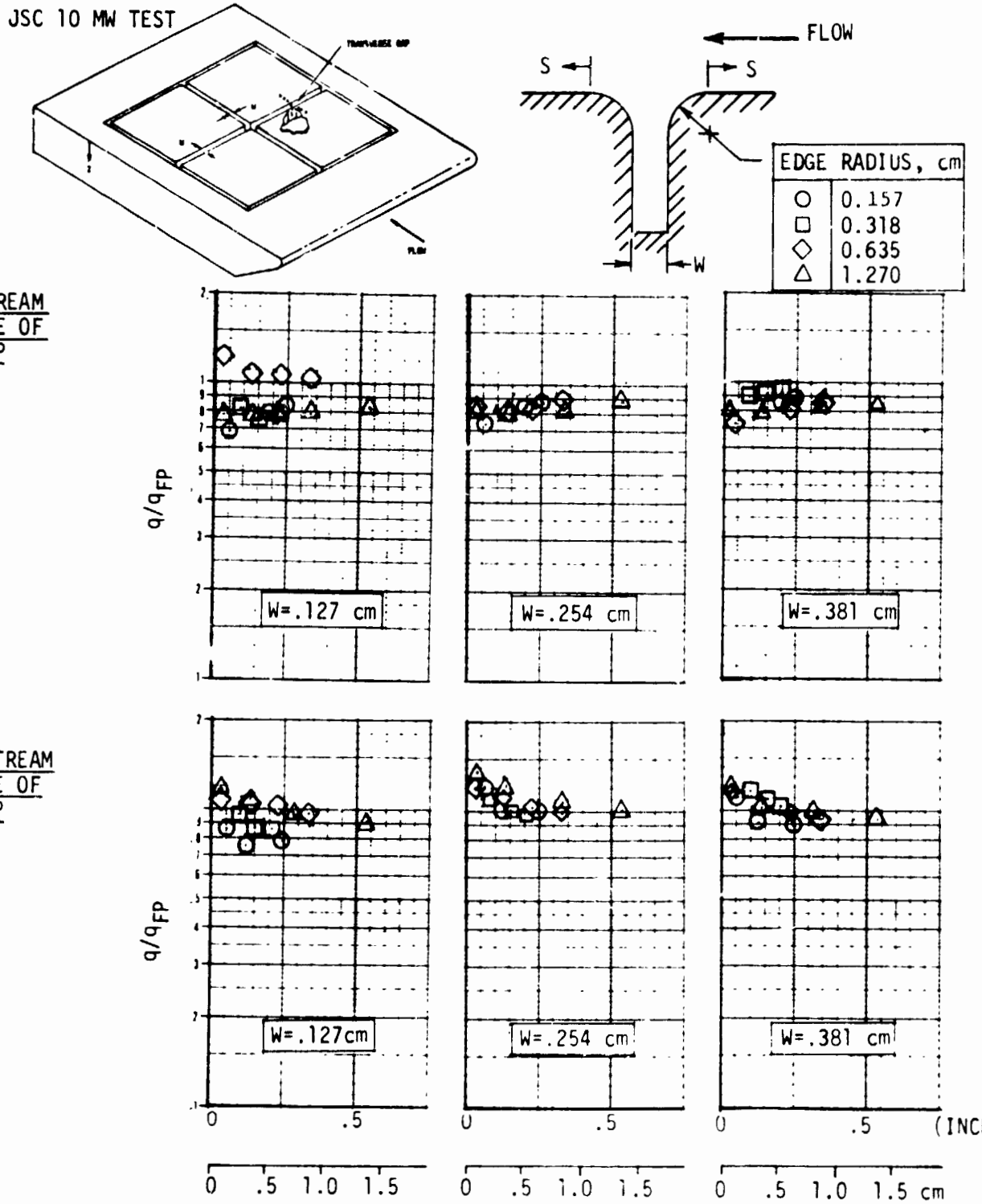

Figure 109

4.5 Analysis of Single In-Line Gap Tests at Ames 3.5 Foot H.W.T. - Data obtained from single in-line gap heating tests conducted in the Ames 3.5 Foot Hypervelocity Wind Tunnel (H.W.T.) were analyzed to assess the effects of tile orientation for several gap width settings. Additionally, the heating patterns for filled and unfilled gaps were examined including the effects of correcting for thermal conduction. Flow conditions were varied to obtain data in the presence of laminar, transitional and turbulent boundary layers.

The test program used a thin skin model inserted into a carrier plate (See Figure 14). Joint configuration was a single, in-line gap which was tested at four flow orientations, three gap widths, four gap depths, and two gap lengths. Some 93 tests were conducted. The test conditions, model description, and data assimilated are discussed in Section 3.5 and Volume II of this report. A complete listing of the runs is given in Figure 15 .

The analyses included evaluation of:

a) Heating patterns for filled and unfilled gaps
b) Correcting for conduction effects in thin skin tiles
c) Gap heating distributions including effects of Reynolds number and gap width
d) Different references for normalization of data
e) Flow orientation effects on in-line gap heating

4.5.1 Heating Patterns in Filled In-Line Gaps - Initial analysis of the in-line gap heating tests consisted of examining the data taken when the gap was filled with dental plaster. The test panel configuration and coordinate system is shown in Figure 14 . Tests were run at unit Reynolds number per meter of 1.57×10^6, 3.32×10^6 and 6.58×10^6. Instrumentation was sufficient to define axial and lateral heating distributions.

The heating distribution in the axial direction (X) adjacent to a filled 0.127 cm gap is shown in Figure 110 for the three Reynolds numbers investigated. The data were measured at a lateral position (Y) of -0.51 cm. The figure shows the influence of boundary layer transition on heating at the higher two Reynolds numbers. The increase in heat transfer coefficient is very significant at the highest Reynolds number.

The heating distribution in the lateral direction (Y) is shown in Figures 111, 112 and 113 for unit Reynolds numbers per meter of 1.57×10^6, 3.32×10^6, and 6.58×10^6 respectively. In each figure, lateral distributions are given for five specific axial distances. Again, the 0.127 cm gap has been filled with dental plaster. It

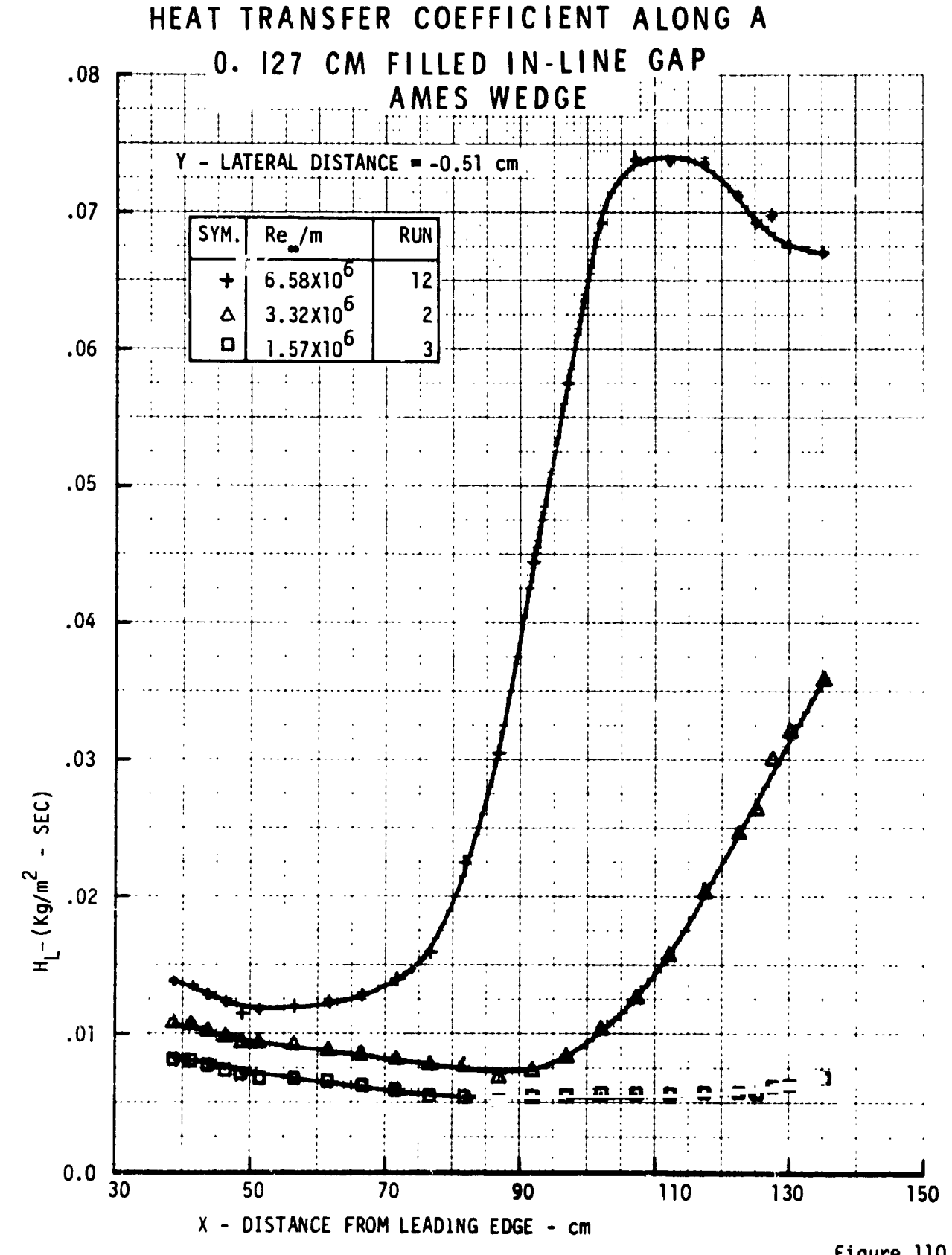
HEAT TRANSFER COEFFICIENT ALONG A
0. 127 CM FILLED IN-LINE GAP
AMES WEDGE
Y - LATERAL DISTANCE = -0.51 cm
SYM. | Re∞/m | RUN
+ | 6.58X10^6 | 12
△ | 3.32X10^6 | 2
□ | 1.57X10^6 | 3
H_L - (Kg/m^2 - SEC)
.08
.07
.06
.05
.04
.03
.02
.01
0.0
30
50
70
90
110
130
150
X - DISTANCE FROM LEADING EDGE - cm

Figure 110

HEAT TRANSFER COEFFICIENT
AMES WEDGE
0.127 CM FILLED IN-LINE GAP GAP
$Re_\infty/M \simeq 1.57 \times 10^6$

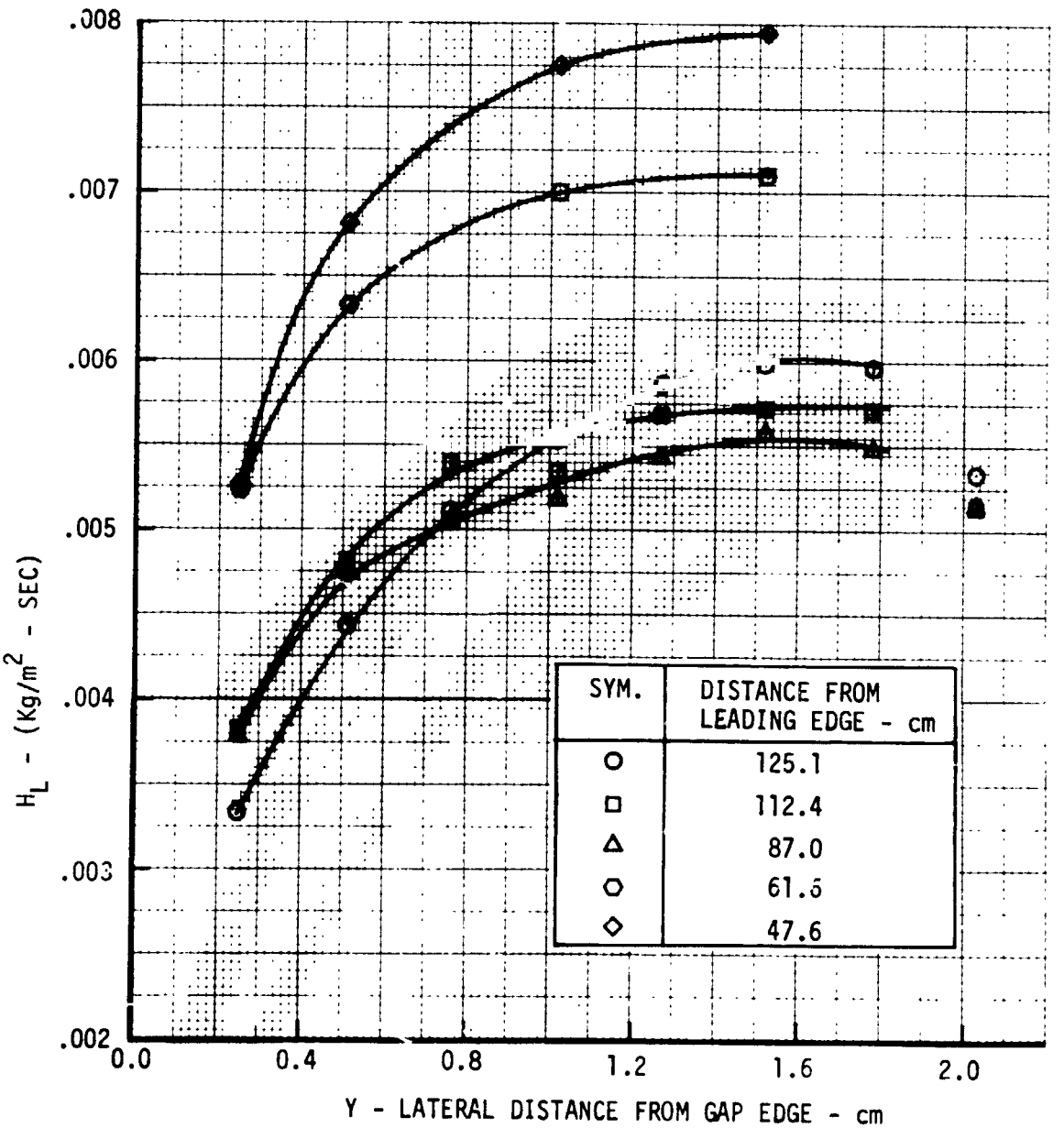

Figure 111

HEAT TRANSFER COEFFICIENT
AMES WEDGE
0.127 CM FILLED IN-LINE GAP

$Re_\infty/M = 3.32 \times 10^6$

SYM.	DISTANCE FROM LEADING EDGE-cm
○	125.1
□	112.4
△	87.0
⬡	61.6
◇	47.6

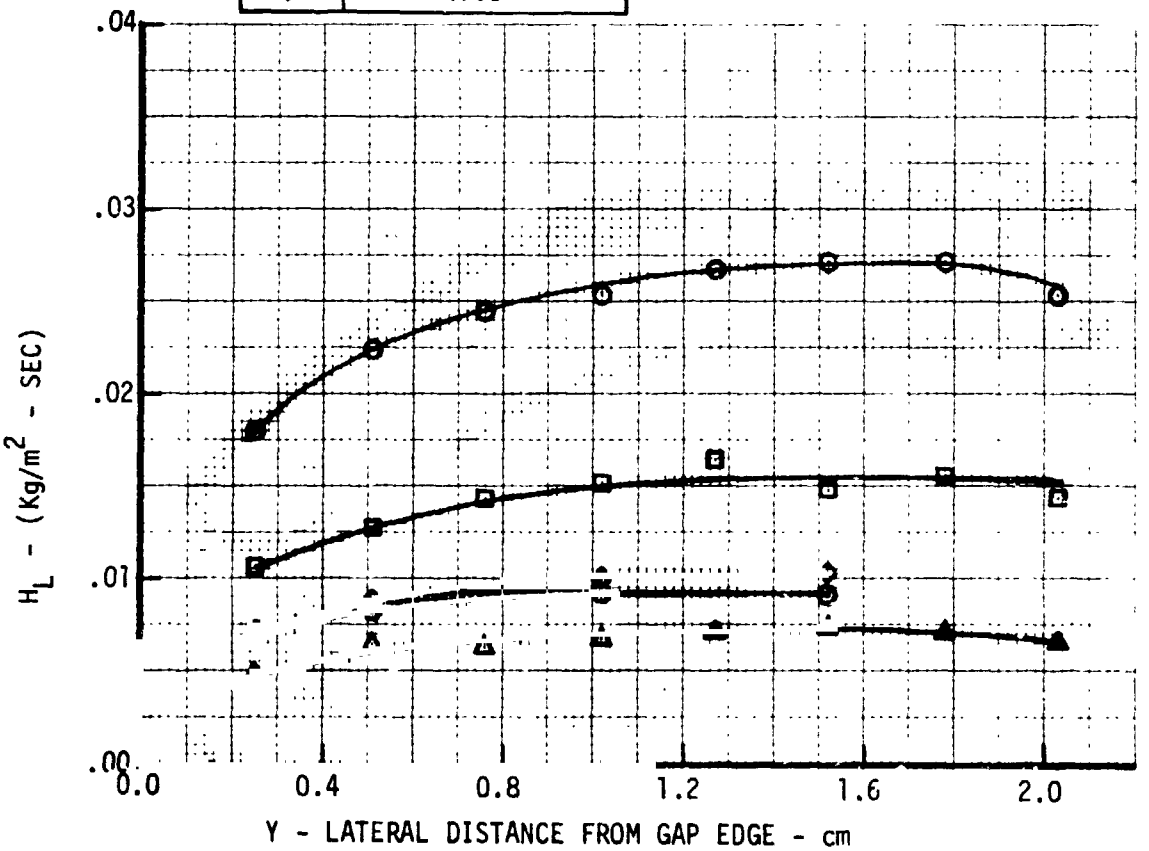

Figure 112

HEAT TRANSFER COEFFICIENT
AMES WEDGE
0.127 CM FILLED IN-LINE GAP

$Re_\infty/M = 6.58 \times 10^6$

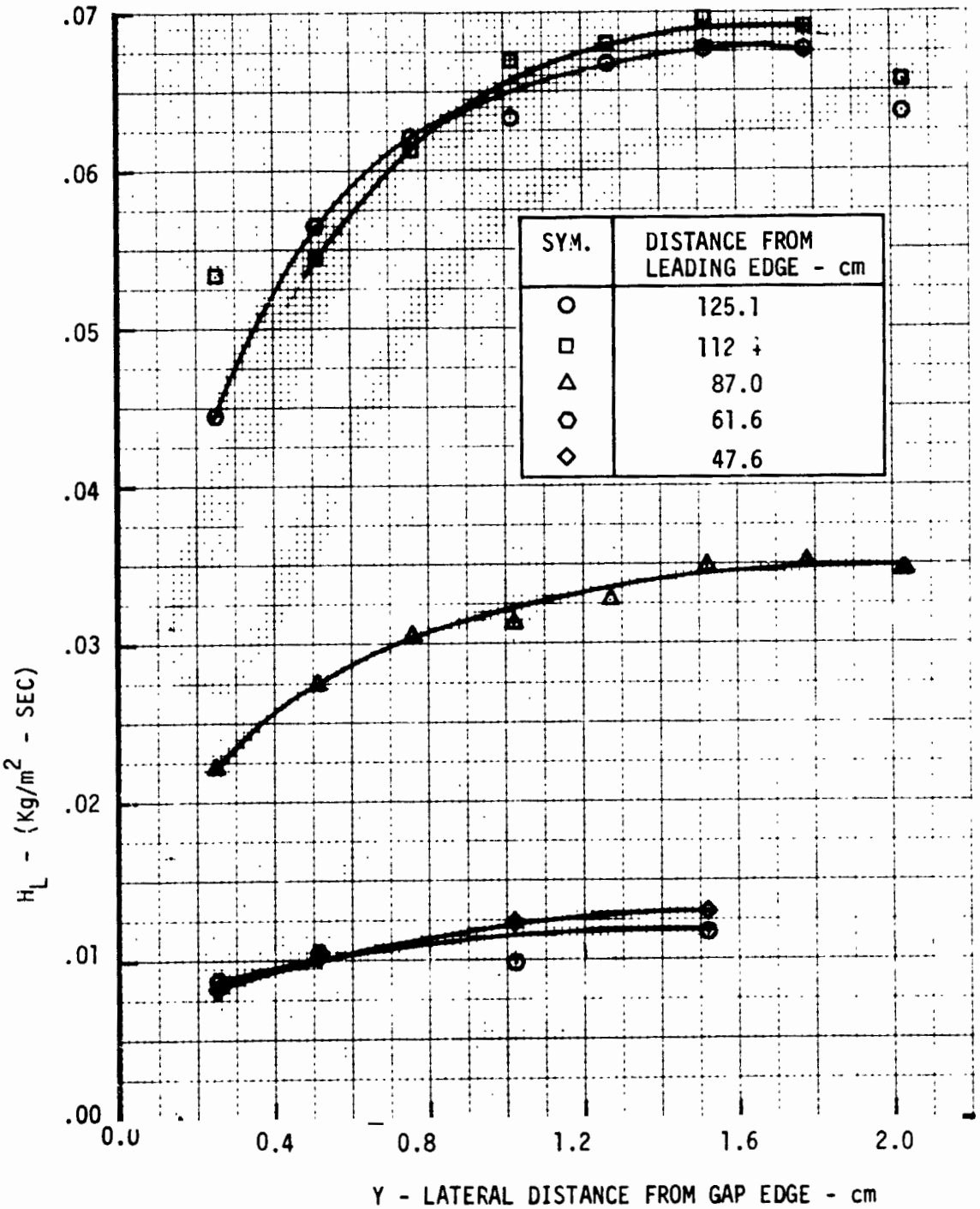

Figure 113

should be noted that Figures 111 thru 113 are not consistent with the axial distribution of Figure 110 in that different instrumentation was employed to obtain the lateral distributions. However, the data presented in Figure 111 for the lowest Reynolds number and at Y = +0.51 cm do agree fairly well with heating measured (Figure 110) on the other side of the filled gap. For all three Reynolds numbers, the lateral heating distributions appear to decrease significantly near the gap, suggesting a heat sink produced by the dental plaster filling the gap. Both finite element analyses and transient conduction effects ($\partial^2 T/\partial Y^2$) were evaluated to explain this discrepancy, but neither could adequately account for the low heating measured near the gap. Finally, Figures 112 and 113 for the two higher Reynolds numbers show streamwise heating distributions indicative of boundary layer transition.

4.5.2 Conduction Effects in Thin Skin Tile - The previous section has shown that the measured surface heat transfer coefficients decrease in the lateral direction (Y) near the in-line gap when the gap is filled with dental plaster. Additional analysis was performed to evaluate conduction in the test article. The data reduction method customarily used in thin skin model testing considers only the temperature rise rates and the local heat storage characteristics of the thin skin material. Thus the thermocouple/recording system is not generally calibrated against known temperatures. It was assumed that this was true for this test and that evaluating conduction effects using second derivatives of measured temperature at the time of insertion would be futile. Consequently, was decided to calculate conservative conduction effects by using temperatures one second after model insertion into the tunnel. These temperatures were calculated assuming isothermal conditions at the time of insertion and determining the temperature rise rate from the measured heating rates. These temperatures were then used to determine the second derivative ($\partial^2 T/\partial Y^2$) with respect to distance and then the transient conduction effects.

Figures 114, 115 and 116 present the measured and conduction corrected heat transfer coefficients for Reynolds number per meter of 1.57×10^6, 3.32×10^6, and 6.58×10^6, respectively. In general, the conduction corrected coefficients are not significantly different from the measured coefficients. In addition, the conduction corrected heating distributions also exhibit the drop off near the filled gap. It was concluded that conduction alone would not explain the lateral heating distribution near the filled gap edge.

HEAT TRANSFER COEFFICIENT
AMES WEDGE
0.127 CM FILLED IN-LINE GAP
$Re_\infty/M = 1.57 \times 10^6$

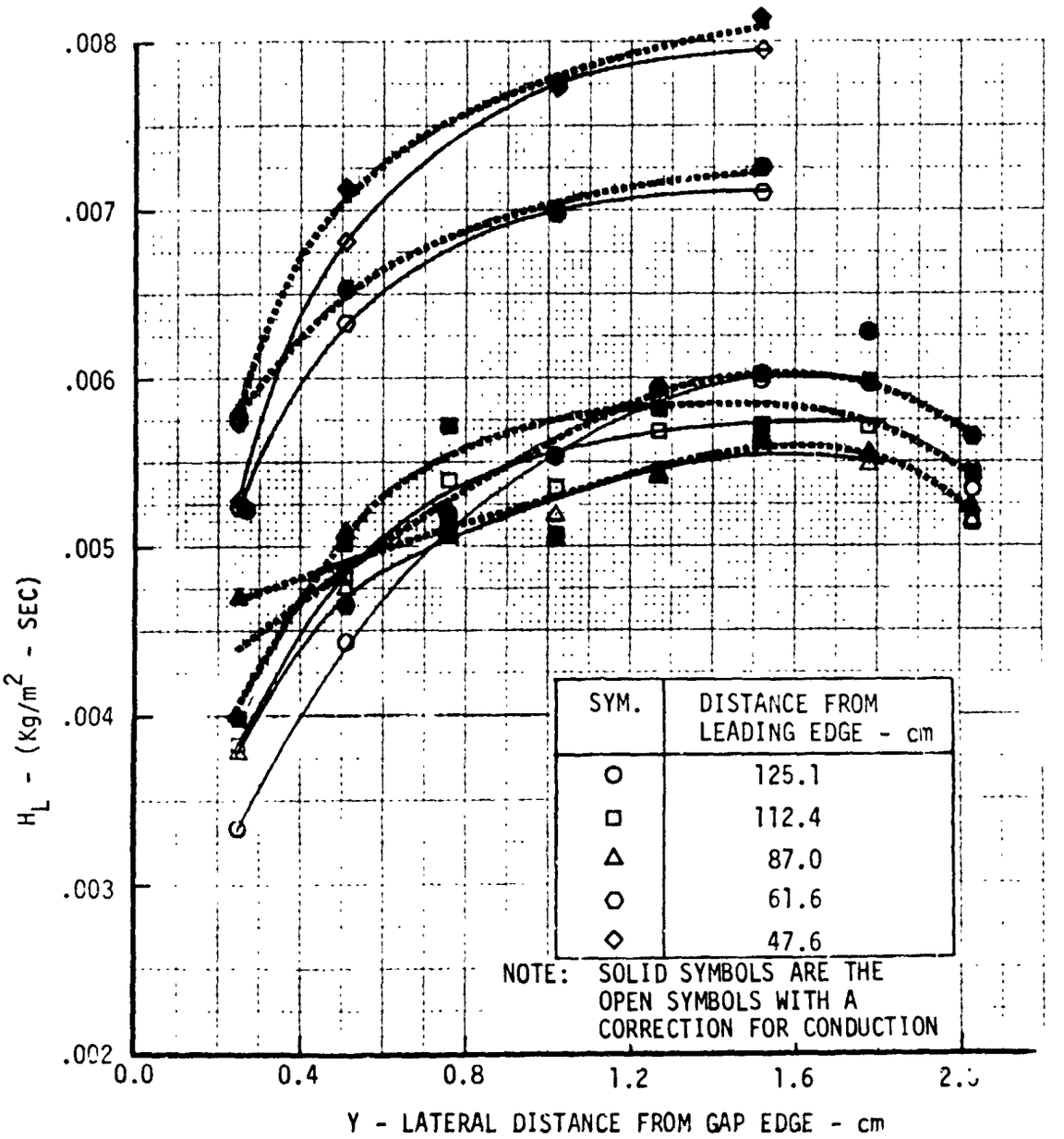

Figure 114

HEAT TRANSFER COEFFICIENT
AMES WEDGE
0.127CM FILLED IN-LINE GAP

$Re_{t_\infty}/M = 3.32 \times 10^6$

SYM.	DISTANCE FROM LEADING EDGE-cm
○	125.1
□	112.4
△	87.0
⬡	61.6
◇	47.6

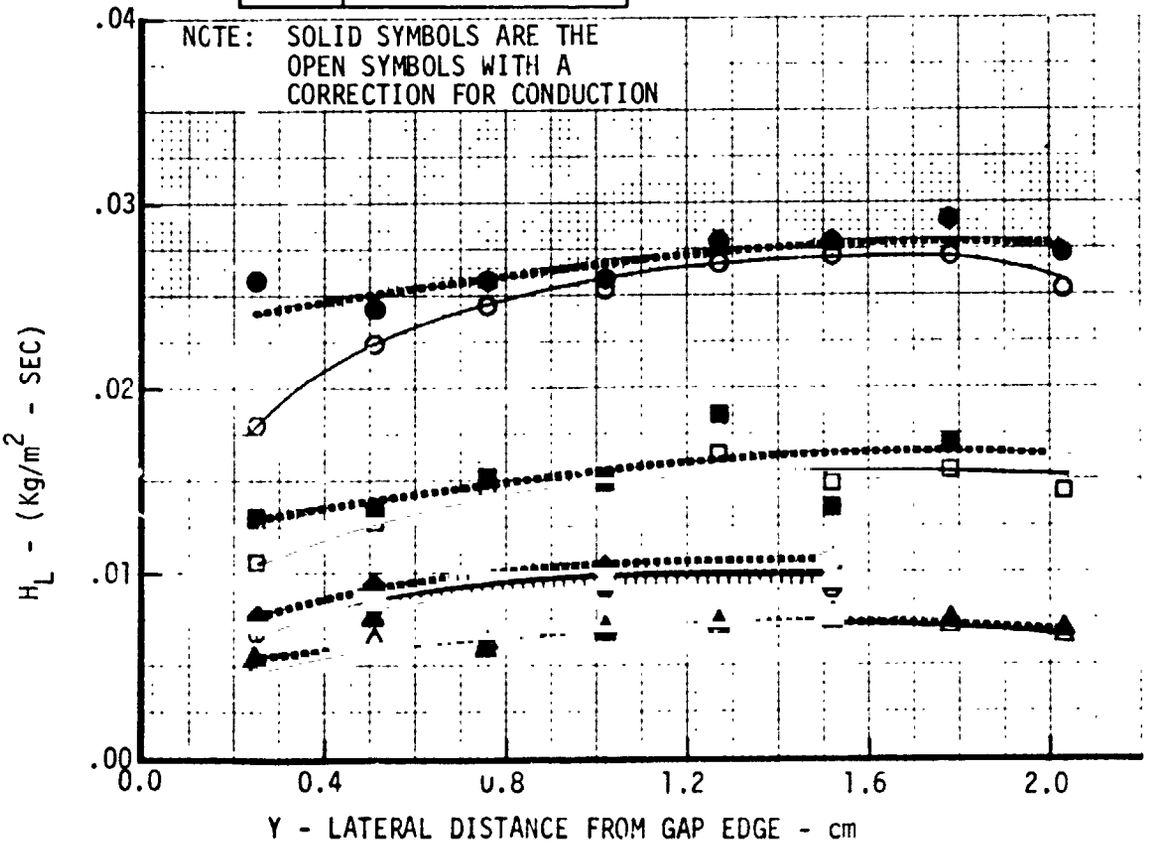

Figure 115

HEAT TRANSFER COEFFICIENT
AMES WEDGE
∘ 0.127 CM FILLED IN-LINE GAP
■ $Re_\infty/M = 6.58 \times 10^6$

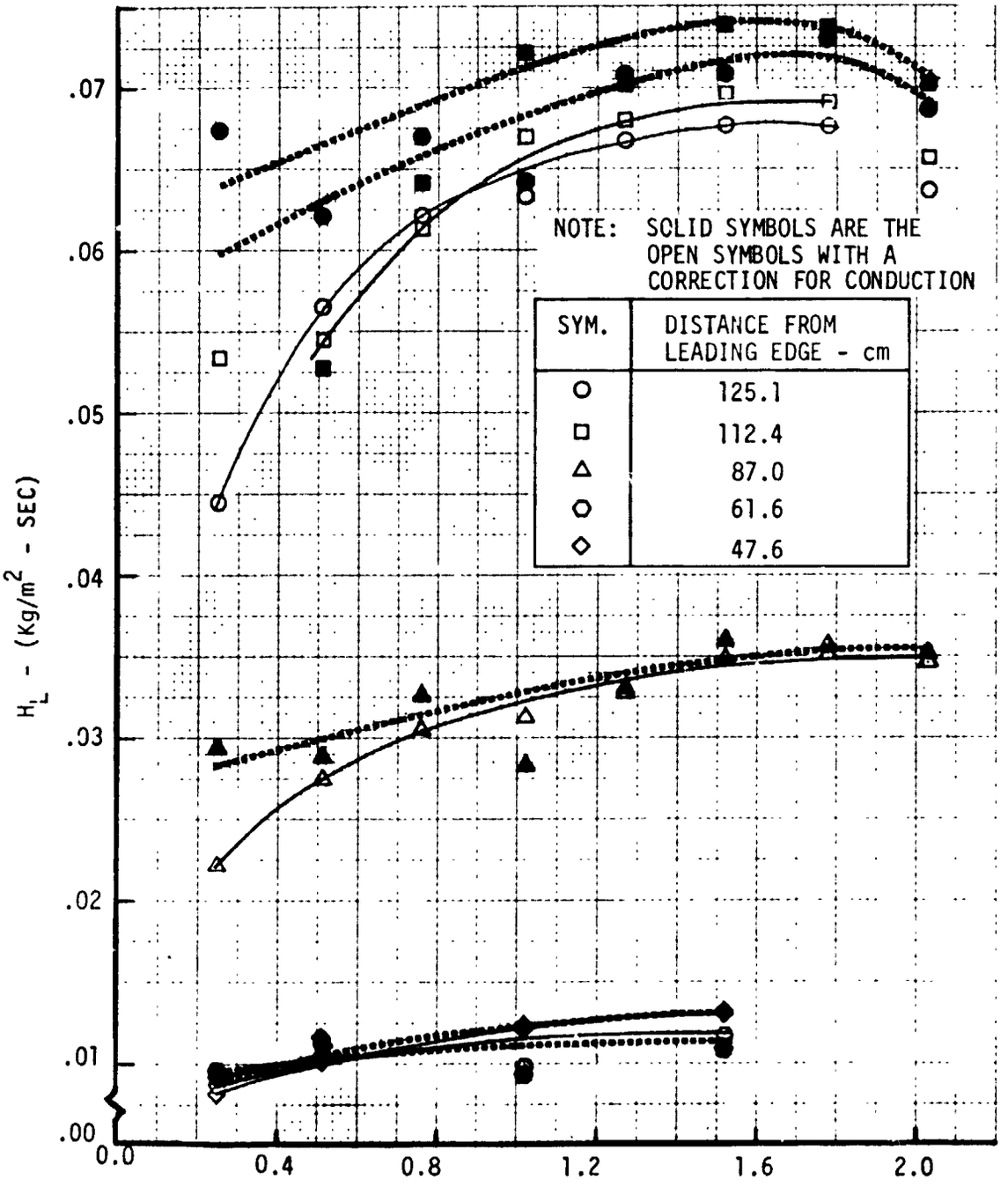

Figure 116

4.5.3 Surface and Gap Heating Distributions - Surface and gap heating distributions in the direction of flow were examined for the Ames in-line gap tests. Both Reynolds number and gap width effects on heating distributions were evaluated. The instrumentation for the runs analyzed consisted of one row of thermocouples along the surface of Y = -0.51 cm and two rows near the top of the gap at Z = 0.25 cm and 0.51 cm. See Figure 14 for the coordinate system definition.

The measured heat transfer coefficients for a gap width of 0.127 cm and Re_∞/m of 1.624×10^6, 3.270×10^6, and 6.359×10^6 are given in Figures 117, 118, and 119 respectively. The surface heating data (Z=0.0) indicates that the boundary layer is either laminar, transitional, or turbulent depending on the distance from the leading edge and Reynolds number. Surface heating decreases with distance up to 90 cm from the leading edge for the low Re_∞/m case (Figure 117) and then gradually increases with distance, indicative of transitional flow. The heating in the gap at Z=0.25 cm shows a similar trend with distance suggesting that gap heating is influenced by surface heating near the gap. The heating at Z=0.51 cm into the gap was too low to determine a trend with distance. The $Re_\infty/m = 3.27 \times 10^6$ data (Figure 118) show surface boundary layer trnasition starting at X=75 cm and ending at approximately X=125 cm. Again the gap heating is significantly affected by the changing surface environment. The heating data for $Re_\infty/m = 6.359 \times 10^6$ (Figure 119) shows a short laminar zone with transition starting at X=50 cm and ending at approximately X=90 cm. The heating in the gap near the beginning of the gap is increasing rapidly with distance. This suggests that the flow has not completely filled the gap. The heating at Z=0.25 cm is approximately equal to the surface heating during the transition zone. The gap heating at both Z=0.25 cm and 0.51 cm follows the surface heating trend for the turbulent surface heating zone. Figures 117 thru 119 illustrate the fact that gap heating is a strong function of the surface heating at the edge of the gap. The trends observed in the surface heating distributions are seen in the gap also.

The heating distributions for a wider gap (0.254 cm) and $Re_\infty/m = 3.138 \times 10^6$ are shown in Figure 120 . The surface heating data (Z=0.0) indicates transition starting at 60 cm from the leading edge and ending at X=120 cm. Transition occurred farther forward for the 0.254 cm gap than for the 0.127 cm gap at the same Reynolds number as seen by comparing Figures 120 and 118. This indicates that the presence of the gap influences the surface heating distribution. The heating in the gap

0. 127 CM IN-LINE GAP HEATING DISTRIBUTIONS

- $Re_\infty/m = 1.624 \times 10^6$
- $M_\infty = 5.1$
- AMES 3.5 FOOT HWT (RUN 6)
- SURFACE HEATING DATA (Z = 0.0) TAKEN AT Y =-0.51 cm

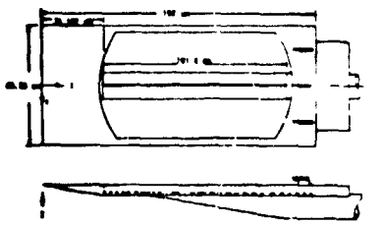

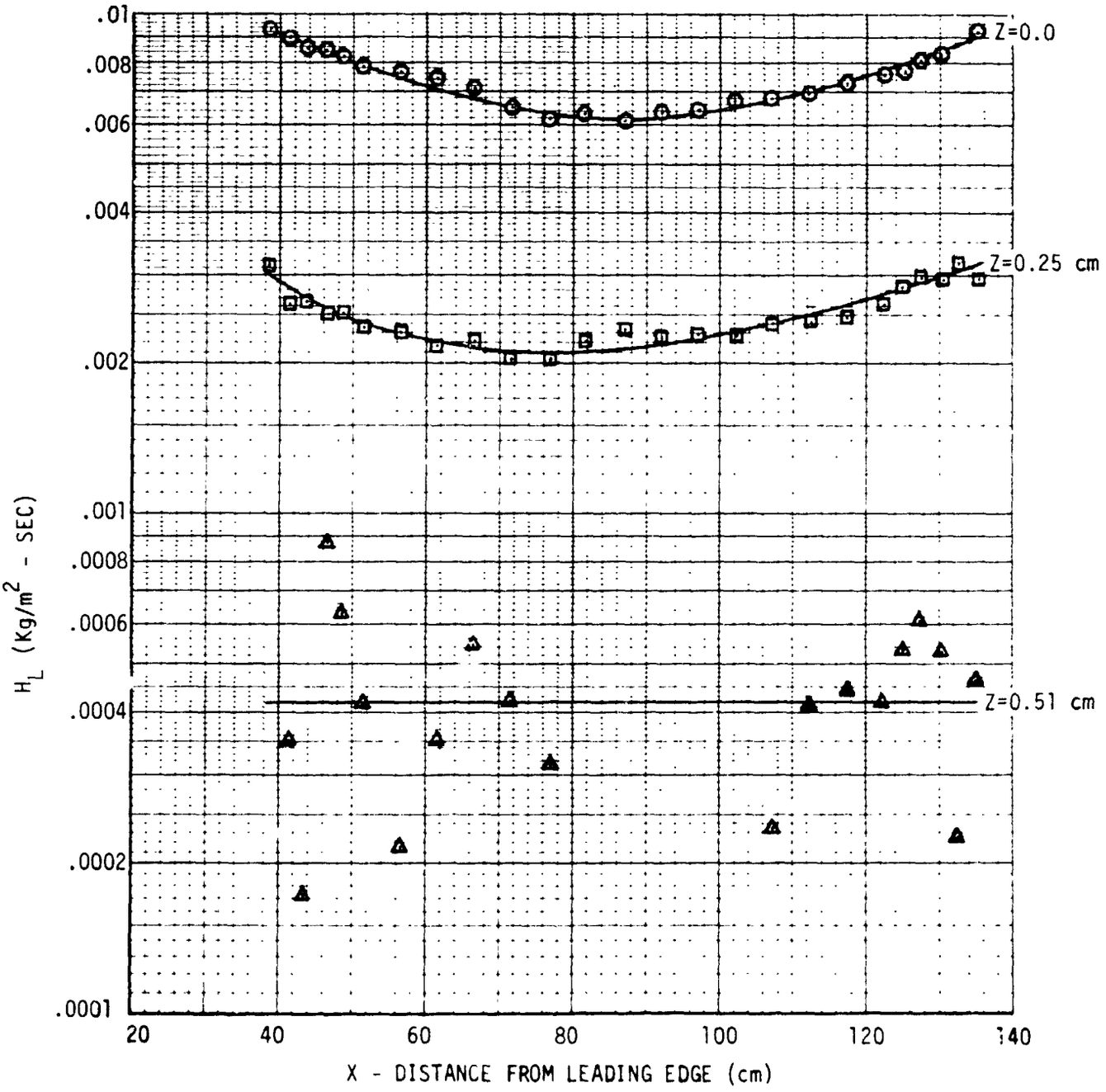

Figure 117

0.127CM IN-LINE GAP HEATING DISTRIBUTIONS

- $RE_\infty/m = 3.270 \times 10^6$
- $M_\infty = 5.1$
- AMES 3.5 FOOT HWT (RUN 7)
- SURFACE HEATING DATA (Z = 0.0; TAKEN AT Y = -0.51 cm

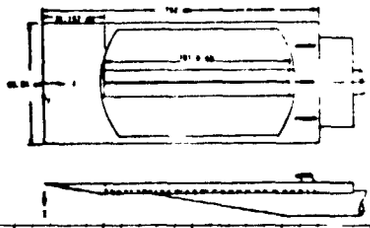

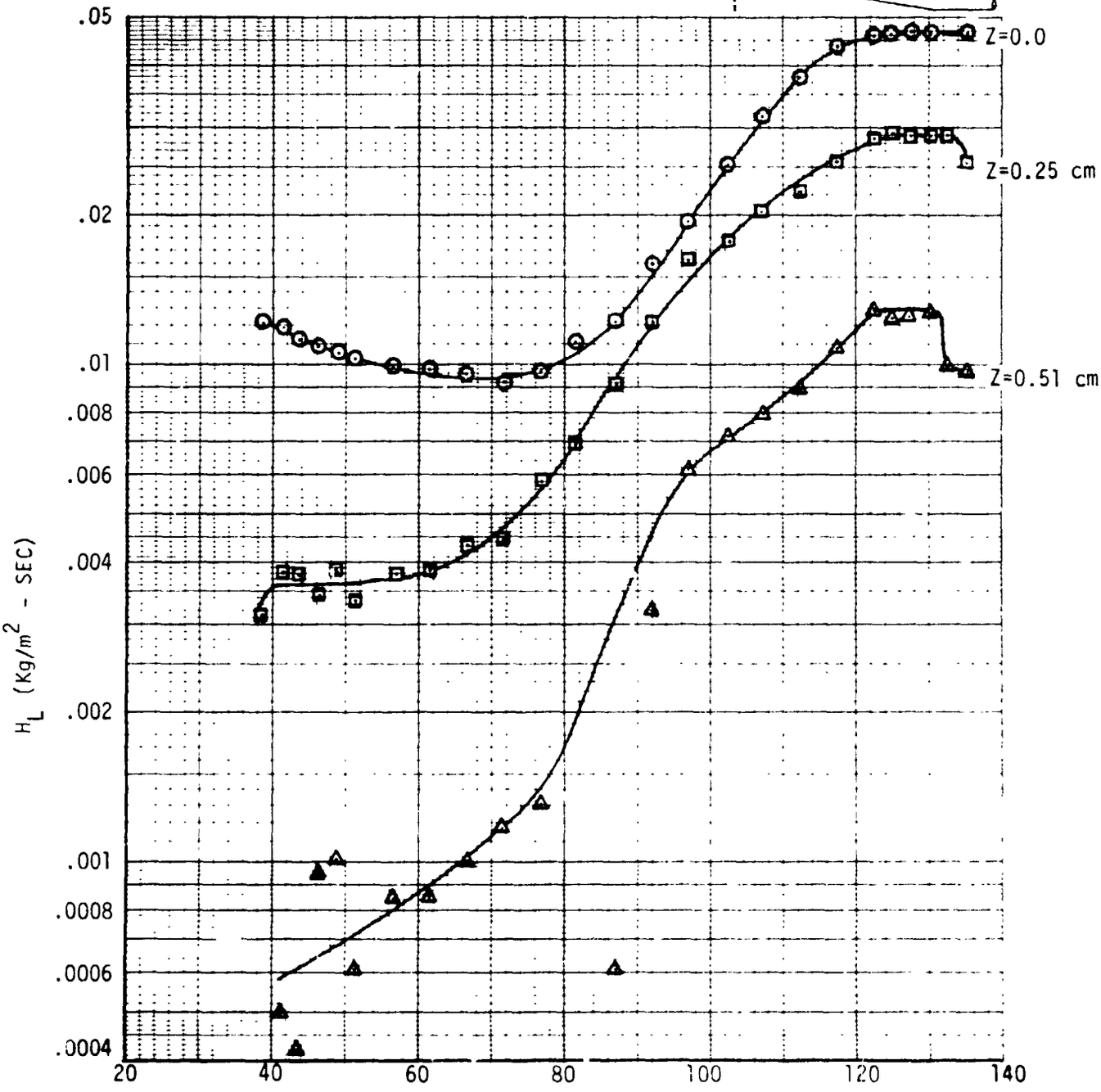

Figure 118

0.127 CM IN-LINE GAP HEATING DISTRIBUTIONS

- $Re_\infty/m = 6.359 \times 10^6$
- $M_\infty = 5.1$
- AMES 3.5 FOOT HWT (RUN 8)
- SURFACE HEATING DATA (Z=0.0) TAKEN AT Y = -0.51 cm

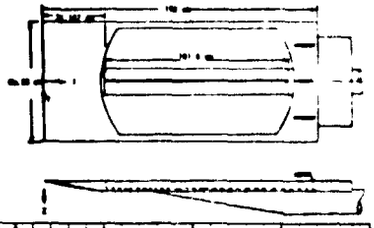

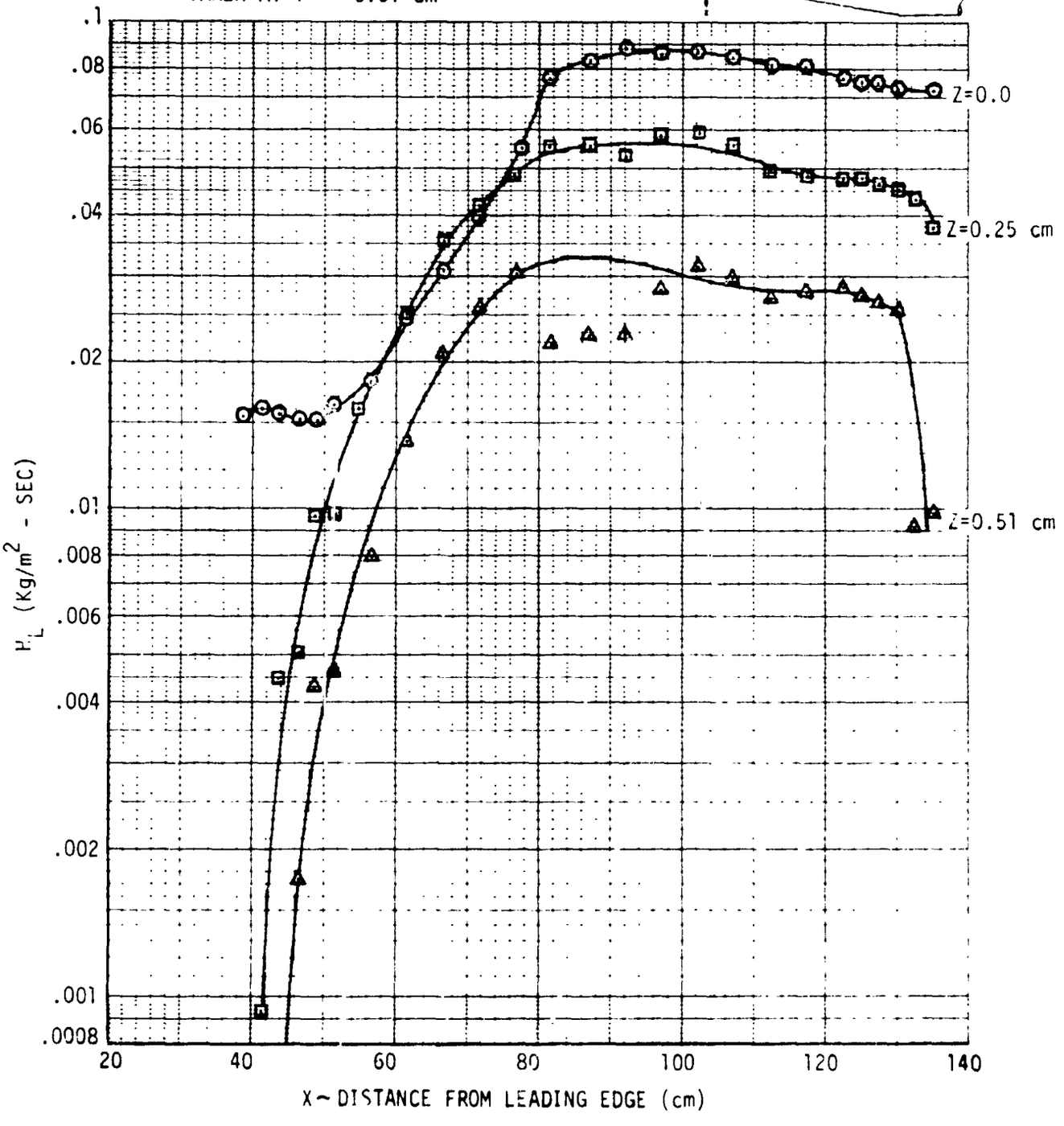

Figure 119

0.254 CM IN-LINE GAP HEATING DISTRIBUTIONS

- $Re_\infty/m = 3.133 \times 10^6$
- $M_\infty = 5.1$
- AMES 3.5 FOOT HWT (RUN 47)
- SURFACE HEATING DATA (Z = 0.0) TAKEN AT Y =-0.51 cm

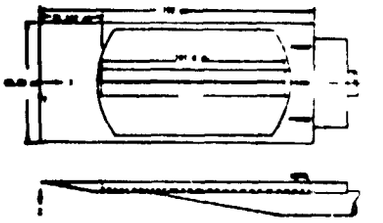

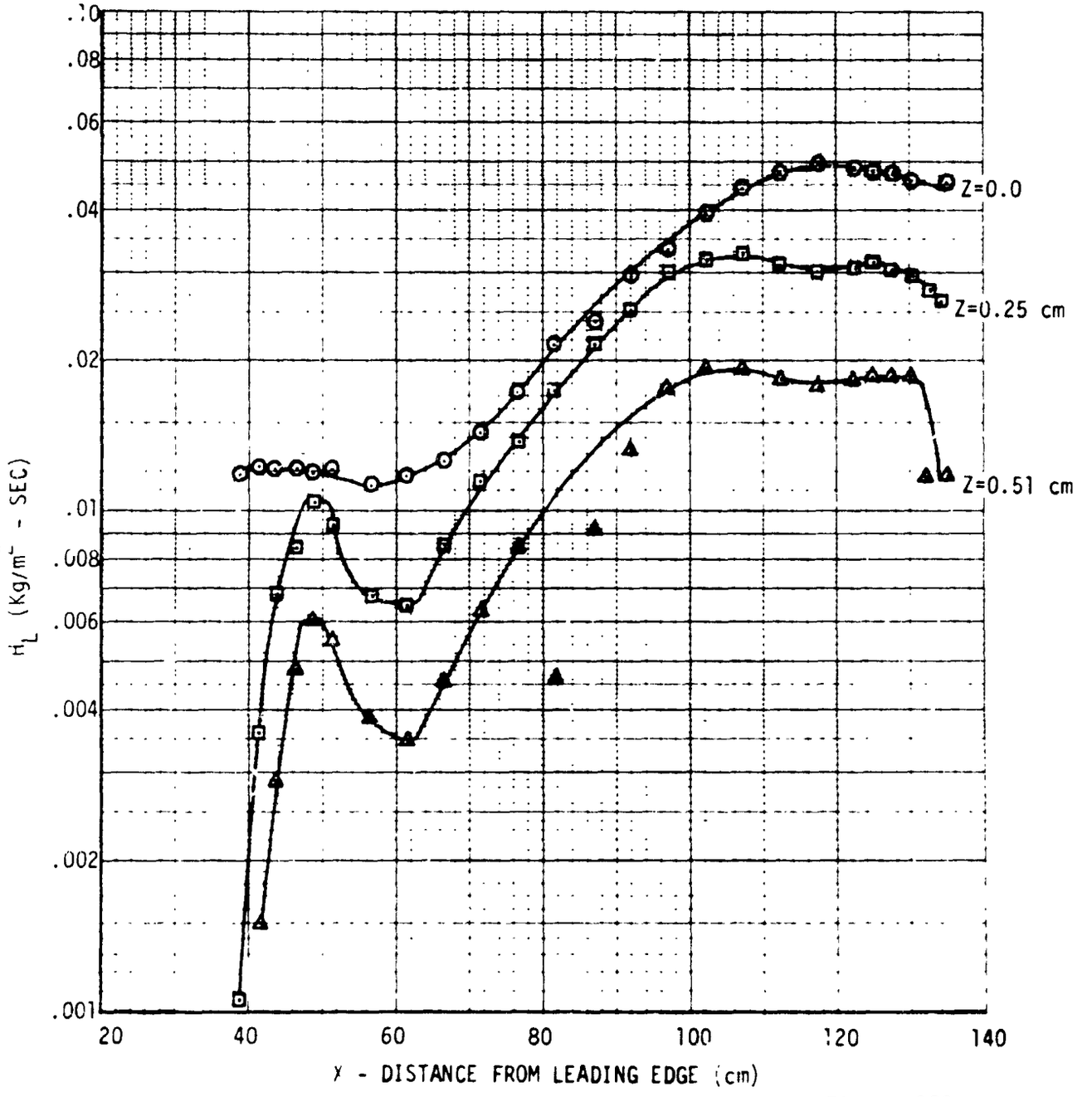

Figure 120

shows a sharp increase and then decrease with distance when the surface boundary layer is laminar. As soon as transition starts the gap heating follows the surface heating trend.

4.5.4 Normalization of Heating Rates - The previous gap heating data from the Ames 3.5 Foot H.W.T. has been ratioed to measured surface heating on a smooth flat plate. However, the data presented in Figures 117 thru 120 indicates that (1) the presence of gaps influences the surface heating near the gap and, (2) the heating in the gap is a strong function of the surface heating near the gap. This suggests that the gap data would correlate better if ratioed to the measured surface heating for the run than if ratioed to the smooth flat plate heating rates.

Figure 121 presents gap heating data for a gap width of 0.127 cm and Re_∞/m of 3.27×10^6 (Run 7) ratioed to both flat plate and measured surface (Z=0.0) heating rates. The ratios are similar up to X=80 cm. The data ratioed to the surface heating forms a ratio which is lower than when it is ratioed to the flat plate heating between X=80 cm and 130 cm. This is due to earlier transition on the gap model than on the smooth flat plate. Figure 122 compares the two gap heating ratios for a gap width of 0.254 cm and $Re_\infty/m = 3.138 \times 10^6$. Again the two ratios are approximately equal until transition occurs on the surface of the test article near the gap (~ 130 cm).

Normalizing the gap heating data to the local surface heating results in a more uniform ratio as a function of distance where the external boundary layer is transitional or turbulent. Because of this, it is concluded that normalizing the gap heating data to the measured surface heating near the gap is the preferred form for correlation purposes.

4.5.5 Flow Orientation Effects on In-Line Gap Heating - Heating data obtained on the Ames long in-line (or axial) gap were segregated according to laminar, transitional or turbulent flow conditions to develop correlations for an in-line gap and an in-line gap at small incidence angles (γ) up to 15 degrees. As discussed above, the presence of the in-line gap promotes boundary layer transition from laminar to a transitional state and finally to fully turbulent flow. Therefore, rather than using the calibration plate heating distribution to determine transition, the heating distribution along the panel measured by the line of thermocouples at a distance of 0.51 cm from the gap was used.

Analyses of the gap heating data for laminar boundary layer are discussed in the following paragraphs. Two sets of data were selected. The data in the first set all have a zero flow incidence angle "γ" while the second set contains the variation in "γ" up to 15 degrees.

0.127 CM IN-LINE GAP HEATING NORMALIZED TO FLAT PLATE AND TILE SURFACE HEATING

- $Re_\infty/m = 3.270X10^6$
- $M_\infty = 5.1$
- AMES 3.5 FOOT HWT (RUN 7)
- FLAT PLATE HEATING DATA FROM CALIBRATION PLATE RUNS
- SURFACE HEATING DATA FROM RUN 7 (y = -0.51cm)

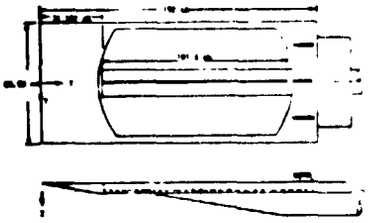

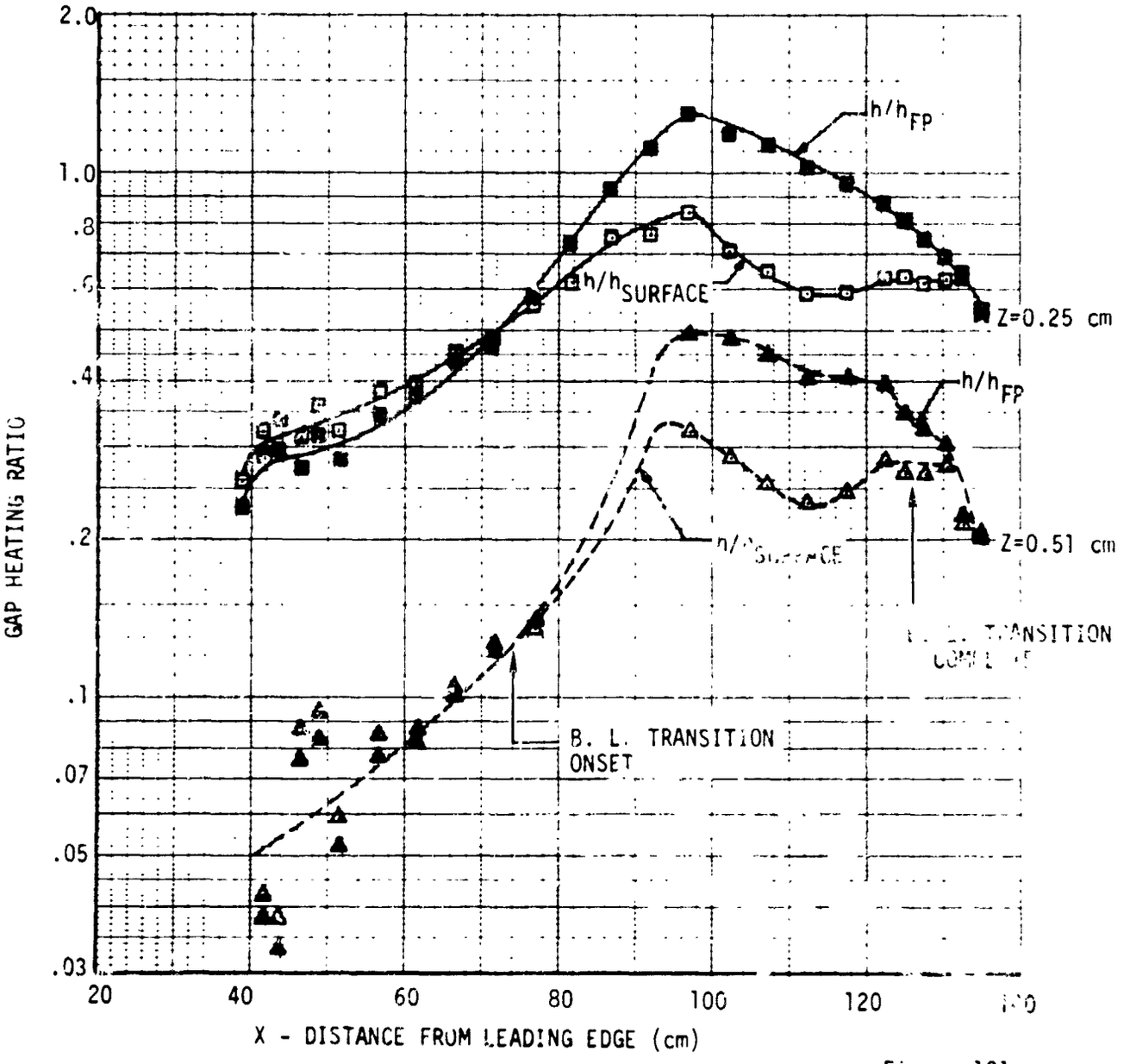

Figure 121

0.254 CM IN-LINE GAP HEATING NORMALIZED TO FLAT PLATE AND TILE SURFACE HEATING

- $Re_\infty/m = 3.138 \times 10^6$
- $M_\infty = 5.1$
- AMES 3.5 FOOT HWT (RUN 47)
- FLAT PLATE HEATING DATA FROM CALIBRATION PLATE RUNS
- SURFACE HEATING DATA FROM RUN 47 (y = - 0.51 cm)

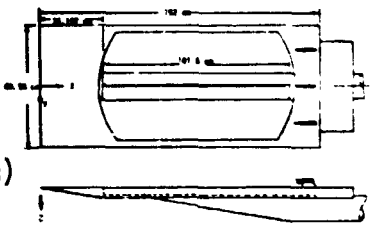

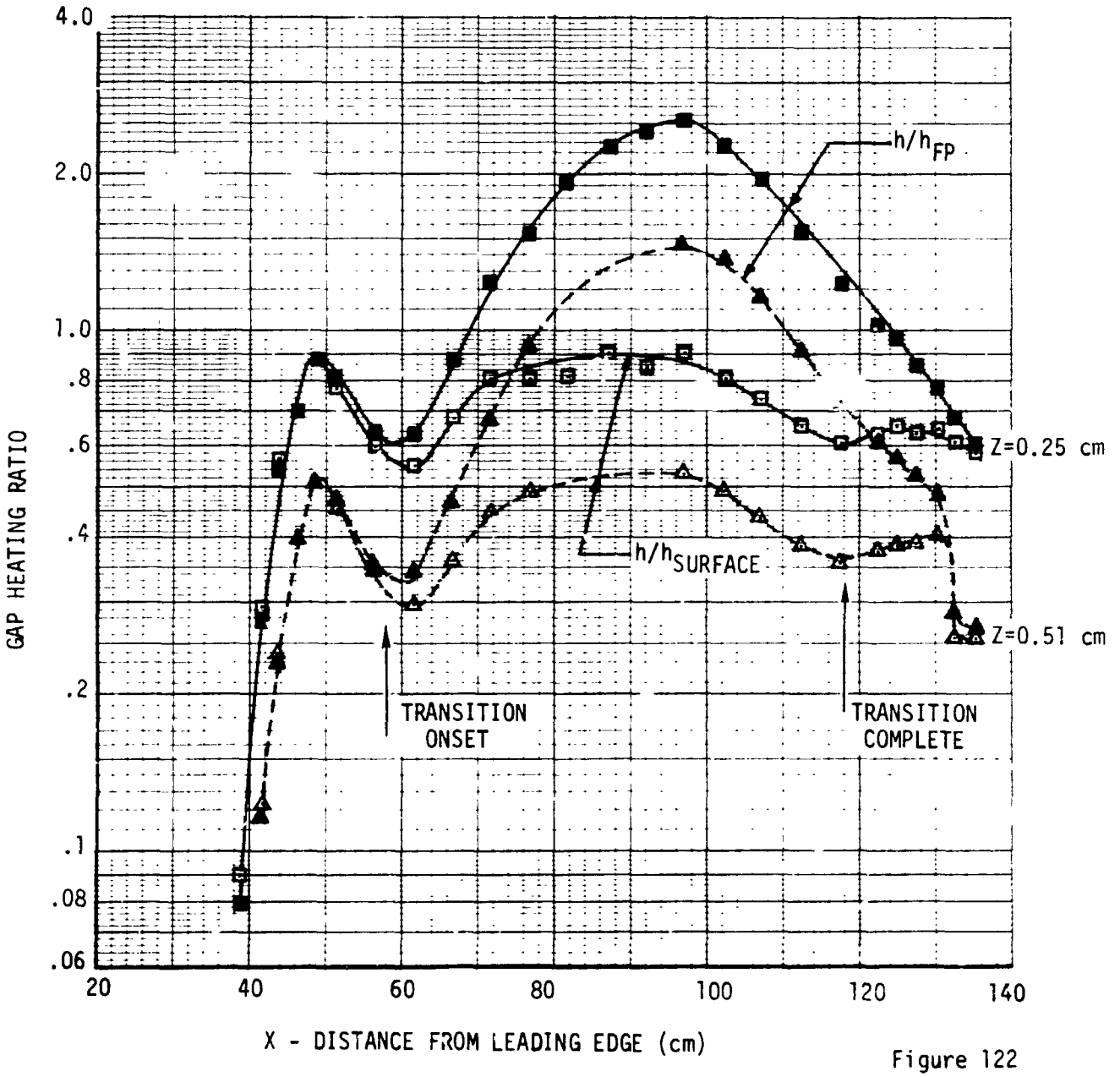

Figure 122

In-Line Gap Heating Laminar Flow, $\gamma = 0°$ - Heating measurements along the gap length were obtained at several depths into the gap for three variations in gap width, four variations in gap depth and three levels of Reynolds number. Data for laminar flow conditions and zero flow incidence are presented in Figures 123 thru 125 . In Figure 123 , heating distributions into the gap are presented for a gap width of 0.127 cm and tile thickness of 2.032 and 3.81 cm. As shown in this figure the heating level appears to increase with Reynolds number and also with axial flow length. Increasing gap depth decreases the heating. Some of the data for the 2.032 cm thick tile was replotted in Figure 124 on different types of graph paper to emphasize the non-linearity of the data.

The effect of gap width on the surface and gap heating distributions is examined in Figure 125 for a tile thickness of 2.032 cm. Reynolds number and axial location were essentially constant for each gap width investigated. As expected, the data indicate that heating increases as gap width is increased, and that heating variation with gap width appears to be non-linear.

In-Line Gap Heating Laminar Flow, $0 \leq \gamma \leq 15^{\circ}$ - The effect of flow orientation angle (γ) on the heating distribution in the in-line gap is shown in Figure 126 and 127 . Figure 126 applies to the low Reynolds number tests, a gap width of 0.127 cm and a tile thickness of 2.032 cm. Curves are presented using both flat plate heating and surface heating as the normalization parameter. As seen, the heating distributions do show a dependency on the flow angle. However, other tunnel conditions and parameters such as distance into the gap, gap width, and unit Reynolds number are larger and tend to overshadow this effect. For example, the runs at $\gamma = 10^{\circ}$ show a sharp increase in heating due to gap width especially at the higher Reynolds number tested, see Figure 127 . Heating on the downstream side of the gap is almost two times that on the upstream side. It is concluded that the presence of the in-line gap at a slight incidence angle cause the boundary layer to be more turbulent similar to a boundary layer transition phenomenon.

IN-LINE GAP HEATING DISTRIBUTION, 3.5 FT AMES H.W.T.

LAMINAR CONDITIONS, γ = 0 DEG

	Re/m (10^6 m^{-1})	X (cm)	T (cm)
○ □ △ ▷ ▽	1.6	61.6	2.032 →
	1.6	47.6	
	3.11	61.6	
	3.11	47.6	
	6.44	47 6	
○ □ △ ▷	1.7	61.6	3.81 →
	1.7	47.6	
	3.40	61.6	
	3.41	47.6	

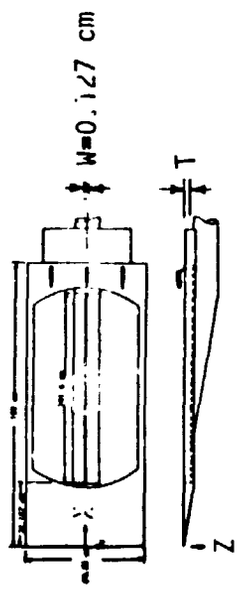

CONDUCTION CORRECTED

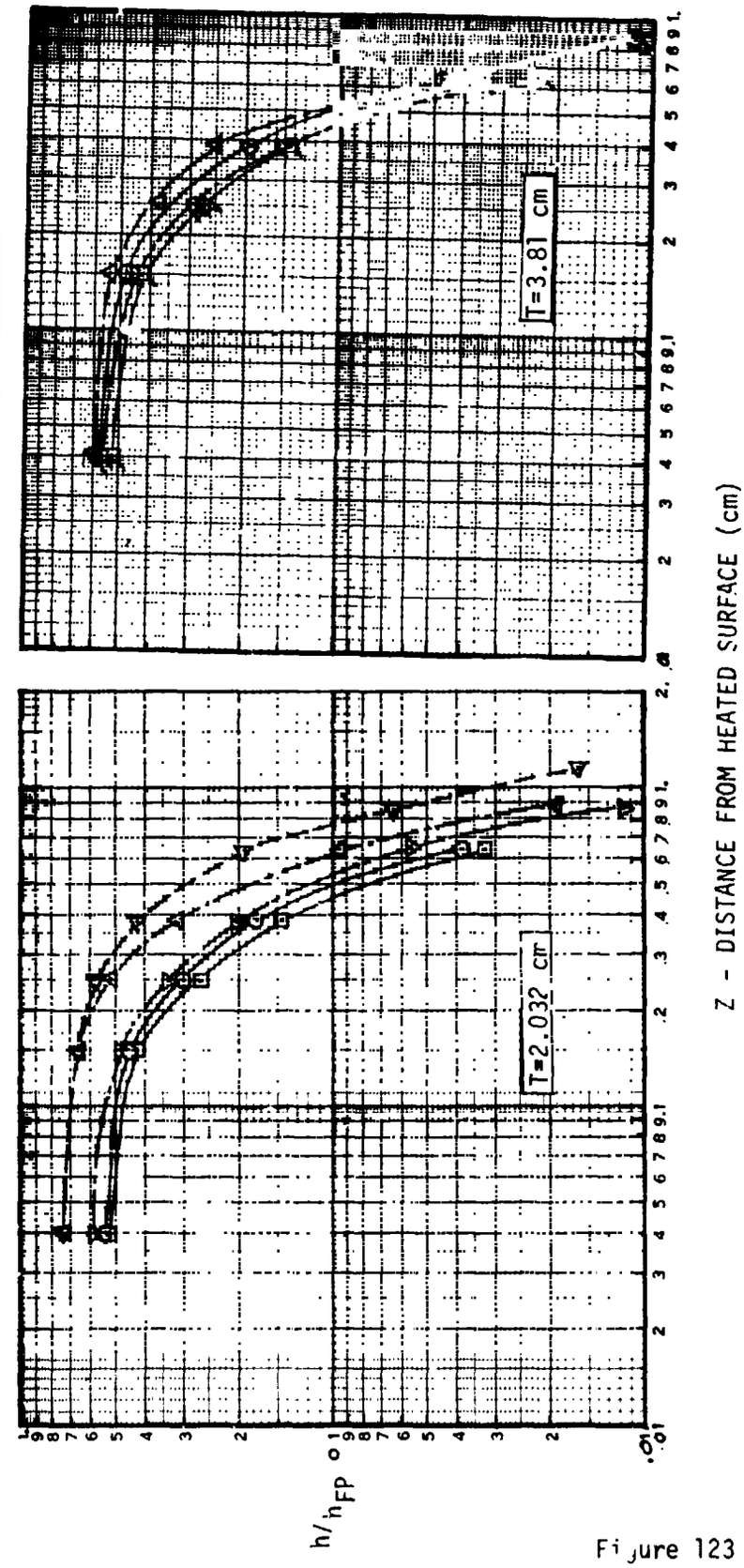

Figure 123

ALTERNATE METHOD OF PRESENTING IN-LINE GAP HEATING DATA

LAMINAR CONDITIONS, γ = 0 DEG

	Re/m (10^6 m^{-1})	X (cm)	T (cm)
○	1.6	61.6	2.032 →
▽	3.11	47.6	
◁	6.44	47.6	

CONDUCTION CORRECTED

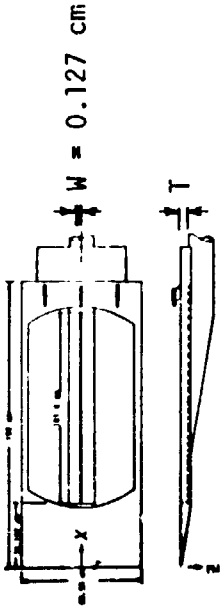

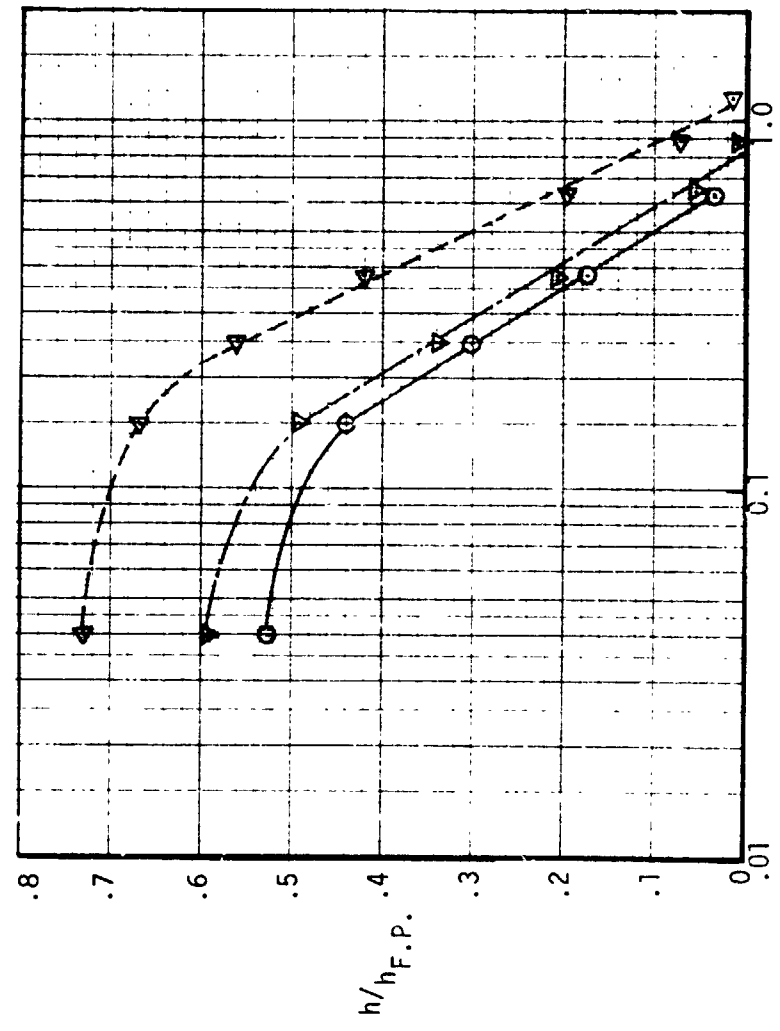

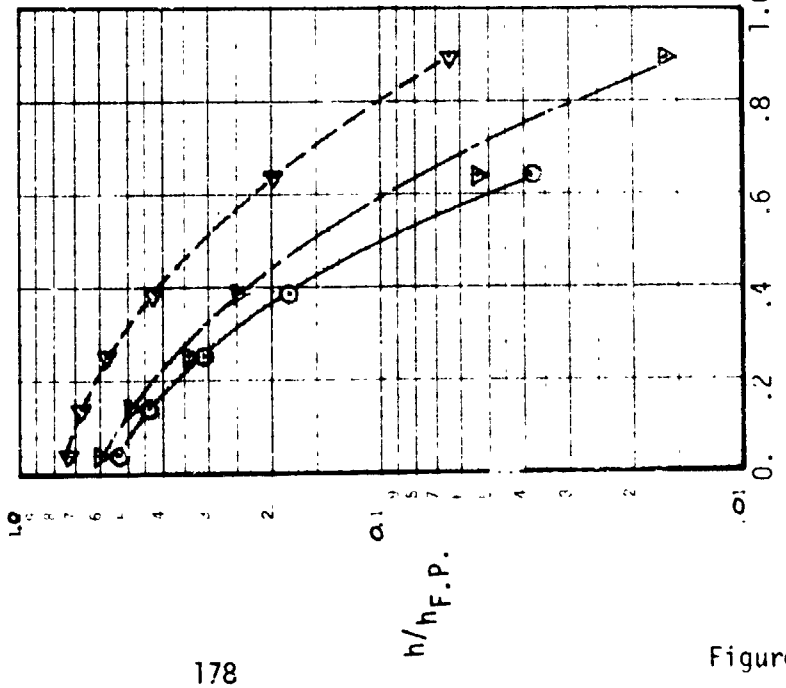

Z - DISTANCE FROM HEATED SURFACE (cm)

Figure 124

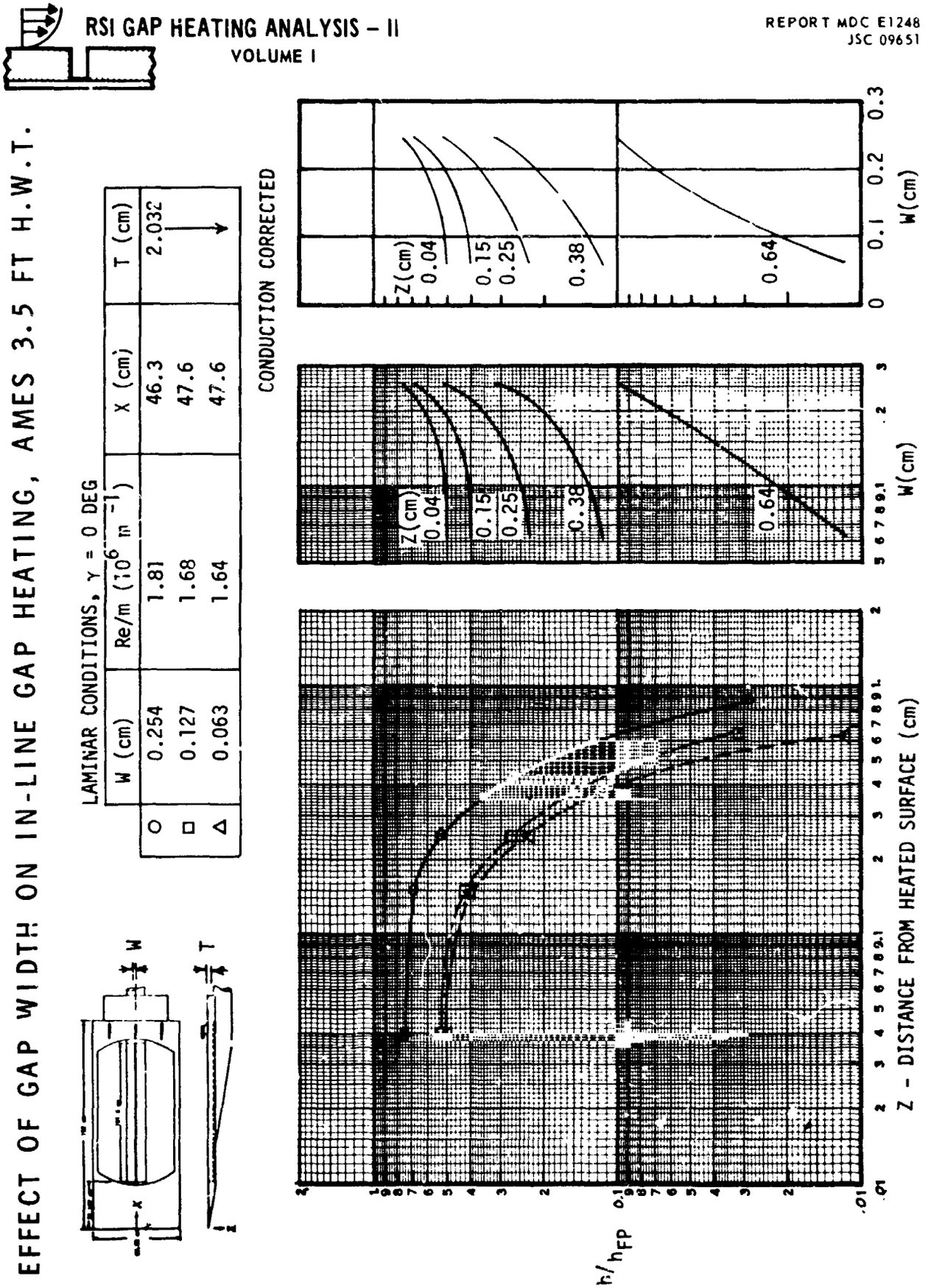
EFFECT OF GAP WIDTH ON IN-LINE GAP HEATING, AMES 3.5 FT H.W.T.
LAMINAR CONDITIONS, γ = 0 DEG
CONDUCTION CORRECTED
W (cm) | Re/m (10^6 m^-1) | X (cm) | T (cm)
○ 0.254 | 1.81 | 46.3 | 2.032
□ 0.127 | 1.68 | 47.6 |
△ 0.063 | 1.64 | 47.6 |
W
T
X
Z(cm)
0.04
0.15
0.25
0.38
0.64
W(cm)
h/h_FP
Z - DISTANCE FROM HEATED SURFACE (cm)

Figure 125

FLOW AT SMALL INCIDENCE ANGLES INCREASES HEATING TO IN-LINE GAPS, LAMINAR CONDITIONS

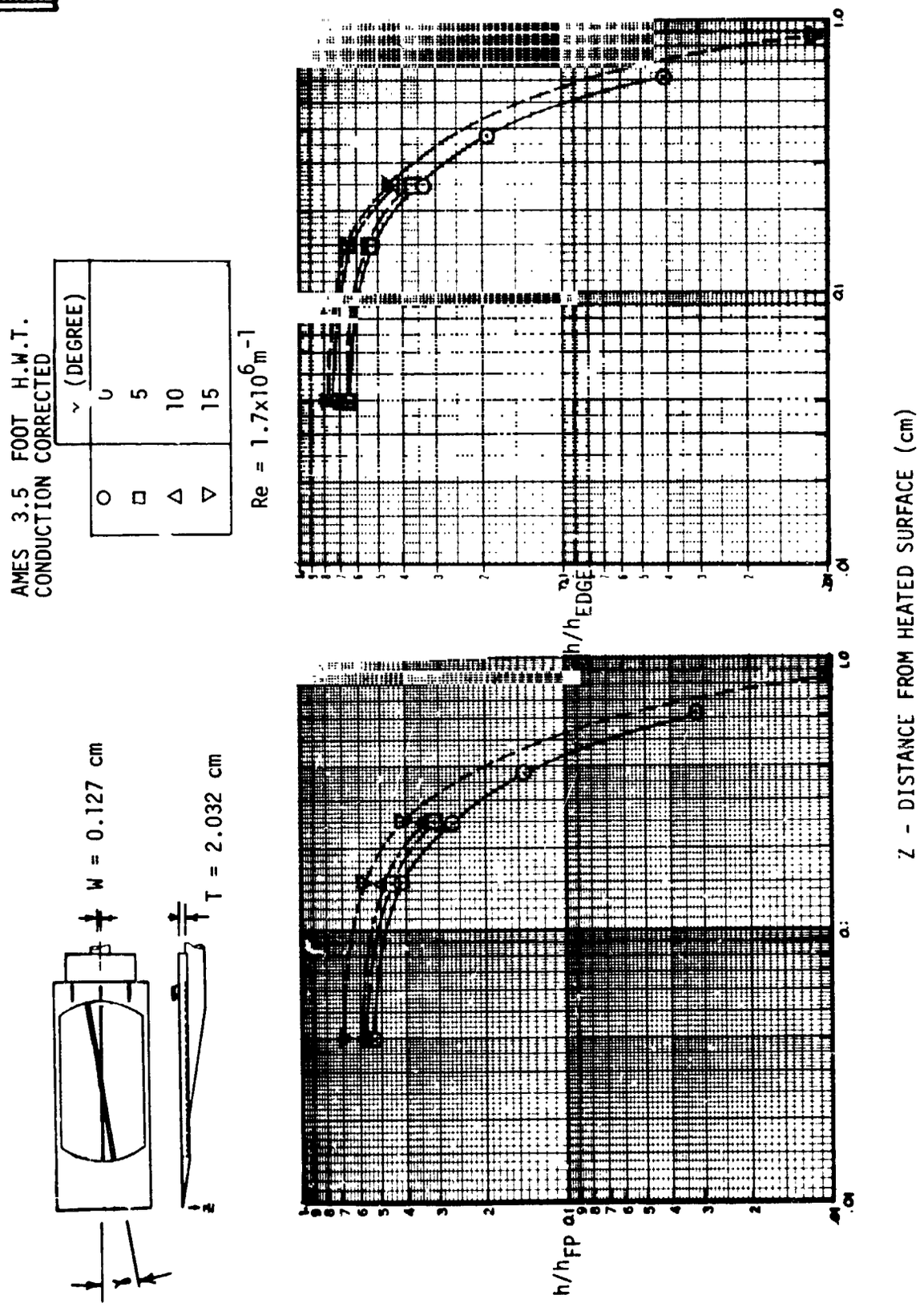

Figure 126

REYNOLDS NUMBER AND GAP WIDTH AFFECT HEATING TO IN-LINE GAP, LAMINAR CONDITIONS

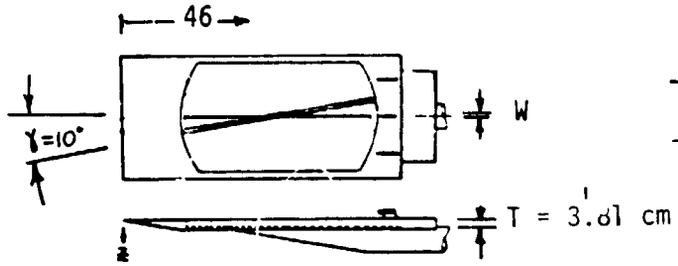

γ = 10 DEGREE
AMES 3.5 FT. H.W.T.

——— Re = $6.6 \times 10^6 m^{-1}$

– – – – – Re = $3.2 \times 10^6 m^{-1}$

CONDUCTION CORRECTED

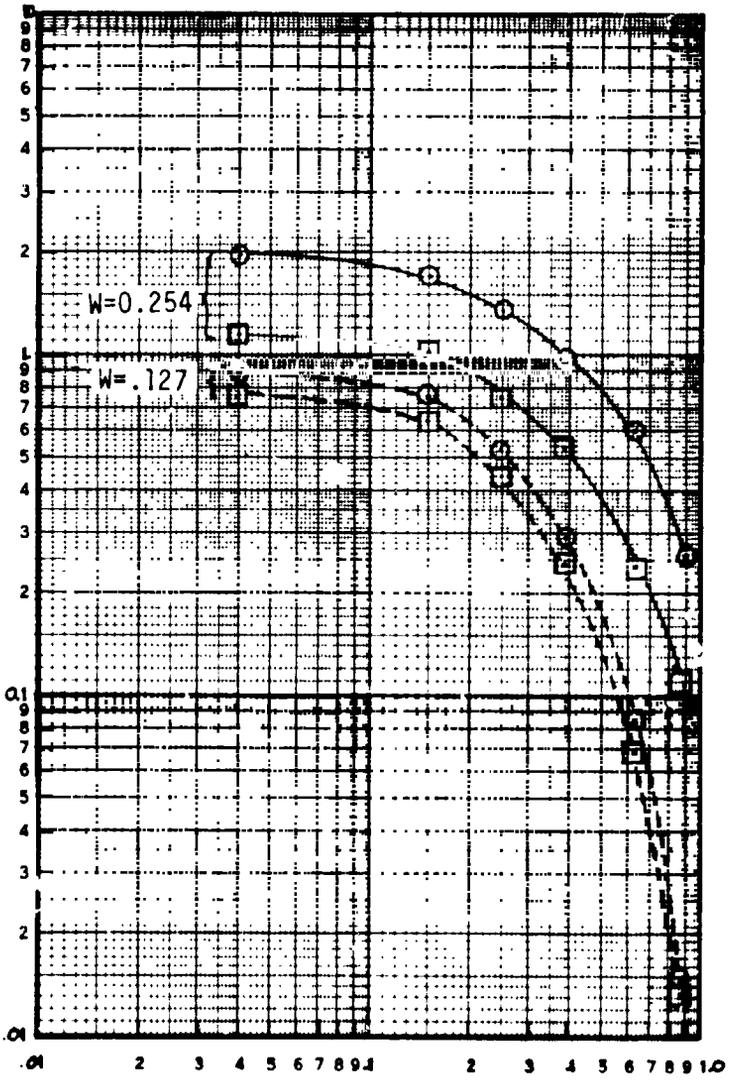

Z - DISTANCE FROM HEATED SURFACE (cm)

Figure 127

4.6 Analysis of LaRC 8 Foot HTST Tests of Gap Heating Panel - Data from the LaRC 8 Foot HTST were analyzed to determine the effects of a large (11) field of tiles on heating patterns at critical locations on the tile when subjected to relatively thin ($0.61 \leq \delta^* \leq 1.43$ cm) turbulent boundary layer. A smooth plate was positioned in the test sled in place of the gap test panel to obtain calibration heating data to determine the degree of flow non-uniformity and as a reference for the gap heating data. The calibration data (Figure 128) showed a minimal deviation on the panel especially in center 25 centimeters where the thin skin tile was located. The heating across the test panel at various X-stations was essentially uniforms with a data spread around a mean. The reference heating curves used in the data analysis are shown in Figure 128 . Reference 3 contains oil flow patterns and additional heating measurements on the test sled which also indicates uniform flow. Flow fences at the sides of the sled were employed during the gap panel tests. Heating patterns were examined for both in-line and staggered tile patterns at three gap widths. Also the increase in gap heating caused by protruding tile were assessed. The panel was instrumented very heavily at the top of the gap so good definition of heating on the radiused portion of the tile could be measured. Test conditions, model description, and data assimilated are discussed in Section 3.6 and Volume II of this report. The central tile (thin skin stainless steel) was held in the same position for all tests so direct comparisons could be made as panel configuration was changed.

4.6.1 Staggered Tiles - One of the most critical gap heating locations is the T-slot where an in-line gap terminates in a transverse gap. Indeed, high heating was experienced (see Figure 129) at the stagnation point.

The radiused portion of the leading edge of the tile experienced a 2.6 fold increase in heating. Instrumentation on either side of the radiused zone substantiate the high heating. Alone the Y = 3.8 cm cut, heating on the forward portion of the tile was more uniform and near the outboard edge of the tile the heating dropped below the smooth plate value. This suggests that the boundary layer flow from the upstream tile protected the downstream tile. It should be pointed out that the heating on the center of the tile was uniform and nearly equivalent to that measured on the calibration plate. This is in contrast to what was measured in the CFHT test facility.

On the aft portion of the tile the heating pattern reversed. Along the tile centerline the heating drops off very pronounsly with distance until at the trailing edge the heating was halved. At the outer edge of the tile, the heating remains nearly constant except for the trailing edge of the tile where high heating

HEATING ON PANEL WITHOUT GAPS (LaRC 8 FOOT HIGH TEMPERATURE STRUCTURES TUNNEL)

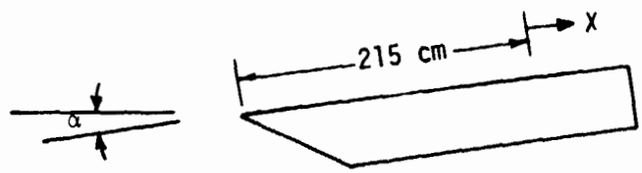

TEST	RUN	COMBUSTOR PRESSURE (N/m^2)	α (DEG)
58	1	7.10×10^6	7.7
58	3	6.55×10^6	0.0
58	4	17.9×10^6	0.08

NOTE
o MEASUREMENTS MADE AT FIVE LATERAL STATIONS ACROSS PANEL

- - - - DATA SPREAD

——— CURVE USED AS REFERENCE FOR GAP TESTS

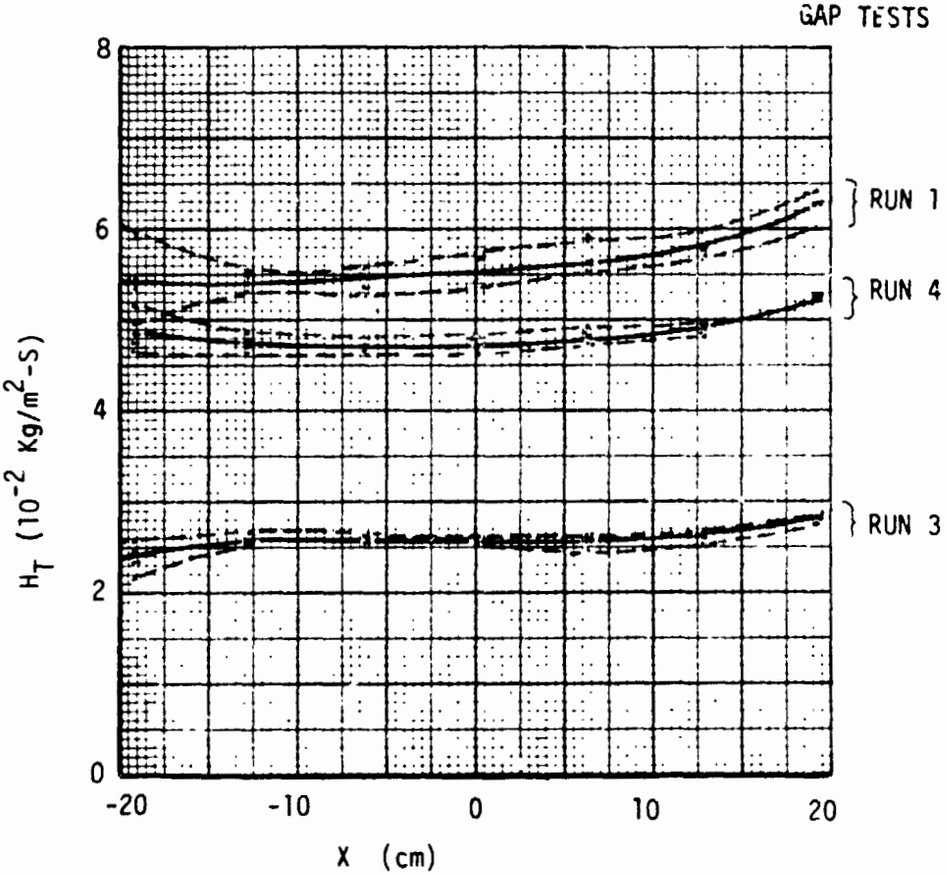

Figure 128

HEATING DISTRIBUTION ON TILE IN 8 FOOT HTST

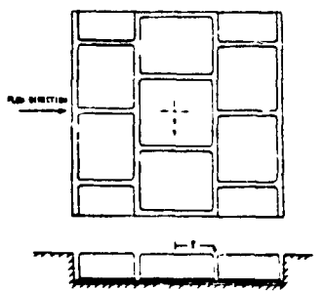

$Re_{/m}$ = 2.067 x 10^6

STAGGERED TILES
GAP WIDTH = 0.178 CM
0.254 CM EDGE RADIUS
TEST 57 RUN 4

○	y = 0
□	y = +3.8 CM
△	y = 7.1 CM
⊿	y = -7.1 CM

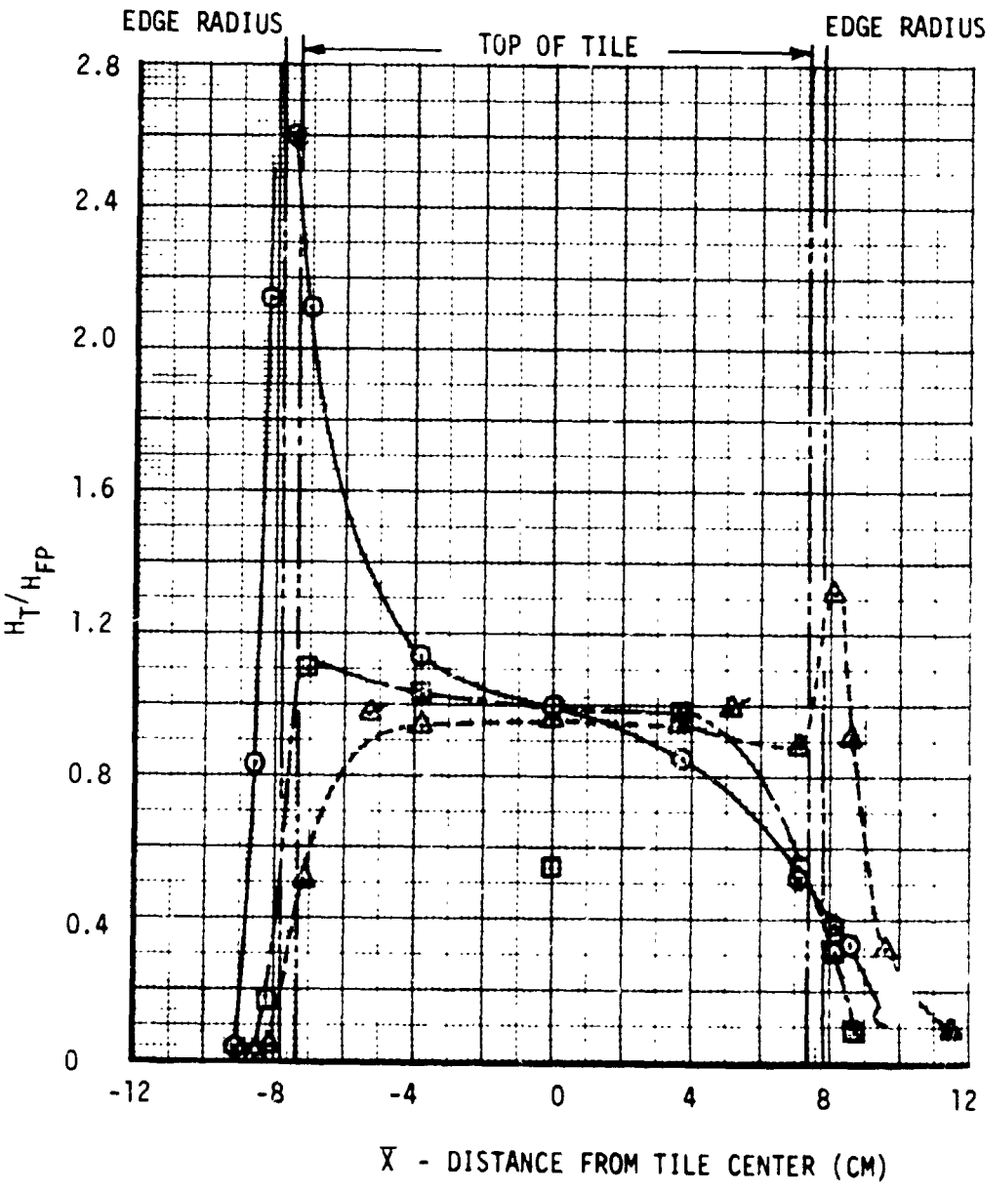

Figure 129

($h_T/h_{FP} \sim 1.3$) was measured. This could be due to an enthalpy dump. Data measured by the same thermocouple for an in-line tile configuration did not record high heating, hence the energy damp effect must be real for the staggered tile configuration.

When the free stream unit Reynolds number was doubled (Figure 130), the heating ratio level increased. Heating ratios increased by as mush as 30%. For all data analyzed the measured heating was ratioed to that measured on a smooth calibration. At the higher Reynolds number condition the edge experienced at heating ratio of 2.9 and the energy damp zone had a ratio of 1.67. These high heating ratios should be of concern when designing a TPS.

In-line Gap - Gap heating distributions at two stations along the in-line gap were examined (Figure 131) to determine the influence of distance along the gap and gap width. As can be noted from the data for the narrower gap (W = 0.102 cm), a significant heating increase was realized at the downstream station. As the gap width increased, heating at the upstream station increase and heating at the downstream station decreased. Again these observations are characteristic of a complicated flow over the tiles and through the gap.

Effect of Gap Width on Heating at Critical Locations - Next the heating at various locations on the tile was examined for a staggered tile pattern (Figure 132) and for an in-line tile pattern (Figure 133). These analyses were performed for several gap widths. As can be seen in Figure 132 for the staggered tiles, the leading edge (T/C 1 and 91) experience significant heating.

Heating ratios as high as 3.2 are imposed on tiles with wide (0.3 cm) gaps. Nominal smooth plate heating experienced at the tile center for all gap widths and the heating at the trailing edge (T/C 65) remains a constant ($h_T/h_{FP} \sim 0.5$) independent of gap width. The energy damp at T/C 17 decreased slightly for the wider gaps (h_T/h_{FP} decreased from 1.3 to 1.1).

4.6.2 In-Line Tiles - The in-line tile pattern also produced interesting heating patterns. As can be seen from Figure 133 the high heating location was on the outboard region of the tile just aft of leading edge rather than on the leading edge at the tile's centerline as was the case for the staggered tiles. The forward corner (T/C 6) of the tile experienced heating ratios of approximately 1.85, with only a modest increase as the gap was opened. At T/C 66, which was on the tile's top near the leading edge, high heating was measured with a stronger dependency on gap width (h_T/h_{FP} of 1.86 to 2.2).

HEATING DISTRIBUTION ON TILE IN 8 FOOT HTST

STAGGERED TILESS

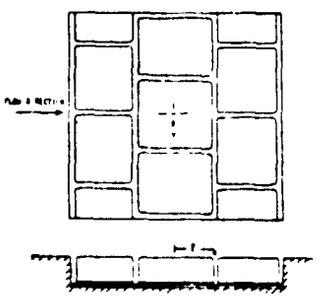

$Re_\infty/_m = 4.82 \times 10^6$
GAP WIDTH = 0.178 CM
0.254 CM EDGE RADIUS

TEST 57 RUN 7

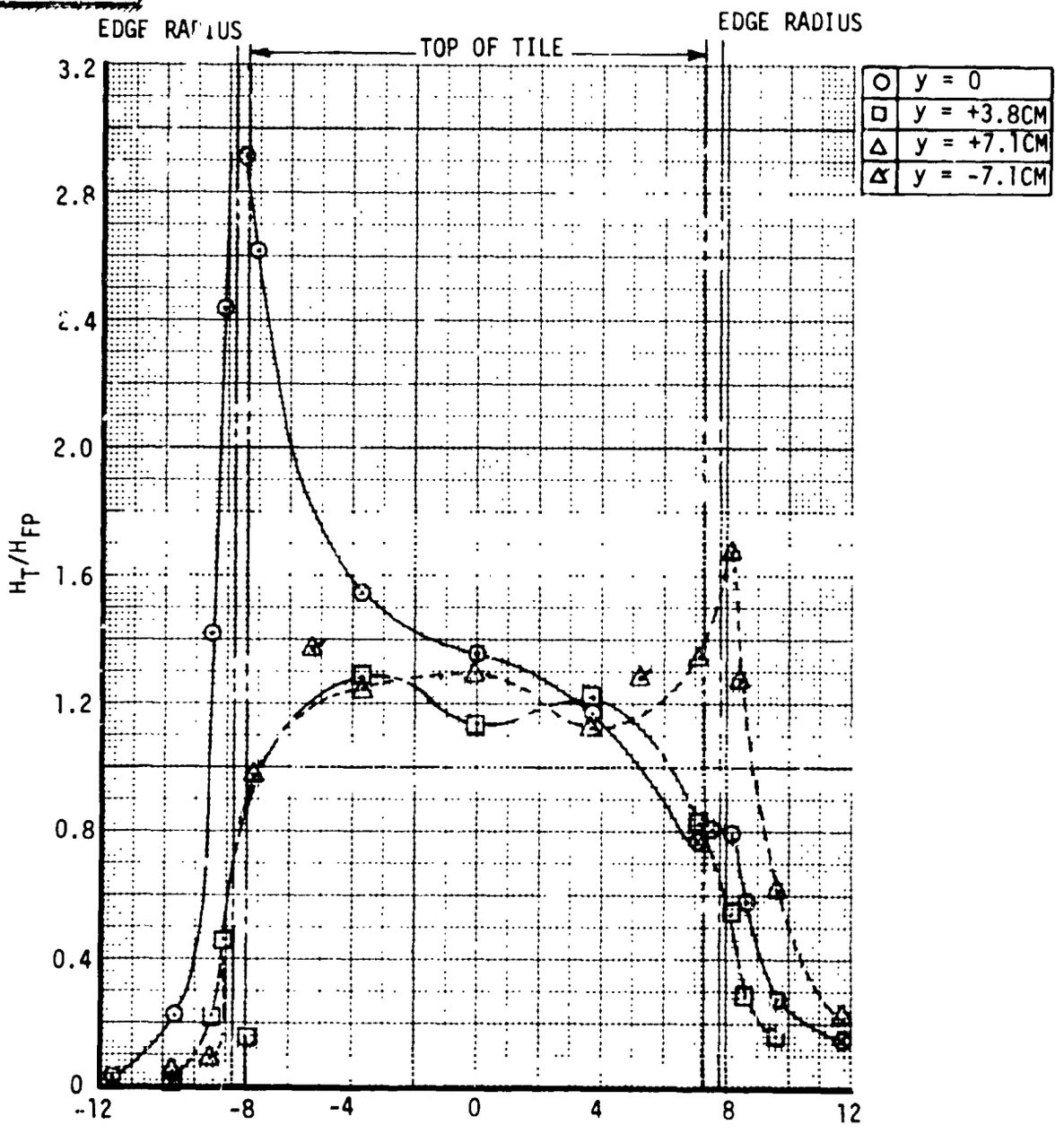

Figure 130

INFLUENCE OF GAP WIDTH ON EDGE HEATING ALONG IN-LINE GAP, 8 FOOT HTST TEST

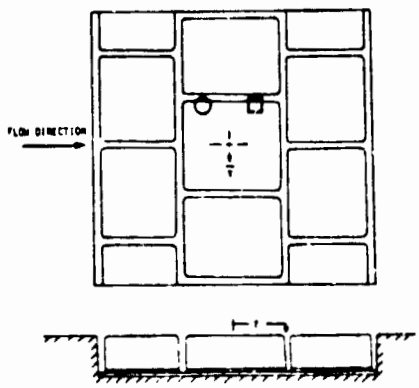

STAGGERED TILES

0.254 cm EDGE RADIUS
W = GAP WIDTH

○	X = -5.26cm
□	X = +5.22cm

TEST 57, RUNS 4, 9 AND 11

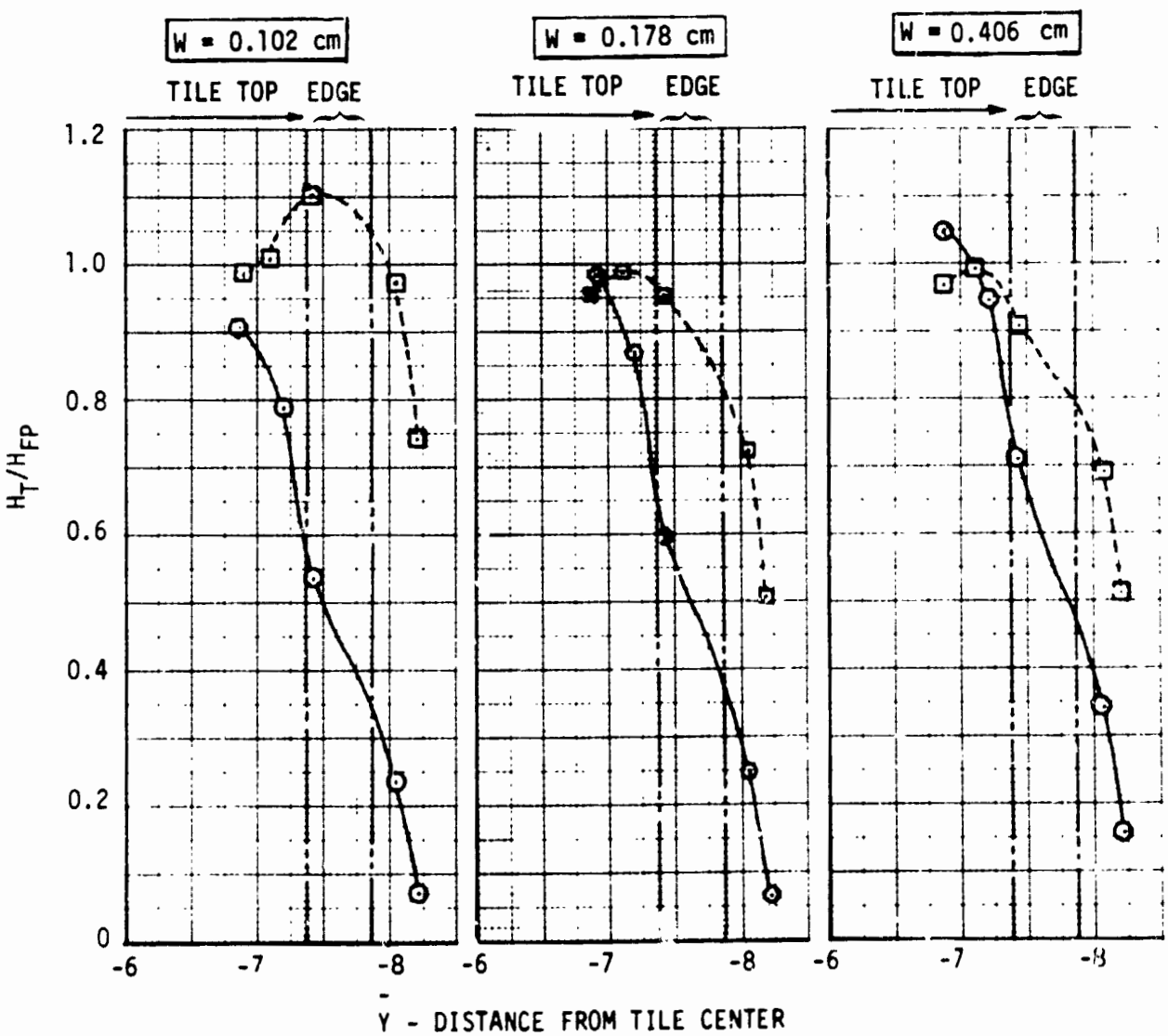

Figure 131

INFLUENCE OF GAP WIDTH ON HEATING OF STAGGERED TILES, 8 FOOT HTST

$Re_\infty/_m = 2 \times 10^6$

7.5° ANGLE OF ATTACK

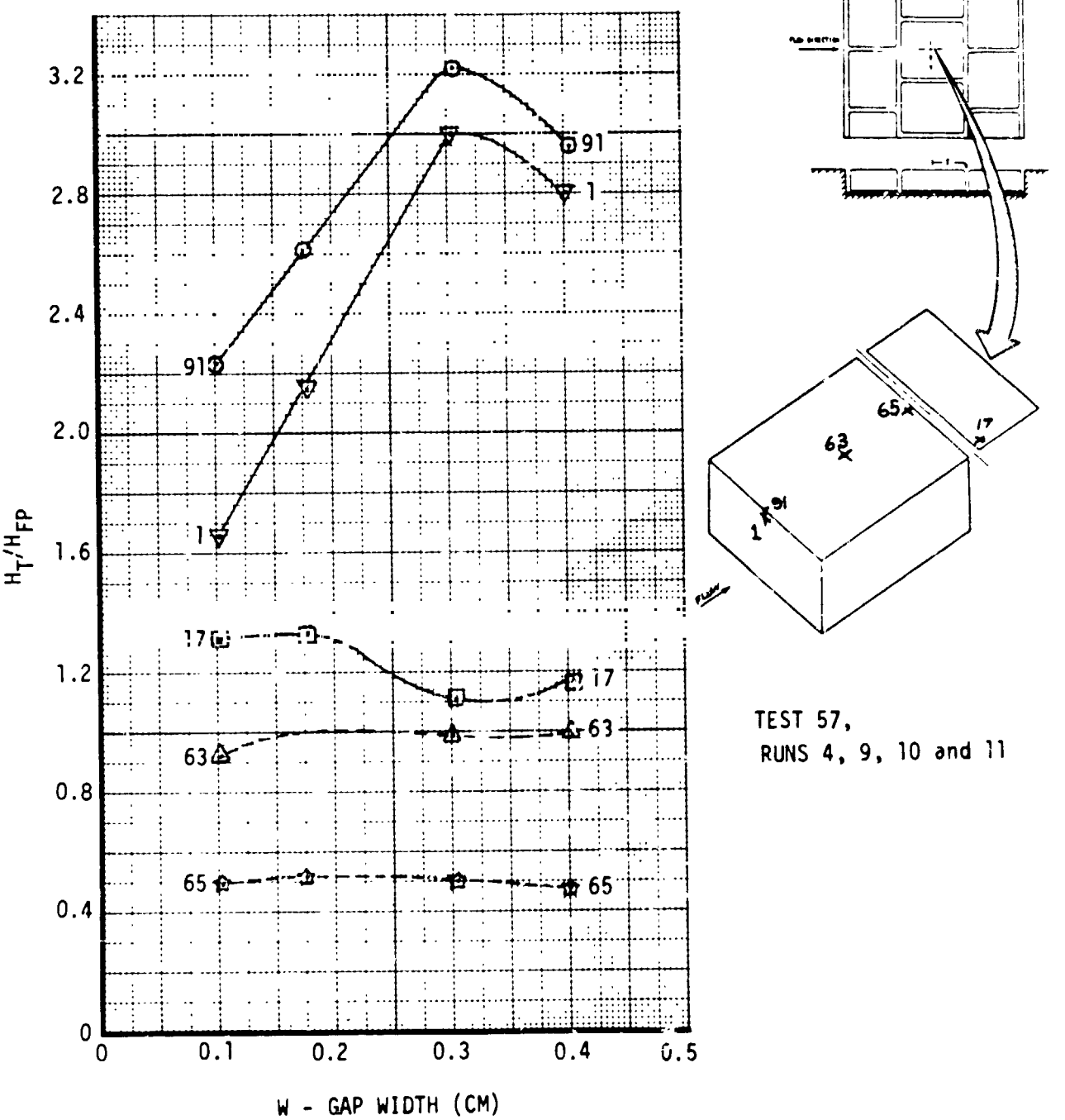

TEST 57,
RUNS 4, 9, 10 and 11

Figure 132

INFLUENCE OF GAP WIDTH ON HEATING OF IN-LINE TILES, 8 FOOT HTST

$Re_{\infty}/_m = 2 \times 10^6$

7.5° ANGLE OF ATTACK

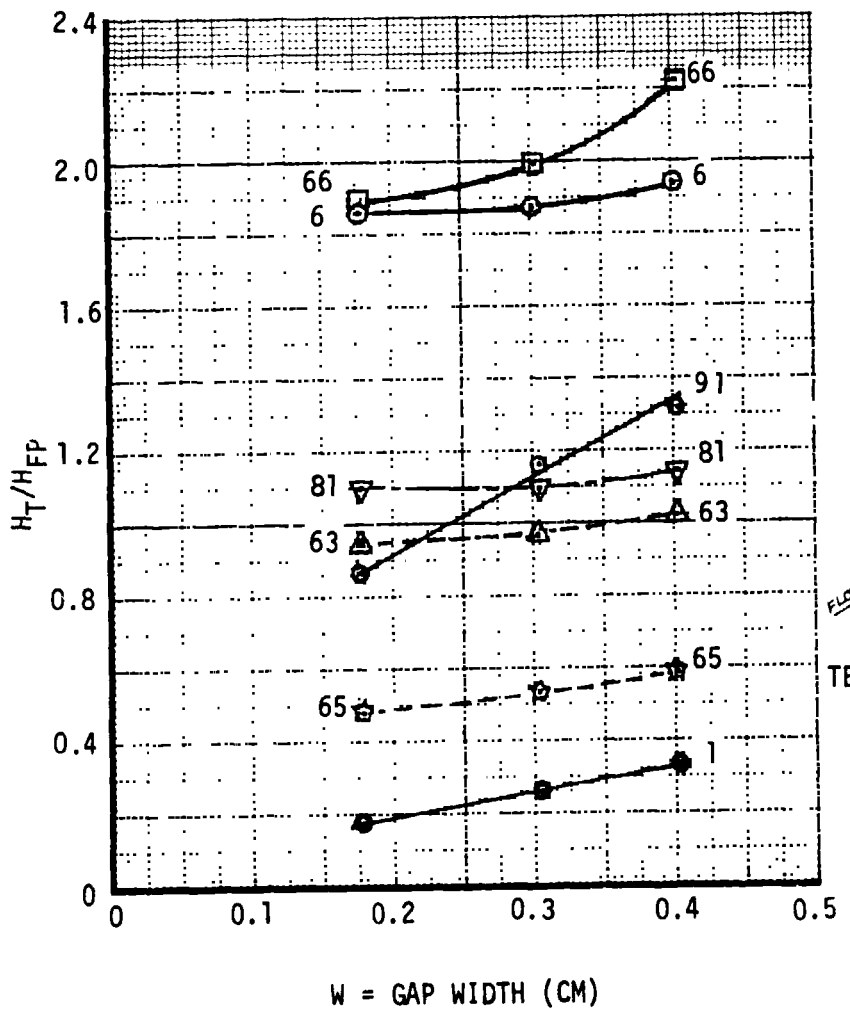

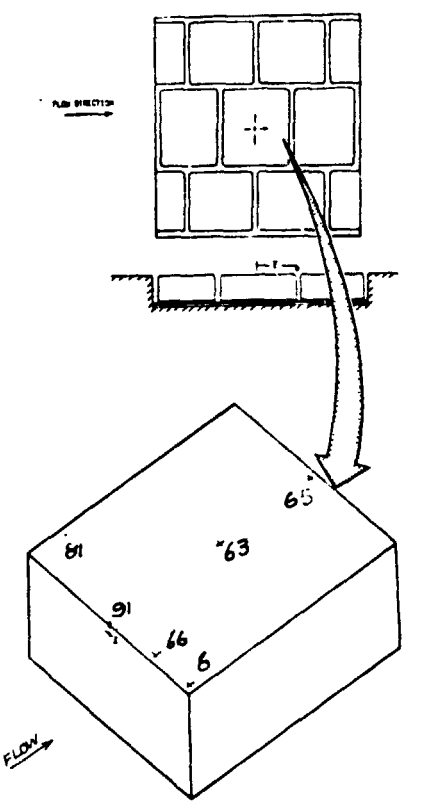

TEST 57, RUNS 13, 14 and 15

C - 3

Figure 133

Heating on the leading edge of the tile at the centerline (T/C 91) also increased with gap width but at a much lower level. For the smaller gap (0.177 cm), T/C 91 recorded less than the smooth plate heating, but showed a strong sensitivity to gap width with a 30% increase in heating over the smooth plate for the widest gap (W = 0.4 cm). Apparently this region of the gap is sheltered for narrow gaps but becomes subjected to the onslaught of the flow for wide gaps. The center of the tile receives, essentially, heating as if there were no gaps. The heating drops off significantly near the trailing edge of the tile as was the case for the staggered tile. This could be due to a local thickening of the boundary layer upstream of a transverse gap. From the data obtained from these tests it should be possible to formulate a flow field model to describe the heating on the top surface of the tile. Figure 134 shows such a flow model. The location and strengths of the crests would be dependent on gap width and the ability of the adjoining gaps to alter crest strength. Of course Reynolds number, Mach number and other flow field parameters would characterize the nominal boundary layer.

4.6.3 Steps - Both in-line and staggered tile patterns were tested with the tiles being flush and with the central tile protruding 0.254 cm into the flow. As can be readily seen from Figure 135, heating on the leading edge of the tile and the forward facing wall experience very high heating. This data indicates that it makes little difference if the tiles are in-line or staggered; essentially the same high heating is experienced when there is a 0.254 cm step. One exception is at the center of the leading edge--the staggered tile receives only a 3.2 heating factor while the in-line tile receives a 3.45 factor. It should be pointed out that the severe heating has "washed" out at the center of the tile where smooth plate heating occurs while the trailing edge is relatively cool ($h_T/h_{FP} \sim 0.5$).

4.6.4 Specific Heat and Conduction Corrections - The preceding analyses were accomplished using data as received on the data tape from the 8 Foot HTST. Examination of the temperature histories such as shown in Figure 136, indicate that there were temperature gradients across the thin skin tile at the time heat transfer coefficients were originally computed. The data reading program was modified to account for thermal conduction in two orthogonal directions. In some instances the heating rates changed by as much as 3.8%. Of course, where there was little or no temperature gradient, the heating rate remained unchanged. Figure 137 shows the change in a heating distribution on the tile when considering thermal conduction.

FLOW MODEL FOR MULTI-GAP PANEL

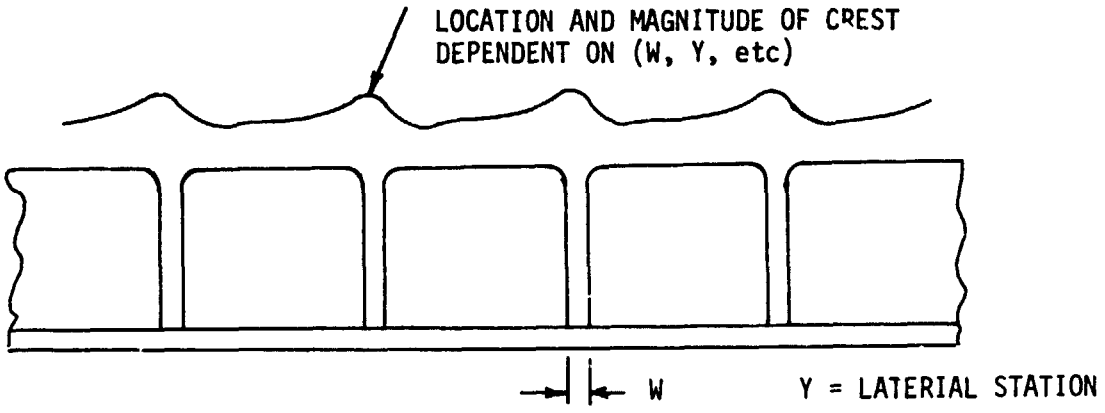

Figure 134

STEPS CAUSE SEVERE HEATING IN-LINE OR STAGGERED TILES, 8 FOOT HTST

$Re_\infty/_m = 2 \times 10^6$

7.5° ANGLE OF ATTACK

-----STAGGERED TILES

_____IN-LINE TILES

0.173 CM GAP

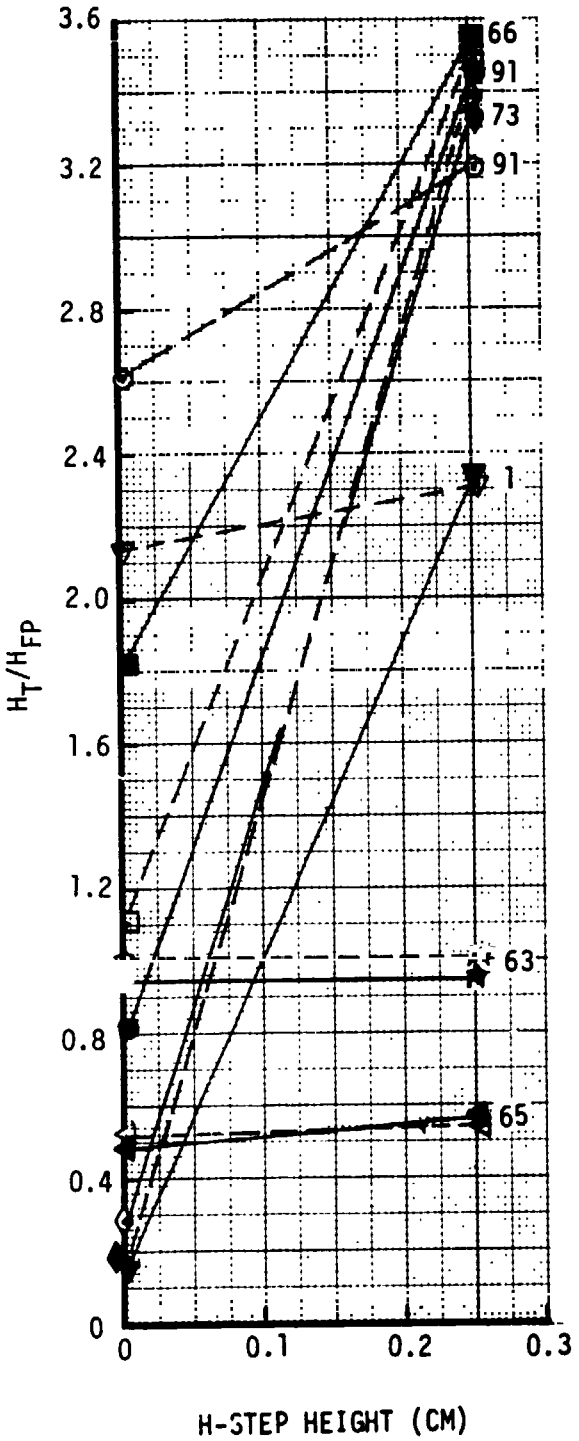

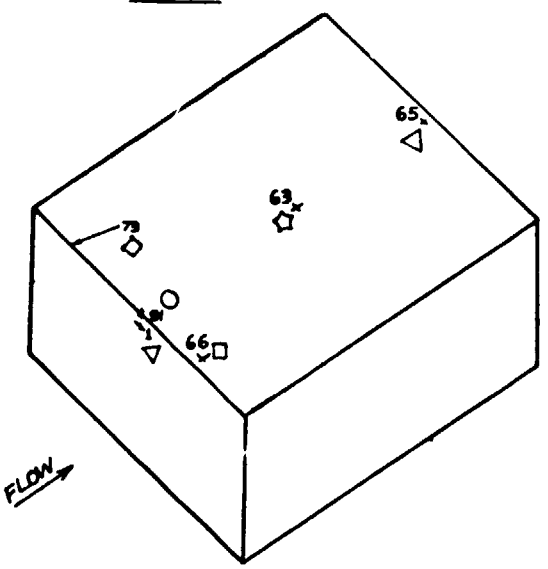

STAGGERED TILES

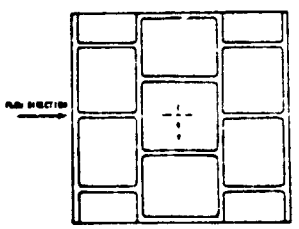

IN-LINE TILES

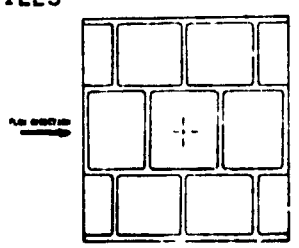

Figure 135

TYPICAL THERMAL RESPONSE OF THIN SKIN METALLIC TILE, 8 FOOT HTST TESTS

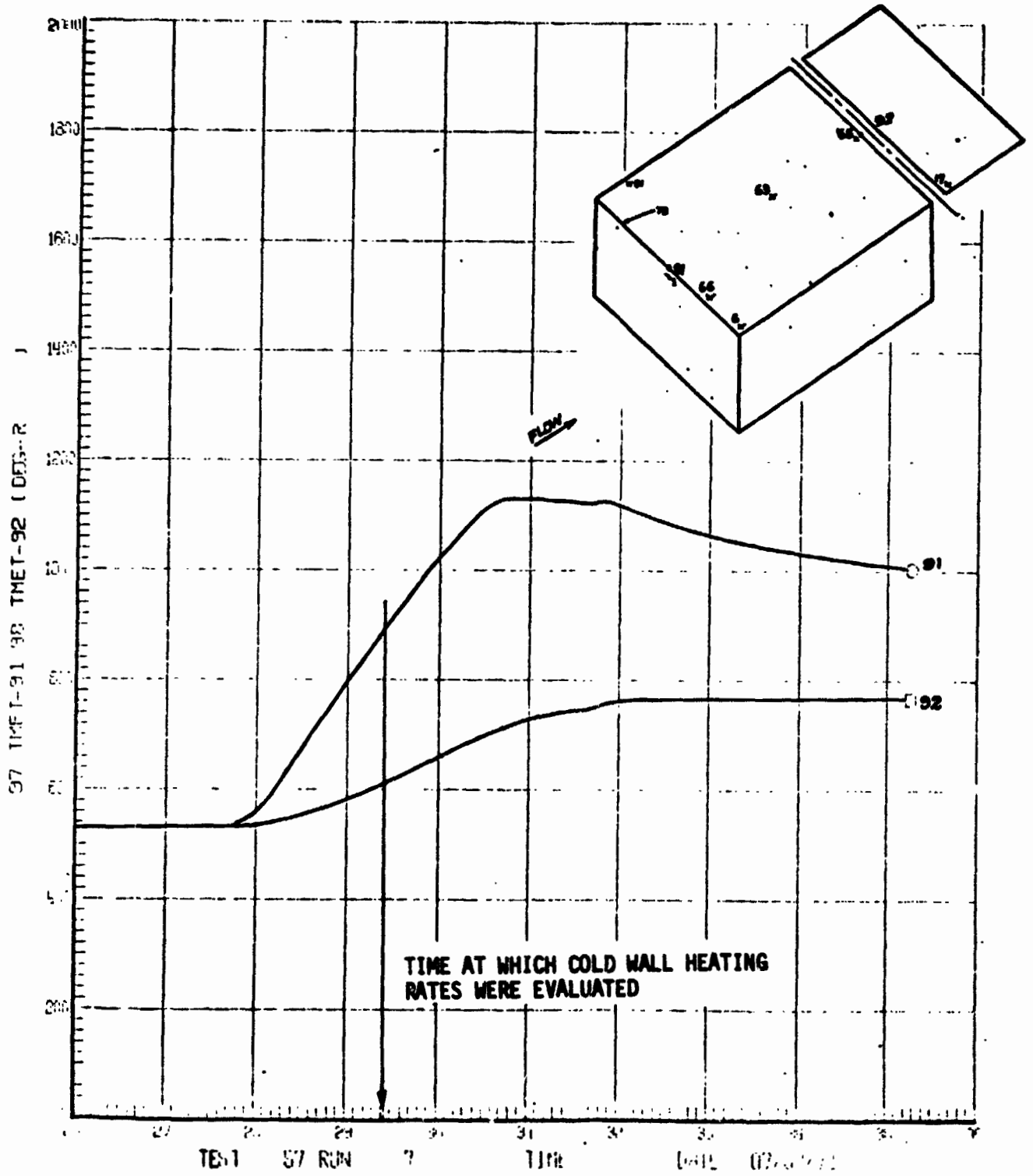

Figure 136

HEATING DISTRIBUTION ON TILE IN 8 FOOT HTST SHOWING CONDUCTION EFFECTS

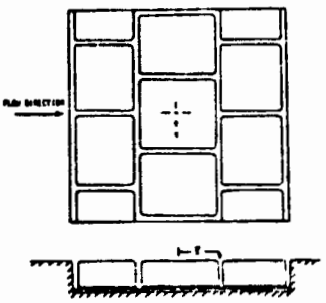

$Re_{/m} = 2.067 \times 10^6$

STAGGERED TILES
GAP WIDTH = 0.178 CM
0.254 CM EDGE RADIUS
TEST 57 RUN 4

○	y = 0
□	y = +3.8 CM
△	y = 7.1 CM
⍙	y = -7.1 CM

SOLID SYMBOLS ARE CONDUCTION CORRECTED - (H_{Tc}/H_{FP})

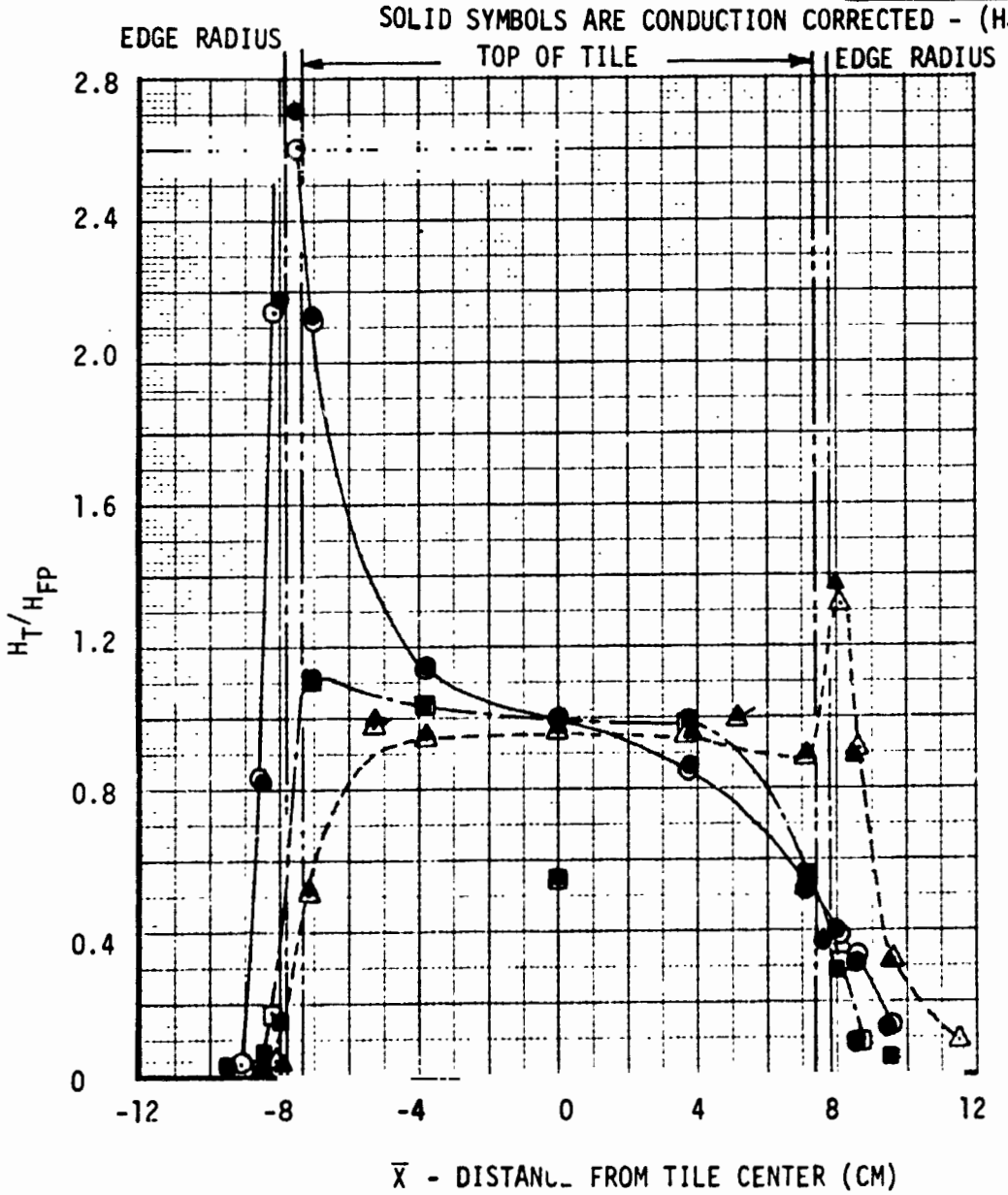

Figure 137

Specific heat measurements on the thin skin tile material and the calibration plate were performed at the conclusion of the test program. This information (Figure 138) was furnished by I. Weinstein of LaRC so that the data could be corrected. The specific heat of the thin skin material was 5.6% higher than that of the calibration plate at room conditions (300°K). In the original data reduction the same specific heat was used for both materials. Hence the heating ratio (h_T/h_{FP}) was 5.6% low. The Data Bank was corrected for both heat storage and thermal conduction effects.

4.6.5 Gap Heating Distributions - The staggered and in-line tile patterns produce significantly different heating distributions on the downstream wall of a gap. Figure 139 shows the sensitivity of gap heating to gap width and Reynolds number for the staggered tiles.

The point analyzed in Figure 139 experiences "T-slot" flow/heating. From the limited test data, it appears that the heating in the gap is proportional to Reynolds number to a power greater than unity. Also the test data indicates that some relief in heating occurs as the gap is opened beyond 0.305 cm. The heating (Figure 140) in the transverse gap for the in-line tiles is much lower than for the staggered tiles. This is because the upstream tile shelters the gap. Gap heating increases with gap width.

This data shows even for very small gaps that the edge radius experiences heating ratios 1.5 or higher. The gap heating for the in-line tiles drops off more rapidly than does the measurements for the staggered tiles. The in-line data suggests an exponential function of (Z) to correlate the heating.

SPECIFIC HEAT MEASURED ON THIN SKIN MATERIALS USED IN LaRC 8 FOOT HTST TESTS

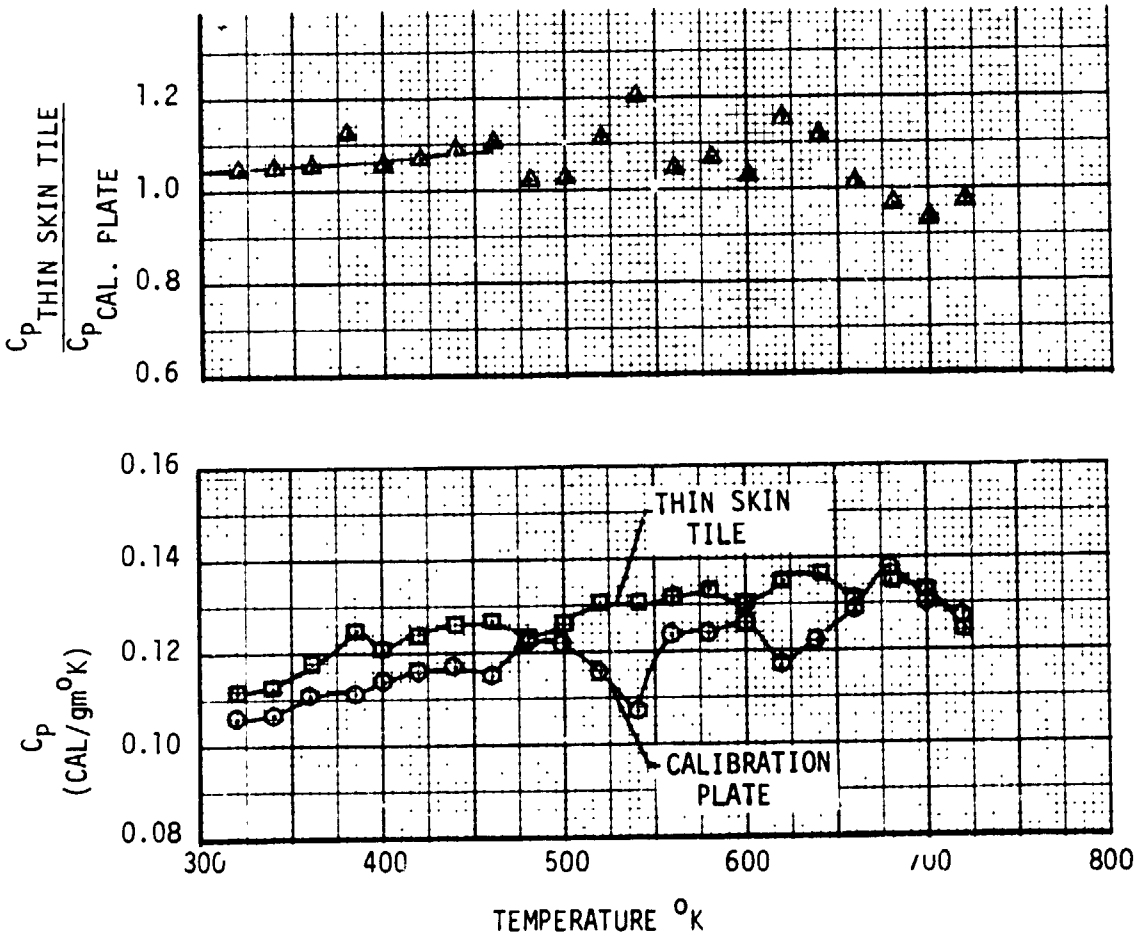

REFERENCE: I WEINSTEIN NASA LaRC, 12-10-74

Figure 138

TRANSVERSE GAP HEATING (STAGGERED TILES)

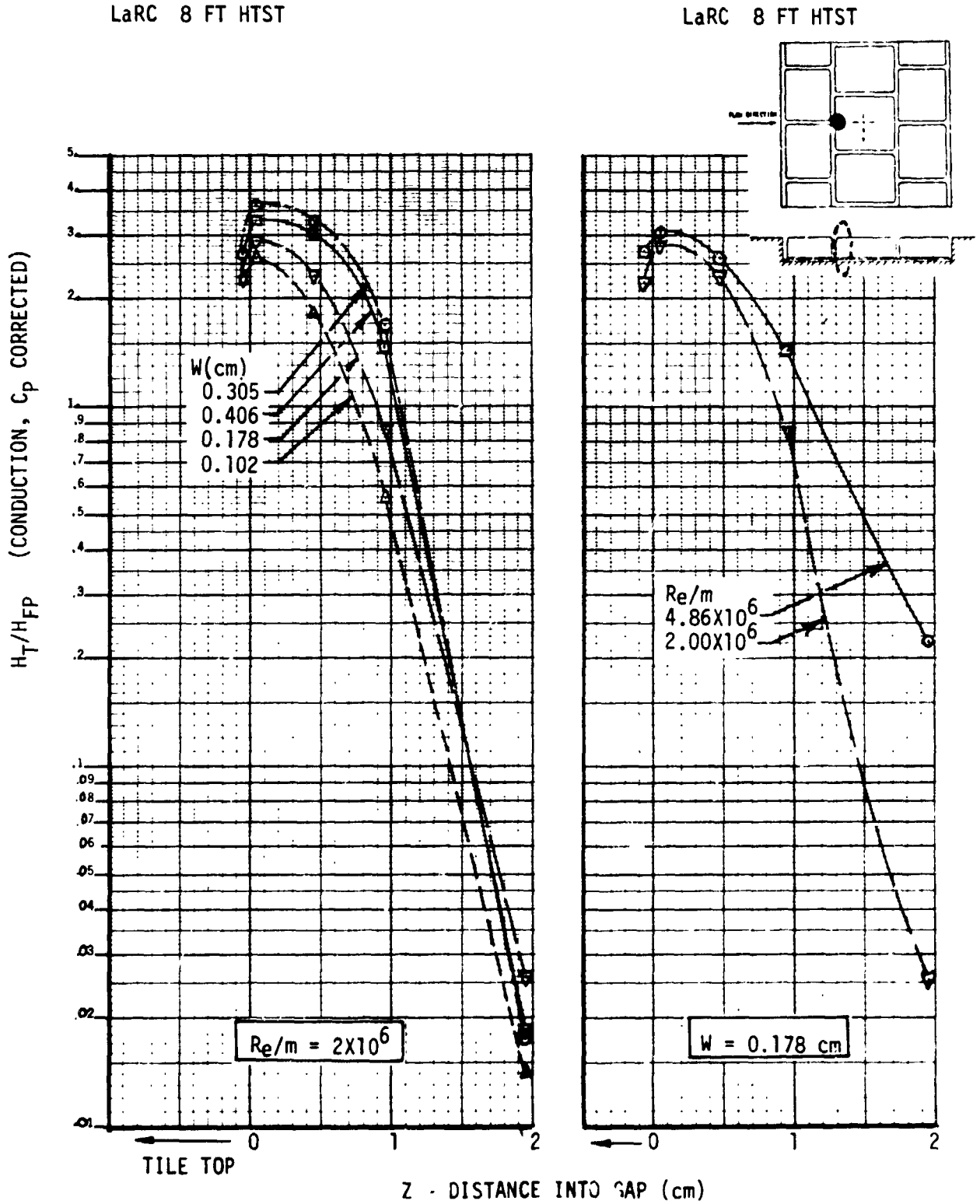

Figure 139

TRANSVERSE GAP HEATING (IN-LINE TILES)

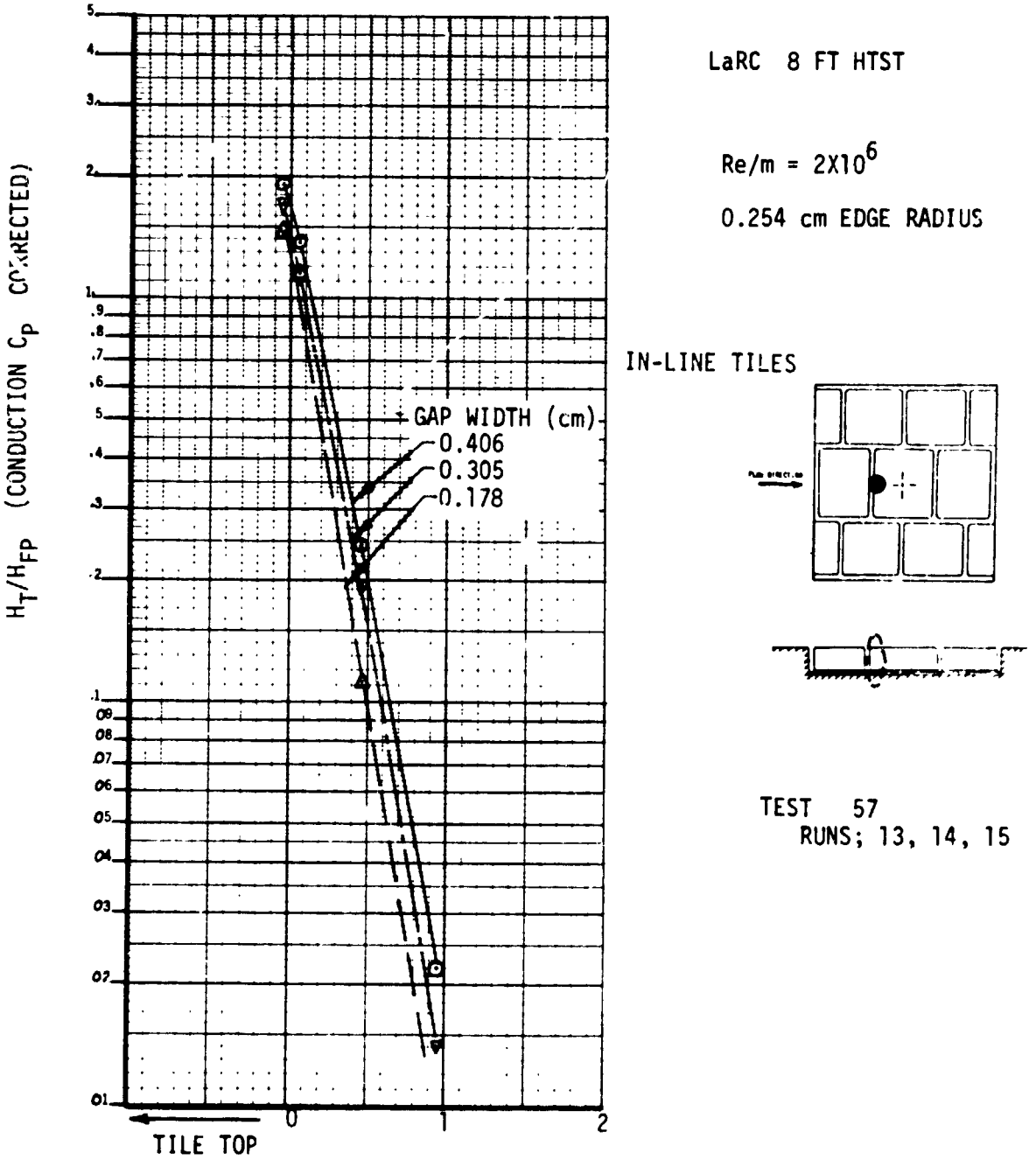

Figure 140

4.7 Analysis of RSI Tile (0.635 cm edge radius) Tests in the AMES Arc Tunnel Turbulent Duct - Temperature response data were collected on Silica RSI tile subjected to high enthalpy turbulent flow. The details of the test facili and the configuration of the test article were described in Section 3.7. The test item temperatures were used to determine sensitivity of the heating rates to gap width and were input to an inverse heat transfer model to find the local heat flux.

Due to misreporting of the thermocouple locations the original attempts to analyze the data proved difficult. However, radiographs of the test panel showing the exact instrumentation locations led to more consistent data analyses. Figure 25 shows the original and corrected thermocouple locations. Figure 141 is a copy of the x-ray of the tile.

Temperature histories of several thermocouples are presented in Figures 142, 143 and 144 for gap widths of 0.0, 0.127, and 0.180 cm, respectively. These data are from tests where T/C #1 was located in the upstream position. The figures show the upstream tile (T/C #4, 6 and 7) running slightly hotter than the downstream tile (T/C #9, 11, and 12). Also, there is a different thermal response pattern for T/C #4, and #9. Several, theories were advanced pertaining to this inconsistency, e.g. differences in local thermal properties or surface irregularities. A mold of the tile surface in the region of the gap showed that T/C #4 protruded through the RSI causing a bump on the surface. Boundary layer disturbances caused by this roughness element could be the cause of the more rapid heating at this location.

Figures 145 and 146 shows the effect of gap width on measured temperatures at 200 seconds in the test for the two flow directions. Thermocouples 4, 6 and 7 indicate consistantly higher temperatures than thermocouples 9, 11, and 12, whether they are in the upstream or downstream position. Examination of T/C #4 and 9 in Figures 145 and 146 indicates that T/C #9 gives consistant trends in both the upstream and downstream position, while T/C #4 gives rather unsystematic results. Therefore, it was decided to use T/C #9 to derive gap heating rates and to blame surface irregularity for the T/C #4 errantry. The shift in level is due to the difference in T/C depth into the slot which was found from the tile x-rays.

A thermal model of the gap and its edge radius was setup to determine effects of edge radius on gap heating using thermal response data measured on the HRSI tiles. The details of the thermal model are illustrated in Figure 147. The model uses hallmark dimensions such as V(2) to define edge radius from which node dimensions are computed.

RADIOGRAPH OF 0.635 CM RADIUS HRSI TILE

AMES RESEARCH CENTER
165KV 55MAM36
X-RAY LAB

VG2 GE300

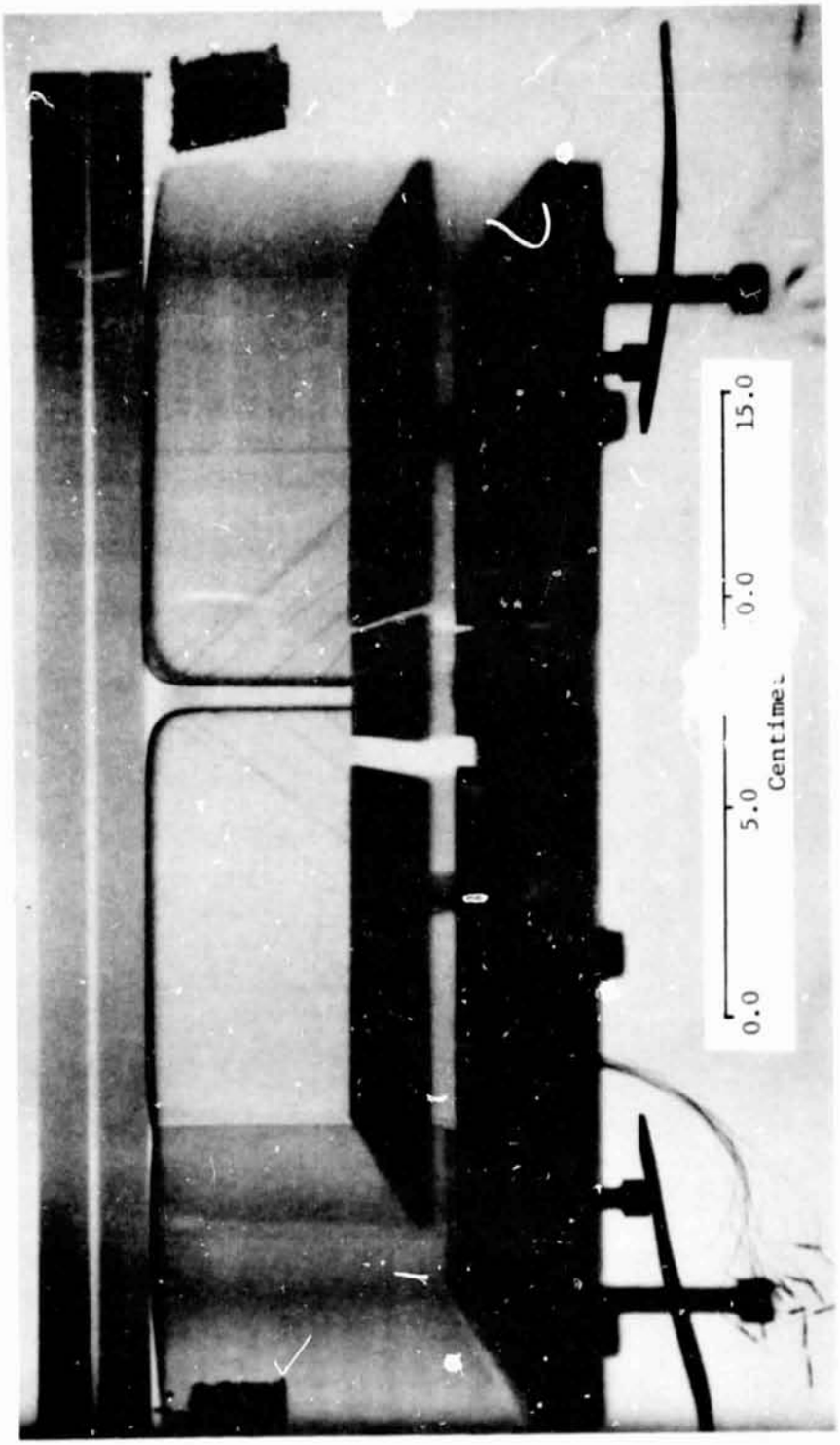

Figure 141

THERMAL RESPONSE OF HRSI TILES AT TRANSVERSE GAP

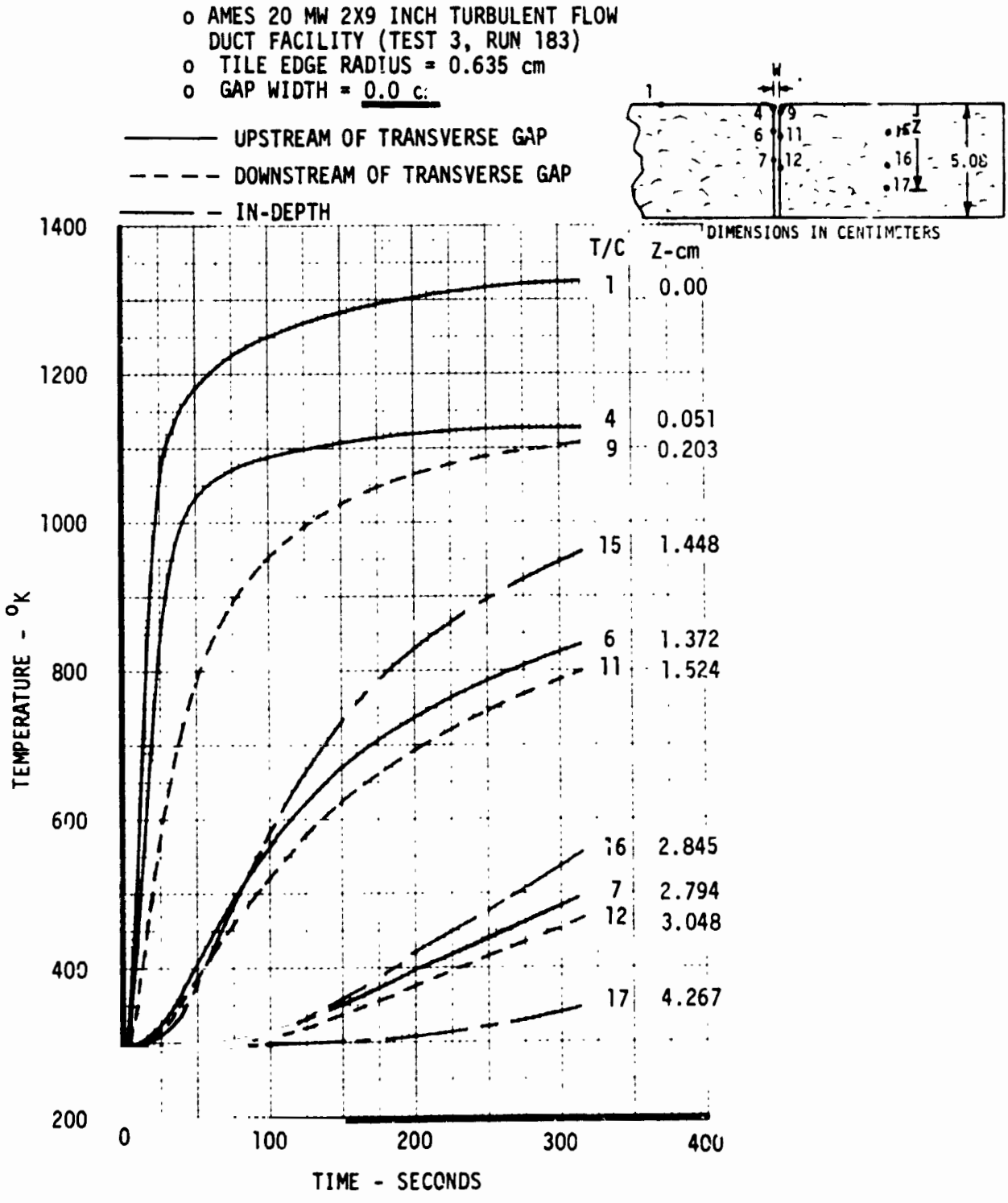

Figure 142

THERMAL RESPONSE OF HRSI TILES AT TRANSVERSE GAP

- o AMES 20 MW 2X9 INCH TURBULENT FLOW DUCT FACILITY (TEST 3, RUN 185)
- o TILE EDGE RADIUS = 0.635 cm
- o GAP WIDTH = 0.127 cm

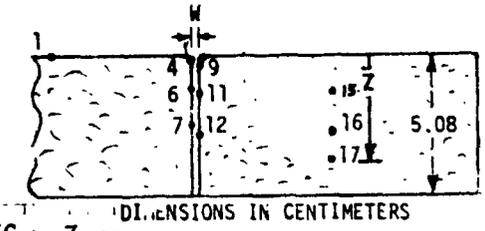

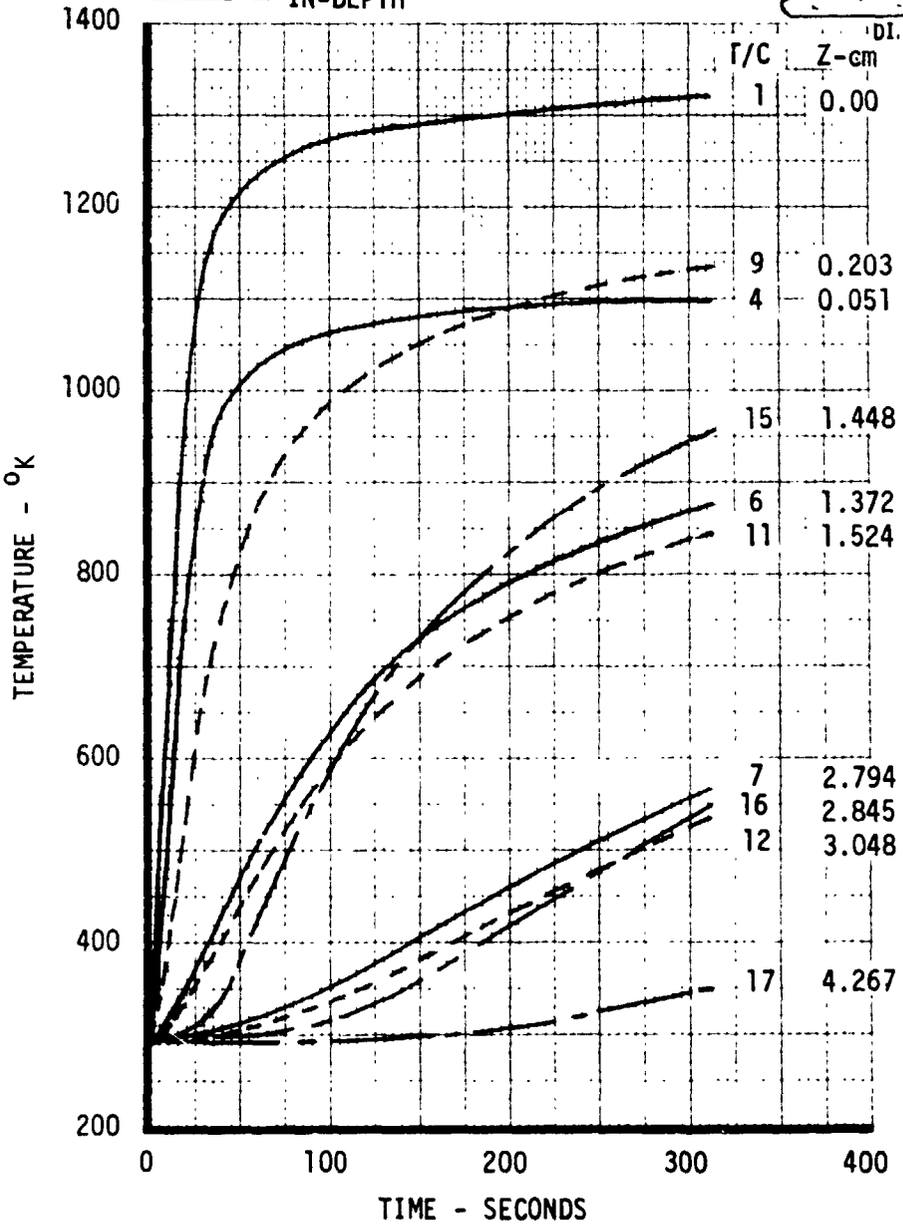

Figure 143

THERMAL RESPONSE OF HRSI TILES AT TRANSVERSE GAP

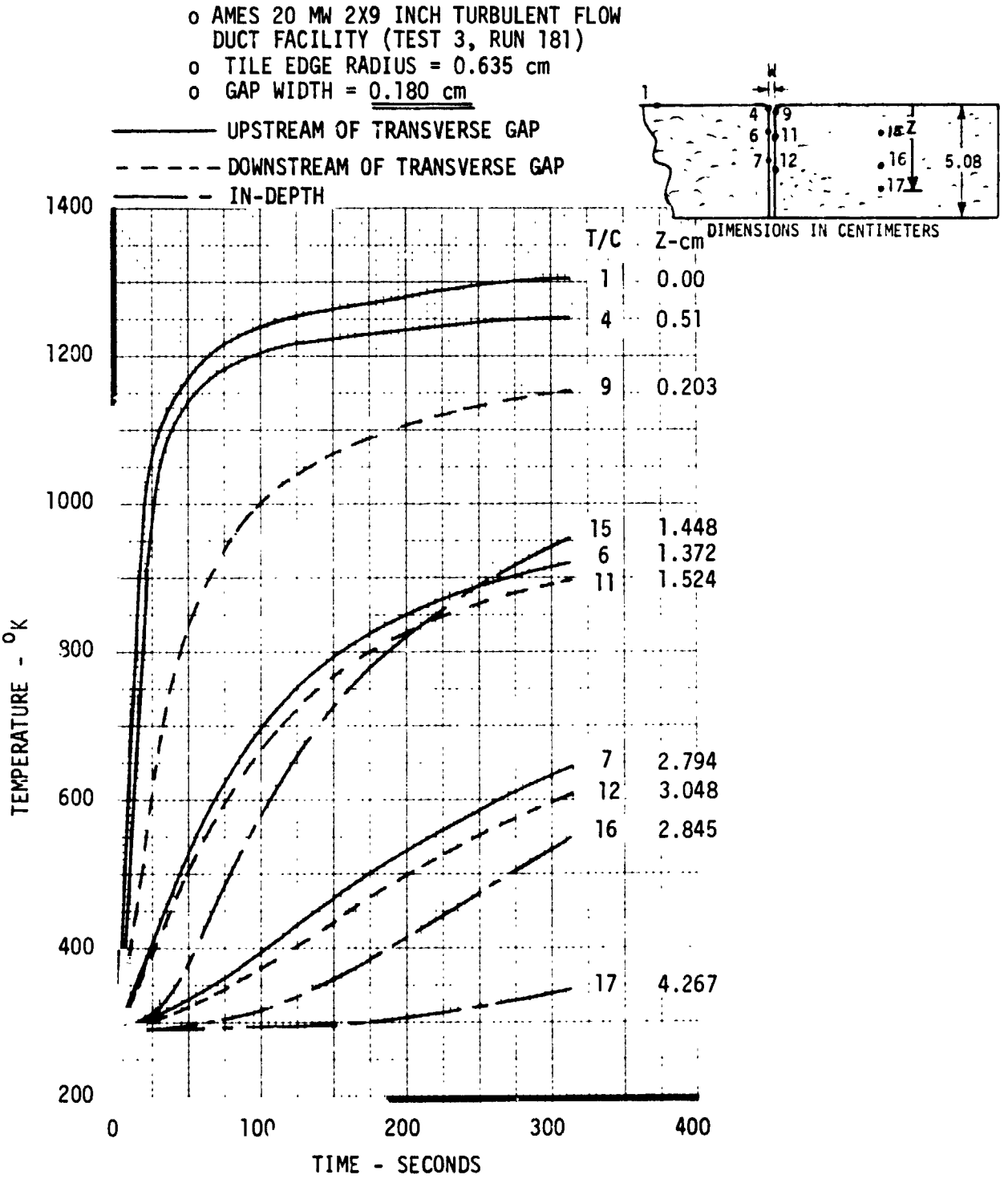

Figure 144

SENSITIVITY OF WALL TEMPERATURES TO GAP WIDTH
AMES 20 MX 2x9 INCH
TURBULENT FLOW DUCT FACILITY

(T/C #1, UPSTREAM)
200 SECONDS, EDGE RADIUS = 0.635 cm

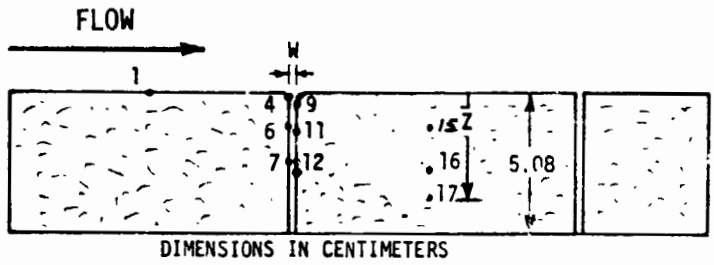

DIMENSIONS IN CENTIMETERS

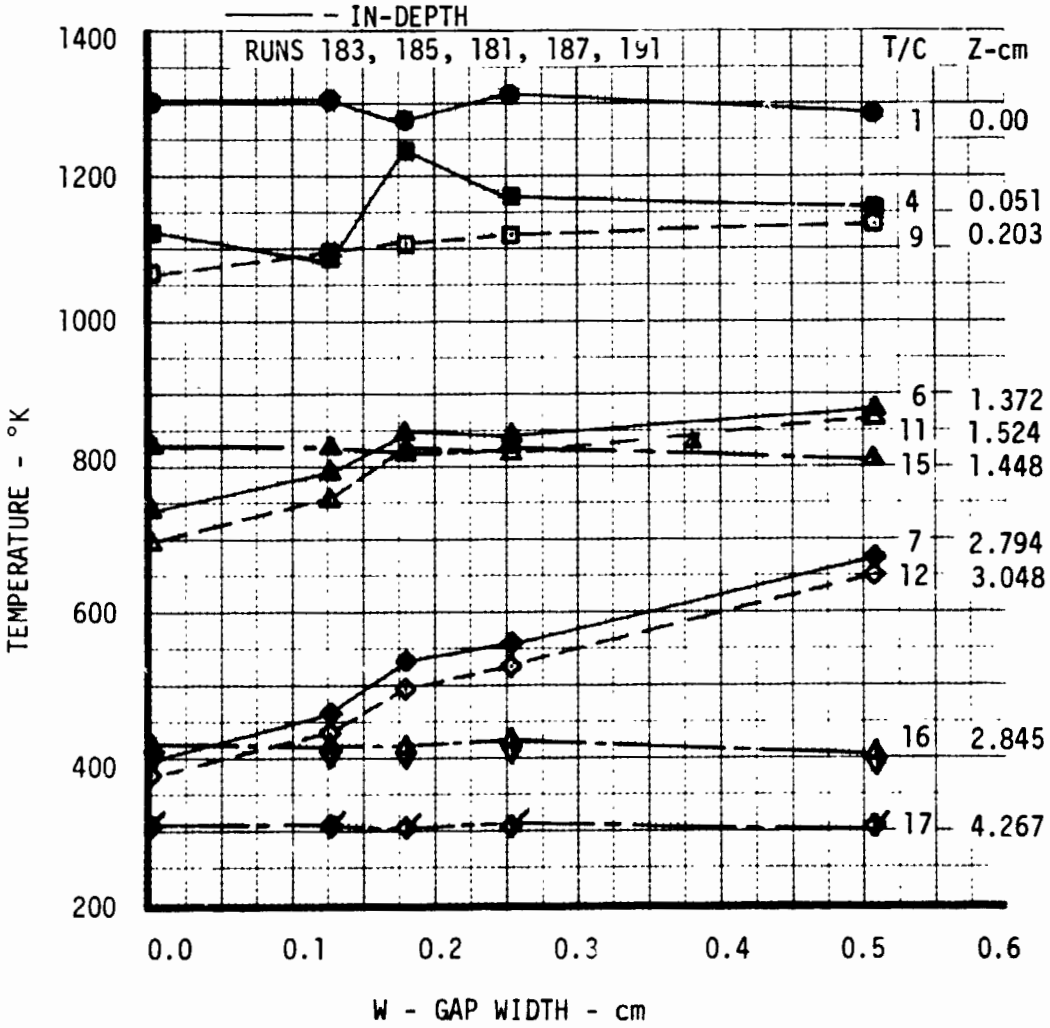

Figure 145

SENSITIVITY OF WALL TEMPERATURES TO GAP WIDTH AMES 20 MW 2x9 INCH TURBULENT FLOW DUCT FACILITY

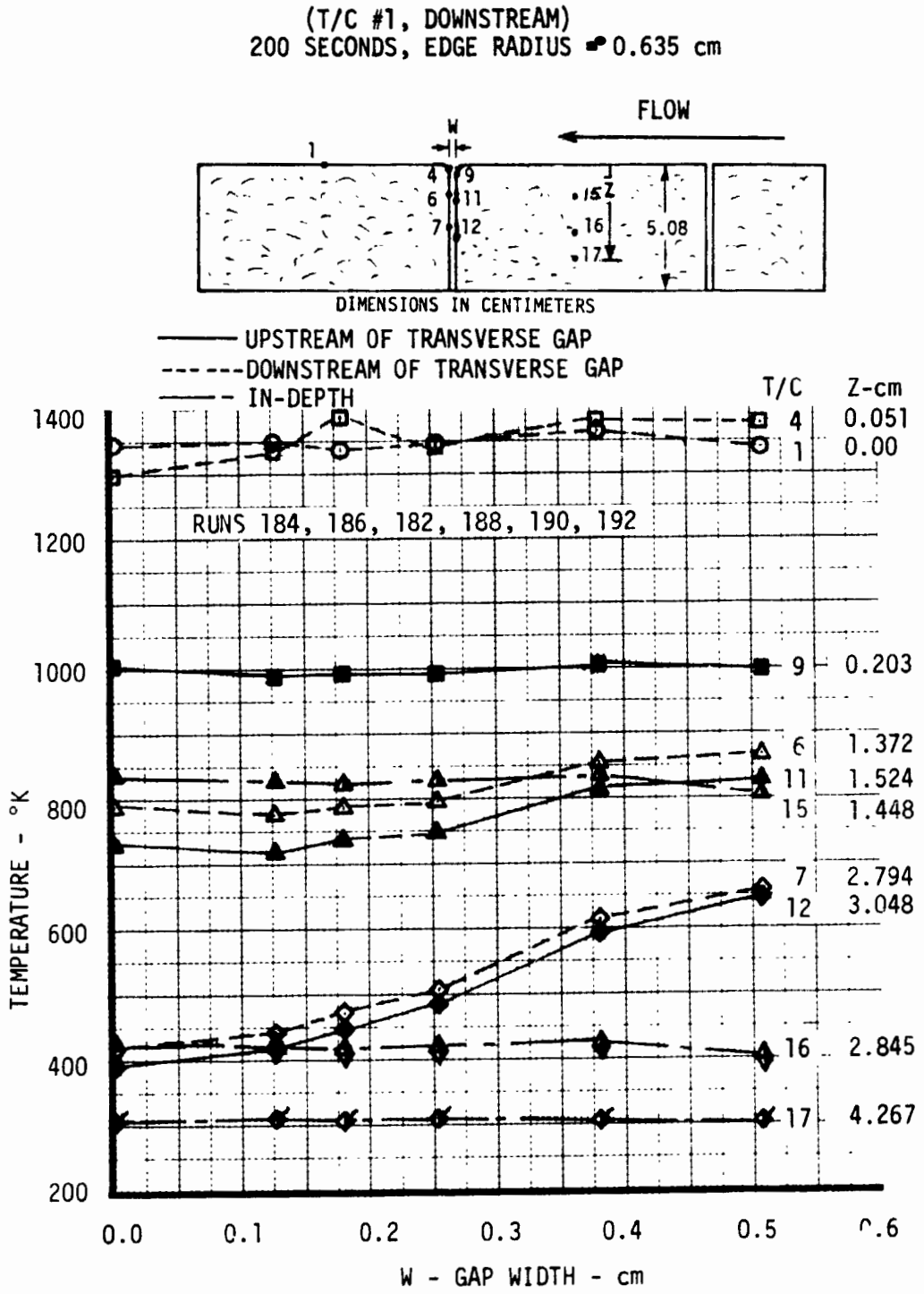

Figure 46

BUTT JOINT TWO-DIMENSIONAL THERMAL MODEL

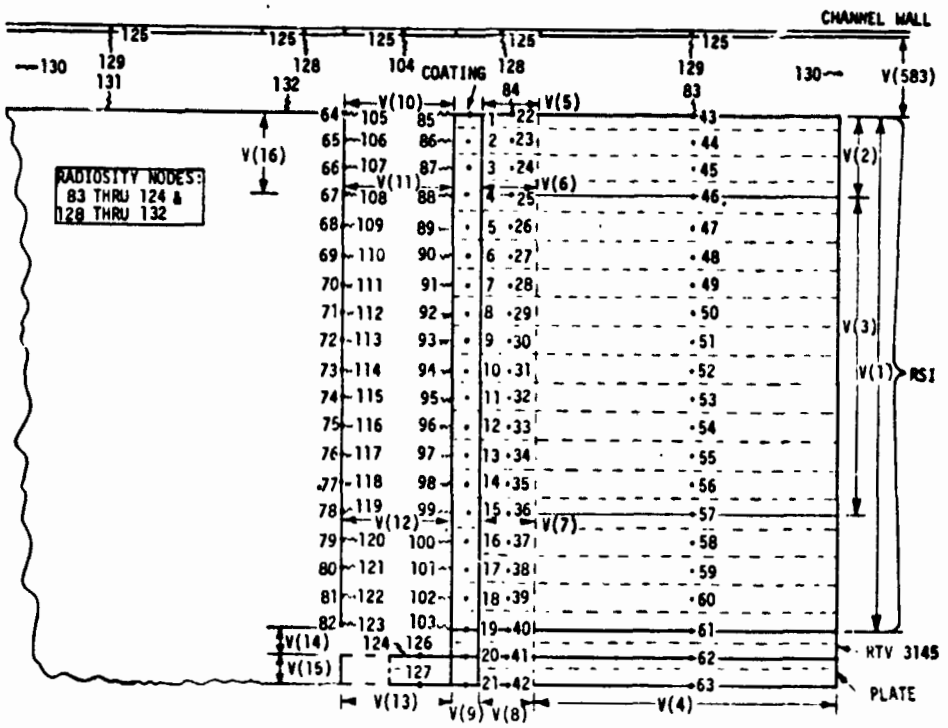

TWO-DIMENSIONAL THERMAL MODEL OF AN RSI TILE JOINT WITH EDGE RADIUS

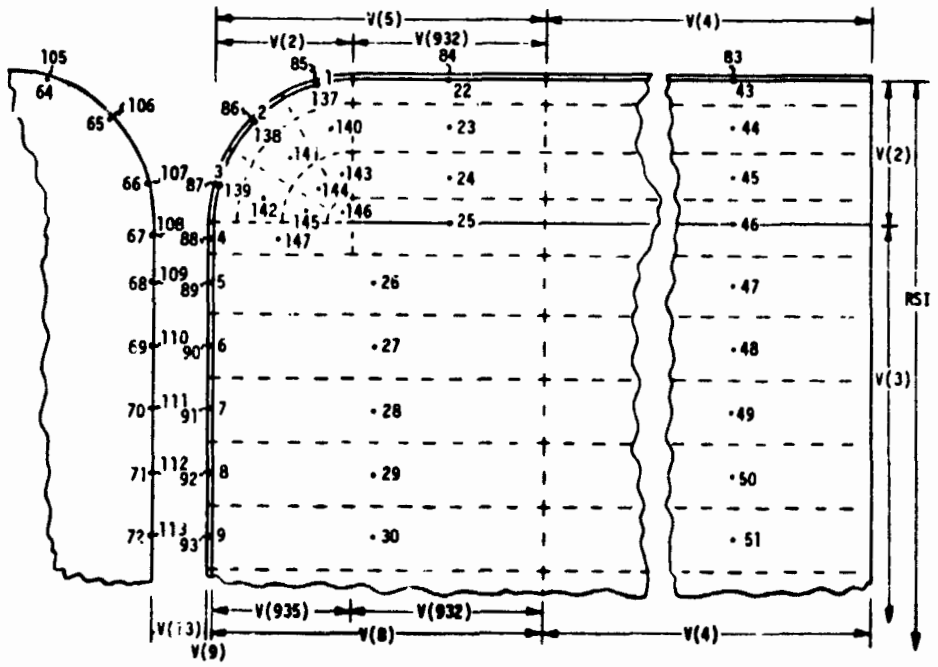

Figure 147

This facilitates comparison of heating data. This thermal model was used to analyze the test data obtained from the AMES Turbulent Duct Facility and for the computation of TPS thermal response during entry.

Figure 148 shows the calculated heating distributions for the downstream face of the transverse gap for four gap widths. The data shows a consistent increase in heating with gap depth. The heat flux predictions along with the data were used in a sensitivity study to determine that there was an error in the thermocouple locations.

Figure 149 indicates the sensitivity of heating to gap depth and width. Also shown on this figure is the error caused by inputing erroneous instrumentation locations into the data reduction analyses. Figure 150 shows the heating distribution in the gap for four gap widths, calculated using the corrected data. Again, heating decreases with depth and increases with width.

BUTT JOINT HEATING DISTRIBUTION HRSI TILES AT TRANSVERSE GAP

- AMES 20 MW 2 X 9 INCH TURBULENT FLOW DUCT FACILITY (TEST 3)
- TILE EDGE RADIUS = 0.635 cm
- DOWNSTREAM WALL OF TRANSVERSE GAP
- DISTRIBUTION AT 160 SEC TEST TIME

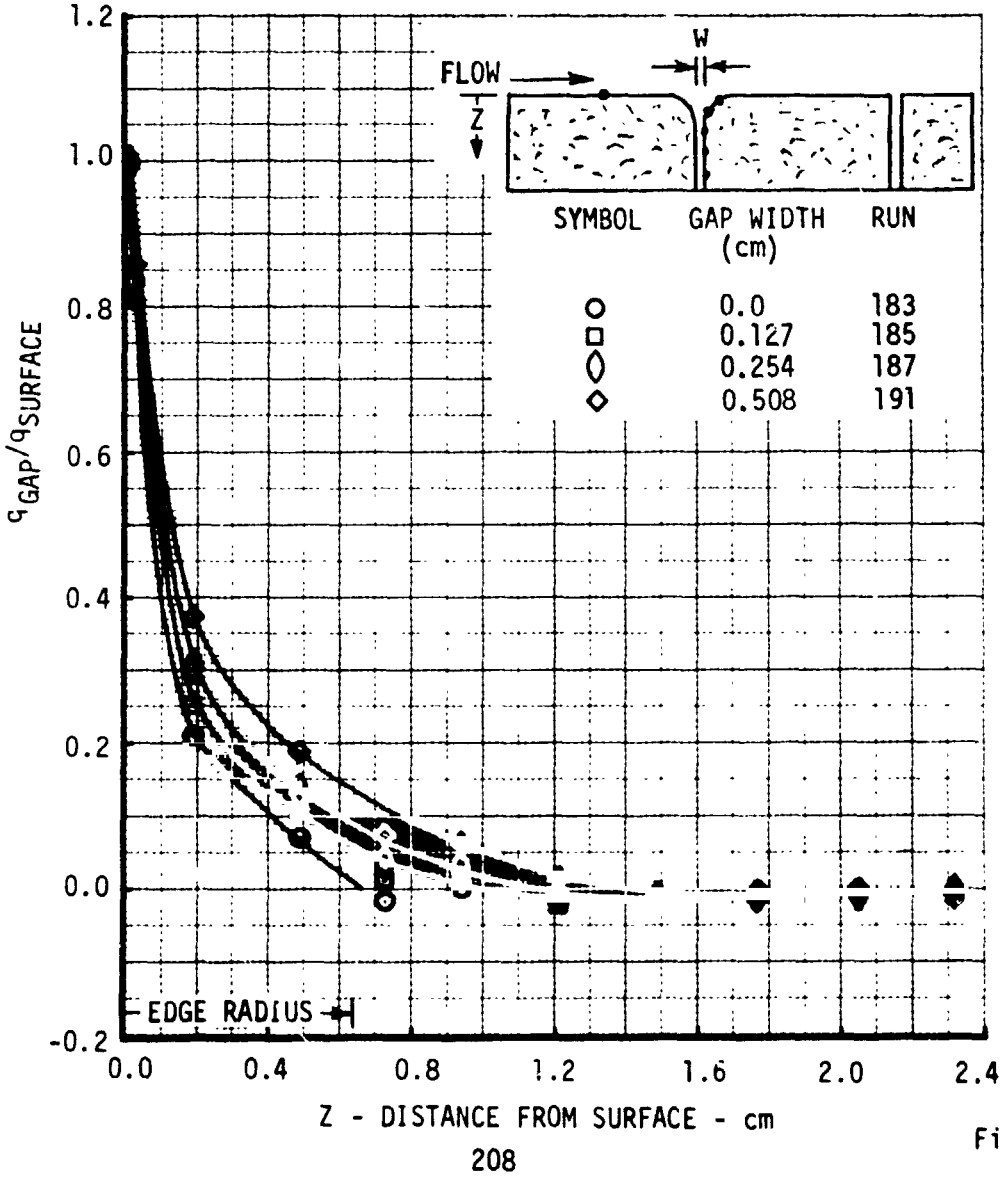

Figure 148

SENSIT'VITY OF T/C LOCATION ON HEATING DISTRIBUTION AT TRANSVERSE GAP BUTT JOINT - HRSI TILES

- AMES 20 MW 2 X 9 INCH TURBULENT FLOW
- DUCT FACILITY (TEST 3)
- TILE EDGE RADIUS = 0.635 cm
- DOWNSTREAM WALL OF TRANSVERSE GAP
- DISTRIBUTION AT 160 SEC TEST TIME

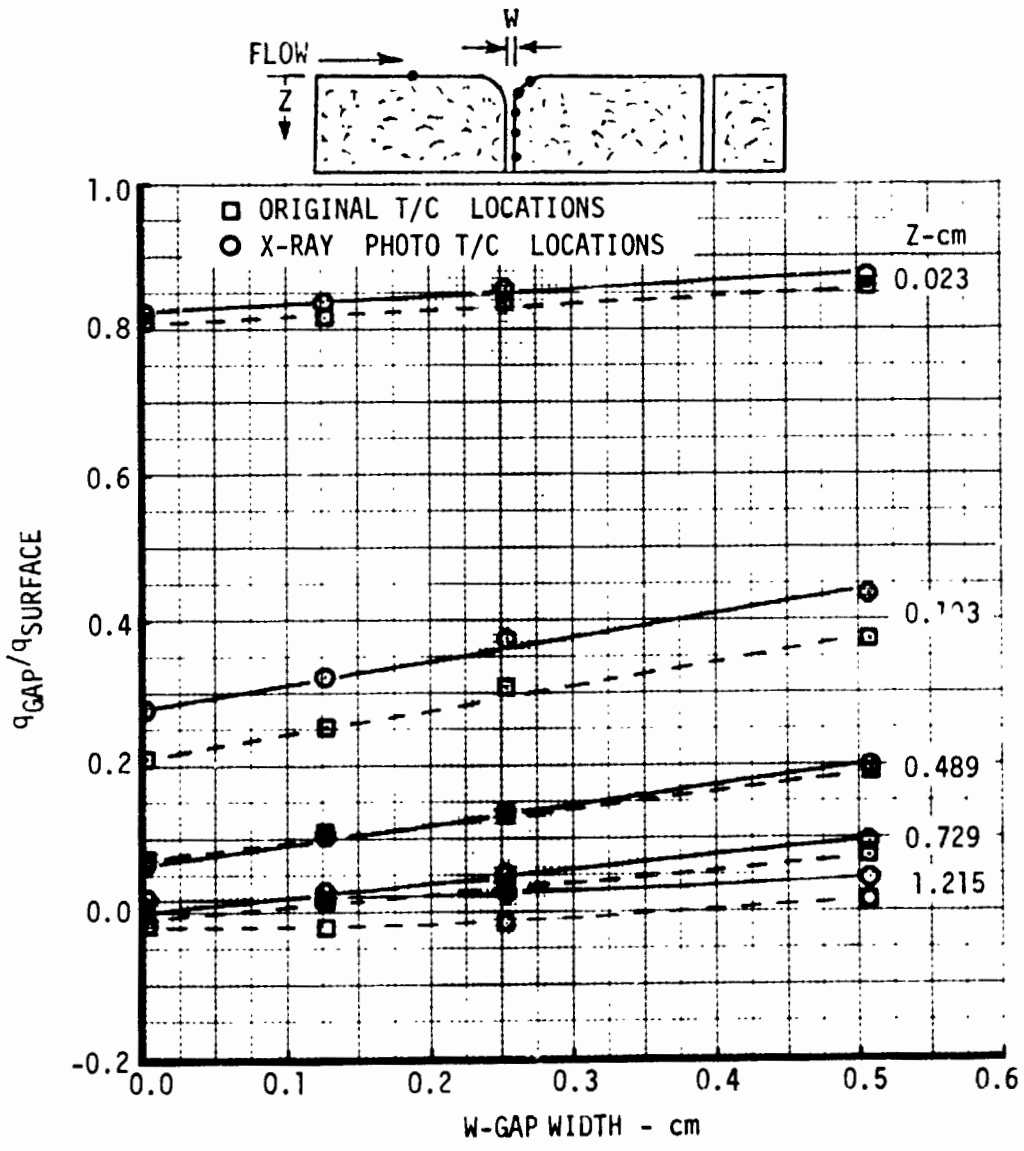

Figure 149

BUTT JOINT HEATING DISTRIBUTION HRSI TILES AT TRANSVERSE GAP

- AMES 20 MW 2 X 9 INCH TURBULENT FLOW DUCT FACILITY (TEST 3)
- TILE EDGE RADIUS = 0.635 cm
- DOWNSTREAM WALL OF TRANSVERSE GAP
- DISTRIBUTION AT 160 SEC TEST TIME

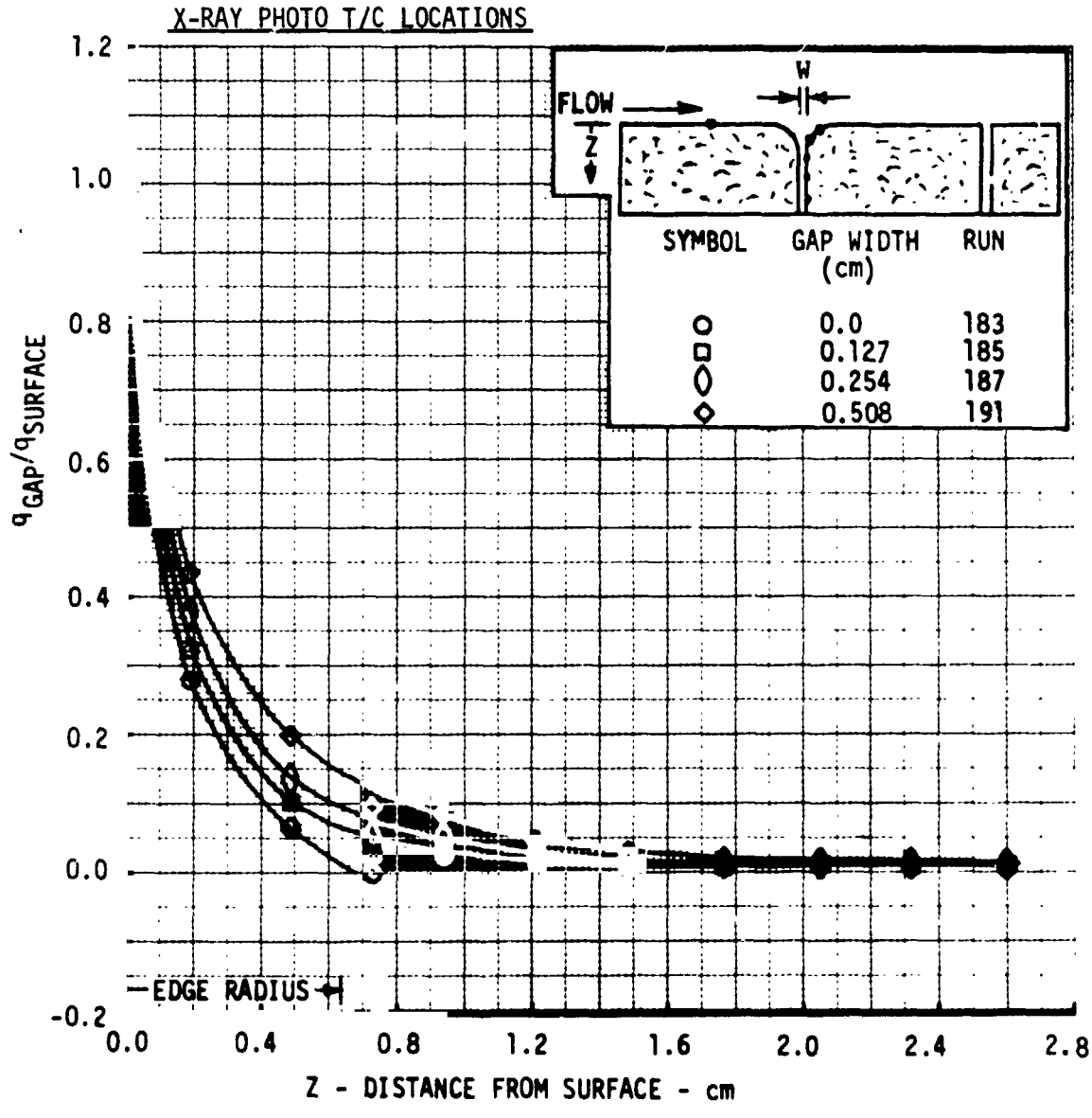

Figure 150

4.8 Boundary Layer Flow Conditions - Boundary layer analyses were performed to characterize the environments at the various tunnel test conditions. Basic boundary layer parameters were computed for use in correlating the heat transfer results from the test facilities. These parameters will aid in extrapolating the test results to Shuttle flight conditions. The basic boundary layer parameters determined for the various test conditions are:

1) Type of boundary layer (laminar, transitional, turbulent)
2) Local unit Reynolds number (edge condition)
3) Local Mach number (edge condition)
4) Displacement thickness (δ^*)
5) Momentum thickness (θ)
6) Laminar sublayer thickness for turbulent boundary layers (δ_s)
7) Temperature ratio across the boundary layer

A summary of the boundary layer analyses that were performed is shown in Figure 151. The details of most of these analyses are contained in Reference 1. Data for the LaRC 8 foot HTST tests and the Ames 20 MW Turbulent Duct tests are contained herein.

Figure 152 contains the displacement (δ^*) and momentum (θ) thicknesses along the HTST panel holder and Figure 153 contains the velocity profiles which were used to obtain sublayer thickness. The displacement thickness on the thin skin tile ranged from 0.61 cm (0.24 inch) to 1.43 cm (0.56 inch) and the momentum thickness ranged from 0.152 cm (0.060 inch) to 0.214 cm (0.084 inch). A nominal momentum thickness (θ = 0.182 cm) was used in the data bank for all tests. It was determined that the displacement thickness and sublayer thickness at the center of the tile could be expressed as a linear function of angle of attack (α) and combustor pressure (P).

Displacement thickness;

$$\delta^*(\text{inch}) = 0.32-0.01674(\alpha-15) -3.53636\text{x}10^{-5}(P-1000)$$

Sublayer Thickness;

$$\ln\left[\delta_L(10^{-4}FT)\right] = \ln 5.8-0.07017(\alpha-15) -4.358\text{x}10^{-4}(P-1202)$$

where α is in degrees
P is combustor pressure (PSI)

FACILITY BOUNDARY LAYER ANALYSES

Facility	Comments
JSC 10 MW (Channel Nozzle)	Equilibrium and nonequilibrium flow in nozzles, (NATA computer program)
LaRC CFHT (Tunnel Wall)	Quadratic relationship between temperature and velocity assumed
LaRC M = 8 VDT (Tunnel Wall)	Measured temperature and pressure profiles used to calculate b.l. parameters
LaRC M = 8 VDT (Freestream)	Exact numerical solution for flat plate b.l. analysis modified transition extent Re used to define transition zone
LaRC 8 ft HTST (0°, 7.5°, 15° α)	Exact numerical solution for flow over test sled
Ames 3.5 ft HWT (Freestream)	Exact numerical solution for flat plate b.l. analysis transition extent Re used to define transition zone
Ames 20 MW Turbulent Duct	Crocco relationship assumed

Figure 151

HTST BOUNDARY LAYER CHARACTERISTICS

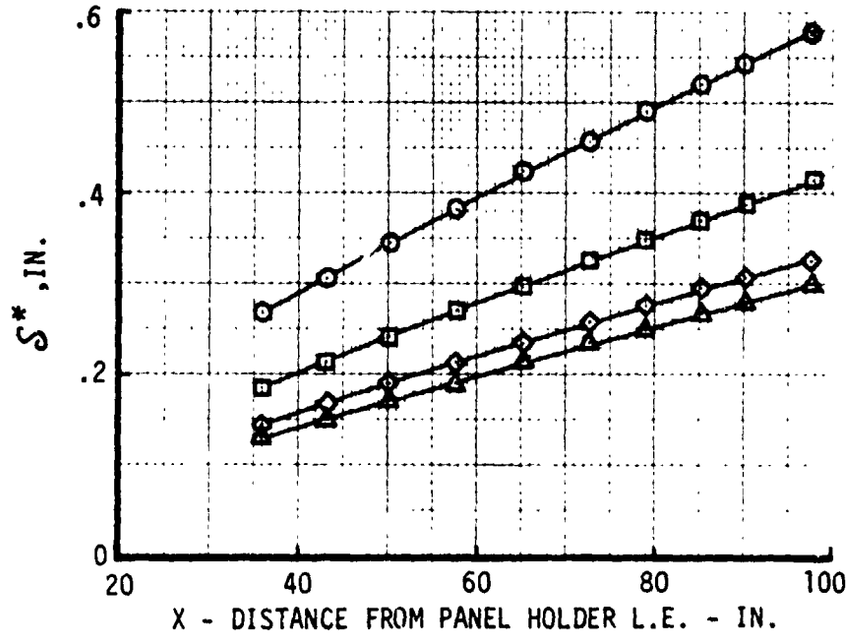

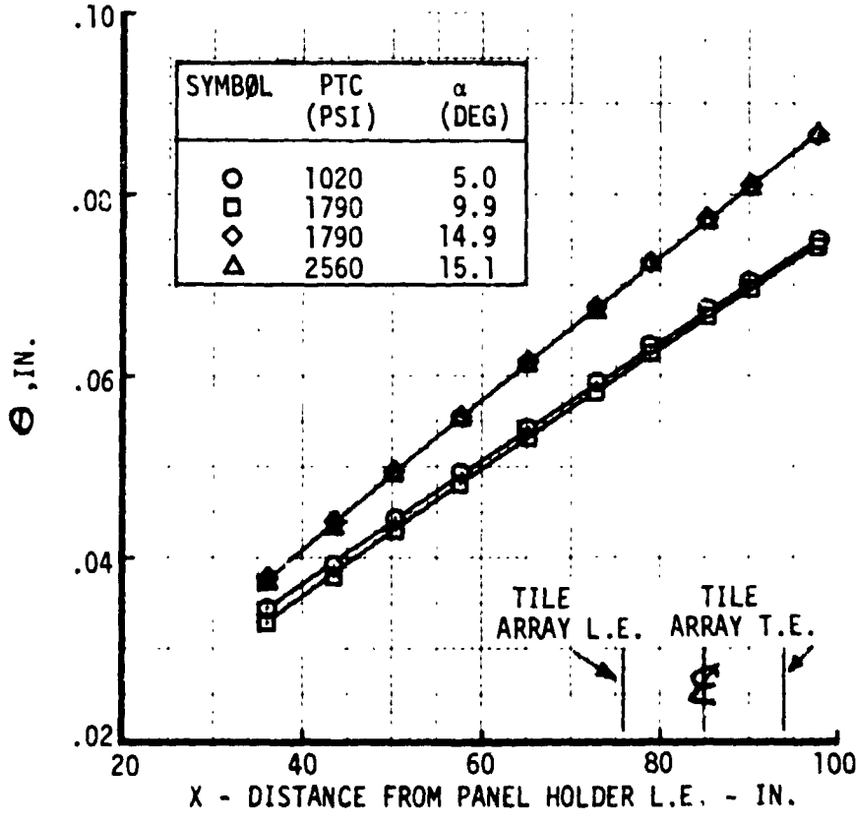

Figure 152

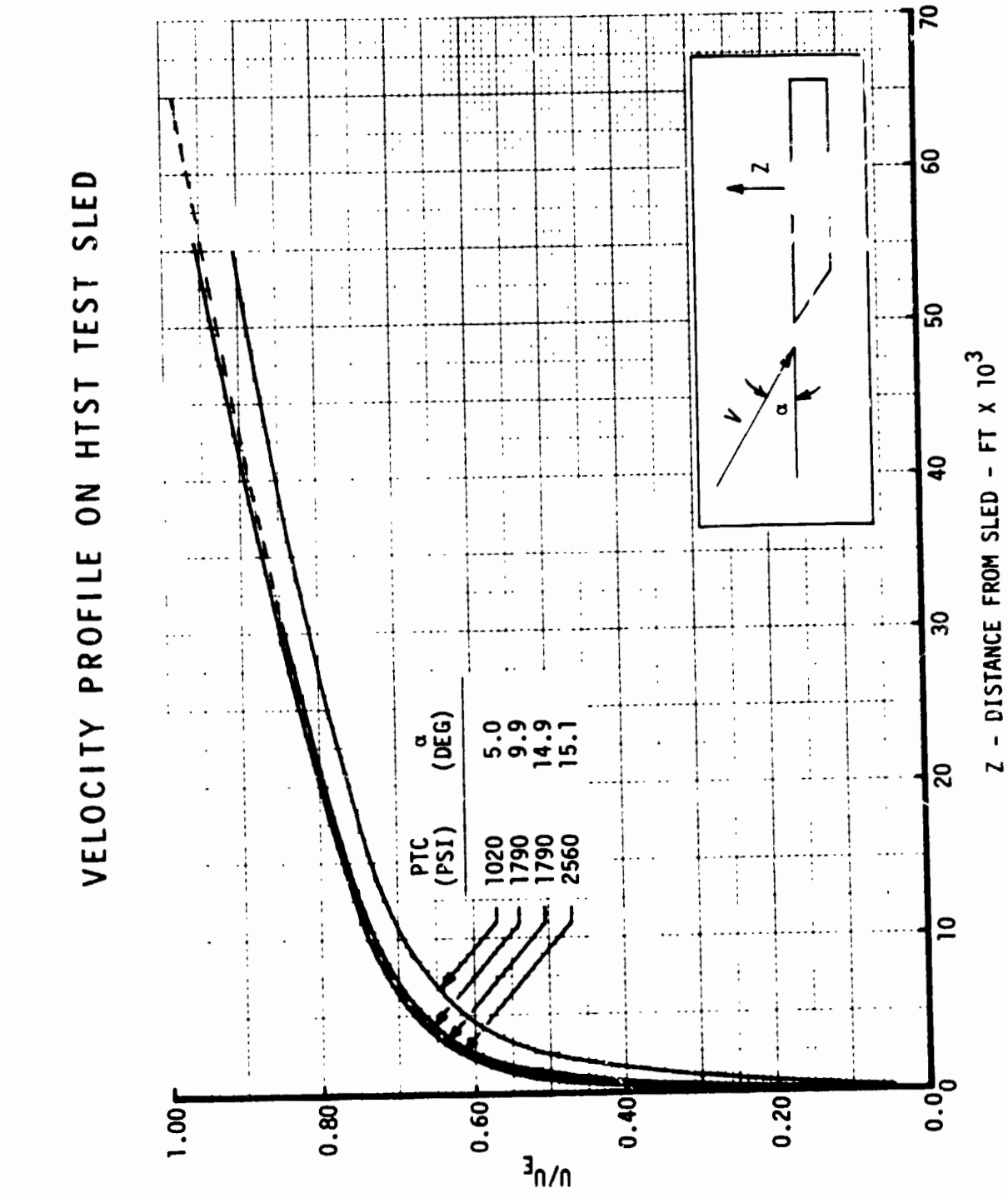
VELOCITY PROFILE ON HTST TEST SLED
PTC (PSI)
α (DEG)
1020 5.0
1790 9.9
1790 14.9
2560 15.1
Z
α
V
1.00
0.80
0.60
0.40
0.20
0.0
u/u_E
0
10
20
30
40
50
60
70
Z - DISTANCE FROM SLED - FT X 10^3

Figure 153

These functions were incorporated into the Data Bank computations. It should be noted that these equations were developed to describe δ^* and θ for a limited set of operating conditions in a particular test program and therefore should not be considered as general correlations.

Details of the Ames Turbulent Duct boundary layer are contained in Reference 4 . Pitot pressure surveys had previously shown the total boundary layer thickness to be about 20 mm for a total enthalpy of 3.7 MJ/kg and a static pressure of 3.5×10^3 N/m^2. Assuming that the Crocco relationship is applicable the momentum and displacement thicknesses are about 2 mm and 5 mm, respectively.

4.9 Comparison of Gap Heating Data from Arc Tunnel and Wind Tunnel Tests - The comparisons performed during Phase I of the heating distributions obtained from arc tunnels and wind tunnels is still valid. These comparisons are contained herein and additional comparisons have been made during Phase II. Comparisons were performed for both transverse gaps and in-line gaps. The gap heating data which have been assimilated come from both an arc tunnel and wind tunnels. Arc tunnels provide high energy (temperature and enthalpy) flow to test articles while wind tunnels provide a considerably lower energy flow. The effect of this difference in flow energy on gap heating was investigated by comparing data from arc and wind tunnels.

4.9.1 Transverse Gap Heating Comparisons - Figure 154 summarizes the gap heating test environments and transverse gap geometry for which data have been assimilated. As can be noted, the wide variety in conditions makes direct comparisons difficult. The check marks denote the data which were selected for comparison. Two gap widths from the JSC 10 MW arc tunnel tests were compared with the wind tunnel data. These gap widths bound the selected gap widths from the wind tunnels. The arc tunnel had the lowest freestream unit Reynolds number of any of the facilities. Therefore, the lowest Reynolds number data available from each wind tunnel facility were selected for comparison. A laminar boundary layer existed in some of the arc tunnels and in some of the wind tunnel tests.

Gap heating data from each wind tunnel test were compared individually with data from the arc tunnel test in Figures 155 thru 162. A comparison of gap heating data from the Ames 3.5 Foot Hypersonic Wind Tunnel and the JSC 10 MW Arc Tunnel is shown in Figure 155. Both tests were conducted in a laminar boundary layer environment with similar edge Mach numbers. Generally good agreement exists in the level of heating down the gap, although the shapes of the heating distributions are different. Figure 156 presents the comparison of gap heating distributions for the arc tunnel and the "freestream" tests in the LaRC Variable Density Tunnel (VDT). Both tests were run with a laminar boundary layer over the test article. The Mach number in the V.D.T. was 8.0 while the Mach number in the arc tunnel was 4.2. Also, the freestream unit Reynolds number is considerably higher in the wind tunnel than in the arc tunnel. The wind tunnel data agree well with the arc tunnel data at a depth into the gap of the 0.7 cm and below. The only data taken higher in the gap were taken at 0.5 cm and here the dimensionless heating was considerably higher than in the arc tunnel. Figure 157 presents the comparison of gap heating obtained using two different panel designs (a HCF panel and a thin skin tile set) tested in the JSC 10 MW Arc Tunnel. The HCF panel was tested in the wall of a channel nozzle

SUMMARY OF GAP HEATING TEST ENVIRONMENTS AND GEOMETRY (TRANSVERSE BUTT JOINT)

TESTING FACILITY	TEST ARTICLE POSITION	GAP DEPTHS (CENTIMETERS)	GAP WIDTHS (CENTIMETERS)	M_∞	Re_∞/m	B.L. STATE
JSC 10 MW ARC TUNNEL (TP2)*	CHANNEL NOZZLE WALL	✓ 3.18 5.08 6.35	.074 ✓.204 ✓.333 .714	✓4.2	✓$.06X10^6$	LAMINAR
AMES 3.5 FOOT WIND TUNNEL	FREE STREAM	1.016 2.032 ✓ 4.064	✓.254	✓5.1	✓$1.6X10^6$ $2.6X10^6$ $4.4X10^6$	LAMINAR
LANGLEY VARIABLE DENSITY WIND TUNNEL	FREE STREAM	✓ 2.54	.159 ✓.318	✓ 8	✓$2.3X10^6$ ↓ $21.8X10^6$	LAMINAR
LANGLEY VARIABLE DENSITY WIND TUNNEL	TUNNEL WALL	✓ 2.54	.159 ✓.318	✓ 8	✓$1.16X10^6$ ↓ $41.4X10^6$	TURBULENT
LANGLEY CONTINUOUS FLOW HYPERSONIC WIND TUNNEL	TUNNEL WALL	✓ 6.35	.13 ✓.23 .46 .71	✓10	✓$3.28X10^6$	TURBULENT
JSC 10 MW ARC TUNNEL WEDGE	FREE STREAM (15° ANGLE OF ATTACK)	✓4.128	.127 ✓.254 .381	✓9.6	✓$1.74X10^3$	LAMINAR
LANGLEY 8 FOOT HIGH TEMPERATURE STRUCTURES TUNNEL	FREE STREAM (0°, 7.5°, 15°, ANGLE OF ATTACK)	✓6.35	0.0 0.10 ✓0.18 ✓0.30 0.41	6.2 ✓↓ 7.0	✓$2.0X10^6$ $4.8X10^6$	TURBULENT
AMES 20 MW 2X9 INCH TURBULENT FLOW DUCT FACILITY	FREE STREAM	✓5.08	0.0 0.127 0.180 ✓0.254 0.381 0.508	✓3.5	✓$0.3X10^6$	TURBULENT

* TP2 - TEST POSITION NUMBER 2

Figure 154

COMPARISON OF TRANSVERSE GAP HEATING (JSC 10 MW AND AMES 3.5 FT)

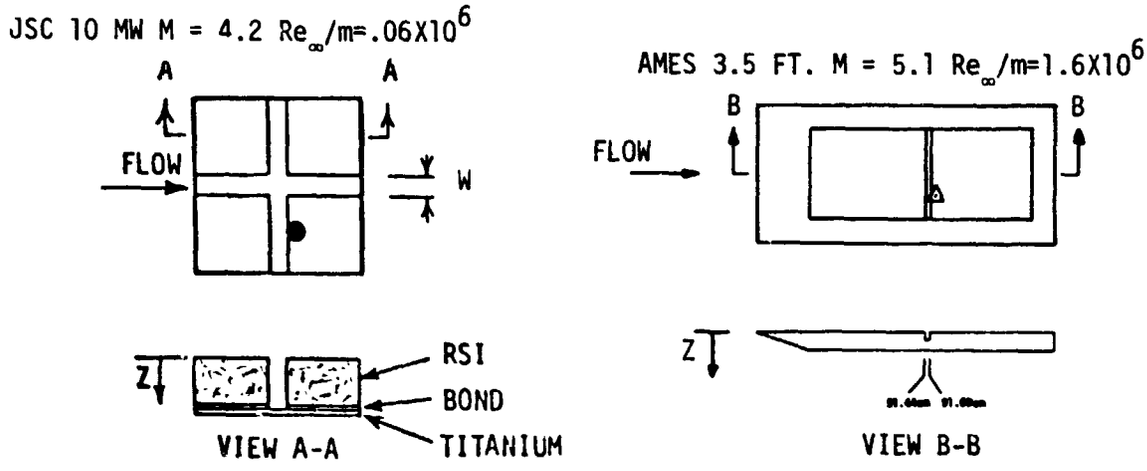

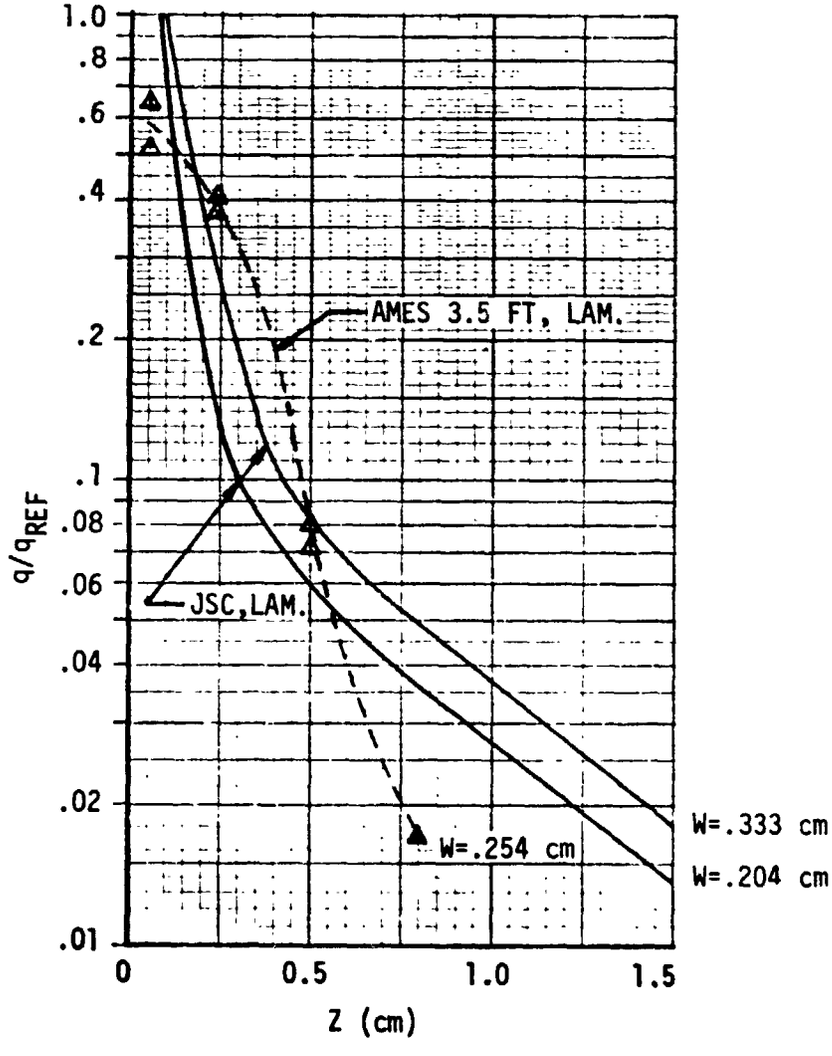

Figure 155

COMPARISON OF TRANSVERSE GAP HEATING (JSC 10 MW AND V.D.T. - FREE STREAM)

JSC 10 MW M = 4.2 $Re_\infty/m=.06X10^6$

M=8 V.D.T. (FREE STREAM) $Re_\infty/m=2.3X10^6$

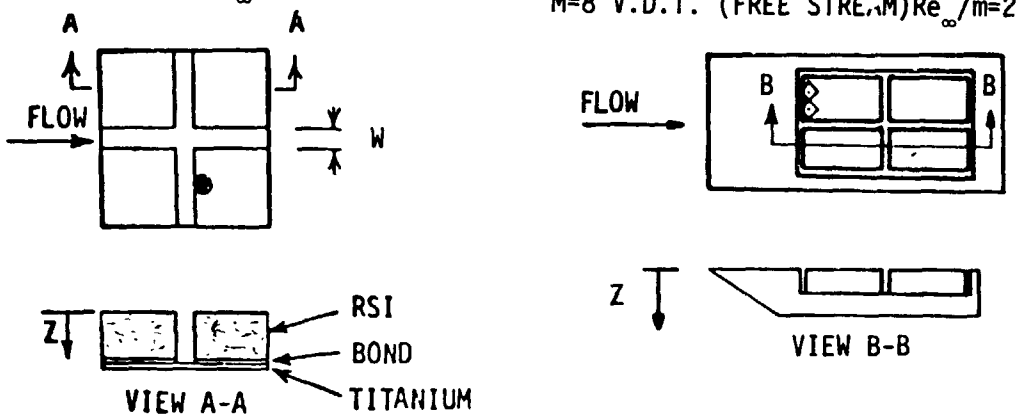

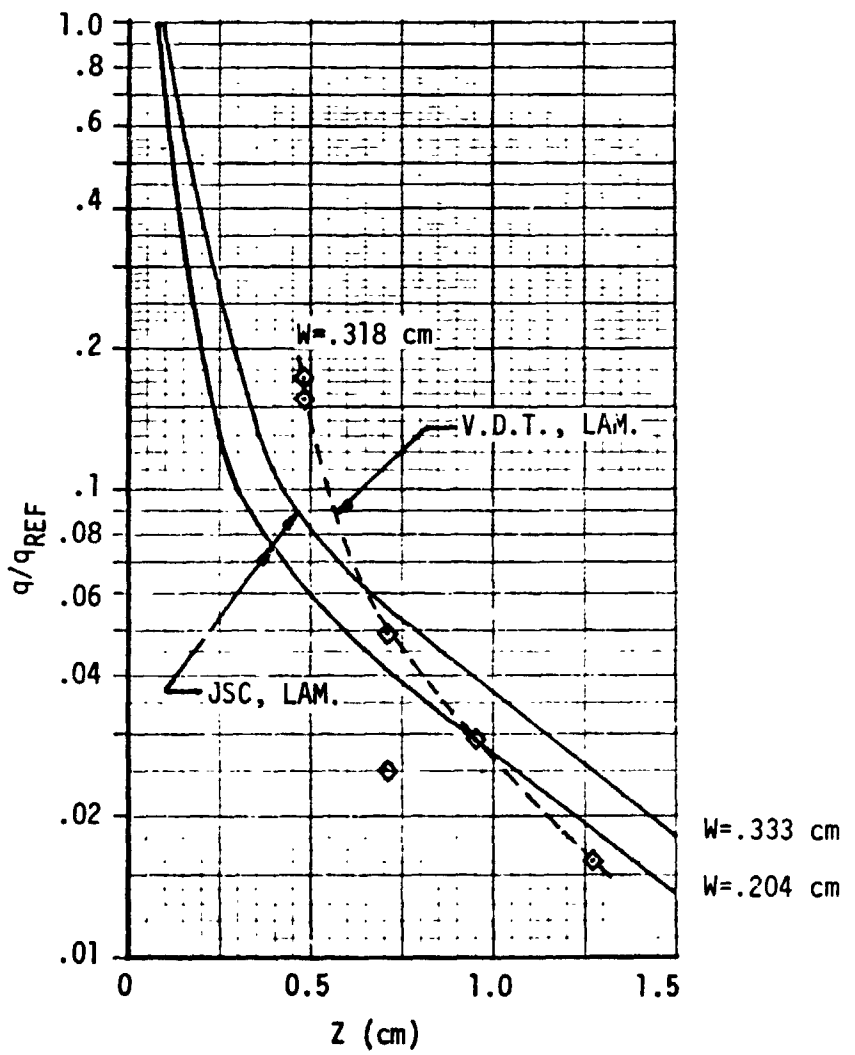

Figure 156

COMPARISON OF TRANSVERSE GAP HEATING JSC 10 MW ARC TUNNEL, LAMINAR FLOW (HCF AND THIN SKIN MODEL)

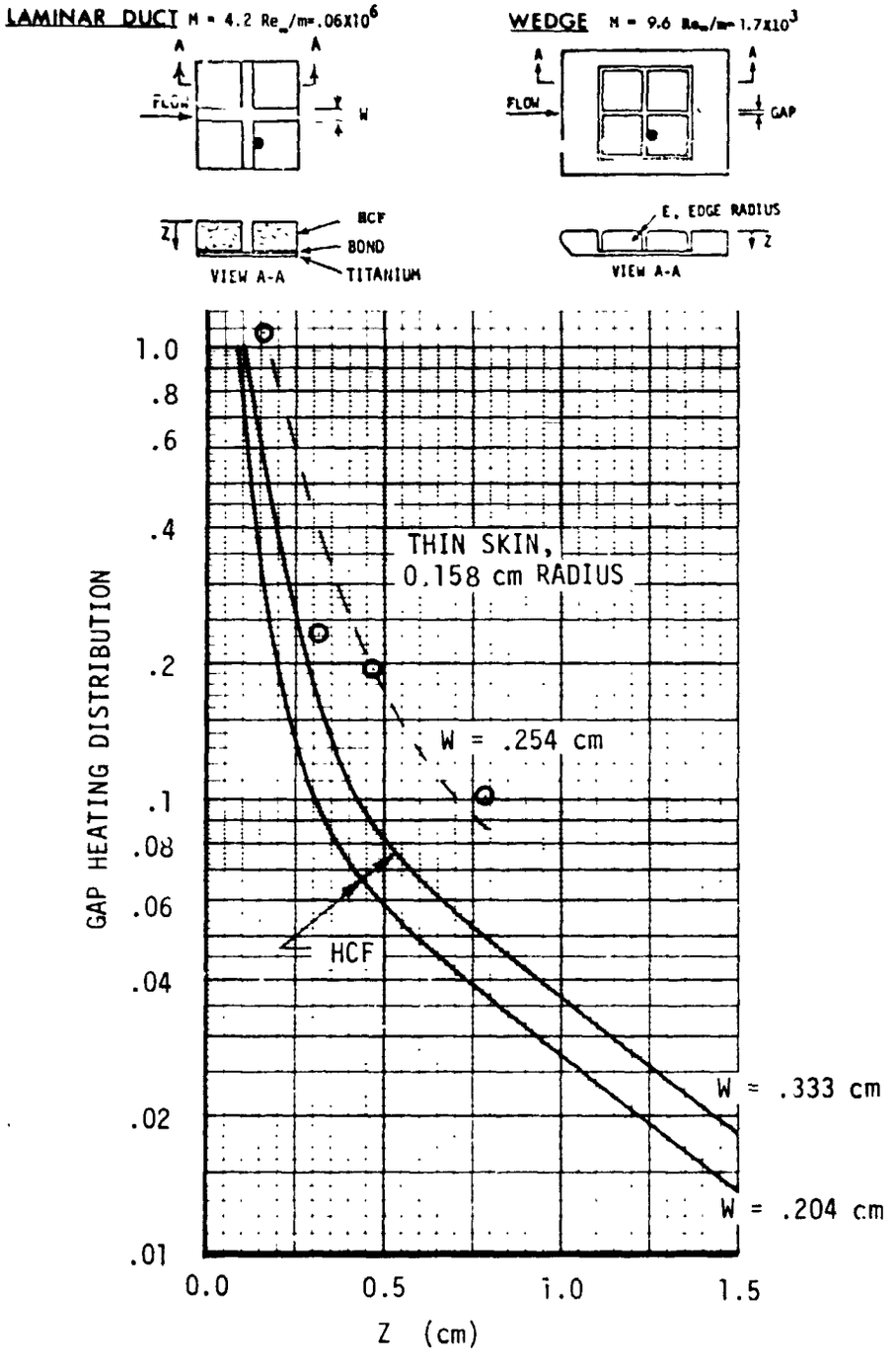

Figure 157

and the thin skin tiles were mounted in a wedge test fixture which was swung into the plume of a free expanding jet. Flow over both test articles was laminar but the Reynolds number and boundary layer thickness was much less for the wedge. This could be the reason for the higher heating measured usint the thin skin tile.

Gap heating data were also taken in the wall of the V.D.T. to expose the test article to a turbulent boundary layer. These data are compared with the arc tunnel data in Figure 158 and are considerably higher than the laminar arc tunnel. Figure 159 compares the arc tunnel data and data taken in the wall of the Mach 10 Continuous Flow Hypersonic Tunnel (CFHT). The boundary layer in the CFHT tests was turbulent and the data for these tests are again higher than the arc tunnel data.

The 8 Foot HTST is a combustion driven facility and the flow over the test panel was turbulent with a relatively thin boundary layer ($0.61 \leq \delta^* \leq 1.43$ cm). Figure 160 is a comparison between HTST data and the channel nozzle data obtained at JSC. Again the turbulent heating for the turbulent flow was higher but a cross-over occured between 0.5 and 0.75 cm into the gap. The heating distributions from the HTST were also compared (Figure 161) with another turbulent test program performed in the CFHT. The boundary layer in the CFHT was much thicker in the HTST tests. The heating in the CFHT was higher also.

Finally the test results for the large edge radiused tiles tested in the JSC 10 MW Arc Tunnel using the wedge and the Ames Turbulent Duct Arc Tunnel is compared in Figure 162. Both these facilities are Arc Tunnels and hence have high enthalpy content. The wedge model employed thin skin tiles whereas the duct model used RSI tiles. The wedge model had laminar flow and the duct produced turbulent flow. The tile exposed to the laminar flow experience a much higher heating than the one in the turbulent boundary layer. Apparently the trend to high gap heating in a turbulent flow is reversed when dealing with large radiused tiles. Additional test programs need to be performed to substantiate this trend.

4.9.2 In-Line Gap Heating Comparisons - Figure 163 lists the data assimilated and used to compare heating measurements obtained in the arc, wind and combustion driven facilities. The same criteria for selecting data employed in the transverse gap applies. Three different test programs were conducted in the JSC 10 MW Arc Tunnel. Figure 164 shows the comparison between results using two RSI materials (HCF a mullite RSI and Ames silica RSI) and the thin skin tile tested in the wedge. The two results from the two RSI materials agree very well whereas the thin skin data is higher. The RSI materials were tested in the same channel nozzle whereas the thin skin tile used a wedge which had the thinner boundary layer. Figure 165 is

COMPARISON OF TRANSVERSE GAP HEATING (JSC 10 MW AND V.D.T. - TUNNEL WALL)

JSC 10 MW M = 4.2 $Re_\infty/m = .06X10^6$

M = 8 V.D.T. (TUNNEL WALL)
$Re_\infty/m = 1.16X10^6$

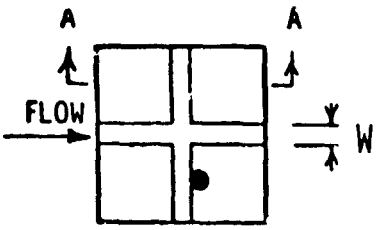

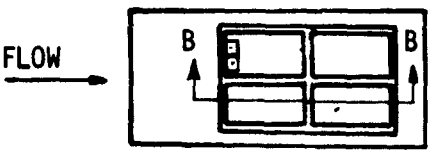

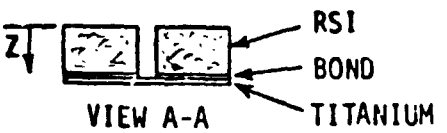

VIEW A-A

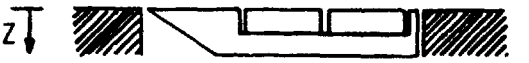

VIEW B-B

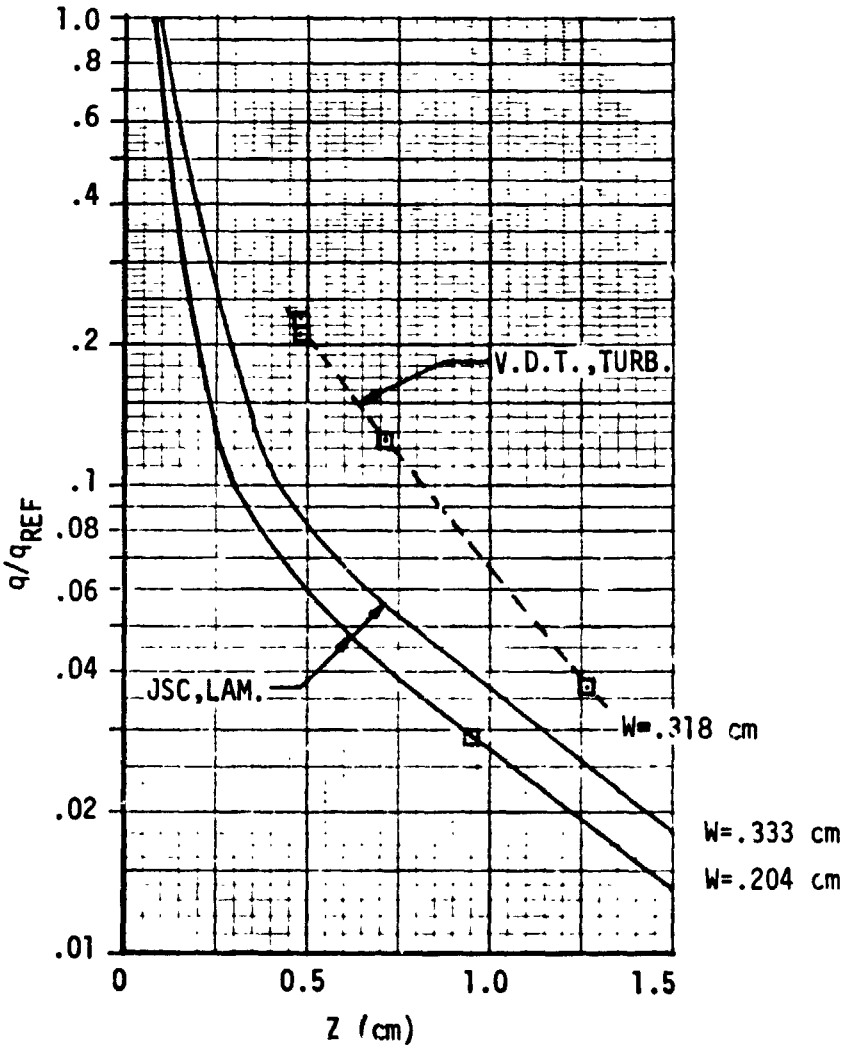

Figure 158

COMPARISON OF TRANSVERSE GAP HEATING (JSC 10 MW AND CFHT)

JSC 10 MW M = 4.2 $Re_\infty/m = .06X10^6$ CFHT M = 10 $Re_\infty/m = 3.28X10^6$

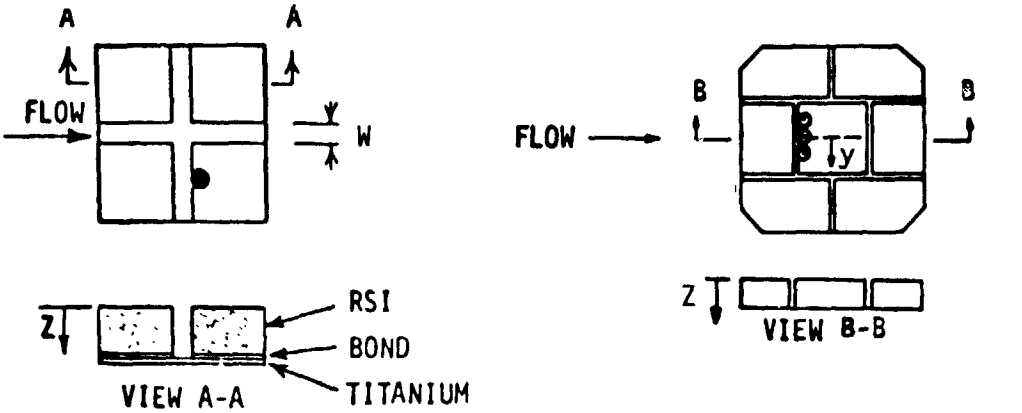

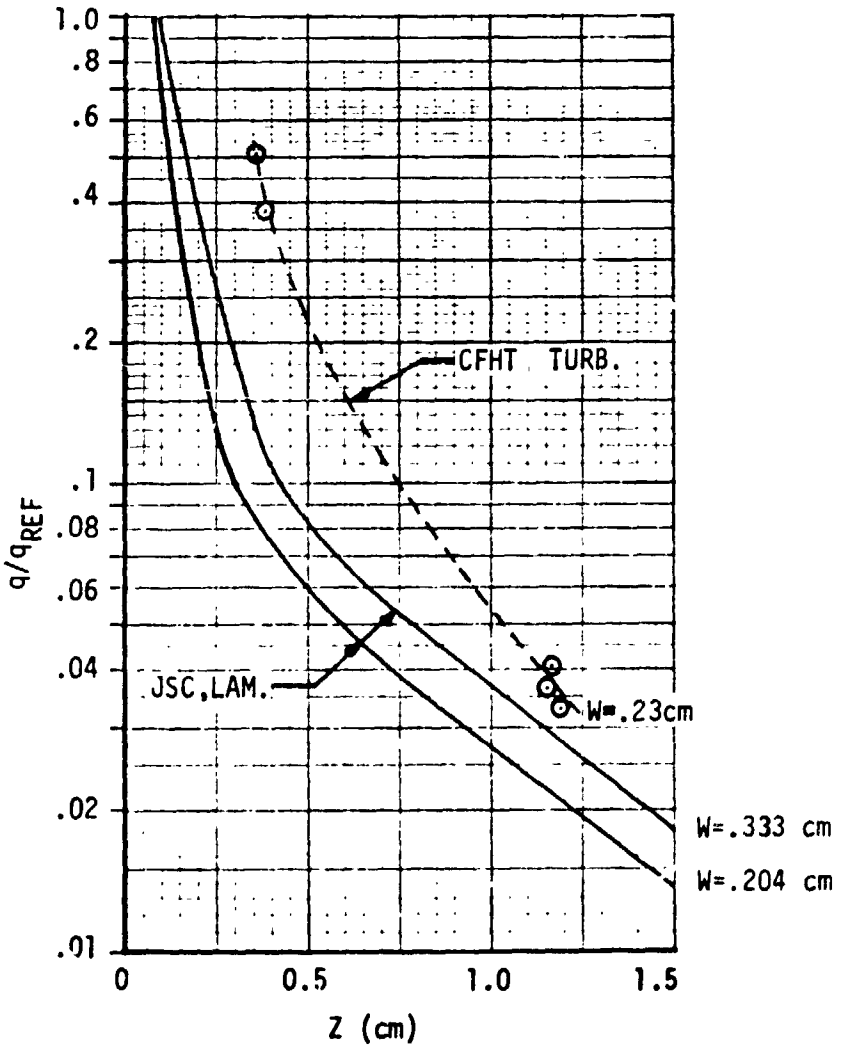

Figure 159

COMPARISON OF TRANSVERSE GAP HEATING JSC 10 MW AND LaRC 8 FOOT HTST T (HCF AND THIN SKIN MODEL)

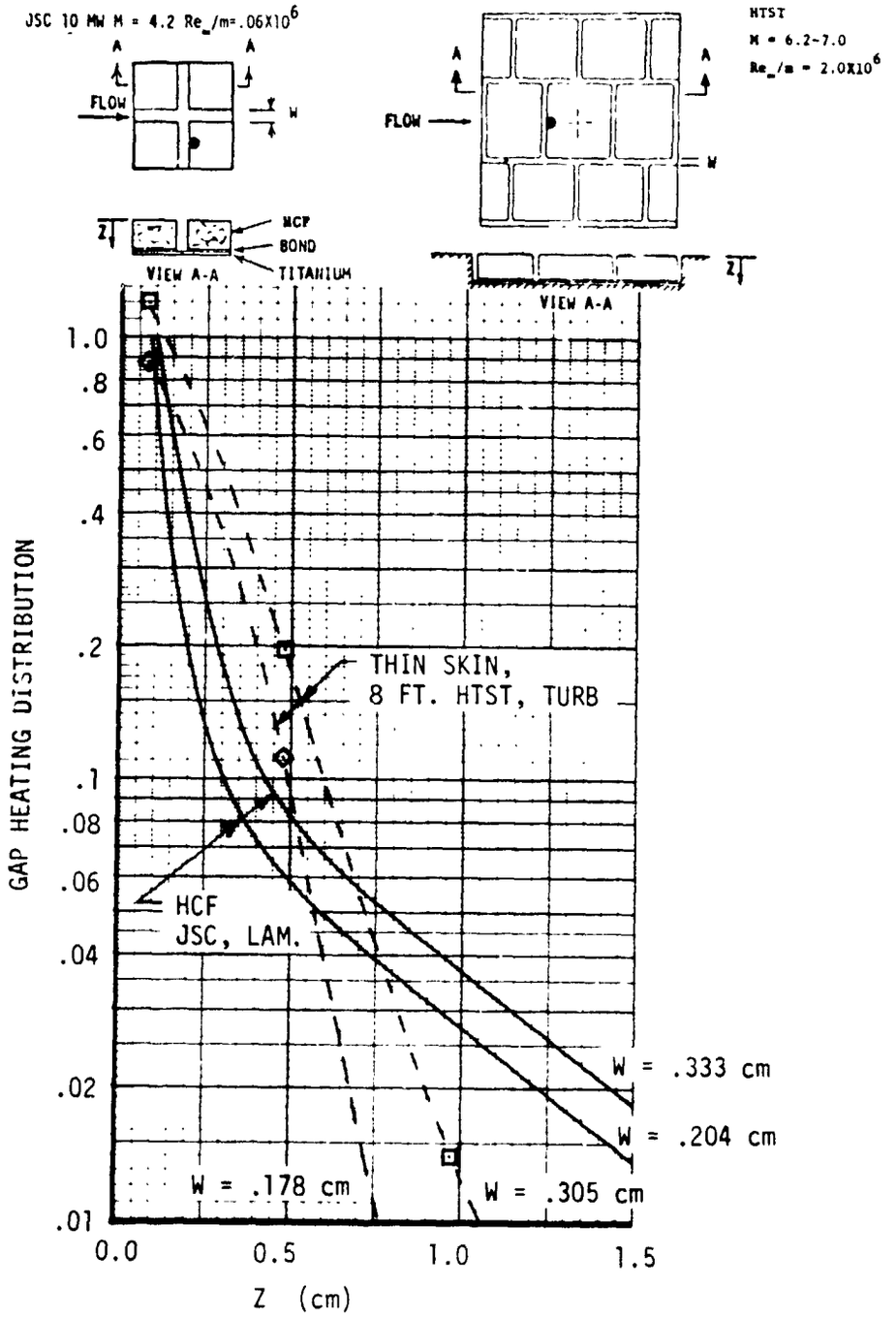

Figure 160

COMPARISON OF TRANSVERSE GAP HEATING G LaRC CFHT AND LaRC 8 FOOT HTST, TURBULENT FLOW (THIN SKIN MODELS)

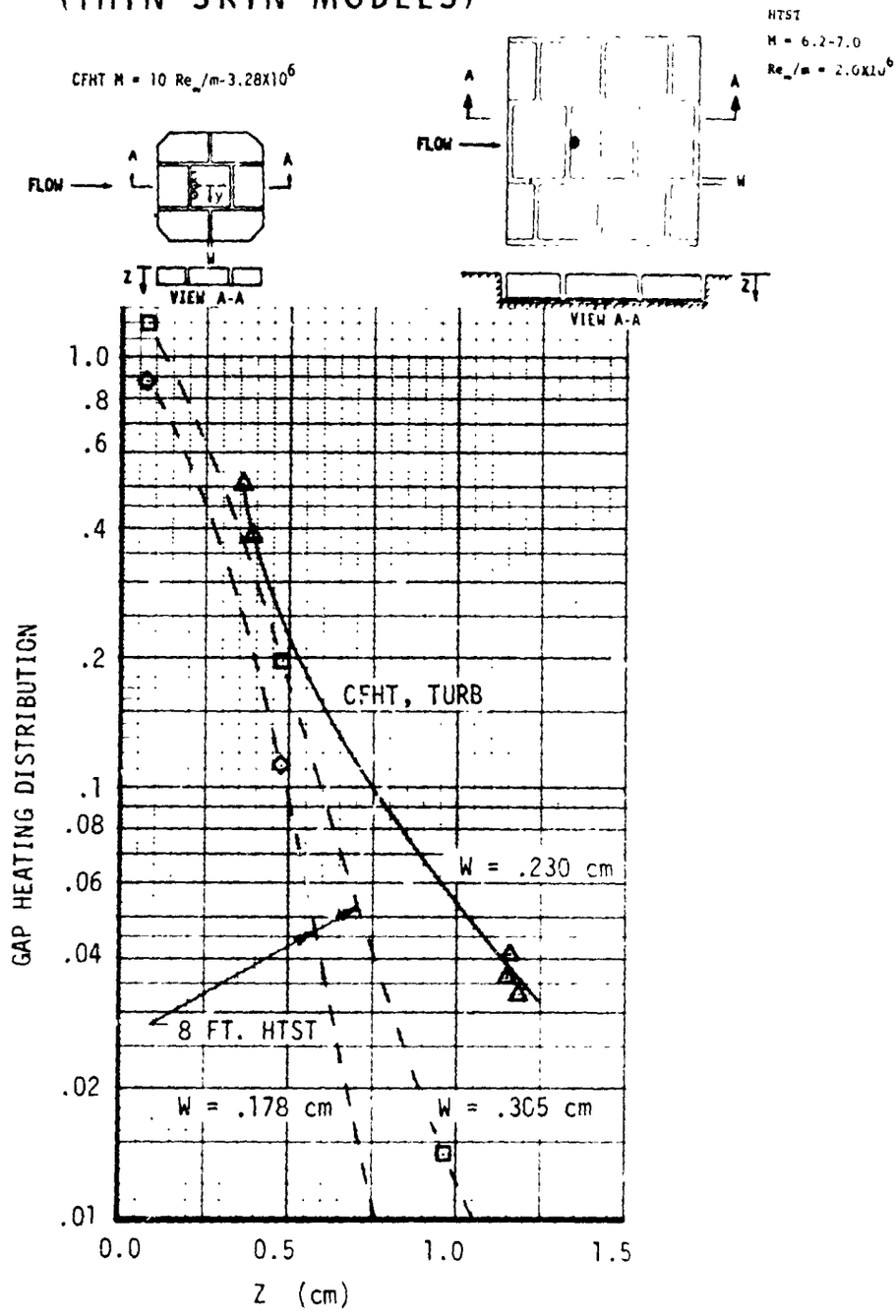

Figure 161

COMPARISON OF TRANSVERSE GAP HEATING JSC 10 MW AND AMES 20 MW TURBULENT DUCT (0.635 CM EDGE RADIUS)

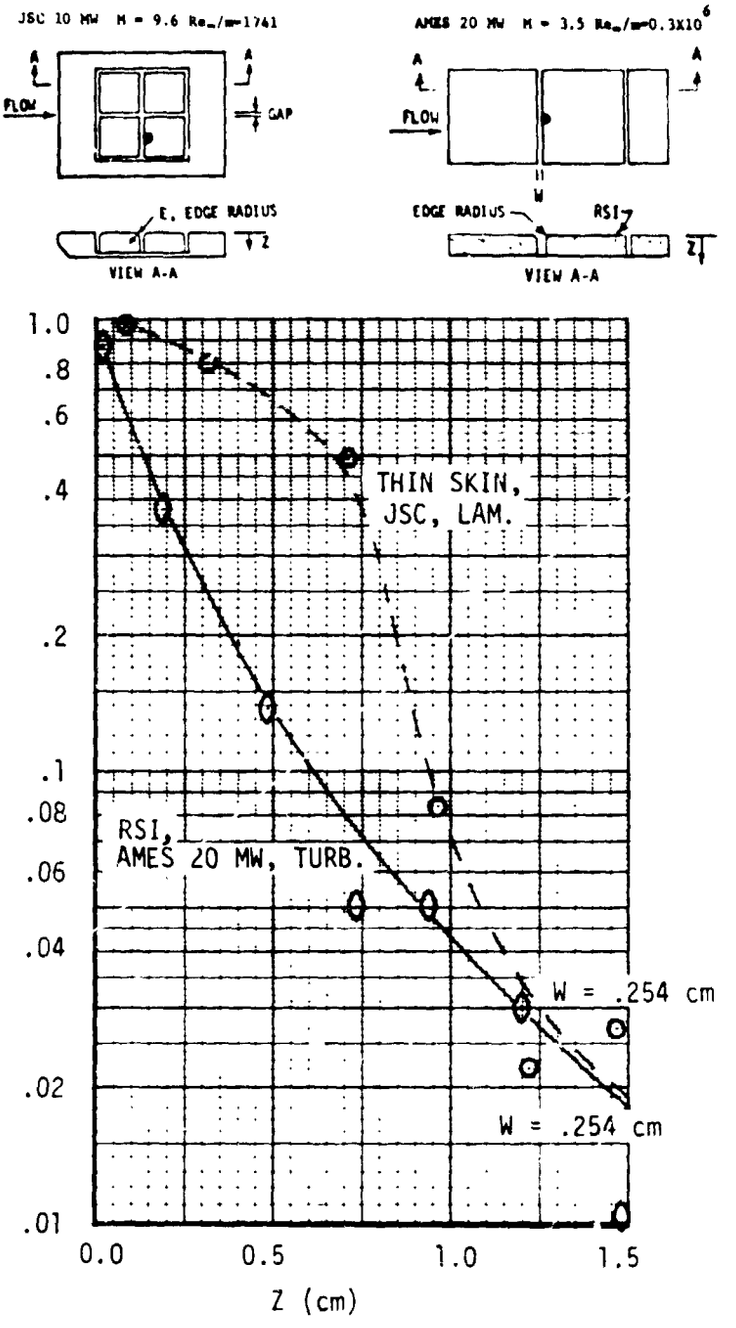

Figure 162

SUMMARY OF GAP HEATING TEST ENVIRONMENTS AND GEOMETRY

(IN-LINE BUTT JOINT)

TESTING FACILITY	TEST ARTICLE POSITION	GAP DEPTHS (CENTIMETERS)	GAP WIDTHS (CENTIMETERS)	M_∞	Re_∞/m	B.L. STATE
JSC 10 MW ARC TUNNEL	CHANNEL NOZZLE WALL	√3.18 5.08 6.35	0.074 √0.204 √0.333 0.714	√4.2	√0.06×10^6	LAMINAR
AMES 3.5 FOOT WIND TUNNEL	FREE STREAM	1.016 2.032 √4.064	√0.254	√5.1	√1.6×10^6 2.6×10^6 4.4×10^6	LAMINAR
LANGLEY CONTINUOUS FLOW HYPERSONIC WIND TUNNEL	TUNNEL WALL	√6.35	0.13 √0.23 0.46 0.71	√10	√3.28×10^6	TURBULENT
JSC 10 MW ARC TUNNEL WEDGE	FREE STREAM (15° ANGLE OF ATTACK)	√4.128	0.127 √0.254 0.381	√9.6	√1.741×10^3	LAMINAR
LANGLEY 8 FOOT HIGH TEMPERATURE STRUCTURES TUNNEL	FREE STREAM (0°, 7.5°, 15° ANGLE OF ATTACK)	√6.35	0.0 0.10 √0.18 √0.30 0.41	6.2 ↓ 7.0	√2.0×10^6 4.6×10^6	TURBULENT
JSC 10 MW ARC TUNNEL	CHANNEL NOZZLE WALL	2.54 √5.08	0.127 √0.254	√3.7-4.5	√$4.5-8.2\times10^4$	LAMINAR
AMES 3.5 FOOT WIND TUNNEL	FREE STREAM	0.0 1.0 √2.0 3.81	0.0 0.127 √0.254	√5.1	√1.64×10^6 3.28×10^6 6.56×10^6	LAMINAR TRANSITIONAL TURBULENT

Figure 163

COMPARISON OF IN-LINE GAP HEATING
JSC 10 MW ARC TUNNEL, LAMINAR FLOW
(HCF, RSI AND THIN SKIN MODELS)

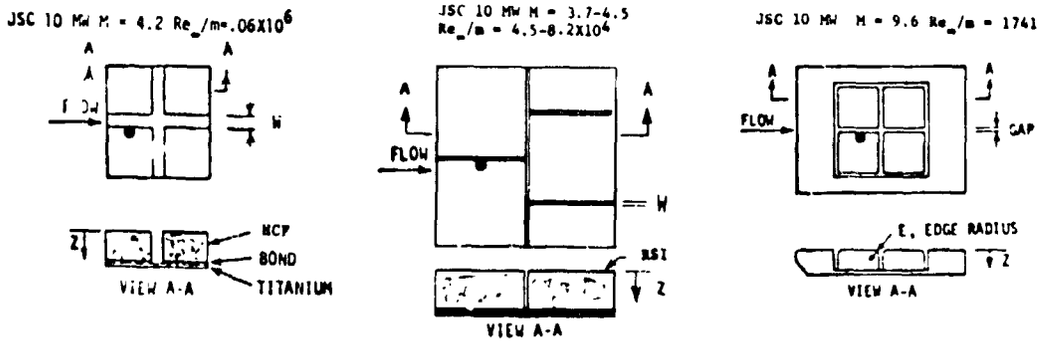

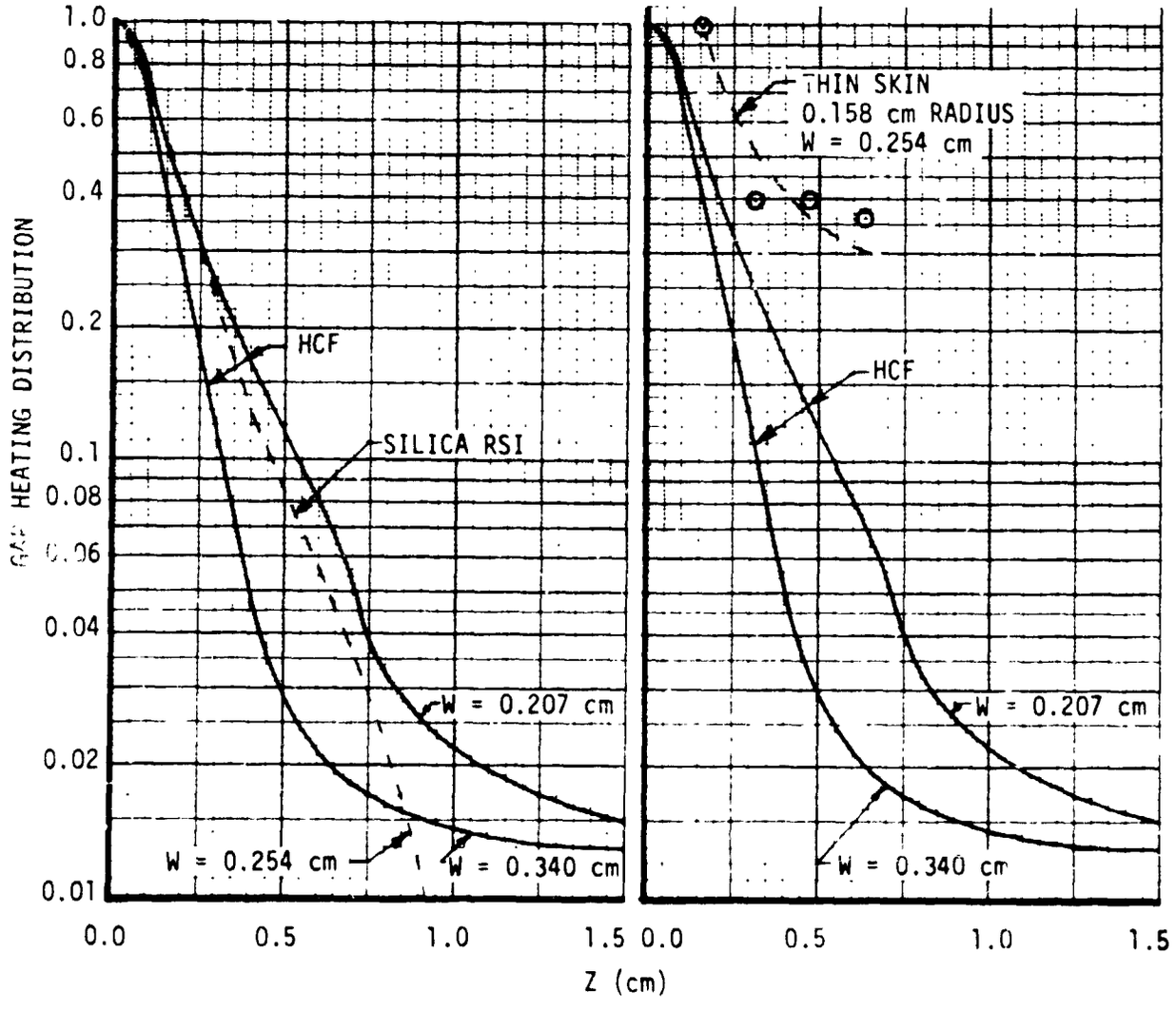

Figure 164

COMPARISON OF IN-LINE GAP HEATING JSC 10 MW AND AMES 3.5 FOOT TUNNEL, LAMINAR FLOW (HCF AND THIN SKIN MODELS)

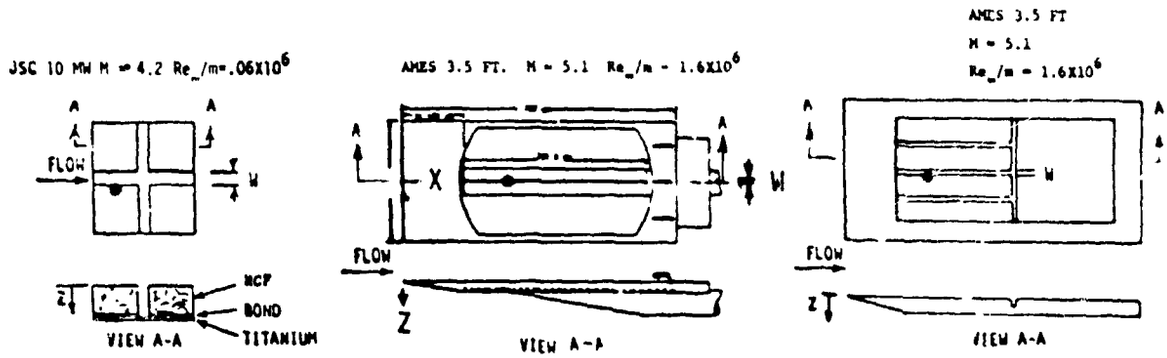

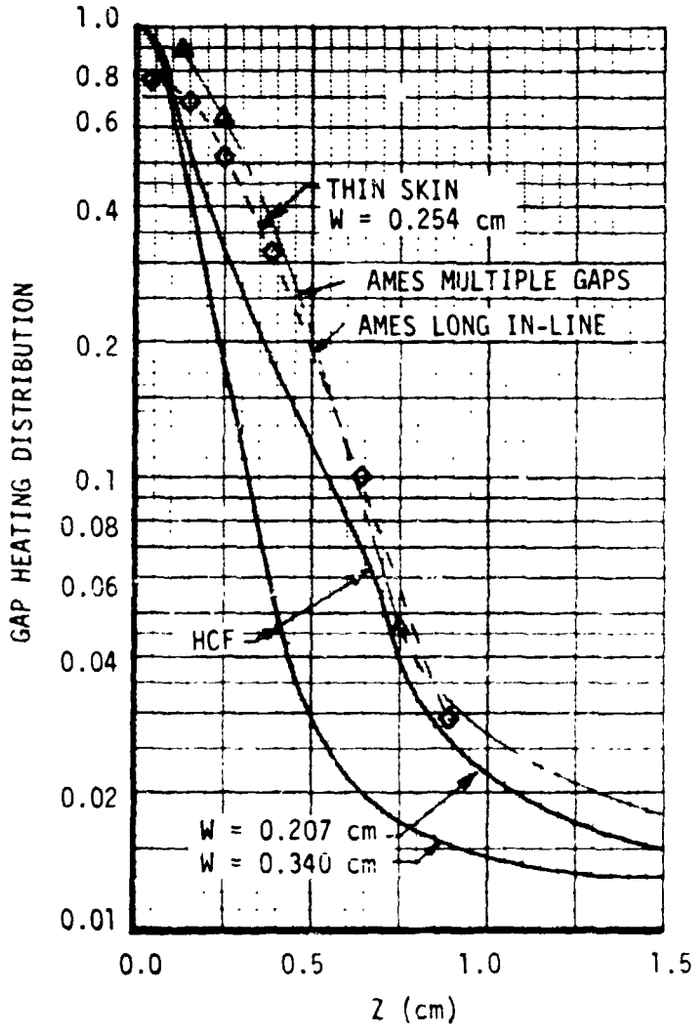

Figure 165

a comparison between the HCF test results and the Ames 3.5 Foot H.W.T. test results. The wind tunnel yielded slightly but consistently higher heating ratios. The shapes of the heating distributions are similar. Figure 166 compares the effect of boundary layer state on in-line gap heating using results from the turbulent CFHT and the laminar JSC Duct. This data, too, shows a higher heating when the boundary layer is turbulent.

The in-line gap heating obtained from the 8 Foot HTST test shows a ignificant higher heating as evident from Figure 167. The HTST heating pattern is also much higher than that obtained from the CFHT which had a much thicker turbulent boundary layer. It should be remembered that a field of eleven tiles was used in the HTST tests whereas the HCF tests employed four tiles. The flow over a tile field could also contribute to increased heating. Further investigations should be conducted to determine if the in-line gap does receive this high heating because it will definitely affect TPS design.

The difference in enthalpy between arc tunnels and wind tunnels does not appear to significantly affect gap heat transfer when normalized by the reference surface heating rate. The laminar wind tunnel data agree reasonably well with the laminar arc tunnel data. However, the boundary layer state does affect the heating in gaps. The data indicate that turbulent boundary layers result in higher dimensionless heating in gaps than laminar boundary layers. These conclusions apply to in-line gaps as well as transverse gap with a noticeable exception where a relatively thin boundary layer maintains high heating deep within the gap. Data also indicates that laminar flow produces higher heating than turbulent flow when the tiles have large edge radius.

COMPARISON OF IN-LINE GAP HEATING JSC 10 MW AND CFHT (HCF AND THIN SKIN MODELS)

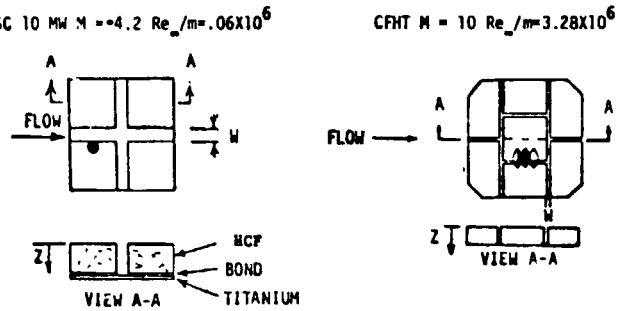

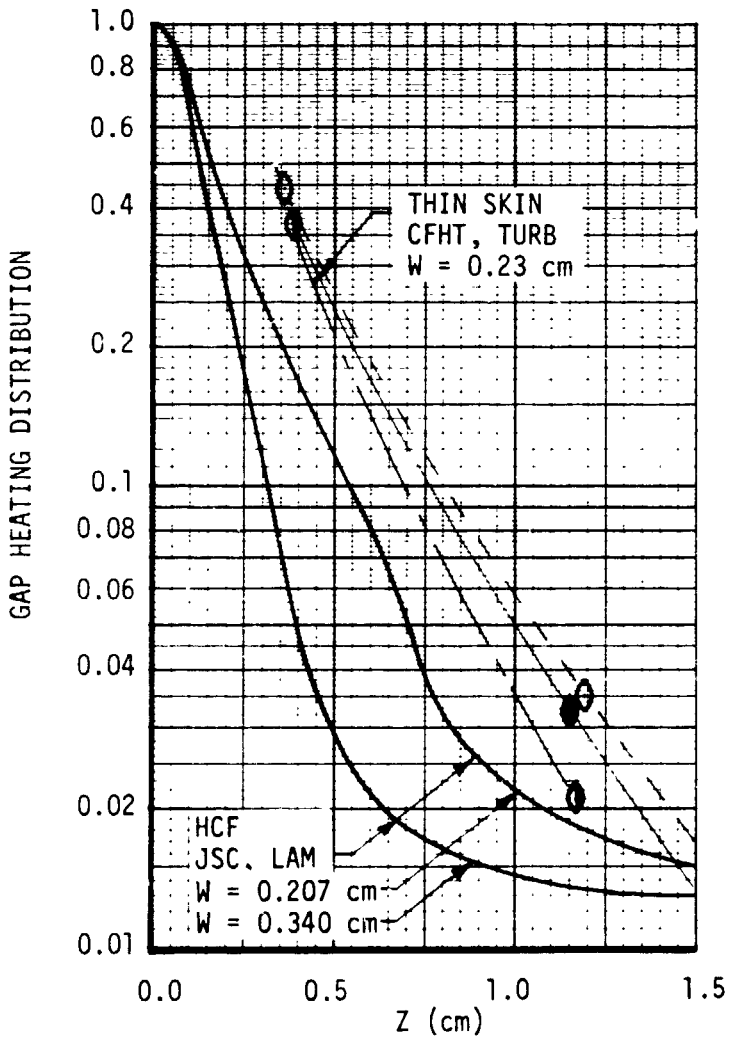

Figure 166

COMPARISON OF IN-LINE GAP HEATING JSC 10 MW AND LaRC 8 FOOT HTST (HCF AND THIN SKIN MODELS)

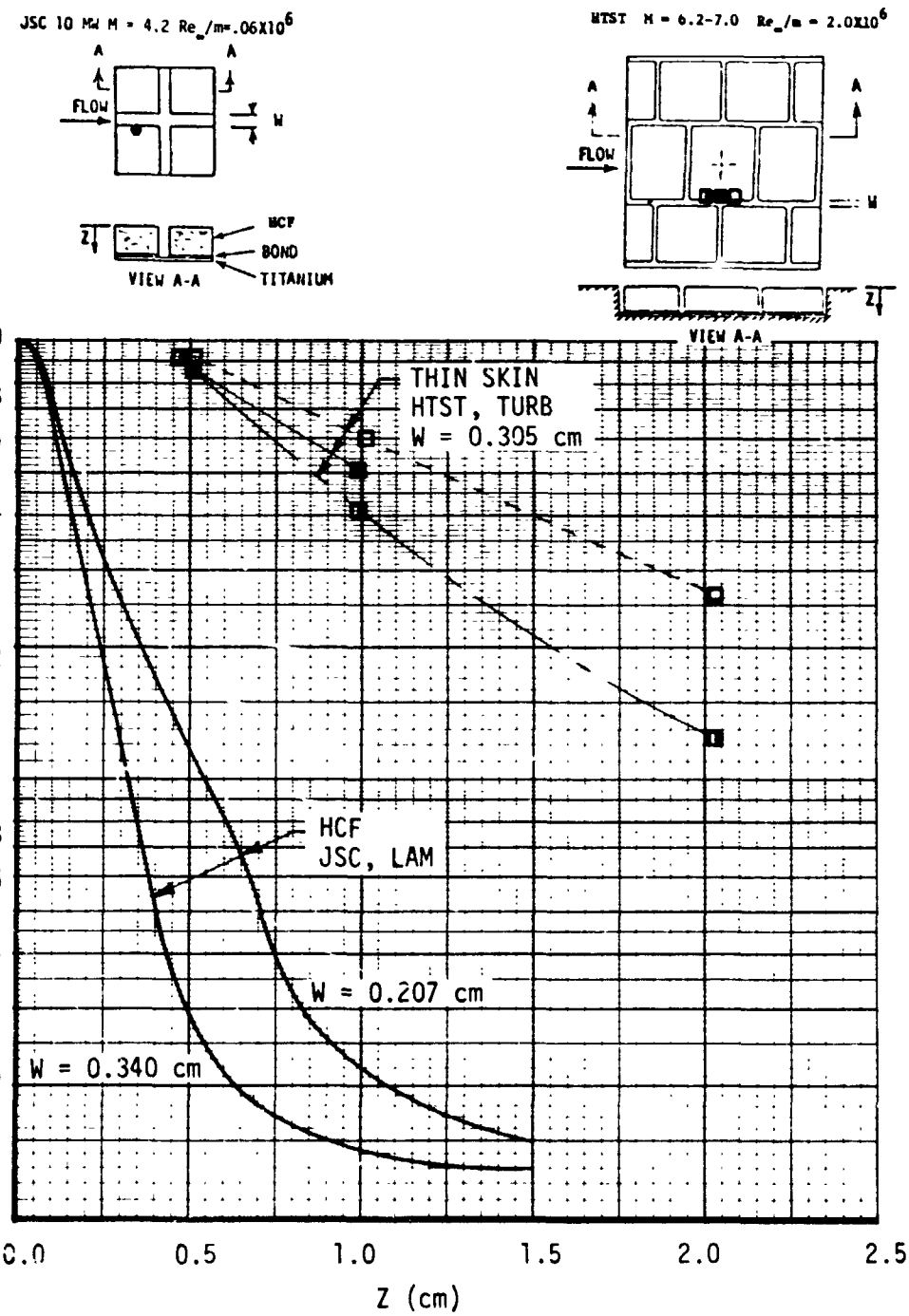

Figure 167

5.0 DATA CORRELATION

The gap heating data were correlated in terms of gap dimensions, location of gap, location in the gap and boundary layer parameters. A general data management system was set up so a common approach could be applied to data from each available source. Test results were ordered, and combined with physical dimensions, instrumentation coordinates and boundary layer parameters to form a data bank. Over 24,000 individual heat transfer measurements were assimilated into a data bank, which is functional on McDonnell Douglas computers. This data management system permitted quick access to data sets with similar attributes and direct input to a MRA (Multiple Regression Analysis) computer program. Correlations were obtained for transverse gaps, in-line gaps, flow angularity, edge radius, and steps in the presence of both laminar and turbulent boundary layers.

5.1 Correlation Method and Data Bank - Test information supplied by each test facility was received on magnetic data tapes, computer tabs, work sheets, and facility test reports. Format and methods of transmitting data were suggested to each facility and where possible these recommendations were incorporated to be consistent with what was most convenient for that facility. Data from each facility were processed into the data bank.

A procedure was set up for ordering data and combining of data with flow field parameters. In the following paragraphs the mechanics of the correlation procedure are described with the aid of a data handling flow chart. Also included in the procedure are discriminators used to select data for correlation using the Multiple Regression Analysis program.

5.1.1 Data Correlation Procedure - Each piece of gap heating data incorporated in the data bank was assigned 24 attributes which provided traceable information about its origin, instrumentation location in the joint, heat transfer parameters and boundary layer parameters. The assigned 24 attributes are listed in Figure 168. Traceable information about test program origin, run number and instrumentation designation constitutes the first attribute word. The system is formulated so that information from other tests can be added to the data bank. Information about the boundary layer flow over the RSI joints was combined with instrumentation location and the gap heating data to complete the data bank. The 24 attributes are also used to select a particular set of data for correlation. The 24 attribute information is stores on magnetic data tape.

The functioning of the data management system is illustrated in Figure 169. For example, results from the CFHT tests stored on a data tape are combined with test

24 ATTRIBUTES WORDS ASSIGNED TO EACH GAP HEATING DATA POINTS

WORD	TYPE	
1	REAL	XX | OYYY . ZZZ ZZZ = T/C OR CHANNEL NUMBER OYYY = RUN NUMBER XX = TEST NUMBER TEST NUMBERS THAT HAVE BEEN ASSIGNED XX = 1, JSC WEDGE TESTS CONDUCTED FOR MDAC-E XX = 2, JSC CHANNEL NOZZLE TESTS CONDUCTED FOR MDAC-E XX = 3, OTHER JSC CHANNEL NOZZLE TESTS XX = 4, JSC, WEDGE EDGE RADIUS, THIN SKIN, C.SCOTT XX = 10, LaRC, CFHT XX = 11, LaRC, MACH 8 V.D.T. XX = 12, AMES TURBULENT DUCT TEST XX = 13, LaRC 8 FOOT HTST XX = 14, 50 MW WEDGE TESTS XX = 15, AMES 3.5 FOOT HWT XX = 16, AMES 3.5 FOOT HWT, IN-LINE GAP
2	INTEGER	GAP CONFIGURATION 1 = BUTT, 2 = CONTOURED, 3 = OVERLAP, 4 = INCLINED
3	INTEGER	INSTRUMENTATION LOCATION 1 = UPSTREAM SIDE OF GAP, 2 = DOWNSTREAM SIDE OF GAP, 3 = IN-LINE 4 = STAGNATION, 5 = TILE TOP, UPSTREAM SIDE OF GAP, 6 = TILE TOP DOWN SIDE OF GAP
4	REAL	x | COORDINATES OF AN INSTRUMENTATION POINT, z = 0
5	REAL	y | AT TOP SURFACE OF THE TILE, x = DISTANCE DOWNSTREAM
6	REAL	z | FROM CENTER OF TILE, y (RIGHTHAND RULE), (cm)
7	REAL	$\bar{x}$, DISTANCE FROM LEADING EDGE OF EACH TILE (cm)
8	REAL	h/h_e
9	REAL	FLOW ORIENTATION (RADIANS)
10	REAL	GAP WIDTH (cm)
11	REAL	STEP HEIGHT (cm)
12	REAL	GAP FLOW LENGTH (cm)
13	REAL	TILE THICKNESS (cm)
14	INTEGER	TILE PATTERN, 0 = STAGGERED, 1 = IN-LINE
15	REAL	LOCAL MACH NUMBER
16	REAL	REYNOLDS NUMBER/METER
17	REAL	MOMENTUM THICKNESS (cm)
18	REAL	DISPLACEMENT THICKNESS (cm)
19	REAL	SUB-LAYER THICKNESS (cm) EDGE RADIUS FOR CARL SCOTT ONLY
20	REAL	HEAT TRANSFER COEFFICIENT (h), (KG/M^2SEC)
21	REAL	h/h_{ref}
22	REAL	STANTON NUMBER
23	REAL	T_{wall}/T_e TEMPERATURE RATIO ACROSS BOUNDARY LAYER
24	INTEGER	BOUNDARY LAYER STATE, 1 = LAMINAR, 2 = TRANSITIONAL, 3 = TURBULENT

Figure 168

DATA HANDLING FOR GAP HEATING CORRELATION

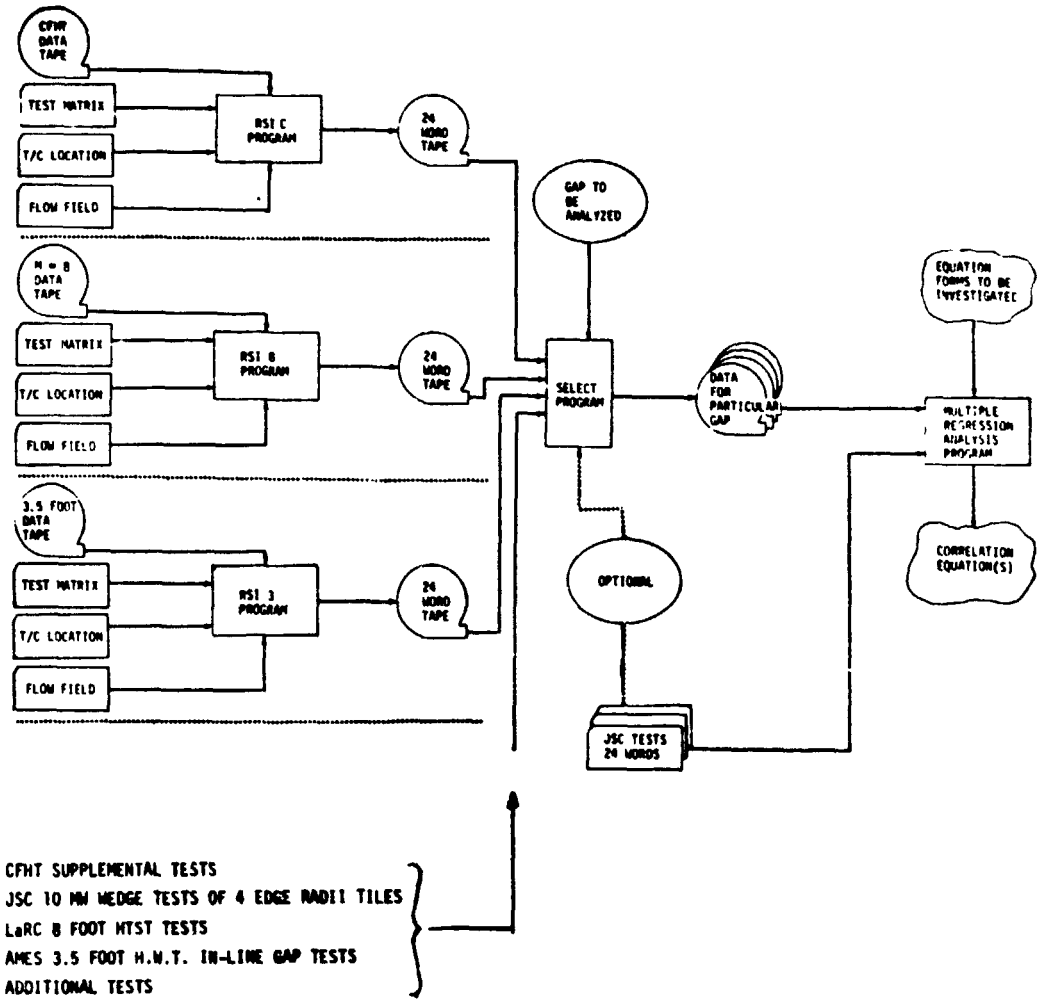

Figure 169

matrix information, T/C coordinates and boundary layer flow field parameters in the "RSI C" program to generate a 24 word attribute tape. Companion tapes from the other tests are prepared in a similar manner. These tapes are then processed by another program which selects data according to a list of discriminators specified for a particular type of gap to be analyzed. Information from the JSC tests contained on data cards can be read by either the "SELECT" program or by the Multiple Regression Analysis (MRA) program. The MRA program processes the selected data and determines the best fit for candidate correlation equations.

A list of 35 discriminators was prepared for selecting data from the 24 attribute tapes for correlation. Figure 170 shows an input form for the "SELECT" program. Upper and lower limit discriminators were used to facilitate the selection process. Tabulations as well as tapes were generated containing the selected data. The tabulated information was valuable for identifing trends, anomalies and for checking data.

Because of the large amount of heating data available for correlation, an automated multiple regression technique was used to obtain consistent-nonbiased correlation equations. The step-wise Multiple Regression Analysis (MRA) computer program (Reference 1) provided information as to the adequacy of the candidate correlation function and the equation coefficients. A modified version of the MRA computer program which accepts information stored in the data bank was used for this study. The principal modifications included accepting information stored in the data and auxiliary statistical analyses. The MRA computes a series of multiple linear regression equations in a stepwise manner. At each step, one parameter is added to the equation. The variable added is the one which makes the greatest reduction in the variance about the mean. Equivalently, it is the parameter which, if it were added, has the highest "F" ratio. Figure 171 lists the form of the correlating equation(s) and the statistical parameters use by the MRA to obtain the most appropriate correlation.

Local heating at the gap ratioed to undisturbed flat plate heating or ratioed to the value on the tile top near the gap edge was designated as the dependent variable for all correlations. Correlations were obtained in terms of natural logarithms of the dependent variable because gap heating experiences a decrease of several orders of magnitude with distance into the gap. For the JSC 10 MW data the ratio was formed using measured convective heating rates. For all other tests the ratio utilized measured convective heat transfer coefficients. The heating rate ratio and heat

VARIABLES AVAILABLE FOR SELECTING DATA

RSI GAP HEATING ANALYSIS

COMPUTER SCIENCES

SELECT INPUT FORM

REQUESTOR _____ DEPT _____

DATE _____ PAGE 1 OF _____

PROBLEM RSI GAP HEATING SCREENING

2	DESCRIPTION (DO NOT KEY PUNCH)	DIMENSION
$LIST		
CASE =	CASE NUMBER	
NFILES =	NUMBER OF FILES TO BE SKIPPED ON TAPE 30 FOR PLACEMENT OF CURRENT CASE	
XLØW =	X-LOWER LIMIT (cm)	
XHIGH =	X-UPPER LIMIT (cm)	
YLØW =	Y-LOWER LIMIT(cm)	
YHIGH =	Y-UPPER LIMIT (cm)	
ZLØW =	Z-LOWER LIMIT (cm)	
ZHIGH =	Z-UPPER LIMIT (cm)	
XBLØW =	$\bar{X}$ LOWER LIMIT (cm)	
XBHIGH =	$\bar{X}$-UPPER LIMIT (cm)	
YBLØW =	$\bar{Y}$-LOWER LIMIT (cm)	
YBHIGH =	$\bar{Y}$-UPPER LIMIT (cm)	
ALPHAL =	FLOW ORIENTATION - LOWER LIMIT (RADIANS)	
ALPHAH =	FLOW ORIENTATION - UPPER LIMIT (RADIANS)	
GAPWL =	GAP WIDTH - LOWER LIMIT (cm)	
GAPWH =	GAP WIDTH - UPPER LIMIT (cm)	
STEPL =	STEP HEIGHT - LOWER LIMIT (cm)	
STEPH =	STEP HEIGHT - UPPER LIMIT (cm)	
GAPFL =	GAP FLOW LENGTH LOWER LIMIT (cm)	
GAPFH =	GAP FLOW LENGTH - UPPER LIMIT (cm)	
THKL =	TILE THICKNESS - LOWER LIMIT (cm)	
THKH =	TILE THICKNESS - UPPER LIMIT (cm)	
IPATN(1) =	TILE PATTERN: 0=STAGGERED, 1=IN-LINE	IPATN(9)
IBL(1) =	BOUNDARY LAYER STATE: 1=LAMINAR, 2=TRANSITIONAL, 3=TURBULENT,	IBL(9)
IGAPC(1) =	GAP CONFIGURATION: 1=BUTT, 2=CONTOURED, 3=OVERLAP, 4=INCLINED	IGAPC(9)
IGLØC(1)	GAP LOCATION: 1=UPSTREAM SIDE OF GAP, 2=DOWNSTREAM SIDE OF GAP,	
	3-PARALLEL, 4-STAGNATION, 5=TILE TOP, UPSTREAM SIDE OF	
	GAP, 6=TILE TOP, DOWNSTREAM SIDE OF GAP	IGLØC(9)
NTØL(1) =	TOTAL NUMBER OF DESIRED DATA POINTS ON EACH TAPE TO BE READ:	
	0 READS ENTIRE FILE	NTØL(9)
IW =	INTERMEDIATE DIAGNOSTIC PRINT-OUT OF FIRST IW DATA POINTS	
HRLØW =	LOWEST ACCEPTABLE HEATING RATE RATIO	
HRHIGH =	HIGHEST ACCEPTABLE HEATING RATE RATIO	
BCASE =	WORD (1) FOR AN INSTRUMENTATION STACK THAT IS TO BE DISCARDED	
HØME =	VALUE OF h/h_o AT TOP OF GAP FOR EACH STACK	
DELTA =	REGION SIZE (cm) ABOUT STACK	
RADLØ =	EDGE RADIUS - LOWER LIMIT (cm)	
RADHI =	EDGE RADIUS - UPPER LIMIT (cm)	
$END		

Figure 170

MULTIPLE REGRESSION ANALYSIS

N = SAMPLE SIZE
Y = DEPENDENT VARIABLE
X_1 = INDEPENDENT VARIABLE
df = DEGREES OF FREEDOM

- STANDARD DEVIATION OF ALL "Y" VALUES: $\sigma = \sqrt{\frac{\Sigma(Y-\bar{Y})^2}{N-1}}$
- CORRELATION EQUATION: $Y = C_0 + C_1 X_1 + C_2 X_2 + C_3 X_3 + \ldots$
- RESIDUAL = $Y_{MEASURED} - Y_{CALCULATED}$
- STANDARD ERROR OF ESTIMATE: $S = \sqrt{\frac{1}{N-df}\sum (Y_{MES} - Y_{CAL})^2}$
- CORRELATION COEFFICIENT: $R = \sqrt{1 - \frac{S^2}{\sigma^2}}$ "R → 1 DENOTES GOOD FIT"
- TOTAL VARIANCE ABOUT MEAN: $S_T^2 = S_{X_1}^2 + S_{X_2}^2 + S_{X_3}^3 + \cdots + S^2_{UNEXPLAINED}$
- F TEST: $F = \frac{S^2_{X_1}}{S^2_{UNEXPLAINED}}$
- TERMS ARE INCLUDED INTO CORRELATION EQUATION STARTING WITH LARGEST "F"
- COEFFICIENTS "C_1", DETERMINED BY LEAST SQUARES

Figure 171

transfer coefficient ratio become identical for high enthalpy flow produced by the JSC 10 MW facility. The independent variables considered in the MRA included boundary layer parameters, gap dimensions, locations in the gap and ratios formed from these quantities. Local flow properties (e.g. Mach number and Reynolds number) were considered as correlation parameters because they affect embedded shock strength, flow expansion angle, boundary layer growth, boundary layer structure, etc. Other independent parameters considered cavity geometry and properties of the mass "captured" by the cavity relative to the structure and energy level of the recirculating flow in the cavity. No individual test program had sufficient variation in free stream conditions to completely evaluate all candidate parameters. Additional experimental data are needed to completely determine the impact of these parameters on gap heating.

In addition to the final function (or equations), intermediate regression equations are obtained after each step in the MRA, giving an indication of which variables are most important. Also, some parameters in the candidate correlation function were rejected because they had no significant effect on the dependent variable (heating ratio).

Statistical information is produced regarding goodness of fit, multiple correlation coefficient (R) and significance of interaction among independent variables. Of particular importance is the standard error of estimate (S) for each step which represents the MRS error of prediction (or confidence band around the regression line). In following selections values of "S" and "R" are used to evaluate candidate function adequacy.

5.1.2 h/h_e Computation - This subsection contains a review of heating ratios available for each set of gap heating data contained within the data bank. This review was conducted approximately midway through the program to establish which data sets contained the gap heating ratioed to the edge value on the tile top. As a result of this review the entire Data Bank was upgraded to include h/h_e. At the same time the effects of thermal conduction were factored into the calculation of the local heat transfer coefficient (see Section 5.1.5).

1) JSC 10 MW Arc Tunnel Channel Nozzle Tests of Mullite RSI tiles

These data were referenced to the calculated surface heating rate from the lone surface thermocouple on the test article which was normally located 0.127 cm from the edge of one of the tiles.

2) JSC 10 MW Arc Tunnel Wedge Tests of Four Edge Radii Tiles

These data were measured on thin skin tiles and were initially referenced to measured smooth flat plate heating at 15° angle-of-attack. It can be shown that the

surface heating on the thin skin tile is significantly different from that measured on the smooth flat plate. The surface heating near the gap is a strong function of surface location and gap width. Therefore h/h_e computations were added to this data set.

3) LaRC Mach 8 Variable Density Tunnel, Wall and Freestream Tests

These data were referenced to the measured surface heating at the most forward location of the test article. They were assimilated during Phase I.

Figure 55 shows data referenced to this surface heating as a function of Re_∞/m with the test article in the freestream position. It can be seen that at higher Reynolds numbers the flow becomes transitional and turbulent. It is felt that the gap heating at these Reynolds numbers would correlate better if referenced to the local surface heating near the gap. Figure 56 shows the heating data referenced to the measured heating at the forward surface thermocouple (point B) when the test article is in the tunnel wall position. The boundary layer is turbulent over the entire test article. The surface heating is nearly constant over the entire surface. Therefore, the reference heating location is not as critical as with the freestream tests. Due to schedule constraints these data were not modified.

4) Ames 3.5 Foot HWT

Two sets of data were received from this test facility. The first set employed a calibration plate insert and four inserts with different gap orientation (see Figure 172). These data were assimilated during Phase I. A set of data for a single in-line gap was assimilated during Phase II. From analyses contained in previous sections, it appears that h/h_e would be a desirable correlation form for these data. The data were originally referenced to the calibration plate data. However, the presence of the gaps has been shown to cause earlier transition on the gap inserts which affects both surface and gap heating. Both sets of data were put in the form of h/h_e.

5) LaRC Mach 10 CFHT Tunnel Wall Tests

These data were referenced to calibration plate heating distributions. The boundary layer is turbulent over the entire length of the test article. This results in nearly uniform heating along the direction of flow for the calibration plate. The heating in the spanwise direction (normal to the flow) increases significantly away from the centerline of the test article.

The data from these tests indicate that the gap heating is related to the heating on the top surface near the gaps. The same trends that apply to the gap

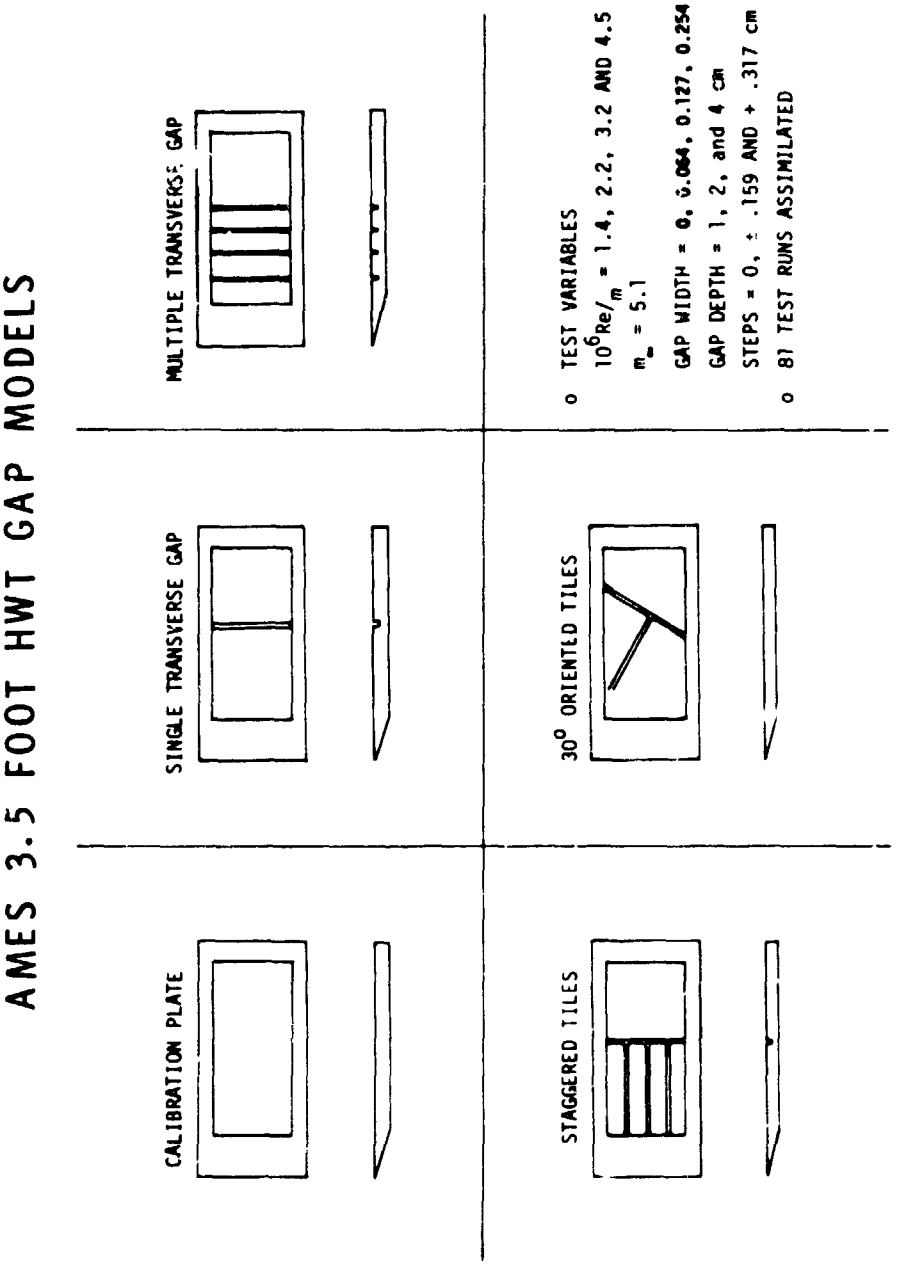
AMES 3.5 FOOT HWT GAP MODELS
MULTIPLE TRANSVERSE GAP
SINGLE TRANSVERSE GAP
30° ORIENTED TILES
CALIBRATION PLATE
STAGGERED TILES
o TEST VARIABLES
$10^6 Re/_m$ = 1.4, 2.2, 3.2 AND 4.5
m_∞ = 5.1
GAP WIDTH = 0, 0.064, 0.127, 0.254 AND 0.508 cm
GAP DEPTH = 1, 2, and 4 cm
STEPS = 0, ± .159 AND + .317 cm
o 81 TEST RUNS ASSIMILATED

Figure 172

heating also apply to the top surface near the edges of the gap. This data appears to correlate better when referenced to edge value. Therefore, h/h_e was added to the Data Bank.

6) LaRC 8 Foot HTST of Gap Model

These data were referenced to both $h/h_{\text{calibration plate}}$ and h/h_{edge}. The test article was tested at 9°, 7.5°, and 15° angles to the flow and two Reynolds number factors. Calibration data are available for only three of the six possible angle-of-attack/Reynolds number combinations.

7) Ames 20 MW Turbulent Duct of Silica Tiles

These data were taken on silica RSI tiles. The data are in the form of thermocouple temperature responses. The heating rates were obtained using the inverse solution technique and the data was already in the form of Q/Q_{surface}.

5.1.3 Boundary Layer Transition - During the course of analyzing each set of data assimilated into this study, the state of the boundary layer over the test panel was determined. Each piece of data was marked as to its boundary layer state, mainly, based on results from tests on smooth calibration plates. The Ames in-line gap tests were handled differently because a continuous row of thermocouples were installed along the top of the panel near the gap and could be used to judge boundary layer transition.

5.1.4 Specific Heat Correction of Thin Skin Data - Where necessary, corrections were applied to the data for differences in specific heat between the calibration plates and the test article. For example the heating data obtained on the top of the thin skin tile material used in the LaRC CFHT test were consistently higher than those measured on a companion calibration plate. The calibration plate was fabricated from a sheet of 304 stainless steel. Nominal values for the specific heat of both materials were used in the data reduction (Cp_{304}=0.12 and Cp_{321}=0.1019 Cal/gm°C). To verify the correctness of these values the specific heat of a coupon cut from the two test articles was measured. The specific heat was measured at LaRC using the same equipment and technique on both specimens. Figure 102 contains the measurements and specific heat ratio. It was necessary to extrapolate down to 300°K where the wind tunnel tests were conducted. The measured specific heat values used for correcting the data are Cp_{304}=0.112 and Cp_{321}=0.1045 Cal/gm°C. This reduces the heating ratio by 9%. The computer program was modified to automatically correct the CFHT data. Figure 103 shows graphically the effects of the specific heat correction on tile heating.

A similar procedure was applied to the specific heat measurements on the thin skin tile and calibration plate material received from I. Weinstein at LaRC. The data are presented in Figure 138. The specific heat of the thin skin material is 5.6% higher than that of the calibration plate at room conditions (300°K). In the original data reduction the same specific heat was used for both materials. Hence the heating ratio (h/h_{FP}) was 5.6% low. Results in the Data Bank were corrected for specific heat.

5.1.5 Conduction Correction of Thin Skin Data - An orthogonal conduction correction for the thin skin tile data was inserted into the data processing programs.

This package arranges adjacent instrumentation so that the second derivatives in both (x) and (y) directions can be computed. The correction on heat transfer coefficient is implemented as follows:

$$h_{corrected} = \frac{1}{T_{AW}-T_W}\left[\rho z C_p \frac{\partial T}{\partial \theta} - kz\left(\frac{\partial^2 T}{\partial x^2} + \frac{\partial^2 T}{\partial y^2}\right)\right]$$

$$h_{corrected} = h_{\substack{HEAT\\STORAGE\\only-}} - \frac{kz}{(T_{AW}-T_W)}\left(\frac{\partial^2 T}{\partial x^2} + \frac{\partial^2 T}{\partial y^2}\right)$$

The procedure is setup so that the order of the temperature curve fit and the number of data points in the least square calculation can be specified. For example, the entire set of heating rates obtained on the thin skin tile tested in the HTST was corrected for thermal conduction in two orthogonal directions. In some instances the heating rates changed by as much as 3.8%. Of course where there was little or no temperature differences indicated by the thermocouples, the heating rate remained unchanged. Figure 101 shows the change in a heating distribution on the tile when considering thermal conduction.

5.2 Correlations Formulated During Phase I - Correlations were obtained for both transverse and in-line gaps for the 10 MW Arc Tunnel at JSC. Transverse gap heating was best described by the following equation, wherein distance into the gap, gap width and the interaction between distance and depth were the most significant variables in the equation.

$$\ln\left(\frac{q_{GAP}}{q_{SURFACE}}\right) = -.3716-5.0249Z+2.5604Z^2+1.0733W-.03797ZT^2-.03654(Z/W) -6.0719(Z/T)^2$$

Equation (9)

Equation 25 was selected as the most descriptive of in-line gap heating. In this correlation, distance into the gap, the ratio of distance to gap width and width were the significant variables

$$\ln\left(\frac{q_{GAP}}{q_{SURFACE}}\right) = -.3319 -4.3979Z+1.5630Z^2-.2295(Z/W)+1.0148W$$

Equation (25)

Sets of data from the CFHT and the Mach 8 tests were submitted to the MRA program to determine the trends with both boundary layer and gap geometry for turbulent flow. The resultant correlation was

$$\frac{h}{h_{REF}} = 0.01384 \quad Z^{(-1.46402W^{-2/7})} \quad \left(\frac{T_W}{T_e}\right)^{-2.549} \quad \left(\frac{Re}{10^6 \text{ meter}}\right)^{-.5362} \quad W^{.7806}$$

Equation (18)

The independent variables have the following ranges

$0.36 \leq Z \leq 5.74$ cm

$0.127 \leq W \leq 0.711$ cm

$0.29 \leq T_W/T_e \leq 0.44$

$1.158X10^6 \leq$ Re (unit Reynolds number, m^{-1}) $\leq 19.37x10^6$

The CFHT data were also analyzed to determine the effects of flow angularity (γ). The following correlation resulted for the transverse gap rotated 90°.

$$\ln\frac{h}{h_{FP}} = -0.1054-3.71478Z+.60432Z^2+1.92179W-.00692Y^2+0.04316YW+.01768YG +.00235\ Y^2Z$$

Equation (12A)

5.3 Correlations for Edge Radius - Sets of four thin skin tiles in a wedge test fixture were inserted into the flow field generated by the JSC 10 MW Arc Tunnel (C. D. Scott, Test Engineer). Four edge radii (0.1575, 0.3175, 0.635 and 1.270 cm) were tested at three gap widths (0.127, 0.254 and 0.381 c). Originally the smallest radius tile was specified in the data we received to have a sharp edge (E = 0.0), so an entire set of correlations were developed using the information. Near the end of this program, information was received that the edge actually had a curvature. Unfortunately, scheduling would only allow reworking one correlation. Multiple Regression Analyses were performed to correlate the heating in the in-line gap both upstream and downstream of the transverse gap, and also on both faces of the transverse gap (see Figure 13). Analyses were performed first for only the vertical walls and then for the vertical wall plus the edge zone on the tile. Approximately 45 data points per gap location were available for the vertical walls and 63 data points when the edge zone was included.

5.3.1 Vertical Wall Correlations - Candidate parameters generated using gap width (W), edge radius (E) and distance into the gap (Z) were used in the correlation of local heating ratioed to the heating on a plate without gaps. Both heating ratio and logarithm of heating ratio were tested. The logarithmic transformation produced the best fit. Three sets of candidate parameters (Figure A1) were used in analysis. The first set which involved (Z) was employed most extensively. The other sets, which contained the surface distance (S) were used to include the data on the radius. The third set included interaction between width and radius.

Figure 173 contains the best function (using set 1 parameters) for the vertical wall data at the four gap locations. Also the data for the all in-line gap were grouped together for an analyses. Similar analyses were performed for the transverse gap and a grand correlation for all vertical wall data. The regression correlation coefficient, standard error of estimate, minimum heating, maximum heat for both measured data and the derived functions are listed in the figure. As can be noted from the figure, the number of parameters was reduced from 39 to a maximum of 8 by the multiple regression analysis procedure. The parameters are listed in each function in the order of significant contributions to the correlation. For example, Z/W was the most significant parameter in Equation 4-1. Each function exhibits a drastic decrease in the heating with distance (Z) into the gap. The effect of edge radius is coupled either with gap width or distance into the gap.

Using the logarithmic transformation of heating ratio produced the best fit. A regression correlation coefficient (R) of 0.9707 with a standard error of estimate (S) of 0.3541 was achieved. The correlating equation for the in-line gap is:

$$\ln \frac{q}{q_{REF}} = 0.20113 - 0.66569 \frac{Z}{W} + 0.01285 \left(\frac{Z}{W}\right)^2 + 3.96410 \left(\frac{E}{Z}\right)^2 - 2.94821 \frac{E}{Z}$$

$$+ 0.15665\, Z^3 + 0.20328 \frac{E}{W} - 0.83354\, (WZ^2)$$

As can be seen from Figure 174, the residuals are distributed uniformly when presented as a function of measured data and also as a function of calculated heating. The fitting of the data was performed using the logarithmic value and hence, Figure 174 should be used to judge the degree of bias in the fit. Figure 175 presents the residuals for the above function transformed into heating ratios. The correlation equation yields a heating ratio that varies from 0.007 to 0.911 as compared with the measured data which varied from 0.006 to 1.020. The correlation function has a standard error of estimate (cartesean) of 0.1190.

To understand the goodness of fit and the data scatter, figures have been prepared which compared the correlations with the reported data. Figures 176 and 177 contain the comparison for the in-line gap, upstream of the transverse gap. Although Equation 4-1 involves seven terms, the curves generated by the equation are smooth with Z, E, and W. Figure 176 is for the extremes of the edge radii tested. For

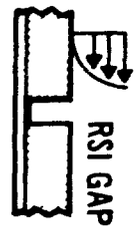

CORRELATION FUNCTIONS FOR GAPS WITH VARIOUS EDGE RADII

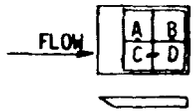

(VERTICAL WALL ONLY)

LOCATION	EQ.NO.	FUNCTION	NO. OF POINTS	R	S	RANGE IN q/q_{FP} (CARTESIAN) MEASURED MIN	MEASURED MAX	FUNCTION MIN	FUNCTION MAX	S^{∇}
A IN-LINE, UP	4-1	$\ln(q/q_{FP}) = 0.20113 - 0.66569\ Z/W + 0.01285(Z/W)^2 + 3.96410(E/Z)^2 - 2.9482(E/Z) + 0.15665(Z^3) + 0.20328\ E/W - 0.83354(WZ^2)$	45	0.9707	0.3541	.006	1.020	.007	.911	.119
	4-2	$\ln(q/q_{FP}) = -0.52977 - 0.40659\ S/W + 13.35856(E/S)^2 + 0.00970(S/W)^2 - 5.37612(E/S) + 0.73183\ W(\ln S)^2$	45	0.9575	0.4137	.006	1.020	.010	1.213	.1354
B IN-LINE, DWN	4-3	$\ln(q/q_{FP}) = -5.60717 - 2.44821\ \ln(Z) + 3.43779(E/Z)^2 + 3.94794\ ZW - 2.24996\ WE^2$	48	.9567	0.4424	.003	.539	.002	.599	.0797
C TRANS, UP	4-4	$\ln(q/q_{FP}) = 1.52373 - 5.4209\sqrt{Z} + 2.06166\ W(E^2) + .00002(Z/E)^2 + 1.04795\ (F/Z)^2$	42	.9344	0.5341	.003	0.740	.004	.583	.1088
D TRANS, DWN	4-5	$\ln(q/q_{FP}) = -4.72221 - 2.60637\ \ln(Z) - 6.73196\ EW + 3.42875(E/Z)^2 + 6.90065\ ZW$	44	.9159	0.5785	.005	1.102	.005	1.677	.1363
C TRANS, UP D DOWN	4-6	$\ln(q/q_{FP}) = -1.32523 - .65551\ \ln(Z) - 0.25169(Z/W) + 2.82815(E/Z)^2 + 0.31381\ Z^3 - 1.96995\sqrt{E} - 1.53064\ W(Z^2)$	86	.9189	.5694	.003	1.102	.006	.772	.127
A IN-LINE; UP B DOWN	4-7	$\ln(q/q_{FP}) = -2.27841 - 1.77052\ \ln(Z) + 2.35783(E/Z)^2 + 1.03455\ \ln(W)$	93	.8413	.8613	.003	1.020	.004	1.011	.157
A IN-LINE & B TRANS. C D	4-8	$\ln(q/q_{FP}) = -1.74875 - 2.62664\ \ln(Z) + 1.98717(E/Z)^2 + 1.26260\ \ln(W) + 0.08062^3 - 0.97971(W/Z)$	179	.8582	.7726	.003	1.102	.007	.891	.1309

NOTE: FOR PURPOSE OF DEVELOPING CORRELATIONS, THE SHARP TILE WAS ASSIGNED AN EDGE RADIUS OF 0.00254 cm

E = EDGE RADIUS (cm)
Z = DISTANCE INTO GAP (cm)
W = GAP WIDTH (cm)
S = SURFACE DISTANCE (cm)

JSC 10MW ARC TUNNEL TESTS (C. D. SCOTT)

E = 0.00254, 0.3175, 0.635 AND 1.27 cm
W = 0.127, 0.254, AND 0.381 cm

R = REGRESSION CORRELATION COEFFICIENT BASED ON NATURAL LOGARITHM

S = STANDARD ERROR OF ESTIMATE BASED ON NATURAL LOGARITHM

S^{∇} = STANDARD ERROR OF ESTIMATE BASED ON CARTESIAN VALUES

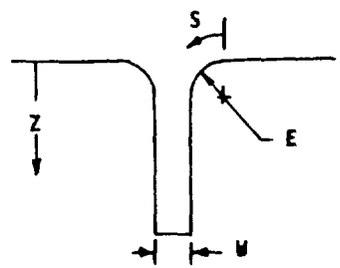

Figure 173

RESIDUALS (ℓn) FOR IN-LINE GAP
JSC 10 MW, EDGE RADIUS TESTS

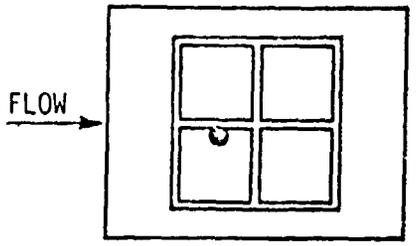

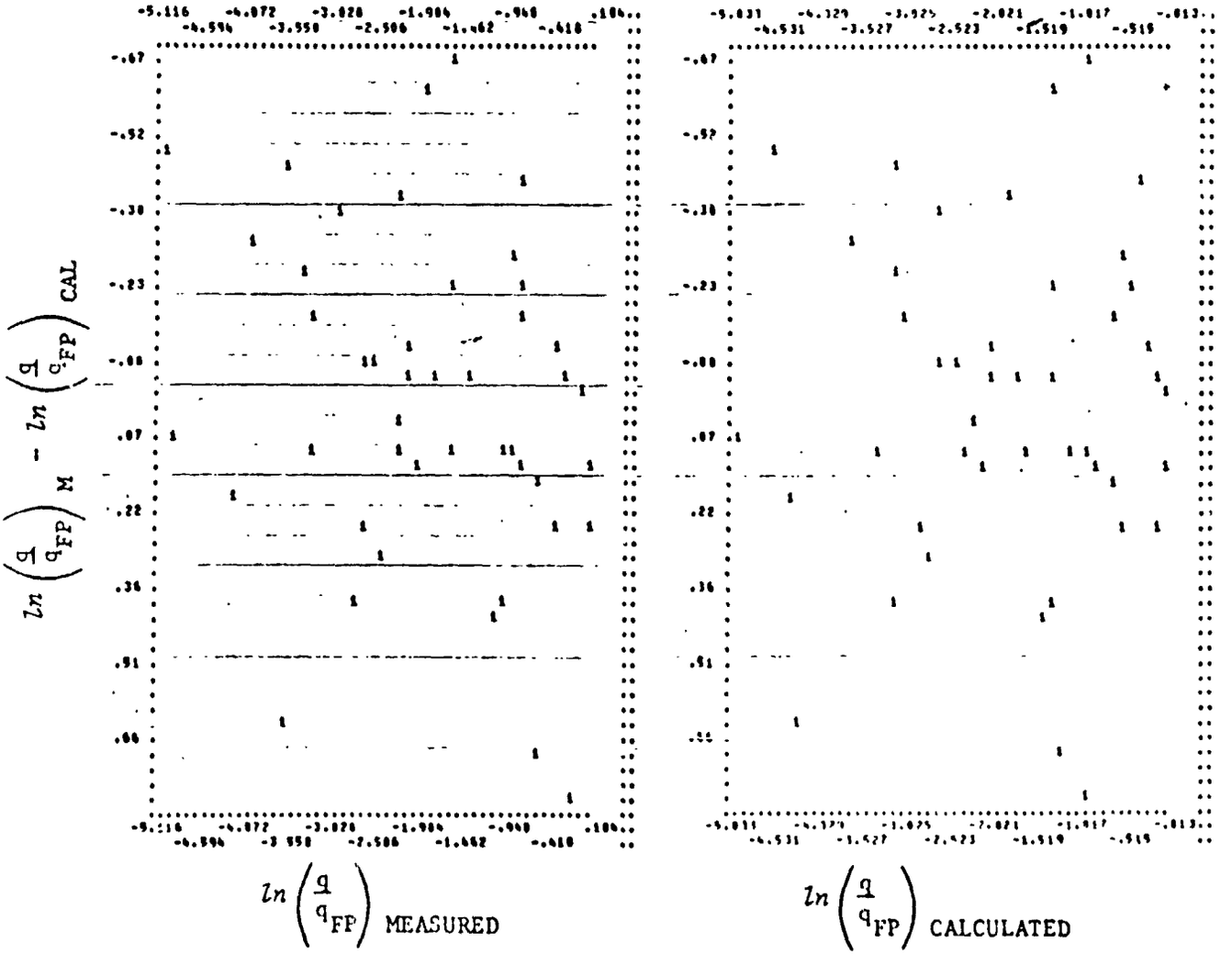

Figure 174

RESIDUALS (CARTESIAN) FOR IN-LINE GAP
JSC 10 MW, EDGE RADIUS TESTS

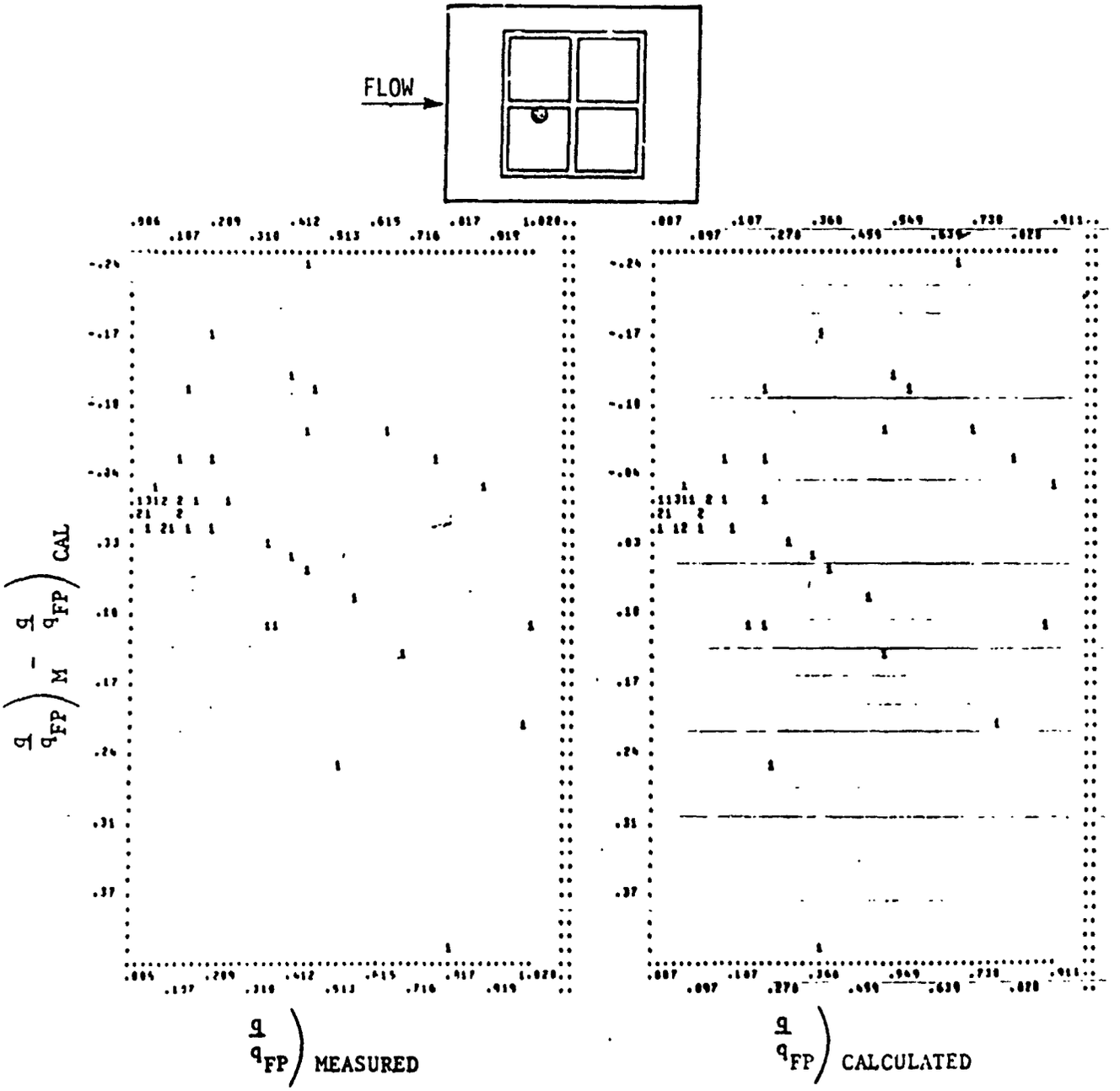

Figure 175

CORRELATION OF IN-LINE GAP HEATING (JSC 10 MW TEST)

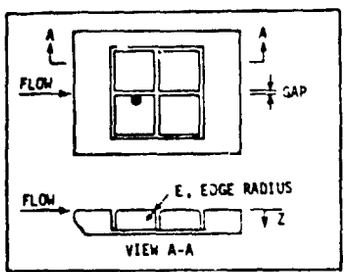

VERTICAL WALL, ONLY

GAP WIDTH (cm)	DATA	EQ. 4-1
0.381	△	– – – – –
0.254	□	– – – –
0.127	○	———

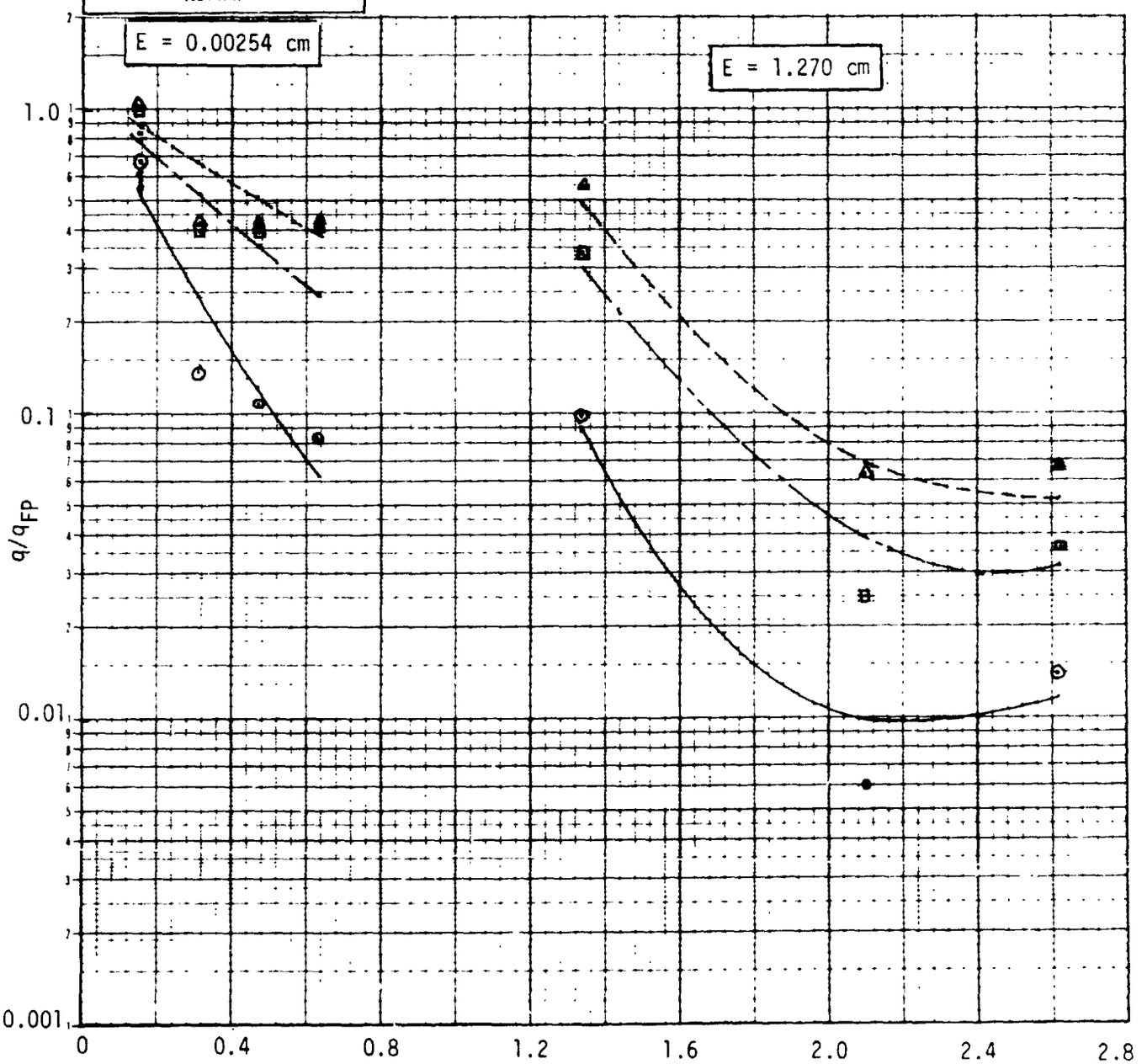

Figure 176

CORRELATION OF IN-LINE GAP HEATING (JSC 10 MW TEST)

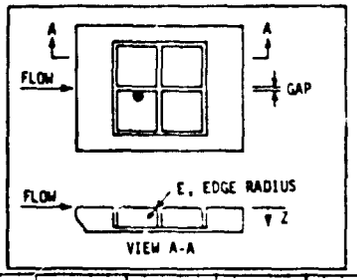

VERTICAL WALL, ONLY

GAP WIDTH (cm)	DATA	EQ. 4-1
0.381	△	– – – –
0.254	□	– – –
0.127	○	———

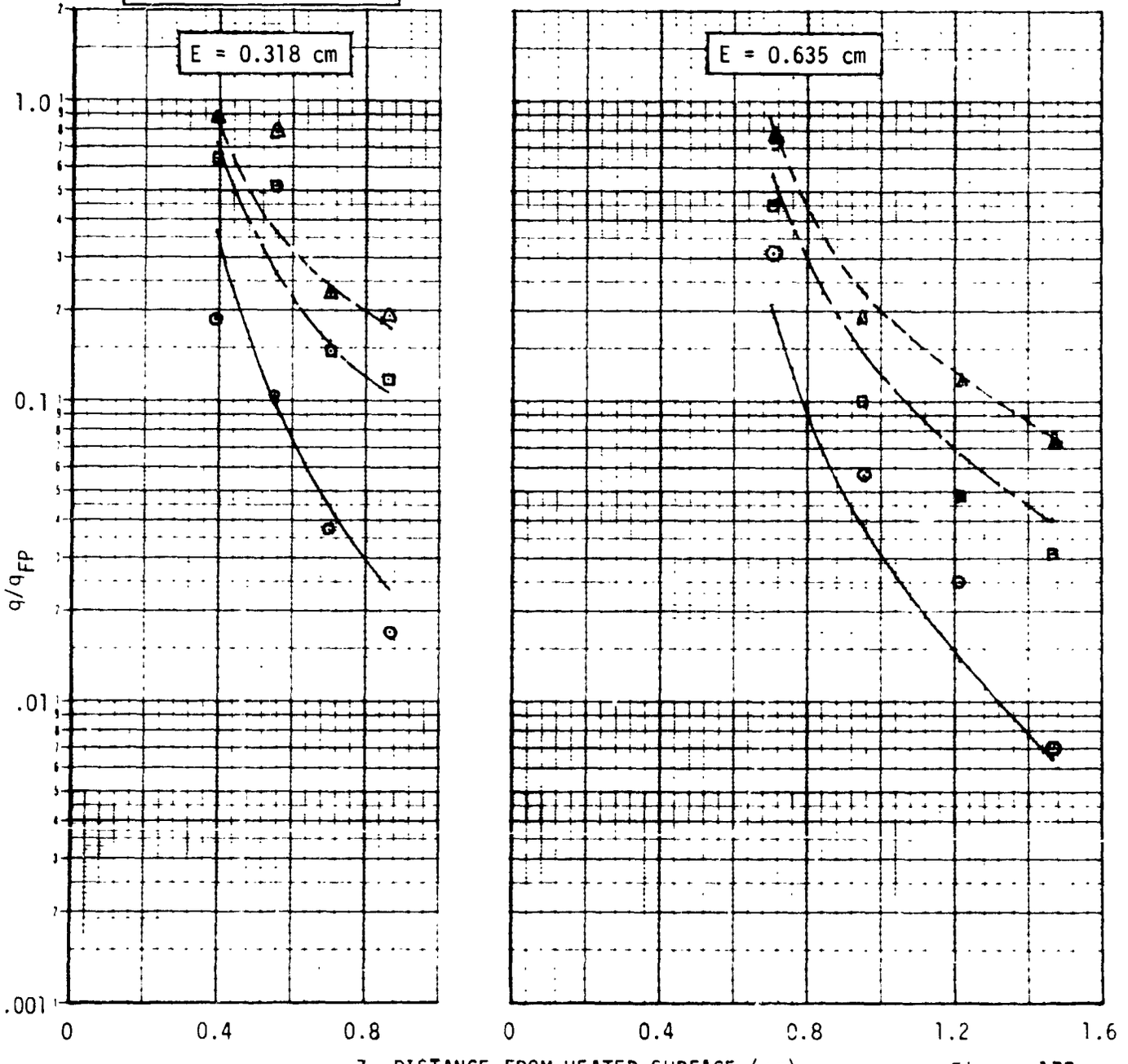

Figure 177

the wide gap (0.381 cm) the function underpredicts the data near the top of the gap. However, while the data scatter is considerable for the lower heating values, the curves pass through the data mean. Figure 177 is for the intermediate edge radii. The curves pass through the data means except for the large edge radius (E = 0.635 cm) at the narrow gap width (W = 0.127 cm) where the function underpredicts the data.

Correlations were also computed for the in-line gap (upstream of the transverse) using surface distance (S) rather than the Z-dimension. These analyses were performed to test the hypothesis that heating is a smooth function of (S). The correlation equation (4-2) for the vertical wall region of the gap is contained in Figure 173. Using (S) as a correlating parameter decreases the number of terms from eight to six at a slight reduction in the goodness of fit.

5.3.2 Correlation for Edge and Wall - The other correlations prepared considered the additional data points for the curved (or edge) portion of the gaps. The best resulting correlation (Equation 4-9, Figure 178) has ten terms. In Figure 179 this correlation is compared with the measured in-line gap data. The S correlation appears able to accomodate heating on the tile edge as well as the vertical portion of the gap with no significant loss in accuracy. Figure 180 compares the best correlation (Equation 4-17, Figure 178) for the transverse gap with the data. Figure 178 presents the correlation of set 3 parameters with the edge and wall data.

5.4 Correlations for Long In-line Gap - Heating data obtained on a long in-line or axial gap was separated according to boundary layer state and correlations were developed for an in-line gap in laminar flow at incidence angles from zero to fifteen degrees.

Two sets of laminar data were selected from the data bank for correlation; the first set consisted of 273 measurements at zero incidence "γ", the second of 635 points at γ between zero and fifteen degrees.

5.4.1 Correlations for Long In-line Gap ($\gamma=0^{\circ}$) - Heating measurements were obtained for three values of gap width and Reynolds number and four gap depths. Attempts to linearize the data proved fruitless so correlations were attempted using independant parameters up to the third order. Figure A1 part 2 contains the variables investigated. Separate analyses were developed for gap heating referenced to the flat calibration plate "h_{FP}" and the edge of the gap "h_{EDGE}". "h_{EDGE}" is the heating rate at y=-0.51 cm on the gap, Side B as illustrated in Figure 14. The resultant equations are presented in Figure 181. The independent parameters are sequenced

CORRELATION FUNCTIONS FOR GAPS WITH EDGE RADIUS (EDGE AND WALL)

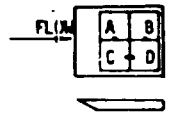

LOCATION		EQ. NO.	FUNCTION	NO. OF POINTS	R	S	RANGE IN q/q_{FP} (CARTESIAN) MEASURED MIN	MEASURED MAX	FUNCTION MIN	FUNCTION MAX	S^{∇}
A	IN-LINE, UP	4-9	$\ln(q/q_{FP}) = .39439 - 0.71672\ S/W + 0.76083\ E/W + 0.01320\ (S/W)^2 + 2.53332\ E^2 \ln S - 3.62726 WE \ln S - 1.33060 E(\ln S)^2 - 0.02602\ (E/W)^2 + 2.53332 WE^2 (\ln S)^2 - 0.51625\ S$	63	.9624	.4171	.006	1.386	.007	1.548	.1698
B	IN-LINE, DN	4-10	$\ln(q/q_{FP}) = -1.21264 - 4.27622S + 0.12501 S^3 + 7.82944E - 2.30047E^2 - 0.39390(E/S)^2 + 1.09199W(\ln S)^2 - 0.060260(S/W)$	66	.9593	.5231	.003	1.040	.002	1.084	.0800
C	TRANS-UP:	4-11	$\ln(q/q_{FP}) = -.313755 - 4.14284 \ln S - 1.42212(\ln S)^2 + 2.27958E + 1.35861E \ln S + 0.33317 \ln W$	57	.9316	.5508	.003	0.750	.007	0.839	.1039
D	TRANS-DN:	4-17*	$\ln(q/q_{FP}) = 0.59775 - 3.67827S + 0.14962 S^3 + 3.05060E - 0.09307(S/W) - 0.27898(E/S)^2$	61	.9440	.5298	.005	1.240	.009	1.376	.1643

NOTE: FOR PURPOSE OF DEVELOPING CORRELATIONS, THE SHARP TILE WAS ASSIGNED AN EDGE RADIUS OF 0.00254 cm

E = EDGE RADIUS (cm)
Z = DISTANCE INTO GAP (cm)
W = GAP WIDTH (cm)
S = SURFACE DISTANCE (cm)

JSC 10MW ARC TUNNEL TESTS (C. D. SCOTT)
E = 0.00254, 0.3175, 0.635 AND 1.27 cm
*E = 0.157, 0.3175, 0.635 AND 1.27 cm
W = 0.127, 0.254, AND 0.381 cm

R = REGRESSION CORRELATION COEFFICIENT BASED ON NATURAL LOGARITHM

S = STANDARD ERROR OF ESTIMATE BASED ON NATURAL LOGARITHM

S^{∇} = STANDARD ERROR OF ESTIMATE BASED ON CARTESIAN VALUES

SET 2 PARAMETERS USED IN ABOVE CORRELATIONS

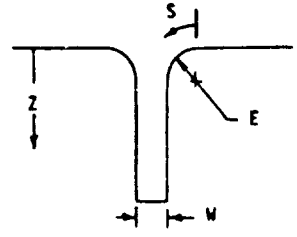

Figure 178
Part 1

CORRELATION FUNCTIONS FOR GAPS WITH EDGE RADIUS (EDGE AND WALL)

(q/q_E) CORRELATION FUNCTIONS FOR GAPS WITH EDGE RADIUS (EDGE AND WALL ZONES)

LOCATION	EQ. NO.	FUNCTION	NO. OF POINTS	R	S	RANGE IN q/q_E (CARTESIAN) MEASURED MIN	MEASURED MAX	FUNCTION MIN	FUNCTION MAX	S^∇	q/q_{FP} R	q/q_{FP} S	q/q_{FP} S^∇
A IN-LINE, UP	4-13	$\ln(q/q_E) = -0.01221-0.41940(S/W)+0.00725(S/W)^2+0.80703(E/S)$ $-0.47496(E/S)^2+0.27744(E/W)-1.07104S+0.04555S^3+$ $0.70519(W+E)^2$	63	.9554	.4364	.006	1.095	.008	2.055	.1182	.9626	.4162	.1718
B IN-LINE, DN	4-14	$\ln(q/q_E) = -1.16773-1.43500S+0.43548\ln E-1.91164\ln S$ $+1.07838(W+E)^2-0.30013(E/S)^2$	66	.9484	.5757	.003	0.979	.002	1.571	.1119	.9529	.5620	.0880
C TRAN, UP	4-15	$\ln(q/q_E) = 0.35564-2.77360S+1.18292E^2+1.83519E^2\ln S$	57	.9175	.5946	.004	1.014	.006	0.987	.1912	.9251	5642	.1401
D TRAN, DN	4-16	$\ln(q/q_E) = 0.42466-5.14719S+0.19450S^3+3.84088(W+E)$ $-0.30623(E/S)^2+2.27613W\ln S-2.18027WE^2$	61	.9563	.4740	.005	0.960	.008	1.200	.1399	.9556	.4830	.1563

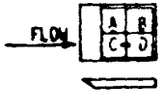

NOTE: FOR PURPOSE OF DEVELOPING CORRELATIONS, THE SHARP TILE WAS ASSIGNED AN EDGE RADIUS OF 0.00254 cm

E = EDGE RADIUS (cm)
Z = DISTANCE INTO GAP (cm)
W = GAP WIDTH (cm)
S = SURFACE DISTANCE (cm)

JSC 10"W ARC TUNNEL TESTS (C. D. SCOTT)

E = 0.00254, 0.3175, 0.635 AND 1.27 cm
W = 0.127, 0.254, AND 0.381 cm

R = REGRESSION CORRELATION COEFFICIENT BASED ON NATURAL LOGARITHM

S = STANDARD ERROR OF ESTIMATE BASED ON NATURAL LOGARITHM

S^∇ = STANDARD ERROR OF ESTIMATE BASED ON CARTESIAN VALUES

SET 3 PARAMETERS USED IN ABOVE CORRELATIONS

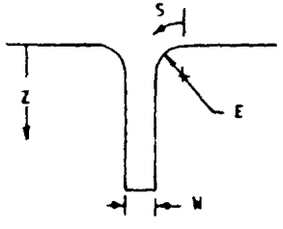

Figure 178
Part 2

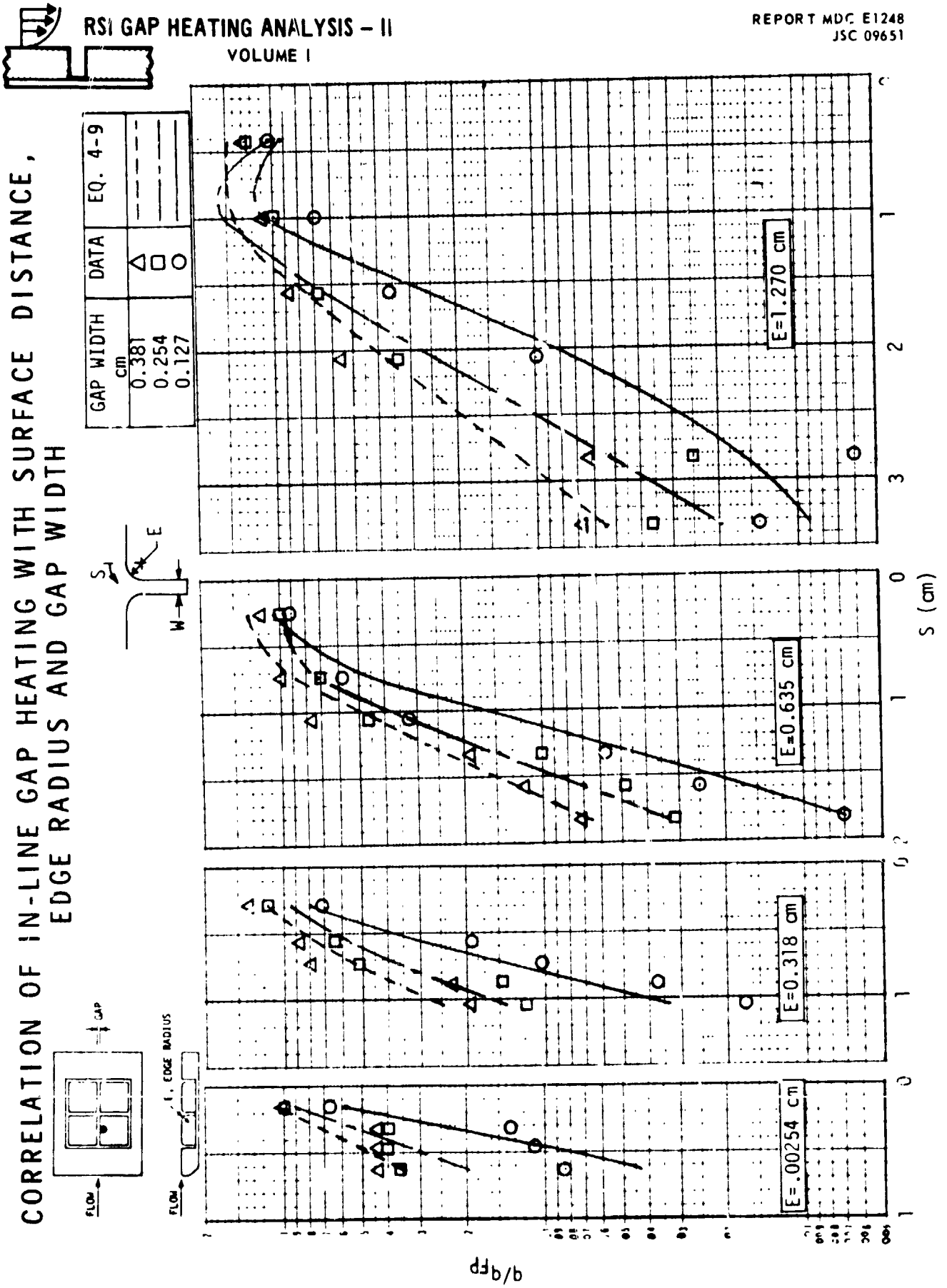
CORRELATION OF IN-LINE GAP HEATING WITH SURFACE DISTANCE, EDGE RADIUS AND GAP WIDTH
GAP WIDTH cm
0.381
0.254
0.127
DATA
EQ. 4-9
E=1.270 cm
E=0.635 cm
E=0.318 cm
E=.00254 cm
S (cm)
GAP
R, EDGE RADIUS
FLOW
FLOW
dfb/b

Figure 179

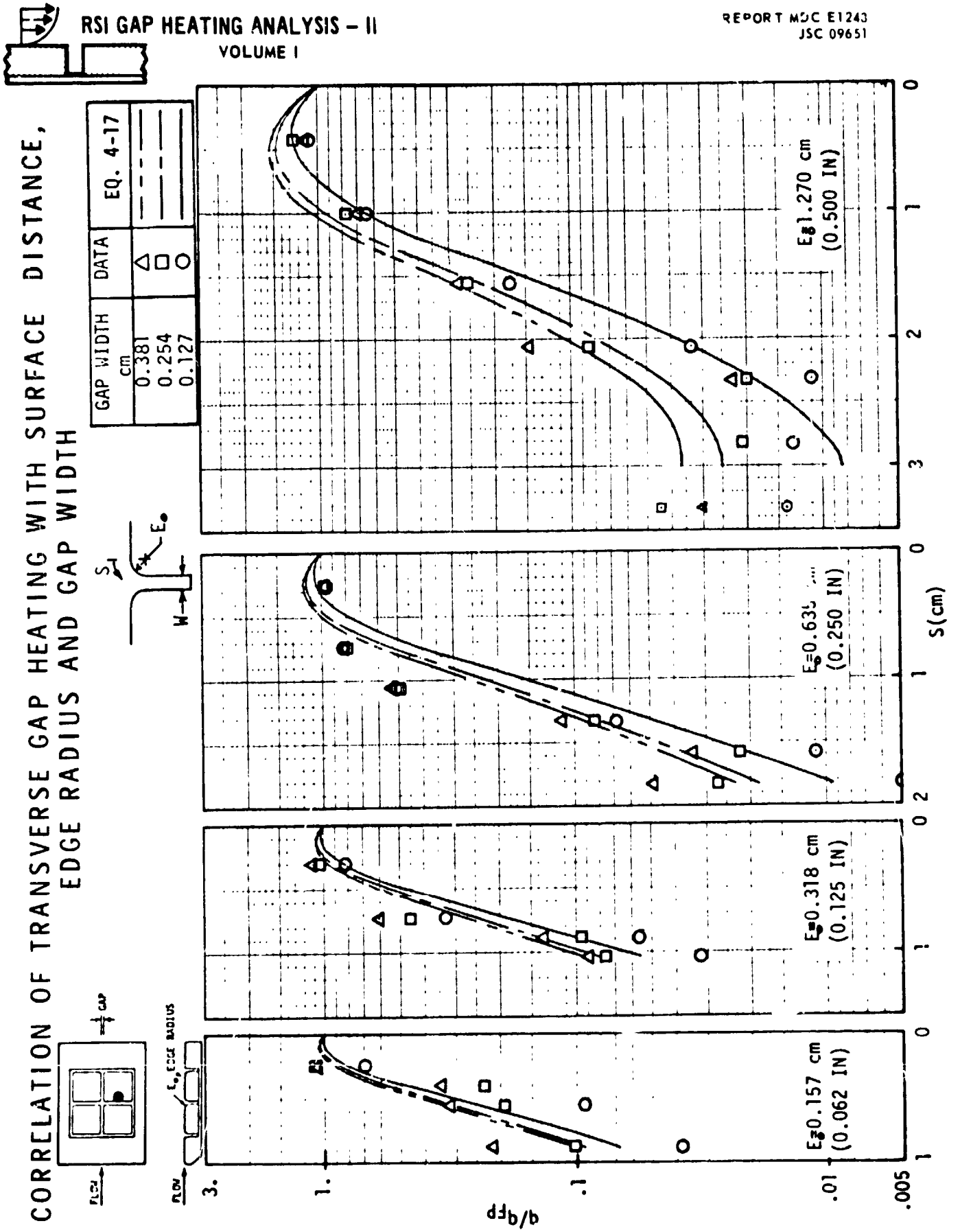
CORRELATION OF TRANSVERSE GAP HEATING WITH SURFACE DISTANCE, EDGE RADIUS AND GAP WIDTH
GAP WIDTH cm
0.381
0.254
0.127
DATA
EQ. 4-17
Eg=1.270 cm (0.500 IN)
Eg=0.635 cm (0.250 IN)
Eg=0.318 cm (0.125 IN)
Eg=0.157 cm (0.062 IN)
S(cm)
q/qfp
3.
1.
.1
.01
.005
FLOW
FLOW

Figure 180

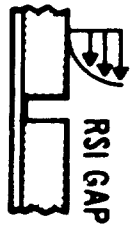

CORRELATION FUNCTIONS FOR IN-LINE GAPS (AMES 3.5 FOOT H.W.T.) LAMINAR, γ = 0 DEGREES

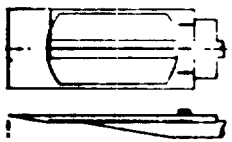

LOCATION	EQ.NO.	FUNCTION	NO. OF POINTS	R	S	RANGE IN $\frac{h}{h_{FF}}$ (CARTESIAN) MEASURED MIN	MEASURED MAX	FUNCTION MIN	FUNCTION MAX	S^{∇}
IN-LINE GAP		$\ln \frac{h}{h_{FF}} = -2.65372-1.9321\ln Z-0.45517(\ln Z)^2$ $-0.57566\ln(Z/W)$	273	.8824	.5677	-	-	-	-	-
	16-1	$\ln \frac{h}{h_{FF}} = 0.70912-1.2942\ln Z-0.52376(\ln Z)^2$ $-1.13475\ln(Z/W)+0.8671\ln(\theta)$ $-0.07728(\ln Z)(\ln W)^2-0.18345\ln(\frac{\delta^*}{L})$ $+0.13155\ln T$		.9137	.4942	.010	1.304	.002	1.215	.1140
IN-LINE GAP		$\ln \frac{h}{h_{EDGE}} = -2.60533-1.53759\ln Z+0.10343(\ln Z)^3$ $-0.52264\ln(Z/W)$		.8907	.5448	-	-	-	-	-
	16-2	$\ln \frac{h}{h_{EDGE}} = 0.58794-0.91294\ln Z+0.11529(\ln Z)^3$ $-1.00779\ln(\frac{Z}{W})+.86146\ln\theta$ $-0.06665\ln Z(\ln W)^2-.15332\ln(\frac{\delta^*}{L})$ $+.13326\ln T$		.9201	.4729	.011	1.388	.005	1.482	.1286

Figure 181

according to their individual dominance in the correlation. Thus, "ℓnZ" was the most significant parameter to both the flat plate and edge referenced correlations. It is interesting to note that while the second order term was the next most dominant parameter for the (h/h_{FP}) equation, $(\ell nZ)^3$ was more important in the other equation.

5.4.2 Correlations for Long In-Line Gaps $(0^o \leq \gamma \leq 15^o)$- Analysis and correlations were performed to determine the effect of flow orientation angle (γ) on the heating distribution in the in-line gaps. Heating measurements were obtained for both walls (Sides A and B) at 0, 5, 10 and 15 degrees. When data from Side A, alone, were considered, there were 516 measurements. Correlations were developed for both data sets using (h/h_{FP}) and (h/h_{EDGE}) as the dependent variable. The resulting functions are listed in Figure 182.

When the gap heating was ratioed to flat plate measurements, the effect of (γ) was masked in the standard deviation (S). The correlation coefficient (R) increased slightly (from 0.9202 to 0.9399) by excluding Side "B" data. This effect can be attributed to a difference in heating on the opposite walls of the gap. When the heating was ratioed to the edge value, the effect of (γ) appears in the correlation (Equation 16-5 and 16-6). Distance into the (Z), gap width (W), momentum thickness (θ), and unit Reynolds number $(Re/10^6)$ contribute more to the correlation equation than does the incidence angle (γ). However, data from one of the low Reynolds number tests did show a dependence on (γ). Data for other tunnel conditions, widths, depths and (γ) must overshadow this effect. For example, the runs at $\gamma = 10°$ show a sharp increase in heating due to gap width expecially at the higher Reynolds number tested. Heating on the downstream side (Side A) of the gap is almost twice that on the upstream side. The data indicate that the presecne of the in-line gap at slight incidence angles causes the boundary layer to become turbulent.

5.5 Correlations for Transverse Gap -(Laminar and Transitional Flow) - Heating rates measured on the downstream wall of a transverse gap were examined for trends with distance into the gap (Z), gap width (W) and unit Reynolds number. Correlations were then developed.

The largest group of data examined were obtained from the Ames 3.5 Foot H.W.T. A total of 668 data points were obtained using transverse gap models with gap depths of 1.02 cm, 2.03 cm and 4.06 cm. Heating rates measured on a smooth calibration plate were used as a reference and also to determine the onset of boundary layer transition from laminar flow. Of the 668 measurements, 316 were for laminar flow.

CORRELATION FUNCTIONS FOR IN-LINE GAPS (AMES 3.5 FOOT H.W.T.) LAMINAR, $0 \leq \gamma \leq 15$ DEGREES

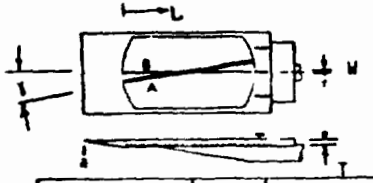

LOCATION	EQ.NO.	FUNCTION	NO. OF POINTS	R	S	RANGE IN q/q_{FP} (CARTESIAN) MEASURED MIN	MEASURED MAX	FUNCTION MIN	FUNCTION MAX	S^{∇}
SIDE A AND SIDE B OF GAP		$\ln\left(\frac{h}{h_{F.P.}}\right) = -1.00604-.96104\ln Z/W$	635	.7950	.7214					
	16-3	$\ln\left(\frac{h}{h_{F.P.}}\right) = 1.88198-2.86909\ln\left(\frac{Z}{W}\right)+.09376\left[\ln\left(\frac{\delta}{L}\frac{Z}{W}\right)\right]^3+.13326\ln(L)$ $+.45139(\ln W)^2-.44674(\ln Z)^2+.60717\ln\theta+1.33939(\ln W)(\ln Z)$ $.10532\ln T$		.9202	.4681	.008	1.873	.002	1.557	.1399
SIDE A OF GAP		$\ln\left(\frac{h}{h_{F.P.}}\right) = -1.01001-.95739\ln Z/W$	516	.8071	.7511					
	16-4	$\ln\left(\frac{h}{h_{F.P.}}\right) = 2.65299-2.98795\ln\left(\frac{Z}{W}\right)+.00215\left[\ln\left(\frac{\delta}{L}\frac{Z}{W}\right)\right]^3+.47890(\ln W)^2$ $-.50150(\ln Z)^2+.69661\ln\theta+1.49684(\ln W)(\ln Z)+.10187\ln T$		.9399	.4371	.008	1.873	.001	1.600	.1362
SIDE A AND SIDE B OF GAP		$\ln\left(\frac{h}{h_{EDGE}}\right) = -.86076-.95264\ln\left(\frac{Z}{W}\right)$	635	.7691	.7790					
	16-5	$\ln\left(\frac{h}{h_{EDGE}}\right) = 4.16869-1.20204\ln\left(\frac{Z}{W}\right)+.09374(\ln Z)^3+.54123(\ln Z)(\ln W)$ $+1.39857\ln\theta-.02029(\ln Z)^2(\ln W)^2+.00026(\ln W)^2(\ln Z)$ $-.39913\ln(Re)+2.64364\gamma-8.30287\gamma^2$		.9029	.5274					
SIDE A OF GAP		$\ln\left(\frac{h}{h_{EDGE}}\right) = -.87502-.95040\ln\left(\frac{Z}{W}\right)$	516	.8044	.7528					
	16-6	$\ln\left(\frac{h}{h_{EDGE}}\right) = 1.48434-1.24928\ln\left(\frac{Z}{W}\right)+.10130(\ln Z)^3+.54690(\ln Z)(\ln W)$ $+.74418\ln\theta-.01992(\ln W)^2\ln Z+2.4384\gamma-7.66436\gamma^2$		.9419	.4281	.010	1.965	.003	2.036	.1556

Results obtained from two test programs conducted in the NASA JSC 10 MW Arc Tunnel facility were also included in the analysis. Seventy eight measurements were used from the HCF type HRSI tiles tested in the Laminar Duct, and eleven measurements were used from a thin skin tile model tested in a wedge test fixture. These heating data were also referenced to heating on a smooth plate. Three HCF tile thicknesses (3.18 cm, 5.08 cm and 6.35 cm) were employed in the Laminar Duct tests. The thin skin tile tests utilized a tile 4.13 cm thick.

In Figure 183, heating measurements from the AMES 3.5 foot H.W.T. are plotted two ways in an effort to obtain the simplest correlation. When plotted on the Log-Log scale the data shows a sharp break which is difficult to describe mathematically. Of note is the inconsistant trend with unit Reynolds number. This inconsistancy whether real or due to experimental technique makes the correlation development more difficult and contributes to the standard error of estimate.

In Figure 184, the heating at two depths into the gap is presented in the two formats. Data from three gap widths (0.127, 0.254 and 0.508 cm) are consolidated on this figure. The trends are flatter on the semi-log scale. It should be pointed out that the curves in the figure are uncorrelated estimates and the presence of several (abnormal) points was neglected. Also, there is an apparent non-monatonic trend with gap width. These observations will manifest themselves in a larger standard error of estimate.

Plots of the NASA-JSC 10 MW Arc Tunnel tests results are contained in other sections of this report.

Correlations for the Laminar/Transitional data set were developed. First the entire set (668) of data from Ames was correlated using Parameter Sets 4 and 6 (Figure A1, part 2). The resulting functions (Equations 15-1, and 15-2) are contained in Figure 185 with a correlation coefficient (R) of less than 0.89. Equation 15-1 was developed from the set of candidate parameters (Set 4) involving the logarithm of boundary layer parameters and physical dimensions of the gap. The wall to boundary layer temperature ratio (T_w/T_e) contributed most to the correlation. Next Parameter Set 6 which contains both logarithmic and non-logarithmic terms was employed in a second correlation (Equation 15-2). Unit Reynolds number, boundary layer displacement thickness as well as physical dimensions contributed to the correlation. The AMES tests were conducted at four unit Reynolds numbers (10^{-6}xRe/m = 1.4, 2.2, 3.3 and 4.5) and had a boundary layer with a displacement thickness of 0.21 to 0.48 cm and a momentum thickness of 0.127 to 0.052 cm. Additional experiments are needed to

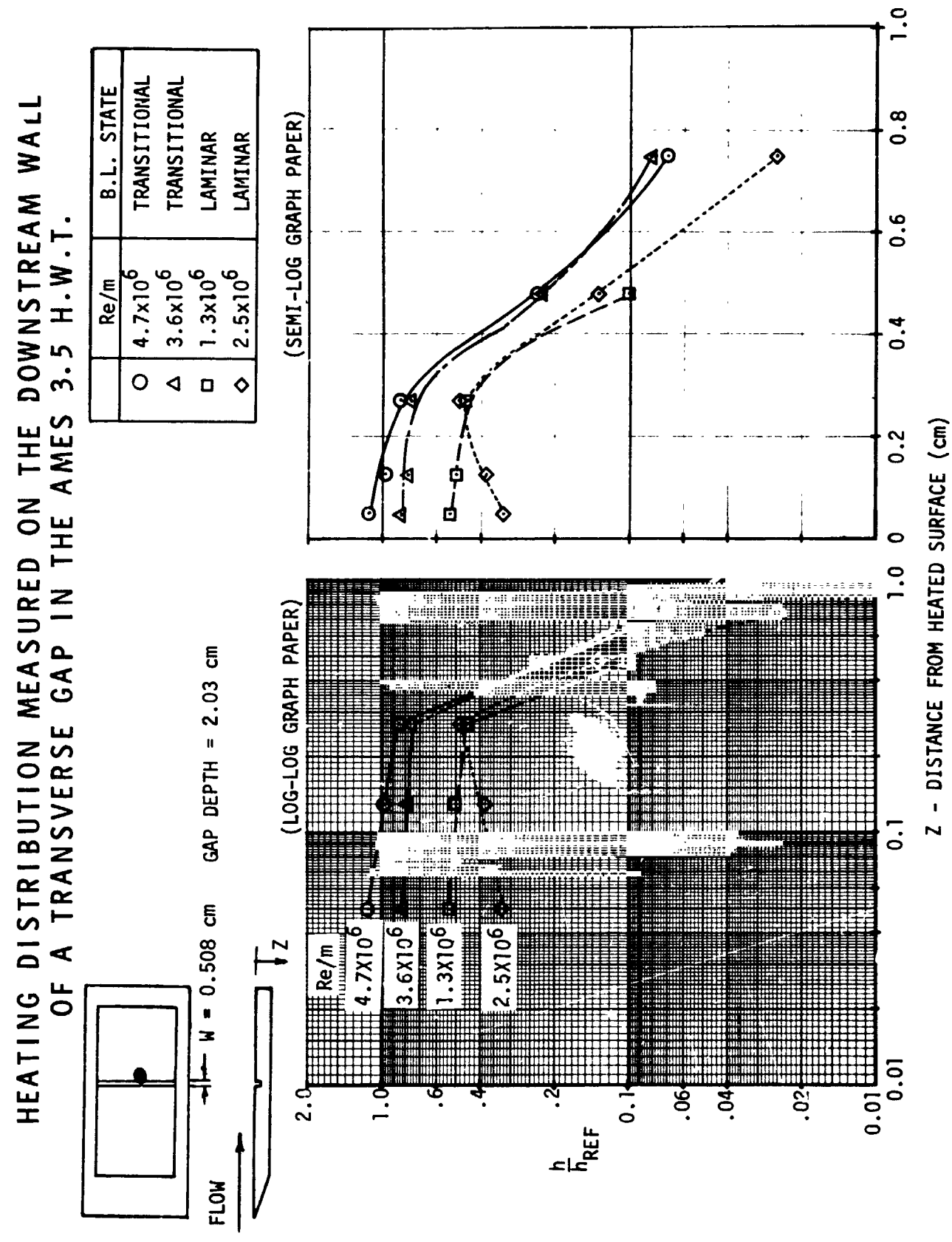
HEATING DISTRIBUTION MEASURED ON THE DOWNSTREAM WALL
OF A TRANSVERSE GAP IN THE AMES 3.5 H.W.T.
Re/m
B.L. STATE
4.7x10^6 TRANSITIONAL
3.6x10^6 TRANSITIONAL
1.3x10^6 LAMINAR
2.5x10^6 LAMINAR
(SEMI-LOG GRAPH PAPER)
(LOG-LOG GRAPH PAPER)
Re/m
4.7X10^6
3.6X10^6
1.3X10^6
2.5X10^6
h/h_REF
Z - DISTANCE FROM HEATED SURFACE (cm)
W = 0.508 cm
GAP DEPTH = 2.03 cm
FLOW
Z

Figure 183

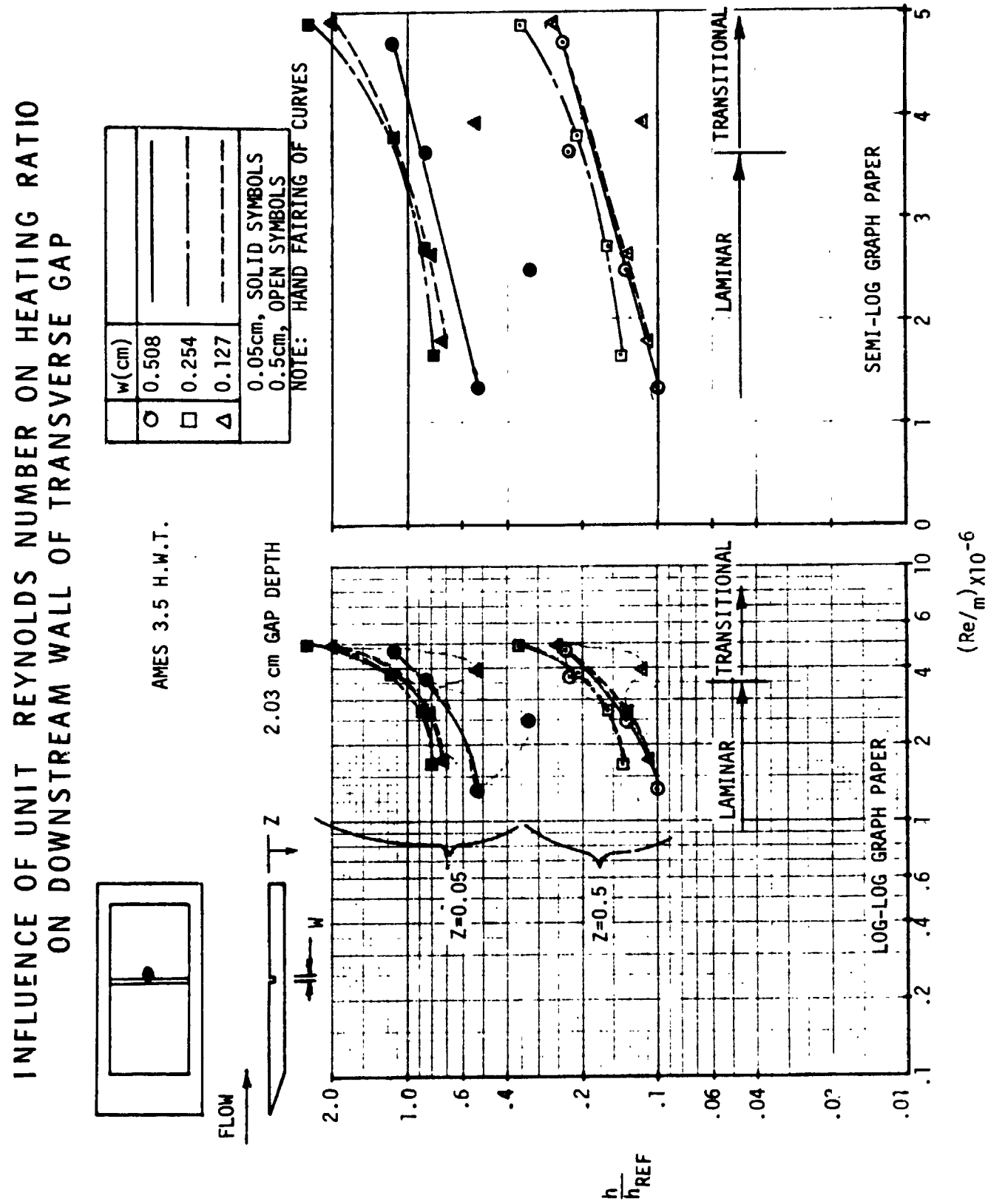
INFLUENCE OF UNIT REYNOLDS NUMBER ON HEATING RATIO ON DOWNSTREAM WALL OF TRANSVERSE GAP
AMES 3.5 H.W.T.
2.03 cm GAP DEPTH
w(cm)
0.508
0.254
0.127
0.05cm, SOLID SYMBOLS
0.5cm, OPEN SYMBOLS
NOTE: HAND FAIRING OF CURVES
FLOW
Z
W
Z=0.05
Z=0.5
LAMINAR
TRANSITIONAL
LOG-LOG GRAPH PAPER
SEMI-LOG GRAPH PAPER
h/h_REF
(Re/m)X10-6

Figure 184

CORRELATION FUNCTIONS FOR TRANSVERSE GAP, LAMINAR AND EFFECTS OF TRANSITION

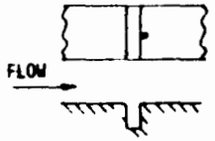

LOCATION	EQ.NO.	FUNCTION	NO. OF POINTS	R	S	RANGE IN q/q_{FP} (CARTESIAN) MEASURED MIN	MEASURED MAX	FUNCTION MIN	FUNCTION MAX	S^2
AMES 3.5 FT LAMINAR & TRANSITIONAL	15-1	$\ln h/h_{REF} = -3.0115-0.91642\ln Z+0.03075\ln Tw/Te -0.2767\ln(Z/W)$	668	.8286	.8708	.005	2.454	.005	1.372	.2904
	15-2	$\ln h/h_{REF} = 11.82018+5.1282Z+1.31368Z^2-.06168T+.70524Re -17.423818*+2.44371\ln\theta+.3001\ln W$	668	.8861	.7230	.005	2.454	.003	1.149	.2181
	15-3	$\ln h/h_{REF} = 0.00668-7.11355Z+2.89517Z^2-.07555Z^3T+0.4872W^2Re +1.04946ZW^2Re-0.08646Z^3WRe$	668	.8995	.6811	.005	2.454	.006	1.236	.2383
AMES 3.5 FT LAMINAR	15-4	$\ln h/h_{REF} = 0.11576-6.53243(Z)+1.91336(Z^2)-0.11154(Z^3WReT) -0.18594(ZT)+0.28963(Z^2Re)+1.65884(ZW^2T)$	316	.9364	.5582	.005	0.878	.004	0.871	.1439
LAMINAR *1. AMES 3.5 FT 2. JSC-HCF 3. JSC-SCOTT	15-5	$\ln h/h_{REF} = -0.40577-6.80369(Z)+1.50570(Z)^2-0.11073(Z^3WReT) +2.91733(W)+0.38987(Z^2Re)+1.79532(Z^2W^2)-0.36933(ZRe) -3.03105(W^2)$	405	.9373	.5494	.005	1.122	.004	1.289	.1451

*1. AMES 3.5 FT TEST (316 MEASUREMENTS)
2. JSC-HCF TESTS (78 MEASUREMENTS)
3. JSC-SCOTT TESTS (11 MEASUREMENTS)

Figure 185

verify the dependency of gap heating on boundary layer parameters. An improved fit was obtained using a parameter set (number 7) assembled from the trends observed in Figures 183 and 184.

Set 7

1) cubic variation with (Z)
2) quadratic variation with (W)
3) linear variation with (Re)
4) linear variation with (T)

$$\ell n\ h/h_{REF} = (a_0+a_1Z+a_2Z^2+a_3Z^3)\ (b_0+b_1W+b_2W^2)(C^0+C_1Re)(D_0+D_1T)$$

The parameters resulting by expanding this expression were used in the Multiple Regression Analysis. Only a small improvement was obtained for the 668 data points (see Equation 15-3).

When Parameter Set 7 was applied to just the laminar data (316 measurements) from Ames, the regression coefficient increased to 0.9364 and the standard error of estimate decreased to 0.1439 (cartesian), Equation 15-4.

The other laminar data was then added to the AMES data and 405 measurements were used to develop Equation 15-5. Distance into the gap (Z) contributed most to the goodness of fit and (W^2) the least. The influence of (Z) is very evident and also enters into the most complicated terms involving (W), (Re) and (T). Figures 186 and 187 are the residual plots for Equation 15-5 and show a uniform spread indicating an unbiased fit. Figure 186 is for the $\ell n(h/h_{REF})$ which was used to develop the correlation and Figure 187 presents the same data in terms of (h/h_{REF}). Figure 188 is a comparison of Equation 15-5 and a sample of measured data. Only a small amount of data from the AMES 3.5 ft. H.W.T. and JSC Arc Tunnel tests is contained on the figure. The preponderance of data is from the AMES Tunnel and hence the correlation passes through the center of the data. Equation 15-5 also describes the data from the JSC Laminar Duct. This is not the case for the wedge test which employed a thin skin metallic tile. Equation 15-5 under predicts the data from the thin skin tile. Figure 189 shows the effect of each gap variable on heating to the downstream wall of a transverse gap.

The correlation study for the transverse gap (laminar flow) was explored further by adding a pseudo heating value of unity to each stack of instrumentation and then generating another correlation. For example, the 405 measurements were obtained from separate 114 stacks of instrumentation. A stack consists of those thermocouples located on the side of a tile at the same X and Y coordinates. The

RESIDUALS (ℓn) FOR DOWNSTREAM SIDE OF TRANSVERSE GAP

∘ LAMINAR FLOW EQUATION 15-5

DATA FROM
1 AMES 3.5 FT H.W.T. (THIN SKIN)
2 JSC - CHANNEL NOZZLE (HCF TILES)
3 JSC - 10MW, WEDGE (THIN SKIN)

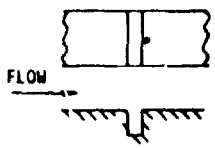

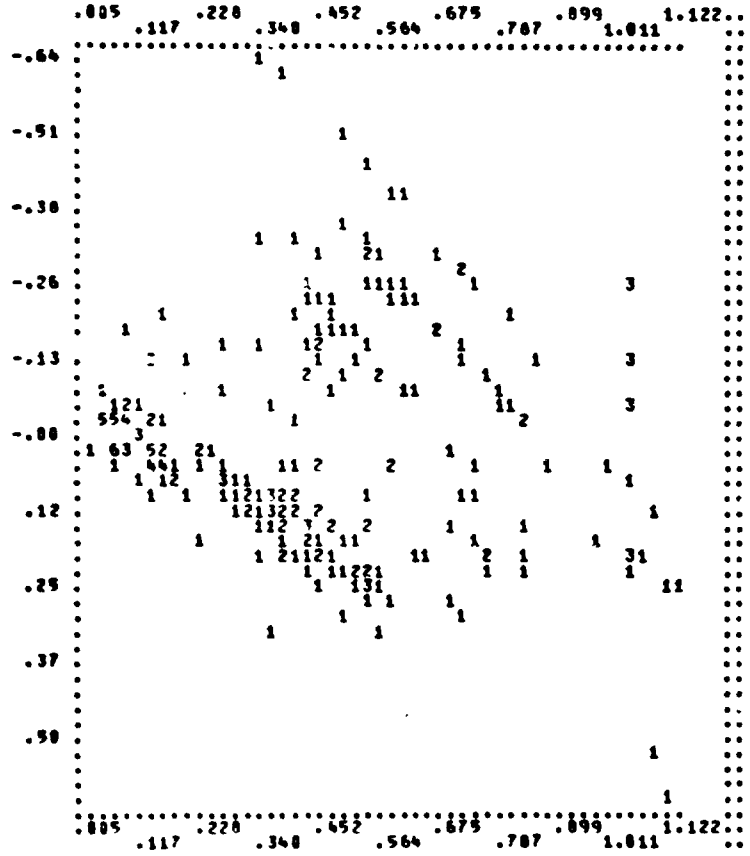

$$\ell n\left(\frac{h}{h_{FP}}\right)_{MEASURED}$$

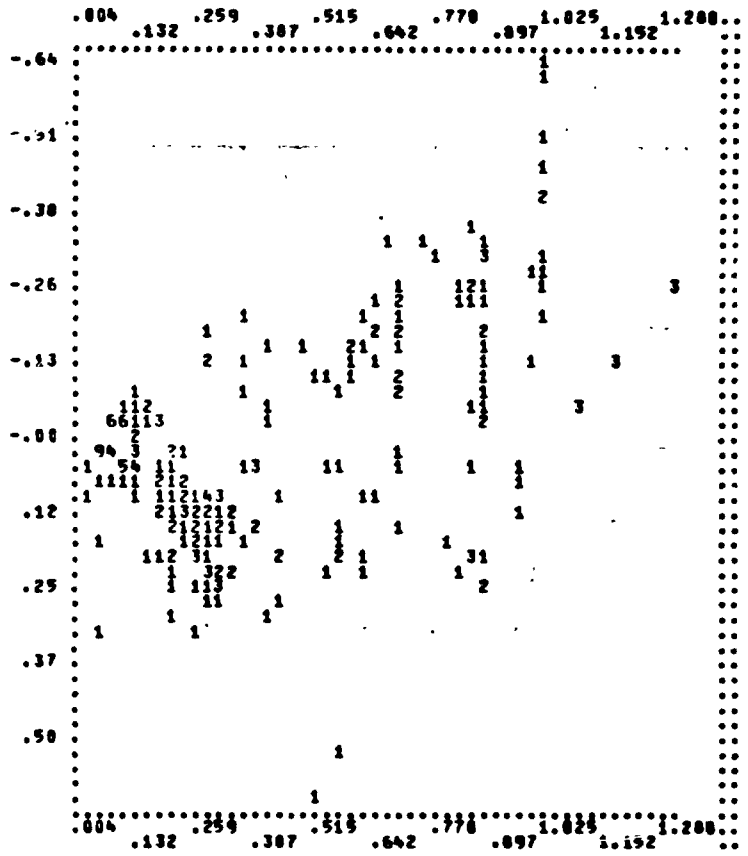

$$\ell n\left(\frac{h}{h_{FP}}\right)_{CALCULATED}$$

$$\ell n\left(\frac{h}{h_{FP}}\right)_{M} - \ell n\left(\frac{h}{h_{FP}}\right)_{CAL}$$

Figure 186

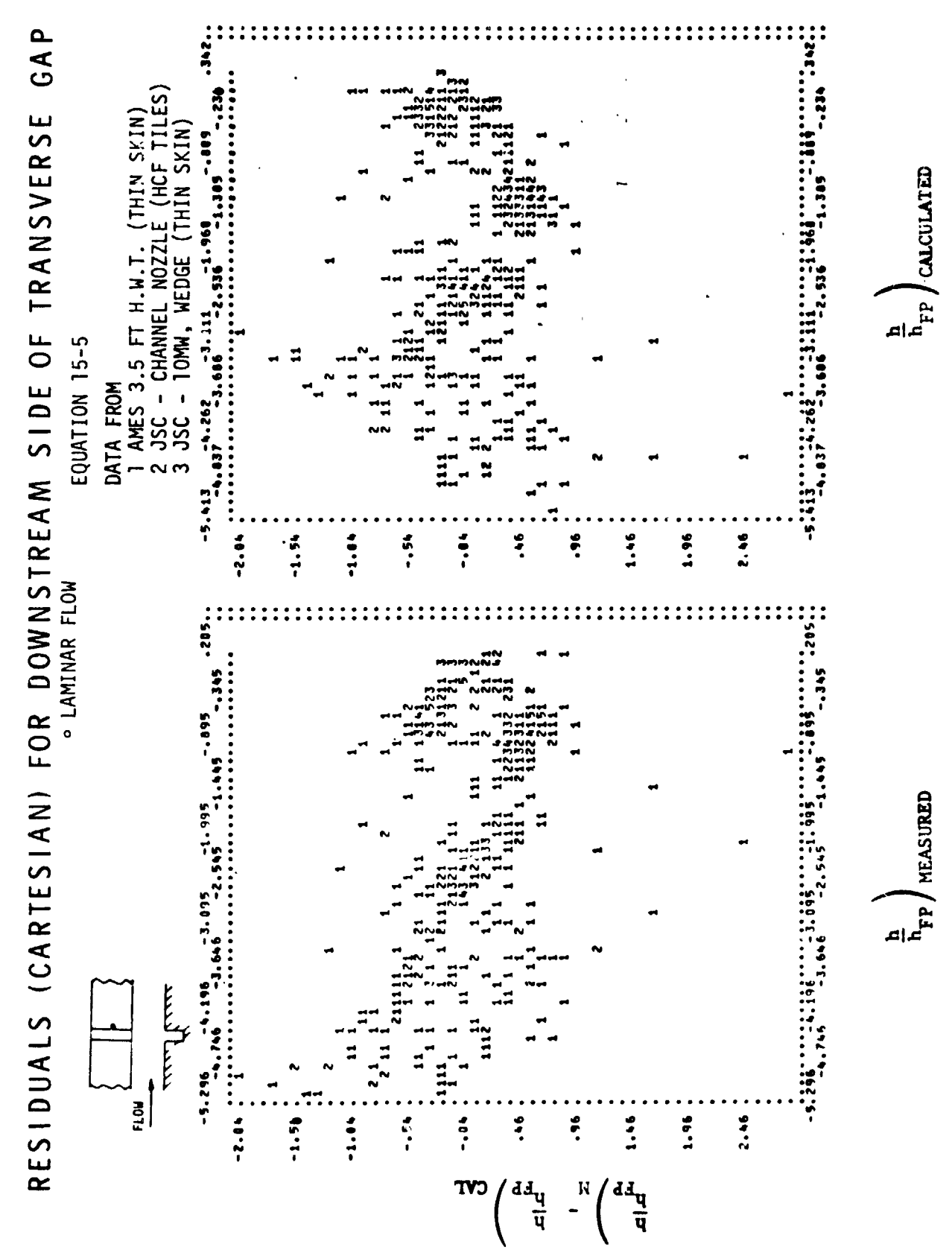
RESIDUALS (CARTESIAN) FOR DOWNSTREAM SIDE OF TRANSVERSE GAP
EQUATION 15-5
o LAMINAR FLOW
DATA FROM
1 AMES 3.5 FT H.W.T. (THIN SKIN)
2 JSC - CHANNEL NOZZLE (HCF TILES)
3 JSC - 10MW, WEDGE (THIN SKIN)
FLOW
$\frac{h}{h_{FP}}$ MEASURED
$\frac{h}{h_{FP}}$ CALCULATED
$\left(\frac{h}{h_{FP}}\right)_{M} - \left(\frac{h}{h_{FP}}\right)_{CAL}$

Figure 187

COMPARISON OF CORRELATION EQ. 15-5 WITH MEASURED TRANSVERSE GAP, LAMINAR BOUNDARY LAYER

		W(cm)	$Re/_m$	T(cm)	EQ. 15-5
AMES 3.5 FT HWT	□	0.508	$1.36X10^6$	2.03	———
	◇	0.508	$2.5X10^6$	2.03	- - - - - -
JSC 10 MW ARC TUNNEL LAMINAR DUCT WEDGE	⬠	0.333	$5.72X10^4$	3.18	——·——·——
	⬠	0.381	$0.17X10^4$	4.13	——·——·——

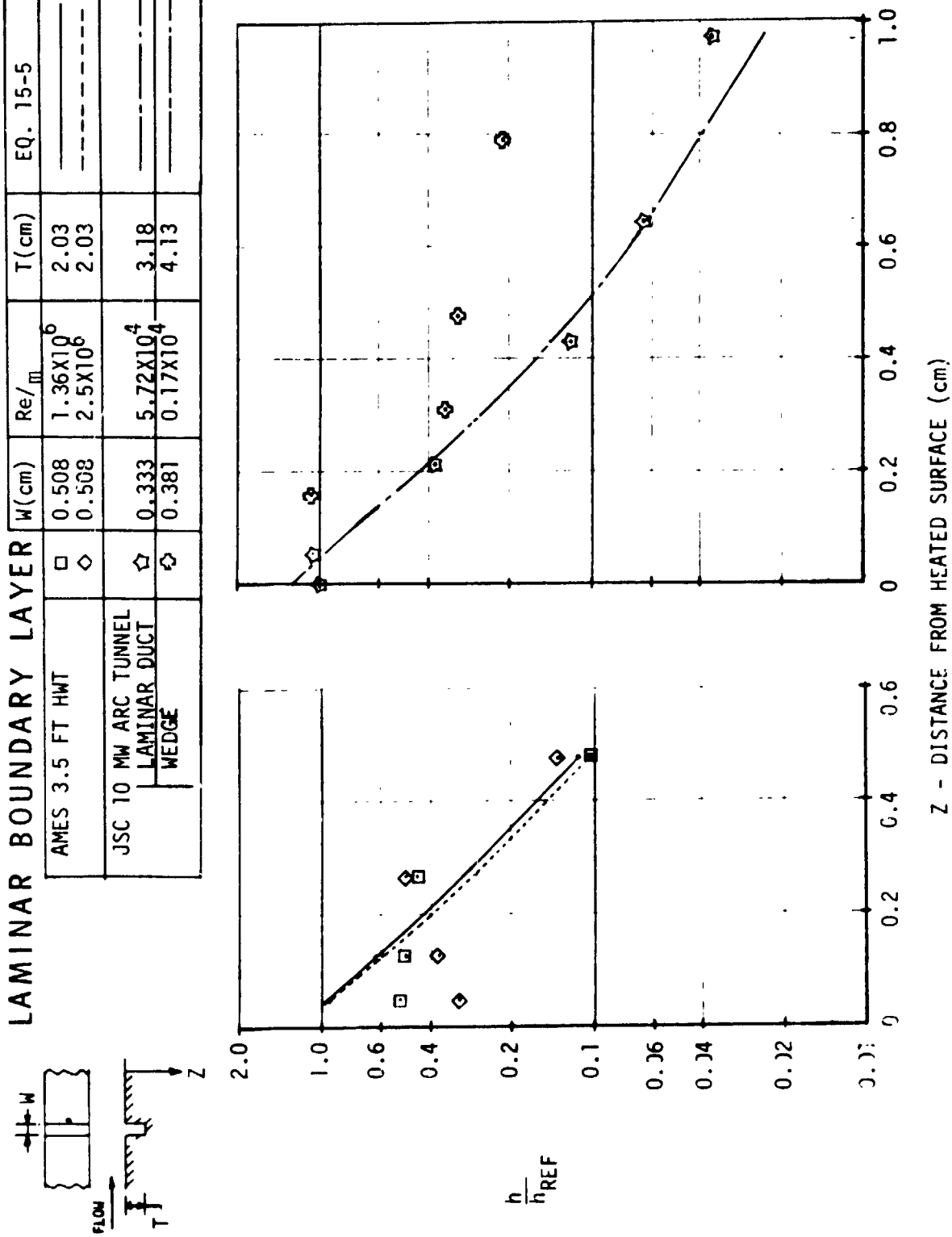

Figure 188

HEATING TRENDS IN TRANSVERSE GAP, LAMINAR FLOW

∘ (EQUATION 15-5)

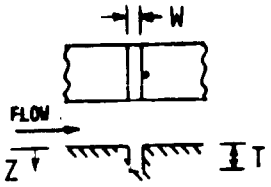

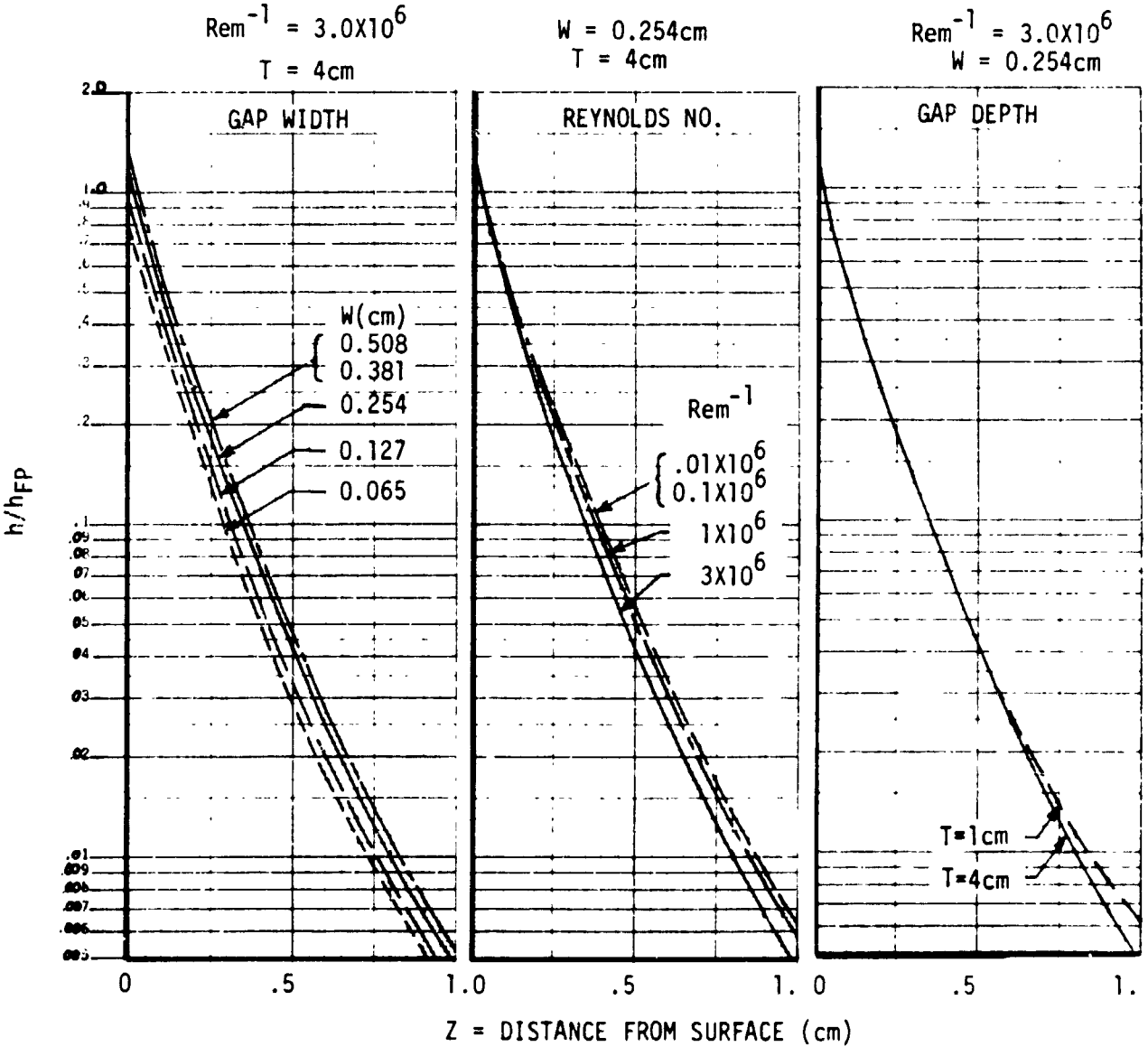

Figure 189

same set of candidate correlation parameters used to generate Equation 15-5 was used. The derived correlation function (Equation 15-6) is contained in Figure 190. The correlation coefficient (R) improved slightly (from 0.9373 to 0.9562) and the standard error of estimate (S^{∇}) decreased (from 0.1451 to 0.1335). Also, a correlation (Equation 15-7) was developed using the gap heating ratioed to the value on the top of the tile near the edge of the gap. The correlation coefficient decreases slightly and the (S^{∇}) increased slightly.

Several correlations were developed for heating on the downstream wall of a transverse gap submerged in a laminar boundary layer. Either Equation 15-5 or 15-6 is suitable for predicting heating in transverse gap.

CORRELATION FUNCTIONS FOR TRANSVERSE GAP, LAMINAR FLOW (HEAT RATIO SET TO UNITY AT TOP OF GAP)

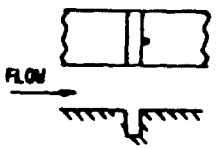

TEST DATA. AMES 3.5 FT, JSC-HOT JSC-SCOTT

LOCATION	EQ.NO.	FUNCTION	NO. OF POINTS	R	S	RANGE IN q/q_{FP} (CARTESIAN) MEASURED MIN	MEASURED MAX	FUNCTION MIN	FUNCTION MAX	S^V
TRANS,DMN	15-6	$\ln(\frac{h}{h_{REF}})$=0.28359-6.29983(Z)+1.62912(Z^2)-0.12191(Z^3WReT) +1.93839(W)+1.91238(ZW)+0.32656(Z^2Re)-0.07403(ZReT) +.41308(Z^2W^2ReT)-0.32656(ZW^2Re)-2.01798(W^2)	522*	0.9562	0.4838	.005	1.122	.004	1.221	0.1335
	15-7	$\ln(\frac{h}{h_E})$=0.1782-5.91662(Z)+1.5483(Z^2)-0.12000(Z^3WReT) +1.93132(ZW^2)+0.25717(Z^2Re+0.53613(Z^3W^2Re) -0.58802(ZWRe)-0.06335(1)+0.11036(WT)	522*	0.9547	0.4878	.004	1.122	.005	1.349	0.1411

* NOTE: 117 HEATING RATIOES OF UNITY WERE ADDED TO THE 405 MEASUREMENTS FOR THIS STUDY

Figure 190

5.6 Correlations for Transverse Gap - Turbulent Flow - Heating measured on the downstream wall of the transverse gaps tested in the LaRC $M_\infty = 8$ Variable Density Tunnel (116 measurements), the LaRC Continuous Flow Hypersonic Flow Tunnel (47 measurements) and in the LaRC 8 Foot High Temperature Structures Tunnel (42 measurements) were used in the Multiple Regression Analysis. Figure 191 contains the resulting correlation function.

CORRELATION FUNCTIONS FOR TRANSVERSE GAP (TURBULENT B.L.)
M_∞ =8, CFHT, HTST TEST DATA

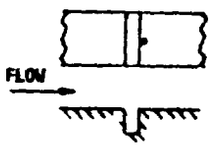

LOCATION	EQ.NO.	FUNCTION	NO. OF POINTS	R	S	RANGE IN q/q_{FP} (CARTESIAN) MEASURED MIN	MEASURED MAX	FUNCTION MIN	FUNCTION MAX	S^∇
DOWNSTREAM SIDE OF TRANSVERSE GAP		$\ln(\frac{h}{h_{FP}})=0.82466-2.83665Z+0.39182Z^2-0.26234W^2T$	205	.6312	.9085	-	-	-	-	-
		$\ln(\frac{h}{h_{FP}})=0.48284-3.29726Z+0.73672Z^2-0.09602ZT-0.25282Re$ $+.26383WReT+0.07219ZRe-0.12309T-.02149Z^3W-2.37974W$	↓	.8596	.7055	.008	.1424	.005	1.264	.1667

5.7 Correlations for Gaps with Steps - Figure 192 shows the effect of step height on heating in a transverse gap. The data indicates that the heating rate increases with both step height and gap width. Separate correlations were developed for gaps with steps for laminar, transitional and turbulent flow. These equations are applicable to the downstream wall of gaps with both rearward and forward facing steps and are shown in Figure 193. The laminar flow correlation was derived using 704 data points mostly from the Ames 3.5 ft tunnel. The transitional correlation was based on 461 data points from Ames and 89 from LaRC Mach 8 tunnel. The turbulent function was based on data from three tests at LaRC. Figure 194 compares the test and calculated values for the LaRC CFHT data for two gap widths. Figure 195 shows data and calculated curves for the Ames laminar flow data. Figure 196 shows the regression residuals for the calculated heating ratios.

The correlation coefficient is low for all three of these fits, especially for the laminar cases. Examination of the data seems to indicate that there is some interaction between gap width, step height and boundary layer thickness not accounted for in the correlation.

EFFECT OF STEP HEIGHT ON HEATING IN TRANSVERSE GAP

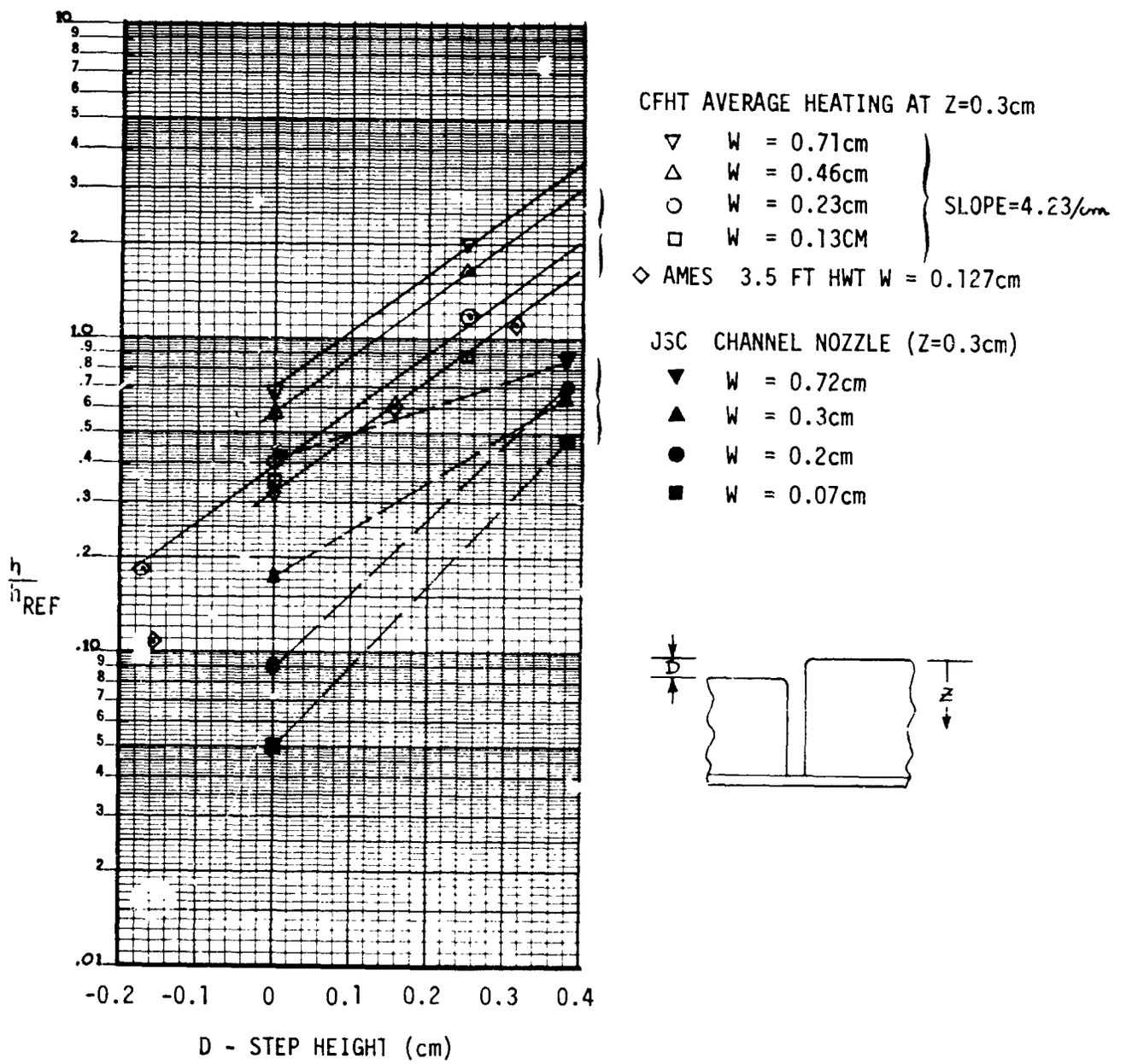

Figure 192

CORRELATION FUNCTIONS DEVELOPMENT FOR STEPS
(LAMINAR FLOW, TRANSITIONAL FLOW AND TURBULENT FLOW)

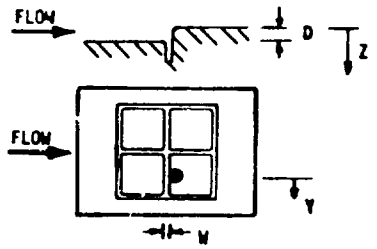

LOCATION	EQ. NO.	FUNCTION	NO. OF POINTS	R	S	RANGE IN q/q_{FP} (CARTESIAN) MEASURED MIN	MEASURED MAX	FUNCTION MIN	FUNCTION MAX	S^{∇}
DOWNSTREAM WALL OF TRANSVERSE GAP (LAMINAR)	17-1	$\ln(\frac{h}{h_{FP}}) = -0.19252-4.24537(Z)+23.52407(ZWD)+1.26103(Z^2)$ $+5.67183(D)-0.00192(Y^2Z)$ $-6.57773(Z^2WD)-11.37065(D^2)$	704(1)	0.8034	0.8970	.010	3.323	.007	1.584	0.396
DOWNSTREAM WALL OF TRANSVERSE GAP (TRANSITIONAL)	17-2	$\ln(\frac{h}{h_{FP}}) = -.65828-4.00086(Z)+1.16511(Z^2)+8.93015(D)-2.63955(D^2)$ $-.01083(Y^2Z^2W)+3.18026(W^2)+.01461(YZ^2)$	550(2)	.8574	.7630	.010	4.788	.007	5.943	.5078
DOWNSTREAM WALL OF TRANSVERSE GAP (TURBULENT)	17-3	$\ln(\frac{h}{h_{FP}}) = -.81624-2.5465(Z)+7.58098(D)+0.35211(Z^2)-0.17100(Y)$ $-1.11972(Z^2D^2)-0.28604(YW)+1.43712(W^2)$	275(3)	0.8301	0.882	.010	3.737	.004	4.174	.5089

Z - VERTICAL DISTANCE INTO THE GAP (cm)
W - GAP WIDTH (cm)
D - STEP HEIGHT (cm)
Y - LATERIAL DISTANCE ALONG GAP

(1) { 566 VALUES FROM AMES 3.5 FOOT TUNNEL; 78 VALUES FROM JSC CHANNEL NOZZLE, MCF DATA; 60 VALUES FROM JSC 10 MW WEDGE }

(2) { 89 VALUES FROM LaRC M_∞ = 8 TUNNEL; 461 VALUES FROM AMES 3.5 FT HWT }

(3) { 109 VALUES FROM LaRC M_∞ = 8; 67 VALUES FROM LaRC 8 FT HIST; 99 VALUES FROM LaRC M_∞ = 10 CFHT }

Figure 193

COMPARISON OF CORRELATION FOR STEPS WITH LaRC CFHT TEST

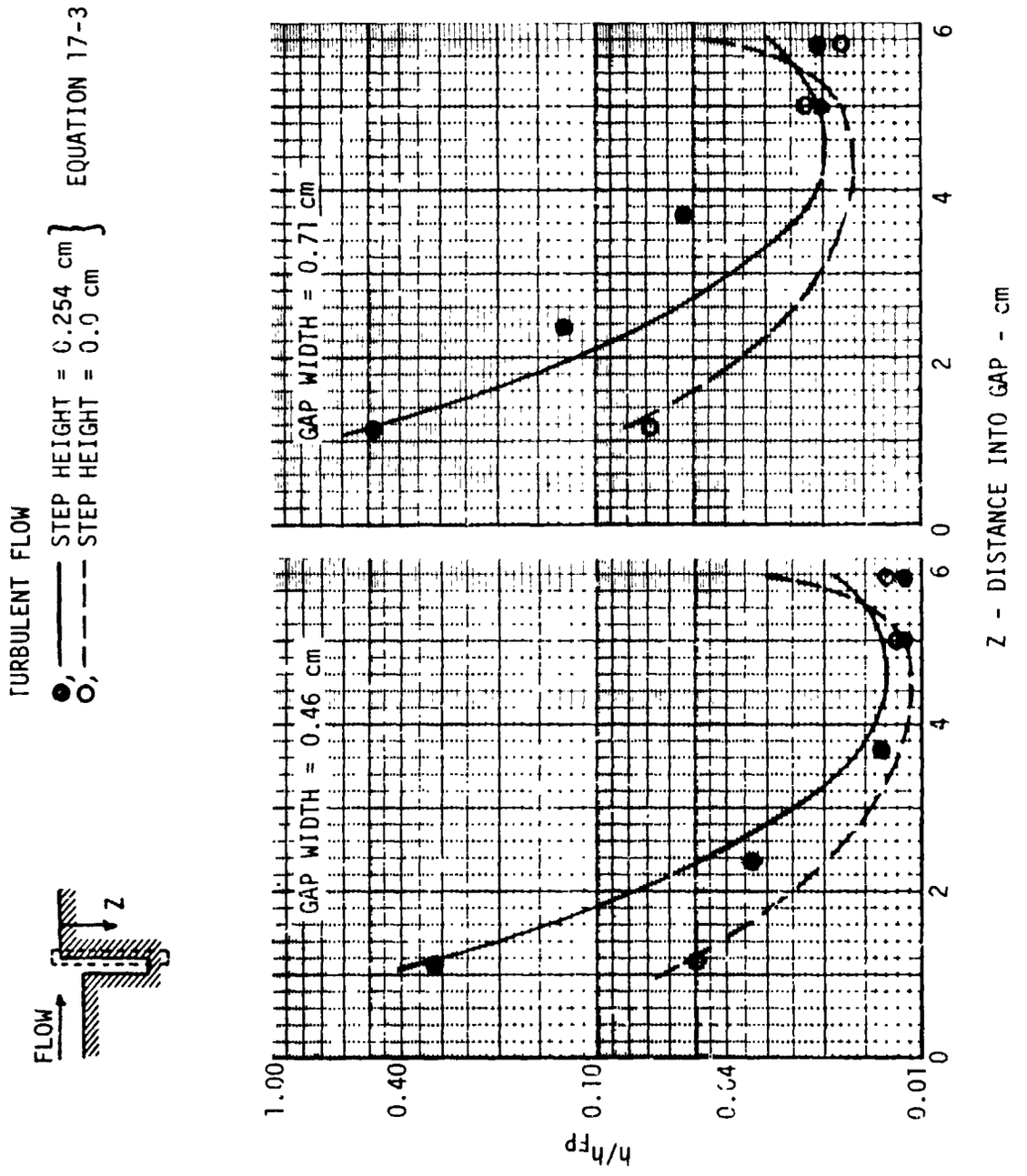

Figure 194

COMPARISON CORRELATION FOR STEPS WITH AMES 3.5 FOOT HWT TESTS

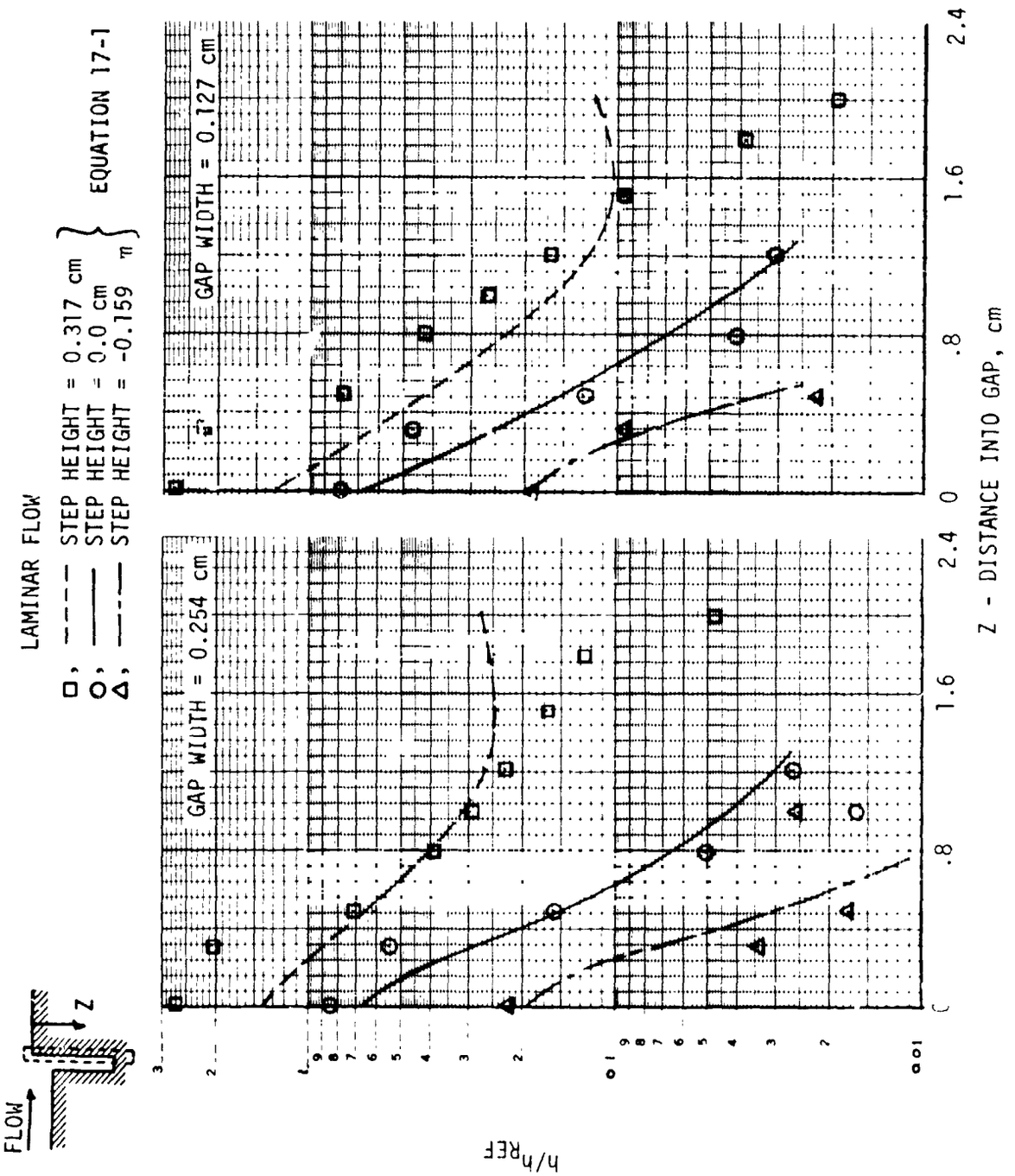

Figure 195

RESIDUALS OF CORRELATIONS FOR GAPS WITH STEPS

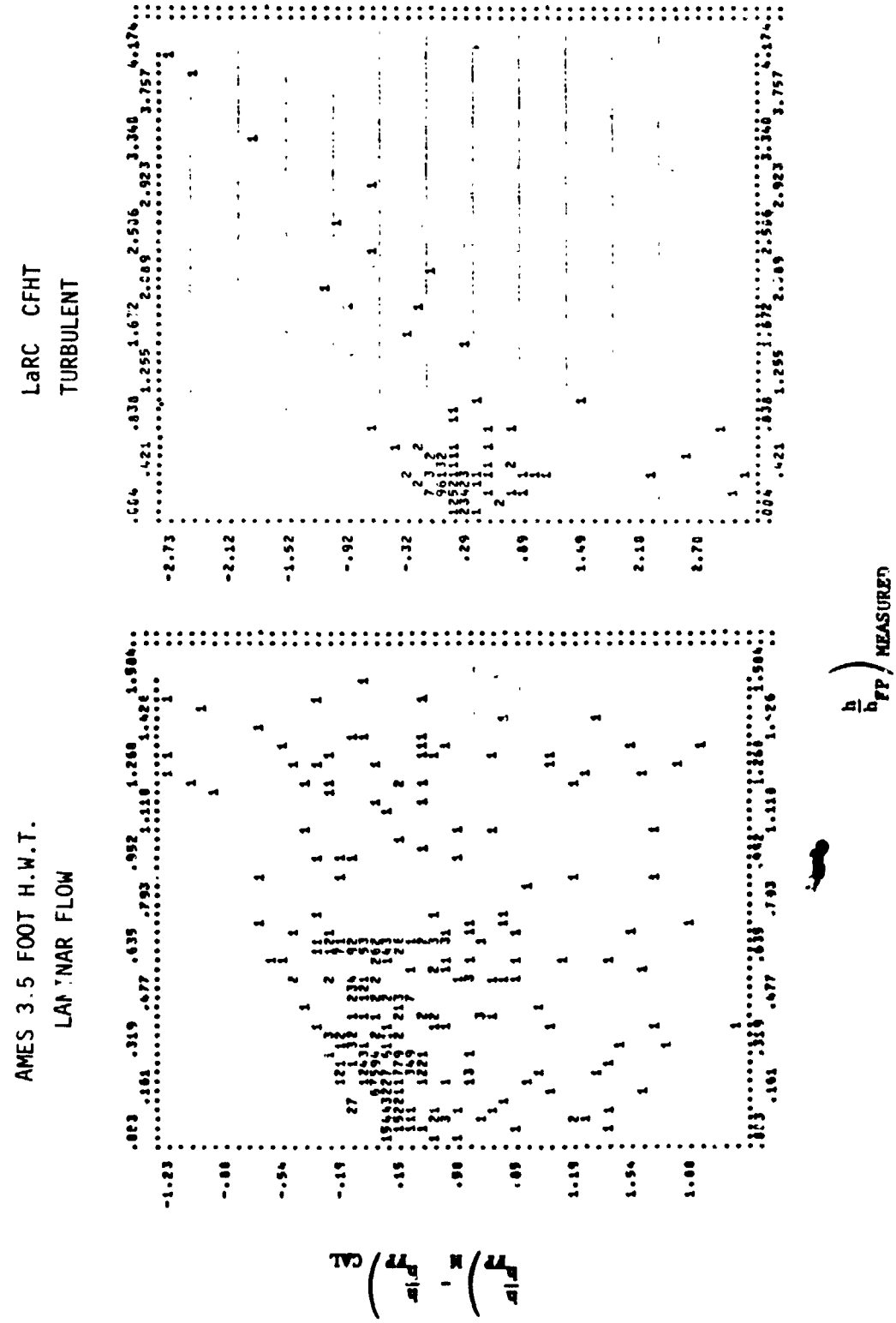

Figure 196

6.0 GAP HEATING CALCULATION PROCEDURE

A general calculation procedure has been developed using available gap heating correlations. This procedure is suitable for sizing TPS, determining system performance and structural temperatures. The calculation procedure is formulated as a set of subroutines which can be used with other thermal model components which describe the thermal characteristics of the gap between tiles, the tiles themselves and the structure. At the present, a set of 24 correlation expressions and control logic have been set up in a group of subroutines so that the package is self contained with well defined interfaces and readily identified input and output. The package is designed to be compatable with general heat transfer computer programs such as the MDAC-E HEATRAN and SINDA. The input list consists of the location within the gap where the convective heating is to be computed, gap geometry descriptors and boundary layer descriptors. Figure 197 describes the interface of the main subroutine with the calling program. In addition to the FORTRAN calling list, a labeled common is used to store the argument list ARGL(25) and other parameters passed between the subroutines within the calculation procedure. The argument list is sized so that the subroutine can be expanded as more correlations are added. The key parameters within the argument list ARGL(25) have preset default values to insure proper functioning of the subroutine in case a parameter is not supplied by the calling program.

The main subroutine "GAPH" is written with an option to input any parameter in the ARGL list when the subroutine is first accessed by using NAMELIST input system. Not all parameters described on the ARGL list are needed at the present time, so the formulation of the desired correlation function should be examined to determine the needed parameters. The features of the subroutine package are highlighted in Figure 198. The parameter "ICØR" can be used to specify a correlation equation or by setting ICØR=0 the logic within GAPH can be used to select the correlation equation.

In Figure 199 the correspondence between correlation sequence number, the equation designation, the gap configuration and flow conditions are tabulated. The designated correlation equations are found earlier in this report. Several correlations were developed during Phase I (ØI) and are included in the gap heating procedure.

In general, the correlations were developed from data measured by instrumentation covering only a finite zone of the gap. Hence, some correlations may yield

GAP HEATING SUBROUTINE "GAPH"

- o FORMULATION IS SETUP FO "GAPH" CAN ACCEPT MANY CORRELATIONS
- o SUBROUTINE WORKS WITH HEATRAN AND SINDA

SUBROUTINE GAPH (J, NTAB, ZZ, Y, QQ)

ARGL IS IN LABLED COMMON/COMGAP/

J = -1 SETS UP SUBROUTINE NAME (HEATRAN, ONLY)
= 0 READS SUBROUTINE INPUT CARDS (HEATRAN, ONLY)
= 1 COMPUTES GAP HEATING

NTAB = NUMBER OF POINTS IN ZTAB (25 MAX)

ZZ = TABLE OF GAP Z-COORDINATES (OR S-COORDINATES) WHERE HEATING RATES ARE TO BE COMPUTED (25 MAX)

S = SURFACE DISTANCE FROM UPPER TANGENCY POINT INTO GAP (cm)

Y = GAP Y-COORDINATES WHERE HEATING IS TO BE COMPUTED (cm)

QQ = TABLE OF COMPUTED HEATING RATES CORRESPONDING TO ZZ TABLE (25 MAX)

ARGL, ARGUMENT LIST (DIMENSIONED TO 25)

ARGL (1) = IBL = BOUNDARY LAYER STATE: 1 = LAMINAR, 2 = TRANSITIONAL, 3 = TURBULENT

ARGL (2) = IGLØC = GAP LOCATION: 1 = UPSTREAM SIDE OF GAP, 2 = DOWNSTREAM SIDE OF GAP, 3 = IN-LINE GAP, 4 = STAGNATION POINT, 5 = TILE TOP, 6 = LONG IN-LINE GAP

ARGL (3) = ICØR = CORRELATION NUMBER TO BE USED: IF ZERO IBL AND IGLØC DETERMINE CORRELATION TO BE USED

ARGL (4) = JOINT CONFIGURATION: 1 = BUTT, 2 = COUNTOURED, 3 = OVERLAP, 4 = INCLINED

ARGL (5) = E = EDGE RADIUS (cm)

ARGL (6) = GAMMA = FLOW ORIENTATION (RADIANS)

ARGL (7) = GAPW = GAP WIDTH (cm)

ARGL (8) = GAPD = GAP DEPTH (cm)

ARGL (9) = STEP = STEP HEIGHT (cm)

ARGL (10) = GAPFL = GAP FLOW LENGTH (cm)

ARGL (11) = HØHLØW = LOWER LIMIT ON HEATING RATIO

ARGL (12) = HØHHI = UPPER LIMIT ON HEATING RATIO

ARGL (13) = AMACH = LOCAL MACH NUMBER

ARGL (14) = REPM = REYNOLDS NUMBER/METER

ARGL (15) = THETA = MOMENTUM THICKNESS (cm)

ARGL (16) = DTHK = DISPLACEMENT THICKNESS (cm)

ARGL (17) = SLYR = SUBLAYER THICKNESS (cm)

ARGL (18) = HFP = HEATING RATE OR HEAT TRANSFER COEFFICIENT FOR LOCAL CONDITIONS ON A SMOOTH VEHICLE

ARGL (19) = TWØTE = T_{WALL}/T_e, TEMPERATURE RATIO ACROSS BOUNDARY LAYER

ARGL (20) = IHØH = HEATING RATIO: 1 = H/H_{FP}, 2 = H/H_E

ARGL (21) To (25) = FOR FUTURE EXPANSION

Figure 197

ORGANIZATION OF GAP HEATING CALCULATION PROCEDURE

1. SUBROUTINE FORMAT (CALL GAPH)
   - 1.1 USER SELECTS CORRELATION OR SUBROUTINE SELECTS CORRELATION
   - 1.2 BRANCH IS MADE TO CORRELATION EQUATION SUBROUTINE
     - 1.2.1 CONSTANTS FOR EQUATION
     - 1.2.2 ON SUCCESSIVE PASSES EQUATION EVALUATED
   - 1.3 IF DISTANCE INTO GAP IS LESS THAN "ZMIN", CONTROLLED EXTRAPOLATION IS USED
   - 1.4 IF DISTANCE INTO GAP IS GREATER THAN "ZMAX" LINEAR EXTRAPOLATION IS USED

2. HEATING DISTRIBUTION CAN BE INPUT THROUGH NAMELIST

3. CORRELATION EQUATION SUBROUTINES ARE NAMED USING EQUATION NUMBER
   EXAMPLE: SUBROUTINE EQ4D14 ← EQUATION 4-14

Figure 198

CORRELATION FUNCTIONS IMPLEMENTED IN GAP HEATING PROCEDURE

CORRELATION SEQUENCE NUMBER "ICØR"	EQUATION DESIGNATION	SOURCE	BOUNDARY LAYER STATE	GAP LOCATION	INFLUENCE OF EDGE RADIUS (cm)	EFFECT OF GAP WIDTH (cm)	FLOW ORIEN-TATION	STEPS	HEATING RATIO
1	TABLE LOOK-UP	DATA INPUT	-	-	-	-	-	-	-
2	TABLE LOOK-UP	C. SCOTT	1	AVG.1&2	0.1575 & 0.3175	0.254	0	0	1
3	4-17	ØII	↓	2	✓	✓	↓	↓	1
4	4-16	↓	↓	2	✓*	✓	↓	↓	2
5	4-9	↓	↓	3,UP	✓*	✓	↓	↓	1
6	4-10	↓	↓	3,DN	✓*	✓	↓	↓	1
7	4-11	↓	↓	1	✓*	✓	↓	↓	1
8	4-13	↓	↓	3,UP	✓*	✓	↓	↓	2
9	4-14	↓	↓	3,DN	✓*	✓	↓	↓	2
10	4-15	↓	↓	2	✓*	✓	↓	↓	2
11	15-5	↓	↓	2	✓*	✓	↓	↓	1
12	9	ØI	↓	2	↓	✓	↓	↓	2
13	25	ØI	↓	3	↓	✓	↓	↓	1
14	18	ØI	3	2	↓	✓	↓	↓	1
15	12A	ØI	3	2	↓	✓	0 TO 90°	↓	1
16	16-1	ØII	1	6	↓	✓	0	↓	1
17	16-2	↓	↓	6	↓	✓	0	↓	2
18	16-3	↓	↓	6,UP&DN	↓	✓	0 TO 15°	↓	1
19	16-4	↓	↓	6, DN	↓	✓	↓	↓	1
20	16-5	↓	↓	6,UP&DN	↓	✓	↓	↓	2
21	16-6	↓	↓	6,DN	↓	✓	↓	↓	2
22	17-1	↓	1	2	↓	✓	0	✓	1
23	17-2	↓	2	2	↓	✓	0	✓	1
24	17-3	↓	3	2	↓	✓	0	✓	1

BOUNDARY LAYER STATE; 1=LAMINAR, 2=TRANSITIONAL, 3=TURBULENT

GAP LOCATION; 1=UPSTREAM SIDE OF GAP, 2=DOWNSTREAM SIDE OF GAP, 3=IN-LINE GAP, 4=STAGNATION, 5=TILE TOP, 6=LONG IN-LINE GAP (UP=UPSTREAM SIDE OF GAP), (DN=DOWNSTREAM SIDE OF GAP)

HEATING RATIO; $1=H/H_{FLAT\ PLATE}$, $2=H/H_{EDGE}$

*; SMALL EDGE RADIUS SPECIFIED AS 0.00254 cm

Figure 199

unrealistic values when extrapolated, especially very near the top of the gap or deep within the gap. For those functions with these tendancies, an extrapolation procedure for the very top zone (A) of the gap and zone (B) within the gap has been implemented. The procedure is depicted in Figure 200. An "SMIN (or ZMIN)" distance defining zone A is contained in the subroutine. A second order equation bridges the "A" zone from S (or Z) = 0 to SMIN. At the S=0 the second order equation passes through $h/h_{REF} = 1$. For the deep zone "B", a correlation cut-off distance SMAX (or ZMAX) is used to anchor a linear extrapolation. The constants for the extrapolation are evaluated in the equation subroutine and transferred back to the main subroutine where the actual extrapolation calculation procedure is implemented.

The calculation procedure is listed in Appendix C. The main subroutine "GAPH" is structured with an input section (NAMELIST), printing of input parameters, logic for selecting correlation function if none is specified and calls to correlation equation subroutines according to sequence number. Each equation subroutine is given a name derived from the "Equation Designation", for example; Equation 4-9 has a subroutine EQ4D9 which contains the formulation of constants which are evaluated during their first access. In turn each equation subroutine calls a function subroutine which actually computes the heating ratio. All equation subroutines are setup with essentially the same calculation flow for easy comprehension by the reader. The subroutine "GAPH" computes heating ratios or actual heating rates if designated for the entire set of S (or Z) values input prior to printing the gap heating distribution. If one of the gap parameters or flow field parameters changes during the course of an analysis of a mission, "GAPH" should be re-called.

TECHNIQUE FOR EXTRAPOLATING CORRELATION FUNCTIONS

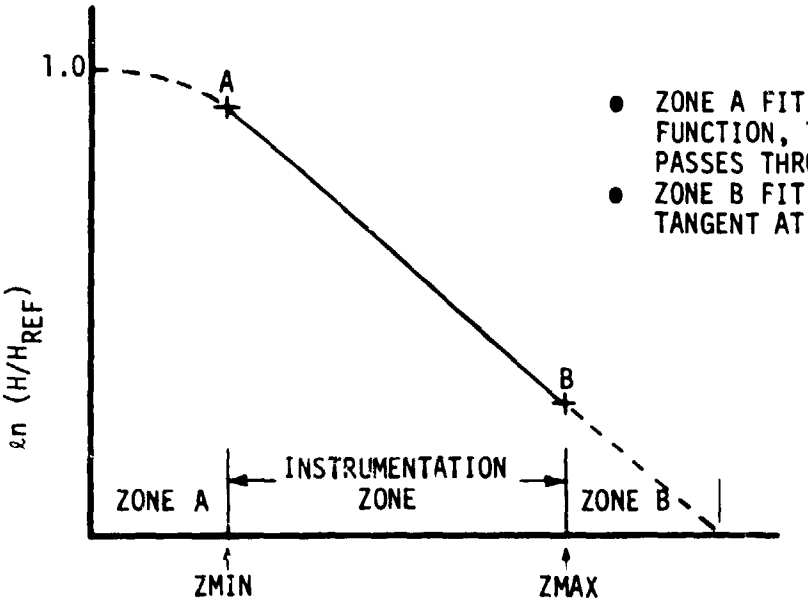

- ZONE A FIT WITH 2ND ORDER FUNCTION, TANGENT AT A AND PASSES THROUGH 1.
- ZONE B FIT WITH LINEAR EQUATION, TANGENT AT B

Figure 200

7.0 INFLUENCE OF GAP HEATING ON TPS SIZING

The effect of gap heating on thermal protection system (TPS) requirements is a major conclusion to be drawn from this study. The thermal protection system for the Shuttle consists of a strain isolation pad (SIP) bonded to the aluminum surface with the RSI tiles bonded to the SIP. Aluminum structure temperature penalties are expected because of the possibility of having large gap widths and tiles with small corner edge radius. The nominal TPS configuration has tiles with edge radii of 0.152 cm and a gap width of 0.254 cm between tiles. The greatest tile thickness increase over a one dimensional model (no gap) was 42% and corresponded to tiles having a corner edge radius of 0.152 cm and a gap width between tiles of 0.508 cm. However, if the tile corner edge radius is increased and the gap width reduced, the tile thickness increase can be reduced to 12%. Heat leakage in the gap is a complex combination of convection, radiation, conduction within the RSI tile and coating, and duration of heat soak.

A set of TPS sizing calculations was made for body point 1040 which is located on the lower surface of the Shuttle fuselage where surface temperatures reach nominally 1278°C. The effect of gap width and edge radius on TPS requirements were investigated. The thermal model used in this analysis is shown on Figure 201 and is basically the same as described in Section 4.7 except for substitution of a radiation heat sink for the channel wall. The RSI used was LI-900, having a density of 144 kgs/m^3 and was covered with waterproof coating. Analyses were performed for the current Shuttle baseline entry trajectory (14414). Figure 202 is the reference heating rate and Figure 203 is the local pressure. The reference heating was converted to a local heating rate using a multiplying factor of 0.3646 and was imposed on the top of the tile with the gap heating correlation applied to the gap walls. The gap heating correlation (Equation 4-17) for a transverse gap submerged in a laminar boundary layer flow was used. This correlation was developed from data measured on thin skin tiles with various edge radii tested in a wedge in the JSC 10 MW Arc Tunnel. The method whereby the correlation was obtained is described in Section 5.2. Figure 204 shows the heating distributions. As can be seen on this figure, the curves do not extend deep into the gap. Figure 205 shows the method of extrapolating the correlation curve toward the bondline. In the gap near the upper surface, a second order curve was fit between an assigned tangency point on Equation 4-17 and passing through $\ln(q/q_{FP})=1.0$ at the tangency point of the edge radius and tile flat surface (S = 0.0). The technique of extending the correlation curves is

THERMAL MODEL OF AN RSI TILE JOINT WITH EDGE RADIUS

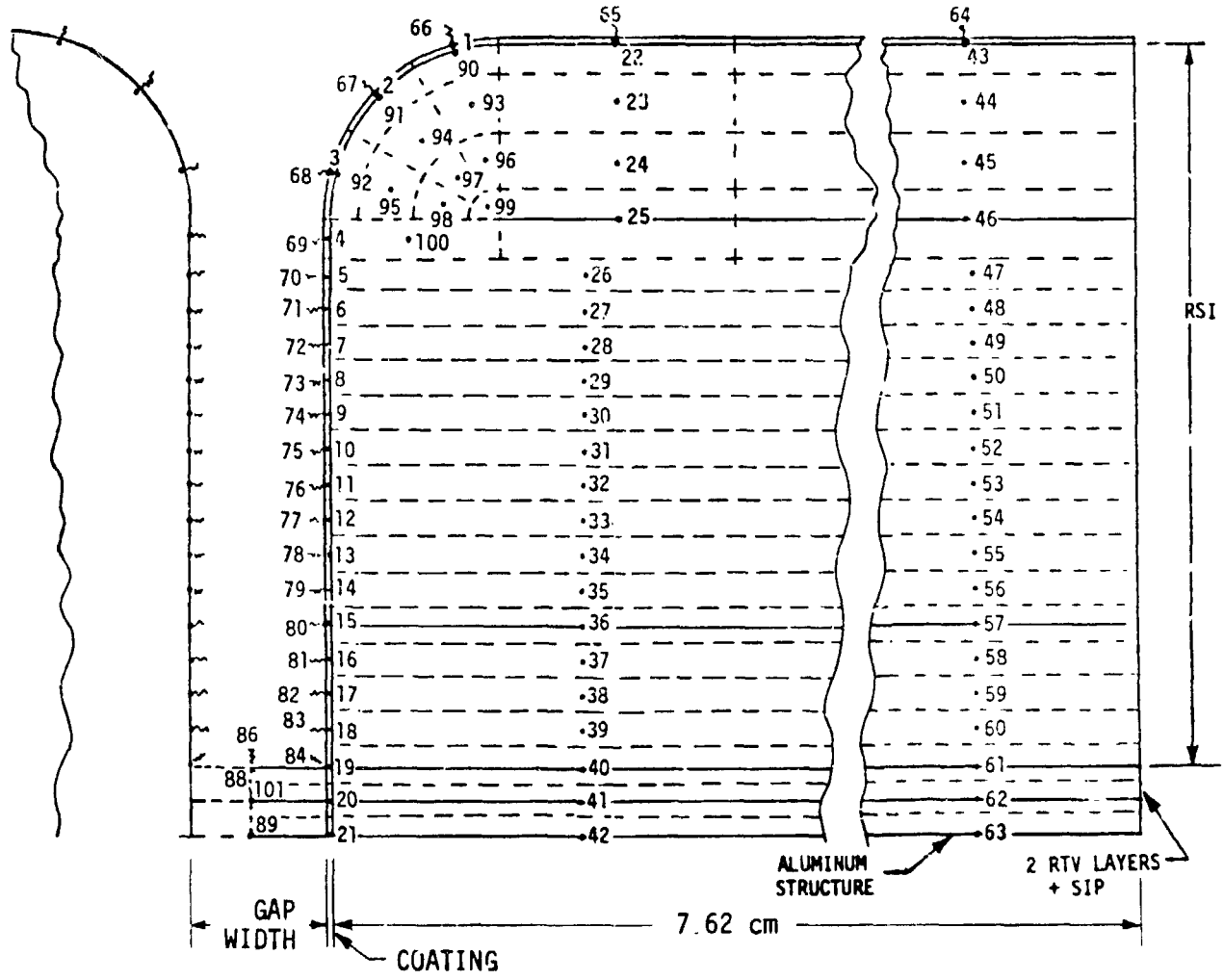

THERMAL MODEL NOTES:

1. CONVECTIVE HEATING ON SURFACE AND GAP WALL
2. COATING THICKNESS = 0.0381 cm
3. COATING EMISSIVITY = 0.80
4. ALUMINUM STRUCTURE = 0.203 cm
5. SIP + RTV ADHESIVE = 0.445 cm

Figure 201

REFERENCE ENTRY HEATING RATE

TRAJECTORY 14414

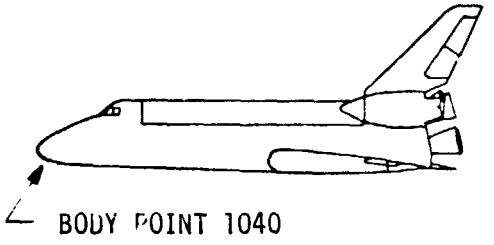

LOCAL HEATING = $\dot{q}_{REF}$ ($\dot{q}_L/\dot{q}_{REF}$)

FOR BODY POINT 1040 = $\dot{q}_{REF}$ * 0.3646

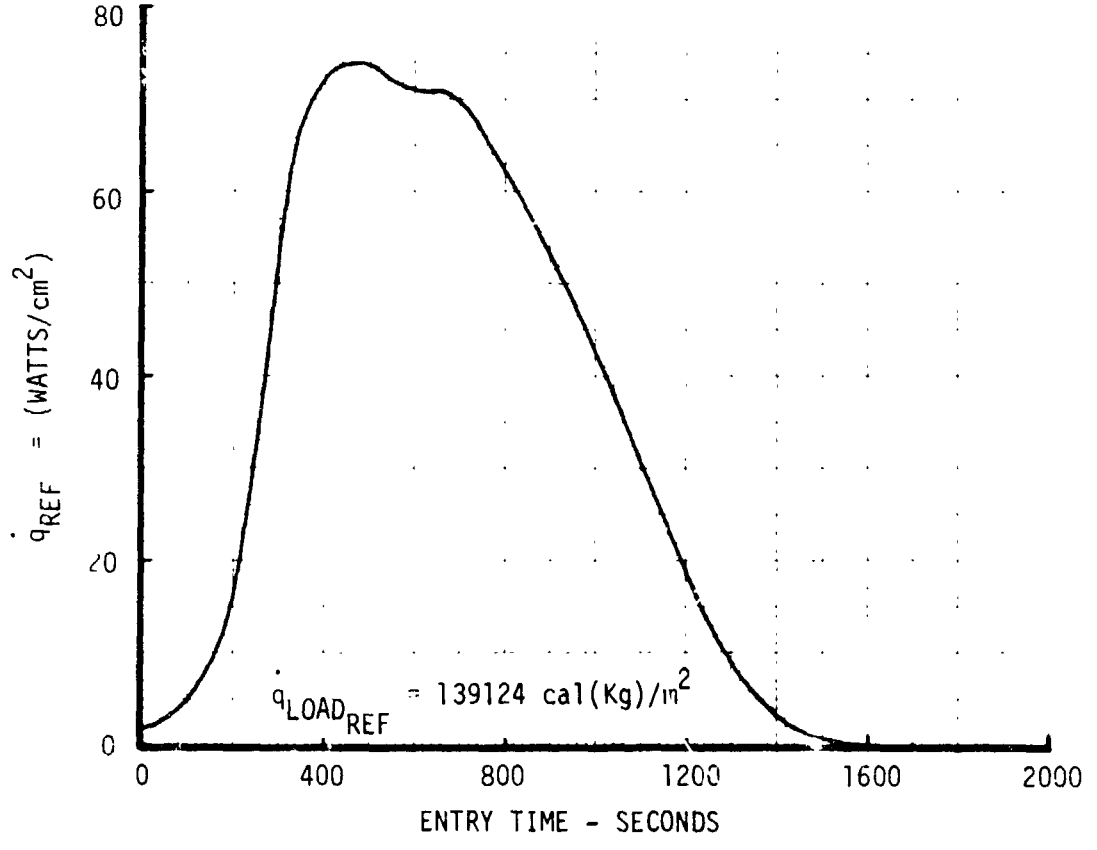

Figure 202

LOCAL PRESSURE ON LOWER SURFACE OF SHUTTLE DURING ENTRY

TRAJECTORY 14414

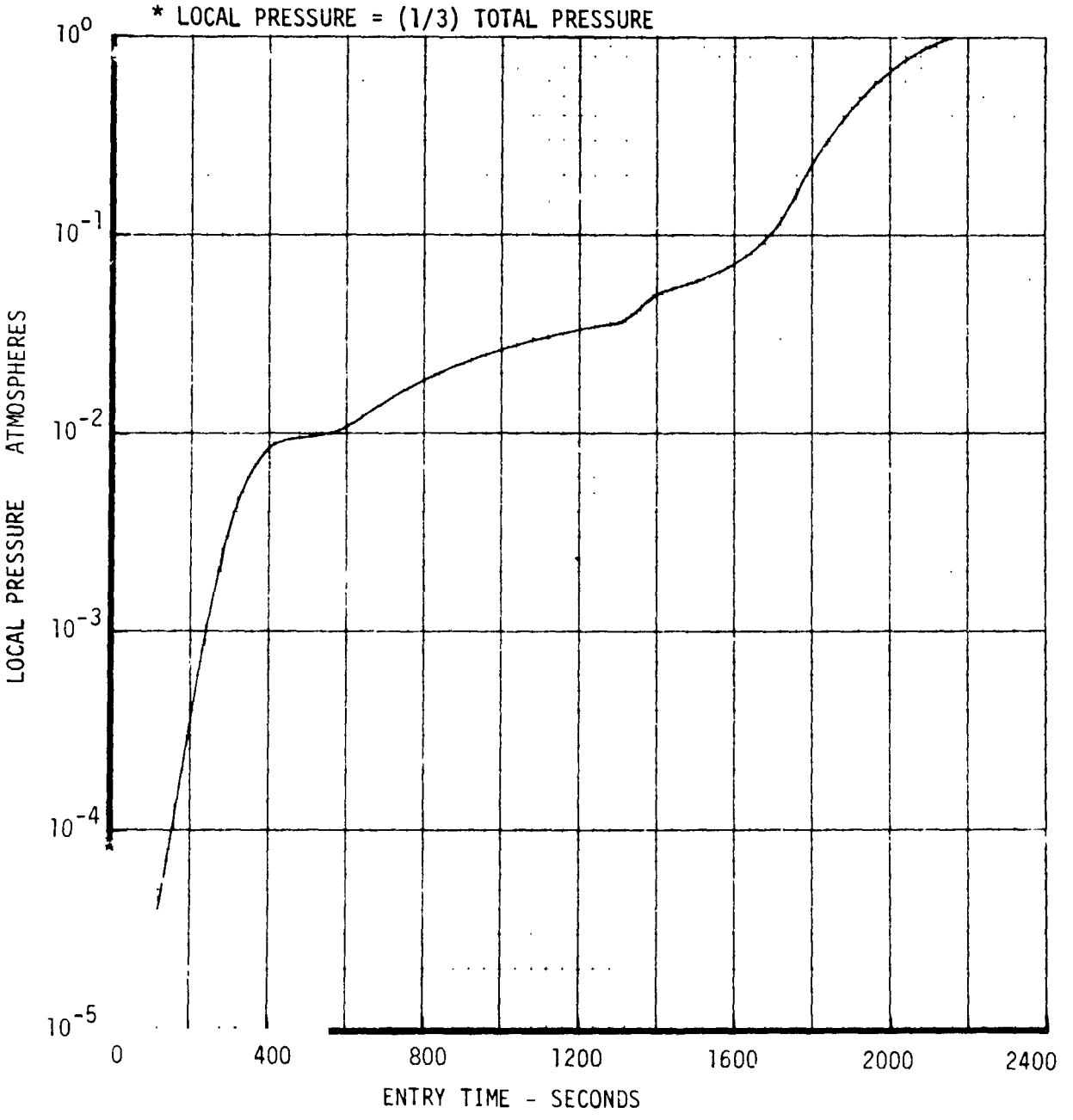

Figure 203

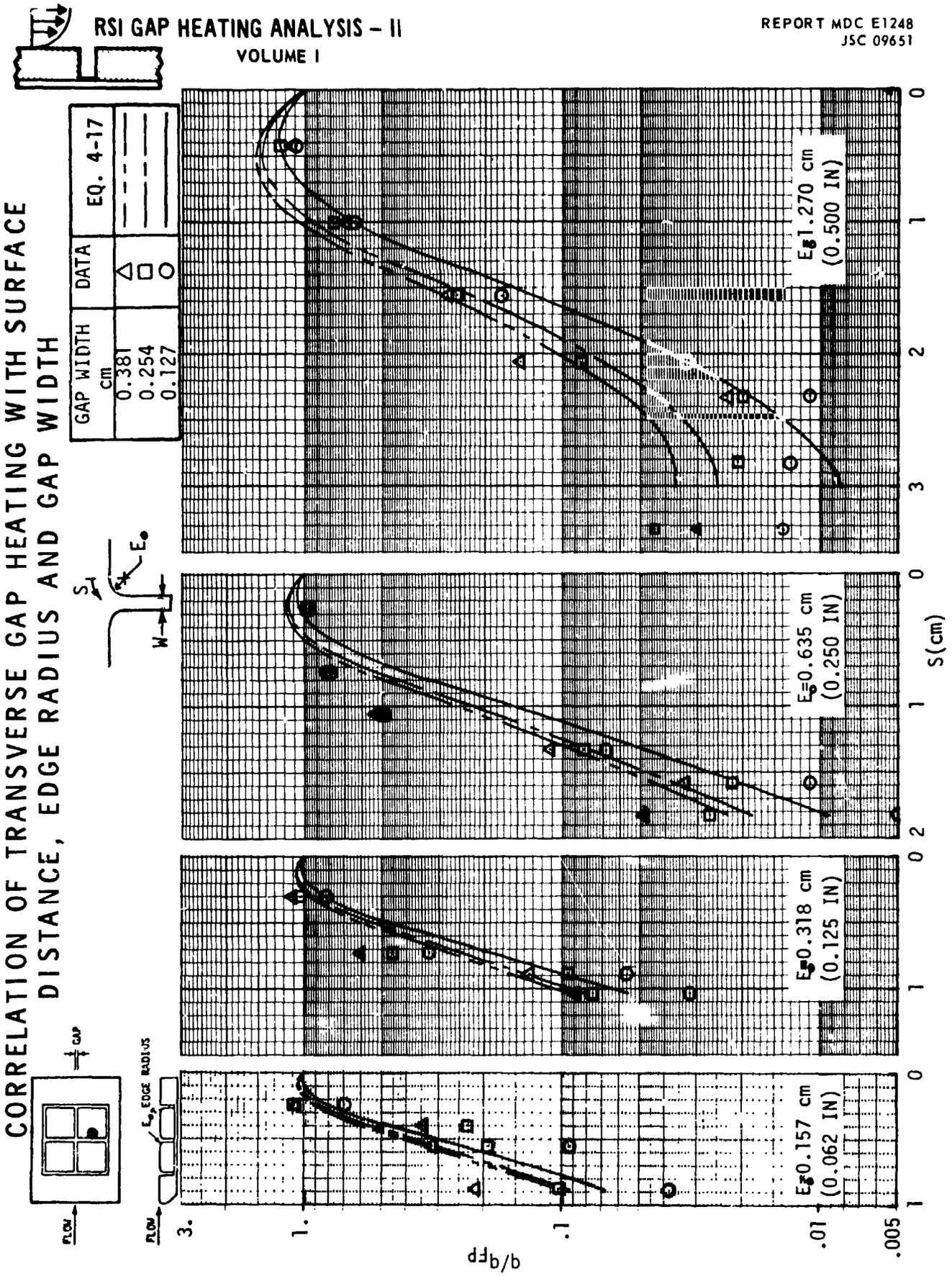
CORRELATION OF TRANSVERSE GAP HEATING WITH SURFACE DISTANCE, EDGE RADIUS AND GAP WIDTH
GAP WIDTH cm
0.381
0.254
0.127
DATA
EQ. 4-17
E=1.270 cm (0.500 IN)
E=0.635 cm (0.250 IN)
E=0.318 cm (0.125 IN)
E=0.157 cm (0.062 IN)
S(cm)
q/q_fp
FLOW
EDGE RADIUS
GAP

Figure 204

TECHNIQUE FOR EXTRAPOLATING CORRELATION FUNCTIONS

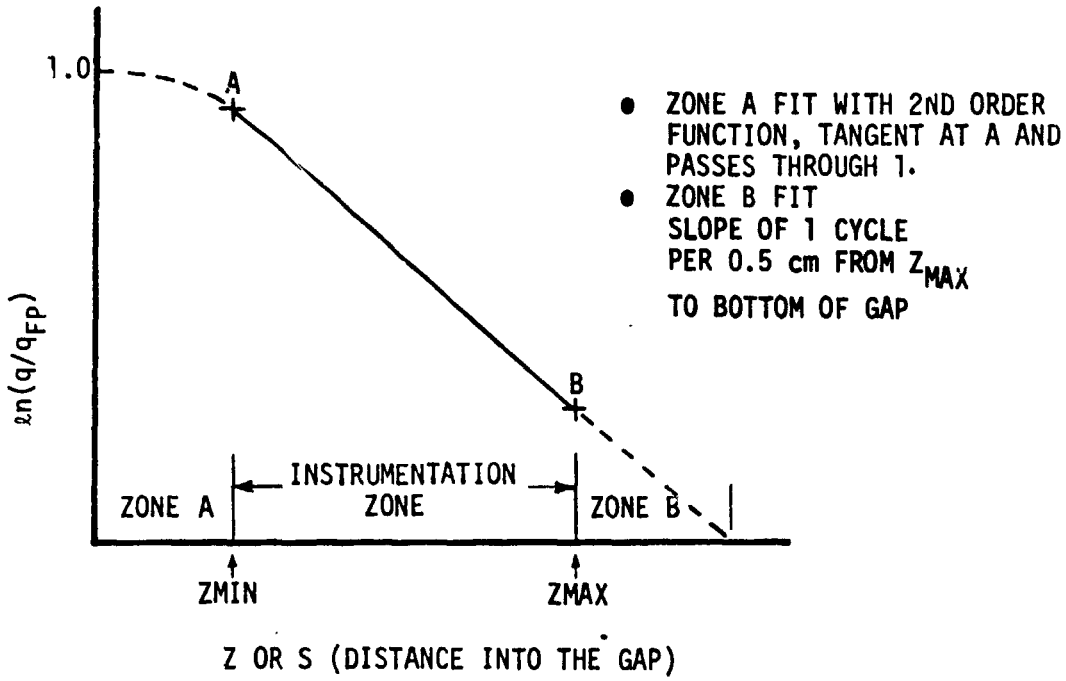

- ZONE A FIT WITH 2ND ORDER FUNCTION, TANGENT AT A AND PASSES THROUGH 1.
- ZONE B FIT SLOPE OF 1 CYCLE PER 0.5 cm FROM Z_{MAX} TO BOTTOM OF GAP

Figure 205

also described in Section 6.0. The local pressure was used to obtain the proper thermal conductivity of LI-900 which is a function of pressure and temperature.

Complete trajectory analyses were performed by computing transient temperatures using the 2-Dimensional thermal model until the aluminum structure (0.203 cm) reaches maximum temperature. Solutions were obtained for gap widths ranging from 0.0 to 0.508 cm and inner edge radius (E_i) ranging from 0.1524 cm to 0.635 cm. The sensitivity of aluminum temperature to tile thickness is shown in Figure 206 for the nominal gap width of 0.254 cm and E_i = 0.152 cm. By comparison, a one dimensional thermal analysis indicates 7.315 cm of RSI would suffice with no gap present. Information from the previous figure is also presented in Figure 207 as the ratio of TPS thickness with a gap to thickness without. Approximately 33% more RSI is needed considering a nominal gap.

Gap width between the RSI tiles has a significant effect on TPS requirements. Figure 208 shows that increasing the gap width from 0.254 cm to 0.508 cm results in a tile thickness increase of seven percent for a tile with an edge radius of 0.152 cm. Figure 209 shows the same information relative to the 1-D thermal model requirements. Likewise, the tile edge radius has a significant effect on TPS requirements as can been seen on Figure 210. Increasing the tile edge radius (not including coating thickness) from 0.152 cm to 0.305 cm reduces the required RSI thickness by five percent for tiles with a gap width of 0.254 cm. Figure 211 shows this information normalized to the 1-D thermal model requirements.

Typical temperature-time history plots (Figures 212, 213, 214) show the response of the tile, the coating on the tile top and gap wall, and in the center of the tile. At the time of peak heating, the in-depth temperatures of the coating in the gap and temperatures in the RSI adjacent to the gap coating (not plotted) are hotter than the in-depth temperature of the RSI toward the center of the tile. This shows the effect of gap heating on temperature.

Figure 215 summarizes the amount and percent change of RSI (LI-900) required to limit the aluminum structure temperature to 177°C for several combinations of gap widths and edge radii. The percent change over a 1-D model (no gap) ranges between 12 and 42%.

ALUMINUM STRUCTURE MAXIMUM TEMPERATURE VS. RSI TILE THICKNESS

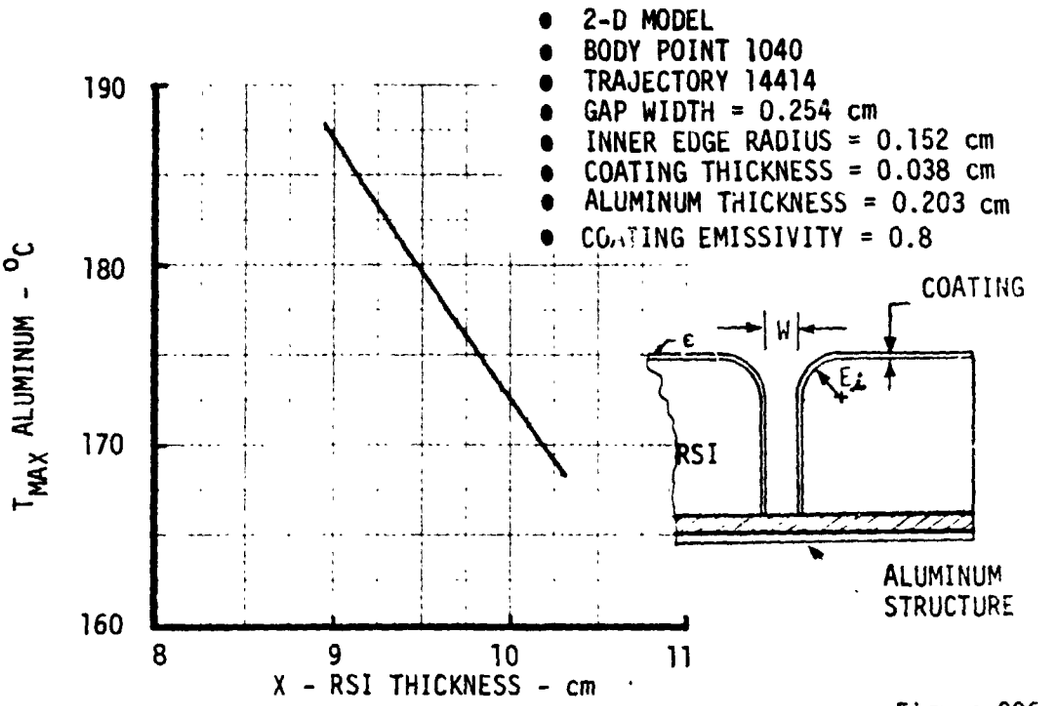

Figure 206

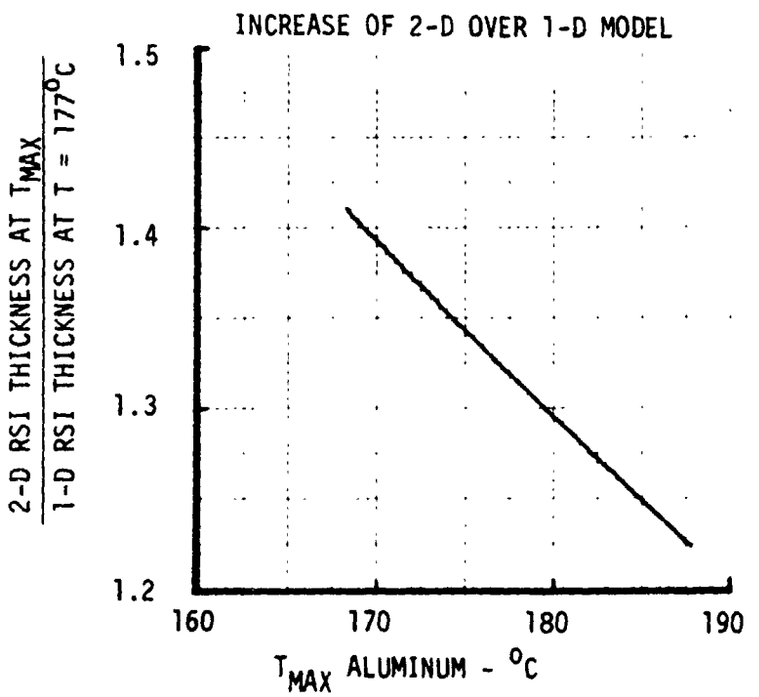

Figure 207

GAP WIDTH EFFECT ON TPS REQUIREMENTS

- 2-D MODEL
- BODY POINT 1040
- TRAJECTORY 14414
- MAXIMUM ALUMINUM TEMPERATURE = 177°C

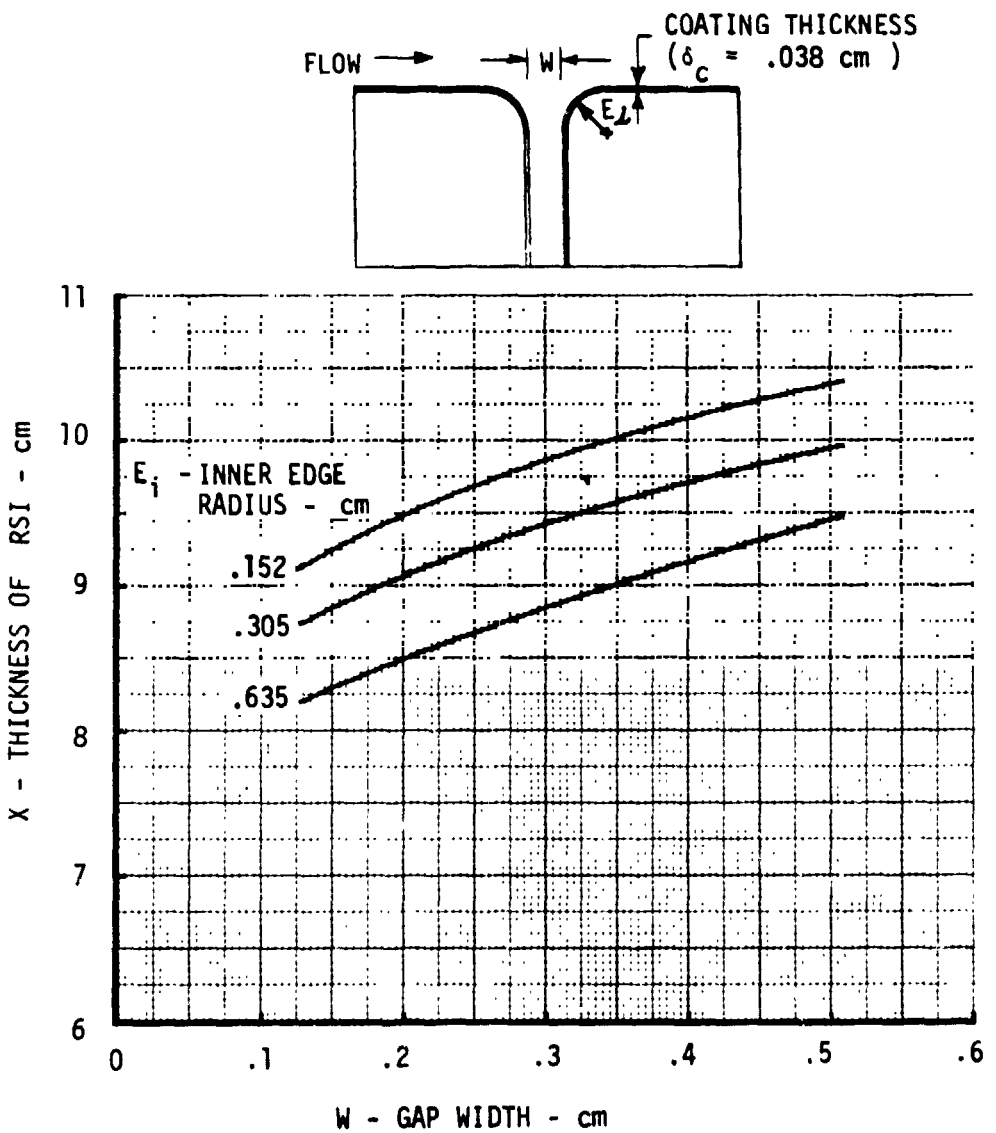

Figure 208

RATIO OF 2-D TO 1-D MODEL FOR VARIOUS GAP WIDTHS AND EDGE RADII

- 2-D MODEL
- BODY POINT 1040
- TRAJECTORY 14414
- MAXIMUM ALUMINUM TEMPERATURE = 177°C

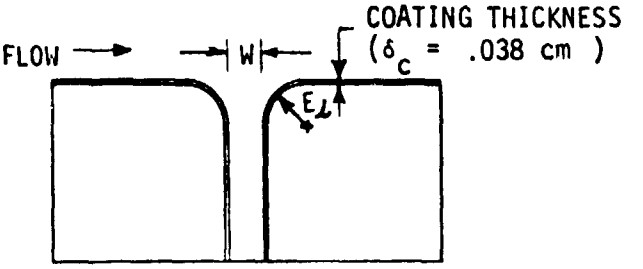

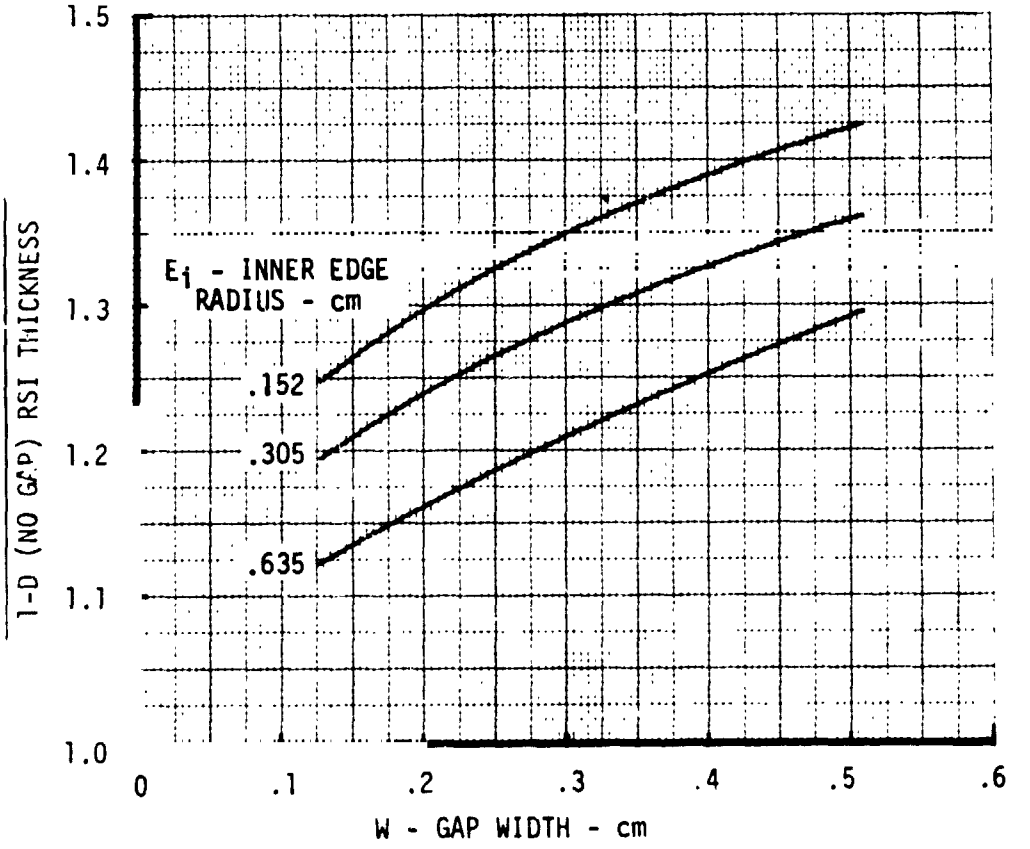

Figure 209

EDGE RADIUS EFFECT ON TPS REQUIREMENTS

- 2-D MODEL
- BODY POINT 1040
- TRAJECTORY 14414
- MAXIMUM ALUMINUM TEMPERATURE = 177°C

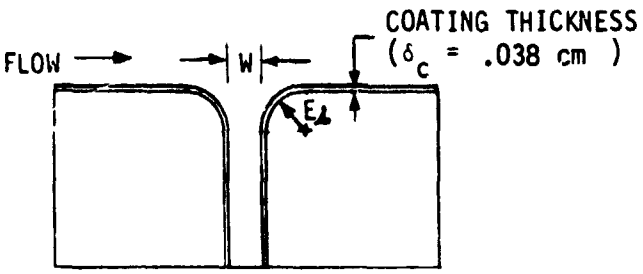

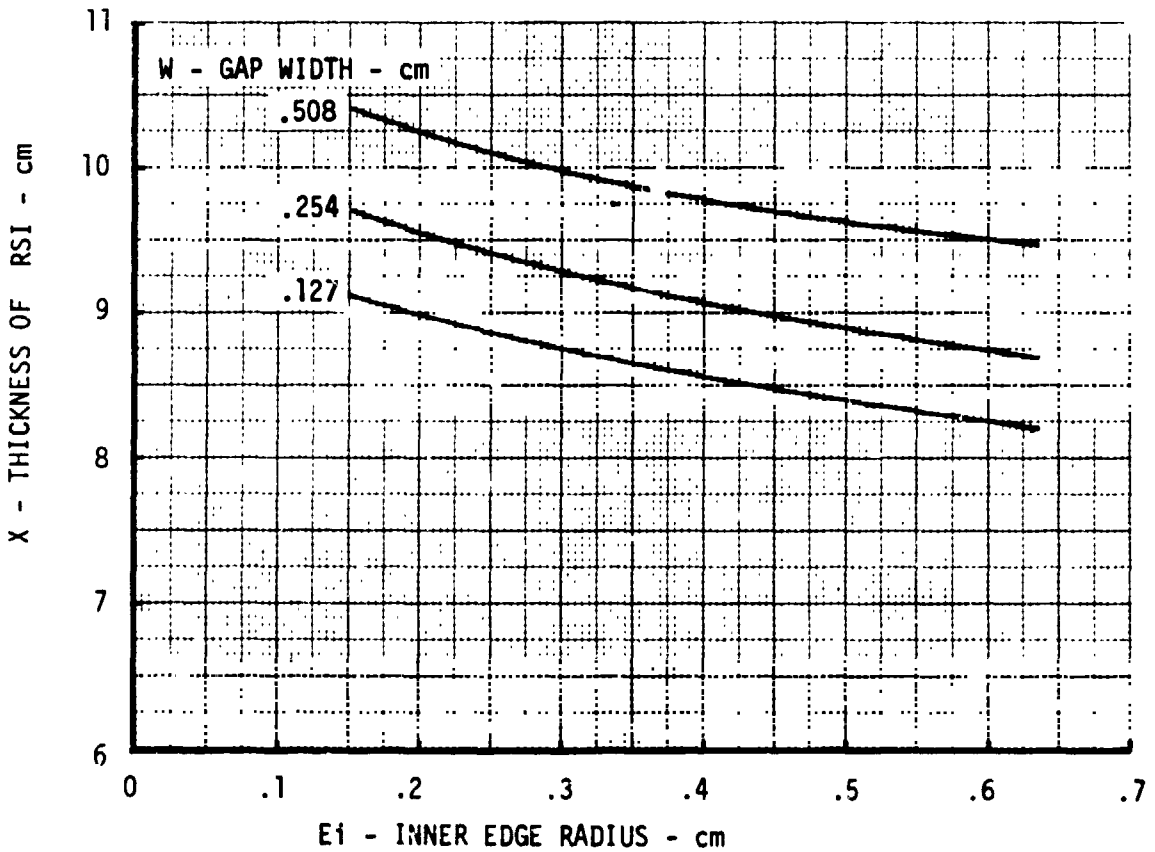

Figure 210

RATIO OF 2-D TO 1-D MODEL FOR VARIOUS GAP WIDTHS AND EDGE RADII

- 2-D MODEL
- BODY POINT 1040
- TRAJECTORY 14414
- MAXIMUM ALUMINUM TEMPERATURE = 177°C

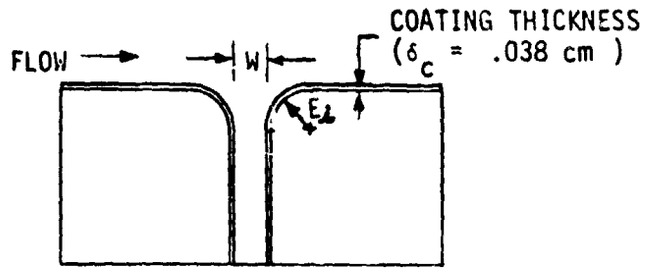

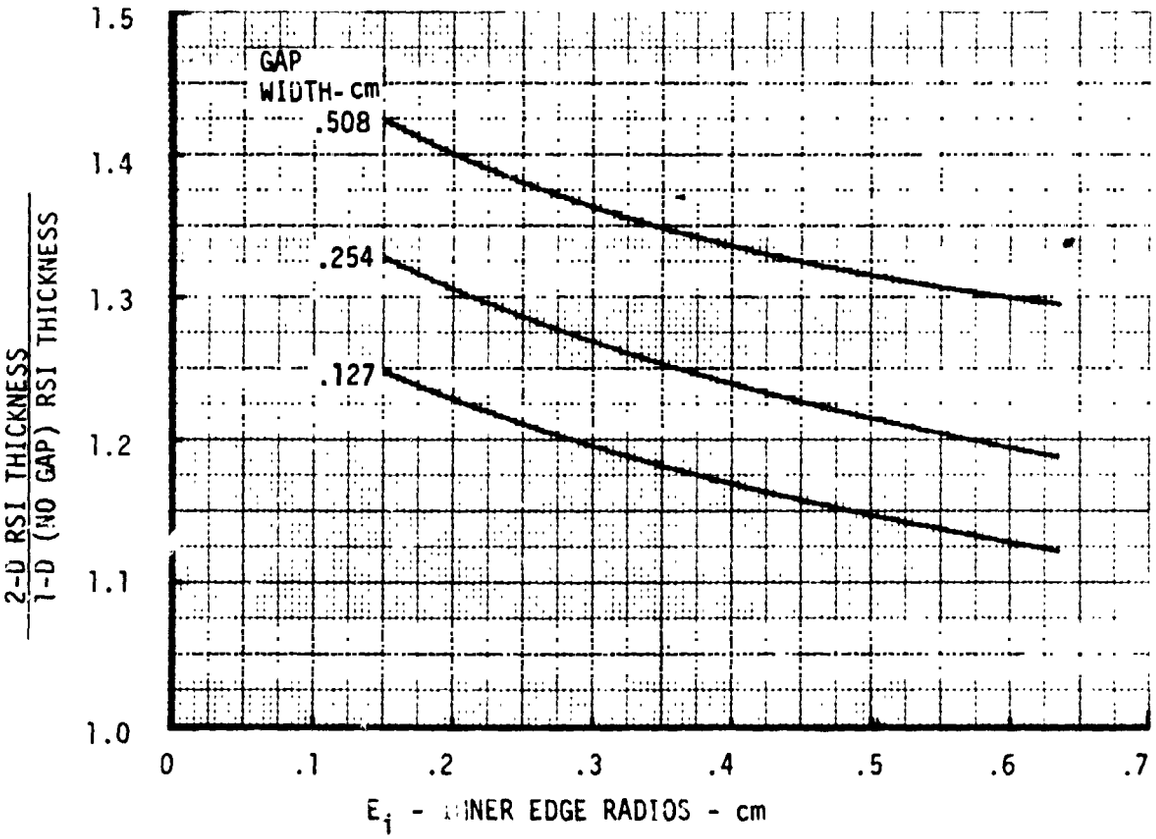

Figure 211

SURFACE, EDGE RADIUS AND ALUMINUM STRUCTURE TEMPERATURES

- BODY POINT 1040
- TRAJECTORY 14414
- GAP WIDTH = 0.254 cm
- INNER EDGE RADIUS = 0.152 cm

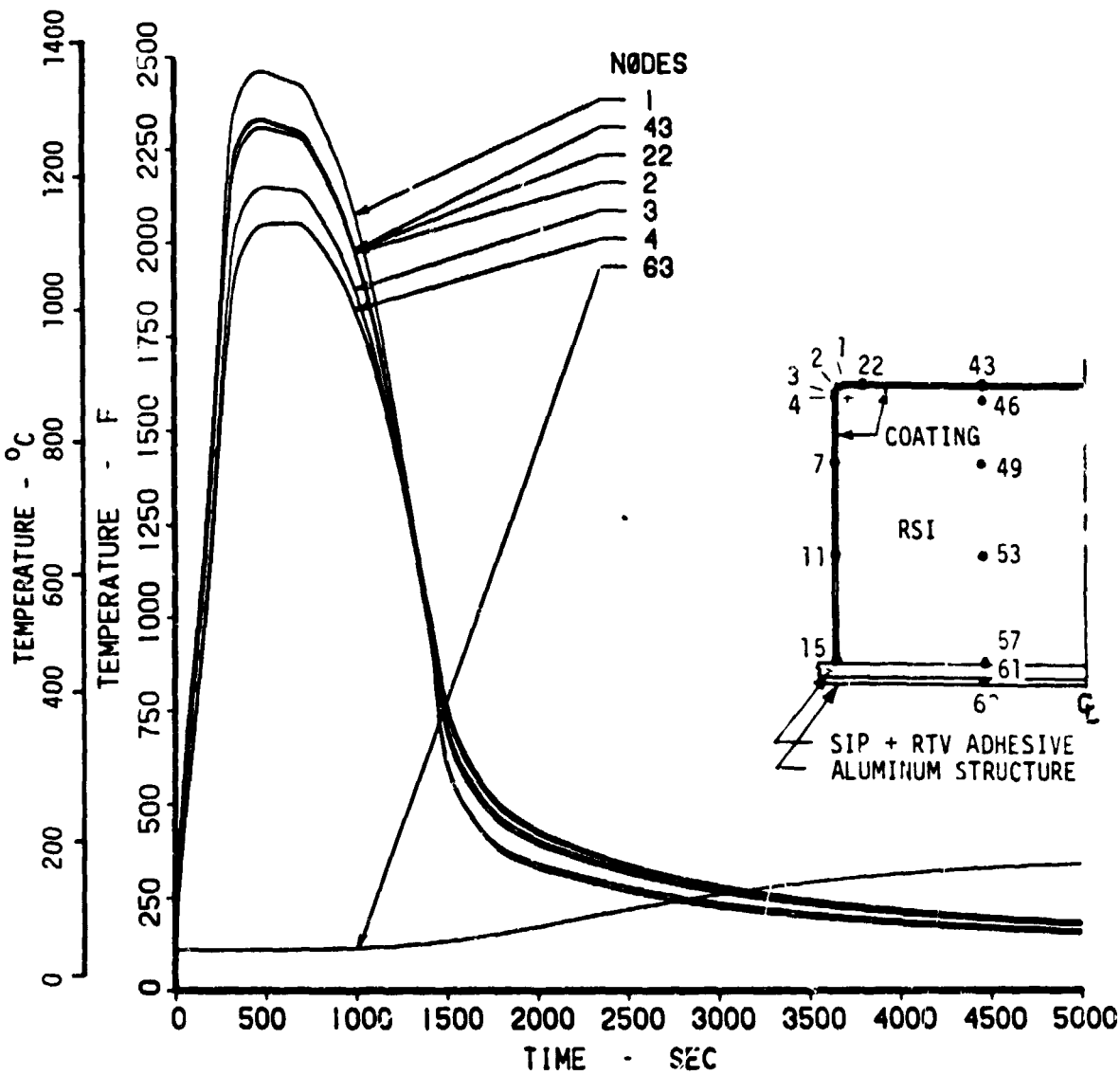

Figure 212

TILE TOP AND GAP WALL COATING TEMPERATURES

- BODY POINT 1040
- TRAJECTORY 14414
- GAP WIDTH 0.254 cm
- INNER EDGE RADIUS = 0.152 cm

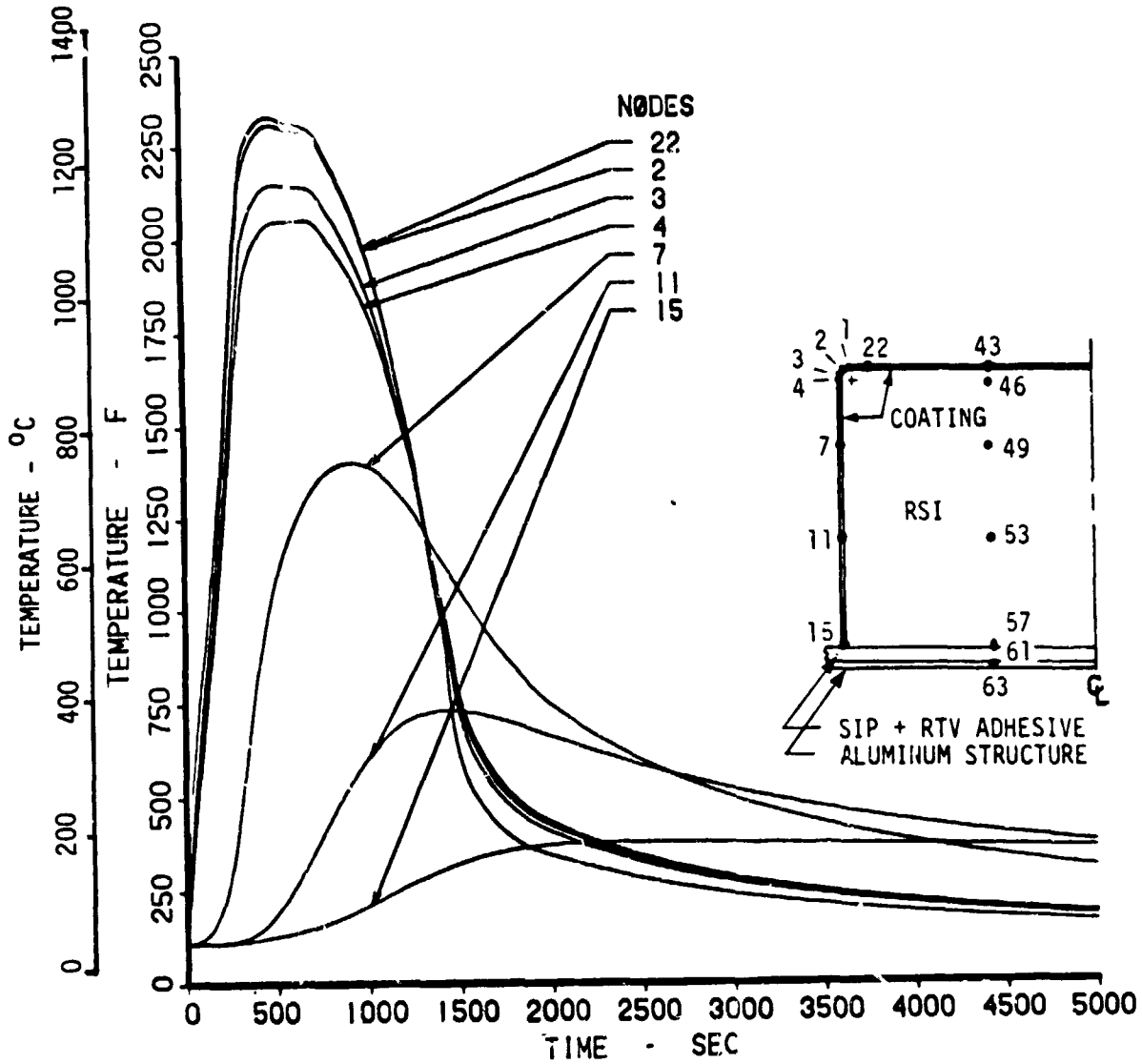

Figure 213

RSI IN-DEPTH TEMPERATURES NEAR CENTER OF TILE

- BODY POINT 1040
- TRAJECTORY 14414
- GAP WIDTH = C.254 cm
- INNER EDGE RADIUS = 0.152 cm

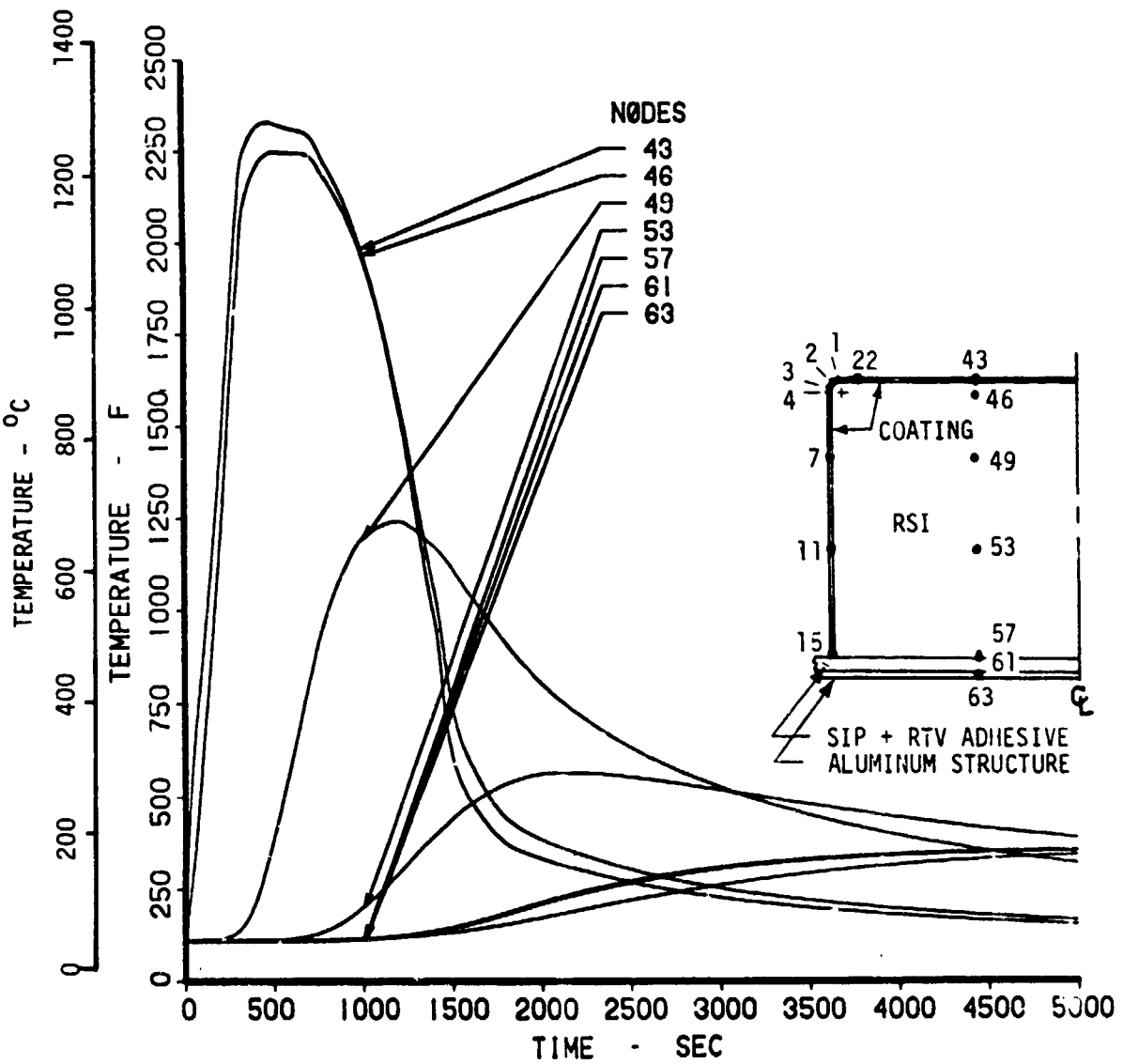

Figure 214

.EFFECT OF TRANSVERSE GAP HEATING ON TPS REQUIREMENTS

ANALYSIS NUMBER	EDGE RADIUS cm, (inch)	GAP WIDTH cm, (inch)	X-RSI cm, (inch)	$X2\text{-}D/_{X1\text{-}D}$
1	1-D MODEL	NO GAP	7.315 (2.880)	-
2	0.152 (0.060)	0.127 (0.050)	9.119 (3.590)	1.25
3	0.305 (0.120)	0.127 (0.050)	8.738 (3.440)	1.19
4	0.635 (0.250)	0.127 (0.050)	8.204 (3.230)	1.12
5	0.152 (0.060)	0.254 (0.100)	9.703 (2.820)	1.33
6	0.305 (0.120)	0.254 (0.100)	9.271 (3.650)	1.27
7	0.635 (0.250)	0.254 (0.100)	8.687 (3.420)	1.19
8	0.152 (0.060)	0.508 (0.200)	10.414 (4.100)	1.42
9	0.305 (0.120)	0.508 (0.200)	9.957 (3.920)	1.36
10	0.635 (0.250)	0.508 (0.200)	9.474 (3.730)	1.30

THE ABOVE RESULTS WERE OBTAINED USING EQUATION 4-17.

Figure 215

8.0 CONCLUSIONS

Convective heating on the surface and within the gaps between representative Space Shuttle RSI tile configurations has been extensively investigated. Data from 10 test programs in 6 NASA facilities provided the experimental base for this investigation, which was conducted in two phases. Major conclusions from this investigation are summarized below.

A number of major conclusions from Phase I were reinforced during Phase II and none was invalidated. Some of these are:

- Gap heating is a three dimensional phenomenon. Both transverse gaps and in-line gaps (as well as gaps of intermediate sweep angles) experienced significant lengthwise and wall-to-wall variations in heating in addition to depthwise variation.
- Interactions exist between gap heating and heating on the top surfaces of tiles.
- Gap heating increases with width; however, for a given width and distance from the tile surface, heating decreases as the gap depth is increased.
- Tiles having forward facing steps experience higher gap heating than tiles with rear-facing steps or no steps.
- Gap cross section geometry is significant for wide gaps (greater than 0.25 cm) and less important for narrow gaps.
- With a turbulent external boundary layer, gap heating at flow incidence angles between 0 and $\pi/2$ is higher than at either 0 or $\pi/2$.

Additional significant conclusions which were drawn from the Phase II studies include:

- In-line gaps promote boundary layer transition. Examination of data from the Ames 3.5 Foot HWT indicates transition is initiated within the gap and propogates outward.
- Gap heating appears to increase more rapidly than tile surface heating as Reynolds number is increased. (A heating increase phenomenon similar to an "energy dump" was observed on a tile trailing edge tested in a turbulent boundary layer at the LaRC 8 Foot HTST.)
- Increasing edge radius is observed to increase gap convective heating slightly. However, lower tile temperatures result, since the heating increase is more than offset by the greater radiant heat rejection afforded by the increased radius.

Data correlation activity during the study yielded 21 equations describing gap heating distributions as functions of boundary layer state and gap geometry. Several of these were originally developed during Phase I and improved by utilizing the larger data base made available during Phase II. Among the more important correlations are the following:

- o Transverse gap correlations which have been improved through the incorporation of additional data
- o Correlations for edge radius
- o Correlations for long in-line gaps including sweep angle effects up to 15 degrees
- o Correlations for gaps with steps

A new gap heating subroutine called GAPH was prepared during Phase II. The subroutine is designed to be compatible with thermal analysis programs such as SINDA and HEATRAN. The subroutine incorporates the correlation equations developed during the study together with internal logic to select the appropriate correlation equation. The desired correlation can also be selected directly by the program user.

Parametric evaluation of gap width and radius effect shows increase in TPS thickness caused by presence of gaps varies between 12% and 42%. Heat rejection by radiation from gap regions is enhanced by increasing tile edge radius. For instance, increasing radius from 0.152 cm to 0.305 cm reduces RSI thickness requirement by 5%.

Finally, though not a study objective, it is worth noting that during the data analysis a persistent tendency existed in all the thin skin tile models for the apparent heat transfer rate on the upper surface to decrease near the tile edge. Tests with filled gaps seem to indicate this does not result from a fluid dynamic phenomenon produced by the gaps. Attempts to explain the mystery on the basis of lateral conduction in the thin skin indicate the magnitude of skin conduction is not sufficiently large to account for the observed effect. The phenomenon remains unresolved.

9.0 RECOMMENDATIONS

Gap heating data from ten test programs in six test facilities provided the basis for this study. The analysis of these data revealed a number of surprises for which satisfactory explanations have not been found. Not all of the unexplained phenomena are of sufficient importance to the Space Shuttle Program or possess sufficient intrinsic merit to deserve further attention. In addition to the unexplained phenomena, the present body of data contains omissions which deserve attention. The recommendations which follow are intended to address significant phenomena which are not understood and to address significant voids in the existing data.

As stated in the Conclusions (Section 8), gap heating is observed to be a three dimensional phenomenon. Significant lengthwise variations in heating rates were observed for all gap orientations in the absence of nominal pressure gradients on tile surfaces. In addition to the observed three-dimensionality of heating within gaps, results from several of the tests show evidence of strong interactions between heating within the gap and adjacent tile surfaces. (Similar results have been observed using teflon models in the Ames facility, Reference 5.) The three dimensional nature of gap heating and its interaction with tile surface heating merits further exploration. Such exploration should employ pressure measurements as well as oil flow and thermal mapping techniques. One or more of the existing test panels could well be modified to perform such an investigation. Also of merit is the development of an analytical computational method for computing flow fields with the gaps between tiles which include viscous effects, real gas effects, pressure gradients, flow field sinks and sources, and heat transfer.

This current program investigated in-line and staggered butt type gaps at flow orientations ranging from 0 to $\pi/2$ radians in the presence of a turbulent external boundary layer (LaRC Mach 10 CFHT Wall Test). Peak heating over large portions of the Shuttle will occur in the presence of a laminar boundary layer at flow inclinations of approximately $\pi/4$. The tests previously conducted in the LaRC CFHT should be repeated with a laminar external boundary layer, using, if possible, the same test apparatus.

The following activities are recommended to be pursued, either individually or (preferably) in conjunction with the above:

- Expand correlation activity to include T slots and the most forward corner on tiles oriented at flow inclination angles in the vicinity of $\pi/4$.
- Investigate the tendency of heat transfer rates measured using thin skin models to decrease near the tile edge.

- Investigate differences between results obtained from thin skin and RSI models by building duplicate models and testing in the same facility. (The need for one of the duplicate models could be satisfied by using results from the current program.)
- Perform gap heating tests using companion RSI tile models each with a different edge radius to further define the benefits (or disadvantages) of radiused tiles especially when exposed to the high enthalpy flow expected during flight.

10.0 REFERENCES

1. "Data Correlation and Analysis of Arc Tunnel and Wind Tunnel Tests of RSI Joints and Gaps," MDC Report E1003, 29 January 1974.

2. "Gap Heating Analysis of Temperature Measured on HRSI (High Temperature Reusable Surface Insulation) TPS (Thermal Protection System) Joint/Gap Panels (Tests, September to November 1973)," MDC Thermodynamics Technical Note No. E242-76.

3. Deveikis, W.D. and Hunt, L.R., "Loading and Heating of a Large Flat Plate at Mach 7 in the Langley 8-Foot High-Temperatures Structures Tunnel," NASA TN D-7275, September 1973.

4. "Symposium on Reusable Surface Insulation for Space Shuttle Volume II - Environmental Testing," NASA TM X-2720, September 1973.

5. Private Communications with Howard K. Larson, NASA-Ames, 29 October 1974.

APPENDIX A

LIST OF CORRELATION PARAMETERS

Figure A-1 presents the lists of the independent correlation parameters submitted to the MRA program. These parameters are divided into seven separate sets so that a particular set could be used in the analysis of a specific gap heating effect.

PARAMETER SETS INVESTIGATED FOR HEATING CORRELATIONS

SET 1

$Z,\ Z,^2\ Z,^3\ \sqrt{Z},\ \ell nZ,$

$E,\ E,^2\ E,^3\ \sqrt{E},\ \ell nE,$

$W,\ W,^2\ W,^3\ \sqrt{W},\ \ell nW,\ W^{1.5}$

$ZE,\ ZW,\ Z(E^2)\ \ Z(W^2),\ Z/E,\ \ E/Z,\ \ (W/Z),\ \ (W/Z)^2$

$EW,\ E(Z^2)\ \ E(W^2),\ Z/W,\ \ E/W,\ \ (W/E),\ \ (W/E)^2$

$W(Z^2),\ W(E^2),\ (Z/E),^2\ \ (E/Z)^2$

$(Z/W)^2,\ \ (E/W)^2$

SET 2

$S,\ S,^2\ S,^3$	$\ell nS,$	$(\ell nS)^2,$	$W\ell nS,$	$W(\ell nS)^2$
$E,\ E,^2$	$\ell nE,$		$E\ell nS,$	$E(\ell nS)^2$
$W,$	$\ell nW,$			$E^2(\ell nS)^2$
	$WE,$		$WE\ell nS,$	$WE(\ell nS)^2$
	$W(E^2),$		$W(E^2)\ell nS,$	$W(E^2)(\ell nS)^2$
$S/W,\ \ E/W,$	$W(S^2),$	$(S/W)^2,$	$(E/W)^2,$ $E/S,$	$(E/S)^2$

SET 3

$S,\ S,^2\ S,^3$	$\ell nS,$	$(\ell nS)^2,$	$W\ell nS,$	$W(\ell nS)^2$
$E,\ E,^2\ 2E,$	$\ell nE,$		$E\ell nS,$	$E(\ell nS)^2$
$W,\ 2W,$	$\ell nW,$			$E^2(\ell nS)^2$
	$WE,$		$WE\ell nS,$	$WE(\ell nS)^2$
	$W(E^2),$		$W(E^2)\ell nS,$	$W(E^2)(\ell nS)^2$
$S/W,\ \ E/W,$	$W(S^2),$	$(S/W)^2,$	$(E/W)^2,$ $E/S,$	$(E/S)^2$
$(W+E),\ (W+E)^2,$	$\ell n(W+E),$	$\ell n(W+E)^2$		
$(W+2E),\ (W+2E)^2,$	$\ell n(W+2E),$	$\ell n(W+2E)^2$		

NOTE: SURFACE DISTANCES ARE ASSIGNED A POSITIVE SIGN FOR PURPOSES OF THE CORRELATION

SET 4

ℓnZ, $(\ell nZ)^2$, $(\ell nZ)^3$

ℓnL, ℓnRe

$\ell n\theta$, $\ell n\,\delta^*$, $\ell n\, T_W/T_E$

$\ell n\ \frac{\delta^*}{L}\frac{Z}{W}$, $\left[\ell n\ \frac{\delta^*}{L}\frac{Z}{W}\right]^2$, $\left[\ell n\ \frac{\delta^*}{L}\frac{Z}{W}\right]^3$

$\ell n\ \frac{\delta}{L}$, $\ell n\ \frac{Z}{W}$,

$\ell n\ W$, $(\ell nW)^2$, $(\ell nZ)\ (\ell nW)$, $(\ell nZ)\ (\ell nW)^2$

$\ell(\ell nZ)^2\ (\ell nW)^2$, $(\ell nZ)^2\ (\ell nW)$

$\ell n\ T$

SET 5

Same as SET 4 with the addition of γ, γ^2, $\ell n\ (COS\gamma)$

---

where: Z = Distance into the gap (cm)

L = Gap length (cm)

Re = Local unit Reynolds number ($10^6 m^{-1}$)

θ = Momentum thickness (cm)

δ^* = Displacement thickness (cm)

W = Gap width (cm)

T = Gap depth (tile thickness), (cm)

γ = Flow incidence angle (radians)

$\frac{T_W}{T_E}$ = Temperature rates across boundary layer (T_W = wall temperature)

SET 6

Same as SET 4 with the addition of Z, Z^2, W. L, Re, θ, δ^*, T_W/T_E

SET 7

1) cubic variation with (Z)
2) quadratic variation with (W)
3) linear variation with (Re)
4) linear variation with (T)

$$\ell n\ h/h_{REF} = (a_o+a_1Z+a_2Z^2+a_3Z^3)(b_o+b_1W+b_2W^2)(C_o+C_1Re)(D_o+D_1T)$$

APPENDIX B

TABULATION OF CORRELATION EQUATION 15-5 [TRANSVERSE GAP, DOWNSTREAM WALL, LAMINAR FLOW]

```
C     PROGRAM GFACT(INPUT=100,OUTPUT,TAPE5=INPUT,TAPE6=OUTPUT)
C     GAP HEATING FACTORS CREATED BY CORRELATION EQ.
C                          MARCH 1975   M.E. CHRISTENSEN
C
      DIMENSION Z(20),M(5), T(4), RE(4), QR(10), EQ(2)
      DATA Z/.001, .01, .05, .1, .15, .2, .25, .3, .4, .5, .6, .7,
     1       .8, .9, 1.0/
     2       1.2, 1.4, 1.6, 1.8, 2.0, 2.5/
      DATA M/ 0.063, 0.127, .254, 0.381, 0.508/
      DATA T/ 1., 2., 3., 4./
      DATA RE/ 0.01, 0.1, 1., 3./
C
      IT=4
      JR=4
      KZ=20
      METHOD=1
      LM=5
      EQ(1)=10H 15-5,LAM.
      EQ(2)=10HTRANS GAP
C
C     TILE THICKNESS
C
      DO 621 I=1,IT
      WRITE(6,960)
      WRITE(6,961) EQ
C
C     REYNOLDS NUMBER
C
      DO 780 J=1,JR,2
      WRITE(6,967)
      WRITE(6,922) T(I), III)
      WRITE(6,963) RE(J),RE(J+1)
      WRITE(6,967)
      WRITE(6,964)
      WRITE(6,968)
      WRITE(6,965) (M(LL),LL=1,LM),(M(LL),LL=1,LM)
      WRITE(6,967)
C
C     Z- DISTANCE
C
      DO 760 K=1,KZ
C
C     GAP WIDTH
      DO 750 L=1,LM
C
      JJ=J-1
      DO 740 KK=1,2
      JJ=JJ+1
      LL=L+5*(KK-1)
      GO TO (600,604),METHOD
C
C     EQUATION 15-5
  600 QR(LL)=-0.40577-6.80369*Z(K)+1.90570*Z(K)*Z(K)
     1       -2.11073*(Z(K)**3)*M(L)*RE(JJ)**T(I)
     2       +1.91713*M(L)**3)*(Z(K)**2)*RE(JJ)
     3       +1.94533*(Z(K)**3)*(M(L)**2)
     4       -0.36933*Z(K)*RE(JJ)

     5       -3.1303105*M(L)*M(L)
      QR(LL)=EXP(QR(LL))
C
      GO TO 740
C
  604 CONTINUE
C
C
  740 CONTINUE
  750 CONTINUE
      IF(QR(1).GE. 0.1)
     1 WRITE(6,966) Z(K), (QR(LL),LL=1,LM),Z(K), (QR(LL+5),LL=1,LM)
      IF(QR(1).LT. 0.1)
     1 WRITE(6,906) Z(K), (QR(LL),LL=1,LM),Z(K), (QR(LL+5),LL=1,LM)
  763 CONTINUE
  780 CONTINUE
  800 CONTINUE
C
      STOP 1
C
  900 FORMAT(1H1)
  901 FORMAT(30X,*EQUATION *2A10)
  902 FORMAT(2(9X,*CAP OPTIM   (I, CM      )=*F10.3))
  903 FORMAT(2(9X,*UNIT REY NO. (RE M=1. *10-6)=*F10.3))
  904 FORMAT(*      Z(OP S)*,*      M      *))
  905 FORMAT(2(*      (CM)   *F7.3,2X))
  906 FORMAT(2(9X,F7.3,2X))
  907 FORMAT(1H )
  908 FORMAT(1H0,5X,*      Z(OR S)*,5(*    M    *))
  909 FORMAT(2(5X,F7.3,1X,5F7.4,1X))
      END
C
```

EQUATION 15-5,LAM.TRANS GAP

GAP DEPTH (T₂ CM)= 1.000
UNIT REY NO. (RE M-1, 10-5)= .010

Z(OR S) (CM)	M .065	M .127	M .254	M .381	M .508
.001	.789	.909	1.122	1.245	1.242
.010	.742	.855	1.055	1.171	1.168
.050	.567	.654	.807	.896	.894
.100	.408	.471	.581	.646	.644
.150	.296	.341	.422	.470	.471
.200	.216	.249	.309	.345	.347
.250	.159	.184	.228	.255	.258
.300	.118	.136	.170	.191	.194
.400	.0665	.0769	.0963	.1043	.1125
.500	.0387	.0447	.0564	.0649	.0681
.600	.0221	.0268	.0341	.0399	.0428
.700	.0142	.0166	.0214	.0254	.0280
.800	.0097	.0116	.0138	.0168	.0191
.900	.0064	.0080	.0092	.0115	.0132
1.000	.0047	.0063	.0081	.0093	.0099
1.200	.0022	.0033	.0045	.0046	.0061
1.400	.0011	.0014	.0022	.0029	.0043
1.600	.0009	.0013	.0022	.0018	.0036
1.800	.0004	.0005	.0010	.0018	.0041
2.000	.0004	.0005	.0009	.0018	.0040
2.200	.0004	.0005	.0009	.0021	.0054

GAP DEPTH (T₂ CM)= 1.300
UNIT REY NO. (RE M-1, 10-6)= .100

Z(OR S) (CM)	M .065	M .127	M .254	M .381	M .508
.001	.789	.909	1.122	1.245	1.242
.010	.742	.855	1.055	1.171	1.168
.050	.567	.653	.806	.895	.893
.100	.407	.469	.580	.644	.644
.150	.295	.340	.421	.468	.469
.200	.215	.248	.307	.343	.345
.250	.158	.183	.227	.254	.256
.300	.117	.135	.169	.189	.192
.400	.0663	.0763	.0955	.1035	.1117
.500	.0383	.0443	.0558	.0643	.0675
.600	.0229	.0266	.0339	.0396	.0424
.700	.0141	.0165	.0212	.0252	.0277
.800	.0090	.0105	.0137	.0167	.0189
.900	.0059	.0069	.0092	.0114	.0136
1.000	.0040	.0047	.0063	.0081	.0099
1.200	.0020	.0024	.0033	.0045	.0060
1.400	.0010	.0014	.0020	.0029	.0043
1.600	.0007	.0009	.0016	.0018	.0036
1.800	.0004	.0006	.0010	.0018	.0040
2.000	.0004	.0005	.0009	.0018	.0040
2.200	.0004	.0005	.0010	.0022	.0057

GAP DEPTH (T₂ CM)= 1.000
UNIT REY NO. (RE M-1, 10-6)= 1.000

Z(OR S) (CM)	M .065	M .127	M .254	M .381	M .508
.001	.789	.909	1.122	1.245	1.242
.010	.742	.862	1.052	1.167	1.165
.050	.554	.643	.793	.881	.879
.100	.395	.455	.563	.625	.625
.150	.283	.326	.403	.449	.450
.200	.204	.235	.292	.325	.327
.250	.149	.172	.213	.239	.241
.300	.110	.126	.157	.177	.180
.400	.0611	.0704	.0883	.1002	.1031
.500	.0354	.0409	.0516	.0594	.0622
.600	.0211	.0247	.0313	.0365	.0390
.700	.0133	.0154	.0198	.0235	.0257
.800	.0086	.0100	.0130	.0157	.0177
.900	.0058	.0068	.0089	.0110	.0127
1.000	.0041	.0047	.0063	.0080	.0096
1.200	.0022	.0028	.0036	.0048	.0062
1.400	.0014	.0017	.0023	.0033	.0048
1.600	.0010	.0012	.0018	.0027	.0044
1.800	.0009	.0011	.0017	.0029	.0055
2.000	.0009	.0011	.0017	.0029	.0059
2.200	.0010	.0012	.0020	.0038	.0087

GAP DEPTH (T₂ CM)= 1.000
UNIT REY NO. (RE M-1, 10-6)= 3.000

Z(OR S) (CM)	M .065	M .127	M .254	M .381	M .508
.001	.788	.908	1.121	1.244	1.241
.010	.734	.846	1.044	1.159	1.156
.050	.538	.620	.766	.852	.849
.100	.370	.426	.527	.585	.585
.150	.258	.297	.367	.420	.409
.200	.182	.209	.259	.289	.291
.250	.130	.150	.186	.208	.210
.300	.094	.109	.135	.152	.154
.400	.0515	.0594	.0732	.0840	.0863
.500	.0287	.0343	.0432	.0497	.0524
.600	.0180	.0208	.0269	.0305	.0324
.700	.0115	.0134	.0172	.0199	.0218
.800	.0078	.0090	.0115	.0137	.0156
.900	.0054	.0064	.0082	.0096	.0110
1.000	.0043	.0048	.0062	.0076	.0089
1.200	.0027	.0031	.0043	.0052	.0065
1.400	.0022	.0025	.0033	.0043	.0057
1.600	.0020	.0022	.0029	.0043	.0057
1.800	.0020	.0022	.0029	.0049	.0071
2.000	.0020	.0022	.0046	.0077	.0111
2.200	.0020	.0023	.0078	.0133	.0226

ECUA.ION 15-5,LAM.TRANS GAP

GAP DEPTH (T₂ CM)= 2.000
UNIT REY NO. (RE M-1, 10-6)= .010

Z(OR S) (CM)	M .065	M .127	M .254	M .381	M .508
.001	.789	.909	1.122	1.245	1.242
.010	.742	.855	1.055	1.171	1.168
.050	.567	.653	.806	.895	.893
.100	.407	.469	.580	.644	.644
.150	.295	.340	.421	.468	.469
.200	.215	.248	.307	.343	.345
.250	.158	.183	.227	.254	.256
.300	.117	.135	.169	.189	.192
.400	.0663	.0763	.0955	.1035	.1117
.500	.0383	.0443	.0558	.0643	.0675
.600	.0229	.0266	.0339	.0396	.0424
.700	.0141	.0165	.0212	.0252	.0277
.800	.0090	.0105	.0137	.0167	.0189
.900	.0059	.0069	.0092	.0114	.0136
1.000	.0040	.0047	.0063	.0081	.0099
1.200	.0020	.0024	.0033	.0045	.0060
1.400	.0010	.0014	.0020	.0029	.0043
1.600	.0007	.0009	.0016	.0018	.0036
1.800	.0004	.0006	.0010	.0018	.0040
2.000	.0004	.0005	.0009	.0018	.0040
2.200	.0004	.0005	.0009	.0021	.0054

GAP DEPTH (T₂ CM)= 2.606
UNIT REY NO. (RE M-1, 10-6)= .100

Z(OR S) (CM)	M .065	M .127	M .254	M .381	M .508
.001	.789	.909	1.122	1.245	1.242
.010	.742	.855	1.055	1.171	1.168
.050	.567	.653	.806	.895	.893
.100	.407	.469	.580	.644	.644
.150	.295	.340	.421	.468	.469
.200	.215	.248	.307	.343	.345
.250	.158	.183	.227	.254	.256
.300	.117	.135	.169	.189	.192
.400	.0663	.0763	.0955	.1035	.1117
.500	.0383	.0443	.0558	.0643	.0675
.600	.0229	.0266	.0339	.0396	.0424
.700	.0141	.0165	.0212	.0252	.0277
.800	.0090	.0105	.0137	.0167	.0189
.900	.0059	.0069	.0092	.0114	.0136
1.000	.0040	.0047	.0063	.0081	.0099
1.200	.0020	.0024	.0033	.0045	.0060
1.400	.0010	.0014	.0020	.0029	.0043
1.600	.0007	.0009	.0016	.0018	.0036
1.800	.0004	.0006	.0010	.0018	.0040
2.000	.0004	.0005	.0009	.0018	.0040
2.200	.0004	.0005	.0009	.0021	.0054

GAP DEPTH (T₂ CM)= 2.000
UNIT REY NO. (RE M-1, 10-5)= 1.000

Z(OR S) (CM)	M .065	M .127	M .254	M .381	M .508
.001	.789	.909	1.122	1.245	1.242
.010	.742	.862	1.052	1.167	1.165
.050	.554	.643	.793	.881	.879
.100	.395	.455	.563	.625	.625
.150	.283	.326	.403	.449	.450
.200	.204	.235	.292	.325	.327
.250	.149	.172	.213	.239	.241
.300	.110	.126	.157	.177	.180
.400	.0611	.0705	.0883	.1000	.1031
.500	.0353	.0409	.0514	.0589	.0616
.600	.0212	.0246	.0311	.0362	.0384
.700	.0133	.0154	.0196	.0231	.0252
.800	.0086	.0100	.0128	.0154	.0179
.900	.0058	.0067	.0087	.0109	.0122
1.000	.0041	.0047	.0061	.0076	.0091
1.200	.0022	.0025	.0034	.0044	.0056
1.400	.0014	.0016	.0022	.0028	.0041
1.600	.0010	.0012	.0016	.0023	.0034
1.800	.0008	.0009	.0013	.0021	.0037
2.000	.0008	.0011	.0015	.0024	.0048

GAP DEPTH (T₂ CM)= 2.000
UNIT REY NO. (RE M-1, 10-6)= 3.000

Z(OR S) (CM)	M .065	M .127	M .254	M .381	M .508
.001	.788	.908	1.121	1.244	1.241
.010	.734	.846	1.044	1.159	1.156
.050	.538	.620	.766	.852	.849
.100	.370	.426	.527	.585	.585
.150	.258	.297	.367	.420	.420
.200	.182	.209	.259	.289	.291
.250	.130	.150	.186	.208	.210
.300	.094	.109	.135	.151	.153
.400	.0514	.0593	.0731	.0833	.0854
.500	.0286	.0341	.0426	.0484	.0503
.600	.0178	.0208	.0258	.0296	.0312
.700	.0115	.0132	.0165	.0191	.0204
.800	.0077	.0088	.0110	.0129	.0140
.900	.0055	.0062	.0078	.0091	.0101
1.000	.0041	.0046	.0058	.0068	.0076
1.200	.0026	.0029	.0035	.0042	.0048
1.400	.0020	.0022	.0028	.0033	.0038
1.600	.0020	.0022	.0028	.0033	.0038
1.800	.0020	.0022	.0028	.0033	.0038
2.000	.0020	.0022	.0028	.0033	.0038
2.200	.0020	.0022	.0028	.0033	.0038

ORIGINAL PAGE IS
OF POOR QUALITY

EQUATION 15-5,LAM.TRANS GAP

GAP DEPTH (T, CM)= 3.000
UNIT REY NO. (RE M-1, 10-6)= .010

Z(OR S) (CM)	W .065	W .127	W .254	W .381	W .508
.001	.749	.909	1.122	1.245	1.242
.010	.742	.855	1.056	1.172	1.169
.050	.567	.694	.807	.896	.894
.100	.407	.471	.581	.646	.646
.150	.295	.346	.422	.470	.471
.200	.215	.248	.309	.345	.347
.250	.158	.183	.228	.255	.258
.300	.117	.135	.170	.191	.194
.400	.0660	.0763	.0965	.1093	.1126
.500	.0383	.0443	.0569	.0643	.0681
.600	.0229	.0266	.0338	.0395	.0428
.700	.0141	.0164	.0211	.0251	.0280
.800	.0085	.0099	.0127	.0156	.0191
.900	.0059	.0069	.0091	.0113	.0135
1.000	.0040	.0047	.0063	.0081	.0099
1.200	.0020	.0024	.0033	.0045	.0061
1.400	.0011	.0014	.0020	.0029	.0043
1.600	.0007	.0009	.0013	.0022	.0036
1.800	.0004	.0005	.0009	.0018	.0030
2.000	.0004	.0005	.0009	.0020	.0034

GAP DEPTH (T, CM)= 3.000
UNIT REY NO. (RE M-1, 10-6)= .100

Z(OR S) (CM)	W .065	W .127	W .254	W .381	W .508
.001	.788	.908	1.121	1.244	1.241
.010	.734	.846	1.044	1.159	1.156
.050	.538	.620	.766	.850	.849
.100	.373	.426	.527	.585	.585
.150	.258	.297	.367	.408	.409
.200	.182	.209	.259	.289	.291
.250	.130	.150	.185	.207	.209
.300	.094	.108	.134	.151	.152
.400	.0513	.0591	.0734	.0827	.0845
.500	.0295	.0339	.0421	.0477	.0493
.600	.0179	.0205	.0264	.0298	.0321
.700	.0114	.0130	.0166	.0182	.0193
.800	.0076	.0086	.0106	.0121	.0128
.900	.0054	.0061	.0073	.0083	.0089
1.000	.0040	.0044	.0052	.0059	.0064
1.200	.0022	.0025	.0031	.0034	.0036
1.400	.0013	.0015	.0020	.0022	.0023
1.600	.0009	.0010	.0015	.0015	.0016
1.800	.0007	.0008	.0011	.0010	.0008
2.000	.0008	.0009	.0012	.0009	.0006

EQUATION 15-5,LAM.TRANS GAP

GAP DEPTH (T, CM)= 4.000
UNIT REY NO. (RE M-1, 10-6)= .010

Z(OR S) (CM)	W .065	W .127	W .254	W .381	W .508
.001	.749	.909	1.122	1.245	1.242
.010	.742	.855	1.056	1.172	1.169
.050	.567	.694	.807	.896	.894
.100	.407	.471	.581	.646	.646
.150	.295	.346	.422	.470	.471
.200	.215	.248	.309	.345	.347
.250	.158	.183	.228	.255	.258
.300	.117	.135	.170	.191	.194
.400	.0660	.0763	.0965	.1093	.1126
.500	.0383	.0443	.0569	.0643	.0681
.600	.0229	.0266	.0338	.0395	.0428
.700	.0141	.0164	.0211	.0251	.0280
.800	.0085	.0099	.0127	.0156	.0191
.900	.0059	.0069	.0091	.0113	.0135
1.000	.0040	.0047	.0063	.0081	.0099
1.200	.0020	.0024	.0033	.0045	.0061
1.400	.0011	.0014	.0020	.0029	.0043
1.600	.0007	.0009	.0013	.0022	.0036
1.800	.0004	.0005	.0009	.0018	.0030
2.000	.0004	.0005	.0009	.0020	.0034

GAP DEPTH (T, CM)= 4.000
UNIT REY NO. (RE M-1, 10-6)= .100

Z(OR S) (CM)	W .065	W .127	W .254	W .381	W .508
.001	.788	.908	1.121	1.244	1.241
.010	.734	.846	1.044	1.159	1.156
.050	.538	.620	.766	.850	.849
.100	.373	.426	.527	.585	.585
.150	.258	.297	.367	.408	.409
.200	.182	.209	.259	.289	.291
.250	.130	.150	.185	.207	.209
.300	.094	.108	.134	.151	.152
.400	.0513	.0591	.0734	.0827	.0836
.500	.0295	.0339	.0421	.0477	.0482
.600	.0179	.0205	.0264	.0298	.0290
.700	.0114	.0130	.0166	.0182	.0182
.800	.0076	.0086	.0106	.0121	.0124
.900	.0054	.0061	.0073	.0083	.0079
1.000	.0040	.0044	.0052	.0059	.0058
1.200	.0022	.0025	.0031	.0034	.0027
1.400	.0013	.0015	.0020	.0022	.0019
1.600	.0009	.0010	.0015	.0015	.0014
1.800	.0008	.0010	.0015	.0010	.0008
2.000	.0009	.0011	.0016	.0009	.0006

APPENDIX C

GAP HEATING CALCULATION PROCEDURE LISTING

A complete discussion of the calculation procedures is contained in Section 6.0. The following 23 pages contain the detail listing of the gap heating calculation procedure. It is written in Fortran IV and consists of a labeled common (COMGAP), a main (QRATIO) and 36 subroutines. A list of program components is shown at the right. QRATIO is a demonstration main program and should be re-written to interface with the other parts of a gap thermal model. A sample output from the procedure is shown at the bottom of this page.

```
 /COMGAP/
QRATIO
GAPM
CSCOTT
EQ41716
QRF
TBLU
EQ4D9
SMAXF
SMINF
QRF4D9
EQ4D10
QRF4D10
QRF4D11
EQ4D11
EQ4D13
QRF4D13
EQ4D14
QRF4D14
EQ4D15
QRF4D15
EQ150=
QRF15D5
EQ9
QRF9
EQ25
EQ18
EQ12A
EQ1601
QRF1601
EQ1602
QRF1602
EQ16D34
QR16D34
EQ16D56
QR16D56
EQ17123
QR17123
```


SAMPLE OUTPUT

TRANSVERSE GAP, DUMN, H/HE, HCF/JSC (EQ.8)
COMPUTED HEATING DISTRIBUTION GAP WIDTH= .254 CM

I	Z(CM)	Q	QRATIO
1	0.00000	.90576	.90576
2	.05000	.40150	.40150
3	.07500	.25165	.25165
4	.10000	.15151	.15151
5	.15000	.04867	.04867
6	.20000	.01331	.01331
7	.30000	.00061	.00061
8	.40000	0.00000	0.00000
9	.50000	0.00000	0.00000
10	.60000	0.00000	0.00000
11	.70000	0.00000	0.00000
12	.80000	0.00000	0.00000
13	.90000	0.00000	0.00000
14	1.00000	0.00000	0.00000

```
      PROGRAM QRATIO(INPUT=100,OUTPUT,TAPE5=INPUT,TAPE6=OUTPUT)
C       GAP HEATING FACTORS GENERATED BY CORRELATION EQ.
C                          MARCH 1975   H.E. CHRISTENSEN
C
C       ---- TEST MAIN
C
      COMMON /COMGAP/ ARGL(25), ZMIN,FMIN,DFDZA, ZMAX, FMAX,DFDZB
      DIMENSION ZZ(25), QQ(25)
      DATA IBL,IGLOC,IGAPC,IHOH/1,2,1,1/
      DATA ZZ /0.0,0.05,0.075,0.10,0.15,0.20,0.30,0.4,0.5,0.6,
     1         0.7,0.8,0.9,1.0,1.2,1.4,1.6,1.8,2.0,2.5,3.0,3.5,4.0/
      DATA NTAB/23/
      DATA ICOR,W, T, REPM /12, 0.254, 4.0, 1.0E+06/

      EQUIVALENCE (ARGL(3),ICOR), (ARGL(7),W),( ARGL(8),T),
     1       (ARGL(14),REPM),(ARGL(1),IBL),
     2       (ARGL(2),IGLOC),(ARGL(4),IGAPC)
C
      ITRIG=1
C
C       ITRIG = -1, ALL PARAMETERS NECSSARY TO SELECT AND EVALUATE
C                   GAP HEATING EQUATION ARE CONTAINED IN  (ARGL)
C
C       ITRIG =  1, NAMELIST INPUT OF ADDITIONAL (ARGL) VALUES.
C
C       ITRIG =  2  IS SET TO (2) BY SUBROUTINES AFTER FIRST PASS.
C
C     DEFAULT--- TRANSVERSE GAP (EQ.9)  HCF/JSC TESTS (EQ.9)  ICOR =12
      CALL GAPH(ITRIG,NTAB,ZZ,Y,QQ)
C
      STOP 1
      END
```

```
      SUBROUTINE GAPH( ITRIG, NTAB, ZZ, Y , QQ )
C
CCC   GAP HEATING CALCULATION METHOD
CCC                                          H.E. CHRISTENSEN  75
CCC
C
      COMMON /COMGAP/ ARGL(25), SMIN,FMIN,DFDSA,SMAX,FMAX,DFDSB
C
      DIMENSION  ZZ(25),          QQ(25), IRGL(25), ZTAB(25),QTAB(25),
     1           SS(25)
      EQUIVALENCE (ARGL,IRGL), (Z,S)
C
      EQUIVALENCE (ARGL(1),IBL), (ARGL(2), IGLOC), (ARGL(3), ICOR),
     1            (ARGL(4),IGAPC),(ARGL(5),E),     (ARGL(6), GAMMA),
     2            (ARGL(7),GAPW ),(ARGL(8),GAPD ), (ARGL(9), STEP ),
     3            (ARGL(10),GAPFL),(ARGL(11),HOHLOW),(ARGL(12),HOHHI),
     4            (ARGL(13),AMACH),(ARGL(14),REPM),(ARGL(15),THETA),
     5            (ARGL(16),DTHK ),(ARGL(17),SLYR ),(ARGL(18),HFP  ),
     6            (ARGL(19),TWOTE),(ARGL(20),IHOH )
C
      DATA SS/-9999./
C
      DATA SMIN,SMAX/-1.E+30, 1.E+30/
      DATA E,GAMMA,GAPW, GAPD, STEP, GAPFL, HOHLOW, HOHHI,AMACH,
     1     REPM,DTHK,SLYR,HFP,TWOTE/
     2     0.0000,0.0,0.254,5.0,0.0,10.0,0.0001,3.0,5.0,1.0E+06,0.1,
     3    0.001,1.0,1.0/
C
CCC   AVERAGED GAP HEATING FROM AMES 3.5 FT H.W.T.
C
      DATA ITQ /12/
C     ZTAB (INCH)
      DATA ZTAB /0.0, 0.01, 0.015, 0.023, 0.036, 0.060, 0.10, 0.14,
     1 0.23, 0.30, 0.50, 5.00/
      DATA QTAB /1.6, 1.2, 1.0, 0.8, 0.6, 0.4, 0.2, 0.1, 0.05, 0.025,
     1 0.0, 0.0/
      DATA  ID /12/
C
CC
      NAMELIST/LIST1/ ARGL,IRGL,IBL,IGLOC,ICOR,E, GAMMA,GAPW,GAPD,
     1           STEP, GAPFL,HOHLOW,HOHHI,AMACH, REPM,DTHK,SLYR,HFP,
     2               TWOTE,IHOH,ZTAB,QTAB,ITQ,NTAB,ZZ,Y,SS
C
CC
      IF(ITRIG.EQ.2) GO TO 10
C
      IF(ITRIG.EQ. -1)  READ(5,LIST1)
      WRITE(6,900)
C
      IF(SS(1).LT.-9990.) GO TO 4
      DO 2 I=1,NTAB
    2 ZZ(I)= SS(I)
    4 CONTINUE
      DO 5 I=1,ITQ
    5 SS(I)=ZZ(I)
C
      WRITE(6,LIST1)
```

```
C
CCC     ----- EQUATION  DECISION
CCC
C
   10 IF(ICOR .GT. 0) GO TO 50
C
CCC
C
      IF(IBL.NE.1 .OR. E.EQ. 0.0) GO TO 12
C
CC    CORRELATIONS FROM EDGE RADIUSED MODELS
      IF(IGLOC.EQ.2  .AND.  IHOH.EQ.1)                          ICOR = 3
      IF(ICOR.NE.ID ) GO TO 50
      IF(IGLOC.EQ.2  .AND.  IHOH.EQ.2)                          ICOR = 4
      IF(ICOR.NE.ID ) GO TO 50
      IF(IGLOC.EQ.3  .AND.  IHOH.EQ.1 .AND.GAPFL.LE. 15.24)     ICOR = 5
      IF(ICOR.NE.ID ) GO TO 50
      IF(IGLOC.EQ.3  .AND.  IHOH.EQ.1 .AND.GAPFL.GT. 15.24)     ICOR = 6
      IF(ICOR.NE.ID ) GO TO 50
      IF(IGLOC.EQ.1  .AND.  IHOH.EQ.1)                          ICOR = 7
      IF(ICOR.NE.ID ) GO TO 50
      IF(IGLOC.EQ.3  .AND.  IHOH.EQ.2 .AND.GAPFL.LE. 15.24)     ICOR = 8
      IF(ICOR.NE.ID ) GO TO 50
      IF(IGLOC.EQ.3  .AND.  IHOH.EQ.2 .AND.GAPFL.GT. 15.24)     ICOR = 9
      IF(ICOR.NE.ID ) GO TO 50
      IF(IGLOC.EQ.1  .AND.  IHOH.EQ.2 )                         ICOR = 10
C
CCC   CORRELATION FOR TRANSVERSE GAP,DOWN-STREAM WALL, LAMINAR (15-5)
C
   12 IF(IBL.EQ.1 .AND. IGLOC.EQ.2)                             ICOR = 11
C
CCC   IN-LINE GAP   HCF/JSC   (EQ.25)
C
      IF(IBL.EQ.1 .AND. IGLOC.EQ.3)                             ICOR = 13
      IF(ICOR.NE.ID ) GO TO 50
C
CCC   TRANSVERSE GAP, DOWN STREAM WALL, TURBULENT (EQ. 18)
C
      IF(IBL.EQ.3 .AND. IGLOC.EQ.2)                             ICOR = 14
      IF(ICOR.NE.ID ) GO TO 50
C
CC    EFFECT OF GAMMA ON TRANSVERSE GAP, TURBULENT  (EQ. 12A)
      IF(IBL.EQ.3 .AND. IGLOC.EQ.2  .AND.GAMMA.NE.0.0)          ICOR = 15
      IF(ICOR.NE.ID ) GO TO 50
      IF(IGLOC.NE.6) GO TO 14
      IF(ICOR.NE.ID ) GO TO 50
C
CC    LONG  IN-LINE GAP CORRELATION     (EQ. 16-1  TO  EQ 16-6)
      IF(GAMMA.EQ. 0.0  .AND. IHOH.EQ.1)                        ICOR = 16
      IF(ICOR.NE.ID ) GO TO 50
      IF(GAMMA.EQ. 0.0  .AND. IHOH.EQ.2)                        ICOR = 17
      IF(ICOR.NE.ID ) GO TO 50
      IF(IGLOC.EQ. 1    .AND. IHOH.EQ.1)                        ICOR = 18
      IF(ICOR.NE.ID ) GO TO 50
      IF(IGLOC.EQ. 2    .AND. IHOH.EQ.1)                        ICOR = 19
      IF(IGLOC.EQ. 1    .AND. IHOH.EQ.2)                        ICOR = 20
      IF(IGLOC.EQ.2     .AND. IHOH.EQ.2)                        ICOR = 21
      IF(ICOR.NE.ID ) GO TO 50
C
CCC   STEPS
C
   14 IF(STEP.EQ.0.0) GO TO 50
      IF(IBL.EQ.1)                                              ICOR = 22
      IF(IBL.EQ.2)                                              ICOR = 23
      IF(IBL.EQ.3)                                              ICOR = 24
C
```

```
C
C       JUATION SELECTED
   50 CONTINUE
      I=1
      Z=ZZ(I)
      GO TO 94
C
   55 IF( S.LT.SMIN) GO TO 70
      IF( S.GT. SMAX) GO TO 80
      GO TO 94
C                    HEATING RATIO EVALUATED
CC
C     SECOND ORDER CURVE FIT BETWEEN SMIN AND S=0
   70 XLNQR = (BMIN    + CMIN*S)*S
      GO TO 90
C
C     LINEAR EXTRAPOLATION INTO GAP BELOW INSTRUMENTATION
   80 XLNQR = FMAX + DFDSB*(S-SMAX)
   90 Q = EXP(XLNQR)
      GO TO 2000
C
CC    -----CONSTANTS COMPUTED DURING ITRIG=1 PASS
CC
CC    BRANCHING TO EQUATION SUBROUTINES
C
   94 GO TO (1010,1020,1030,1040,1050,1060,1070,1080,1090,1100,
     1        1110,1120,1130,1140,1150,1160,1170,1180,1190,1200,
     2        1210,1220,1230,1240,1250,1260,1270),ICOR
C
CCC
CCCC
CCCCC
C
C     TABLE LOOK-UP
 1010 IF(ITRIG.EQ.2) GO TO 1012
      WRITE(6,901)
      DO 1011 K=1,ITQ
      WRITE (6,950) K,ZTAB(K),QTAB(K)
 1011 CONTINUE
      ITRIG = 2
      IMEM = 2
      GO TO 55
 1012 CALL TBLU(IDUM,IMEM,Z,ZTAB,Q,QTAB)
      GO TO 2000
C     SCOTT AVERAGE OF TRANSVESE GAP LP AND DOWN WALLS
C
 1020 IF(ITRIG.EQ.2) GO TO 1022
      WRITE(6,902)
      IR = 1
      IF(E.GE. 0.3048 ) IR = 2
      GO TO 55
 1022 CALL CSCOTT(IR,S,Q)
      GO TO 2000
C
CCC
CCCC
C     TRANSVERSE GAP, DOWN  (EQ.4-17), LAMINAR,  (H/HFP)
C
 1030 IF(ITRIG.EQ.1) WRITE(6,903)
      CALL EQ41716(ITRIG,S,Q,ICOR)
      GO TO 2000
C
CC    TRANSVERSE  GAP, DOWN  (EQ.4-16),LAMINAR, (H/HE)
C
 1040 IF(ITRIG.EQ.1) WRITE(6,904)
      CALL EQ41716(TRIG,S,Q,ICOR)
      GO TO 2000
C
C     IN-LINE GAP UP-STREAM OF JUNCTION, LAMINAR (H/HFP),EQ.4-9
 1050 IF(ITRIG.EQ.1) WRITE(6,905)
      CALL EQ409(ITRIG,S,Q,ICOR)
      GO TO 2000
C
```

```
C       IN-LINE GAP  DWN-STREAM,LAMINAR (H/HFP), EQ.4-10
 1060   IF(ITRIG.EQ.1) WRITE(6,906)
        CALL EQ4010(ITRIG,S,Q,ICOR)
        GO TO 2000
C
C       TRANSVERSE GAP, UPSTREAM, LINEAR (H/HFP), (EQ.4-11)
 1070   IF(ITRIG.EQ.1) WRITE(6,907)
        CALL EQ4D11(ITRIG,S,Q)
C        GO TO 2000
CCC
C       IN-LINE GAP (H/HE), UP, (EQ. 4-13)
C
 1080   IF(ITRIG.EQ.1) WRITE(6,908)
        CALL EQ4D13(ITRIG,S,Q)
        GO TO 2000
C
CC      IN-LINE GAP (H/HE), DOWN,( EQ.4-14)
 1090   IF(ITRIG.EQ.1) WRITE(6,909)
        CALL EQ4D14(ITRIG,S,Q)
        GO TO 2000
C
CC      TRANSVERSE GAP(H/HE), UP (EQ.4-15)
C
 1100   IF(ITRIG.EQ.1) WRITE(6,910)
        CALL EQ4D15(ITRIG,S,Q)
        GO TO 2000
C
CC      TRANSVERSE GAP, DOWN, H/HFP, LAMINAR, 3TEST PROGRAMS,(EQ 15-5)
C
 1110   IF(ITRIG.EQ.1) WRITE(6,911)
        CALL EQ15D5(ITRIG,S,Q)
        GO TO 2000
C
C       TRANSVERSE GAP, DOWN, H/HE, HCF/JSE(EQ.9)
C
 1120   IF(ITRIG.EQ.1) WRITE(6,912)
        CALL EQ9(ITRIG,S,Q)
        GO TO 2000
C
CC      IN-LINE GAP(H/HE) ,HCF/JSC (EQ.25)
C
 1130   IF(ITRIG.EQ.1) WRITE (6,913)
        CALL EQ25(ITRIG,S,Q)
        GO TO 2000
C
C       TRANSVERSE GAP TURBULENT (CFAT,M=8), (EQ. 18)
 1140   IF(ITRIG.EQ.1) WRITE (6,914)
        CALL EQ18(ITRIG,S,Q)
        GO TO 2000
C
CC       INFLUENCE OF GAMMA, TRANSVERSE GAP  (EQ. 12A)
C
 1150   IF(ITRIG.EQ.1) WRITE(6,915)
        CALL EQ12A (ITRIG,Z,Y,Q)
        GO TO 2000
C
C
CCC
C       H/HFP , LONG IN-LINE GAP , LAMINAR,  GAMMA=0  (EQ.16-1)
C
 1160   IF(ITRIG.EQ.1) WRITE(6,916)
        CALL EQ16D1(ITRIG,Z,Q)
        GO TO 2000
C
CC      H/HE ,  LONG IN-LINE GAP,  LAMINAR,  GAMMA=0   (EQ.16-2)
C
 1170   IF(ITRIG.EQ.1) WRITE(6,917)
        CALL EQ16D2(ITRIG,Z,Q)
        GO TO 2000
C
```

```
C       H/HFP,  LONG IN-LINE GAP, LAMINAR, GAMMA UP TO 15, SIDES A/B EQ16-3
C
 1180   IF(ITRIG.EQ.1) WRITE(6,918)
        CALL EQ16034(ITRIG,Z,Q)
        GO TO 2000
C
CC      H/HFP, LONG IN-LINE GAP, LAMINAR, GAMMA UP TO 15, SIDE A (EQ.16-4)
C
 1190   IF(ITRIG.EQ.1) WRITE (6,919)
        CALL EQ16034(ITRIG,Z,Q)
        GO TO 2000
C
CC      H/HE,  LONG IN-LINE GAP, LAMINAR, GAMMA UP TO 15,SIDES A/B EQ.16-5
C
 1200   IF(ITRIG.EQ.1) WRITE (6,920)
        CALL EQ16056(ITRIG,Z,Q)
        GO TO 2000
C
CC      H/HE, LONG IN-LINE GAP, LAMINAR, GAMMA UP TO 15,SIDE A (EQ.16-6)
C
 1210   IF(ITRIG.EQ.1) WRITE (6,921)
        CALL EQ16056(ITRIG,Z,Q)
        GO TO 2000
 1220   IF(ITRIG.EQ.1) WRITE(6,922)
        CALL EQ17123(ITRIG,Z,Y,Q)
        GO TO 2000
 1230   IF(ITRIG.EQ.1) WRITE(6,923)
        CALL EQ17123(ITRIG,Z,Y,Q)
        GO TO 2000
 1240   IF(ITRIG.EQ.1) WRITE(6,924)
        CALL EQ17123(ITRIG,Z,Y,Q)
        GO TO 2000
 1250   CONTINUE
 1260   CONTINUE
 1270   CONTINUE
C
CC
C
 2000   CONTINUE
        IF(ITRIG.EQ.2) GO TO 2010
C
C
        ITRIG = 2
        CMIN = -(FMIN -SMIN*DFDSA)/(SMIN*SMIN)
        BMIN =  (FMIN-CMIN*SMIN*SMIN)/SMIN
        GO TO 55
 2010   CONTINUE
C
C
        IF(Q.LT. HOHLOW) Q =0.0
        IF(Q.GT. HOHHI) Q=HOHHI
C
        QQ(I) = Q
        IF( I.EQ. NTAB) GO TO 3000
        I = I+1
        Z = ZZ(I)
        GO TO 55
 3000   WRITE(6,952) GAPW
        DO 3010 I=1,NTAB
        QR = QQ(I)
        QQ(I) = QQ(I)*HFP
        WRITE(6,954) I,ZZ(I),QQ(I),QR
 3010   CONTINUE
        RETURN
```

```
900 FORMAT(*1 USER SUPPLIED PARAMETERS TO GAP HEATING DISTRIBUTION*)
901 FORMAT(* HEATING RATIO INPUT TABLE*/*    I    Z(CM)    QRATIO*/)
902 FORMAT(* AVERAGED GAP HEATING IN TRANSVERSE GAP (C.SCOTT DATA)*)
903 FORMAT(* CORRELATION  OF TRANSVERSE GAP ,E-EFFECT(EQ.4-17)*)
904 FORMAT(* CORRELATION  OF TRANSVERSE GAP ,E-EFFECT(EQ.4-16 H/HE)*)
905 FORMAT(* IN-LINE GAP,H/HFP, UP-STREAM OF JUNCTION (EQ. 4-9)*)
906 FORMAT(* IN-LINE GAP,H/HFP, DW-STREAM OF JUNCTION (EQ. 4-10)*)
907 FORMAT(* TRANSVERSE CAP,UP, H/HFP (EQ. 4-11)*)
908 FORMAT(* IN-LINE GAP,UP, H/HE   (EQ.4-13)*)
909 FORMAT(* IN-LINE GAP,DN H/HE   (EQ.4-14)*)
910 FORMAT(* TRANSVERSE GAP,UP, H/HE   (EQ. 4-15)*)
911 FORMAT(* TRANSVERSE GAP,DWN, H/HFP, LAMINAR (EQ.15-5)*)
912 FORMAT(* TRANSVERSE GAP, DOWN, H/HE , HCF/JSC (EQ.9)*)
913 FORMAT(* IN-LINE GAP (H/HE), HCF/JSC (EQ.25)*)
914 FORMAT(* TRANSVERSE GAP TURBULENT CFHT,M=8 (EQ.18) *)
915 FORMAT(* TRANSVERSE GAP TURBULENT CFHT,M=8 (EQ.18) *)
916 FORMAT(* H/HFP, LONG IN-LINE GAP, LAMINAR,GAMMA=0 (EQ.16-1)*)
917 FORMAT(* H/HE, LONG IN-LINE GAP, LAMINAR,GAMMA=0 (EQ.16-2)*)
918 FORMAT(* H/HFP,LONG IN-LINE GAP,LAMINAR,GAMMA=UP TO 15, SIDES A/B
   1 (EQ.16-3)*)
919 FORMAT(* H/HFP, LONG IN-LINE GAP, LAMINAR,GAMMA UP TO 15, SIDE A
   1 (EQ.16-4)*)
920 FORMAT(* H/HE, LONG IN-LINE GAP, LAMINAR,GAMMA UP TO 15, SIDES A/B
   1 (EQ. 6-5)*)
921 FORMAT(* H/HE, LONG IN-LINE GAP, LAMINAR,GAMMA UP TO 15, SIDE A
   1 (EQ.16-6)*)
922 FORMAT(* TRANSVERSE STEP, LAMINAR FLOW*)
923 FORMAT(* TRANSVERSE STEP, TRANSITION  *)
924 FORMAT(*TRANSVERSE STEP, LTURBULENT   *)
950 FORMAT(I4,2F10.5)
952 FORMAT(*   COMPUTED HEATING DISTRIBUTION  GAP WIDTH=*F8.3,* CM*/
   1*    I    Z(CM)         Q          QRATIO*)
954 FORMAT(I4,3F10.5)
    END
```

```
      SUBROUTINE CSCOTT(IR,SCM,QR)
C
CCC   GAP HEATING DISTRIBUTION DATA FROM CARL SCOTT
CCCCC
CCC   ----  FOR GAP WIDTH = 0.10 INCH
CCCCC
CCC   Q/QREF = F(S,EDGE RAD)      (DIMENSIONS ARE IN INCHES)
C
      DIMENSION SCOTTS(18,2),SCOTTQ(18,2)
      DIMENSION CS0(2),CS1(2),CS2(2),CS3(2)
      DATA ISCOTT / 18 /
      DATA SCOTTS / -100.0, -0.26, -0.14, -0.10, -0.08, -0.04, -0.02,
     1     -0.01, 0.0, 0.06, 0.10, 0.16, 0.20, 0.28, 1.0, 2.0,
     2     10.0, 100.0,
     3     -100.0, -0.30, -0.20, -0.15, -0.10, -0.06, -0.02, 0.0, 0.02,
     4     0.06, 0.10, 0.15, 0.20, 0.22, 0.30, 0.36, 0.40, 100.0 /
      DATA SCOTTQ / 0.93, 0.93, 0.94, 0.96, 0.99, 1.02, 1.03, 1.00,
     1     0.96, 0.80, 0.48, 0.36, 0.24, 0.0, 4*0.0,
     2     0.95, 0.95, 0.96, 0.97, 0.98, 1.00, 1.02, 1.01, 0.98, 0.95,
     3     0.90, 0.80, 0.55, 0.45, 0.27, 0.08, 0.0, 0.0 /
      DATA CS0 / 0.965, 0.975 /
      DATA CS1 / 0.035, 0.025 /
      DATA CS2 / 0.06, 0.30 /
      DATA CS3 / 2.88, 2.575 /
      S = SCM/2.54
      IF(S.LT.SCOTTS(2,IR)) GO TO 156
      CALL TBLU(IDUM,IMEM,ISCOTT,S,SCOTTS(1,IR),QR,SCOTTQ(1,IR))
      GO TO 157
  156 QR = CS0(IR)-CS1(IR)*COS(PI*(-S-CS2(IR))/CS3(IR))
  157 CONTINUE
      RETURN
      END
```

```
      SUBROUTINE EQ41716(ITRIG,S,QR,ICORR)
C
CCC   GAP HEATING DISTRIBUTION USING EQUATIONS 4-17 AND 4-16
CCC
CCC   ICORR = 3,  EQUATION 4-17
CCC   ICORR = 4,  EQUATION 4-16
C
      COMMON / COMGAP / ARGL(25),SMIN,FMIN,DFDSA,SMAX,FMAX,DFDSB
      DIMENSION C(5)
      EQUIVALENCE (ARGL(5),E),(ARGL(7),W),(ARGL(21),T)
      DIMENSION XE(4),XSMAX(4),XSMIN(4)
      DATA XE / 0.15748, 0.318, 0.635, 1.270 /
      DATA XSMIN / 0.400, 0.540, 0.810, 1.350 /
      DATA XSMAX / 0.900, 1.050, 1.850, 3.000 /
      DATA IS / 4 /
   11 FORMAT(6X,12HCOEFFICIENTS,2X,5F10.5/6X,10HSMIN,QRMIN,4X,2F10.5/
     1    6X,10HSMAX,QRMAX,4X,2F10.5)
   12 FORMAT(6X,9HCMIN,BMIN,5X,2F10.5)
C
CCCCC F = C1+C2*S+C3*S**3+C4/S**2+C5*LN(S)   =  LN(Q/QREF)
CCCCC
C     ----- INITIALIZE
      IF(ITRIG.GE.2) GO TO 100

      IF(ICORR.EQ.4) GO TO 20
C
CCC   -----CONSTANTS FOR EQUATION 4-17
C
      C(1) = 0.59775+3.05060*E
      C(2) = -3.67827-0.09307/W
      C(3) = 0.14962
      C(4) = -0.27898*E*E
      C(5) = 0.0
      GO TO 40
C
CCC   ----- CONSTANTS FOR EQUATION 4-16
C
   20 CONTINUE
      C(1) = 0.42466+3.84088*(W+E)-2.18027*W*E*E
      C(2) = -5.14719
      C(3) = 0.19450
      C(4) = -0.30623*E*E
      C(5) = 2.27613*E
C
CCC   DETERMINE VALUES AT S EXTREMES OF CORRELATION
CCC   ----- INTERPOLATE TO OBTAIN SMAX AND SMIN = F(E)
C
   40 CONTINUE
      IMEM = 2
      CALL TBLU(IDUM,IMEM,IS,E,XE,SMAX,XSMAX)
      CALL TBLU(IDUM,IMEM,IS,E,XE,SMIN,XSMIN)
      QRMAX = QRF(C,SMAX)
      ALNQRMX = ALOG(QRMAX)
      DALNQS = 2.0*(T-SMAX)*ALOG(0.10)
      DFDSB = DALNQS
C     ----- COEFFICIENTS FOR CORRELATION
CCC         AT LOW END OF CURVES
CCC         MATCHING DFDS AT SMIN
C
      DFDSA = C(2)+3.0*C(3)*SMIN*SMIN-2.0*C(4)/(SMIN**3)+C(5)/SMIN
      FMIN = ALOG(QRMIN)
      GO TO 160
C
CCC   DETERMINE GAP HEATING RATIO
C
  100 CONTINUE
      QR = QRF(C,S)
C
CCC   -----  DALNQS = SLOPE OF 1 CYCLE PER 0.5 CM FROM SMAX TO T
C
  160 RETURN
      END
```

```
      FUNCTION QRF(C,S)
C
C     CORRELATION EXPRESSION TO EQUATIONS 4-17 AND 4-16
C
      DIMENSION C(1)
      XLNQR = C(1)+C(2)*S+C(3)*S*S*S+C(4)/(S*S)+C(5)*ALOG(S)
      QRF = EXP(XLNQR)
      RETURN
      END
```

```
      SUBROUTINE TBLU(IDUM,I,IT,X,XTAB,Y,YTAB)
C
C     ONE DIMENSIONAL TABLE LOOKUP WITH A MEMORY
C
      DIMENSION XTAB(1),YTAB(1)
C     FIND BRACKET
      IF(X.LT.XTAB(IT-1)) GO TO 8
      I=IT
      GO TO 30
    8 IF(XTAB(I).GT.X) GO TO 20
   10 I=I+1
      IF(I.EQ.IT) GO TO 30
      IF(XTAB(I).GT.X) GO TO 30
      GO TO 10
C
   20 IF(XTAB(I-1).LE.X) GO TO 30
      I=I-1
      IF(I.EQ.2) GO TO 30
      GO TO 20
   30 CONTINUE
C     I DESIGNATES THE XTAB POINT TO THE RIGHT
      AB=(X-XTAB(I))/(XTAB(I-1)-XTAB(I))
      Y=AB*YTAB(I-1)+(1.0-AB)*YTAB(I)
      RETURN
      END
```

```
      SUBROUTINE EQ4D9(ITRIG,S,Q)
C
CCC   IN-LINE GAP, UPSTREAM OF INTERSECTION, LAMINAR,  (Q/QFP)
CCCCC                                                 H.E.CHRISTENSEN 75
CCCCC E = EDGE RADIUS (CM)
CCCCC W = GAP WIDTH   (CM)
CCC   S = SURFACE DISTANCE INTO GAP (CM)
C
      COMMON /CONGAP/ ARGL(25),SMIN,FMIN,DFDSA,SMAX,FMAX,DFDSB
      EQUIVALENCE (ARGL(5),E), (ARGL(7),W)
      DIMENSION C(5)
      IF(ITRIG.GE.2) GO TO 100
C
CCC   -----CONSTANTS FOR EQUATION 4-9
C
      C(1) = 0.39439 +0.76083*E/W -0.02602*E*E/(W*W)
      C(2) = -0.71672/W-0.51625
      C(3) = 0.0132/(W*W)
      C(4) = 2.53332*E*E -3.62726*W*E
      C(5) = -1.33060*E + 2.53332*W*E*E
C
CCC   ----- INTERPOLATE TO OBTAIN SMIN AND SMAX
C
      SMIN = SMINF(E)
      SMAX = SMAXF(E)
C
      QRMIN = QRF4D9(C,SMIN)
      FMIN  = ALOG(QRMIN)
      QRMAX = QRF4D9(C,SMAX)
      FMAX  = ALOG(QRMAX)
      DFDSA = C(2) + 2.0*C(3)*SMIN + C(4)/SMIN + 2.0*C(5)*(ALOG(SMIN))/
     1        SMIN
      DFDSB = C(2) + 2.0*C(3)*SMAX +C(4)/SMAX + 2.0*C(5)*(ALOG(SMAX))/
     1        SMAX
C
      RETURN
C
  100 Q = QRF4D9(C,S)
      RETURN
      END



      FUNCTION SMAXF(E)
C
CCC   MAX. SURFACE DISTANCE FOR INSTRUMENTATION IN C. SCOTT TESTS
C
      DIMENSION XE(4),XSMAX(4)
      DATA XE    / 0.00254, 0.318, 0.635, 1.270/
      DATA XSMAX / 0.900  , 1.050, 1.850, 3.000 /
      DATA IS,IMEM /4,2/

      CALL TBLU(IDUM, IMEM,IS,E,XE,AB  , XSMAX)
      SMAX = AB
      RETURN
      END



      FUNCTION SMINF(E)
C
CCC   MIN. SURFACE DISTANCE FOR INSTRUMENTATION IN C.SCOTT TESTS
C
      DIMENSION XE(4), XSMIN(4)
      DATA XE    / 0.00254, 0.318, 0.635, 1.270/
      DATA XSMIN / 0.400  , 0.540, 0.810, 1.350/
      DATA IS,IMEM /4,2/

      CALL TBLU(IDUM,IMEM,IS,E,XE,AB, XSMIN)
      SMIN = AB
      RETURN
      END
```

```
      FUNCTION QRF409(C,S)
C                              CORRELATION FUNCTION  4-9
      DIMENSION C(1)
      ALNS  = ALOG(S)
      XLNQR = C(1) + (C(2) + C(3)*S)*S +(C(4)+ C(5)*ALNS)*ALNS
      QRF409 = EXP(XLNQR)
      RETURN
      END




      SUBROUTINE EQ4D10(ITRIG,S,Q)
C
CC    IN-LINE GAP, DOWNSTREAM OF INTERSECTION,LAMINAR,  (Q/QFP)
CCC                                                    H.E. CHRISTENSEN 75
CCC   E=EDGE RADIUS (CM)
CCC   W=GAP  WIDTH  (CM)
CCC   S= SURFACE DISTANCE INTO GAP(CM)
C
      COMMON/COMGAP/ ARGL(25),SMIN,FMIN,DFDSA,SMAX,FMAX,DFDSB
      EQUIVALENCE (ARGL(5),E),(ARGL(7),W)
      DIMENSION C(5)
      IF(ITRIG.GE.2) GO TO 100
C
CCC   ----- CONSTANTS FOR EQUATION 4-10
C
      C(1) =-1.21264 +(7.82944 - 2.30047 *E)*E
      C(2) =-0.060260/W -4.27622
      C(3) =  0.12501
      C(4) =-0.39390*E*E
      C(5) =  1.09199*W
C
CC    ----- INTERPLETE TO OBTAIN SMIN AND SMAX
C
      SMIN = SMINF(E)
      SMAX = SMAXF(E)
C
      QRMIN = QRF4D10(C,SMIN)
      FMIN  = ALOG(QRMIN)
      QRMAX = QRF4D10(C,SMAX)
      FMAX  = ALOG(QRMAX)
C
      DFDSA = C(2) + 3.0*C(3)*SMIN*SMIN -2.0*C(4)/(SMIN**3)+ 2.0*C(5)*
     1        ALOG(SMIN)/SMIN
      DFDSB = C(2)+ 3.0*C(3)*SMAX*SMAX -2.0*C(4)/(SMAX**3)+ 2.0*C(5)*
     1        ALOG(SMAX)/SMAX
C
      RETURN
C
  100 Q = QRF4D10(C,S)
      RETURN
      END




      FUNCTION QRF4D10(C,S)
      DIMENSION C(1)
      XLNQR = C(1)+(C(2) +C(3)*S*S,*S + C(4)/(S*S) + C(5)*((ALOG(S))*2)
      QRF4D10 = EXP(XLNQR)
      RETURN
      END
```

```
      SUBROUTINE EQ4D11(ITRIG,S,Q)
C
C     TRANSVERSE GAP UP-STREAM WALL, LAMINAR, (Q/QFP)
C                                                    H.E.CHRISTENSEN
C     E = EDGE RADIUS (CM)
C     W = GAP WIDTH   (CM)
C     S = SURFACE DISTANCE INTO GAP  (CM)
C
      COMMON / COMGAP/ ARGL(25),SMIN,FMIN,DFDSA,SMAX,FMAX,DFDSB
      EQUIVALENCE (ARGL(5),E), (ARG (7),W)
      DIMENSION C(3)
C
      IF(ITRIG.GE.2) GO TO 100
C
C     -----CONSTANTS FOR EQUATION 4-11
C
      C(1) =-0.313755 + 2.27958*E + 0.33317*ALOG(W)
      C(2) =-4.1428   + 1.35861*E
      C(3) =-1.42212
      SMAX = SMAXF(E)
      QRMAX = QRF4D11(C,SMAX)
      FMAX = ALOG(QRMAX)
      SMIN = SMINF(E)
      QRMIN = QRF4D11(C,SMIN)
      FMIN = ALOG(QRMIN)
C
      DFDSA = C(2)/SMIN   + 2.0*C(3)*ALOG(SMIN)/SMIN
      DFDSB = C(2)/SMAX   + 2.0*C(3)*ALOG(SMAX)/SMAX
C
  100 Q = QRF4D11(C,S)
      RETURN
      END



      FUNCTION QRF4D11(C,S)
      DIMENSION C(1)
      AB = ALOG(S)
      XLNQR = C(1)+(C(2)+ C(3)*AB)*AB
      QRF4D11 = EXP(XLNQR)
      RETURN
      END
```

```
      SUBROUTINE EQ4D13(ITRIG,S,Q)
C
CC    IN-LINE GAP, UPSTREAM OF INTERSECTION, LAMINAR, (Q/QE)
CCC
C
      COMMON /COMGAP/ ARGL(25),SMIN,FMIN,DFDSA,SMAX,FMAX,DFDSB
      EQUIVALENCE (ARGL(5),E), (ARGL(7),W)
      DIMENSION C(6)
      IF(ITRIG.GE.2) GO TO 100
C
CC    -----CONSTANTS FOR EQUATION 4-13
C
      C(1) =-0.01221 +0.27744*E/W + 0.70519*((E+W)**2)
      C(2) =-1.37104 -0.41940/W
      C(3) = 0.00725/(W*W)
      C(4) = 0.04555
      C(5) = 0.80703*E
      C(6) =-0.47496*E*E
C
C
      SMIN = SMINF(E)
      SMAX = SMAXF(E)
      QRMIN= QRF4D13(C,SMIN)
      FMIN = ALOG(QRMIN)
      QRMAX = QRF4D13(C,SMAX)
      FMAX = ALOG(QRMAX)
      DFDSA= C(2)+ 2.0*C(3)*SMIN + 3.0*C(4)*SMIN*SMIN -C(5)/(SMIN*SMIN)
     1       -2.0*C(6)/(SMIN**3)
      DFDSB= C(2)+2.0*C(3)*SMAX + 3.0*C(4)*SMAX*SMAX - C(5)/(SMAX*SMAX)
     1       -2.0*C(6)/(SMAX**3)
C
      RETURN
C
  100 Q = QRF4D13(C,S)
      RETURN
      END
```

```
      FUNCTION QRF4D13(C,S)
C                          CORRELATION FUNCTION 4-13
      DIMENSION C(1)
      XLNQR= C(1)+(C(2)+(C(3)+C(4)*S)*S)*S +(C(5)+ C(6)/S)/S
      QRF4D13 = EXP(XLNQR)
      RETURN
      END
```

```
      SUBROUTINE EQ4D14(ITRIG,S,Q)
C
CCC
CCC   IN-LINE GAP, DOWNSTREAM OF INTERSECTION, LAMINAR,(Q/QE)
C
      COMMON/COMGAP/ ARGL(25),SMIN,FMIN,DFDSA,SMAX,FMAX,DFDSB
      EQUIVALENCE (ARGL(5),E), (ARGL(7),W)
      DIMENSION C(5)
C
      IF(ITRIG.GE.2) GO TO 100
C
CCC   -----CONSTANTS
C
      C(1)=-0.16717 + 1.45275*((W+E)**2) + 0.42637*ALOG(E)
      C(2)=-2.6609
      C(3)= 0.06483
      C(4)= 0.33840*E*E
      C(5)=-1.3285
C
      SMIN = SMINF(E)
      SMAX = SMAXF(E)
C
      QRMIN= QRF4D14(C,SMIN)
      FMIN = ALOG(QRMIN)
      QRMAX = QRF4D14(C,SMAX)
      FMAX  = ALOG(QRMAX)
C
      DFDSA = C(2) + 3.0*C(3)*SMIN*SMIN -2.0*C(4)/(SMIN**3) + C(5)/SMIN
      DFDSB = C(2) + 3.0*C(3)*SMAX*SMAX - 2.0*C(4)/(SMAX**3)+ C(5)/SMAX
C
      RETURN
C
  100 Q = QRF4D14(C,S)
      RETURN
      END
```

```
      FUNCTION QRF4D14(C,S)
C                          CORRELATION FUNCTION 4-14
      DIMENSION C(1)
      XLNQR = C(1) + (C(2) + C(3)*S*S)*S + C(4)/S + C(5)*ALOG(S)
      QRF4D14 = EXP(XLNQR)
      RETURN
      END
```

```
      SUBROUTINE EQ4D15(ITRIG,S,Q)
C
CC    TRANSVERSE GAP (UP-STREAM SIDE), LAMINAR, (Q/QE)
C
      COMMON /COMGAP/ ARGL(25),SMIN,FMIN,DFDSA,SMAX,FMAX,DFDSB
      EQUIVALENCE (ARGL(5),E),(ARGL(7),W)
      DIMENSION C(3)
C
      IF(ITRIG.GE.2) GO TO 100
C
CC    -----CONSTANTS
C
      C(1)= 0.35564 + 1.18292*E*E
      C(2)=-2.7736
      C(3)= 1.83519*W*E*E
C
      SMIN = SMINF(E)
      SMAX = SMAXF(E)
C
      QRMIN= QRF4D15(C,SMIN)
      FMIN = ALOG(QRMIN)
      QRMAX= QRF4D15(C,SMAX)
      FMAX = ALOG(QRMAX)
      DFDSA = C(2) + C(3)/SMIN
      DFDSB = C(2) + C(3)/SMAX
C
      RETURN
C
  100 Q = QRF4D15(C,S)
      RETURN
      END



      FUNCTION QRF4D15(C,S)
C                          CORRELATION FUNCTION  4-15
      DIMENSION C(1)
      XLNQR = C(1) + C(2)*S + C(3)*ALOG(S)
      QRF4D15 = EXP(XLNQR)
      RETURN
      END
```

```
      SUBROUTINE EQ15D5(ITRIG,Z,Q)
C
CC    TRANSVERSE GAP, DOWNSTREAM WALL(LAMINAR)  (H/HFP)    (EQ 5-15)
C
      COMMON /COMGAP/ ARGL(25),ZMIN,FMIN,DFDZA, ZMAX, FMAX, DFDZ3
      EQUIVALENCE (ARGL(5),E),(ARGL(7),W),(ARGL(8),T),(ARGL(14),REPM)
      DIMENSION C(4)
      RE = REPM/(1.0E+06)
C
      IF(ITRIG.GE.2) GO TO 100
C
CC    -----CONSTANTS FOR EQ.15-5
C
      C(1)=-0.40577 + 2.91733*W -3.03105*W*W
      C(2)=-6.80369 - 0.36933*RE
      C(3)= 1.5057 + 0.38980*RE + 1.79532*W*W
      C(4)=-0.11073*W*RE*T
C
      ZMIN  = -1.E+30
      ZMAX  = 4.0
      WRITE(6,900) ZMAX
      QRMAX = QRF15D5(C,ZMAX)
      WRITE(6,900)ZMAX,C,QRMAX
      FMAX  = ALOG(QRMAX)
C
C
      DFDZB = C(2) + (2.0*C(3)      + 3.0*C(4)*ZMAX)*ZMAX
      WRITE(6,900) DFDZB
C
      RETURN
C
  100 Q = QRF15D5(C,Z)
      RETURN
  900 FORMAT(*  ZMAX,C,QRMAX*/8E13.3)
      END


      FUNCTION QRF15D5(C,Z)
C                          CORRELATION FUNCTION 15-5
      DIMENSION C(1)
      XLNQR = C(1) + (C(2)+(C(3)+C(4)*Z)*Z)*Z
      QRF15D5 = EXP(XLNQR)
      RETURN
      END



      SUBROUTINE EQ9(ITRIG,Z,Q)
C
CC    TRANSVERSE GAP, LAMINAR (EQ9) HCF TESTS AT JSC
C
      COMMON/COMGAP/ ARGL(25), ZMIN,FMIN,DIFDZA,ZMAX,FMAX,DFDZB
      EQUIVALENCE (ARGL(7),W), (ARGL(8),T)
      DIMENSION C(3)
C
      IF(ITRIG.GE.2) GO TO 100
C
CC    ----- CONSTANTS
C
      C(1) =-C.3716 +1.0733*W
      C(2) =-5.0249 -0.3797*T*T -0.03654/W
      C(3) =2.5604 -6.-719/(T*T)
C
      RETURN
C
  100 Q = QRF9(C,Z)
      RETURN
      END
```

```
      FUNCTION QRF9(C,Z)
C                              CORRELATION EQUATION 9
      DIMENSION C(1)
      XLNQR = C(1) + (C(2) + C(3)*Z)*Z
      QRF9 = EXP(XLNQR)
      RETURN
      END


      SUBROUTINE EQ25(ITRIG,Z,Q)
C
CC    IN-LINE GAP, HCF TESTED AT JSC   (H/HFP), LAMINAR
C
      COMMON/ COMGAP/ ARGL(25),ZMIN,FMIN,DFDZA,ZMAX,FMAX,DFDZB
      EQUIVALENCE (ARGL(7),W)
      DIMENSION C(3)
C
CC    ----- CONSTANTS
C
      C(1) =-0.3319 + 1.0148*W
      C(2) = -4.3979  - 0.2295/W
      C(3) = 1.563
C
      RETURN
C
  100 Q = EXP( C(1) + (C(2) + C(3)*Z)*Z)
      RETURN
      END


          SUBROUTINE EQ18(ITRTG,Z,Q)
C
CC    TRANSVERSE GAP (CFHT M=10, VDT M=8)  TURBULENT FLOW (EQ.18)
C
      COMMON/COMGAP/ ARGL(25),ZMIN,FMIN,DFDZA,ZMAX,FMAX,DFDZB
      EQUIVALENCE (ARGL( 7),W), (ARGL(19), TWOTE), (ARGL(14),REPM)
      DIMENSION C(3)
C
C
      IF(ITRIG.GE.2) GO TO 100
C     ----- CONSTANTS FOR EQUATION 18
C
C     C(1) = 4.28021 -0.53620*(ALOG(REPM/1.0E+06)) +0.7806*ALOG(W)
      C(2) = 1.46402*(W**(-2.0/7.0))
      C(3) =-2.549
C
      RETURN
C
  100 Q = EXP(C(1)+C(2)*ALOG(Z) + C(3)*ALOG(TWOTE))
      RETURN
      END


      SUBROUTINE EQ12A(TRIG,Z,Y,Q)
C
CC     INFLUENCE OF FLOW ANGLE ON TRANSVERSE GAP HEAT (TURB),(H/HFP)
C
      COMMON /COMGAP/  ARGL(25),ZMIN,FMIN,DFDZA,ZMAX,FMAX,DFDZB
      EQUIVALENCE (ARGL(7),W), (ARGL(6),G)
C
      IF(ITRIG.GE.2) GO TO 100
C
CC    ----- CONSTANTS
C
      C = -0.1504 + 1.92179*W
C
      RETURN
C
  100 Q = EXP(C -3.714*Z +0.50432*Z*Z -0.00692*Y*Y +0.04316*Y*W
     1        + 0.1768*Y*G + 0.00235*Y*Y*Z)
      RETURN
      END
```

```
      SUBROUTINE EQ16D1(ITRIG,Z,Q)
C
CC    H/HFP, LONG IN-LINE GAP, LAMINAR, GAMMA=0 (EQ.16-1)
C
      COMMON /COMGAP/ ARGL(25),ZMIN,FMIN,DFDZA,ZMAX,FMAX,DFDZB
      EQUIVALENCE (ARGL(7),W),(ARGL(8),T), (ARGL(10),GAPFL),
     1            (ARGL(15),THETA),(ARGL(16),DTHK)
C
      DIMENSION C(5)
C
      IF(TRIG.GE.2) GO TO 100
C
CC    ----- CONSTANTS
C
      C(1) = 0.70912 +0.13155*ALOG(T)+1.13475*ALOG(W) +0.18345*ALOG(G/PF
     1       L)
      C(2) =-1.2942  -1.13475         -0.07728*((ALOG(W))**2)
      C(3) =-0.52376
      C(4) = 0.8671
      C(5) =-0.1835
C
C
      ZMIN = 0.04
      ZMAX = 3.5
      QRMIN = QRF16D1(C,ZMIN)
      FMIN  = ALOG(QRMIN)
C
      QRMAX = QRF16D1(C,ZMAX)
      FMAX  = ALOG(QRMAX)
C
      DFDZA =        C(2)/ZMIN + 2.0*C(3)*ALOG(ZMIN)/ZMIN
      DFDZB=         C(2)/ZMAX + 2.0*C(3)*ALOG(ZMAX)/ZMAX
C
      RETURN
C
  100 Q = QRF16D1(C,Z)
      RETURN
      END



      FUNCTION QRF16D1(C,Z)
C
CC                          EQ 16-1
C
      DIMENSION C(1)
      COMMON /COMGAP/ ARGL(25), ZMIN,FMIN,DFDZA,ZMAX,FMAX,DFDZB
      EQUIVALENCE  (ARGL(15),THETA), (ARGL(16),DTHK)
      AB = ALOG(Z)
      XLNQR = C(1) + (C(2)+C(3)*AB)*AB + C(4)*ALOG(THETA) + C(5)*ALOG(
     1        DTHK)
      QRF16D1=EXP(XLNQR)
      RETURN
      END
```

```
      SUBROUTINE EQ16D2(ITRIG,Z,Q)
C
C     H/HE; LONG IN-LINE GAP, LAMINAR,GAMMA=0 (EQ16-2)
C
      COMMON /COMGAP/ ARGL(25),ZMIN,FMIN,DFDZA,ZMAX,FMAX,DFDZB
      EQUIVALENCE (ARGL(7),W), (ARGL(8),T), (ARGL(10), GAPFL),
     1            (ARGL(15),THETA), (ARGL(16),DTHK)
C
      DIMENSION C(5)
C
      IF(ITRIG.EQ.2) GO TO 100
C
C     -----CONSTANTS
C
      C(1) = 0.58794 +1.00779*ALOG(W)-0.19332*ALOG(GAPFL)
     1       +0.13326*ALOG(T)
      C(2) =-0.91294 -1.00779 -0.06665*((ALOG(W))**2)
      C(3) = 0.86146
      C(4) = -0.19332
      C(5) = 0.11529
C
      ZMIN = 0.04
      ZMAX = 3.5
      QRMIN= QRF16D2(C,ZMIN)
      FMIN = ALOG(QRMIN)
C
      QRMAX= QRF16D2(C,ZMAX)
      FMAX = ALOG(QRMAX)
      DFDZA = C(2)/ZMIN + 3.0*C(5)*((ALOG(ZMIN))**3)
      DFDZB = C(2)/ZMAX + 3.0*C(5)*((ALOG(ZMAX))**3)
C
      RETURN
C
  100 Q =QRF16D2(C,Z)
      RETURN
      END



      FUNCTION QRF16D2(C,Z)
C
C
C                              EQ 16-2
      DIMENSION C(2)
      COMMON/COMGAP/ ARGL(25),ZMIN,FMIN,DFDZA,ZMAX,FMAX,DFDZB
      EQUIVALENCE    (ARGL(15),THETA),(ARGL(16),DTHK)
      AB = ALOG(Z)
      XLNQR = C(1) + C(2)*AB + C(3)*ALOG(THETA) + C(4)*ALOG(DTHK)
     1        + C(5)*AB*AB*AB
      QRF16D2 = EXP(XLNQR)
      RETURN
      END
```

```
      SUBROUTINE EQ16D34(ITRIG,Z,Q)
C
CCC
CCC   H/HFP, IN-LINE GAP, LAMINAR , GAMMA UP TO 15
CCC
CCC   ICOR = 18 --- EQ. 16-3,  SIDE A AND B
CCC   ICOR = 19 --- EQ. 16-4,  SIDE A
C
      COMMON /COMGAP/  ARGL(25), ZMIN, FMIN, DFDZA, ZMAX, FMAX, DFDZB
C
      EQUIVALENCE (ARGL(3), ICOR), (ARGL(7), W), (ARGL(10), GAPFL),
     1           (ARGL(15),THETA),(ARGL(16),DTHK),(ARGL(8),T)
      DIMENSION C(5)
      IF(ITRIG.GE.2) GO TO 100
      AB    = ALOG(W)
      IF(ICOR.EQ.19) GO TO 10
C
CCC   ----- CONSTANTS FOR EQ. 16-3
C
      C(1) = 1.88198 +2.86909*W +0.13326*ALOG(GAPFL)+ 0.45139*AB*AB
     1      +.10532*ALOG(T) +0.60717*ALOG(THETA)
      C(2) =-2.86909+1.33939*AB
      C(3) =-0.44674
      C(4) = 0.00376
      C(5) = DTHK/(GAPFL*W)
      GO TO 20
C
CCC   ----- CONSTANTS FOR EQ. 16-4
C
   10 C(1) = 2.65299 + 2.98795*AB +0.4789*AB*AB +0.69661*ALOG(THETA)
     1      +0.10187*ALOG(T)
      C(2) =-2.65239 +1.49684*AB
      C(3) =-0.50150
      C(4) = 0.00215
      C(5) = DTHK/(GAPFL*W)
C
   20 ZMIN = 0.04
      ZMAX = 3.8
      QRMIN= QR16D34(C,ZMIN)
      FMIN = ALOG(QRMIN)
      QRMAX= QR16D34(C,ZMAX)
      FMAX = ALOG(QRMAX)
C
      DFDZA= C(2)/ZMIN + 2.0*C(3)*ALOG(ZMIN)/ZMIN +
     1       3.0*C(4)*((ALOG(C(5)*ZMAX))**2)/(C(5)*ZMIN)
C
      RETURN
C
  100 Q = QR16D34(C,Z)
      RETURN
      END
```

```
      FUNCTION  QR16D34 (C,Z)
C
CCC   EQ.16-3   AND  EQ.16-4
C
      DIMENSION C(5)
      AB = ALOG(Z)
      ALNQ = C(1) +(C(2)+ C(3)*AB)*AB + C(4)*((ALOG(C(5)*Z))**3)
      QR16D34 = EXP(ALNQ)
      RETURN
      END
```

```
      SUBROUTINE EQ16D56(ITRIG,Z,Q)
C
CCCCC
      H/HE, IN-LINE GAP, LAMINAR, GAMMA UP TO 15
CCCCC
      ICOR = 20 --- EQ. 16-5   SIDES A AND B
      ICOR = 21 --- EQ. 16-6   SIDE A
C
      COMMON /COMGAP/  ARGL(25), ZMIN, FMIN, DFDZA, ZMAX, FMAX, DFDZB
C
      EQUIVALENCE (ARGL( 3), ICOR  ), (ARGL(7),H     ), (ARGL(15),THETA)
     1           ,(ARGL( 6),GAMMA  ), (ARGL(14),REPM)
C
      DIMENSION C(3)
C
      IF(ITRIG.GE.2)GO TO 100
C
      AB = ALOG(H)
      BC = ALOG(THETA)
C
      IF(ICOR.EQ.21) GO TO 10
C
CCC   ----- CONSTANTS FOR EQ. 16-5
C
      C(1) = 4.16869 +1.20204*AB +1.39857*BC -0.39913*ALOG(REPM/1.0E+06)
     1       +(2.64364 - 8.30287*GAMMA)*GAMMA
      C(2) =-1.20204 +0.54123*AB +0.00026*AB*AB
      C(3) = 0.9374
C
      GO TO 20
C     ----- CONSTANTS FOR EQ. 16-6
C
   10 CONTINUE
      C(1) = 1.48434 +1.2492*AB + 0.74418*BC
     1       +(2.4384 - 7.964*GAMMA)*GAMMA
      C(2) =-1.2492  +0.54690*AB
      C(3) = 0.10130
C
   20 ZMIN = 0.04
      ZMAX = 3.8
      QRMIN=  QR16D56(C,Z)
      FMIN = ALOG(QRMIN)
      QRMAX=  QR16D56(C,Z)
      FMAX = ALOG(QRMAX)
C
      DFDZA = C(2)/ZMIN + 3.0*C(3)*((ALOG(ZMIN))**2)/ZMIN
      DFDZB = C(2)/ZMAX + 3.0*C(3)*((ALOG(ZMAX))**2)/ZMAX
C
      RETURN
C
  100 Q = QR16D56(C,Z)
      RETURN
      END



      FUNCTION  QR16D56(C,Z)
C
C     CORRELATION EQUATIONS  16-5 AND 16-6
      AB = ALOG(Z)
      ALNQR = C(1)+(C(2)+C(3)*AB*AB)*AB
      QR16D56 = EXP(ALNQR)
      RETURN
      END
```

```
      SUBROUTINE EQ17123(ITRIG,Z,Y,Q)
C
CC    TRANSVERSE GAP WITH FORWARD FACING STEP  (DOWN STREAM WALL)
CC
CC    ICOR = 21   LAMINAR        EQ. 17-1
CC    ICOR = 22   TRANSITION     EQ. 17-2
CC    ICOR = 23   TURBULENT      EQ. 17-3
C
      COMMON /COMGAP/ ARGL(25), ZMIN, FMIN, DFDZA, ZMAX, FMAX, DFDZB
C
      EQUIVALENCE (ARGL( 7),W     ),(ARGL(9), D),
     1            (ARGL( 1),IBL)
C     D = STEP HEIGHT (CM)
C     W = GAP WIDTH (CM)
C
      DIMENSION C(3)
C
      IF(ITRIG.GE.2) GO TO 100
C
      IF(IBL.NE.1)  GO TO 10
C
CC    -----LAMINAR FLOW CONSTANTS
C
      C(1) =-0.19252 +(5.67183-11.37065*D)*D
      C(2) =-4.24537 +23.52407*W*D -0.00192*Y*Y*Z
      C(3) = 1.26103 -6.57773*W*D
      GO TO 30
   10 IF(IBL.NE. 2) GO TO 20
C     -----TRANSITIONAL FLOW CONSTANTS
C
      C(1) =-0.65828 + 8.93015*D - 2.63955*D*D + 3.18026*W*W
      C(2) =-4.00086
      C(3) = 1.16511 - 0.01083*Y*Y*W +0.01461*Y
      GO TO 30
C
CC    -----TURBULENT  FLOW  CONSTANTS
C
   20 C(1) =-0.81624 +7.58098*D +0.17100*Y -0.28604*Y*W +1.43712*W*W
      C(2) =-2.5465
      C(3) = 0.35211 - 1.11972*D*D
C
   30 CONTINUE
      ZMIN =-1.0E+30
      ZMAX = 3.8
      QMAX = QR17123(C,ZMAX)
      FMAX = ALOG(QMAX)
C
      RETURN
C
  100 Q = QR17123(C,Z)
      RETURN
      END




      FUNCTION QR17123(C,Z)
C        STEP HEATING CORRELATION  EQ.17-1 , EQ.17-2, EQ.17-3
CC
      DIMENSION C(3)
      QR17123 = EXP(C(1) +(C(2)+C 3)*Z)*Z)
      RETURN
      END
```

APPENDIX D

The units used in this volume are SI Units, except Section 2 where the raw data presented was in English Units. Conversion factors required for units used herein are given in the following table:

Physical quantity	U.S. Customary Unit	Conversion factor (*)	SI Unit
Convective Heating Rate	Btu/ft^2-sec	1.134×10^4	$Watts/m^2$
Convective Heat Transfer Coefficient Based on $Taw/T_t = 0.895$	lbm/ft^2-sec	4.88	Kg/m^2-S
Enthalpy	Btu/lbm	2.324×10^3	J/Kg
Heat Transfer Coefficient	Btu/ft^2-sec-^oF	2.042×10^4	$Watts/m^2$-^oC
Length	in.	2.54×10^{-2}	m
Length	ft.	0.305	m
Pressure	lbf/ft^2	47.88	N/m^2
Pressure	lbf/ft^2	47.88×10^3	KN/m^2
Pressure	lbf/ft^2	47.88×10^6	MN/m^2
Reynolds Number	Re/ft	3.28	Re/m
(RHO V)1 Freestream Density - Velocity Product	lbm/ft^2-sec	4.88	Kg/m^2-S
Temperature	^oF	$5/9(^oF-32)$	^oC
Temperature	^oF	$5/9(^oF+460)$	^oK

*Multiply value in U.S. Customary Unit by conversion factor to obtain equivalent value in SI Unit.